



XA0055000

IAEA-TECDOC-1149

Experimental tests and qualification of analytical methods to address thermohydraulic phenomena in advanced water cooled reactors

*Proceedings of a Technical Committee meeting
held in Villigen, Switzerland, 14–17 September 1998*

31 / 27



INTERNATIONAL ATOMIC ENERGY AGENCY

IAEA

May 2000

IAEA SAFETY RELATED PUBLICATIONS

IAEA SAFETY STANDARDS

Under the terms of Article III of its Statute, the IAEA is authorized to establish standards of safety for protection against ionizing radiation and to provide for the application of these standards to peaceful nuclear activities.

The regulatory related publications by means of which the IAEA establishes safety standards and measures are issued in the **IAEA Safety Standards Series**. This series covers nuclear safety, radiation safety, transport safety and waste safety, and also general safety (that is, of relevance in two or more of the four areas), and the categories within it are **Safety Fundamentals**, **Safety Requirements** and **Safety Guides**.

- **Safety Fundamentals** (silver lettering) present basic objectives, concepts and principles of safety and protection in the development and application of atomic energy for peaceful purposes.
- **Safety Requirements** (red lettering) establish the requirements that must be met to ensure safety. These requirements, which are expressed as 'shall' statements, are governed by the objectives and principles presented in the Safety Fundamentals.
- **Safety Guides** (green lettering) recommend actions, conditions or procedures for meeting safety requirements. Recommendations in Safety Guides are expressed as 'should' statements, with the implication that it is necessary to take the measures recommended or equivalent alternative measures to comply with the requirements.

The IAEA's safety standards are not legally binding on Member States but may be adopted by them, at their own discretion, for use in national regulations in respect of their own activities. The standards are binding on the IAEA for application in relation to its own operations and to operations assisted by the IAEA.

OTHER SAFETY RELATED PUBLICATIONS

Under the terms of Articles III and VIII.C of its Statute, the IAEA makes available and fosters the exchange of information relating to peaceful nuclear activities and serves as an intermediary among its members for this purpose.

Reports on safety and protection in nuclear activities are issued in other series, in particular the **IAEA Safety Reports Series**, as informational publications. Safety Reports may describe good practices and give practical examples and detailed methods that can be used to meet safety requirements. They do not establish requirements or make recommendations.

Other IAEA series that include safety related sales publications are the **Technical Reports Series**, the **Radiological Assessment Reports Series** and the **INSAG Series**. The IAEA also issues reports on radiological accidents and other special sales publications. Unpriced safety related publications are issued in the **TECDOC Series**, the **Provisional Safety Standards Series**, the **Training Course Series**, the **IAEA Services Series** and the **Computer Manual Series**, and as **Practical Radiation Safety and Protection Manuals**.

***Experimental tests and qualification of
analytical methods to address
thermohydraulic phenomena in
advanced water cooled reactors***

*Proceedings of a Technical Committee meeting
held in Villigen, Switzerland, 14–17 September 1998*



INTERNATIONAL ATOMIC ENERGY AGENCY

IAEA

May 2000

The originating Section of this publication in the IAEA was:

Nuclear Power Technology Development Section
International Atomic Energy Agency
Wagramer Strasse 5
P.O. Box 100
A-1400 Vienna, Austria

**EXPERIMENTAL TESTS AND QUALIFICATION OF
ANALYTICAL METHODS TO ADDRESS THERMOHYDRAULIC PHENOMENA IN
ADVANCED WATER COOLED REACTORS**

IAEA, VIENNA, 2000
IAEA-TECDOC-1149
ISSN 1011-4289

© IAEA, 2000

Printed by the IAEA in Austria
May 2000

FOREWORD

Worldwide there is considerable experience in nuclear power technology, especially in water cooled reactor technology. Of the operating plants, in September 1998, 346 were light water reactors (LWRs) totalling 306 GW(e) and 29 were heavy water reactors (HWRs) totalling 15 GW(e). The accumulated experience and lessons learned from these plants are being incorporated into new advanced reactor designs. Utility requirements documents have been formulated to guide these design activities by incorporating this experience, and results from research and development programmes, with the aim of reducing costs and licensing uncertainties by establishing the technical bases for the new designs. Common goals for advanced designs are high availability, user-friendly features, competitive economics and compliance with internationally recognized safety objectives.

Large water cooled reactors with power outputs of 1300 MW(e) and above, which possess inherent safety characteristics (e.g. negative Doppler moderator temperature coefficients, and negative moderator void coefficient) and incorporate proven, active engineered systems to accomplish safety functions are being developed. Other designs with power outputs from, for example, 220 MW(e) up to about 1300 MW(e) which also possess inherent safety characteristics and which place more emphasis on utilization of passive safety systems are being developed. Passive systems are based on natural forces and phenomena such as natural convection and gravity, making safety functions less dependent on active systems and components like pumps and diesel generators.

In some cases, further experimental tests for the thermohydraulic conditions of interest in advanced designs can provide improved understanding of the phenomena. Further, analytical methods to predict reactor thermohydraulic behaviour can be qualified for use by comparison with the experimental results. These activities should ultimately result in more economical designs.

The Technical Committee Meeting on Experimental Tests and Qualification of Analytical Methods to Address Thermohydraulic Phenomena in Advanced Water Cooled Reactors was convened to review the current status and the remaining needs in this area. The meeting was hosted by the Paul Scherrer Institute, Villigen, 14–17 September 1998.

The IAEA officer responsible for this publication was J. Cleveland of the Division of Nuclear Power.

EDITORIAL NOTE

This publication has been prepared from the original material as submitted by the authors. The views expressed do not necessarily reflect those of the IAEA, the governments of the nominating Member States or the nominating organizations.

The use of particular designations of countries or territories does not imply any judgement by the publisher, the IAEA, as to the legal status of such countries or territories, of their authorities and institutions or of the delimitation of their boundaries.

The mention of names of specific companies or products (whether or not indicated as registered) does not imply any intention to infringe proprietary rights, nor should it be construed as an endorsement or recommendation on the part of the IAEA.

The authors are responsible for having obtained the necessary permission for the IAEA to reproduce, translate or use material from sources already protected by copyrights.

CONTENTS

SUMMARY	1
CONDENSATION TESTS AND QUALIFICATION OF MODELS (Session 1)	
Effect of pool turbulence on direct contact condensation at a steam/water interface.....	13
<i>J.D. Jackson, C.L. Zhao, S. Doerffer, J.E. Byrne, H. Falaki</i>	
Characterization of direct contact condensation of steam jets discharging into a subcooled water	21
<i>Chul-Hwa Song, Seok Cho, Hwan-Yeol Kim, Yoon-Young Bae, Moon-Ki Chung</i>	
Experimental research on in-tube condensation in the presence of air.....	39
<i>A. Tanrikut, O. Yesin</i>	
Effects of non-condensable gas on the condensation of steam.....	53
<i>J.D. Jackson, P. An, A. Reinert, M. Ahmadijead</i>	
Evaluation of the condensation phenomenon in presence of non-condensable gases for PCCS related geometry	83
<i>V. Faluomi</i>	
Modelling containment passive safety systems in advanced water cooled reactors	97
<i>L.E. Herranz, M.H. Anderson, M.L. Corradini, J.L. Muñoz-Cobo</i>	
DATA AND MODELS FOR CRITICAL HEAT FLUX (CHF) AND POST-CHF HEAT TRANSFER (Session 2)	
Experiments on critical heat flux for CAREM reactor.....	109
<i>C.M. Mazufri</i>	
Enhancing the moderator effectiveness as a heat sink during loss of coolant accidents in CANDU-PHW reactors using glass-peened surfaces	121
<i>T. Nitheanandan, R.W. Tiede, D.B. Sanderson, R.W.L. Fong, C.E. Coleman</i>	
Uncertainty of evaluations of flow film boiling heat transfer coefficient	139
<i>A.A. Ivashkevitch, P.L. Kirillov, V.V. Sergeev, I.P. Smogalev, V.N. Vinogradov</i>	
Dispersed flow film boiling heat transfer of flowing water in vertical tubes — CIAE steady state data and prediction methods	155
<i>Chen Yuzhou, Chen Haiyan</i>	
PASSIVE SYSTEMS FOR FLUID AND HEAT TRANSPORT (Session 3)	
Effectiveness of passive systems tested in the NOKO facility	167
<i>E.F. Hicken, H. Jaegers, M. Fethke, L. Rossner</i>	
The DIVA programme: General presentation and first results	179
<i>P. Dumaz, B. Duc</i>	
A flashing driven moderator cooling system for CANDU reactors: Experimental and computational results.....	189
<i>H.F. Khartabil</i>	
Natural circulation in an integral CANDU test facility.....	201
<i>P.J. Ingham, J.C. Luxat, A.J. Melnyk, T.V. Sanderson</i>	
Natural circulation performance in nuclear power plants	213
<i>F. D'Auria, G.M. Galassi, M. Frogheri</i>	
Boiling induced mixed convection in cooling loops	221
<i>J.U. Knebel, G. Janssens-Maenhout, U. Müller</i>	
Thermal hydraulic research on next generation PWRs using ROSA/LSTF	233
<i>T. Yonomoto, Y. Anoda</i>	

EXPERIMENTS AND ANALYSIS OF PASSIVE SAFETY SYSTEMS (Session 4)

EC-sponsored research activities on innovative passive safety systems.....	249
<i>J. Martin Bermejo, G. van Goethem</i>	
TEPSS related PANDA tests (ESBWR).....	267
<i>M. Huggenberger, C. Aubert, T. Bandurski, J. Dreier, O. Fischer, H.J. Strassberger, G. Yadigaroglu</i>	
SWR 1000 related containment cooling system tests in PANDA	277
<i>J. Dreier, C. Aubert, M. Huggenberger, H.J. Strassberger, G. Yadigaroglu</i>	
Modelling of particular phenomena observed in PANDA with GOTHIC	287
<i>Th. Bandurski, F. Putz, M. Andreani, M. Analytis</i>	
Modifications of the κ - ϵ model in GOTHIC near physical boundaries.....	299
<i>G.Th. Analytis, M. Andreani</i>	
RELAP5 capabilities in thermal-hydraulic prediction of SBWR containment behaviour: PANDA steady state and transient tests evaluation.....	315
<i>V. Fahuomi, S.N. Aksan</i>	
TEPSS – Technology enhancement for passive safety systems.....	327
<i>J. Hart, W.J.M. Slegers, S.L. de Boer, M. Huggenberger, J. López Jiménez, J.L. Muñoz-Cobo Gonzalez, F. Reventós Puigjaner</i>	
Post test analysis of TEPSS tests -P2-, -P3-, -P5- and -P7- using the system code RELAP5/MOD 3.2	337
<i>D. Luebbesmeyer</i>	
Relevant results of pre- and post-test analysis of P3 and P6 PANDA experiments.....	353
<i>L. Batet, F. Reventós</i>	

QUALIFICATION OF ANALYTICAL METHODS AND CODES (Session 5)

RELAP5 analysis of PACTEL injection tests.....	367
<i>G.R. Kimber, J.N. Lillington</i>	
FLICA-IV: An advanced code for advanced water cooled reactor.....	377
<i>A. Bergeron, D. Caruge, E. Royer</i>	
Primary coolant circuit coastdown and thermosyphon mode under failure of forced circulation in the Indian PHWR	391
<i>P. Pramod, A. Dubey, H.P. Rammohan, S.S. Bajaj</i>	
TRAC analyses and GIRAFFE tests for PCCS performance prediction	401
<i>K. Kataoka, K. Arai, S. Yokobori</i>	

APPLICATION OF METHODS IN DESIGN AND SAFETY ANALYSES (Session 6)

Uncertainty methodology applied to large break LOCA analysis	421
<i>C.F. Freire, E. Kuramoto, G. Seeberger, S. Blank</i>	
Application of data analysis techniques to nuclear reactor systems code to accuracy assessment.....	427
<i>R.F. Kunz, G.F. Kasmala, C.J. Murray, J.H. Mahaffy</i>	
Analysis of excessive increase in secondary steam flow transient in Chashma nuclear power plant.....	441
<i>Intsar-ul-Haq</i>	
Analysis of SGTR in AP-600 by RELAP5/MOD3.2 code	447
<i>F. D'Auria, G. Fruttuoso, G.M. Galassi, F. Oriolo, I. Bassanelli</i>	
List of Participants	465

SUMMARY

1. BACKGROUND

For advanced water cooled reactors, some key thermohydraulic phenomena are critical heat flux (CHF), post-CHF heat transfer, pressure drop under low flow and low pressure conditions, flow and heat transport by natural circulation, condensation of steam in the presence of non-condensable gases, thermal stratification and mixing in large pools, gravity driven re-flooding, and potential flow instabilities. To investigate the thermohydraulic behaviour of advanced designs, experimental facilities have been constructed and operated by various organizations supporting the design, testing, and certification of advanced water cooled reactors, as well as by organizations assessing the safety performance of these designs.

The nuclear industry and regulatory bodies have developed thermohydraulics codes for predicting reactor performance under normal, transient and accident conditions. These codes are used for plant design, evaluations of thermal margins, establishment of emergency procedures and operator training. These codes essentially solve mass, momentum and energy balance equations and include detailed representations of thermohydraulic relationships and thermophysical properties. The main code development efforts focus on modelling especially thermohydraulic phenomena in the primary system, in large pools of water, and in the containment. Clearly the performance of these codes is dependent on the accuracy and consistency of the representations of the thermohydraulic relationships and thermophysical properties data contained in the codes.

Extensive qualification programmes have been carried out to demonstrate the applicability of the codes in predicting reactor performance. These have been conducted in national and international contexts at four levels, involving the use of fundamental experiments, separate effects test facilities (SETF), integral test facilities (ITF), and plant data.

Experimental data have been extensively compared with code predictions including Committee on the Safety of Nuclear Installations (CSNI), international standard problems developed by the OECD Nuclear Energy Agency and IAEA standard problem exercises.

The present situation in relation to the development, qualification and use of system codes, can be summarized as follows:

- Passive components and systems represent a challenge for thermohydraulic codes. New models have been or are being developed in the following areas in order to qualify the codes:
 - non-equilibrium mixtures involving subcooled and saturated water, saturated and superheated steam;
 - low velocity natural circulation;
 - initiation of passive systems;
 - effects of non-condensables on steam condensation;
 - water circulation in pools;
 - rapid condensation caused by interfacing steam and subcooled water;
- The codes have reached an acceptable degree of maturity though their reliable application is still limited to the validation domain;
- Code validation criteria and detailed qualification programmes have been established [1, 2];

- Methodologies to evaluate the “uncertainty” (i.e. the error) in the prediction of nuclear plant behaviour by system codes have been proposed and are being tested;
- The topics of user effect (i.e. influence of code users on the predictions), nodalization qualification, quantification of code accuracy (i.e. ranking of the error in the comparison between measured and calculated trend), have been dealt with and experience is currently available;
- Activities co-ordinated by the CSNI have been recently completed including:
 - a state of the art report on thermohydraulics of emergency core cooling [3];
 - establishment of the separate effects tests-code validation matrix including the identification and the definition of the phenomena that must be predicted by codes;
 - the set-up of the integral test facility code validation matrix;
 - documentation of lessons learned from the execution of the International Standard Problem exercises.

The IAEA has published several reports on advanced water cooled reactor designs and the related experimental tests and analytical methods development to address thermohydraulic phenomena [4–11]. Also, an IAEA co-ordinated research project on thermohydraulic relationships for advanced water cooled reactors was conducted from 1995–1998 with the aim (a) to systematically list and evaluate the requirements for thermohydraulic relationships in support of advanced water cooled reactor systems during normal and accident conditions, and provide details of their database where possible, and (b) recommend a consistent set of thermohydraulic relationships for selected phenomena such as CHF and post-CHF heat transfer, and pressure drop, including low flow and low pressure conditions, for advanced water cooled reactors.

As reported at the IAEA Technical Committee Meeting on Progress in Development and Design Aspects of Advanced Water Cooled Reactors [5] convened in Rome in 1991, it is clearly recognized that incorporation of passive systems into advanced designs brings the need for experimental investigations and modelling activities over a wide range of conditions appropriate for initiation and operation of the systems and for conditions appropriate to testing of the systems. Considerable progress achieved in experimental tests and analyses of heat removal systems was reported in an IAEA Technical Committee meeting [7] convened in Piacenza, Italy, in 1995. Although proof of predicted performance in support of design certification has been the major goal of such testing, more complete understanding of the basic heat transfer phenomena would be very worthwhile for thorough understanding. This is especially important for passive heat transport systems which rely on small driving forces at low pressure thereby requiring comprehensive testing to assure that conditions resulting in system initiation and conditions affecting system reliability and performance are thoroughly understood. Further, it was the general consensus at the Piacenza meeting that testing of heat removal systems at large scale integral test facilities should continue to provide an extensive experience base in system behaviour and data for qualification of computer codes. The Piacenza meeting also emphasized that the question of extrapolability of the test results to larger sized plants which rely on the same phenomena should be addressed, because larger plants could potentially bring economic advantages.

2. OBJECTIVE AND SCOPE

The objective of the Technical Committee Meeting on Experimental Tests and Qualification of Analytical Methods to Address Thermohydraulic Phenomena in Advanced Water Cooled

Reactors was to provide a forum to present and discuss activities related to (1) the establishment of qualified experimental data bases on thermohydraulic phenomena which cover ranges of parameters relevant to advanced water cooled reactors, (2) qualification of analytical methods and codes, and (3) application of these methods in design and analyses of advanced water cooled reactors. Another aim was to identify areas and research needs where international co-operation can be beneficial.

Papers were solicited on the following topics:

(A) Experimental tests and qualification of analytical methods addressing:

- CHF for advanced water reactors;
- post CHF heat transfer for advanced water reactors;
- pressure drop under low flow, low pressure conditions;
- natural circulation;
- BWR natural-circulation flow instabilities;
- heat transport in pools under non-equilibrium conditions;
- rapid condensation caused by interfacing steam and subcooled water;
- effects of non-condensables on steam condensation;
- initiation and functioning of passive systems.

(B) Application of computer models to predict performance of components and systems in which the above phenomena occur.

3. CONDUCT OF THE MEETING

The Technical Committee meeting was organized by the Department of Nuclear Energy and hosted by the Paul Scherrer Institute, Villigen, Switzerland, 14–17 September 1998. It was conducted within the frame of activities of the IAEA's International Working Groups on Advanced Technologies for Light Water Reactors and Heavy Water Reactors (the IWG-LWR and IWG-HWR).

There were 50 participants representing 22 Member States and the European Commission. The Member States represented were: Argentina, Belgium, Brazil, Canada, China, France, Germany, Hungary, India, Israel, Italy, Japan, the Republic of Korea, Mexico, the Netherlands, Pakistan, the Russian Federation, Spain, Switzerland, Turkey, the United Kingdom, and the United States of America.

The meeting Chairman was Nusret Aksan of the Paul Scherrer Institute, Villigen, Switzerland.

4. RESULTS

Several advanced water cooled reactor designs incorporate passive systems for condensing steam. Although condensation of steam has been studied extensively in the past for many industrial applications, several experiments on steam condensation have been, and are being, carried out by the nuclear industry. It is important to have assurance that the passive systems for steam condensation are effective during all sequences in which they are required to function. Further, high quality experimental data are necessary to validate modern thermohydraulic computer codes used to predict the performance of the passive systems.

The condensation process can occur either by direct contact between steam and subcooled water or on walls separating the steam from cooler media. These two condensation processes are quite different. Further it is well known that the condensation process can be heavily effected by the presence of non-condensable gases. In water cooled reactor containments, non-condensables are always present in relatively high concentrations. Non-condensables may also be present in the primary circuit of water cooled reactors during certain phases of accident sequences.

For several advanced water cooled reactor designs, steam is condensed under accident conditions by injecting it directly into water pools. This occurs, for example, when the reactor primary system is depressurized through depressurization valves to the in-containment refuelling water storage tank, and when the pressurizer safety relief valves are opened to discharge into a water tank. To properly design the depressurization system, including the steam spargers, to assure its structural integrity, it is necessary to understand this direct contact condensation phenomena. This is influenced by the pressure, mass flux, steam and pool temperature, as well by the geometry and orientation of the discharge nozzle.

Direct condensation has been investigated at the Korea Atomic Energy Research Institute for steam discharge into sub-cooled water. These tests were performed to simulate the condensation during the depressurization of advanced systems (e.g. the Korean Next Generation Reactor, and others) through valves into an in-containment refuelling water storage tank (IRWST). Test results were used to examine the accuracy of various correlations for modelling of condensation. The tests were performed over a wide range of steam mass flow and water pool temperatures.

Condensation by direct contact at a horizontal interface between saturated steam and a pool of water has been investigated at the University of Manchester in the United Kingdom. The tests were performed in a small vertical cylindrical section which was operated at ambient pressure. Measurements were made of direct contact condensation heat transfer at a relatively undisturbed interface between the saturated steam and the water. Additional tests examined the effect of turbulence in the water pool on the condensation process, and a correlation was derived relating the heat transfer coefficient to the turbulent velocity just below the interface.

Several advanced designs incorporate passive systems for steam condensation within tubes cooled externally. The presence of non-condensable gases can greatly inhibit condensation inside tubes due to build up of these gases at the heat transfer interface. The decrease in condensation resulting from the presence of non-condensable gas (air) has been investigated experimentally at the Middle East Technical University (METU) of Ankara, Turkey in co-operation with the Turkish Atomic Energy Authority. The degradation in heat transfer coefficient is strongly dependent on the specific geometrical conditions in addition to the thermohydraulic conditions, and therefore requires testing under conditions appropriate to the geometry of the system. For the specific configuration examined by METU, comparisons of code predictions with measured data typically showed differences in the range of 5 to 50%. For this phenomena, comparisons of experimental results with code predictions generally show this type of difference, currently resulting in the need to either test full scale components, or to design systems with considerable margin to cover the uncertainties.

Recent experiments to examine the effects of non-condensable gas (air) have been carried out at the University of Manchester in the United Kingdom. Heat was removed from flowing steam-air mixtures by a condensing plate cooled by water. The ratio between steam and air flow in the atmosphere inside the test vessel could be varied as well as the inclination of the

condensing plate. These experiments extend the data base with the goal of improving the empirical input to thermohydraulics codes used for assessments systems for removing heat from reactor containments.

Although reactor design organizations incorporate different condensing system designs for containment cooling, all of these systems rely on steam condensation to assure that the containment pressure remains within acceptable bounds. Experiments and analyses of steam condensation in these systems are conducted at several research institutes to assure sufficient knowledge of system performance. Comparisons between experimental data and different prediction models have been conducted in the Department of Nuclear Fission, CIEMAT, Spain with satisfactory agreement between experiment and model predictions.

The introduction of passive systems for fluid and heat transport is a key feature of a number of advanced water cooled reactor designs. For these systems it is necessary to demonstrate that they operate as intended and operate reliably under a wide range of conditions. Specifically, in passive systems for fluid and heat transport, the driving forces may be small under certain conditions due to small temperature gradients.

Several thermohydraulic phenomena (e.g. mixing, stratification, natural circulation) are important in passive systems for fluid and heat transport, and occur under different conditions in advanced designs compared to present generation plants. It is necessary to establish sufficient, qualified, experimental data to ensure thorough understanding of the phenomena, and to provide a base of data for qualification of calculational tools.

The accurate prediction of critical heat flux (CHF) and film boiling heat transfer in fuel rod bundles is important to assure that temperature limits on fuel and cladding are not exceeded. Predictions of CHF and film boiling heat transfer are performed with empirical correlations derived from experimental data. Film boiling may be encountered during the blowdown and reflood phases of Loss-of-Coolant Accidents. Because the maximum temperature of the fuel is primarily determined by heat transfer in the film boiling regime, accurate calculation of CHF and film boiling heat transfer is important. For new designs that rely on passive heat transfer, it is necessary to accurately predict these phenomena at low flow and low pressure conditions. Several experiments have been conducted to obtain data under these conditions, and new correlations have been developed. Further, look-up tables for CHF and film boiling heat transfer coefficients have been developed. Tables can be conveniently updated as new, qualified, data become available, but like correlations, tables can not be used with confidence for ranges where the data base is limited.

Considerable work on investigating the behaviour of passive systems has been conducted with cost shared projects sponsored by the European Commission. These projects benefit from the collective experience of research from several co-operating facilities and are focused on developing and assessing innovative passive systems. Most projects include both experimental and analytical activities and are directed mainly at studying the important phenomena associated with heat removal from the core and from the containment. The experiments are carried out at large scale integral test facilities (e.g. PANDA, NOKO and PACTEL) in Europe. Several large thermohydraulics codes are used (e.g. ATHLET, CATHARE, TRAC, RELAP5) to assist in selecting the proper test conditions, and are being compared with experimental results in qualification efforts. The codes are also used to predict the behaviour of the actual plant systems.

At the Paul Scherrer Institute, recent testing with the PANDA facility has focused on examining the response of the passive containment cooling system (PCCS) of the European Simplified Boiling Water Reactor, the passive building condenser (BC) and the passive isolation condenser (IC) of the Siemens SWR-1000, and a containment plate condenser (CPC). The tests generally showed that these systems behave as expected, providing long term heat removal capability. Test results for the integral behaviour of the system (reactor plus containment) have been used to validate the TRACG code for transient analyses of BWR behaviour. The results of integral tests, including tests which investigated condenser behaviour with non-condensables, carried out at PANDA have also been compared with the RELAP5 code which generally calculated the results of the tests sufficiently accurately. The tests involving passive containment cooling have also been modelled with the containment code GOTHIC. In addition, GOTHIC has been used at the Paul Scherrer Institute to study certain phenomena such as heated gas jet and plume behaviour, gas mixing, and stratification with the conclusion that GOTHIC is a suitable tool for modelling 3-D phenomena observed in the PANDA tests that cannot be adequately modelled with lumped parameter and 1-D system codes.

During recent years, several facilities (e.g the NOKO facility of Forschungszentrum, Juelich, Germany, the PANDA facility of Paul Scherrer Institute, Switzerland, the ROSA-V facility of the Japan Atomic Energy Research Institute, and SPES of ENEA, Italy) have been used to experimentally study the effectiveness of passive heat removal systems incorporated into advanced water cooled reactor designs. These facilities have provided considerable data for use in validating models employed in computer codes. To provide data acceptable for code qualification it is essential that the experiments are well instrumented.

The behaviour of the emergency condenser of the Siemens SWR-1000 reactor has been investigated at the NOKO facility of the Jülich Research Centre, Germany. The objective of the activity has been to provide data for the assessment of the thermohydraulic effectiveness of passive decay heat removal from the core to the containment.

Natural circulation is an important phenomena in advanced water cooled reactor designs. Useful data on natural circulation have been accumulated from experimental facilities at several institutes including the following: the Lobi-Mod-2 facility of the Joint Research Centre, Ispra; the SPES facility of ENEA, Italy; the BETHSY facility at Grenoble; the Semiscale Mod-2A facility in Idaho, USA; the PKL-III facility of Siemens, Germany, and the LSTF/ROSA-IV facility of JAERI. The base of data from these facilities is suitable for evaluating natural circulation performance for different plant designs. Evaluations carried out at the University of Pisa have used this experience base to confirm the suitability of passive systems incorporating core makeup tanks as embodied in the AP600 design and in the PACTEL facility, which simulates a WWER-440 plant.

Decay heat removal from CANDU reactors has been investigated by Atomic Energy of Canada, Ltd. Under certain conditions, decay heat can be removed from the CANDU core by natural single- or two-phase natural circulation in the primary loop. Many experiments have been conducted in the RD-14M integral test facility of AECL's Whiteshell laboratories. Results show that significant natural convection flows can be established; these data provide a useful information source for development and qualification of physical models.

Heat removal from the moderator in conventional CANDU reactor designs is achieved by use of pumps to circulate the moderator to heat exchangers. However, circulation of the moderator could be achieved passively by natural convection in a flashing driven loop. This is

under investigation by AECL. Loop stability at low power is improved with greater mixing within the calandria.

For the CANDU design, the heavy water in the calandria provides a backup heat sink for the reactor core in the unlikely event of a loss of coolant accident. Enhancing the CHF value for the calandria tube reduces the heat-up of the fuel under these conditions. Research has been carried out at AECL to improve the surface characteristics of the calandria tubes in such a way as to increase the CHF significantly.

To better understand the phenomena associated with passive systems for fluid and heat transport, thermohydraulic experiments have been conducted by the Japan Atomic Energy Research Institute with the ROSA-V Large Scale Test Facility (1/48 scale full height, full pressure mock-up of a typical large, 4-loop, PWR). The test data are also useful in assessing and improving computer codes. Passive systems modelled by ROSA-V include a gravity driven injection system, a conventional (nitrogen pressurized) accumulator injection system, and a flashing driven injection system. ROSA has been used to examine the response of passive systems to a small break LOCA(SBLOCA) and a low pressure steady state natural circulation test; the tests have shown that the primary loop can be depressurized by the secondary side automatic depressurization system to the pressure allowing actuation of the gravity driven injection system, with subsequent long term cooling by natural circulation. A feature of the results was complex non-uniform flow behaviour in the steam generator U tubes. Careful modelling was required with the RELAP5 code in order to model this non-uniform behaviour.

The PACTEL facility of VTT Energy, Finland, is used to investigate the behaviour of passive core cooling systems within the programme of the European Commission. PACTEL is a scaled full height model of a Russian WWER-440 reactor. The facility has been modified by installation of a core makeup tank (CMT) to examine the thermohydraulic phenomena expected during the operation of this component (the CMT is part of the AP-600 design as well as other advanced designs). Tests to study the effects of condensation in the CMT have been conducted, and results have been compared with predictions made by AEA technology using the RELAP5 code. Basically, the capability of the code-nodalisation in reproducing the measured scenario was demonstrated. Results showed that the modelling of wall condensation requires further attention. The general conclusion is that RELAP5 is suitable for analysis of passive injection systems with CMTs, although some improvements in the modelling of the condensation process would be beneficial.

The FLICA-4 code is under development by CEA-Saclay in France to model phenomena in core thermohydraulics. It can be coupled with existing codes (e.g. CATHARE) for system studies or with neutronics codes for simulating coupled neutronic-thermohydraulic phenomena, such as the coupling of reactivity and temperature. The code is in the development/qualification stage.

The Nuclear Power Corporation of India has developed a model for the simulation of a loss of flow event in a 225 MW(e) Indian HWR: and the codes capability to reproduce a plant transient involving a variation of core flow rate has been demonstrated. To verify the capability of the code to predict natural circulation performance will require comparison with experimental data, probably from test loops.

The GIRAFFE facility at Toshiba's Ukishima site in Japan is a full height test facility simulating the SBWR containment with a passive containment cooling system. All main

components of the SBWR, that are assumed to play a role following an accident, are part of the facility. Experimental data has been used both to confirm the design of the SBWR, and to examine the capability of the best-estimate code, TRAC, in predicting the transient behaviour of the system. Separate effects tests have been conducted to determine the effects of nitrogen on steam condensation, and integral tests have been performed to validate the degradation model. Also, integral tests have been conducted to investigate the behaviour of the containment with its passive cooling system. These tests showed that the system could condense the steam generated by decay heat maintaining the containment pressure well below the design pressure. Results of these and other tests have qualified TRAC for predicting the performance of the passive containment cooling system, in the presence of hydrogen, following a loss of coolant accident.

Scaled experiments and analytical work are being carried out at Forschungszentrum Karlsruhe, Germany, to examine passive cooling or core debris following a core melt accident through the SUCO programme with a phased series of experiments investigating the effectiveness of sump cooling in future light water reactors. This includes investigations of heat exchanger configuration. Detailed modelling with the computational fluid dynamics code CFX 4.1 is carried out to model the boiling phenomena.

Steam injectors offer a promising means of passively using steam as an energy source to pump cold water from a pressure lower than the steam to a higher pressure. Heat available from steam condensation can be partly converted into mechanical work useful for pumping the liquid. A steam injector consists of a steam nozzle to partially convert steam enthalpy into kinetic energy, a water nozzle to distribute inlet liquid around the steam, a mixing section for heat, mass and momentum transfer from the steam to water, resulting in condensation at a higher pressure than the inlet steam, and a diffuser. Steam injectors are considered for advanced water cooled reactors for providing high pressure makeup water — e.g. as high pressure injection or for emergency feedwater. Tests have been carried out by CEA to obtain data for qualification of the CATHARE computer code.

Important developments are underway to utilize computational fluid dynamics (CFD) codes for modelling of the behaviour of passive systems of advanced water cooled reactors. With the rapid increases in computing speed, these detailed codes can bring further understanding to complex thermohydraulic behaviour of such systems. It is important to realize that there is still need to use empirical correlations in such modelling. Therefore there is a need to gather accurate experimental data both to improve the correlations and increase the base of data for code qualification.

5. CONCLUSIONS AND RECOMMENDATIONS

As a result of the discussions at the meeting, the following general conclusions and recommendations can be stated:

- (1) Some years ago, it was considered that application of passive safety systems for advanced water cooled reactor designs was limited to small to medium size plants (less than about 700 MW(e)). This has now changed as a result of further design activities and experimental testing. Now passive systems are also being incorporated into designs of 1000 MW(e) and above.
- (2) Both passive or active systems, or combinations of active and passive systems can meet safety requirements. The selection needs to be made with the aim of simplification, and

achievement of reliability, safety and economic goals. For passive systems especially, uncertainties in phenomenology result a tendency to incorporate considerable margins into system designs. However, this typically carries a cost penalty. Better knowledge of phenomena can help both to achieve more economical designs as well as adequate assurance that the systems will function as intended.

- (3) For passive systems, developers of nuclear power plants need to assure that sufficient data exist for code qualification, and that the effects of degradation mechanisms on system performance are well understood. For example, the effects of degradation mechanisms such as aging and flow blockages on system reliability should be thoroughly understood. Also, "unexpected" experimental results should be carefully investigated. For example, if condensation does not start near the expected time in an experiment, the test should be repeated, perhaps with additional instrumentation, so that the reasons for the first results are clearly understood.
- (4) Close communication and co-ordination between experimentalists and analysts is highly important to help ensure that the experimental data are truly relevant to advanced water reactor development. The acquisition of experimental data should proceed in parallel with code development and application.
- (5) A considerable base of data for condensation heat transfer including non-condensables has been accumulated over fifty years. Although there had been increased activity in recent years in this field, because of the importance of this phenomenon to advanced water cooled reactors, there remains a need for a thorough literature survey, and for a review and consolidation of the existing data. Because such data are very dependent on thermohydraulic conditions and system geometry, a proper review should start with plant design and anticipated operational and accident conditions.
- (6) For advanced water cooled reactors, relative to currently operating plants, there is an increased need for 3-dimensional codes for modelling the thermohydraulic phenomena. It is also important that appropriate data (e.g. for 3-dimensional jets) be obtained for development and qualification of these codes.
- (7) In order to use experimental data for code qualification, it is important to have proper instrumentation to capture and understand the important phenomena, and for use in performing uncertainty analyses of the experimental results.
- (8) Thermohydraulic computer codes are sufficiently validated for current plants in order to perform meaningful uncertainty analyses. For advanced plants with passive systems, the importance of certain phenomena (e.g. tracking of non-condensables, condensation with non-condensables, mixing and condensation in large pools, natural circulation, temperature stratification and turbulence) is much increased and more experiments and work on the codes for performing calculations of thermohydraulic behaviour is required before methodologies relying on best-estimate predictions and uncertainty analyses can be qualified.
- (9) Code users must have a thorough understanding of the physics and the abilities and limitations of the codes that they are using. They require proper training on use of the code to eliminate "user's effects". The training should include topics such as selection of nodalisation schemes, and qualification and use of appropriate numerical methods.

- (10) Capabilities of computational fluid dynamics codes are improving and provide detailed flow information where this is needed. However, careful attention is required to ensure that the appropriate physical phenomena are included e.g. (interfacial heat transfer, drag, and other phenomena). Computing times would tend to be very large and may be unpractical for large 3-dimensional problems involving natural convection and significant interfacial heat and mass transfer.
- (11) There is interest in convening a general review meeting of the topic of the experimental tests and qualification of analytical methods to address thermohydraulic phenomena in advanced reactors on about a 4 year cycle. There is also a need to focus on specific topics by convening groups of experts in the special technical areas.

REFERENCES

- [1] ORGANIZATION FOR ECONOMIC CO-OPERATION AND DEVELOPMENT, CSNI Separate Effects Tests Matrix for Thermal-Hydraulic Code Validation, CSNI report, OECD/NEA/GD(94)/82 (1994).
- [2] ORGANIZATION FOR ECONOMIC CO-OPERATION AND DEVELOPMENT, CSNI Integral Test Facility Validation Matrix for The Assessment of Thermal-Hydraulic Codes for LWR LOCA and Transients, CSNI report, OECD/NEA/GD(97)12, (CSNI report 132/revision 1) (1996).
- [3] ORGANIZATION FOR ECONOMIC CO-OPERATION AND DEVELOPMENT, State of The Art Report on Thermohydraulics of Emergency Core Cooling in Light Water Reactors, OECD/CSNI report no. 161 (1989).
- [4] INTERNATIONAL ATOMIC ENERGY AGENCY, Terms for Describing New, Advanced Nuclear Power Plants, IAEA-TECDOC-936, Vienna (1997).
- [5] INTERNATIONAL ATOMIC ENERGY AGENCY, Progress in Development and Design Aspects of Advanced Water Cooled Reactors, IAEA-TECDOC-677, Vienna (1992).
- [6] INTERNATIONAL ATOMIC ENERGY AGENCY, Status of Advanced Containment Systems for Next Generation Water Reactors, IAEA-TECDOC-752, Vienna (1994).
- [7] INTERNATIONAL ATOMIC ENERGY AGENCY, Progress in Design, Research and Development and Testing of Safety Systems for Advanced Water Cooled Reactors, IAEA-TECDOC-872, Vienna (1996).
- [8] INTERNATIONAL ATOMIC ENERGY AGENCY, Status of Advanced Light Water Reactor Designs, IAEA-TECDOC-968, Vienna (1997).
- [9] INTERNATIONAL ATOMIC ENERGY AGENCY, Advances in Heavy Water Reactor Technology, IAEA-TECDOC-984, Vienna (1997).
- [10] INTERNATIONAL ATOMIC ENERGY AGENCY, Technical Feasibility and Reliability of Passive Safety Systems for Nuclear Power Plants, IAEA-TECDOC-920, Vienna (1996).
- [11] Juhn, P.-E., et al., "IAEA activities on passive safety systems, and overview of international developments" paper presented at 14th Int. Conf. on Passive and Engineered Safety Systems in Nuclear Installations, Pisa, Italy, 1997.

CONDENSATION TESTS AND QUALIFICATION OF MODELS

(Session 1)

Chairman

E.F. Hicken
Germany

NEXT PAGE(S)
left BLANK



EFFECT OF POOL TURBULENCE ON DIRECT CONTACT CONDENSATION AT A STEAM/WATER INTERFACE

J.D. JACKSON, C.L. ZHAO, S. DOERFFER, J.E. BYRNE, H. FALAKI

Nuclear Engineering Laboratories,

School of Engineering,

University of Manchester,

Manchester, United Kingdom

Abstract

Measurements of direct contact condensation heat transfer have been made for the case where the process takes place at the horizontal interface between saturated steam and a pool of water in a vertical cylindrical test section. A submerged vertical jet of subcooled water was injected upwards on the axis to promote the condensation and water was withdrawn at the same rate from the bottom of the pool. In conjunction with the above study, measurements of the turbulent velocity fluctuations just below a free surface produced by the injection of a vertical submerged jet have been measured using hot film anemometry on an isothermal air-water test facility of similar geometry for similar flow conditions at ambient temperature. A correlation is proposed in terms of a Stanton number based on turbulent velocity fluctuation near the interface on the liquid-side. Our results are in good agreement with those of others for similar configurations when compared in terms of condensation Stanton number.

1. INTRODUCTION

Condensation of vapour in direct contact with a liquid plays a key role in various branches of engineering and can be of particular importance in water cooled nuclear reactor design and safely assessment ([1] and [2]). The condensation rate is limited by the effectiveness of the process of diffusion of heat from the interface to the bulk liquid. This is critically dependent on the intensity of turbulence in the liquid. Although various correlations have been proposed for the interfacial transport rate ([3] and [4]), based usually on a combination of experimental data and simplistic models, detailed information concerning the liquid-side heat transport mechanisms is still limited. Sonin and co-workers ([5] and [6]) have conducted experimental studies of direct contact condensation in which turbulence was generated below a steam-water interface in a vertical cylindrical test section by the injection of a vertical submerged jet of subcooled water. However, those workers only carried out tests for one fixed ratio of test section diameter to jet diameter ($D/d_j=24$). A further study of condensation due to the injection of a submerged jet towards a steam-water interface in a cylindrical test section was reported recently by Byrne and Falaki ([7]). In their experiments the main emphasis was on measurements of heat transfer under conditions where the free surface was in a highly agitated state with sharp pressure bursts occurring regularly following the entrainment of steam in the water.

The purpose of the investigation reported here was to make measurements of direct contact condensation heat transfer at a relatively undisturbed interface between saturated steam and water and to study its dependence on the turbulence in the water. In the present study, condensation heat transfer measurements have been made using a similar configuration to that of Sonin et al, but covering a much wider range of diameter ratios ($D/d_j = 3.19-12.77$). Condensation heat transfer coefficients have been determined using a calorimetric method. Using that approach it was possible to obtain results for quiescent (burst-free) conditions. In conjunction with the heat transfer study described here, turbulent velocity fluctuations have been measured by means of hot film anemometry using an isothermal air-water facility having a test section of similar geometry to that of the condensation heat transfer test facility. The results obtained from the combined study show that for similar conditions the condensation heat transfer coefficient at a steam-water interface is proportional to the r.m.s. turbulent velocity just below the air-water interface. Our results are in good agreement in terms of condensation Stanton number with those of others who have studied direct contact condensation heat transfer using similar configurations.

2. EXPERIMENTAL STUDIES

As already mentioned, two separate investigations have been undertaken, one involving heat transfer measurements and the other involving turbulence measurements.

The heat transfer study was carried out using the apparatus shown in Figure 1. The test facility was constructed from pyrex glass fittings and was surrounded by perspex protection walls. Steam was generated in a boiler by heat supplied from four electrical immersion heaters. The water in the test section was turbulent due to the injection of a vertical submerged jet of subcooled water some distance below the free surface. The degassing column was operated under vacuum during the experiments to continuously extract non-condensable gas from the circulating water. Figure 2 shows a schematic of the test section. The water issuing from the submerged nozzle in the test section was directed vertically upwards towards the steam-water interface which was maintained at a chosen level above the nozzle exit. Water was removed steadily from the bottom of the test section at the same rate. Measurements were made for a range of water levels above the nozzle exit, a range of values of injection jet velocity, several nozzle sizes and using two test sections of different diameter. For a particular jet velocity, the experiment proceeded in steps changing the water level. Initially the water level was set well above the nozzle exit and the steam-water interface was undisturbed and flat. With decrease of the water level, the surface gradually became wavy. Beyond a certain point, condensation 'bursts' occurred intermittently as steam became entrained in the water and condensed very rapidly. When this happened, a pressure spike was generated, the free surface broke up explosively and water splashed upwards for a short period. With further reduction of water level and/or increase of jet velocity, the condensation bursts occurred more frequently until a condition was achieved during which violent bursts occurred continuously. On the basis of the frequency F_b of occurrence of condensation bursts, the experimental results have been classified into three distinct modes: a quiet condensation mode (no condensation bursts, $F_b=0$); an intermittent burst condensation mode ($0 < F_b < 2$ Hz); and a continuous burst condensation mode ($F_b > 2$ Hz). In the present paper, we focus on results obtained in the quiet condensation mode. The system pressure was maintained at 1.2 bar. Non-condensable gas which collected near the interface was bled off by raising the interface up to a steam bleed pipe (see Fig. 2) just prior to a condensation heat transfer measurement being made.

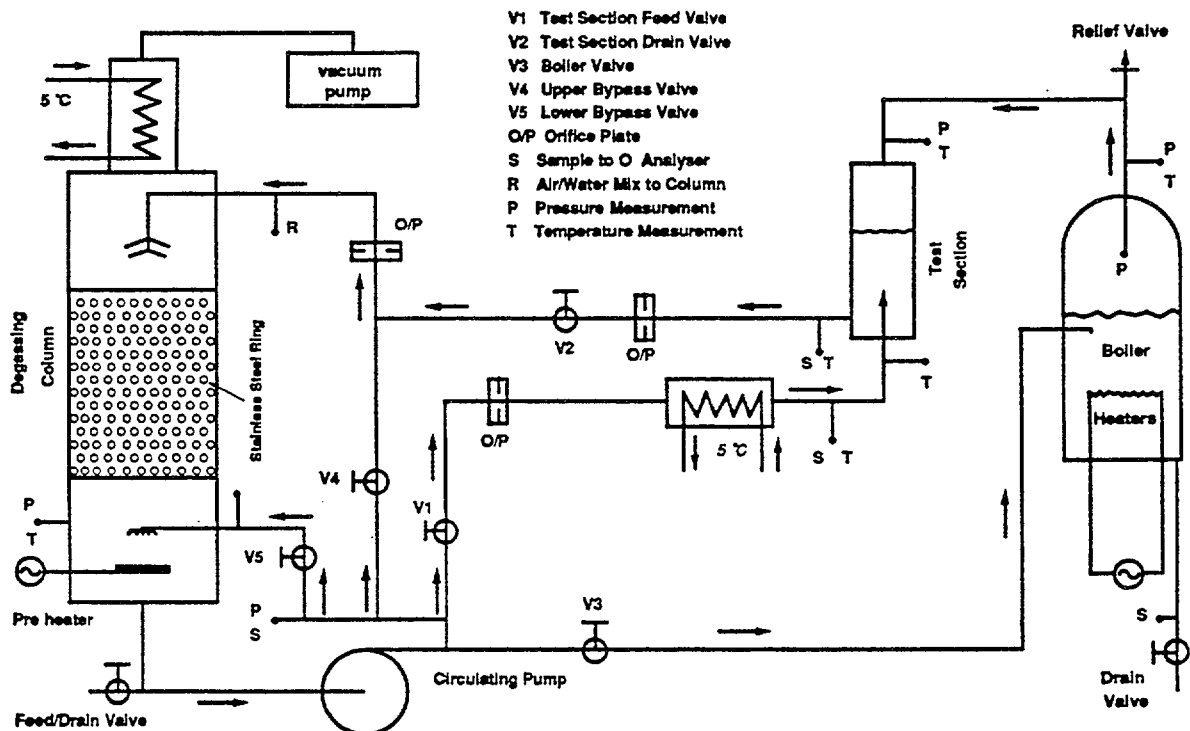


Figure 1. Schematic Diagram of Condensation Rig

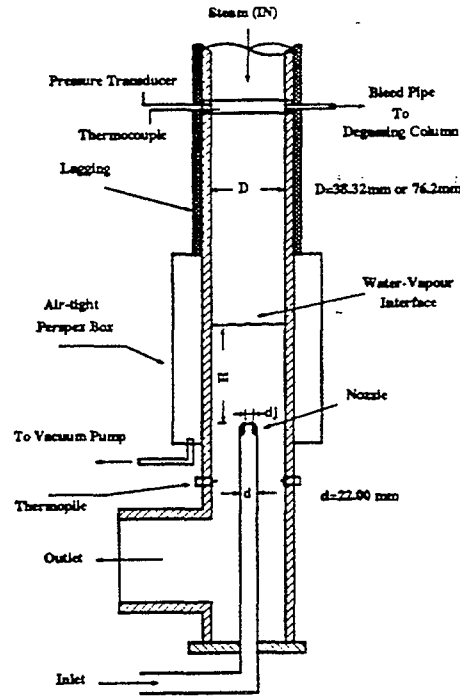


Figure 2. The Arrangement for Vertical Injection in the Test Section

A calorimetric method, based on the measurement of the water flow rate and temperature rise between the outlet and inlet of the test section, was used to determine the rate of heat transfer. The temperature rise was measured using a thermopile made from ten thermocouples connected in series. This enabled reliable values of condensation heat transfer coefficient to be obtained even for the quiet mode of condensation. For steady-state operation without bursts, the temperature rise across the test section was in the range 0.5K to 4K. The resolution of the thermopile was about $\pm 0.025\text{K}$. Under quiet mode conditions the measured condensation heat transfer coefficient proved to be proportional to the jet velocity to decay exponentially with increase of water level above the injection nozzle.

In conjunction with the above study, measurements of turbulent velocity fluctuations were made using hot film anemometry on an isothermal air-water test facility having a test section of similar geometry. The flow conditions covered were similar to those in the condensation experiments. A closed circuit flow system containing deionised water was used (see Figure 3). The header tank was positioned approximately 18 metres above the bottom tank to provide the head to drive the flow. The flow of water into the main test section was controlled by inlet valve V1 and outlet valve V2. The water flow to the calibration test section was controlled by inlet valves V3, V4, and outlet valve V2. The water flowrates were measured by two rotameters. Satisfactory accuracy of the hot film anemometer measurements was achieved by regular probe calibration using the arrangement shown in Figure 4 and careful control of water purity and temperature. Turbulent velocity fluctuation measurements made with the probe just below free surface showed that the r.m.s. turbulent velocity was also proportional to jet velocity and that it decayed exponentially with increase of the level of water above the nozzle exit. The following relationship between the r.m.s. turbulent velocity (U_{rms}) and the system parameters was found to fit the results satisfactorily:

$$U_{rms} = 21.2U_j \frac{d_j + 0.2(d - d_j)}{D} \exp \left[\frac{H}{d_j} \left(-0.07 - 1.15 \frac{d_j}{D} - 0.47 \frac{d_j^2}{D^2} \right) \right]$$

for $3.19 < D/d_j < 24$ (1)

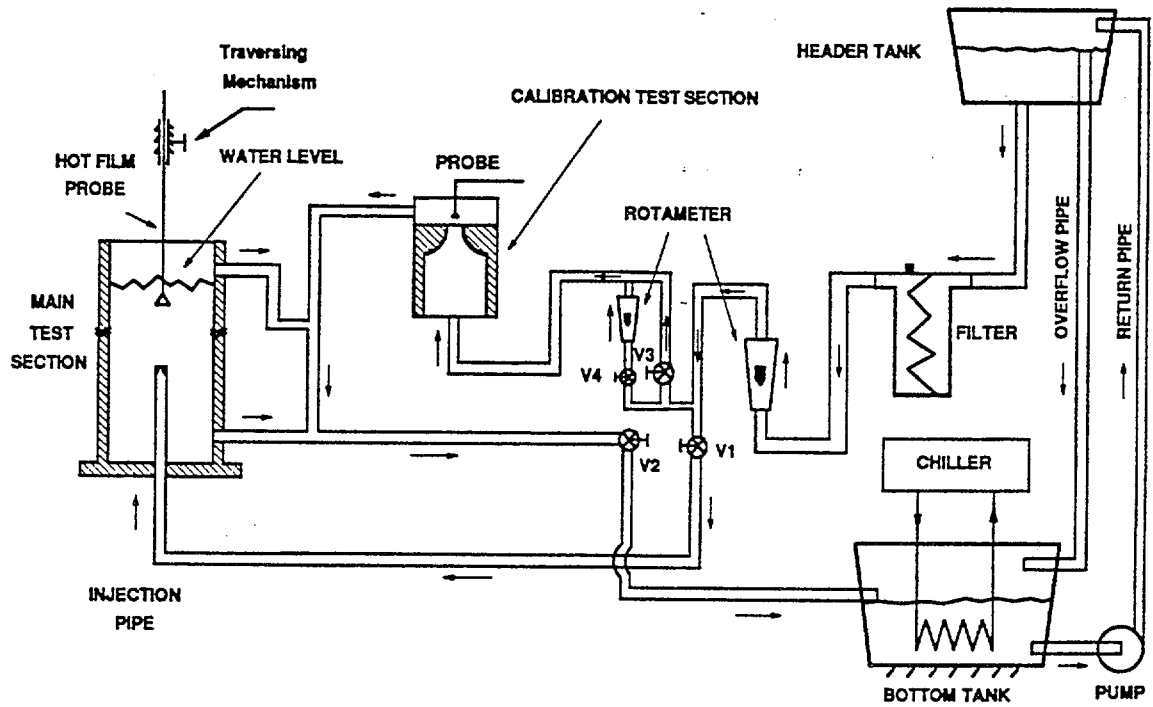


Figure 3. Schematic Diagram of Air/Water Rig

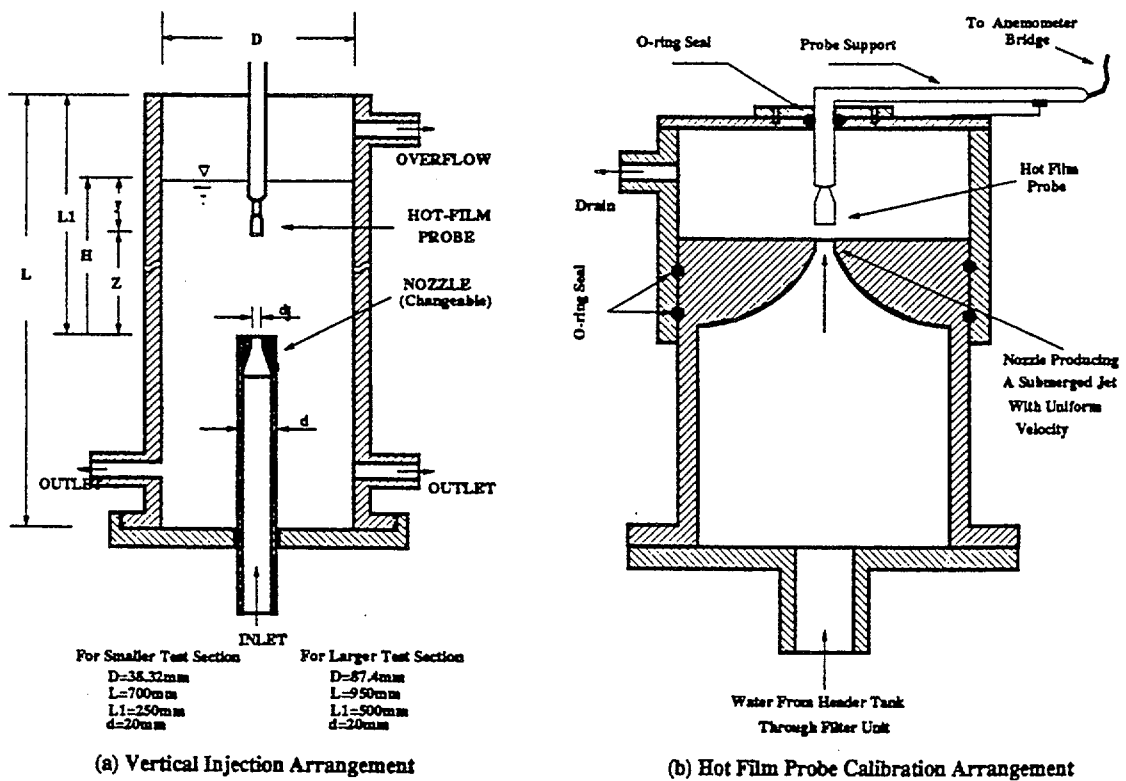


Figure 4. The Arrangement of Hot Film Probe in the Test Section

In the above relationship U_j is the jet velocity, H is the water level above the nozzle exit, D is the test section diameter, d is the injection pipe outside diameter and d_j is the jet diameter.

3. DISCUSSION OF RESULTS

Figure 5 shows that the condensation heat transfer coefficients are well correlated when plotted against r.m.s. turbulent velocity calculated using equation (1). It can be seen that

$$h = 50 U_{rms} \quad (2)$$

Expressing our results in terms of a Stanton number (based on the r.m.s. turbulent water velocity near the interface) we obtain:

$$St = \frac{h}{C_{pb} \rho_b U_{rms}} = 0.01195$$

$$\text{for } 7.5 < Pr_b < 8.5 \quad (3)$$

C_{pb} and ρ_b are the specific heat and density, respectively, on the liquid side at the bulk temperature of the water. Pr_b is the Prandtl number based on bulk liquid properties.

A comparison of our results with those of others on the basis of condensation Stanton number is shown in Table 1. From the table, it can be seen that for vertical injection, similar values of Stanton numbers are obtained where the configurations are similar. Sonin and co-workers obtained the following Stanton number correlation using their data from an experiment with a test section on which the ratio D/d_j was 24:

$$St = 0.019 Pr_b^{-0.33} \quad (4)$$

$$\text{for } 1 < Pr_b < 6$$

If we substitute a typical value of Prandtl number from our experiments ($Pr_b=8.0$) into Eq.(4), we obtain $St=0.0100$. This is not very different from the value of 0.01195 found in the case of our rather more constrained configurations ($D/d_j=3.19 - 12.77$).

However, for configurations which differ significantly from ours (such as those of Thomas and Jensen and Yuen), the Stanton number values are different. This is presumably because the levels of turbulent fluctuation near the interface were very different in those studies. Thomas made measurements of steam condensation at a steam-water interface, using a vertical submerged jet system similar to ours, but with much reduced nozzle submergence and jet velocity. The Stanton number which he obtained from his data was somewhat smaller than those obtained in the studies of Sonin et al and the present study. Jensen and Yuen conducted experiments on steam condensation at a steam-water interface in a horizontal co-current water-steam channel flow where the liquid-side turbulence was induced mainly by shear stress exerted by the flowing steam. The Stanton number obtained from their experiments was significantly higher than that found in the present study.

Conclusions

The heat transfer coefficients at the water-steam interface on the direct contact condensation test facility are proportional to the values of r.m.s. turbulent velocity just below the interface on the air/water test facility for similar conditions and geometry. Heat transfer can be correlated in terms of a Stanton number based on the turbulent velocity fluctuation on the liquid-side near the interface. When compared on this basis, our results are in good agreement with those of others who have carried out experiments for similar configurations.

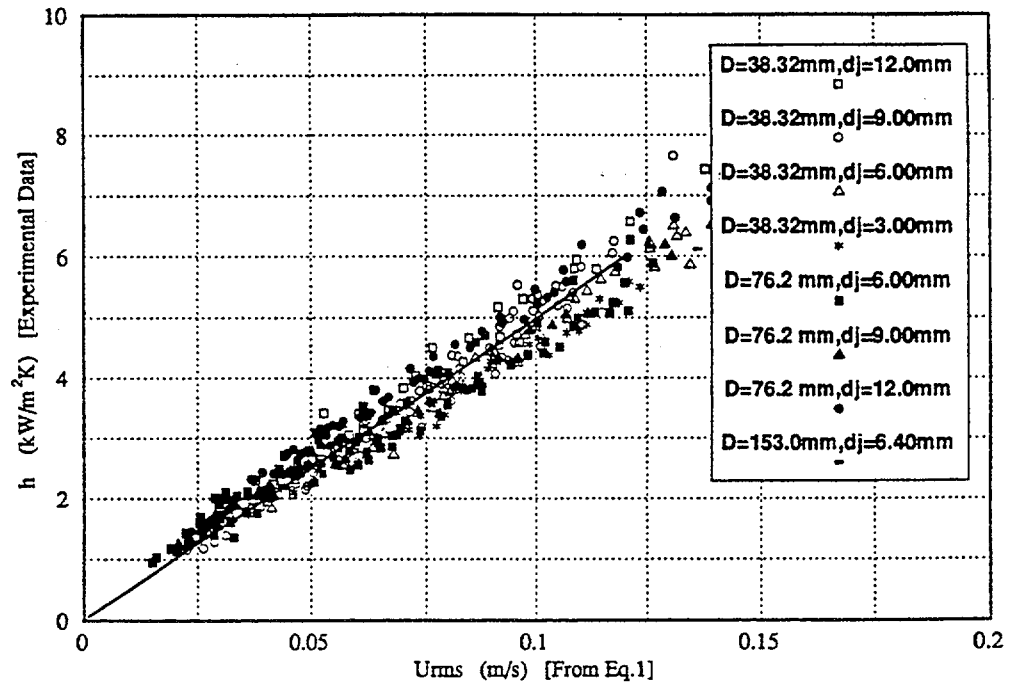


Figure 5 The Correlation of Condensation Heat Transfer Coefficient Using the r.m.s. Turbulent Velocity

Table 1 Summary of Condensation Stanton Number for Different Flow Configurations

Flow Configuration	Reference	Jet Submergence H/D	Test Section Diameter to Jet Diameter D/d _j	Bulk Prandtl Number Pr _b	Turbulence Measurement Technique	Condensation Stanton Number St
Submerged vertical jet directed to water-vapour interface	Present Study	3.91 - 4.96	3.193 - 12.77 (D=38.32mm)	7.5 - 8.5	Hot Film Anemometry	0.01195
		3.67 - 5.25	6.35 - 12.7 (D=76.2mm)			
As above	Sonin et al (1986) Brown et al (1990)	3.1 - 4.2	24 (D=153mm)	1.0 - 6.0	Flow Visualisation and Laser Doppler Velocimetry	0.0113 (Pr _b =5.4)
As above with low jet submergence	Thomas (1979)	0.3 - 1.3	23.62 - 94.34 (D=300mm)	1.9	Hot Film Anemometry	0.00782
Horizontal cocurrent channel flow of steam and subcooled water	Jensen and Yeun (1982)			6.2	Laser Doppler Velocimetry	0.019

Nomenclature

d_j	jet diameter. [mm]
d	injection pipe outside diameter. [mm]
D	test section diameter. [mm]
H	water level above jet exit. [mm]
U_j	jet velocity. [m/s]
U_{rms}	r.m.s. turbulent velocity. [m/s]
F_b	frequency of pressure bursts. [Hz]
H	condensation heat transfer coefficient. [kW/m ² K]
St	Stanton number.
Pr	Prandtl number.

REFERENCES

- [1] BROWN et al, 1989, Vapour Condensation at a Turbulent Liquid Surface in System with Possible Space-based Application, AIAA-89-2846.
- [2] KIRCHNER W and BANKOFF S.G., 1985, Condensation Effects in Reactor Transients, Nucl. Sci. & Eng., Vol.89, pp.310-321.
- [3] THOMAS R.M., 1979, Condensation of Steam on Water in Turbulent Motion, Int. J. Multiphase Flow, Vol.5, pp.1-15.
- [4] JENSEN R.J. and YUEN M.C., 1982, Interphase Transport in Horizontal Stratified Concurrent Flow, NUREG/CR-2334, USNRC.
- [5] SONIN et al, 1986, Vapour Condensation onto a Turbulent Liquid – I. The Steady Condensation Rate as a Function of Liquid-side Turbulence, Int. J. Heat & Mass Transfer, Vol.29, pp.1319-1338.
- [6] BROWN et al, 1990, Rate Correlation for Condensation of Pure Vapour on Turbulent, Subcooled Liquid, Int. J. Heat & Mass Transfer, Vol.33, pp.2001-2018.
- [7] BYRNE J.E. and FALAKI H.R., 1990, Direct Contact Condensation of Steam on Subcooled Water, Proceedings of the 9th Int. Heat Transfer Conference, Jerusalem, Israel, Vol.4, pp.289.

NEXT PAGE(S)
left BLANK

CHARACTERIZATION OF DIRECT CONTACT CONDENSATION OF STEAM JETS DISCHARGING INTO A SUBCOOLED WATER

CHUL-HWA SONG, SEOK CHO, HWAN-YEOL KIM,
YOON-YOUNG BAE, MOON-KI CHUNG
Korea Atomic Energy Research Institute,
Taejon, Republic of Korea



XA0055002

Abstract

Direct contact condensation of steam jets discharging into a subcooled pool water has been experimentally investigated using five different sizes of horizontal nozzle over a wide range of steam mass flux and pool temperature conditions. Condensation phenomena have been observed visually and by taking pictures of steam jets using a video camera. Three kinds of steam jet shape were typically observed, which are dependent on the steam mass flux and pool temperature. The jet expansion ratio and the jet length as well as the condensation heat transfer coefficients were determined. The effect of steam mass flux, pool temperature, and nozzle diameter on these parameters were also discussed. The axial and radial temperature distributions in steam jet and in surrounding pool water as well as the dynamic pressure at the tank wall were measured under various test conditions. In addition, the relation between steam condensation and dynamic pressure at the tank wall was also discussed, which is dependent also on the steam mass flux and pool temperature.

1. INTRODUCTION

Direct contact condensation (DCC) phenomena can occur in various equipments of nuclear power plant such as a reactor drain tank of the pressurized water reactor (PWR) or a pressure suppression pool of the boiling water reactor (BWR) during normal operation or accidental situation. Understanding of the DCC phenomena is especially important in the design of advanced PWRs such as AP600, System 80+ or KNGR (Korea Next Generation Reactor) since the phenomena are expected to occur in a in-containment refuelling water storage tank (IRWST) when the reactor depressurization system valves or the pressurizer safety valves are open to discharge steam into the tank through spargers. In order to properly design the steam spargers for ensuring the structural integrity of associated equipments or systems and their safe operation, it is essential to understand well the DCC phenomena. Therefore, understanding of the condensation of steam discharged from a single nozzle into a pool water will provide a formal basis for analyzing more complicated phenomena occurring around steam spargers, which consist, in general, of multiple holes.

Even though a lot of studies on DCC phenomena has been previously investigated theoretically and experimentally due to its wide applications, details of the phenomena are not well understood. Among these experimental works, empirical correlation of the heat transfer coefficient was proposed by Aya & Nariai [1] at low steam mass flux conditions, by Young et al. [2] and Fukuda [3] for an intermediate range of steam mass flux. And Cumo et al. [4], Kerney et al. [5] and Chun et al. [6] developed the correlation for a wide range of steam mass flux conditions.

Empirical correlation of the steam jet length was proposed by Del Tin et al. [7] and Stanford & Webster [8] for relatively low steam mass flux conditions, and Kerney et al. [5], Weimer et al. [9] and Chun et al. [6] for high steam mass flux conditions. However, the correlations for high steam mass flux conditions are not agreeable with each other. Simpson & Chan [10] investigated basic mechanism of steam jet condensation at relatively low mass flux,

and observed that the dynamics of subsonic jets are quite different from those of sonic jets. Weimer et al. [9], Tsai & Kazimi [11], and Chen & Faeth [12] investigated theoretically the steam jet penetration. They proposed simple models or expression for jet penetration distance. However, it is shown that the prediction of steam jet length varies with main assumptions employed.

Condensation regime maps, which are mostly dependent on the steam mass flux and pool temperature, were proposed, among others, by Nariai & Aya [13] for low steam mass flux and by Fukuda [3] for an intermediate range of steam mass flux in vertical nozzles. And Young et al. [2] also proposed a condensation regime map for an intermediate range of steam mass flux in a horizontal nozzle. Chun et al. [6] extended the steam mass flux ranges to 1500 kg/m²-s for small horizontal nozzles. The condensation mode can be, in general, classified into five regions: chugging, transitional, condensation oscillation, bubbling and stable condensation regions. Most of these maps, however, were constructed under relatively low range of steam mass flux conditions. Cumo et al. [4] and Del Tin et al. [14] proposed stability boundaries between stable and unstable behavior of vapor core for an intermediate range of steam mass flux conditions with small diameter nozzles.

The present study deals with the experiments on condensation phenomena of steam discharging into a subcooled water pool in order to investigate detailed mechanism of the DCC phenomena and to find major parameters affecting the condensation. Five different horizontal nozzles with the internal diameter in the range of 5 ~ 20 mm were used under various test conditions of the steam mass flux in the wide range of 70 ~ 1190 kg/m²-s and the pool water temperature in the range of 20 ~ 95 °C. Three different kinds of steam jet shape were observed, which include the conical, ellipsoidal and divergent types. Several jet parameters were measured or estimated, which include the temperature distributions in the jet and in the surrounding pool water, the jet expansion ratio and dimensionless jet length, the average heat transfer coefficients, and the dynamic pressure at the wall. Only for the case of stable steam jets, the shape of steam jet was analyzed to determine the jet expansion ratio, the dimensionless jet length and the average heat transfer coefficients. However, the dynamic pressure pulse induced by a steam jet condensing in pool water was measured for both stable and unstable steam jets.

For the stable steam jet, both conical and ellipsoidal shapes could be observed depending on the steam mass flux and pool temperature as well as nozzle diameter. The expansion ratio and dimensionless steam jet length tend to increase with the steam mass flux and pool temperature, and the average heat transfer coefficient tends to increase as the pool temperature and nozzle size are decreased and the steam mass flux is increased. Empirical correlations for the dimensionless steam jet length and the average heat transfer coefficient are presented as functions of the steam mass flux and the condensation driving potential. It was found that the dynamic pressure measured at the tank wall is closely related to the condensation phenomena, which are influenced by the steam mass flux and pool water temperature.

2. EXPERIMENTAL METHOD

Direct contact condensation phenomena were experimentally investigated in the test facility as schematically shown in Fig. 1. The experimental facility consists of a steam generator, a quenching tank, a steam supply line, a preheat line, and valves and instruments. The steam generator with electric heaters of 300 kW produces steam continuously with the dryness higher than 99 %. The maximum operating pressure is 1.03 MPa and the maximum

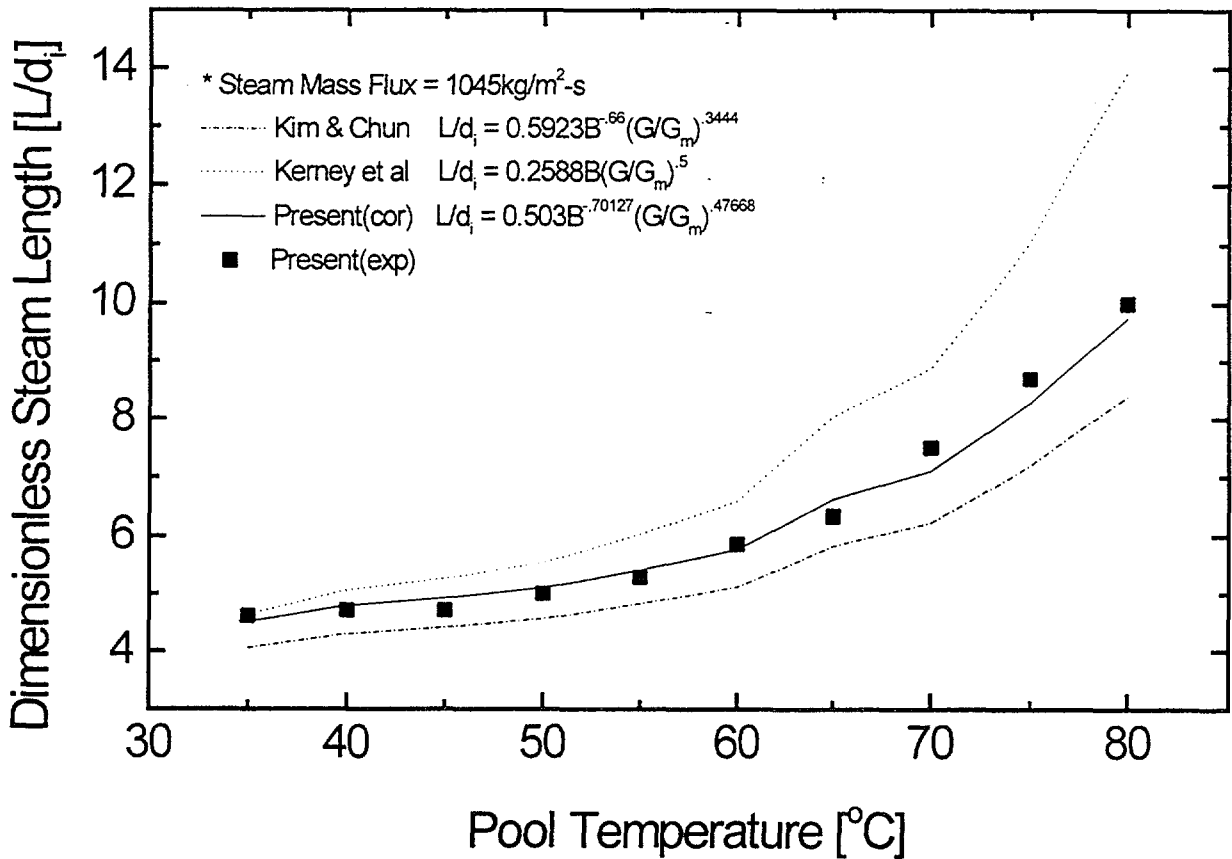


Fig. 1. Schematic diagram of the experimental apparatus .

steam flow rate is 0.1 kg/sec. Subcooled water is contained in a quenching tank equipped with two plexiglasses for visual observation and video camera imaging. The quenching tank is a horizontal cylindrical tank, which is open to atmosphere, with the diameter and length of 1 m and 1.5 m, respectively. The size of the steam supply line between the steam generator and the discharge nozzle is 1 inch. The preheat line which by-passes the steam flow meter is installed at the steam supply line in order to avoid a steam flow meter failure which might occur due to a sudden temperature increase at the initial operation of steam supply. The steam supply line is heated by trace heaters and insulated in order to maintain the supplied steam saturated with 100% dryness during testing.

A vortex type of steam flow meter, a manual flow control valve, a drain valve, an isolation valve, a pressure transmitter, and a thermocouple are installed in the steam supply line. Five thermocouples are also installed inside the quenching tank to measure the pool temperature, and the dynamic pressure sensors of the piezo-electric type are installed at the tank wall. A temperature sensor traverse unit, which consists of 15 thermocouples, is installed to measure the temperature distributions in the steam jet and in the surrounding pool water. And a video camera with halogen lamps is used for taking pictures of steam jets. All signals except video images are processed using the data acquisition system, which consists of an IBM-compatible PC and a 16-bit A/D converter, and video images are analyzed later by means of an image processing software. All the instrumentations were calibrated before testing. Especially the calibration of vortex flow meter was made using the so-called constant volume method and by measuring the weight of overflow after condensing it in the pool.

Five horizontal steam injection nozzles with the hole diameters of 20, 15.5, 10.15, 7.1, and 5 mm were tested for various combination of steam mass flux and pool temperature. The steam mass flux is controlled with the manual flow control valve installed in the steam supply line. The initial pool temperature can be controlled by the heat addition from the discharged steam. The steam injection nozzle is initially submerged about 30 cm below the free surface of the pool water. When the steam generator isolation valves are open, the water and air inside the steam supply line are discharged first. After clearing out the water and air in the line, the steam from the steam generator is continuously discharged into the pool. At the initial stage of steam discharge, it was observed that some dissolved gas in the pool is changed to a lot of tiny gas bubbles, which make video camera imaging unclear. As the pool temperature is increased to higher than 30 °C, tiny gas bubbles disappear.

Since steam jets become unstable and divergent in case of the pool temperature above about 80 °C, so the test run for evaluating the heat transfer area, jet expansion ratio, and jet length was limited to the stable jet conditions where the interfacial surface of steam and water is relatively clear, and they are in the range of 20 ~ 80 °C of the pool temperature and 250 ~ 1190 kg/m²-s of steam mass flux. However, the dynamic pressure measurement was performed at both the stable and unstable condensation modes. In case of dynamic pressure measurements, the location of the injection nozzle was moved to the center of the quenching tank, which gives the distance between the injection nozzle exit and the pressure sensor location to be about 75 cm.

Table 1 shows the test conditions for investigating the shape of steam jet. The number of test run becomes smaller for larger nozzle diameter cases, since the test conditions are limited to higher steam mass flux cases which exclude the chugging and condensation oscillation modes in this study.

TABLE I. TEST CONDITIONS

Nozzle I.D.	Steam mass flux	Pool temperature
[mm]	[kg/m ² -s]	[°C]
20	250 ~ 300 (250 ~ 280)*	20 ~ 95 (35 ~ 50)
15.5	250 ~ 500 (250 ~ 440)	20 ~ 95 (35 ~ 75)
10.15	250 ~ 850 (300 ~ 825)	20 ~ 95 (35 ~ 80)
7.1	460 ~ 1050 (460 ~ 1050)	20 ~ 95 (35 ~ 80)
5.0	870 ~ 1240 (870 ~ 1188)	20 ~ 95 (35 ~ 80)

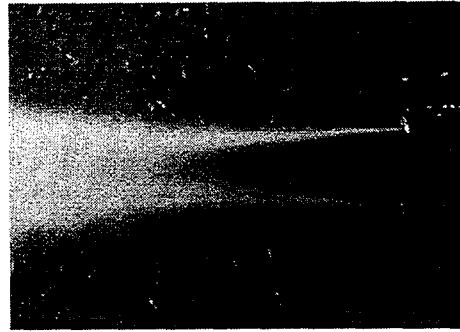
* Value in parenthesis () corresponds to the stable condensation case.

From several pre-test runs of temperature distribution measurement at both the upper and lower parts of steam jet and surrounding pool water, it was confirmed that the temperature distribution is symmetric, which means that the buoyancy force is negligible compared to the steam inertia force. So, the temperature was measured only at the upper part of steam jet and surrounding pool water for characterizing the steam jet shapes and condensation phenomena.

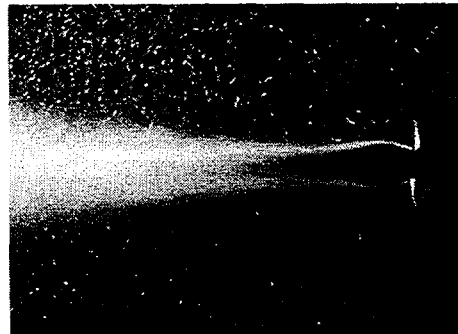
3. EXPERIMENTAL RESULTS AND DISCUSSION

3.1. Steam jet shape

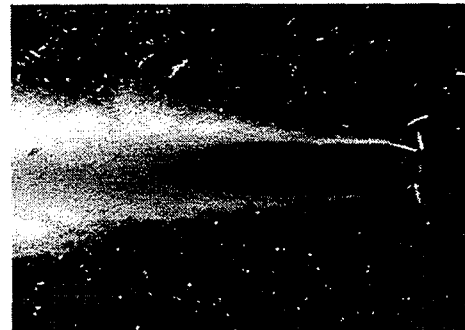
As typically shown in Fig. 2, three different shapes of steam jet were typically observed under the test conditions considered in this study. In general, the *conical* shape of steam jet was observed at smaller steam mass flux and lower pool temperature, whereas the *ellipsoidal* shape of steam jet was observed at relatively higher range of steam mass flux and pool temperature in relatively small diameter nozzles. Both shapes are *stable* in view of their condensation mode. The *divergent* shape of steam jet was observed with the increase of pool



(a) Conical Shape [$d = 15\text{mm}$, $T_{\text{pool}} = 35\text{ }^{\circ}\text{C}$, $G = 350\text{ kg/m}^2\text{-sec}$]



(b) Ellipsoidal Shape [$d = 7\text{mm}$, $T_{\text{pool}} = 40\text{ }^{\circ}\text{C}$, $G = 920\text{ kg/m}^2\text{-sec}$]



(c) Divergent Shape [$d = 10\text{mm}$, $T_{\text{pool}} = 80\text{ }^{\circ}\text{C}$, $G = 600\text{ kg/m}^2\text{-sec}$]

FIG. 2 . Typical shapes of steam jet discharged from horizontal nozzles.

temperature, and this case showed a random and *unstable* variation of jet cavity shape, which makes it difficult to determine the parameters to characterize the steam jet. In case of the stable condensation, the conical shape of steam jet was always observed for the 20 mm nozzle and the ellipsoidal shape was always observed for the 5 mm nozzle. For the rest of nozzle sizes, both cases of jet shape could be observed depending on the test condition.

The jet expansion ratio, which is defined as the ratio of the maximum jet diameter (δ) and the nozzle internal diameter (d_i), is calculated for the case of ellipsoidal shape of steam jet. Fig. 3 shows the expansion ratio versus pool temperature for the nozzle injection diameter of 5 mm. As the mass flux and pool temperature increase, the expansion ratio is increased. The effect of nozzle size on the jet expansion ratio was not so large under the same condition of steam mass flux and pool temperature, and its varying tendency was observed very similar irrespective of the nozzle size. The expansion ratio is shown to be in the range of 1.05 ~ 2.31 over the whole test runs. Here, the axial location could be estimated from the video images, as typically shown in Fig. 2, due to the fact that the outer diameter of the nozzle can be used as a reference length scale in the image, which corresponds to 25.4 mm in all cases of nozzle size.

The interfacial configuration between water and steam is clearly observed from the nozzle exit to the location of complete expansion, and Weimer et al. [9] named this region as an isentropic expansion region in their analysis of the steam jet condensation. But it was observed in this experiment that the heat transfer could occur at the interfacial region upstream of the maximum expansion location by considering that the expansion ratio is

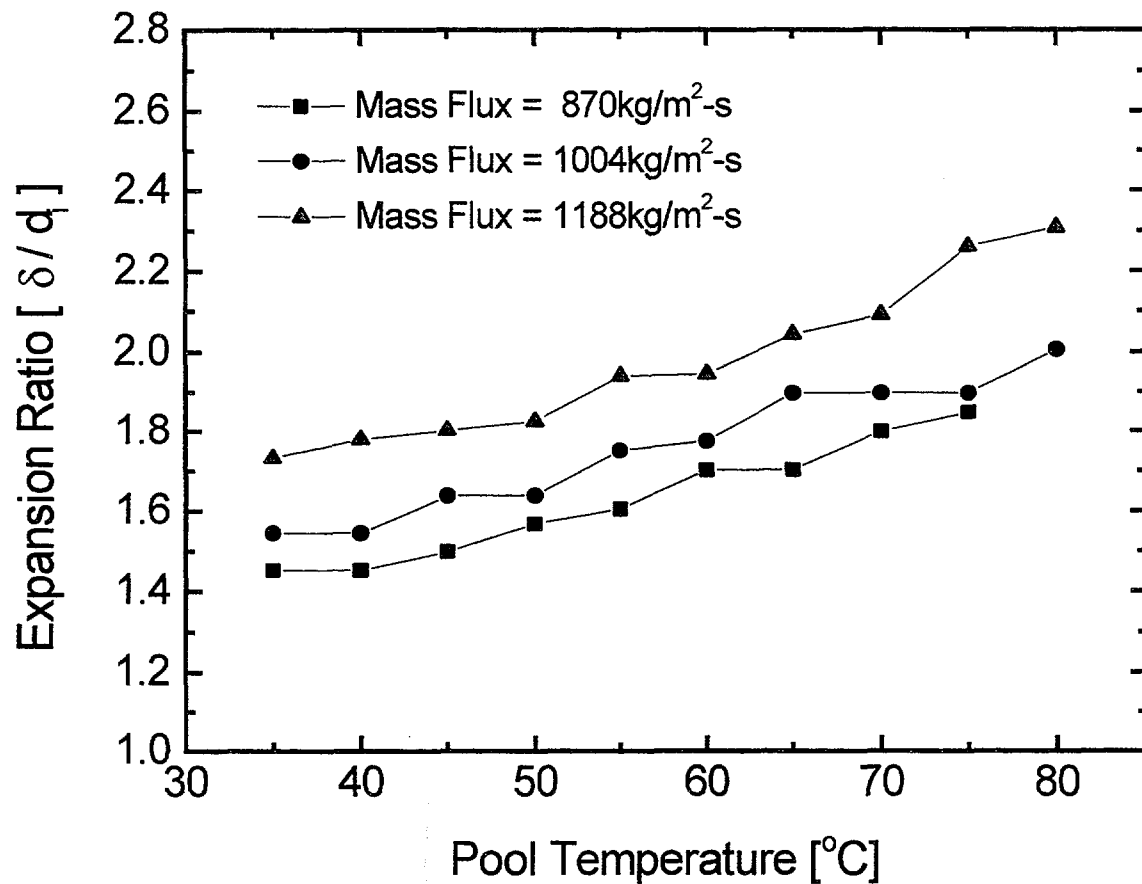


FIG. 3. Jet expansion ratio vs. pool tempere for 5 mm nozzle.

changed even at the same mass flux with the variation of pool temperature. Downstream of the maximum expansion location, there occurs a two-phase mixture at the interface between water and steam regions. The content of water in the mixture region becomes larger due to a lot of water entrainment as the discharged steam goes through the tip of steam jet cavity. This kind of two-phase mixture existing downstream of the maximum expansion location could be observed in all cases of the ellipsoidal jet and it was clearly observed around the jet cavity tip of a divergent jet shape, as typically shown in Fig. 2(c).

3.2. Steam jet length

The dimensionless steam jet length (L/d_i), which is defined as the ratio of the jet length (L) to the nozzle internal diameter (d_i), is calculated for all the stable jet conditions shown in Table 1. It seems to be valuable to express the dimensionless steam jet length in terms of operating parameters, since the steam jet is confined in the pool for complete condensation. The dimensionless steam jet length can be evaluated either by analyzing the video images of steam jet or by measuring the temperature profiles along the nozzle axis (Kudo et al. [15]). Even though both methods are available in this experiment, the image analysis method was adopted since the uncertainty of determining the tip of the jet cavity can be relatively reduced (Del Tin et al. [14]). It is, however, difficult to estimate the exact tip location of steam jet cavity when the pool temperature is increased since the shape of steam jet is very unstable and reveals the characteristics of a divergent jet type.

Fig. 4 shows the dimensionless steam jet length versus pool temperature for the nozzle diameter of 7.1 mm. As the mass flux and pool temperature increase, the jet length is

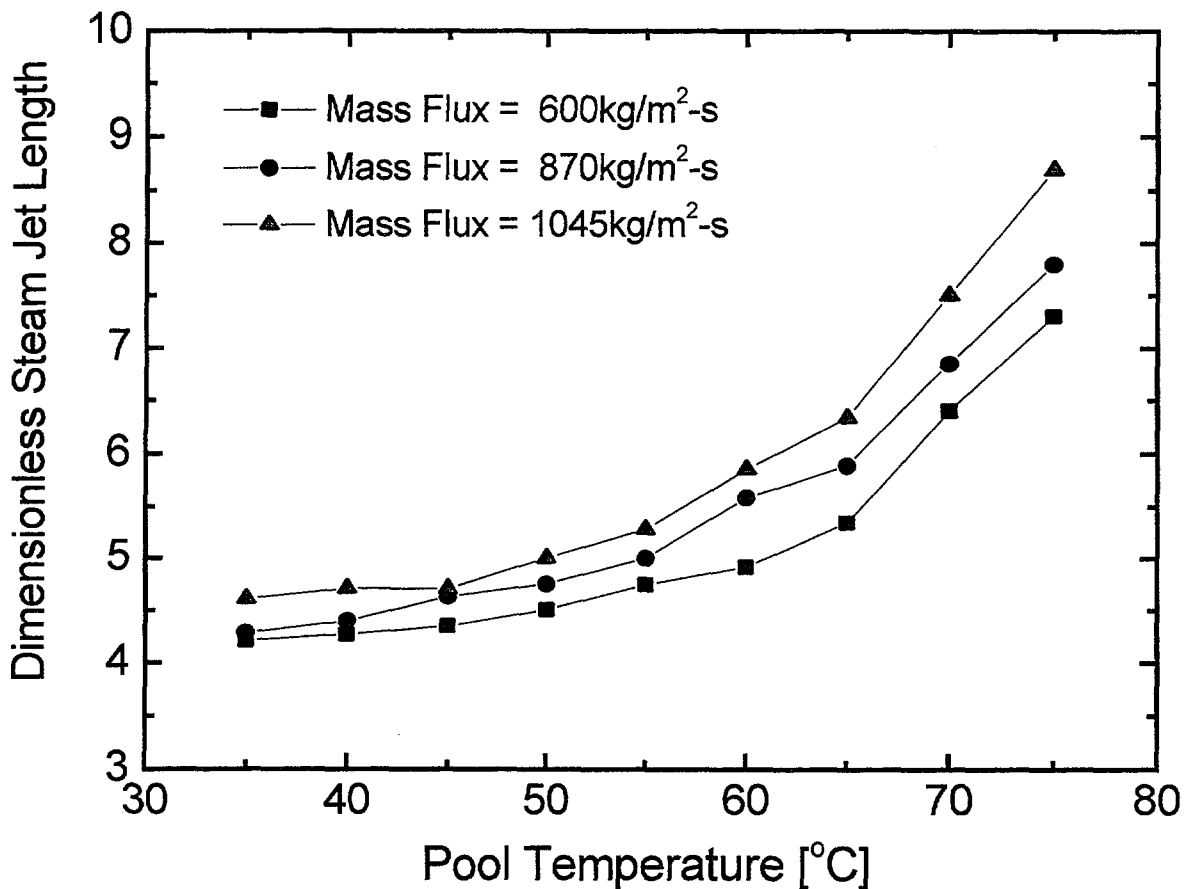


FIG. 4. Dimensionless steam jet length vs. pool temperature for 7.1 mm nozzle.

increased, and its varying tendency is shown very similar irrespective of nozzle sizes. Under the same mass flux and pool temperature condition, the effect of nozzle size on the jet length ratio is not so large. The dimensionless steam jet length is shown to be in the range of 2.05 ~ 11.3 for the whole test runs.

The jet length can be expressed by introducing the dimensionless parameters, B and G/G_m , as reported by Kerney et al. [5]. Here B is the condensation driving potential expressed by $B = C_p (T_s - T_i) / (h_s - h_i)$, and G/G_m is the dimensionless mass flux. Here G_m is equal to 275 kg/m²-s which corresponds to the critical steam mass flux at atmospheric discharge condition. With the negligible effect of nozzle size, the following correlation is obtained based on the present experimental data:

$$L / d_i = 0.503 B^{-0.70127} (G/G_m)^{0.47688} . \quad (1)$$

Comparison of the measured jet length with the correlated one in dimensionless form is shown in Fig. 5, which shows that most of the measured data lies within the range of +/- 15 % of the correlation. In Fig. 6, the present experimental data and the correlation of the dimensionless steam jet length are compared with other correlations by Chun et al. [6] and Kerney et al. [5]. The resultant tendency of the jet length ratio obtained is consistent with the results of Weimer et al.[9] and Chun et al. [6]

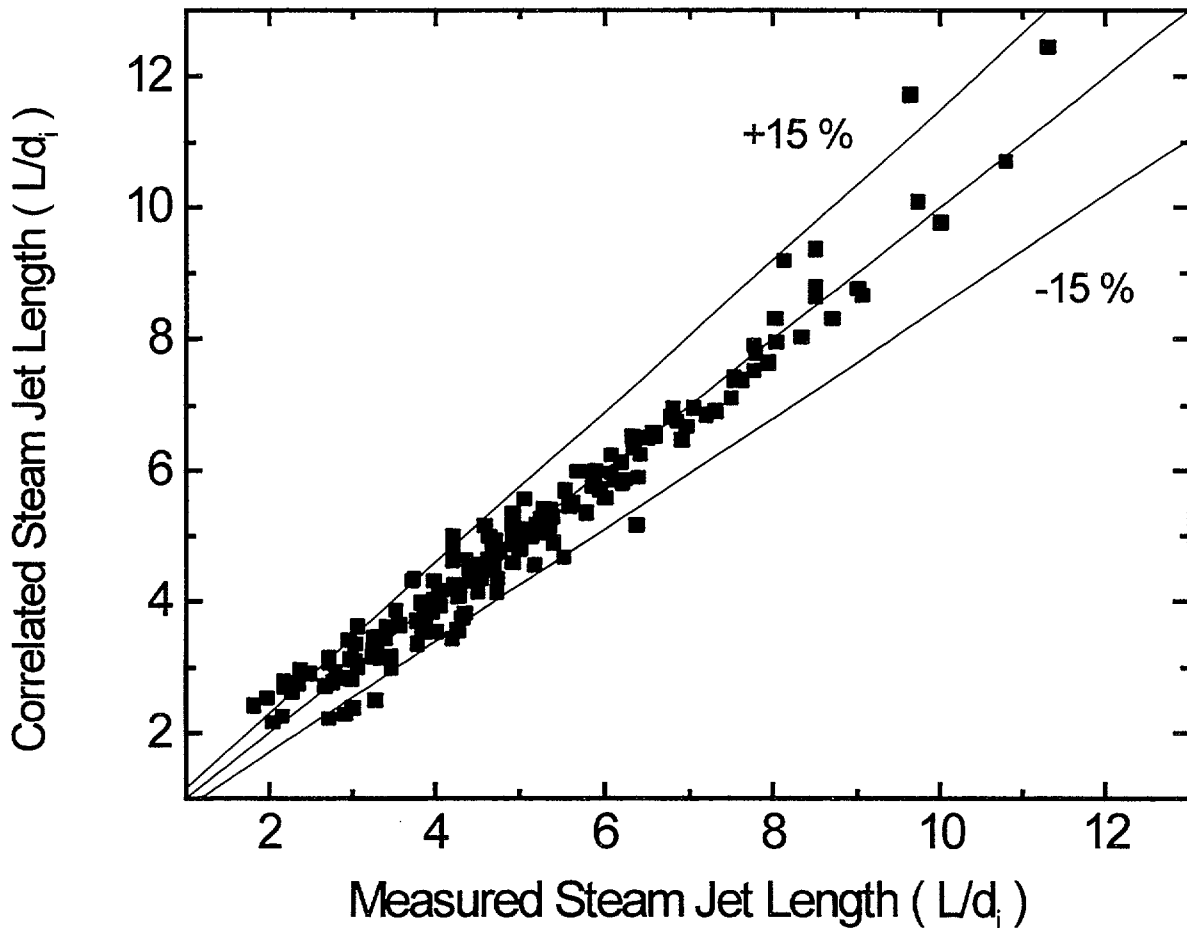


FIG. 5. Comparison of measured and correlated steam jet lengths.

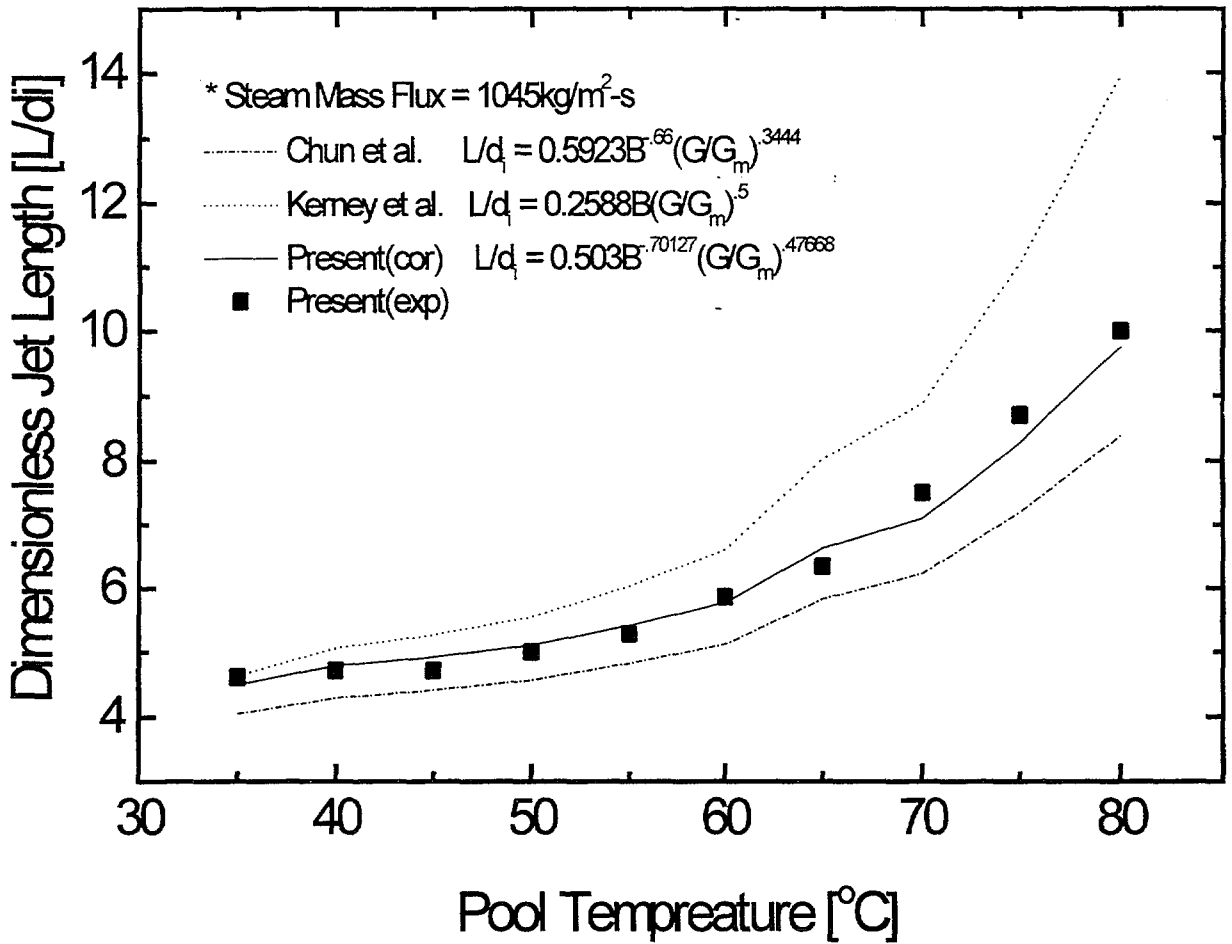


FIG. 6. Comparison of the present work with other correlations of steam jet length.

3.3. Heat transfer coefficient

The average heat transfer coefficient is defined by

$$Q = G A_e (h_s - h_f) = h A (T_s - T_f), \quad (2)$$

where G , A_e , h_s and h_f are the steam mass flux, nozzle exit area, steam enthalpy and water enthalpy, respectively and h , A , T_s and T_f are the heat transfer coefficient, jet surface area, steam temperature and water temperature, respectively. As done by Aya & Nariai [1], smooth surface configuration at steam-water interfaces was assumed in the evaluation of the heat transfer coefficient, since it is extremely difficult to estimate the exact surface area contributing to the heat transfer. Even though the assumption may cause some uncertainties, it is believed that the order of magnitude in the heat transfer coefficient does not change significantly. The steam temperature is obtained by averaging the temperature profile along the nozzle axis, and the water temperature is obtained by averaging the measurements from five thermocouples installed inside the tank to measure the pool temperature.

It is observed that the average heat transfer coefficient is in the range of 1.24 ~ 2.05 MW/m²-°C for the whole test runs. These range of the heat transfer coefficient are higher than the case of subsonic steam jet (below 1 MW/m²-°C in Simpson & Chan [10]), but smaller than the case of superheated steam jet (about 3 MW/m²-°C in Cumo et al. [4]). The average heat transfer coefficient can be expressed by introducing again the dimensionless parameters, B

and G/G_m , as previously discussed. With the negligible effect of nozzle size, the following correlation is obtained from the present data:

$$h = 1.4453 C_p G_m B^{0.03587} (G/G_m)^{0.13315} \quad (3)$$

It can be interpreted from Eq. (3) that the average heat transfer coefficient increases as the pool temperature is decreased and the steam mass flux is increased.

Fig. 7 shows the measured average heat transfer coefficient versus the correlated one expressed by Eq. (3). Most of the measured data lies within the range of $\pm 20\%$. The effect of nozzle size, which might be expressed in terms of dimensionless jet length, is excluded in the correlation, since the number of test nozzles in the present study are small compared with the other parameters and the jet length is, in general, not known *a priori*. Experimental data shows, however, the tendency such that the average heat transfer coefficient increases as the nozzle size is decreased when the pool temperature and steam mass flux are constant.

3.4. Axial temperature distribution

The temperature distribution along the nozzle axis is shown in Figs. 8 and 9 for the 20 mm and 10.15 mm nozzles, respectively. Figure 8 shows the trend typical of conical jet shapes, whereas Figure 9 shows the trend typical of ellipsoidal jet shapes. As previously mentioned, the stable mode of steam jet shows two different shapes; one is conical and the other is ellipsoidal by depending on the steam mass flux and pool temperature. As shown in Fig. 8 and 9, there are two regions characterized by the temperature variation along the nozzle axis with regard to the pool temperature.

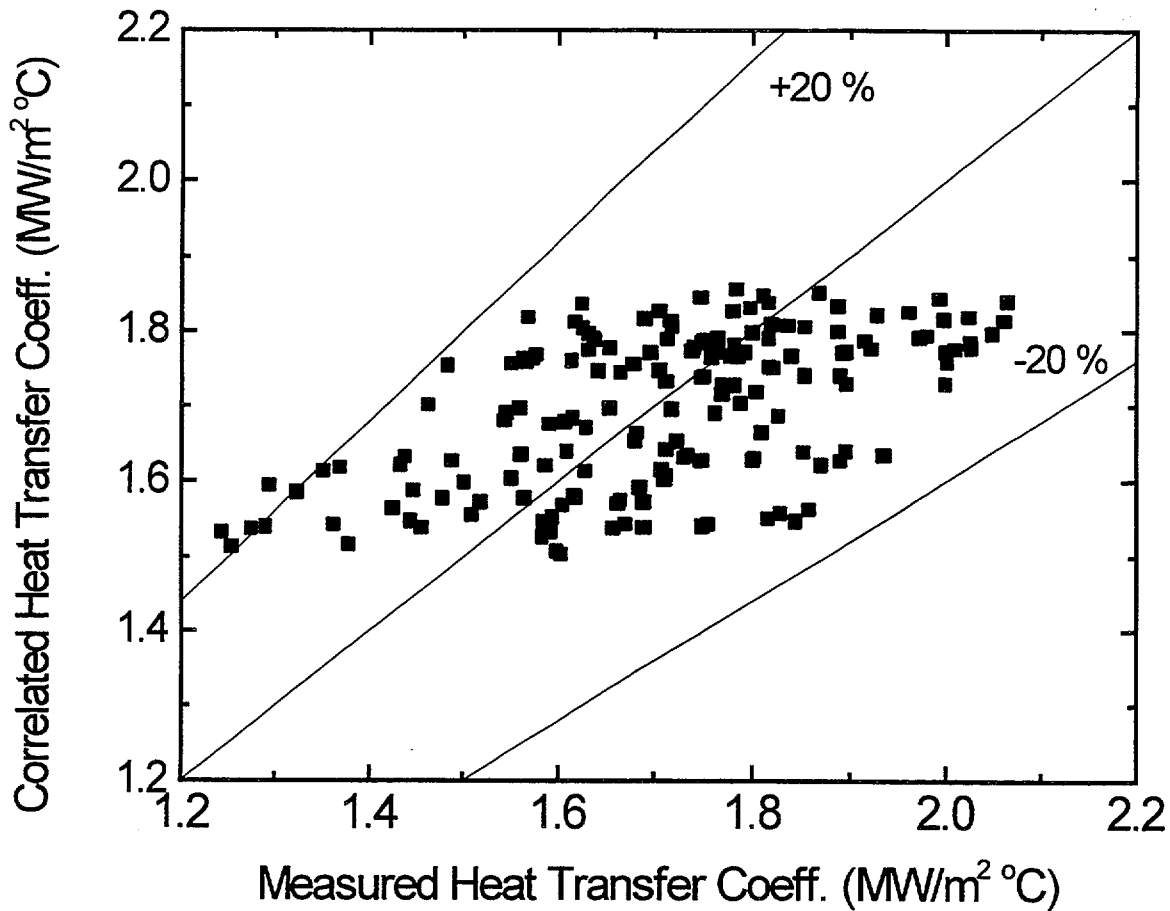


FIG. 7. Comparison of measured and correlated heat transfer coefficients.

In case of the conical jet shape, as typically shown in Fig. 8 for the 20 mm nozzle with the mass flux of $280 \text{ kg/m}^2\text{-s}$, it can be seen that the temperature variation is almost independent of the pool temperature near the nozzle exit. And the magnitude of its variation is not so large in this region. The centerline temperature shows similar trends irrespective of the pool temperatures and steam mass flux. In case of ellipsoidal jet, however, where the jet diameter is increased due to the jet expansion, the temperature tends to decrease first and then increase near the nozzle exit region as typically shown in Fig. 9 for the 10.15 mm nozzle with the mass flux of $600 \text{ kg/m}^2\text{-s}$. The magnitude of temperature variation is about 25°C in this region. Downstream of the maximum jet expansion location, the temperature tends to decrease again. The jet expansion effect on the center line temperature profiles was observed in the nozzles with the diameter of 15.5, 10.15, 7.1 and 5 mm at high steam mass flux conditions even though the critical steam mass flux, at which the jet expansion effect is revealed, is dependent on the nozzle size.

The difference in the variation of centerline temperature profiles along the jet axis for two different jet shapes indicates that the jet temperature is affected by the jet expansion and compression, which occurs at the under-expanded steam jet. Near the jet cavity tip, the temperature variation is strongly dependent on the pool temperature, which means that subcooled water is entrained into the jet cavity. The temperature profile is steeper as the pool temperature is lower, which indicates that the jet length is shorter at a lower pool temperature. Similar trend for the temperature variation has been observed by Del Tin et al. [14].

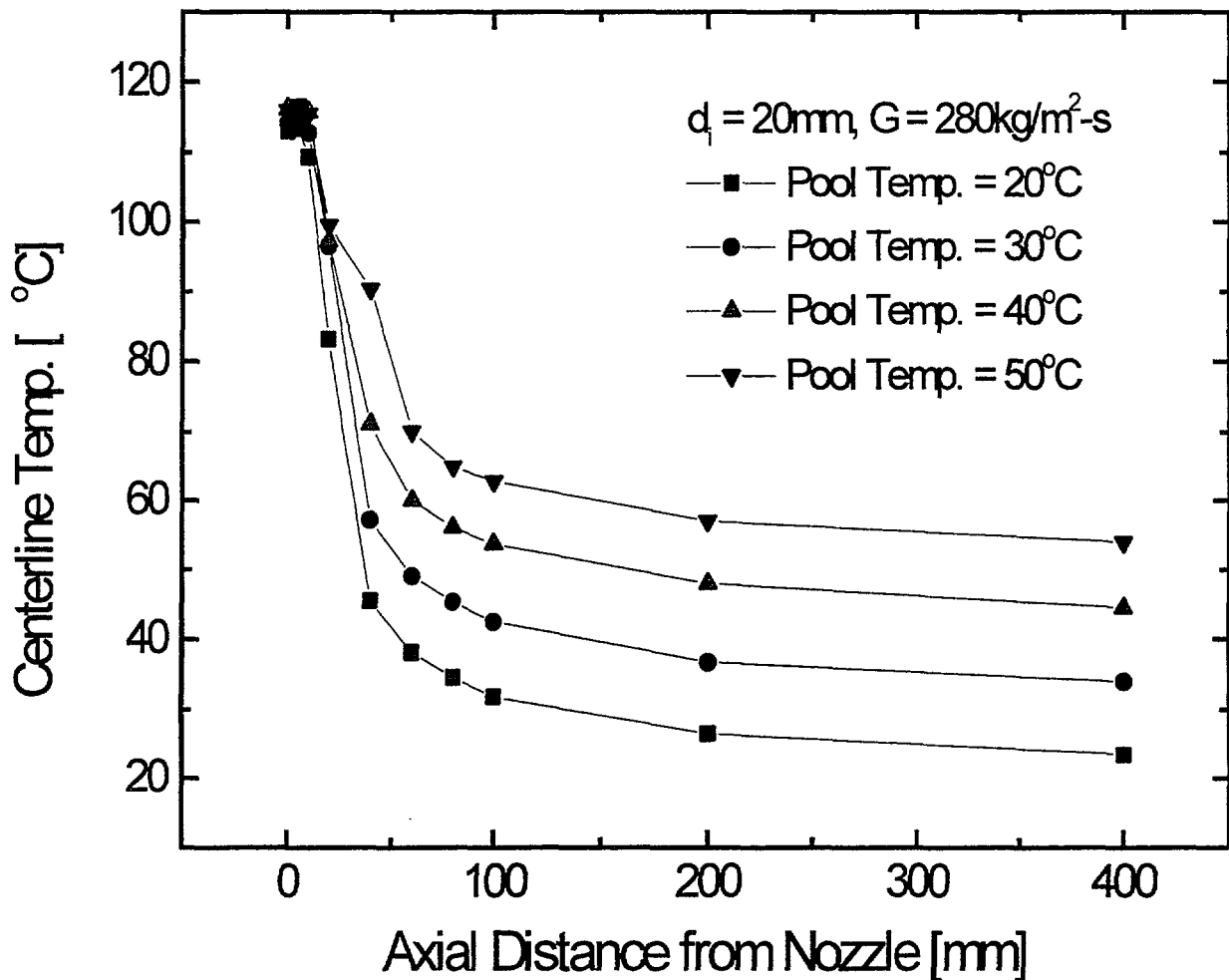


FIG. 8. Axial temperature profiles in steam jets: $d_i = 20 \text{ mm}$, $G = 280 \text{ kg/m}^2\text{-s}$.

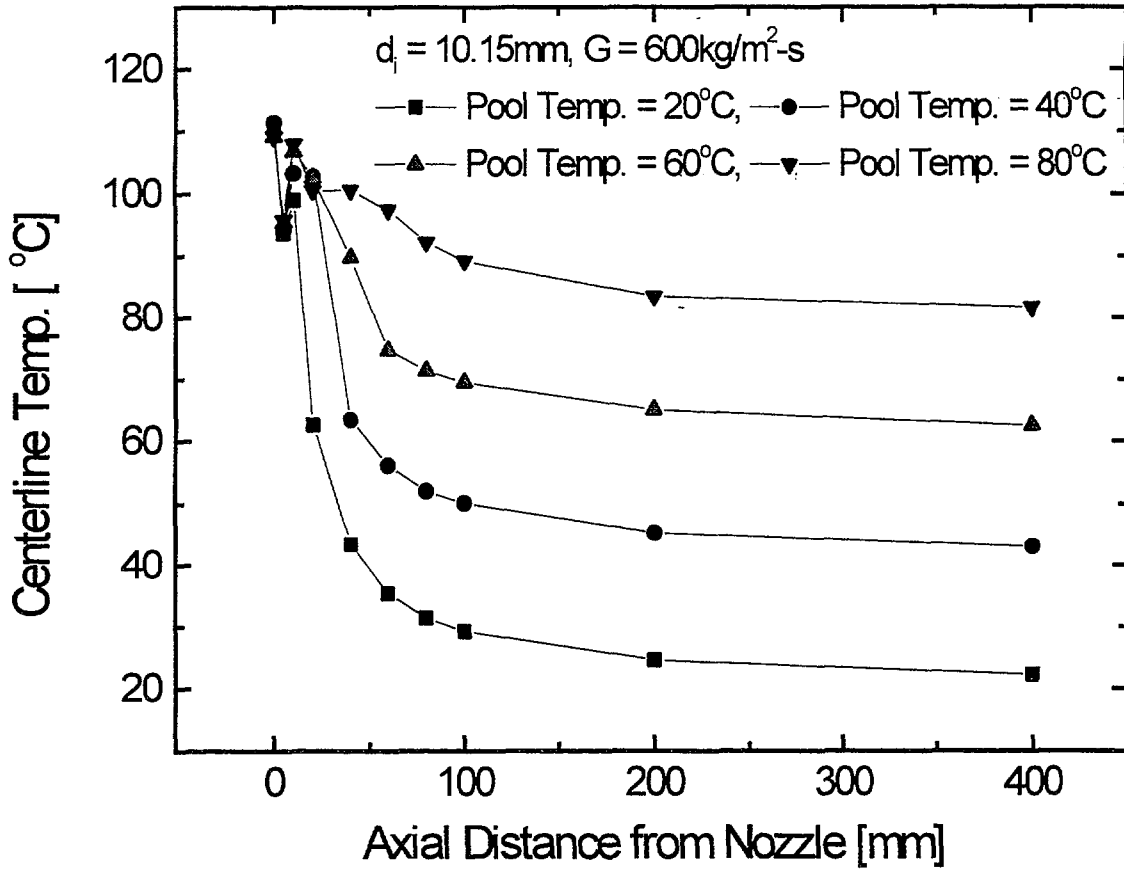


FIG. 9. Axial temperature profiles in steam jets: $d_i = 10.15 \text{ mm}$, $G = 600 \text{ kg/m}^2\text{-s}$.

3.5. Radial temperature distribution

Radial temperature variations at some pre-fixed axial locations are shown in Figs. 10 and 11 for the 20 mm nozzle with the steam mass flux of $280 \text{ kg/m}^2\text{-s}$ and for the 10.15 mm nozzle with the steam mass flux of $600 \text{ kg/m}^2\text{-s}$ at the pool temperature of 40°C , respectively. As previously discussed, the steam jet shape is conical for the 20 mm nozzle and ellipsoidal for the 5 mm nozzle.

In case of conical jet shape, as typically shown in Fig. 10, it can be seen that the radial temperature indicates its maximum value at the nozzle centerline and then decreases toward the mean temperature of pool water. In case of ellipsoidal jet shape as typically shown in Fig. 11, however, there shows that the radial temperature increases first and then decreases to the outer radial location inside the jet near the nozzle exit for the 10.15 mm nozzle. Considering the expansion and compression of under-expanded steam jet, as discussed in previous section, the variation of the radial temperature in steam jet is well understood.

Based on the results of experimental data, as typically shown in Figs. 10 and 11, the radial temperature profile of steam jet is independent of the pool temperature near the nozzle exit region. In the other region, however, the radial temperature decreases from the centerline to the outer radial location and is strongly dependent on the average pool temperature.

3.6. Characteristics of dynamic pressure

Figs. 12 and 13 shows the variation of the dynamic pressure amplitude with the steam mass flux and the pool temperature for 10.15 mm and 20 mm nozzles, respectively. It was

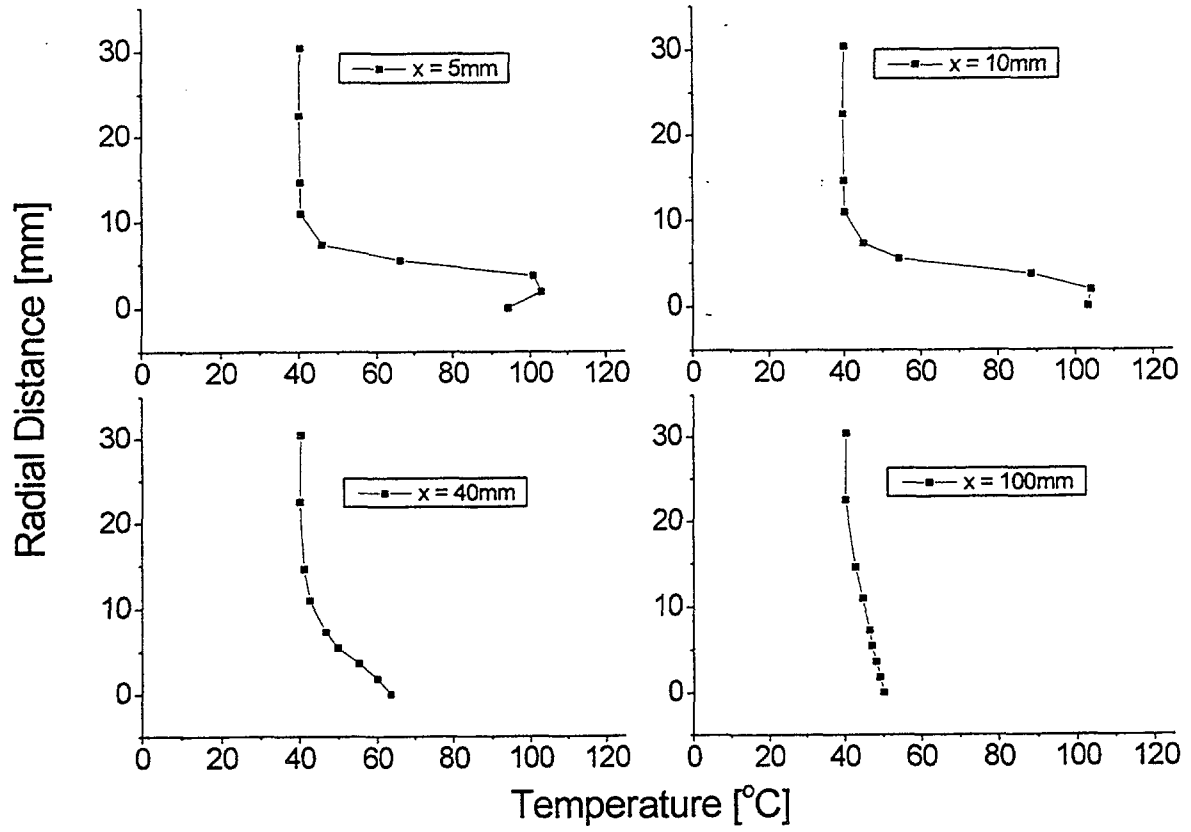


FIG. 10. Radial temperature profiles in conical steam jets: $d_i = 20$ mm, $G = 280$ kg/m²-s, $T_f = 40$ °C.

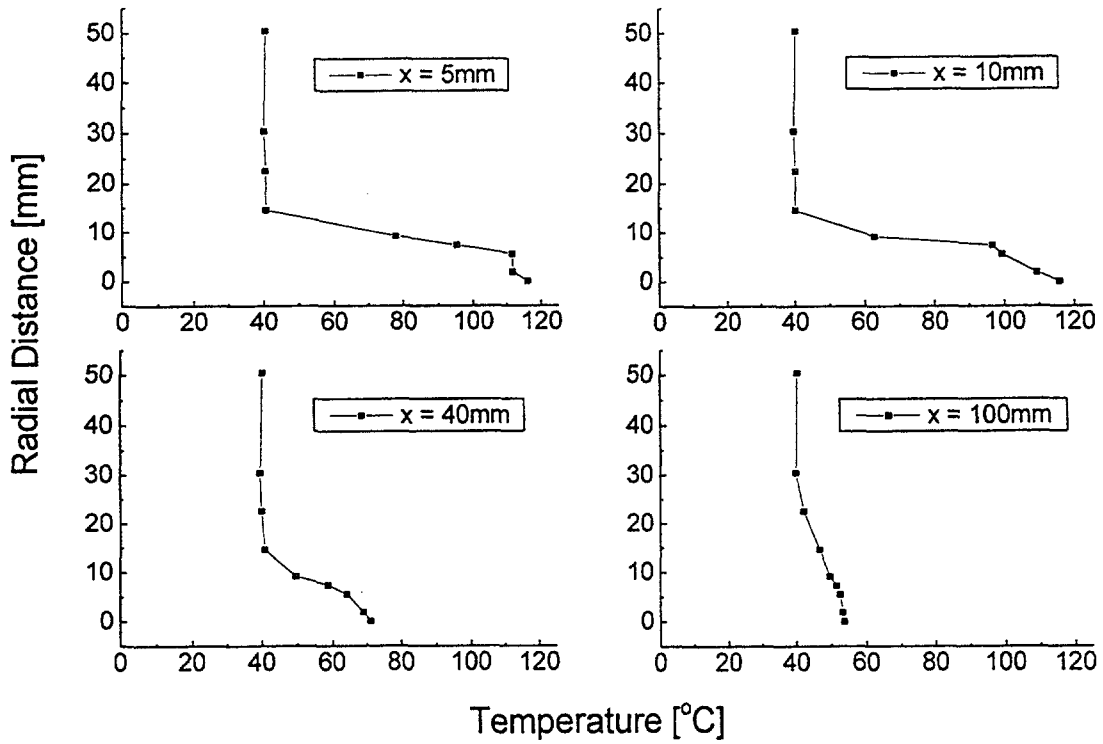


FIG. 11. Radial temperature profiles in ellipsoidal steam jets: $d_i = 10.15$ mm, $G = 600$ kg/m²-s, $T_f = 40$ °C.

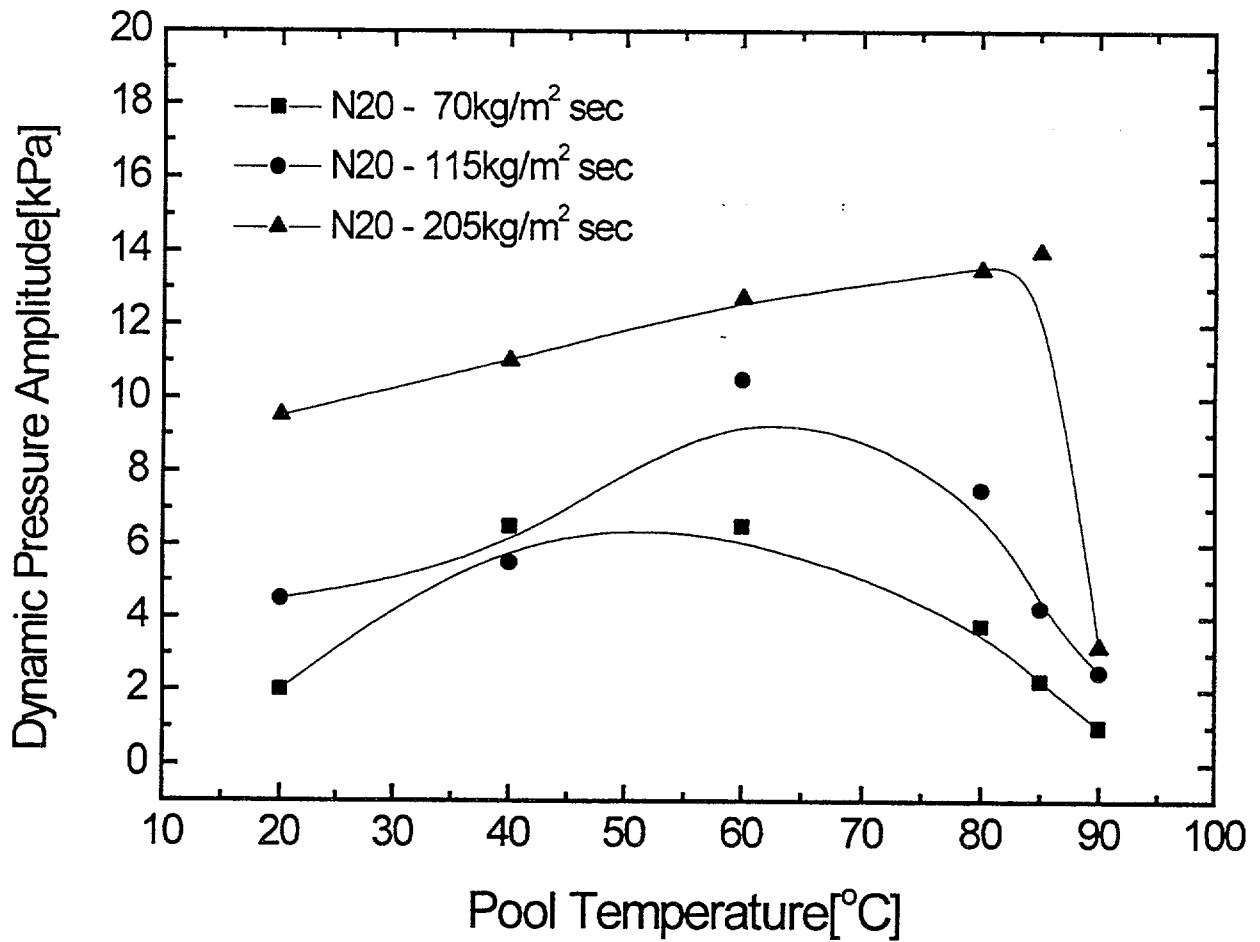


FIG. 12. Variation of the dynamic pressure at the wall : $d_i = 20$ mm.

observed that the shape of steam jet cavity is rather random and the condensation mode is very oscillatory at the steam mass flux smaller than $270 \text{ kg/m}^2\text{-s}$ in the entire range of pool temperature tested. It can be thought that this instability is mainly due to the steam discharge pressure lower than the choking pressure and due to small steam discharging velocity at the nozzle exit [9,10]. With the steam mass flux higher than $300 \text{ kg/m}^2\text{-s}$, however, the steam jet becomes stable and the shape of steam jet was observed to be conical or ellipsoidal depending on the steam mass flux and the pool temperature.

With the above-mentioned observation in mind, it is interesting to note that the characteristics of dynamic pressure is very closely related to the steam mass flux, which determines the stability of steam jet, that is, it depends mainly on whether or not the flow condition at the nozzle exit is in choking. As shown in Fig.12, the dynamic pressure at lower steam mass flux ($< 270 \text{ kg/m}^2\text{-s}$), which corresponds to oscillatory condensation, shows larger amplitude than that at higher steam mass flux ($> 270 \text{ kg/m}^2\text{-s}$), as typically shown in Fig. 13, corresponding to stable condensation.

It can be seen from Figs.12 and 13 that the peak of dynamic pressure varies differently with the steam mass flux. These differences are mainly due to the state of the flow condition at the nozzle exit as discussed above rather than the nozzle size itself. At lower steam mass flux ($< 270 \text{ kg/m}^2\text{-s}$), the peak amplitude increases with the steam flux as shown in Fig. 12 for the 20 mm nozzle. At higher steam mass flux, however, the trend is reversed as shown in Fig. 13 for the 10.15 mm nozzle.

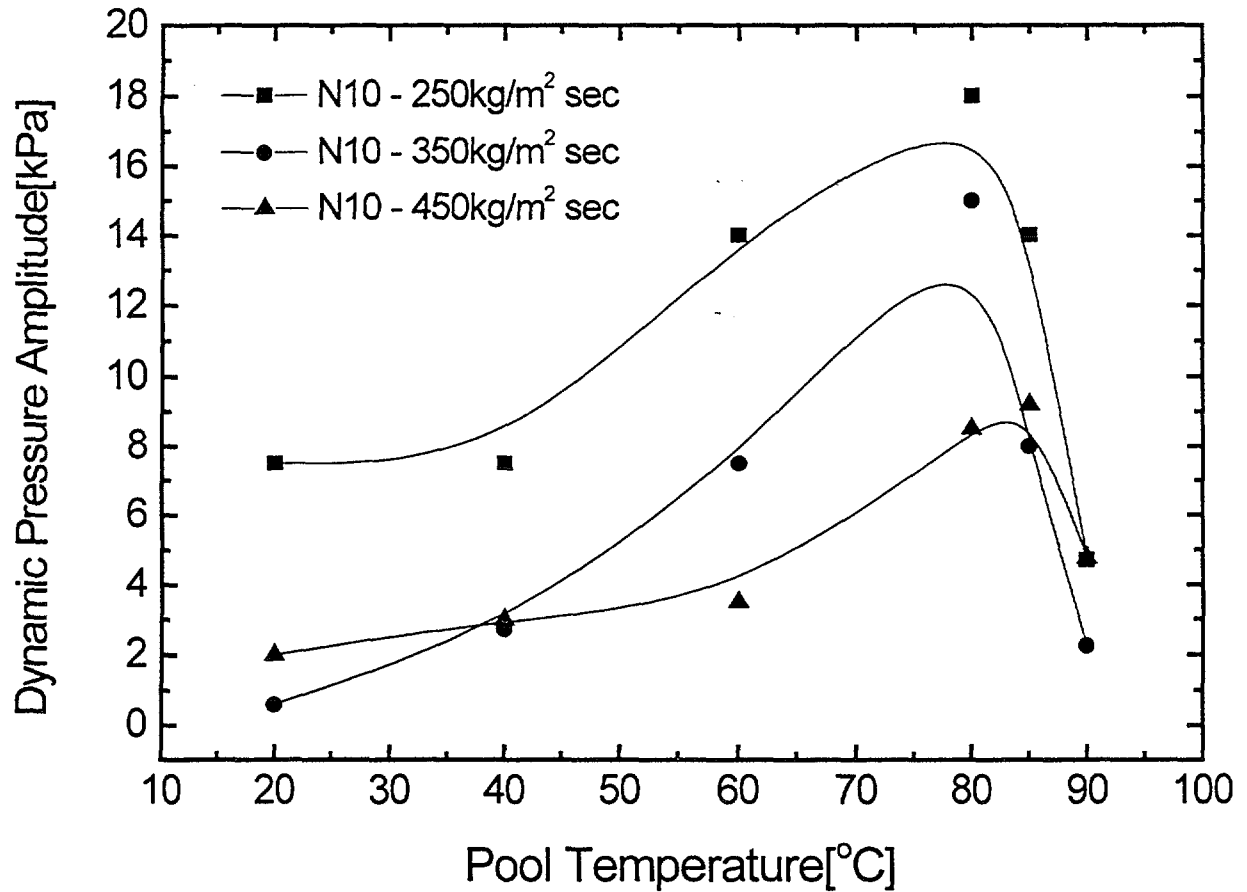


FIG. 13. Variation of the dynamic pressure at the wall: $d_i = 10.15$ mm.

As shown in Figs. 12 and 13, the amplitude of pressure pulse is increased as the pool temperature increases, then it reaches a peak, after which it decreases rapidly before the pool water becomes saturated for both stable and unstable condensation cases. It is also interesting to note that the dynamic pressure in the pool shows a peak at a finite subcooling of about 20 °C, and approaches to a very small value as the subcooling is decreased. This trend is very similar to that observed by Sonin [16] and Chan [17].

IV. CONCLUSION

Experimental investigations on direct contact condensation of steam discharging into subcooled pool water have been performed for five different horizontal nozzles under various conditions of pool water temperature and steam mass flux. For the stable steam jet, conical shape of steam jet is typically observed in case of smaller mass flux and lower pool temperature, and ellipsoidal shapes in case of larger mass flux and higher pool temperature. Inside the jet near the nozzle exit, the axial and radial temperatures are independent of the pool water temperature. Especially, the temperature fluctuations for both the axial and radial directions are observed in this region due to the jet expansions in case of the ellipsoidal shape of jet.

The jet expansion ratio is in the range of 1.05 ~ 2.3 and tends to increase as the steam mass flux and pool temperature are increased. The effect of nozzle size on the expansion ratio is observed not so large. The dimensionless steam jet length is in the range of 2.05 ~ 11.3 and tends to increase as the steam mass flux and pool temperature is increased. The effect of

nozzle size on the dimensionless steam jet length is also observed not so large. The average heat transfer coefficient is found to be in the range of $1.24 \sim 2.05 \text{ MW/m}^2 \cdot ^\circ\text{C}$ and tends to increase as the pool temperature and nozzle size is decreased and the steam mass flux is increased. Empirical correlations for the dimensionless steam jet length as well as the average heat transfer coefficients are presented as functions of the steam mass flux and condensation driving potential.

The dynamic pressure shows the trend which is mainly dependent on the steam mass flux and pool water temperature. The magnitude of the dynamic pressure in pool water shows a peak at a finite subcooling of around 20°C , and becomes smaller as the subcooling is decreased. The peak value of dynamic pressure varies differently with the steam mass flux: At low steam mass flux, the peak magnitude increases with increasing steam mass flux, whereas at higher steam mass flux, the trend is reversed.

NOMENCLATURE

A	: heat transfer area, m^2
A_e	: nozzle exit area, m^2
B	: condensation driving potential, $C_p (T_s - T_f) / (h_s - h_f)$
C_p	: water specific heat, $\text{J/kg} \cdot ^\circ\text{C}$
d_i	: nozzle internal diameter, m
δ	: width of the steam jet at its maximum location, m
G	: steam mass flux, $\text{kg/m}^2 \cdot \text{s}$
G_m	: critical steam mass flux at atmosphere, $\text{kg/m}^2 \cdot \text{s}$
h	: average heat transfer coefficient, $\text{W/m}^2 \cdot ^\circ\text{C}$
h_s	: steam enthalpy, J/kg
h_f	: water enthalpy, J/kg
L	: steam jet length, m
T_f	: water temperature, $^\circ\text{C}$
T_s	: steam temperature, $^\circ\text{C}$

REFERENCES

- [1] AYA, I. and NARIAI, H., "Evaluation of Heat Transfer Coefficient at Direct Condensation of Cold Water and Steam", Nucl. Eng. & Des., Vol. 131 (1991), pp. 17-24.
- [2] YOUNG, R.J., YANG, S.K. AND NOVONTY, J.L., "Vapor Liquid Interaction in a High Velocity Vapor Jet Condensing in a Coaxial Water Flow", Proc. 5th Int. Heat Transfer Conf., Tokyo, Vol. 3 (1974), pp. 226-230.
- [3] FUKUDA, S., "Pressure Variation due to Vapor Condensation in Liquid (II): Phenomena at Large Vapor Mass Flow Rate", J. Atomic Energy Soc. Japan, Vol. 24, No. 6 (1982), pp. 466-474.
- [4] CUMO, M., FARELLO, G.E. AND FERRARI, G.E., "Heat Transfer in Condensing Jets of Steam in Water", Proc. 6th Int. Heat Transfer Conf., Toronto, Vol. 5 (1978), pp. 101-106.

- [5]KERNEY, P.J., FAETH, G.M. AND OLSON, D.R., "Penetration Characteristics of Submerged Jet," AICHE J., Vol. 18, No. 3 (1972), pp. 548-553.
- [6]CHUN, M.H., KIM, Y.S. AND PARK, J.W., "An Investigation of Direct Condensation of Steam Jet in Subcooled Water", Int. Comm. Heat & Mass Transfer, Vol. 23, No. 7 (1996), pp. 947-958.
- [7]DEL TIN, G., LAVAGNO, E. AND MALANDRONE, M., "Thermal and Fluid-Dynamic Features of Vapor Condensing Jets", Heat & Technology, Vol. 1, No. 1 (1983), pp. 13-35.
- [8]STANFORD, L.E. AND WEBSTER, C.C., "Energy Suppression and Fission Product Transport in Pressure Suppression Pools", ORNL-TM-3448 (1972).
- [9]WEIMER, J.C., FAETH, G. M. AND OLSON, D.R., "Penetration of Vapor Jets Submerged in Subcooled Liquids", AICHE J., Vol. 19, No. 3 (1973), pp. 552-558.
- [10]SIMPON, M. E. AND CHAN, C. K., "Hydraulics of a Subsonic Vapor Jet in Subcooled Liquid", J. of Heat Transfer, Vol. 104 (1982), pp. 271 ~ 278.
- [11]TSAL, S.S. AND KAZIMI, M.S., "The Potential for Penetration of a Hot Vapor Jets into a Subcooled Liquid", ASME 76-WA/HT-78 (1976)
- [12]CHEN, L.D. AND FAITH, G.M., "Condensation of Submerged Vapor Jets in Subcooled Liquids", J. Heat Transfer, Vol. 104 (1982), pp. 774-780.
- [13]NARIAI, H. AND AYA, I., "Fluid and Pressure Oscillations Occurring at Direct Contact Condensation of Steam Flow with Cold Water", Nucl. Eng. & Des., Vol. 95 (1986), pp. 35-45.
- [14]DEL TIN, G., LAVAGNO, E. AND MALANDRONE, M., "Pressure and Temperature Measurements in Vapor Condensing Jets", Proc. 7th Int. Heat Transfer Conf., Munchen, Vol. 6 (1982), pp. 159-164.
- [15]KUDO, A, EGUSA, T. AND TODA, S., "Basic Study of Vapor Suppression," Proc. 5th Int. Heat Transfer Conf., Tokyo, Vol. 3 (1974), pp. 221-225.
- [16]SONIN, A. A., "Suppression Pool Dynamics Research at MIT", NUREG/CP-0048 (1984), pp. 400 ~ 421.
- [17]CHAN, C. K., "Dynamical Pressure Pulse in Steam Jet Condensation", Proc. 6th Int. Heat Transfer Conf., Toronto (1978), pp. 395 ~ 399.

NEXT PAGE(S)
left BLANK



EXPERIMENTAL RESEARCH ON IN-TUBE CONDENSATION IN THE PRESENCE OF AIR

A. TANRIKUT

Nuclear Computing and Design Group,
Turkish Atomic Energy Authority,
Kavaklıdere Ankara

O. YESIN

Mechanical Engineering Department,
Middle East Technical University,
Ankara

Turkey

Abstract

In this research work, in-tube condensation in the presence of air is investigated experimentally for different operating conditions, and inhibiting effect of air is analyzed by comparing the experimental data of air/steam mixture with the data of corresponding pure steam cases, with respect to temperature, heat flux, and heat transfer coefficient. The test matrix covers the range of; $P=2-6$ bar, $Re_v=45000-94000$, and $X_i=0\%-52\%$. The inhibiting effect of air manifests itself as a remarkable decrease in centerline temperature ($10\text{ }^{\circ}\text{C}-50\text{ }^{\circ}\text{C}$), depending on inlet air mass fraction. However, the measured centerline temperature is suppressed compared to the predicted one, from the Gibbs-Dalton Law, which indicates that the centerline temperature measurements are highly affected by inner wall thermal conditions, possibly due to narrow channel and high vapor Reynolds number. Even at the lowest air quality (10%) the reduction of the heat flux is 20% while it reaches up to 50% for the quality of 40%. Maximum percent decrease of the heat transfer coefficient was observed in runs with the system pressure of 2 bar; 45% and 65%, for the air mass fraction of 10% and 28%, respectively.

1. INTRODUCTION

The introduction of nuclear power becomes an attractive solution to the problem of increasing demand for electricity power capacity in Turkey. Thus, Turkey is willing to follow the technological development trends in advanced reactor systems. A part of our long term research and development efforts is planned to concentrate on passive cooling systems. The primary objectives of the passive design features are to simplify the design, which assures the minimized demand on operator, and to improve plant safety. The research on passive systems mainly comprises the computer code assessment studies and includes the applications for both old and new generation reactor systems. To accomplish these features the operating principles of passive safety systems should be well understood by an experimental validation program. Such a validation program is also important for the assessment of advanced computer codes which are currently used for design and licensing procedures. The condensation mode of heat transfer plays an important role for the passive heat removal applications in the current nuclear power plants (e.g. decay heat removal via steam generators in case of loss of heat removal system) and advanced water-cooled reactor systems. But it is well established that the presence of noncondensable gases can greatly inhibit the condensation process due to build-up of noncondensable gas concentration at the liquid/gas interface. The isolation condenser of passive containment cooling system of the simplified boiling water reactors is a typical application area of in-tube condensation in the presence of noncondensable gases. An experimental study which could enable us for the fundamental investigation of condensation in the presence of air was planned in cooperation with the Mechanical Engineering Department of the Middle East Technical University (METU), Ankara, in the frame of a project between the Turkish Atomic Energy Authority (TAEA) and METU. The project is

partially sponsored by the International Atomic Energy Agency (IAEA) under the Coordinated Research Program (Contract No: 8905/R0) which is entitled "*Thermohydraulic Relationships for Advanced Water Cooled Reactors*". The experimental program covers a wide range of steam and steam/air mixture flow rates under forced convection conditions and has the purpose to investigate the inhibiting effect of air on steam condensation process.

2. DESCRIPTION OF THE METU CONDENSATION TEST FACILITY

The test facility, named as METU Condensation Test Facility (METU-CTF), was installed at the Mechanical Engineering Department of METU [1]. The experimental apparatus consisting of an open steam or steam/gas system and an open cooling water system is depicted in the flow diagram of Figure 2.1.

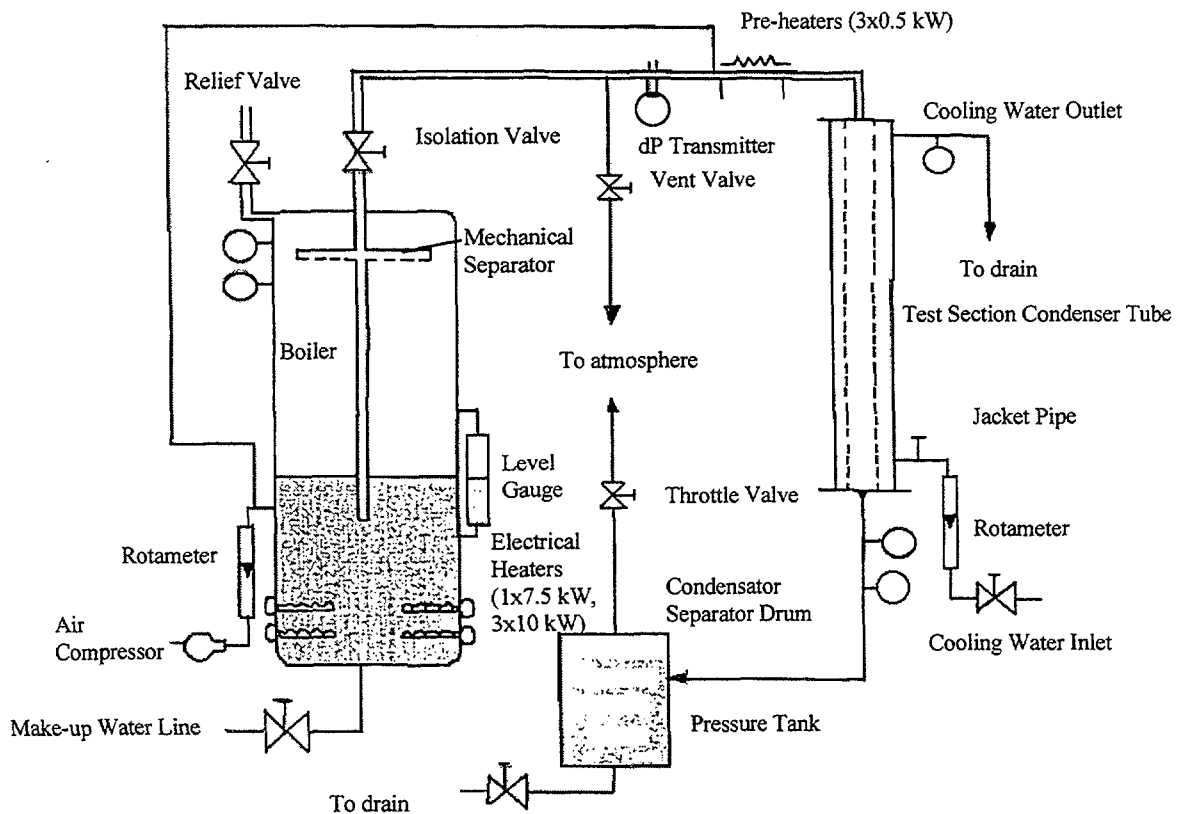


FIG. 2.1. The flow diagram of the METU-CTF.

Steam is generated in a boiler (1.6 m high, 0.45 m ID) by using four immersion type sheathed electrical heaters. Three of these heaters have a nominal power of 10 kW each and the fourth one has a power of 7.5 kW, at 380 V. All the heaters can be individually controlled by switching on or off. One of these heaters, i.e. the one with 7.5 kW power, is connected to a variac for continuous control of power. The boiler tank was designed to withstand an internal pressure of 15 atm (at $T=20\text{ }^{\circ}\text{C}$) and was tested at this pressure. The maximum operating pressure of the tank is 10 atm. To ensure dry steam at the exit of the boiler, a mechanical separator directly connected to the exit nozzle was installed. However, electrical pre-heating

with three heaters (0.5 kW per heater) is also available at the entrance of the test to increase the temperature of steam, so that steam is guaranteed to be 100% dry. The boiler tank was thermally insulated to reduce environmental heat loss.

Compressed air can be supplied either to the boiler tank (directly to the water) or to the steam line via a nozzle (after the orifice meter) on the horizontal part of the pipe which connects the boiler and the test section. Preference was given to the first method, i.e. injection to the boiler, during most of the experiments since system behavior is more stable compared to the second method, when air mass flow rate is increased. When air injection was performed by the second method (to the horizontal piping), air injected passes through the preheating section so that local steam condensation was avoided at the entrance of the test section due to thermal inequilibrium of steam and air.

The pipe connecting the boiler tank and the test section has a length of approximately 2 m and an ID of 38.1 mm. The pipe was connected to the boiler tank via an isolation valve. This isolation valve (38.1 mm ID) is used to isolate the boiler until inside pressure of the tank is increased to a pre-determined level. The measurements performed on this part of the experimental facility are: mass flow rate via a differential pressure transmitter and temperature. There are three electric heaters (0.5 kW each at 220 V) installed to the horizontal part of the piping between the orifice meter and the test section. The pipe connecting the boiler and the test section was thermally insulated.

The test section is a heat exchanger of countercurrent type, that is steam or steam/gas mixture flows downward inside the condenser tube (inner tube) and cooling water flows upward inside the jacket pipe (outer pipe).

The condenser tube consists of a 2.15 m long seamless stainless steel tube with 33/39 mm ID/OD and is flanged at both ends with sealing materials. The condenser tube was flanged to the inlet (33.5/42.6 mm ID/OD) and exit (33.5/42.6 mm ID/OD) pipes of the test section. The total length of the inlet pipe from the horizontal part of the pipe section down to the condenser tube is approximately 33 cm ($10 \times d_i$, where d_i is the inner diameter of the tube) and this length is long enough for the mixture flow to become fully developed before entering the condenser. It should also be noted that some uncertainties (such as irregular film development or dropwise condensation) associated with the liquid film development at the entrance of the condenser tube are expected to occur in this development region since the entrance region was not thermally insulated. A pressure measurement port was located at the vertical part of the inlet pipe flanged to the condenser tube. A total of 13 holes (1.5 mm diameter) were drilled with an angle of 30° at different elevations along the condenser tube length to fix the thermocouples for inner wall temperature measurements. The condenser tube was tested at 10 atm pressure to check that inner wall of the tube was not pierced during the drilling process. The outlet of the condenser tube is connected to a tank via exit part of the test section. This tank is used to keep the system pressure at a constant level by controlling the flow rate of steam or air/steam mixture through a valve connected to the tank. The measured parameters at the exit of the test section are pressure and temperature.

The jacket pipe surrounding the condenser tube is made of sheet iron and has a length of 2.133 m and 81.2/89 mm ID/OD. The cooling water is supplied via a nozzle which has been welded on the jacket pipe. Similarly, cooling water outlet consists of a nozzle which is connected to the building water discharge system. Inner diameter of all these nozzles is 12.7 mm. A total of 15 holes (1.5 mm diameter) were drilled radially at different elevations for installation of the thermocouples to be used for cooling water temperature measurements. The measured cooling water temperature is used to determine heat flux profile along the annulus region. The jacket pipe was thermally insulated to reduce environmental heat losses.

3. EXPERIMENTAL TEST MATRIX

The experimental test matrix [1] consists of two parts: pure steam runs and air/steam mixture runs. It is to be noted that the mass flow rate measurement was performed by using a differential pressure transmitter (orifice meter) so that in each set of experimental run, differential pressure, rather than mass flow rate, was set to an almost constant predetermined value while changing system pressure. In air/steam mixture runs, system pressure (P) and steam mass flow rate (\dot{m}_v) settings are kept close to those set before during pure steam runs. The reason of selection of steam mass flow rate as a fixed parameter, rather than total mixture mass flow rate, in air/steam mixture runs is to fix the amount of steam at the entrance of the test section to be able to make better comparison with the data of pure steam runs and to understand inhibiting effect of air as a noncondensable gas. However, the total mass flow rate (mass flow rate of air + vapor) was increased compared to the pure steam runs and this should be taken into account when analyzing the experimental data. The experimental test matrices are given in Tables I and II. In these tables; Re_v is vapor Reynolds number, \dot{m}_{cw} is mass flow rate of cooling water, and X_{air} is air quality, at the inlet of the test section.

4. EXPERIMENTAL RESULTS AND DISCUSSION

4.1. Temperature distribution

Temperature measurements were performed at three different locations in the radial direction of the test section [1]: at the centerline and inner wall of the condenser tube, and at the annulus of the jacket pipe. The centerline temperature simply gives the information for the state of vapor, flowing downward, along with the system pressure measured at the inlet of the test section. The temperature measurement in the jacket pipe, on the other hand, enables the prediction of the local heat flux distribution inside the condenser tube. It is expected that for pure steam runs, the measured centerline temperature should be the saturation temperature at the corresponding system pressure measured at the inlet, by assuming that differential pressure along the channel is small enough (~0.3 bar at the system pressure of 5 bars, and much smaller for lower system pressure settings). Moreover, when air/vapor mixture flows along the test section, the centerline temperatures indicate the existence of air at the core of the condenser tube since the vapor temperature is lower than the saturation temperature corresponding to the total system pressure due to partial pressure of vapor which decreases with increasing quality of air, as Gibbs-Dalton Law states. Measured inner wall temperature values also indicate the effect of the presence of air as a noncondensable gas, by following the

TABLE I. TEST MATRIX FOR PURE STEAM EXPERIMENTAL RUNS

Code	P (bar)	\dot{m}_v (kg/s)	Re_v	\dot{m}_{cw} (kg/s)	X_{air}
RUN-1.2.1	1.829	1.808×10^{-2}	54770	0.221	0.0
RUN-1.3.1	3.029	2.314×10^{-2}	66875	0.223	0.0
RUN-1.4.1	3.959	2.721×10^{-2}	76645	0.226	0.0
RUN-1.5.1	4.837	3.101×10^{-2}	85675	0.225	0.0
RUN-1.6.1	5.452	3.419×10^{-2}	93365	0.226	0.0

TABLE II. TEST MATRIX FOR AIR/STEAM EXPERIMENTAL RUNS

Code	P (bar)	\dot{m}_v (kg/s)	Re_v	\dot{m}_{cw} (kg/s)	X_{air}
RUN-2.2.1R2	1.919	1.853×10^{-2}	56228	0.232	0.095
RUN-2.2.1	1.919	1.771×10^{-2}	53748	0.198	0.099
RUN-3.2.1	1.956	1.865×10^{-2}	56879	0.236	0.191
RUN-4.2.1	2.01	2.055×10^{-2}	62949	0.232	0.275
RUN-2.3.1R1	2.93	2.428×10^{-2}	70801	0.232	0.092
RUN-2.3.1	2.969	2.306×10^{-2}	66771	0.23	0.099
RUN-3.3.1	2.901	2.366×10^{-2}	69543	0.231	0.189
RUN-4.3.1	3.16	2.664×10^{-2}	78258	0.238	0.279
RUN-5.3.1R	3.13	1.804×10^{-2}	53938	0.237	0.421
RUN-2.4.1	3.982	2.833×10^{-2}	80253	0.234	0.097
RUN-3.4.1	3.90	2.77×10^{-2}	79188	0.223	0.193
RUN-4.4.1	3.94	2.987×10^{-2}	85898	0.231	0.274
RUN-5.4.1	3.94	2.193×10^{-2}	63663	0.253	0.369
RUN-6.4.1	3.906	1.526×10^{-2}	45195	0.253	0.519
RUN-2.5.1	4.312	2.918×10^{-2}	82043	0.237	0.097
RUN-6.5.1	4.36	1.881×10^{-2}	54476	0.253	0.43
RUN-2.6.1	5.257	3.386×10^{-2}	93388	0.234	0.098

trend of centerline temperature, i.e. higher the percentage of air lower the centerline and inner wall temperatures. In fact, air, presumably homogeneously mixed with vapor at the entrance of the test section, then tends to accumulate at the interface of liquid film and air/vapor mixture which, consequently, causes a corresponding reduction of partial pressure of vapor at the interface. In turn, this reduces the saturation temperature at which condensation takes place. The net effect is to lower the effective thermal driving force thereby reducing the heat transfer rate. The accumulation of air at the interface is the principal reason for the mass diffusion resistance in radial direction which causes lower condensation rates. The mechanism of air accumulation at the interface of air/vapor and liquid film can be explained on the following physical grounds: The vapor that is to be condensed is carried towards the wall of the condenser tube and it also carries with it some amount of air. Since the condensate film is impermeable to air, it must be removed from the interface at the same rate as it arrives, at steady-state conditions. However, the rate of diffusive flow depends on the concentration gradient and sufficient amount of gas should be accumulated at the interface to sustain the balance between the convective inflow and diffusive back-flow.

To demonstrate the effect of presence of air, the measured temperature profiles, for the case of $P=4$ bar, are presented in Figures 4.1, 4.2 and 4.3 corresponding to $X_{air}=0\%$, 28% and 52%, respectively. The pure vapor run results show that the measured centerline temperature (T_c) trend closely follows the saturation temperature (T_s) line and always remains below of it

($\Delta T_{\max} \sim 4$ °C) even at the bottom of the test section. It should be noted that experimental runs with the system pressure of 4 bar were performed at the condition of higher vapor Reynolds number compared to runs with lower system pressure (Tables I and II) and this in turn causes the thermocouples to be wetted by the condensed liquid film droplets. The temperature differences of $T_{c-\text{sat}}$ (saturation temperature of zero air quality) and T_c are: 24–29 °C and 42–48 °C for the cases of $X_i = 28\%$ and 52% , respectively. The difference between the predicted (from the Gibbs-Dalton Law, T_s) and the measured (T_c) centerline temperatures come out to be 1–5 °C, 13–21 °C, and 15–31 °C, for $X_i = 0\%$, 28%, and 52%, respectively. Among the results presented, the experimental results pertaining to the case with $X_i = 52\%$ represents a special case concerning the inlet vapor Reynolds number ($\sim 41,000$), which is about half of other runs at the same pressure setting. The distribution of T_s shows a marked decrease towards the bottom of tube due to increase in X_{air} , steeper than other runs. Moreover, a sharp decrease in all measured temperatures (T_c , T_w) are observed for the case with $X_i = 52\%$, i.e. more than 40 °C, relative to the pure vapor case.

4.2. Heat flux distribution

To calculate local heat transfer coefficients, the local air/vapor mixture temperature, local inner wall temperature, and the local heat flux must be known. The local air/vapor mixture and inner wall temperatures were measured directly, and the local heat flux was obtained from the measured coolant temperature profile [1]. Hence dT_{cw}/dx was computed from an exponential fit of the measured coolant temperature as a function of axial distance, and the local heat flux was determined from:

$$q''(x) = -\frac{\dot{m}_{cw} c_p}{\pi d_i} \frac{dT_{cw}(x)}{dx} \quad (1)$$

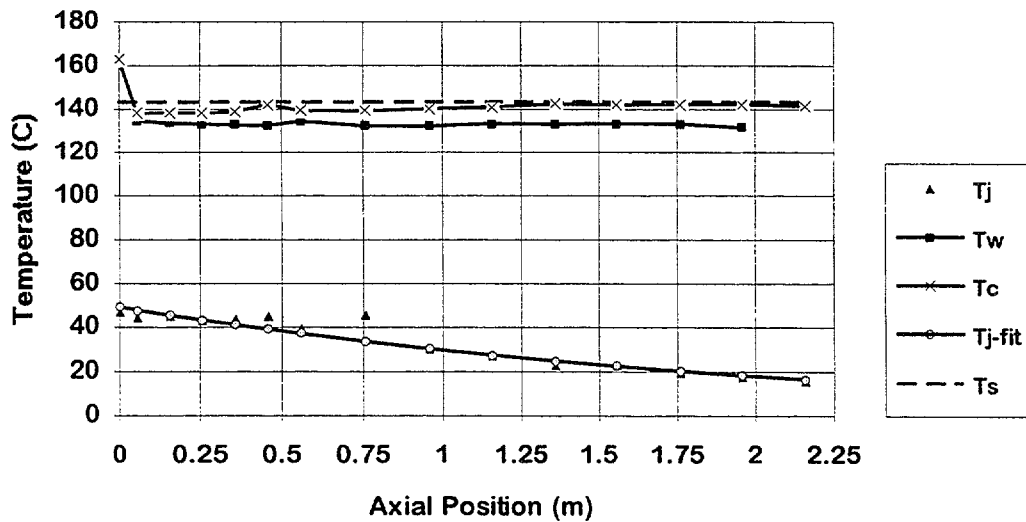


FIG. 4.1. Temperature distribution ($P=4$ bar, $Re_v=76645$, $X_i=0\%$).

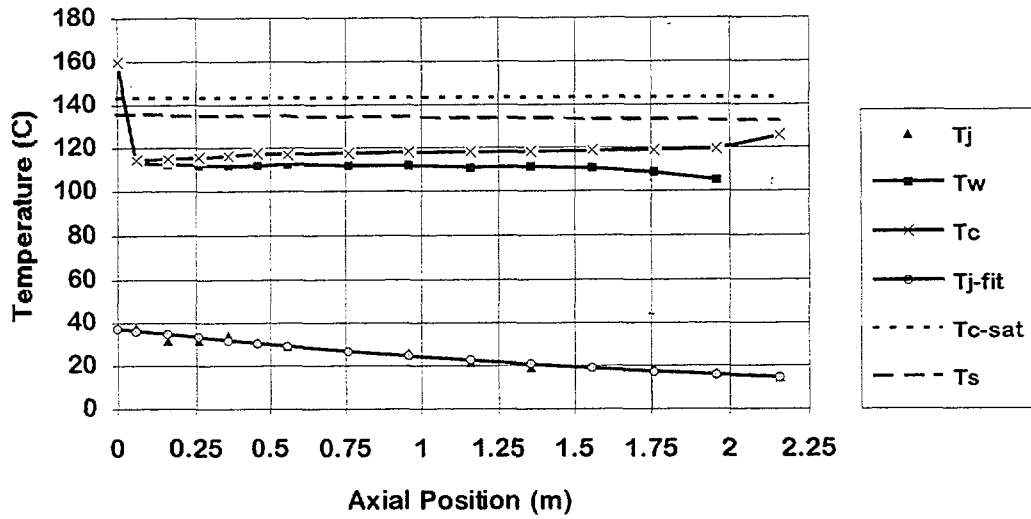


FIG. 4.2. Temperature distribution ($P=4$ bar, $Re_v=85898$, $X_i=28\%$).

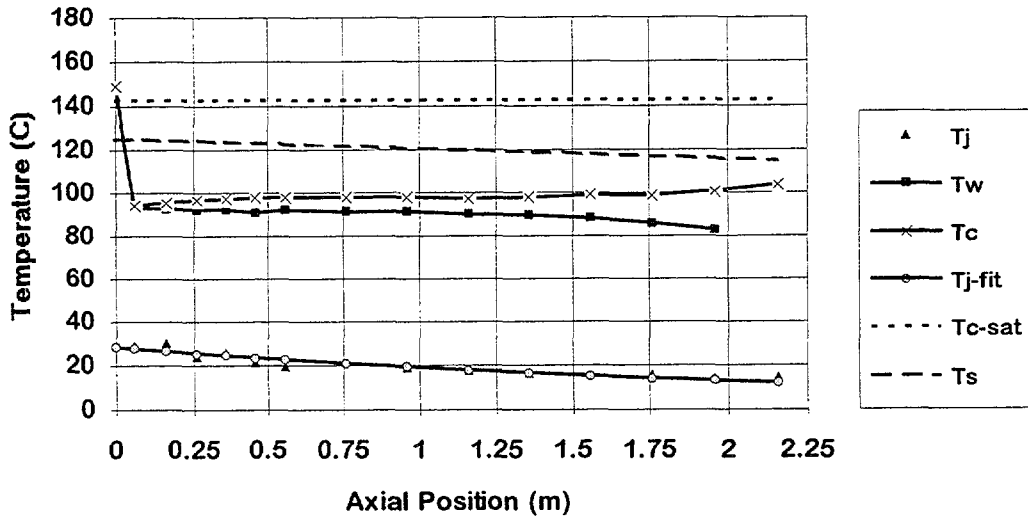


FIG. 4.3. Temperature distribution ($P=4$ bar, $Re_v=45195$, $X_i=52\%$).

where

- \dot{m}_{cw} is the mass flow rate of cooling water (kg/s),
- c_p is the constant pressure specific heat (J/kg °C),
- d_i is the inner diameter of the condenser tube (m),
- $dT_{cw}(x)/dx$ is the local axial temperature gradient (°C/m).

The heat flux distributions for experimental runs corresponding to the system pressures of 2 and 4 bar, and including pure vapor and different mixtures of air and vapor, are presented in Figures 4.4 and 4.5. It is clear in all figures that the heat flux drastically decreases as inlet air mass fraction increases. This situation is the evidence for how some amount of air, mixed with vapor, degrades the performance of the heat exchanger. The percent decrease in

heat flux, at the middle of the test section (~ 1 m from the top), is summarized as follows (corresponding pure vapor cases are taken as the reference for each system pressure):

- $P_n=2$ bar: 20% ($X_i=10\%$), 24% ($X_i=20\%$), 45% ($X_i=30\%$)
- $P_n=3$ bar: 19% ($X_i=10\%$), 24% ($X_i=19\%$), 30% ($X_i=28\%$), 48% ($X_i=42\%$)
- $P_n=4$ bar: 22% ($X_i=10\%$), 24% ($X_i=20\%$), 28% ($X_i=29\%$), 37% ($X_i=37\%$)
44% ($X_i=52\%$)
- $P_n=5$ bar: 24% ($X_i=10\%$), 75% ($X_i=43\%$)
- $P_n=6$ bar: 27% ($X_i=10\%$)

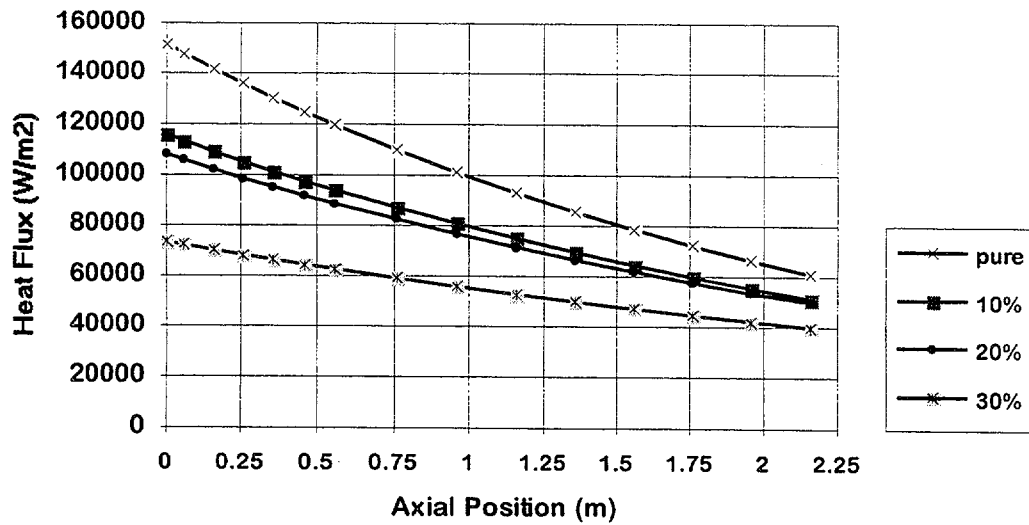


FIG. 4.4. Heat flux distribution along the condenser tube ($P=2$ bar, $Re_v=54000-63000$).

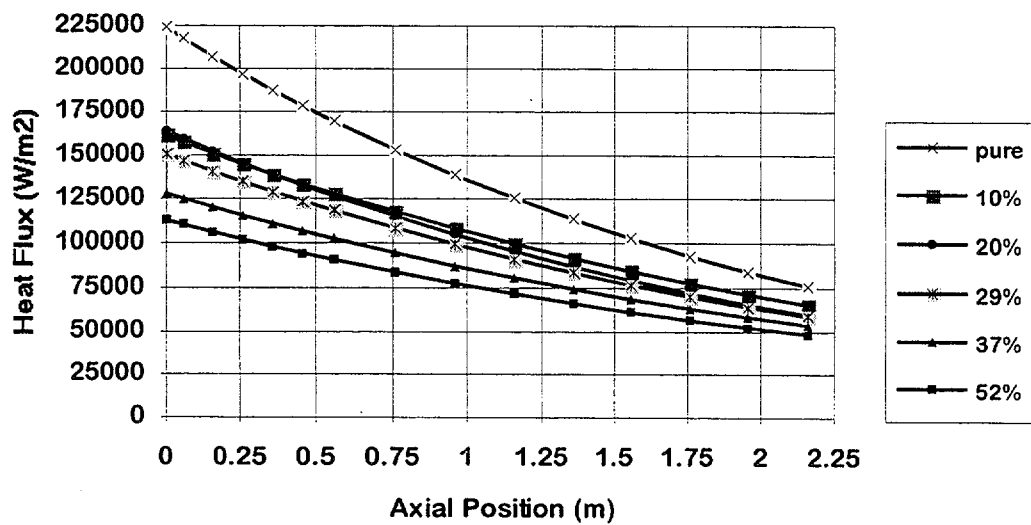


FIG. 4.5. Heat flux distribution along the condenser tube ($P=4$ bar, $Re_v=77000-86000$ for $X_i=0\%, 10\%, 20\%, 29\%$ and 37% , and $Re_v=45000$ for $X_i=52\%$).

Another point to be emphasized is that the difference in heat flux values corresponding to the air/vapor mixture and pure vapor cases get closer to each other towards the bottom of the condenser tube due to diminishing condensation rate as the result of increased condensate film thickness and air mass fraction. The local heat flux is increased by system pressure along with vapor mass flow rate. This is observed by other investigators [1] as well and can be attributed to the increase in wall subcooling degree which enhances the thermal driving force for heat transfer. Moreover, higher system pressure associated with the higher inlet temperature leads to a greater number of molecular collisions helping in the diffusive transport of energy. However, the dependency of the wall subcooling degree, either measured or predicted from the Gibbs-Dalton Law, on system pressure is such that the wall subcooling degree remains nearly the same for the same inlet air mass fraction and for the different system pressure. This implies that the vapor mass flow rate may dominate over system pressure, concerning the effect on local heat flux, for cases with air/vapor mixture. The situation is rather different in pure vapor runs, that is increase in system pressure has a strong effect on enhancement of predicted, and even measured, wall subcooling degree. The comparison concerning the effect of system pressure on local heat flux for the inlet air quality of 30% is shown in Figure 4.6.

4.4. The heat transfer coefficient

The experimental local heat transfer coefficient was obtained from [1]

$$h(x) = \frac{q''(x)}{(T_c(x) - T_w(x))} \quad (2)$$

where

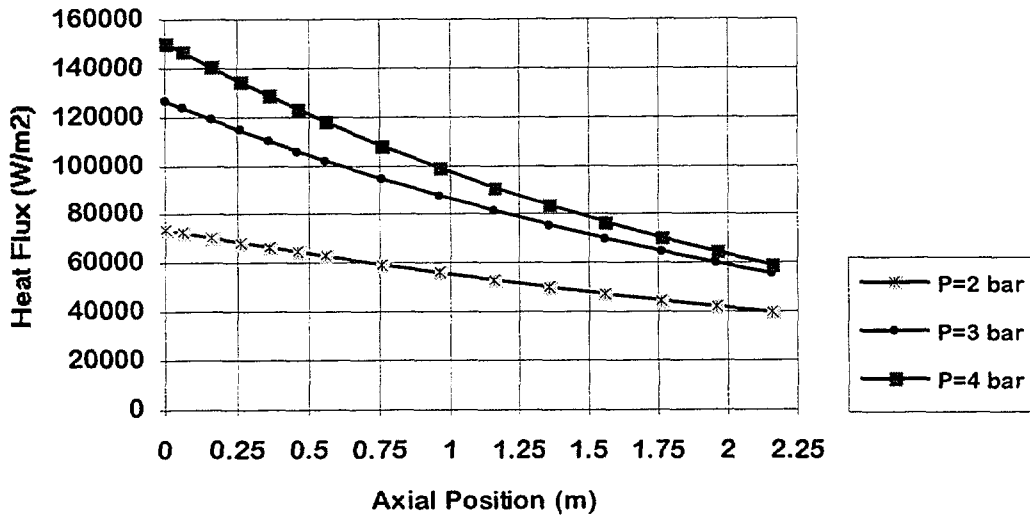


FIG. 4.6. Effect of system pressure ($X_i=30\%$).

$T_c(x)$ is the curve fitted value of the measured centerline temperature ($^{\circ}\text{C}$),

$T_w(x)$ is the curve fitted value of the measured inner wall temperature of the condenser tube ($^{\circ}\text{C}$).

As seen in the Figs. 4.7 and 4.8, existence of air in vapor suppresses the heat transfer coefficient. The percent of suppression, compared to the corresponding pure vapor case, highly depends on the system pressure and therefore on the vapor flow rate, as well as inlet air mass fraction. Since the temperature difference ($T_c - T_w$), namely the measured wall subcooling degree, is nearly constant ($\sim 5-8^\circ\text{C}$) for all runs, the heat transfer coefficient is mainly governed by the heat flux. When results given for $X_1=10\%$ and 28% are compared to the pure vapor case, at a nominal pressure of 2 bar, a maximum deviation of -45% and -65% is observed within an axial distance of 1 m, respectively. The results also reveal that the estimated effective condensation length, for pure vapor run, is not more than 1.25 m, which is about 60% of the total length, when the axial location at which heat transfer coefficients (pure and air/vapor mixture) are getting closer, is considered. From this, the effective condensation length of the air/vapor mixture case may be considered same as the pure vapor case.

All results presented up to this point are based on the measured temperature difference ($T_c - T_w$) as given in Equation (2). However, the bulk temperature (T_s) at the core of the condenser tube, as predicted by the Gibbs-Dalton Law, reveals the fact that the inequality $T_c < T_s$ always exists for the experimental cases with air/vapor mixture and even for some pure vapor runs. This situation shows that the measured centerline temperature (T_c), somehow, was affected by the inner wall thermal conditions. It is thought that thermocouples used for the centerline temperature measurements were continuously attacked by detached liquid droplets or patches from the inner surface of the tube due to turbulence initiated by high vapor flow. Besides this, narrow channel is another factor to be considered for such centerline temperature measurements, i.e. there is not sufficient distance between the film developed on the inner surface of the tube and the thermocouples fixed to a guide wire. This observation leads us to the question whether T_c or T_s is to be used for calculating the heat transfer coefficient, from the known heat flux values. It should be noted that when preference has been given to T_s , the heat transfer coefficient would represent the conditions of air mixed with dry vapor, at the core of the tube. To understand the effect of above given interpretation on the method of determining the wall subcooling, an analysis was performed for the ratio of the estimated heat

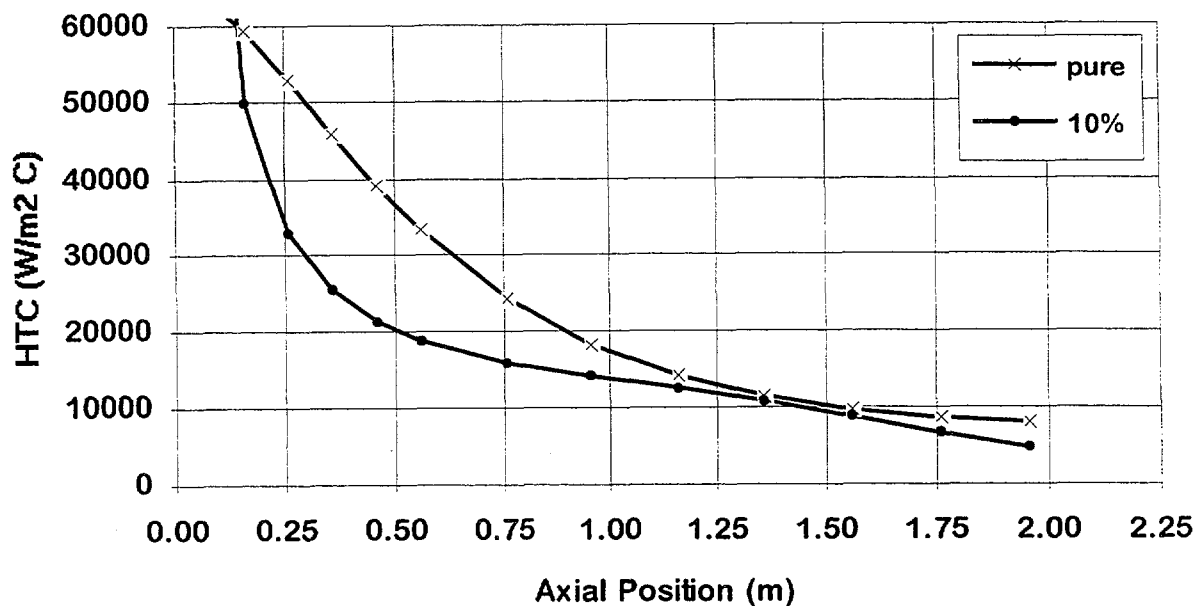


FIG. 4.7. Heat transfer coefficient distribution ($P=2$ bar).

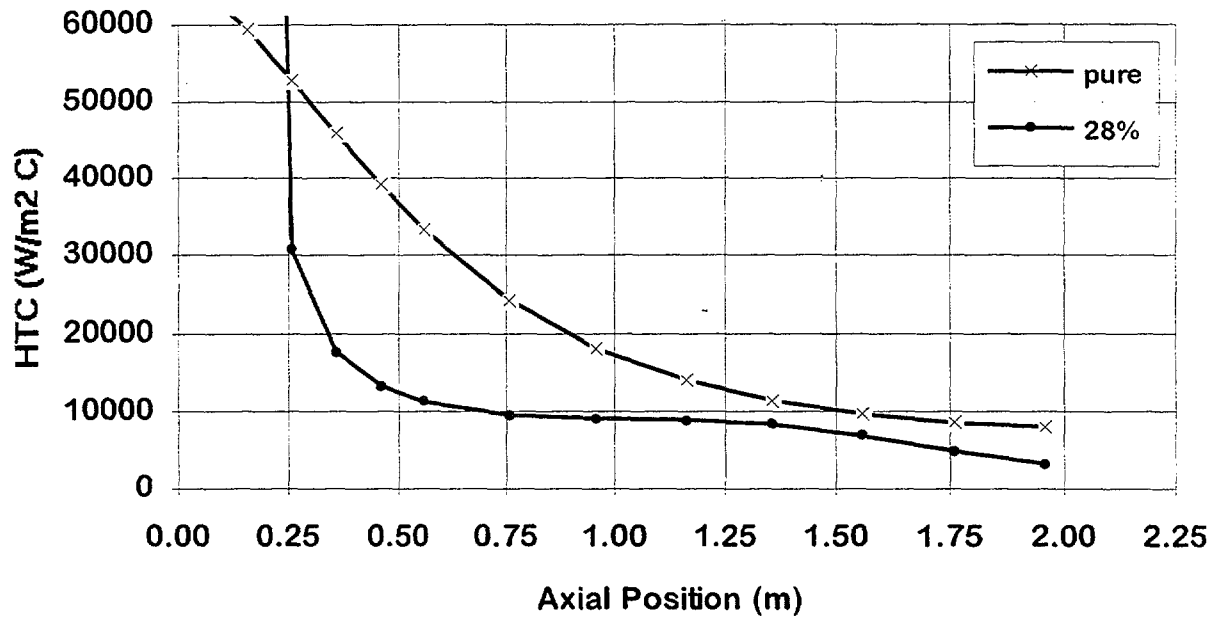


FIG. 4.8. Heat transfer coefficient distribution ($P=2$ bar).

transfer coefficient (h') and the experimental one (h). The ratio of the heat transfer coefficients determined from the two methods is equal to

$$\frac{h'(x)}{h(x)} = \frac{(T_c(x) - T_w(x))}{(T_s(x) - T_w(x))} \quad (3)$$

since heat flux is same. The heat transfer coefficient ratio for $P=5$ bar is presented in Fig. 4.9.

This figure shows that as inlet air mass fraction increases the ratio (h'/h) decreases, for the same system pressure, and this behavior is same for other experiments with the system pressure of 2, 3, 4, and 6 bar as well. That is to say, increase in air mass fraction leads to deviation from the measured heat transfer coefficient. However the ratio increases smoothly towards the bottom of the tube due to increase in measured centerline temperature (T_c). Another observation is that the heat transfer coefficient ratio, calculated for the pure vapor cases, decreases as system pressure, and therefore vapor Reynolds number, increases due to liquid droplet detachment from the inner surface of the tube which becomes increasingly dominant as vapor mass flow rate increases. Contrary to the pure vapor cases, the effect of system pressure and mass flow rate of vapor seems not so much pronounced for air/vapor mixture cases.

4.5. Comparison with theory

A set of simulations was performed by using the RELAP5/mod3 thermal-hydraulic system analysis computer code [2], used for safety and system analyses of nuclear power plants. The code solves six equations (mass, momentum, and energy) for two-phase and one equation (mass) for noncondensable gas. The heat transfer solution scheme of the code also includes condensation of vapor containing noncondensable gas, such as air, hydrogen, nitrogen, helium. The default model used currently is the Shah-Colburn-Hougen model. The Shah model replaces the Nusselt model for pure steam condensation if the heat transfer

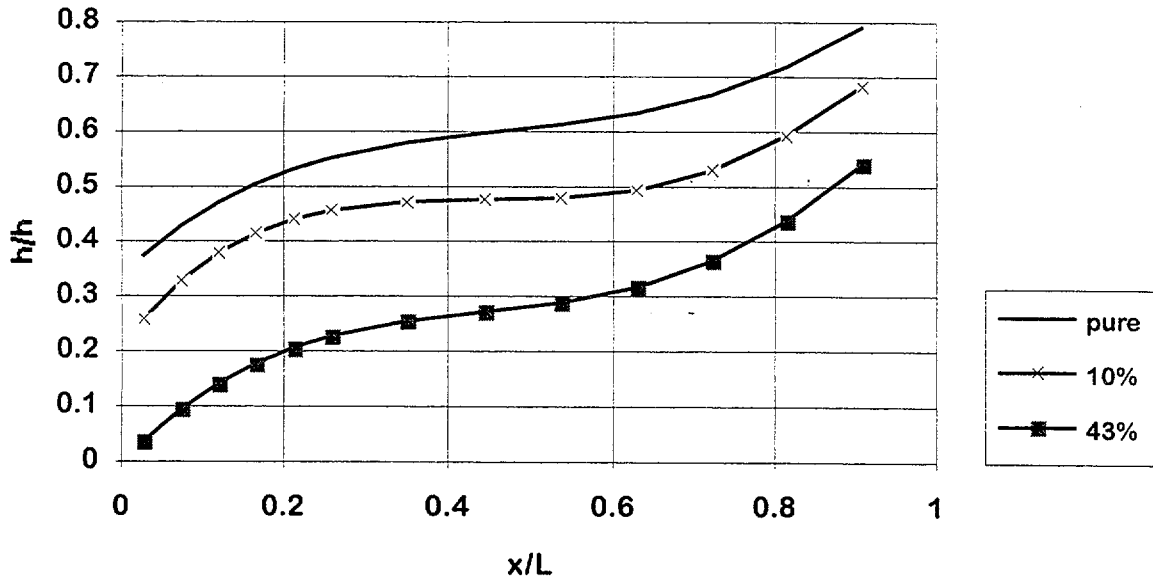


FIG. 4.9. Ratio of Heat Transfer Coefficients based on T_c and T_s ($P=5$ bar)

coefficient calculated by this model is greater than that of Nusselt model. The Colburn-Hougen diffusion model, used for taking into account the inhibiting effect of a noncondensable gas, involves an iteration process to solve for the steam saturation temperature at the interface between the steam/gas boundary layer and water film. As seen in Fig. 4.10, the RELAP5 code overestimates the heat flux from about 5% to 50%. Problems associated with the prediction of condensation heat transfer rates are; 1- assumption of the code for *dry vapor* in the core of a condenser tube may not necessarily reflect the physics there however simplifies the analysis, 2- superheated steam can affect the condensation process when a noncondensable gas is present.

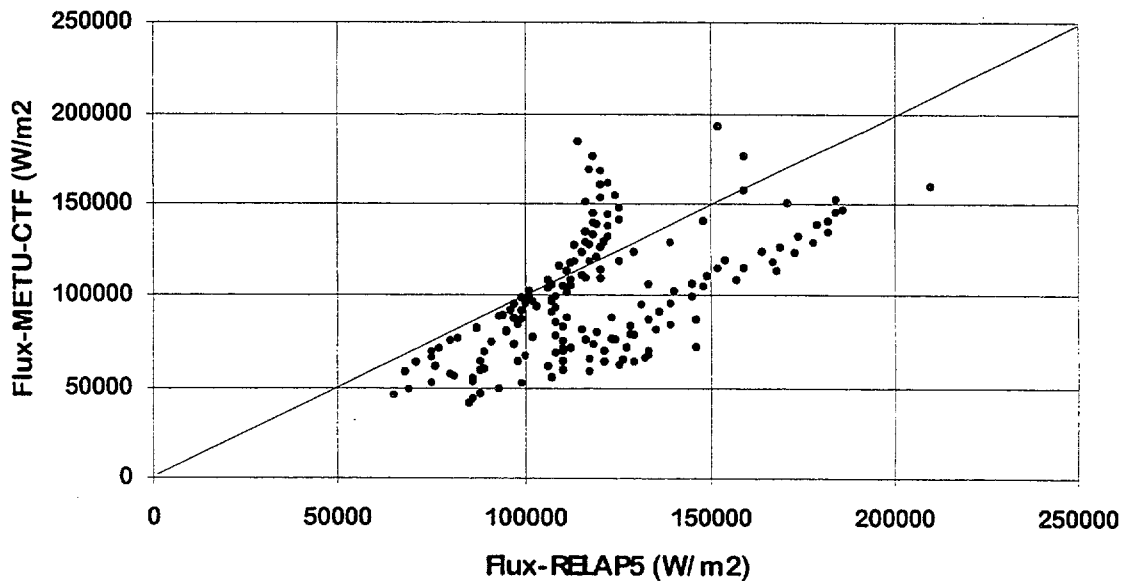


FIG. 4.10. Comparison of METU-CTF data and shah-colburn-hougen model.

5. CONCLUSION

When pure vapor runs are considered as the reference for comparison, first indicator of effect of air is the remarkable decrease in centerline and inner wall temperatures. Comparisons show that difference between saturation temperature, corresponding to the pure vapor case, and measured centerline temperatures varies between 10 °C and 50 °C, depending on inlet air mass fraction. In other words the temperature difference increases considerably as air mass fraction increases. However, the experimental data reveal the fact that thermocouples used for the centerline temperature measurements were wetted by detached liquid droplets from the surface so that centerline temperature trend closely follows that of inner wall, with a difference of about 1–10 °C. This situation indicates that centerline temperatures were highly affected by inner wall thermal conditions, possibly due to narrow channel and high vapor flow rate. It is found that there is a drastic decrease in the performance of the heat exchanger as the inlet air mass fraction increases. Even at the lowest inlet mass fraction (10%) cases, the decrease in heat flux is as high as ~20% while it reaches up to about 50% when the air mass fraction is increased to about 40%. The inhibiting effect of air on condensation manifests itself as a reduction in heat transfer coefficient. However, the inhibiting effect of air diminishes as system pressure and vapor flow rate increases. Maximum percent decrease was observed in runs with the system pressure of 2 bar, i.e. 45% and 65%, for air mass fraction of 10% and 28%, respectively. As discussed previously, the heat transfer coefficient can be based on either the measured centerline temperature (T_c) or on the predicted one (T_s). The heat transfer coefficient considerably decreases when T_s is used since T_s is always greater than T_c . The ratio of the heat transfer coefficients computed from these two methods shows that the increase in air mass fraction leads to larger deviation from the measured one calculated by T_c . The computer codes assume dry vapor in the core of the condenser tube so that care should be given in assessing the predicted results since this assumption may not reflect the physics inside the tube.

REFERENCES

- [1] TANRIKUT, A., In-tube Condensation in the Presence of Air, Ph.D. Thesis, Dept. of Mechanical Eng., Middle East Technical University, Ankara (1998).
- [2] RELAP5/MOD3 Code Manual, Code Structure, System Models and Solution Methods, Idaho National Engineering Laboratory, NUREG/CR-5535, Vol. 1, (1995).

NEXT PAGE(S)
left BLANK



EFFECTS OF NON-CONDENSIBLE GAS ON THE CONDENSATION OF STEAM

J.D. JACKSON, P. AN, A. REINERT, M. AHMADINEJAD

Nuclear Engineering Laboratories,
School of Engineering,
University of Manchester,
Manchester, United Kingdom

Abstract

The experimental work reported here was undertaken with the aim of extending the database currently available on the condensation of steam in the presence of non-condensable gases and thereby improving the empirical input to thermal-hydraulic codes which might be used for design and safety assessment of advanced water-cooled nuclear reactors. Heat was removed from flowing mixtures of steam and air in a test section by means of a water-cooled condensing plate. The test facility constructed for the study incorporates a degassing unit which supplies water to a boiler. This delivers steam steadily to a mixing chamber where it joins with a flow of preheated air. The mixture of steam and air is supplied to the bottom of a cylindrical test section in which it flows upwards over a double sided condensing plate which can be vertical, inclined or horizontal. The rate at which heat is removed by cooling water flowing through internal passages in the plate can be determined calorimetrically knowing the flow rate of the water and its temperature rise. After commissioning experiments had shown that reliable measurements of condensation heat transfer rate could be made using the test facility, a programme of development work followed in the course of which three different designs of condensing plate were evaluated in turn. The version eventually used in the main programme of experiments which followed was made from copper. However, its surfaces were coated with a thin layer of nickel and then with one of chromium. It was found that such a surface consistently promoted dropwise condensation and showed no signs of deterioration after lengthy periods of use. The rate of heat removal from pure steam and from mixtures of steam and air in varying proportions was measured as a function of plate sub-cooling for a variety of plate orientations.

1. Introduction

Passive decay heat removal systems will play an important part in the future in improving the safety of nuclear reactors of advanced design. Feasibility studies for nuclear reactors utilising such concepts have highlighted the need to improve our understanding of a number of aspects of heat transfer and thermal hydraulics. The influence of non-condensable gas on steam condensation is one of the topics on which further research is needed.

The inhibiting effect of non-condensable gas on the condensation of steam has long been recognised (see Ref. [1]) and much has been written on this topic. Some relevant papers on the influence of gas on the condensation of steam on plane surfaces are listed at the end of this paper (Refs. [2] to [23]). However, it is clear that there is a need for further basic experimental data. The present study was initiated to extend the existing database.

Work began on the project in 1996 with the design and construction of a test facility. That task was completed by the end of 1996. Calibration of the instrumentation and the commissioning of the test facility began in 1997 and by the middle of that year some preliminary experiments had been carried out. Photographs of the test facility at that stage of the project are shown on Plates 1 and 2. In the light of the experience obtained in the course of those experiments some modifications were made to the test facility and condensing plates of improved design were developed. A detailed programme of experiments was then carried out.

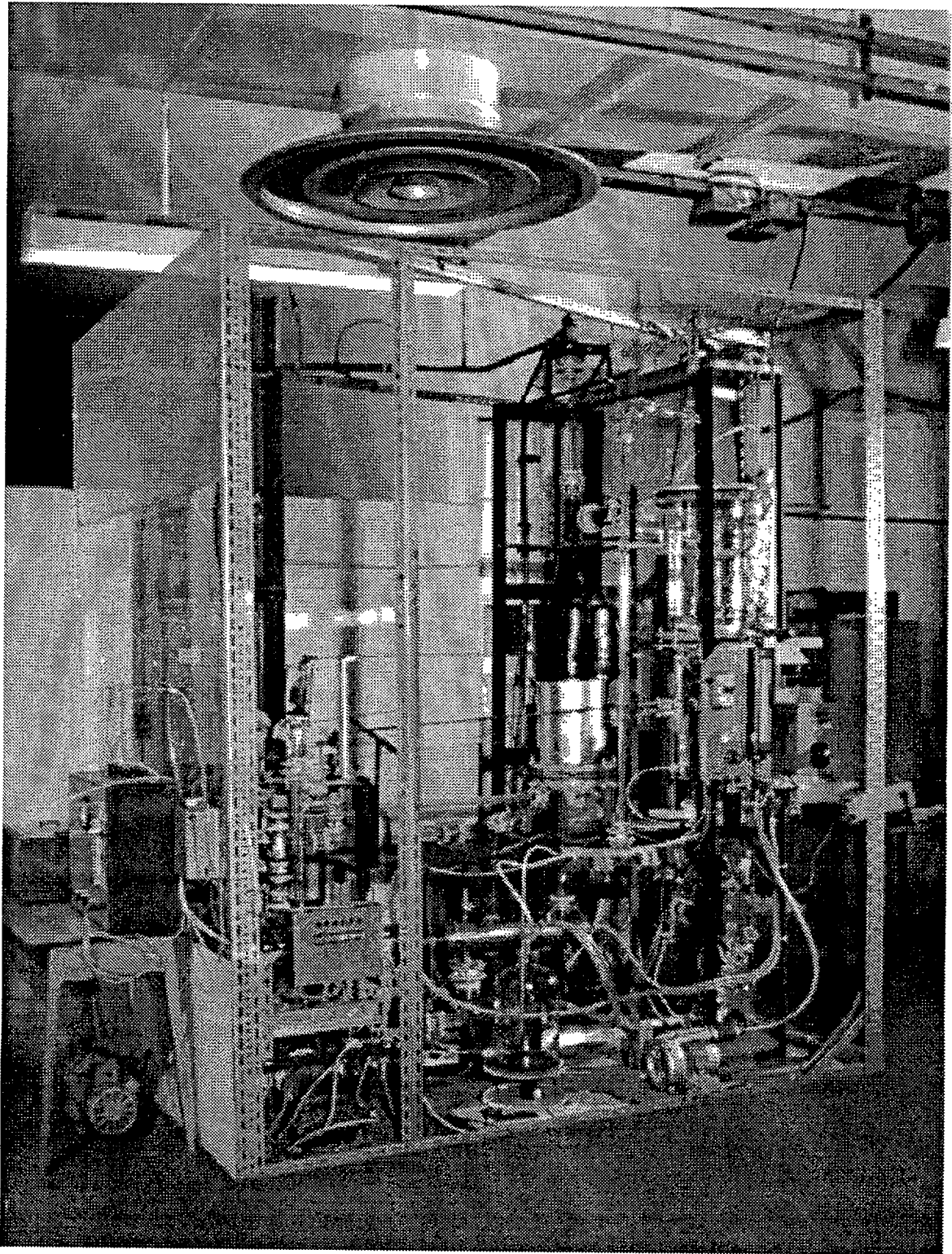


Plate 1

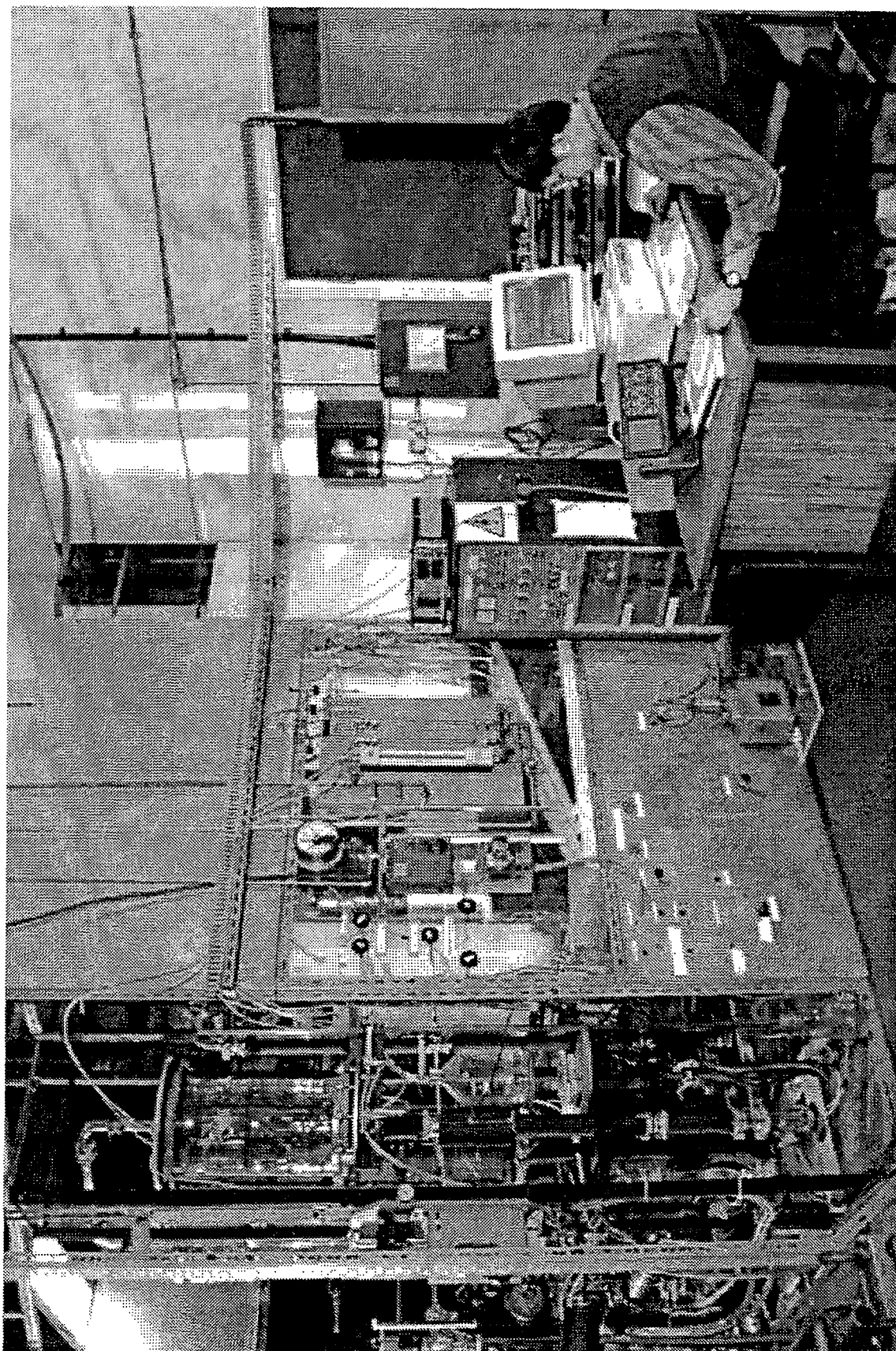


Plate 2

2. Description of the test facility

2.1. General description

Figure 1 shows a schematic diagram of the test facility. The degassing system is used to provide a supply of water for use in the steam boiler. The boiler generates steam steadily at a rate which is controlled by the power input to the electrical immersion heaters. On leaving the boiler and passing through a separator section, the steam flows into the mixing chamber where it joins a flow of air which has been preheated so as to cause the vapour in the resulting mixture entering the test section to be in the dry saturated condition. The test section is a cylindrical vessel with a water-cooled condensing plate suspended within it. The mixture of air and steam leaving the test section passes to a shell and tube heat exchanger where the residual steam is fully condensed. Condensate collected from the test section, the shell and tube heat exchanger and the separator is returned to the water degassing system.

2.2. Degassing system

The degassing system consists of a cylindrical packed bed column, a vacuum pump, a circulating pump, associated pipelines and an oxygen content analyser. The column is made of pyrex glass, as also are the various pipelines. It contains many small stainless steel rings stacked in the form of a bed of height 1.5 m and diameter 0.23 m. Water delivered by the circulating pump is sprayed onto the bed of rings from a distributor at the top. Mounted vertically above the degassing column is a condenser which is supplied with cooling water from a chiller unit. The top of the condenser is connected to a vacuum pump. The degassing system is able to reduce the oxygen concentration in the water to a fraction of a milligram of oxygen per kilogram of water. Sampled water can be passed to an oxygen content analyser (type Kent EIL-9435) for the purpose of checking the amount of oxygen in it.

2.3. Steam supply system

The boiler shell, which is also made of pyrex glass, is a cylindrical vessel of diameter 0.3 m and height 1.4 m having a domed top. It contains four electrical immersion heaters, each rated at 9 kW, which are mounted vertically within it on a stainless steel base. The power supplied to these heaters can be controlled independently. The electrical system is equipped with safety overload and over-temperature protection circuits. An over-pressure safety valve set at a gauge pressure of 0.2 bar is fitted to the top of the boiler. Degassed water can be supplied to the boiler, as needed, via a feed line made of pyrex glass. The boiler is instrumented so that the steam delivery temperature and pressure can be measured. Under conditions of maximum power input, water is evaporated in the boiler at a rate of about 0.015 kg/s. Steam produced by the boiler passes through a thermally insulated U shaped section which acts as a separator. Water collects at the bottom of the downward leg from where it drains to a sump. The steam passes upwards from the separator to the steam/air mixing chamber.

2.4. Air supply system and steam/air mixing chamber

Air drawn from the laboratory by a small centrifugal blower passes through a filter and an electrical preheater. The flow rate can be adjusted manually using a control valve. It is measured using a rotameter. Dry steam from the boiler and hot air from the preheater flow into a pyrex glass tube containing number of horizontal perforated plates which serves as a mixing chamber.

2.5. Test section

Figure 2 shows a schematic of the test section, which is of diameter 0.3 m and height 0.6 m and is also made of pyrex glass. Within it a water-cooled condensing plate is suspended from the top by an arrangement which allows the plate orientation to be varied. Figure 3 shows the cooling water system for the condensing plate.

The steam/air mixture enters the test section through the base and flows upwards over the condensing plate. On the base there are two condensate collectors. The outside one collects any

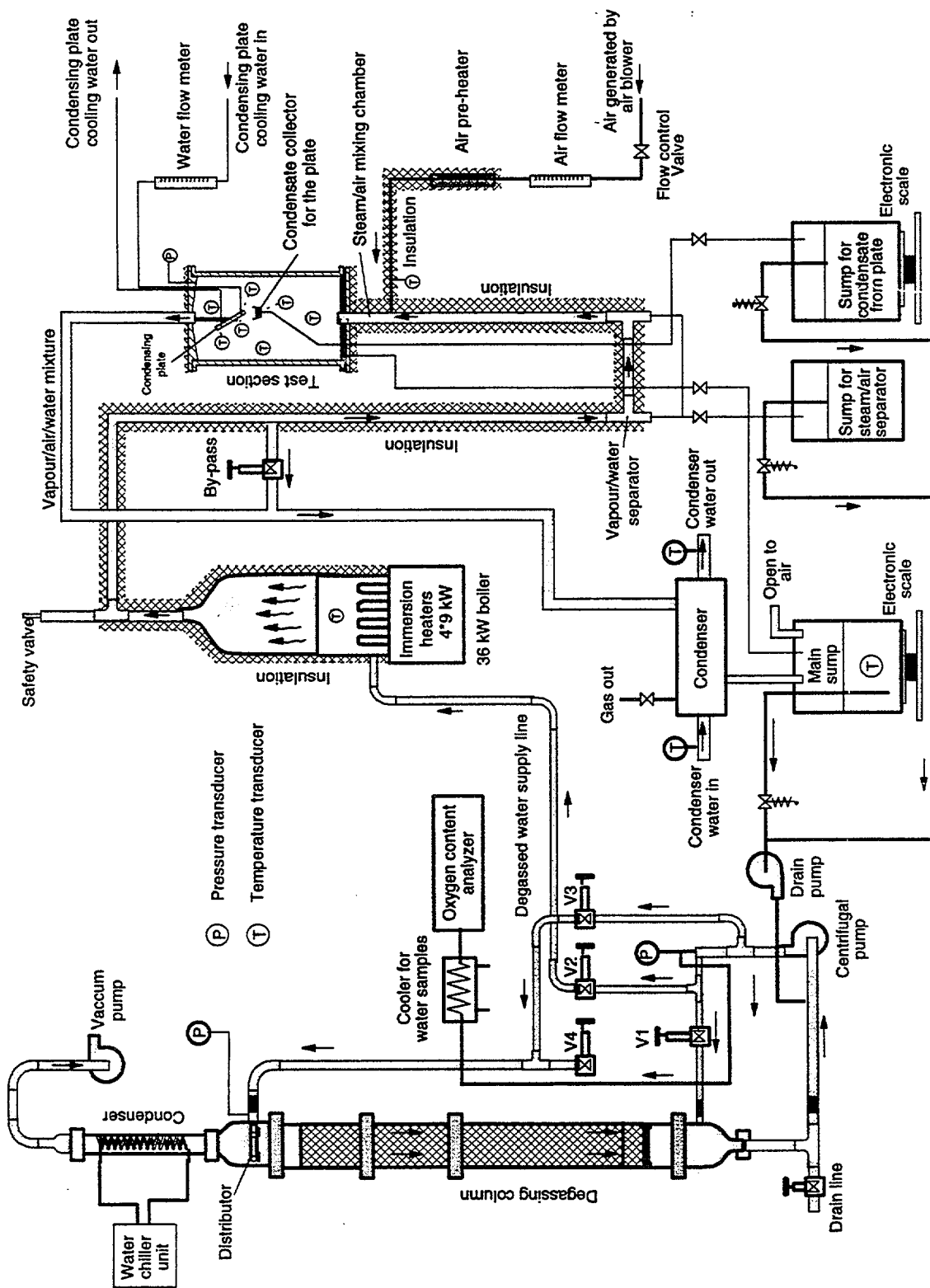


Figure 1: The test facility

The diagram illustrates a closed-loop water cooling system. The main loop consists of a high-pressure pump at the top right, connected to a water tank. From the water tank, the flow goes through a heat exchanger (indicated by a zigzag line) and then through a control valve. The water then enters a test section (a rectangular box with a diagonal line inside). After exiting the test section, the water passes through a flow cell (a circle with a dot) and a rotameter (a vertical tube with horizontal markings). The flow then goes through another control valve and back to the high-pressure pump. A bypass line with a control valve connects the water tank directly to the test section. An air-cooled radiator is connected to the bottom of the test section and the water tank, with arrows indicating air flow. Labels include: Controlled flow rate, temperature; Flow cell; Rotameter; Control valve; High pressure pump; Water tank; Heat exchanger; Bypass line; Test section; Air cooled radiator; Control valves; Water to and from laboratory cooling water system.

Figure 3: Condensing plate cooling system

condensate which is formed on the test section wall. This is minimal because the heat loss to the surroundings is small. The central collector catches condensate which falls from the condensing plate. This drains to a sump. The rate at which condensate is produced can be determined from measurements of the weight of the sump and contents. These are made using an electronic scale. The mixture of residual vapour and air leaves the test section at the top and is ducted through pyrex glass tubing to a water-cooled shell and tube heat exchanger in which the steam is completely condensed.

2.6. Condensing plates

Three different designs of condensing plate have been used in the course of this study. The initial one (see Figure 4) was manufactured from aluminium. When, after some time, it was found that the surface condition was showing signs of deteriorating the aluminium plate was replaced by one made of copper with nickel coated surfaces (see Figure 5). The internal passages for cooling water were modified so as to reduce flow resistance and improve the uniformity of cooling. In the course of further tests the surface condition of this plate was also found to be deteriorating. A third type of plate, was designed and manufactured (see Figure 6). The material was again copper but this time the surfaces were first coated with a thin layer of nickel and then with one of chromium. Also, a novel arrangement of internal passages was used with a view to achieving improved cooling. Commissioning tests showed this plate to have a stable surface condition and also to be satisfactory from the point of view of uniformity of temperature.

2.7. Cooling water system

In the case of the tests performed using the initial plate, the cooling water was taken directly from the laboratory cooling water system. The sub-cooling of the plate was varied by adjusting the water flow rate. This arrangement was later replaced by another one (see Figure 3, earlier) which enabled the sub-cooling to be controlled by varying water flow rate and water temperature independently. The various condensing plates were each instrumented to enable the temperature rise of the cooling water flowing through them to be measured using thermocouples situated at entry and exit. Thus, knowing the cooling water flow rate and its temperature rise the rate of heat transfer could be determined.

2.8. Shell and tube heat exchanger

The residual vapour in the mixture of steam and air leaving the test section is completely condensed in a water-cooled shell and tube heat exchanger made of stainless steel. The condensate produced passes to a sump. When the contents exceed a certain value, a pump and magnetic valve is activated causing the water in it to be returned to the degassing column.

2.9. Measurements

The measurements made are listed below:

- Rate of flow of condensate from the shell and tube condenser to the main sump. This is measured using a load cell in conjunction with the data acquisition system.
- Rate at which condensate is produced on a condensing plate. This is also measured using a load cell in conjunction with the data acquisition system.
- Rate of flow of cooling water through the condensing plate. This is measured using a rotameter and a flow turbine.
- Pressures in the steam delivery line and the test section. These are measured using pressure gauges.
- Temperature of the condensing plate. This is measured using several calibrated K-type thermocouples.
- Temperatures of the steam/air mixture flowing into and out of the test section. These are measured using two calibrated K-type thermocouples.

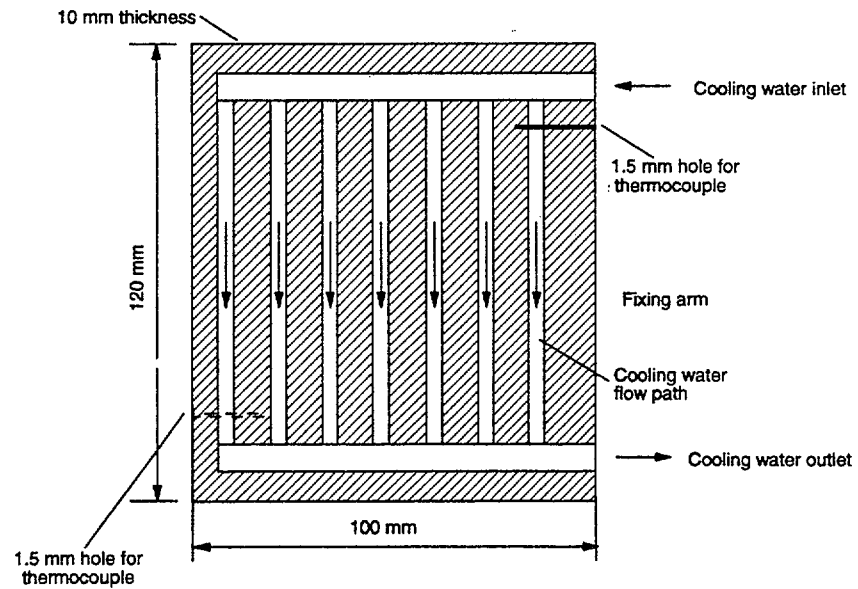


Figure 4: Initial condensing plate

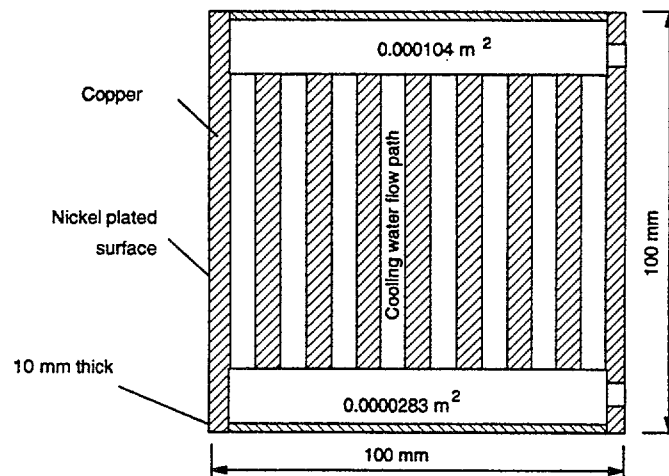


Figure 5: Second condensing plate

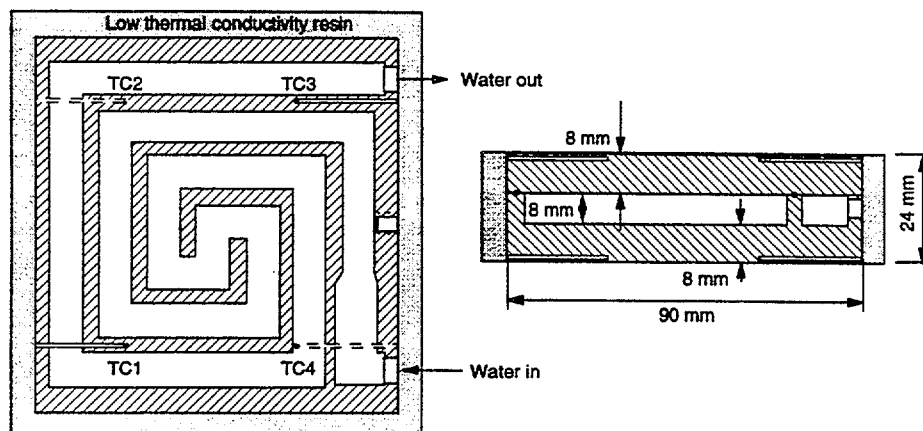


Figure 6: Final condensing plate

- Temperature of condensate leaving the test section. This is measured using a calibrated K-type thermocouple situated in the condensate collector.
- Rate of flow of air injected into the steam. This is measured using a rotameter and a flow cell.
- Temperature of the air injected into the steam. This is measured using a calibrated K-type thermocouple situated near the air injection nozzle.
- Temperatures of the cooling water at inlet to and outlet from the condensing plate. These are measured using two calibrated K-type thermocouples mounted in the flow passages at inlet and outlet.
- Electrical power supplied to the boiler immersion heaters. This is determined from measurements of current and voltage.

2.10. Data acquisition system

A computer-based system consisting of a 16 channel scanner, a precision digital voltmeter and an IBM compatible PC is used for signal monitoring and data acquisition. It takes the signals from the test facility, stores them, and displays updated information on a monitor.

3. Commissioning of the Test Facility

3.1. Commissioning tests

In the course of commissioning the test facility, checks were carried out to ensure that all the measurement devices were functioning properly and to assess the accuracy with which the measurements could be made using them. A number of calibration tests were performed. Particular care was taken in the case of temperature measurement. All the thermocouples on the test facility were calibrated against a standard platinum resistance thermometer.

The test facility was first brought into service with the aluminium condensing plate installed in the test section. It was initially operated with a fixed electrical power input to the boiler supplying steam steadily at atmospheric pressure to the test section without air injection. Condensate from the condensing plate was collected in the test section and from the sump of the shell and tube heat exchanger which condenses the residual steam leaving the test section. No water was supplied to the boiler whilst this test was in progress. The whole procedure was repeated for a number of values of electrical power input to the boiler covering the full working range. These measurements enabled the total rate of heat removal from the condensing plate and the heat exchanger to be determined for each value of power input to the boiler. By subtracting this from the electrical power input to the boiler, the heat loss from the test facility to the surroundings was found. This turned out to be quite small (about 1 kW) and did not vary much from test to test because the temperature of the boiler and test section did not change. These tests demonstrated that the rate of production of steam in the boiler could be readily determined from a knowledge of the electrical power input to the boiler by simply subtracting the estimated rate of heat loss from it and assuming that the remainder was used to evaporate water in the boiler.

Next, experiments were performed to study the accuracy with which condensation heat transfer could be determined. Measurements of the rate at which condensate was collected from the condensing plate enabled a check to be made on the accuracy of the calorimetric method of determining heat removal from the plate. Figure 7 shows a comparison of the rates of heat transfer determined by the two different methods. It can be seen that they are in very good agreement with each other.

4. Preliminary Experiments Using the Initial Condensing Plate

4.1. Condensation heat transfer measurements with pure steam

(i) Effects of varying the steam flow rate and the plate orientation

Initially experiments were performed with the plate vertical supplying pure steam at atmospheric pressure to the test section at 3.5 g/s by applying a power of 9 kW to the immersion heaters in the

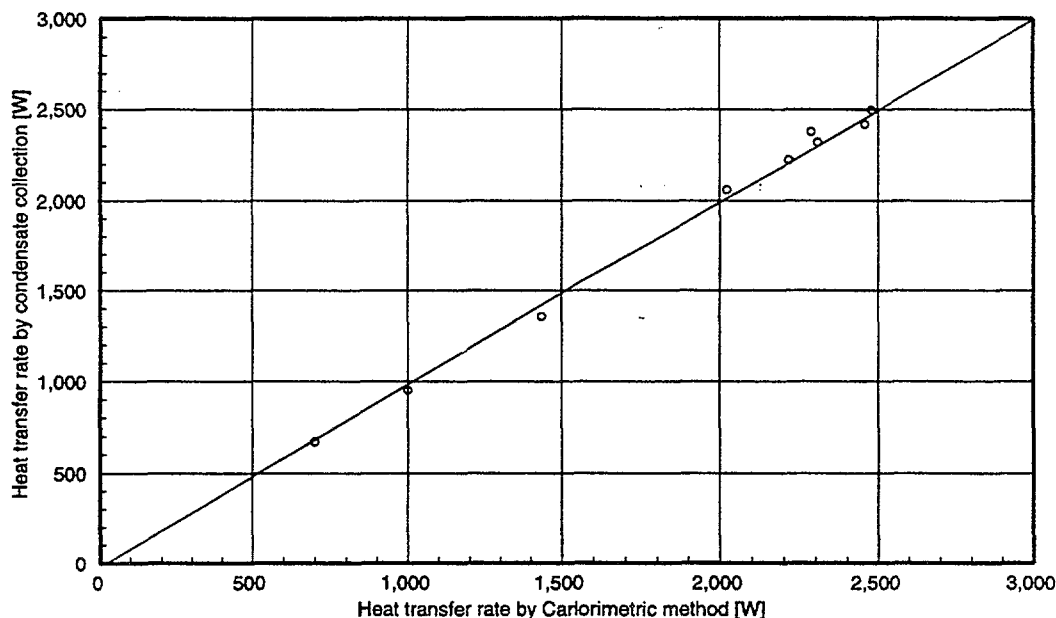


Figure 7: Comparison of heat transfer rate measured by the calorimetric and the direct condensate collection methods with initial plate

boiler. The subcooling of the plate was varied by adjusting the flow rate of cooling water passing through it. Figure 8 shows the results. Further experiments were then performed with the power input to the boiler increased to 18 kW, giving a steam flow rate of 7.2 g/s. Next, similar experiments were carried out with the plate inclined at 45° and then, finally, with the plate in the horizontal position. Figure 9 shows the results obtained for all three cases. It can be seen that there is a clear difference between the rate of heat transfer for the three different orientations of the plate. As might have been anticipated, the rate of heat transfer is highest for the vertical case, slightly reduced for the inclined case and very much reduced for the horizontal case. Some effect of varying the steam flow rate can be seen, but this is small.

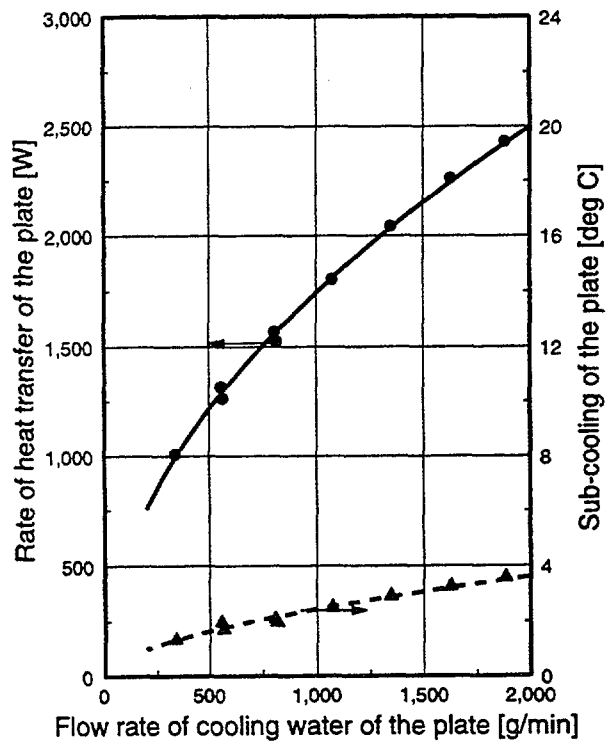
(ii) Effect of reducing the steam pressure

Experiments to study the effect of reducing the steam pressure were performed next. Measurements were made at pressures of 0.75 bar and 0.60 bar. The results are shown on Figure 10 where it can be seen that there was a systematic reduction of rate of heat transfer as the steam pressure was reduced.

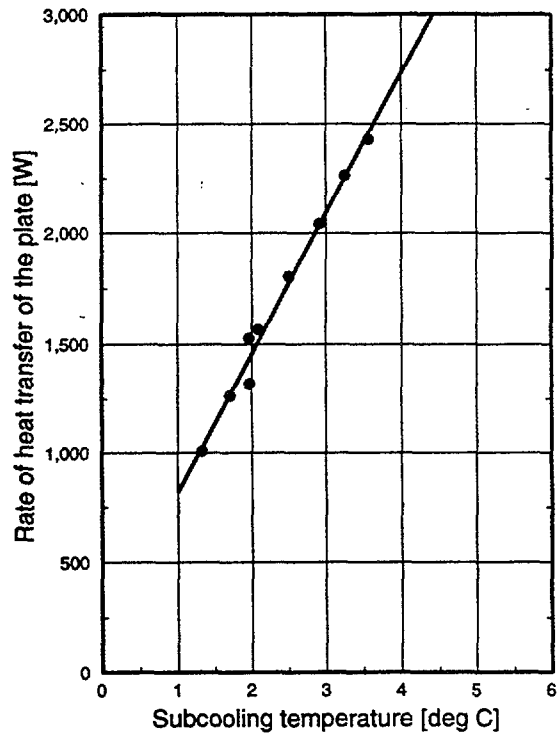
Some limitations of the initial condensing plate design became apparent in the course of these tests. Only a very limited range of subcooling could be covered and it was clear, therefore, that larger cooling passages were needed. A further cause for concern was the fact that the two thermocouples on the plate gave readings which differed significantly. However, in spite of these limitations, it was decided to continue to use this condensing plate for further commissioning tests.

4.2 Measurements with mixtures of air and steam

Experiments were performed next supplying mixtures of air and steam at atmospheric pressure to the test section. Results were obtained for the vertical, inclined and horizontal cases with values of air flow rate of 0.5 g/s, 1.0 g/s and 1.5 g/s and steam flow rates of 3.5 g/s and 7.2 g/s. They are shown on Figures 11 and 12, where it can be seen that for each inclination there is a strong and systematic reduction of heat transfer with increase of air concentration. These experiments demonstrated that the air supply system was functioning satisfactorily and that the test facility was capable of yielding useful information. However, they highlighted the limitations of the arrangement for cooling the condensing plate referred to earlier. Also, visible stains became apparent on the condensing plate indicating that its surface condition was changing. This gave rise to concern about the repeatability of the results which could be obtained using this plate.



(a) Rate of heat transfer and subcooling



(b) Rate of heat transfer vs. subcooling

Figure 8: A typical result for initial plate in vertical position with power input to boiler 9 kW (vapour flow rate: 3.5 g/s)

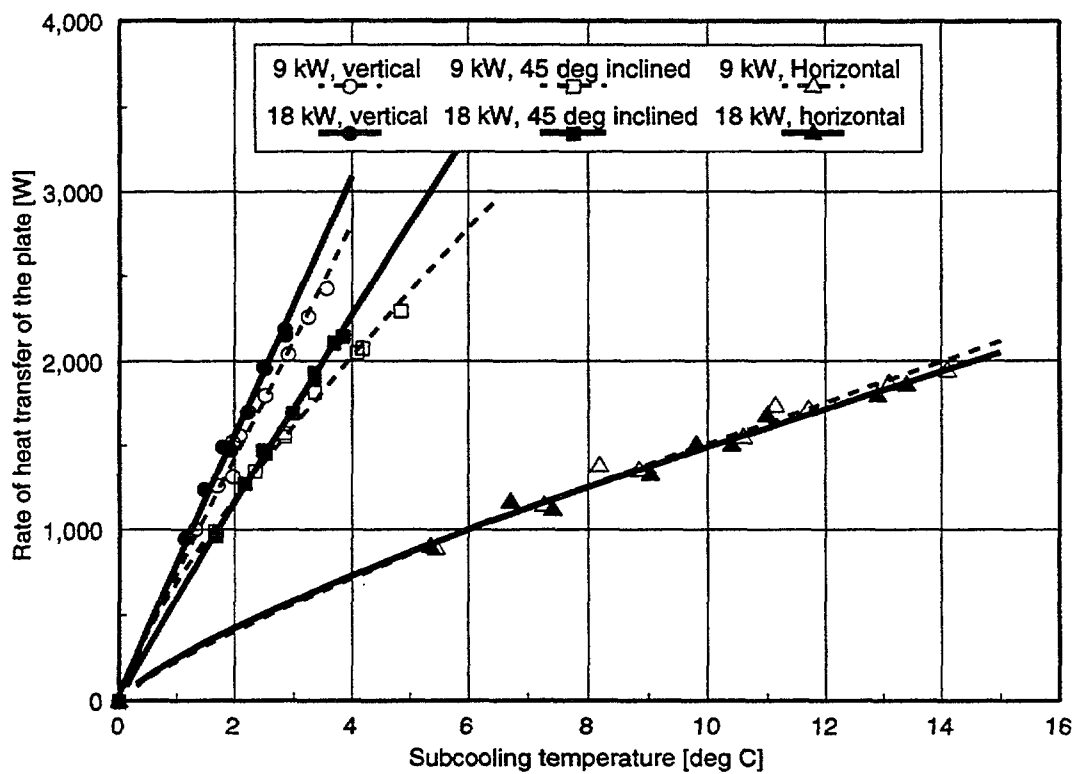


Figure 9: Effect of plate inclination on rate of heat transfer

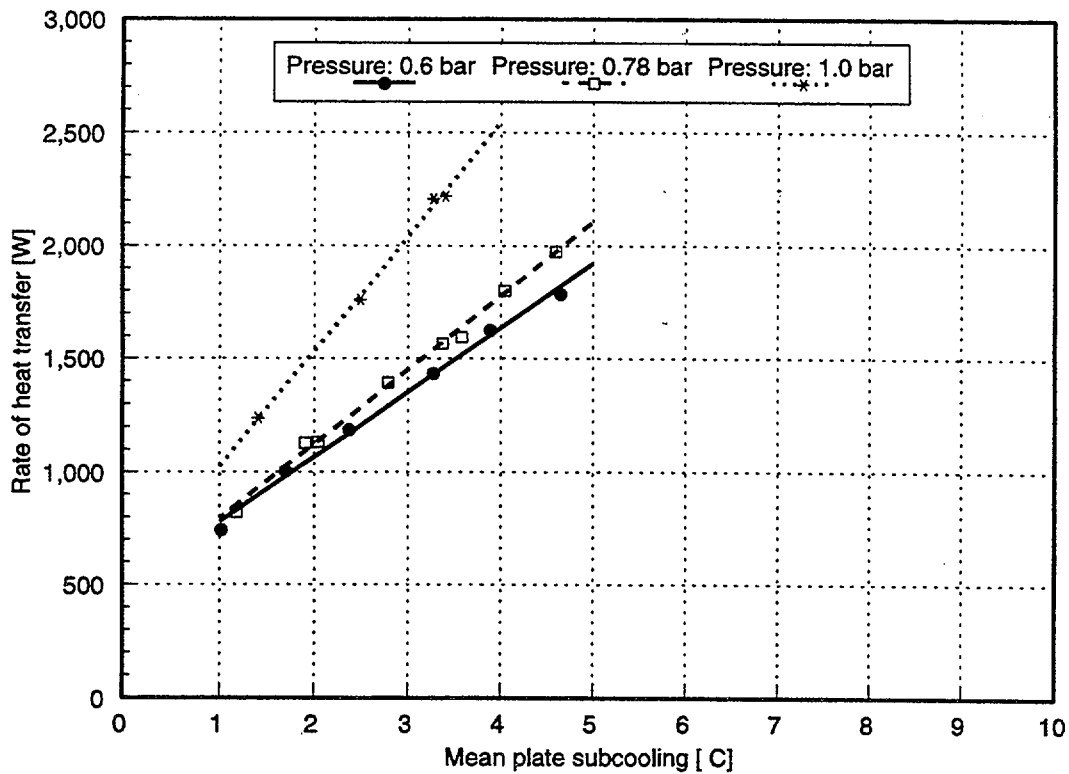


Figure 10: Effect of steam pressure on rate of heat transfer (vertical plate, power input to boiler: 9 kW, steam flow rate 3.5 g/s)

5. Development of an Improved Condensing Plate

As a result of the experience gained with the initial condensing plate, it was decided to manufacture a new one using copper rather than aluminium. Four thermocouples were embedded within it to measure the surface temperature and the arrangement of internal cooling passages was changed to reduce the flow resistance. The outside of the plate was coated with nickel with a view to improving the stability of its surface condition. In addition, a new cooling system was installed on the test facility which enabled the temperature of the cooling water to be controlled. Once this was done the test facility was brought into service again. Figure 13 shows the results of commissioning experiments to check the accuracy of heat transfer measurement using the new plate and the new cooling system.

A lengthy programme of experiments followed, firstly supplying pure steam and then mixtures of steam and air. Some typical results (obtained with plate inclined at 45°) are shown on Figure 14. It was found that a much greater range of subcooling could be covered. However, the plate temperature did not prove to be as uniform as expected. Furthermore, after quite a number of tests had been completed there was again evidence of discolouration of the plate and lack of repeatability of results due to deterioration of surface condition.

An interesting feature of the results obtained is that with pure steam supplied to the test section the rate of heat transfer increases very rapidly as the subcooling is increased up to about ten degrees after which it suddenly stops changing. A further feature is the very large reduction of heat transfer caused by injecting small amount of air into the steam. It became obvious that more sensitive control over air injection was needed.

After careful analysis of the plate-cooling problem, a new condensing plate having a very different arrangement of internal cooling passages was designed, manufactured and installed in the test section (see Figure 6, earlier). It was manufactured in two halves using copper. These were brased together in a furnace after the grooves for the cooling passages had been machined on them. To address the problem of obtaining a stable surface condition the condensing surfaces were firstly coated with a thin layer of nickel and then with one of chromium. The air injection arrangements were

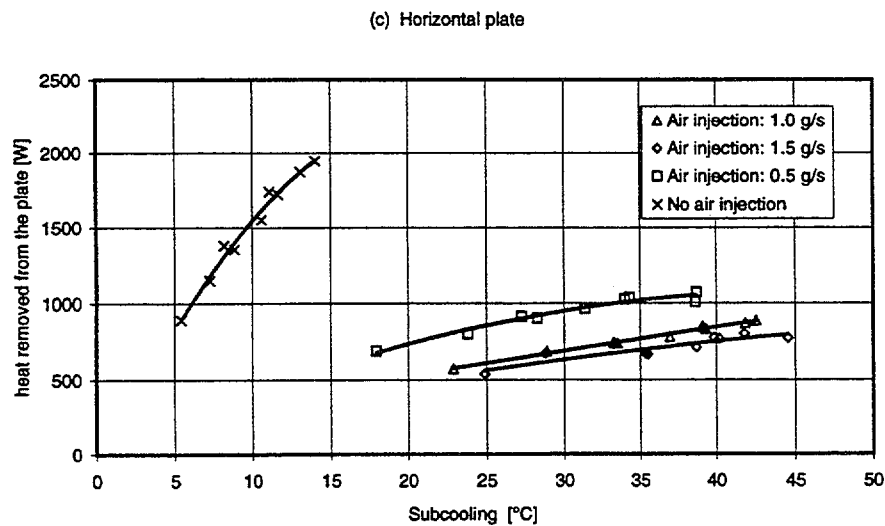
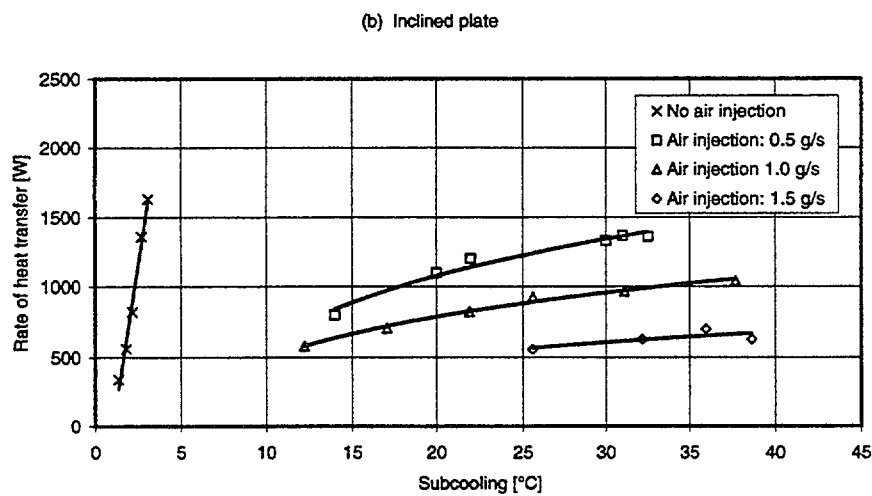
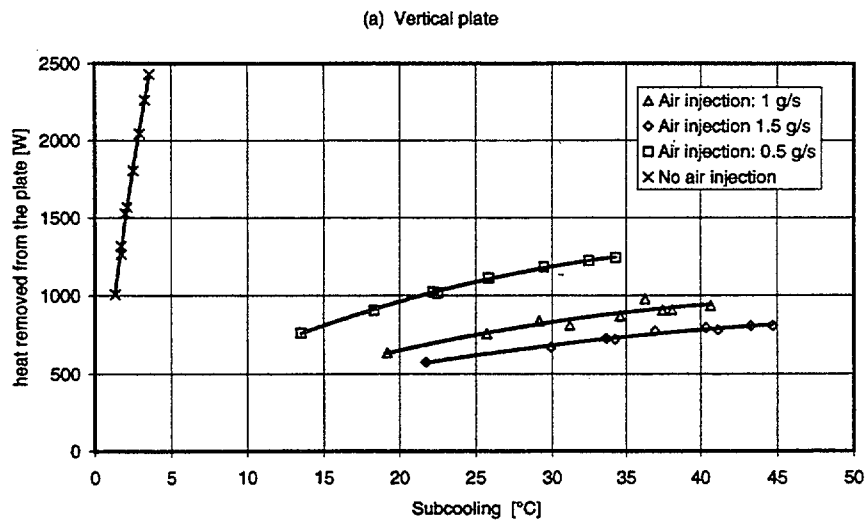
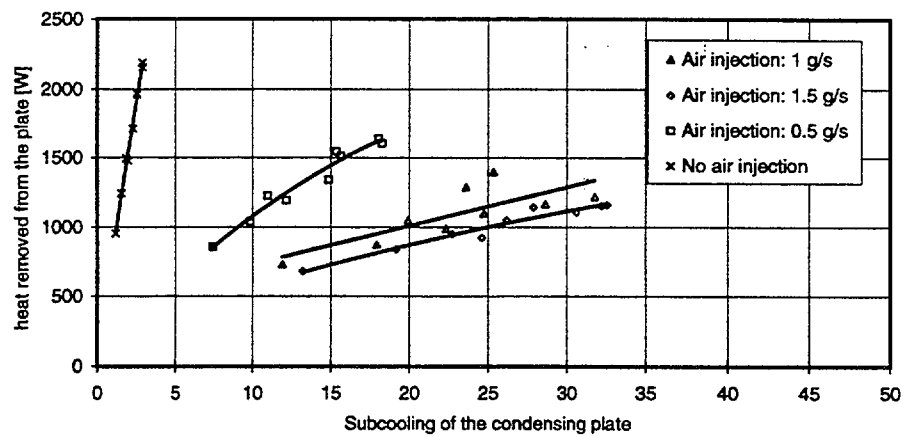
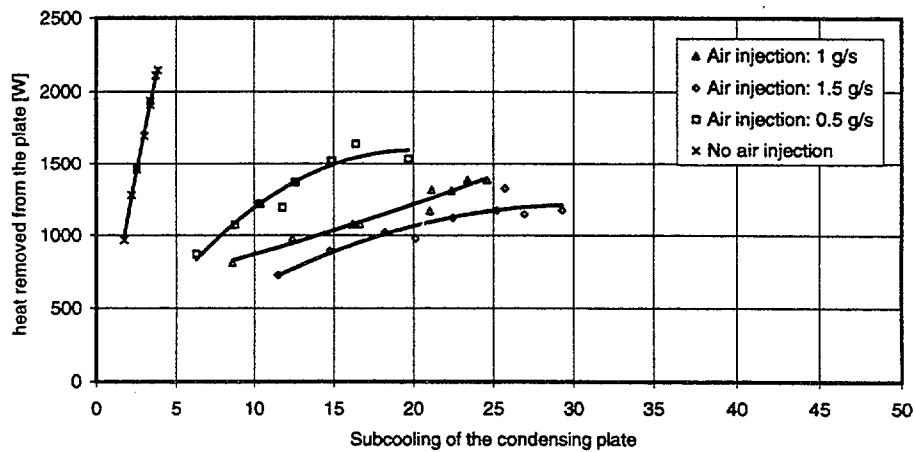


Figure 11: Effect of air injection on rate of heat transfer (Power input to boiler: 9kW, Vapour flow rate: 3.5 g/s)

(a) Vertical plate



(b) Inclined plate



(c) Horizontal plate

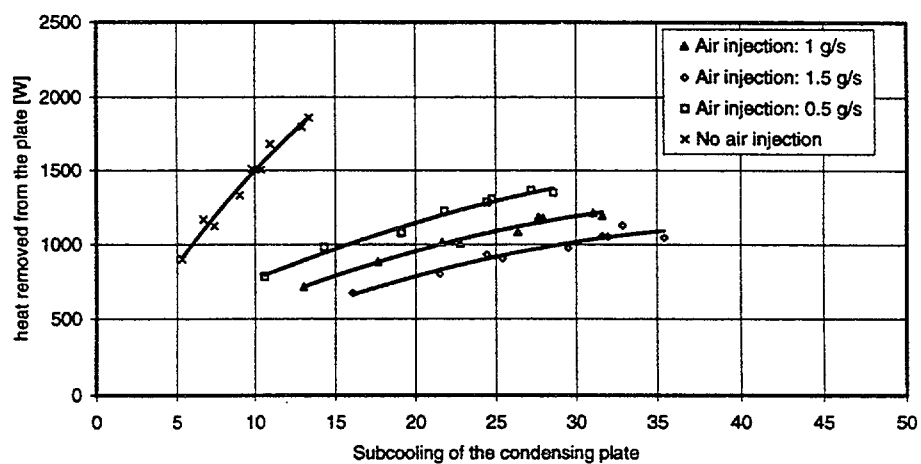


Figure 12: Effect of air injection on rate of heat transfer (Power input to boiler: 18kW, Vapour flow rate: 7.4 g/s)

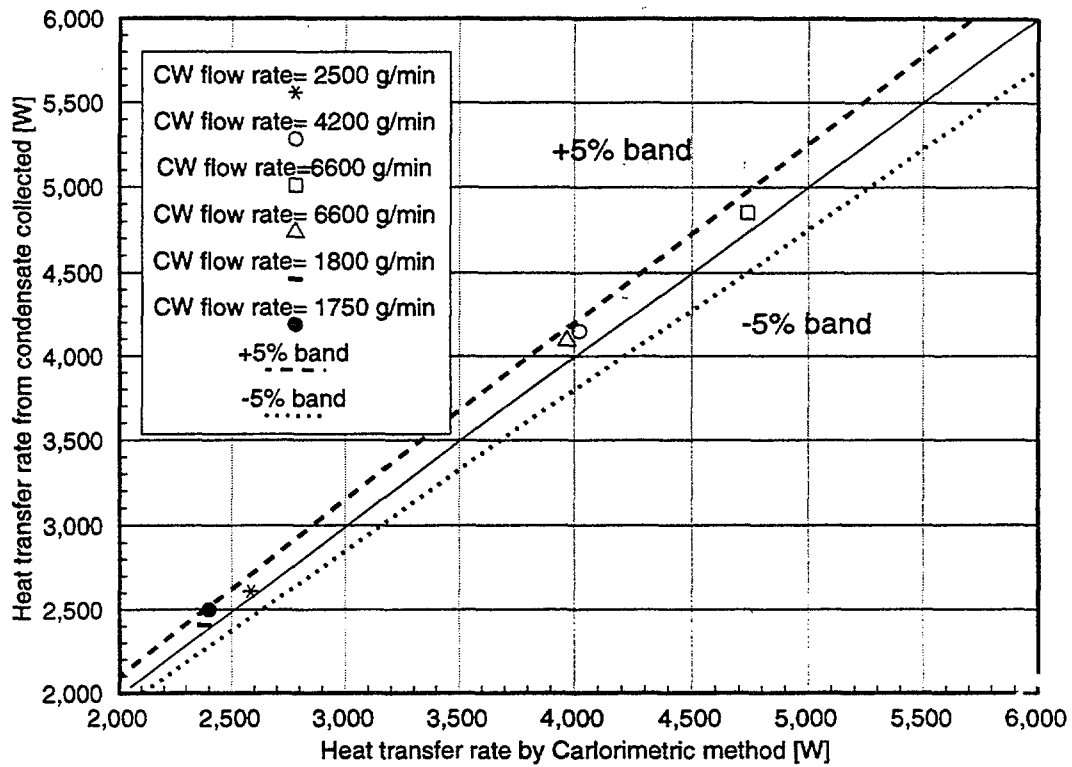


Figure 13: Comparison of heat transfer measured by the carlorimetric and the direct condensation collection method

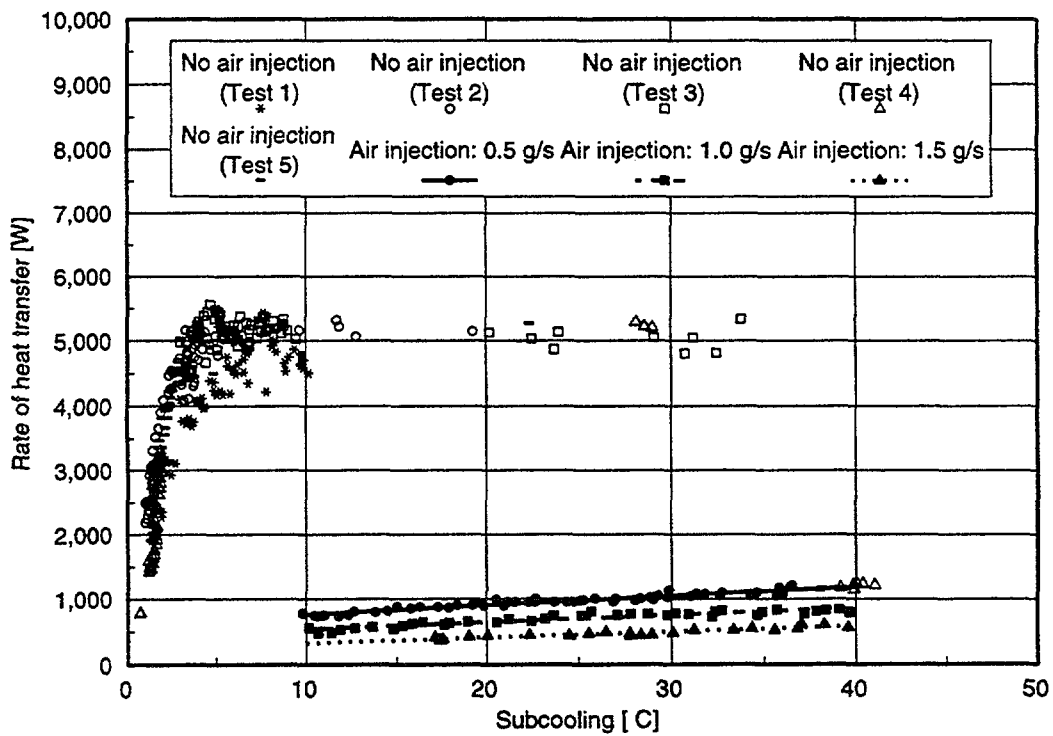


Figure 14: Rate of heat transfer for inclined condensing plate with and without air injection (Vapour flow rate: 3.5 g/s)

modified to enable greater control to be exercised at low flow rates. Commissioning tests were then carried out to study the effects of these changes. These experiments showed that the uniformity of temperature was significantly improved with this plate and that accurate and repeatable heat transfer results could be obtained. The mode of condensation promoted on the surfaces was dropwise and there was no evidence of any deterioration of surface condition after a lengthy period of use. In the following section of this report a series of investigations of condensation heat transfer made using this plate are reported.

6. Main Programme of Experimental Work

6.1. Experiments promoting condensation on both surfaces

In the first investigation, experiments were performed promoting condensation on both surfaces of the plate. Measurements were made using pure steam and also mixtures of steam and air. Power inputs of 9 kW, 18 kW, and 27 kW were supplied to the boiler, giving steam flow rates \dot{m}_s of 3.5 g/s, 7.4 g/s and 11.4 g/s. Air was injected into the steam at rates in the range 0.02 g/s to 1.0 g/s. Results were obtained for three different orientations of the plate, vertical, inclined at 45° and horizontal. The results are presented on Figures 15, 17 and 19, respectively, as rate of heat transfer \dot{Q} versus subcooling ΔT for a number of values of air injection rate \dot{m}_a . On these figures, the curves for condensation with mixtures of steam and air were produced using an equation of the form $\dot{Q} = C\Delta T^p \dot{m}_a^q$, with values of the coefficient C and the indices p and q chosen to give the best fit to the experimental data for each steam flow rate \dot{m}_s and plate orientation. Comparisons between the experimental and curve-fitted values of \dot{Q} for the three different orientations are shown on Figures 16, 18 and 20, respectively, along with the corresponding equations. It can be seen that in general the fit to the data is good.

With the plate vertical or inclined at 45° droplets of condensate formed very rapidly at many points on the surfaces and coalesced to form rivulets. These ran off the plate leaving the surface clear so that further dropwise condensation could occur. The process was repeated continuously all over the surface in a very dynamic manner. When pure steam was supplied to the test section the rate of heat transfer increased steadily with increase of subcooling and then remained constant beyond a certain value because it was no longer possible for additional steam to reach the condensing plate.

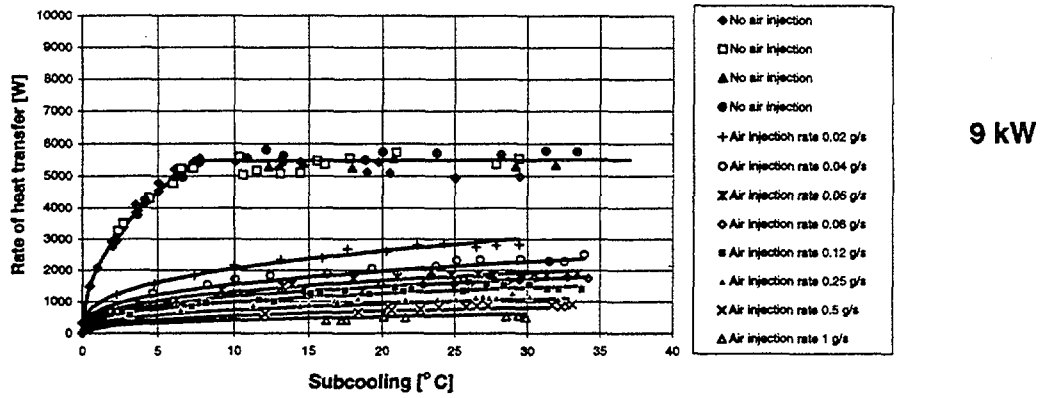
When mixtures of steam and air were supplied to the test section, the presence of a very small amount of air inhibited the heat transfer process markedly. The rate of heat transfer continued to fall as the concentration of air was raised, but less and less strongly. The limit on heat transfer found with pure steam as subcooling was increased was not reached in the experiments with air present in the steam.

A good overall description of the results shown on Figures 15 and 17 from the experiments with mixtures of steam and air for the vertical and inclined cases is given by the equation.

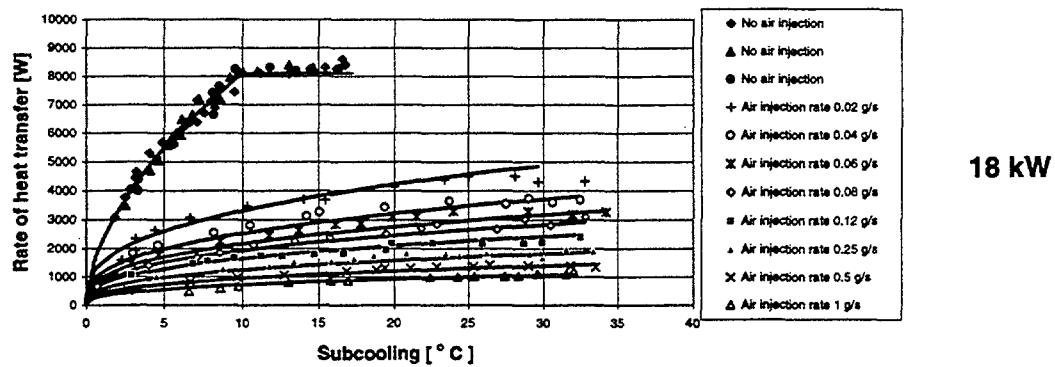
$$\dot{Q} = C\Delta T^{0.36} \dot{m}_a^{-0.38} \dot{m}_s^{0.85}, \quad (1)$$

with the coefficient C taking the value 63.7 for the vertical plate and 60.1 for the inclined one. Comparing these values it can be seen that the total rate of heat transfer with the plate inclined is only slightly lower than with it vertical. The dependence of rate of heat transfer on air injection rate is very similar for these two orientations (\dot{Q} varying with \dot{m}_a in a rather non-linear manner). The same can be said of the variation with steam flow rate (this time with \dot{Q} increasing almost in proportion to \dot{m}_s). A measure of the effectiveness of heat transfer is provided by the ratio $\dot{Q}/\Delta T$ and, it can be seen from Equation 1 that this falls with increase of subcooling as $\Delta T^{-0.64}$.

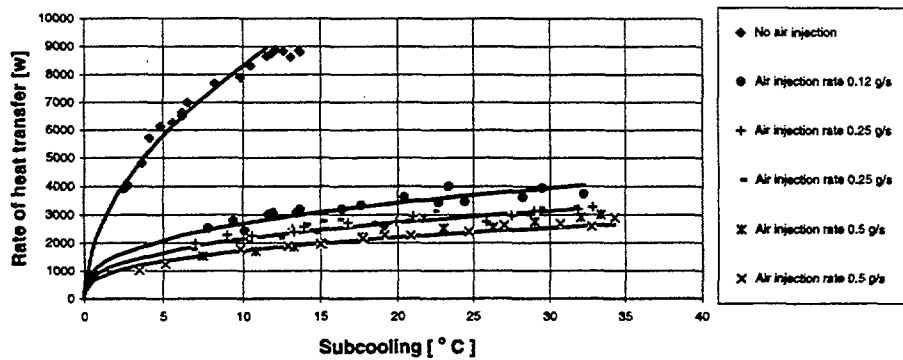
With the plate horizontal, condensate was not able to leave the plate so readily and parts of the upper and lower surfaces were covered with liquid for a significant proportion of the time. Whereas the rates of heat removal for the inclined case were only slightly smaller than for the vertical case they were much lower when the plate was horizontal. For this orientation, the trends with increase of steam flow rate and air injection rate were not completely systematic.



a) Vapour flow rate = 3.5 g/s

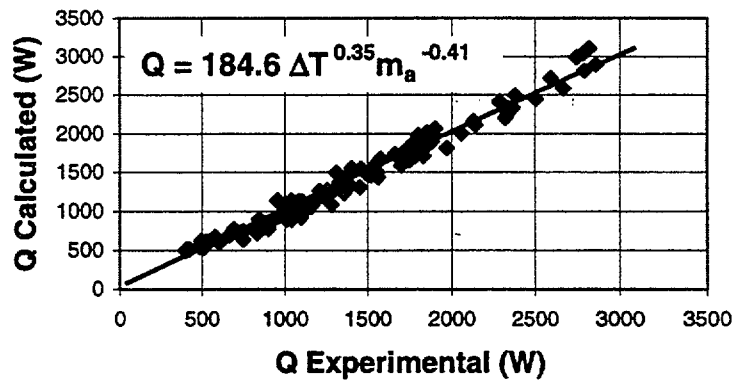


b) Vapour flow rate = 7.4 g/s

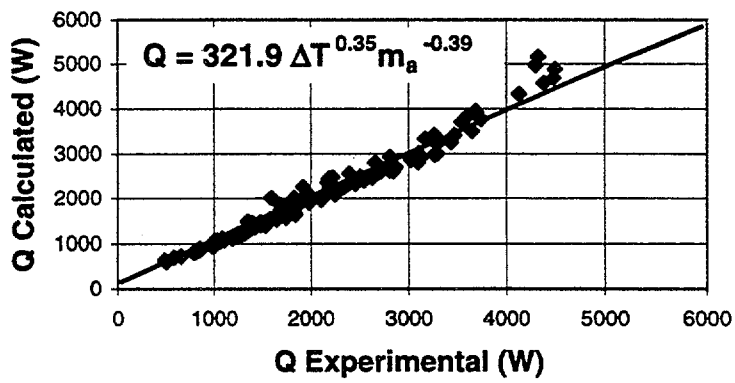


c) Vapour flow rate = 11.4 g/s

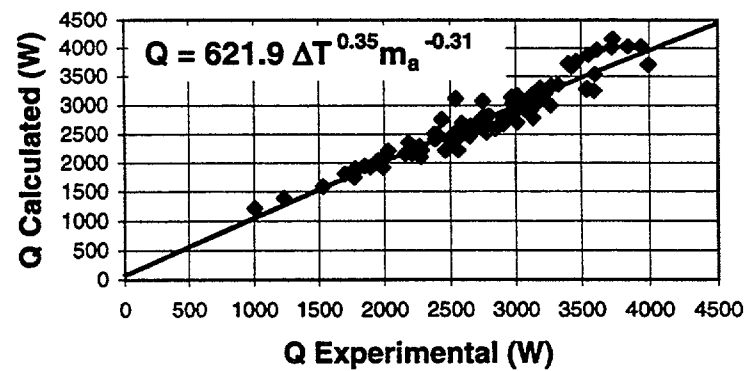
Figure 15: Effect of subcooling, air injection rate and vapour flow rate on rate of heat transfer for the double-sided vertical case with the final plate.



a) Vapour flow rate=3.5 g/s

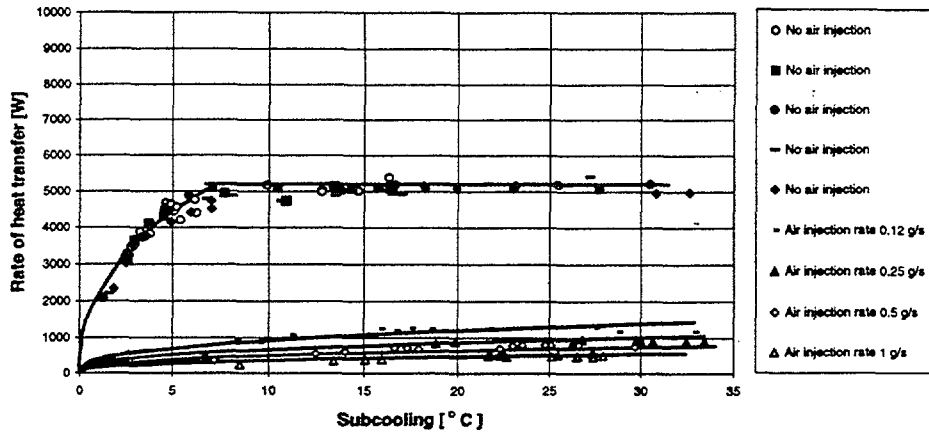


b) Vapour flow rate=7.4 g/s

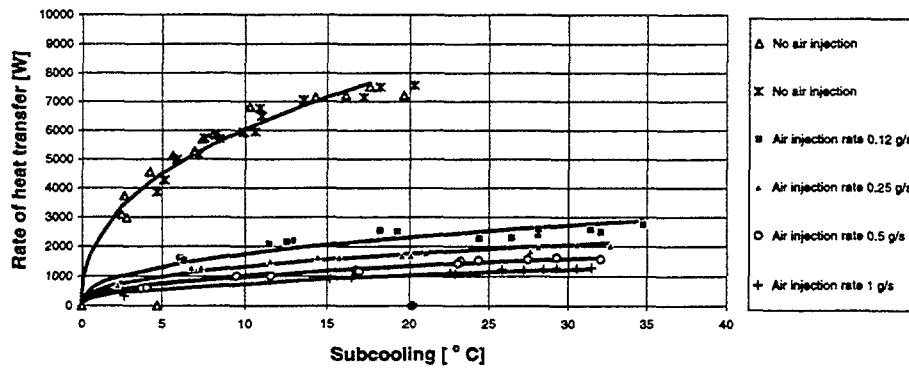


c) Vapour flow rate=11.4 g/s

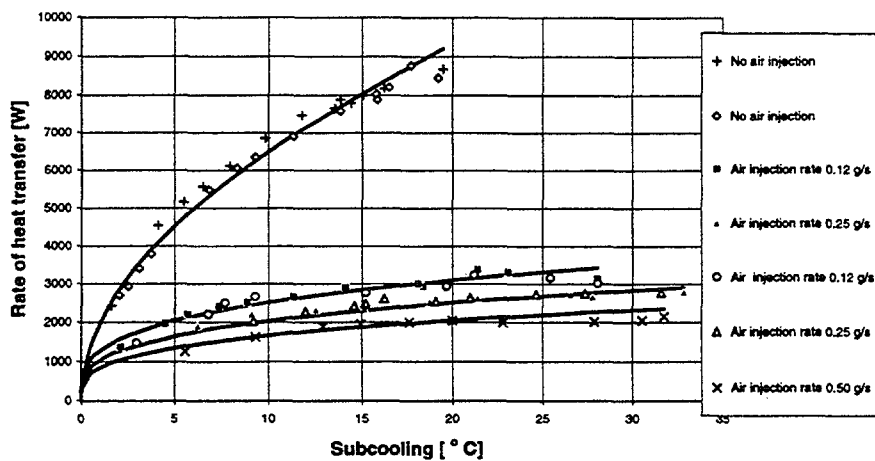
Figure 16: Comparision of experimental and curve-fitted values of heat transfer



a) Vapour flow rate = 3.5 g/s

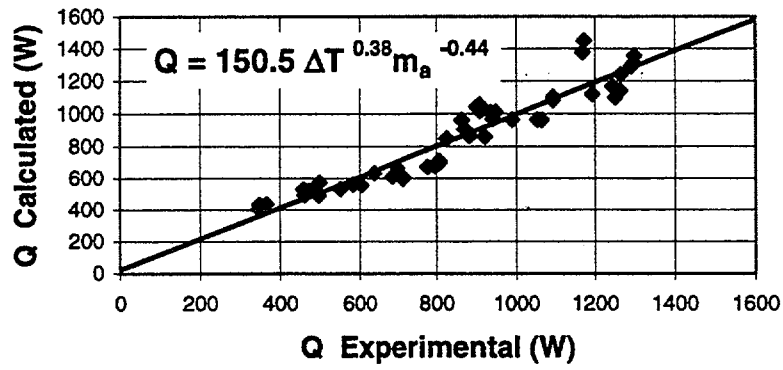


b) Vapour flow rate = 7.4 g/s

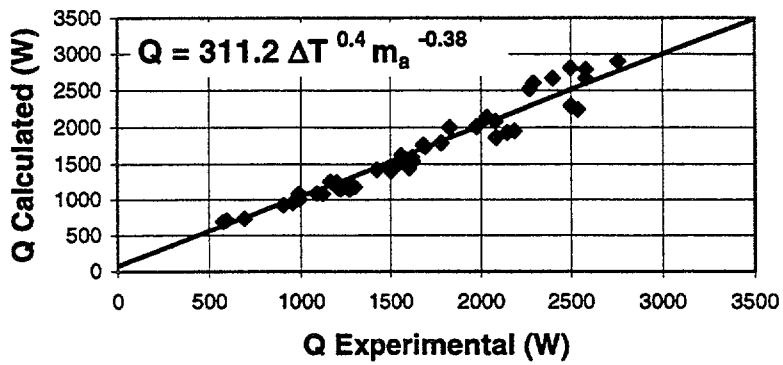


c) Vapour flow rate = 11.4 g/s

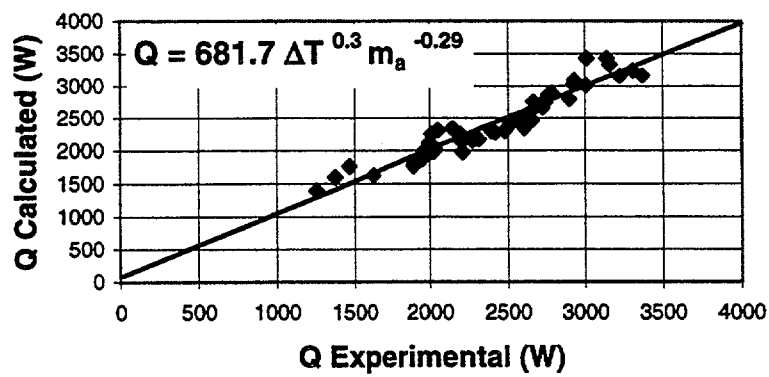
Figure 17: Effect of subcooling, air injection rate and vapour flow rate on rate of heat transfer for the double-sided inclined at 45° case.



a) Vapour flow rate=3.5 g/s



b) Vapour flow rate=7.4 g/s



c) Vapour flow rate=11.4 g/s

Figure 18: Comparison of experimental and curve-fitted values of heat transfer

A satisfactory overall description of the set of results for mixtures of steam and air shown on Figure 19 is given by the equation

$$\dot{Q} = 73.3 \Delta T^{0.35} \dot{m}_a^{-0.32} \dot{m}_s^{0.7} \quad (2)$$

From this it can be seen that the influences of air injection rate and steam flow rate are both slightly weaker than for the vertical and inclined cases. The overall rate of heat transfer for the horizontal case is generally lower by about 20% than for the vertical and inclined cases.

These experiments with a double-sided plate did not allow the contributions of the upper and lower surfaces to be separated. Clearly, in the case of condensation on horizontal or slightly inclined surfaces the process of condensation will be different on the two surfaces and the upward facing and downward facing cases should be studied separately. It was with this in mind that the experiments reported in the next section were conducted with the plate only promoting condensation on one surface.

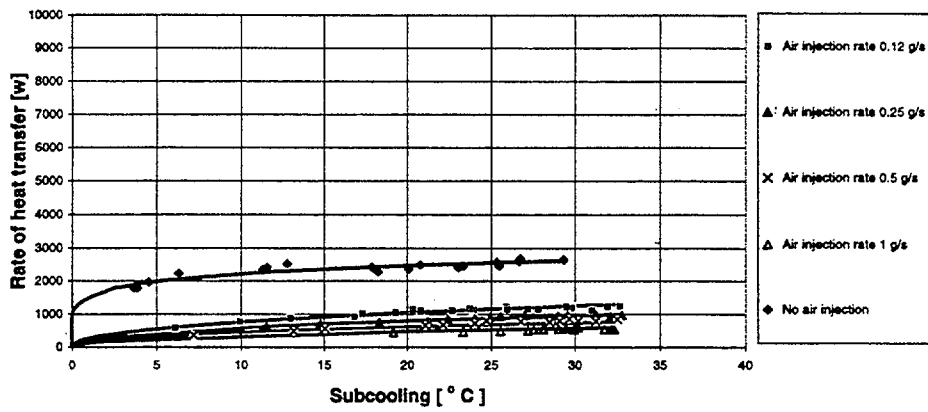
6.2. Experiments promoting condensation on one surface only

The condensing plate was thermally insulated on one face by covering it with a sheet of perspex 5mm thick. A programme of experiments was then carried out with the plate horizontal, inclined at 5° and inclined at 20°, firstly with the condensing surface facing upwards and then with it facing downwards. Experiments were only performed for one value of steam flow rate (7.4 g/s, boiler power input 18 kW). The results for the upward and downward facing cases are shown on Figures 21 and 23, respectively.

The data for condensation of steam in the presence of air have again been fitted separately for each orientation of the plate by an equation of the form $\dot{Q} = C \Delta T^p \dot{m}_a^q$. Comparisons between the experimental and curve-fitted values of \dot{Q} for the various orientations of the plate are shown on Figures 22 and 24 along with the corresponding equations.

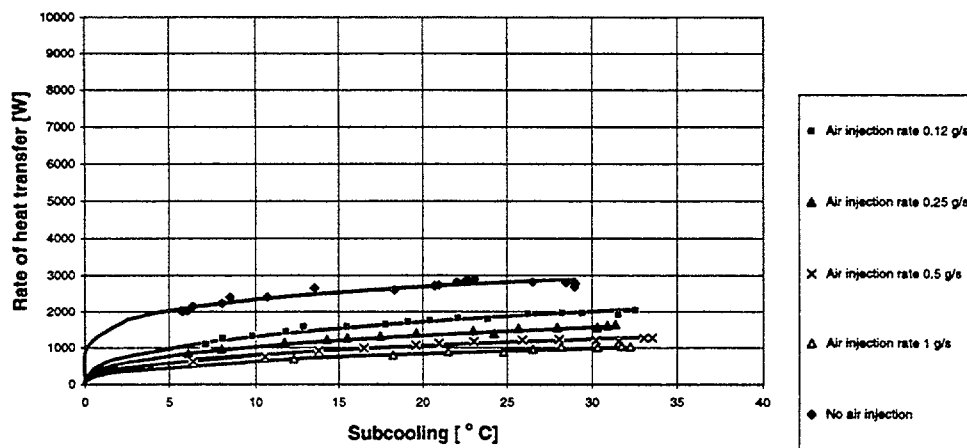
It can be seen from Figures 21(a) and 23(a) that with pure steam and the plate inclined at 20° to the horizontal the rates of heat transfer are clearly higher for the upward facing case than for the downward facing one. This must be due to the rivulets of condensate running off the surface more readily. However, with the plate mounted horizontally, or inclined at only 5°, the rates of heat transfer are greatly reduced and there is no clear cut difference between the rates of heat transfer for the upward and downward facing cases. However, an irregular variation of rate of heat transfer with subcooling is evident in the upward facing case and this is indicative of flooding of the surface.

As can be seen from Figures 21(b), (c) and (d) and Figures 23(b), (c) and (d), the pattern of behaviour with mixtures of steam and air is quite different. There is a systematic reduction in rate of heat transfer with increase of air concentration and also with reduction of plate inclination. The values are consistently higher for the downward facing case, presumably as a result of the upward flow of steam towards the plate helping to control the build up of air near it.



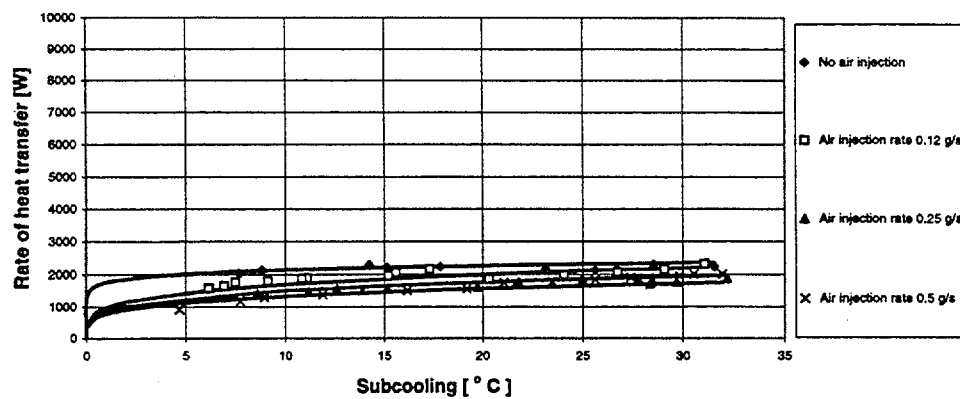
9 kW

a) Vapour flow rate = 3.5 g/s



18 kW

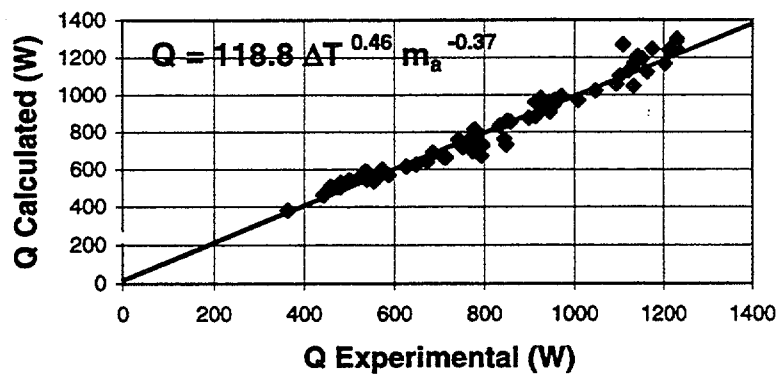
b) Vapour flow rate = 7.4 g/s



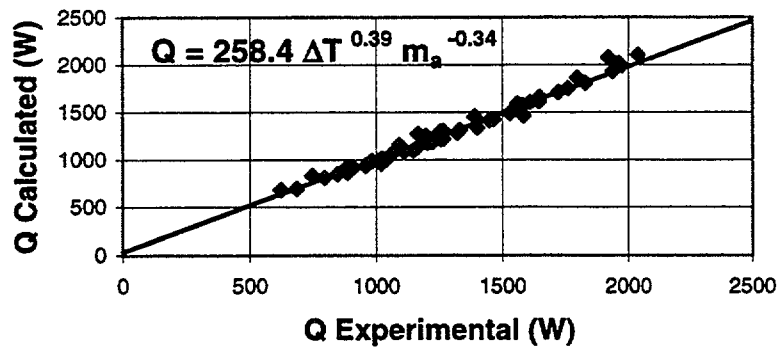
27 kW

c) Vapour flow rate = 11.4 g/s

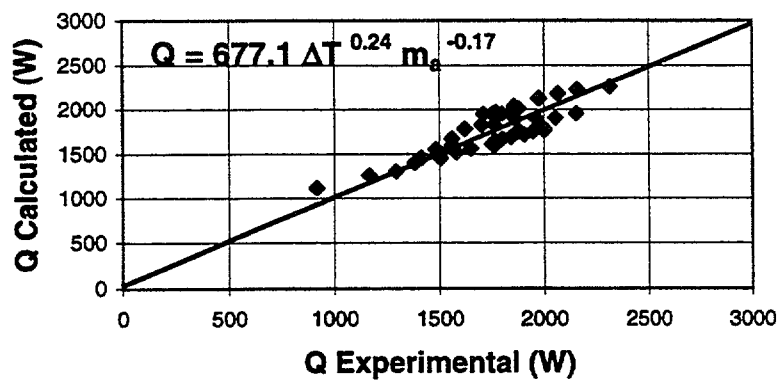
Figure 19: Effect of subcooling, air injection rate and vapour flow rate on rate of heat transfer for the double-sided horizontal plate.



a) Vapour flow rate=3.5 g/s



b) Vapour flow rate=7.4 g/s



c) Vapour flow rate=11.4 g/s

Figure 20: Comparison of experimental and curve-fitted values of heat transfer

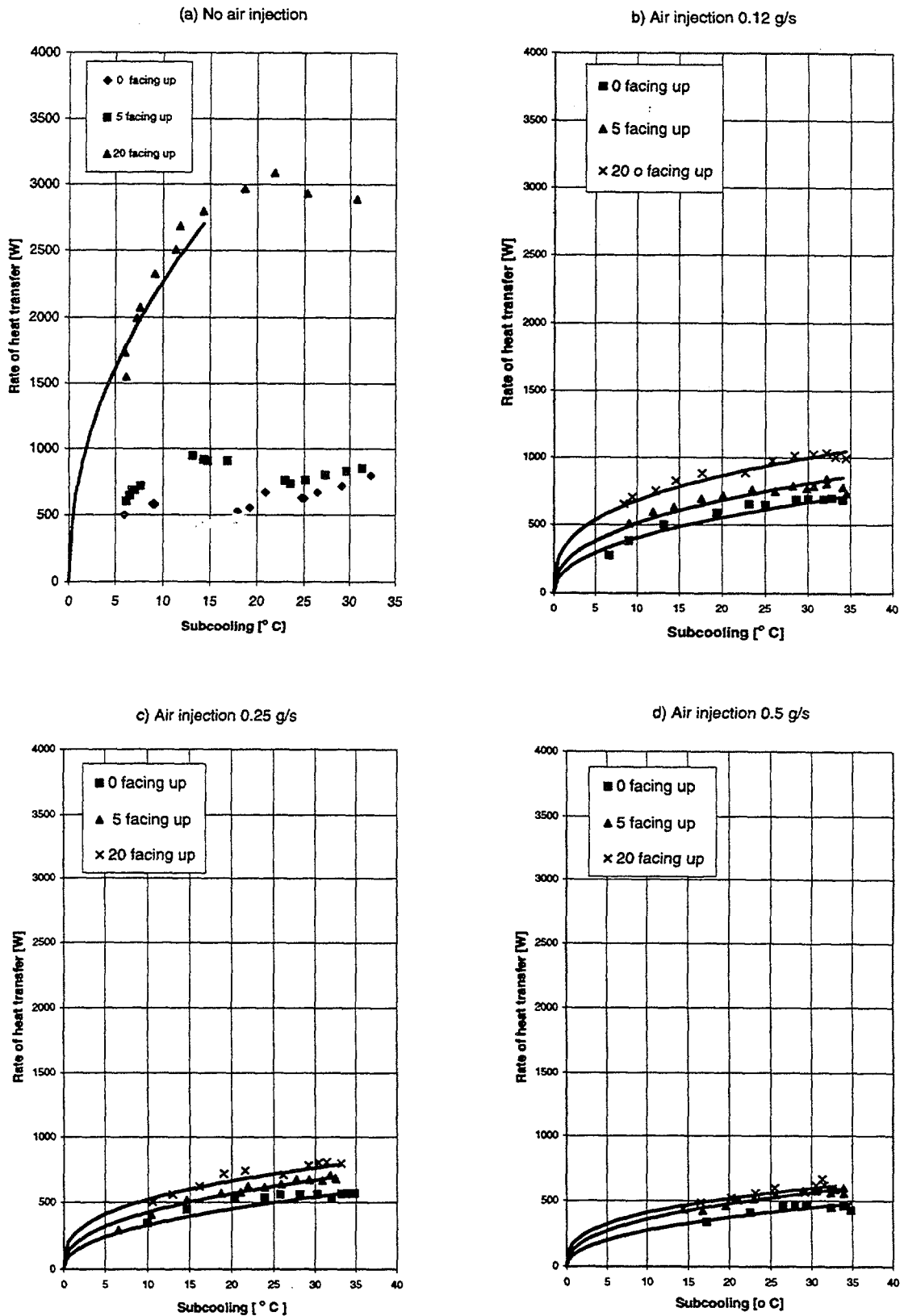
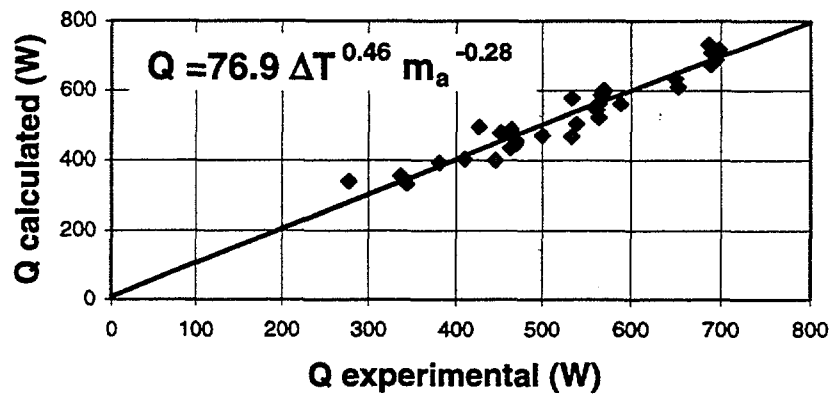
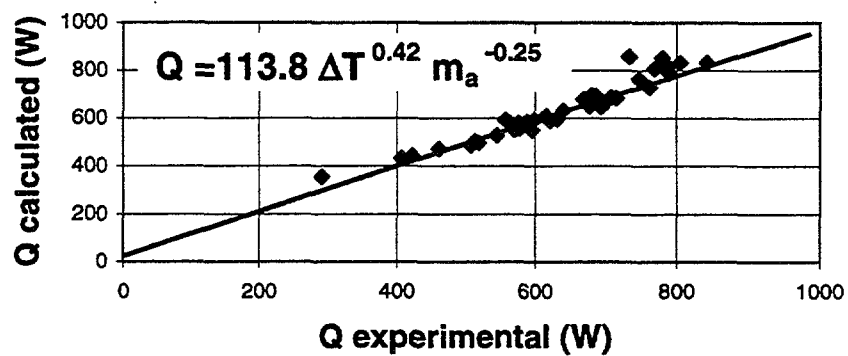


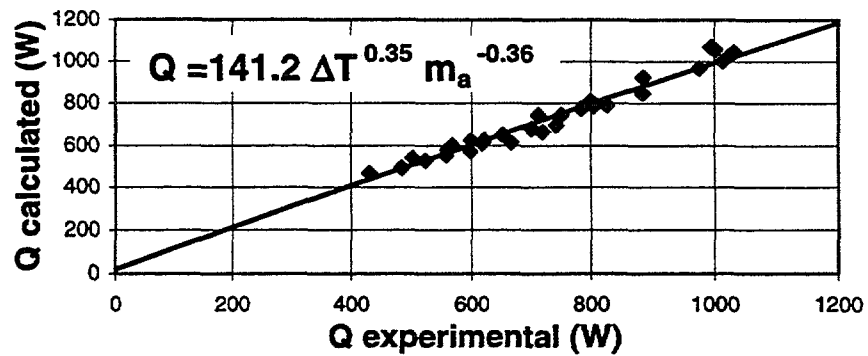
Figure 21: Effect of subcooling, air injection rate and orientation on rate of heat transfer (upward facing single sided plate, power input to the boiler 18 Kw, vapour flow rate 7.4 g/s)



a) 0° facing up



b) 5° facing up



c) 20° facing up

Figure 22: Comparison of experimental and curve-fitted values of heat transfer

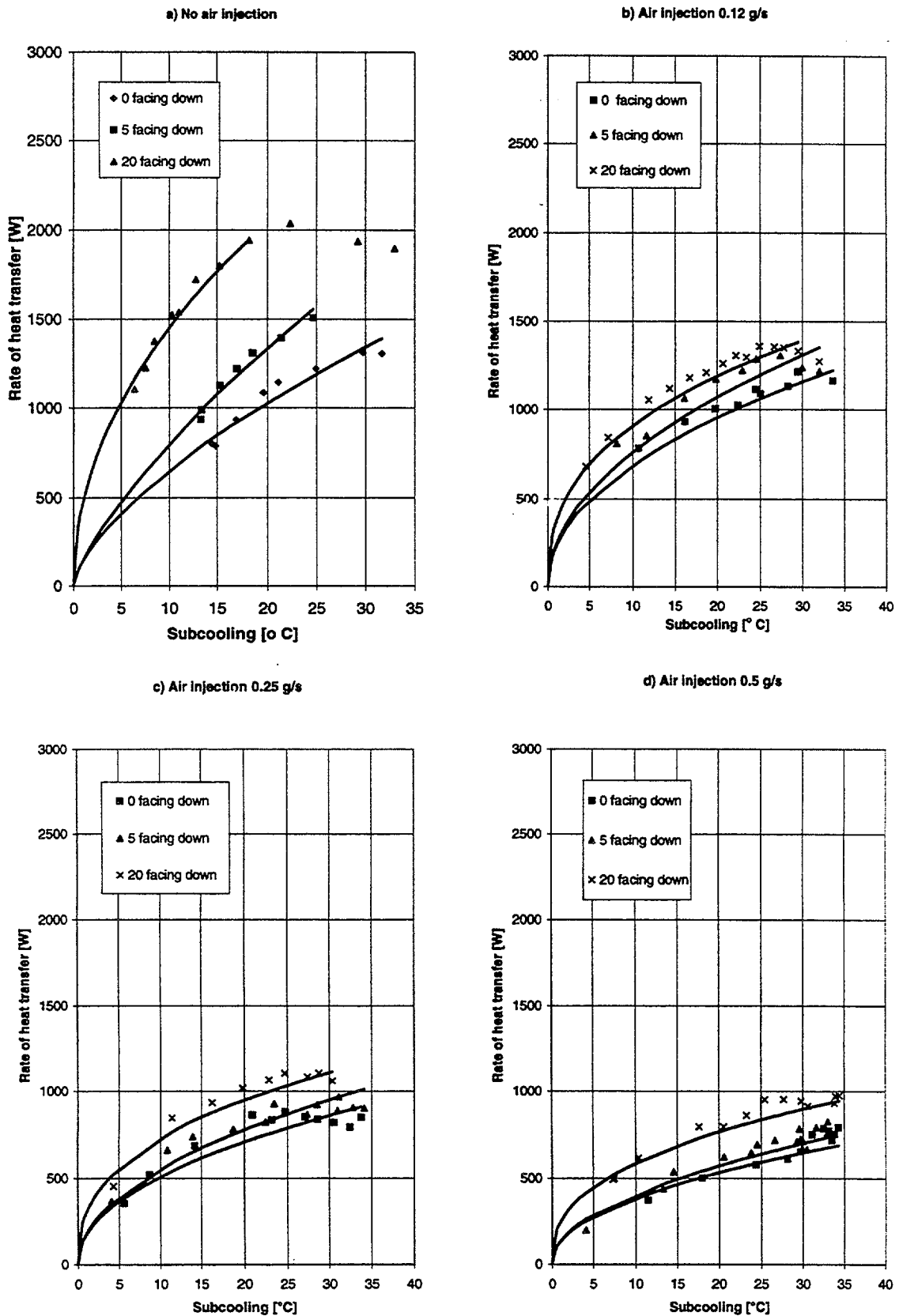
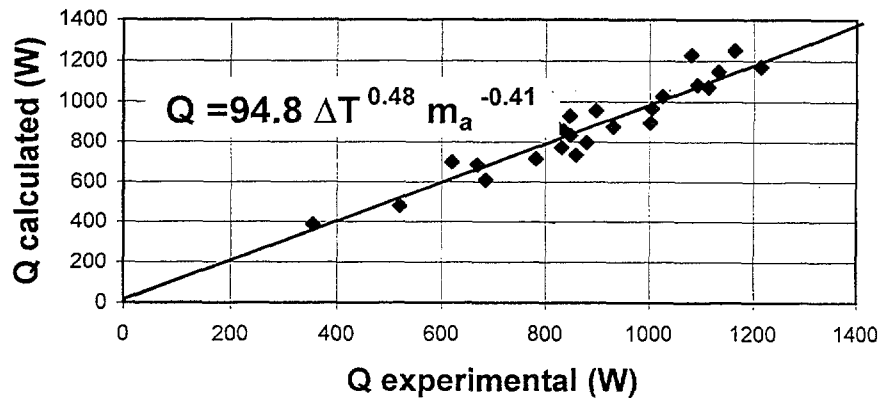
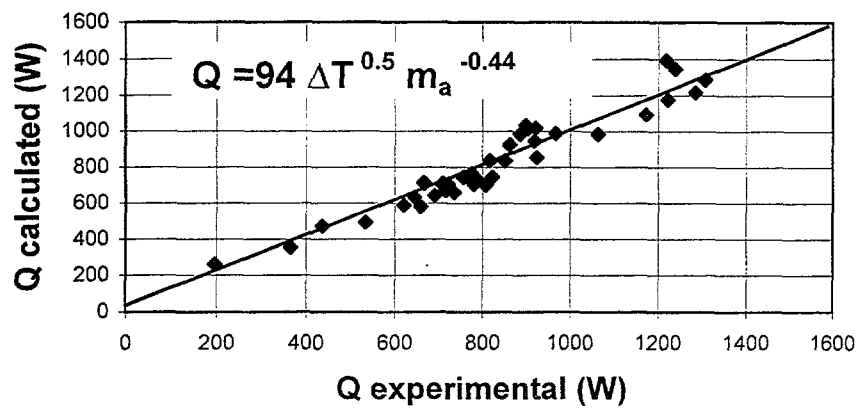


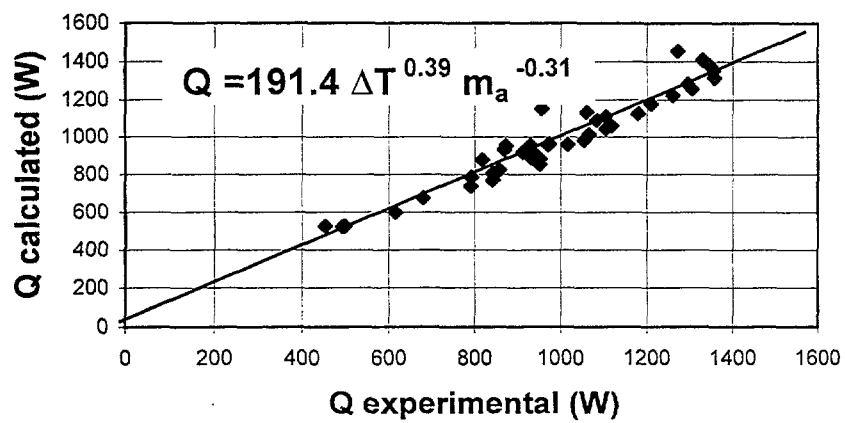
Figure 23: Effect of subcooling, air injection rate and orientation on rate of heat transfer (downward facing single plate, power input to the boiler 18 Kw, vapour flow rate 7.4 g/s)



a) 0° facing down



b) 5° facing down



c) 20°C facing down

Figure 24: Comparison of experimental and curve-fitted values of heat transfer

Conclusions

The chromium-plated condensing plate used in the present study proved to be very satisfactory. It consistently promoted dropwise condensation and the surface condition showed no signs of deteriorating after a lengthy period of use. The novel arrangement of cooling passages enabled a satisfactory uniformity of plate temperature to be achieved.

The experiments using pure steam with the plate mounted vertically in the test section promoting condensation on both sides showed that the heat transfer rate increased steadily up to a certain value as subcooling was increased after which ceased to increase as a result of a limit being reached on the rate at which steam could get to the plate. The degree of subcooling at which this occurred and the limiting value of heat transfer rate both increased as the rate of flow of steam through the test section was increased.

The associated experiments with mixtures of steam and air using the double-sided vertical plate showed that even a very small amount of air present in the steam caused a large reduction in rate of heat transfer. This influence varied in a very non-linear manner becoming less and less sensitive to the amount of air present as the concentration was increased.

With the plate mounted at 45° promoting condensation from steam or mixtures of steam and air on both sides, heat was removed at almost the same rate as for the vertical case and the pattern of behaviour with increase of steam flow rate and air concentration was very similar.

With the plate mounted horizontally the rates of heat transfer achieved were greatly reduced as a result of the condensate not draining easily from the plate. This was particularly evident in the case of condensation of pure steam where the rate of heat transfer actually fell the steam flow rate was increased due to flooding of the upper surface with condensate.

With the plate promoting condensation on one surface only and mounted at an angle of 20° to the horizontal, the rate of heat transfer from pure steam was higher for the upward facing case. With the angle of inclination reduced from 20° to 5° , or with the plate mounted horizontally, the rate of heat transfer was considerably lower due to condensate not draining from the plate so readily. There was then no clear cut difference between the results for the upward and downward facing cases except that the variation with subcooling became rather irregular with the condensing surface facing upwards due to flooding of the surface.

Using mixtures of steam and air, the rates of heat transfer reduced systemically as the concentration of air was increased and also as the inclination of the plate was reduced. The rate of heat transfer was higher in the downward facing case as a result of the upward flow of steam towards the plate aiding the removal of air from the condensing surface.

Further Work

A follow on programme of experiments with the surface condition of the plate modified so that it promotes filmwise condensation under all conditions has been initiated.

REFERENCES

- [1] REYNOLDS, O., On the condensation of a mixture of air and steam upon cold surfaces, Proc. Roy. Soc. 144, (1873).
- [2] HERR, J.E., KADAMBI, J.R. and ROHATGI, U.S., Condensation in presence of non-condensable gases, Proc. ASME 165, 77-86, (1993).
- [3] HUHTINIEMI, I., BARRY, J.J. and CORRADINI, M.L., Condensation in the presence of a non-condensable gas - The effect of surface orientation, AIChE Symposium Series, 85 250-210, (1989).

- [4] NUSSELT, W., The condensation of steam on cooled surfaces, Chemical Engineering Fundamentals Vol. 1, No. 2 ISSN 0723-0966, 6-19, (1982)
- [5] OTHMER, D.F., The condensation of steam, Ind. Engng. Chem. Vol. 21, No. 6 576-583, (1929).
- [6] VOTTA, F. JR. and WALKER, C.A., Condensation of vapour in the presence of non-condensing gas, AIChE Journal Vol. 4, No. 4 413-417, (1958).
- [7] ROSE, J.W., Condensation of a vapour in the presence of a non-condensing gas, JHMT, Vol.12 233-237, (1969).
- [8] COLBURN, A.P. and HOUGEN, O.A., Design of cooler condensers for mixtures of vapours with non-condensing gases, Ind. Engng. Chem. Vol. 26, No. 11 1178-1182, (1934).
- [9] CORRADINI, M.L., Turbulent condensation on a cold wall in the presence of a non-condensable gas, Nuclear Technology, Vol. 64 186-195, (1984).
- [10] DEHBI, A.A., GOLAY, M.W. and KAZIMI, M.S., The effects of non-condensable gases on steam condensation under turbulent natural convection conditions, Massachusetts Institute of Technology, Cambridge, MA, Report No. MIT-ANP-TR-004, (1991).
- [11] HENDERSON, C.L. and MARCHELLO, J.M., Film condensation in the presence of a non-condensable gas, ASME JHT Vol. 91 447-450, (1969).
- [12] MORI, Y. and HIJIKATA, K., Free convective condensation heat transfer with non-condensable gas on a vertical surface, IJHMT Vol. 16 2229-2240, (1973).
- [13] SPARROW, E.M. and LIN, S.H., Condensation heat transfer in the presence of non-condensable gas, ASME JHT Vol. 86 430-436, (1964).
- [14] VIEROW, K.M. and SCHROCK, V.E., Condensation in a natural circulation loop with non-condensable gases: Part 1 - Heat Transfer, Proc. ICMF, Tsukuba, Japan 183-186 (1991).
- [15] PETERSON, P.F., SCHROCK, V.E. and KAGEVAMA, T., Diffusion layer theory for turbulent vapour condensation with non-condensable gases, Transactions of ASME JHT Vol. 115 998-1003, (1993).
- [16] ANDERSON, M.H. and CORRADINI, M.L., Condensation in the presence of non-condensable gases: AP600 containment simulation, NURETH-7, Saratoga Springs, NY, USA 1519-1534, (1995).
- [17] ASANO, K. and NAKANO, Y., Forced convection film condensation of vapours in the presence of non-condensable gas on a small vertical flat plate, JCHE of Japan, (1978).
- [18] CHO, D.C. and STEIN, R.P., Steam condensation on the underside of a horizontal surface, Proc. of Third Int. Topical meeting on nuclear power plant thermal hydr. and operations, Seoul, Korea, 1988.
- [19] HENDERSON, C.L. and MARCHELLO, J.M., Film condensation in the presence of a non-condensable gas, Transactions of ASME, JHT Vol. 91(3) 447-450, (1969).
- [20] AL-DIWANY, H.K. et al., Free convection film condensation of steam in the presence of non-condensing gas, IHMT, Vol. 16, (1973).
- [21] LEE, W.C. et al., Forced convection film condensation on a horizontal tube with and without non-condensing gas, IHMT, Vol. 27, (1984).
- [22] GERSTMANN et al., Laminar film condensation on the underside of horizontal and inclined surfaces, IHMT, Vol. 10, (1967).
- [23] LEDUC, C. COSTE, P., BARTHEL, V. and DESLANDES, H., The modelling of wall condensation with non-condensable gases for the containment codes, NURETH-7, Saratoga Springs, NY, USA 1456-1477, (1995).

<p style="text-align: center;">NEXT PAGE(S) left BLANK</p>
--

EVALUATION OF THE CONDENSATION PHENOMENON IN PRESENCE OF NON-CONDENSIBLE GASES FOR PCCS RELATED GEOMETRY



XA0055005

V. FALUOMI

Dipartimento di Costruzioni Meccaniche e Nucleari,
University of Pisa,
Pisa, Italy

ABSTRACT

This paper presents a summary of results obtained analyzing the condensation phenomenon through the use of some selected models calculating the heat transfer coefficient during condensation in presence of non-condensable gases (air).

To achieve this goal, after selecting some widely used and qualified models, these were implemented in the CMTC (Computer Model for Correlations Test) computer code to evaluate their performances in a round tube geometry type. The CMTC code basically provides to the condensation models, (integrating the mass, energy and momentum equations over a control volume) the local values of fluid parameter (as mass flow rates, steam and gas properties, and so on) needed to determine the local heat transfer coefficient and the power exchanged between primary and secondary side of a PCC-like component.

After the model was assessed against experimental data, some parametrical studies were performed taking as reference the geometry of PCC component of a SBWR plant, with some expected conditions after a accident transient.

Some of the models were also implemented in the RELAP5/Mod3.2 code, to analyze the interactions among code structure and model responses, and the implementation was assessed using the previously mentioned experimental data. The following results were achieved:

- The CMTC code used to predict the condensation phenomenon in the considered geometry was successfully assessed, and overall acceptable performances were obtained in the prediction of experimental data considered;

- The parametrical analyses carried on for different postulated conditions of work of PCCs component showed some large spread of results, especially in the region of low non-condensable concentration in the steam bulk flow (less than 10%);

- The application of some of the selected models in the RELAP5/Mod3.2 showed a general underestimation of the heat transfer coefficient, mainly due to the overestimation of the effect of non-condensable gases in the condensation phenomenon;

- The comparison of the results obtained with the simple computer program used to test the selected models and the RELAP5 code are in acceptable agreement, making possible to use the program as a standard base to test new models and perform fast parametrical analyses.

ACKNOWLEDGMENT

The Author thanks Dr. Nusret Aksan, from the Thermal-Hydraulics Laboratory of Paul Scherrer Institut, for the hospitality as well as for technical support, needed for the study. The Author is also grateful to Dr. Michele Andreani, Dr. G. Th. Analytis and Dr. Dirk Luebbesmeyer, from the Thermal-Hydraulics Laboratory of Paul Scherrer Institut, for the interesting technical discussions about the results. Finally, the Author thanks Trevor Dury, from the Thermal-Hydraulics Laboratory of Paul Scherrer Institute, for the great help in improving the English of the manuscript.

1. INTRODUCTION

In the framework of safety analyses of Light Water Reactors (LWR), film condensation problems may be encountered in several situations. Concerning the presence of non-condensable in the vapor flow, it has been established that this can greatly inhibit the condensation process/1/. This phenomenon results in an accumulation of a non-condensable gas at the liquid/gas interface leading to a decrease in the corresponding vapor partial pressure and thus the interface temperature at which the condensation occurs.

In the new advanced passive boiling water reactor design (SBWR and ESBWR), the main component of the Passive Containment Cooling System (PCCS) is the Isolation Condenser (IC). The function of the IC is to

provide the ultimate heat sink for the removal of the Reactor Coolant System sensible heat and core decay heat. In performing this function, the IC must have the capability to remove sufficient energy from the reactor containment in order to prevent the containment from exceeding its design pressure shortly following design basis events and to significantly reduce containment pressure in the longer run.

After a loss of coolant accident, the steam/air mixture from the reactor containment may flow to the IC which will then reject decay heat to a pool of water. The steam condenses in downward flow through a bundle of tubes and the condensate drains back to the reactor pressure vessel. During the condensation of the vapor in presence of non-condensable gases, the condensed liquid flows in an annular film adjacent to the cooled tube wall and the vapor/gas mixture flows through in the center of the tube. The bulk motion of the core sweeps away the non-condensable gas leading to a lower buildup of the gas concentration at the interface, and at the same time the shear stress exerted by the gas leads to a thinning of the condensate film^{2/}. Both these factors lead to an increase in the heat transfer coefficient compared to the free convection in absence of non-condensable gases. In the IC the heat transfer coefficient vary greatly along the length of the tube. The decrease in the rates of heat and mass transfer with distance down the tube is mainly caused by the progressively increasing air fraction and the decreasing flow velocity, resulting from progressive dehumidification of the mixture.

Since the rate of heat transfer is strongly coupled to the hydrodynamic characteristics of the PCCs, a detailed knowledge of the variation of local heat transfer coefficient is necessary in order to predict the overall performance of the PCCS and to optimize the design of the IC.

In this work, the behaviour of a selected number of condensation models are analyzed through the use of a simple computer code, called CMTC (Computer Model for Testing Correlations). This code integrates, numerically, the mass, momentum and energy equations in their steady state form making use of a "control volume" scheme. The considered geometry is the round tube geometry. The integration of these equations provide the model analyzed with the local conditions needed to evaluate the heat transfer coefficient for condensation in presence of non-condensable gases.

The main feature of this code is the capability to handle different condensation models (up to 10 different models) to be able to do extensive comparisons among the different approaches for the condensation phenomenon. The assessment of this computer code is performed calculating two different experiments run in the University of Berkeley by J. Kuhn^{3/}. The results of this assessment and some statistics about the different responses of the models analyzed are also discussed.

The next step is the parametrical analysis of the different models using, as reference, the expected conditions on a SBWR containment after a Loss of Coolant Accident for different concentration of air in the steam, the models were used to evaluate their performances in the extraction of the decay heat from the core. As reference, a decay heat of 30 MW (corresponding to a 1.8% of the nominal SBWR core thermal power) was used, and conditions with concentrations of air in the condensing flow ranging from 0.01 % to 100% (flow saturated of air) were investigated. Ten values of system pressure were considered, starting from 1 bar (corresponding to the transient start) up to 10 bar. The model results and the safety issues related to the results obtained are presented and commented. Lastly, some of the models selected for this study were implemented in the RELAP5/Mod 3.2^{4/} thermal-hydraulic code, to evaluate the suitability of the model to be used in the system codes, and the suitability of the CMTC code to be used as a platform to test new models and to perform fast parametrical analyses for PCCS-like components. In the conclusions some notes about the code performance and the further development of the presented activity will be introduced.

2. DESCRIPTION OF COMPUTER MODEL

2.1 Generalities

The computer model used to simulate the behaviour of a PCC tube bundle for the analyses discussed in this paper is based on a steady state and one-dimensional numerical integration of the basic flow equations (mass, momentum and energy equations)^{5/} along a stream of volumes simulating the tube bundle. The secondary side of the PCC component is represented by a symmetric stream of control volumes exchanging heat with the primary side. No axial heat conduction through the tube wall is modeled, and a simple cylindrical geometry is used to model the radial heat conduction between primary and secondary side of PCC component.

The general scheme and the main parameters used to simulate a PCC like component is represented in Fig. 2.1. The non-condensable gas taken as reference for this study is air. The pressure drops, primary and secondary heat transfer coefficients are calculated through empirical correlations, as well as the properties of air. For the steam properties, a polynomial interpolation of tabulated values for saturated conditions is used.

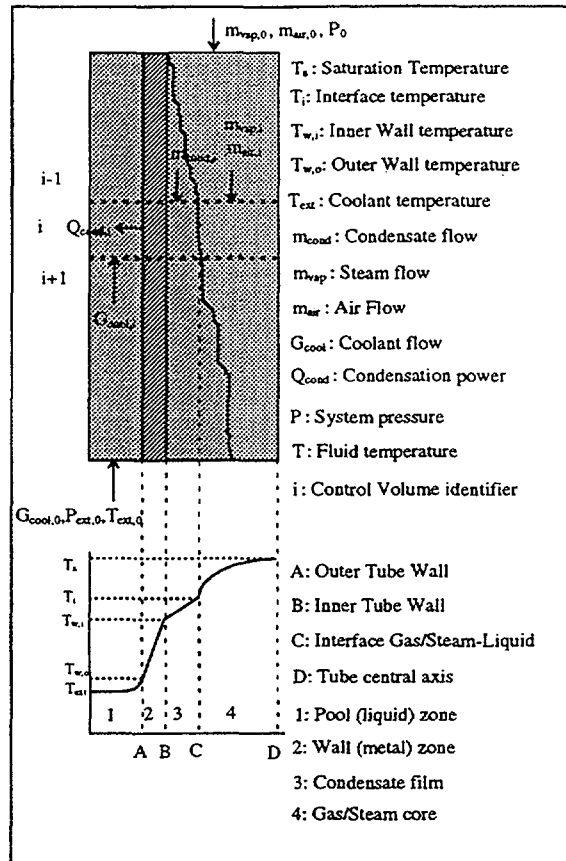


Fig. 2.1: Schematization of PCC component used to implement the CMTC code

2.2 Numerical solution

The numerical solution is based on a iterative solution of the flow equation for each control volume of the primary side. An additional iteration is performed in the secondary side to match the total energy exchanged between the primary and the secondary side and the energy extracted by the coolant on the secondary side of the loop^{6f}. Following the numerical scheme is fully exploited:

1. Using the inlet conditions in the primary side and guess the rest of system variables assuming full condensation, the first control volume is solved;
2. Using the results for the previous volume, the values for the actual volumes are calculated;
3. For each volume, two iterations are performed:
 - the first iteration is used to calculate the correct amount of condensate flow, matching the condensation heat flux (primary side) with the conduction heat flux (using a previous value of the secondary side tube wall temperature);
 - the second iteration, using the previous value of condensate, recalculates the secondary side tube wall temperature, using a previous value of secondary side liquid temperature;
4. Once all the control volumes of the stack are calculated, the energy extracted on the secondary side is compared with the heat exchanged between primary and secondary side. The procedure restart iteratively from point 1 till convergence is reached in this step.

2.3 Constitutive equations

To calculate some quantities needed to solve the flow equations, constitutive equations are used. These are mainly empirical or semiempirical correlations, based on a number of experiments regarding a certain phenomenon, like pressure drop, heat transfer coefficient and so on. In the case of this study, three phenomena are evaluated using constitutive equations:

- pressure drop in the primary side;
- condensation heat transfer coefficient in the primary side;
- subcooled boiling in the secondary side.

Because the main object of this computer model is that to investigate the effect of use of different condensation models, more emphasis is given to this aspect. This means that, the program is such that it can handle different condensation models and, for each model, calculate the values of the parameters inside and outside the condensing tubes, starting from selected boundary conditions.

The pressure drop model is a simple implementation of a homogeneous two-phase friction coefficient, based on definition of two-phase viscosity /7/. This choice is derived by the fact that, as already shown in Ref. /6/ the pressure drops in the condensing tubes are so little that the influence of the model is negligible.

Concerning the subcooling heat transfer model for the secondary side of the condensing tubes, the standard Chen correlation is used. Differently than in the case of condensation models, the choice of the model for the secondary heat transfer coefficient is of fundamental importance to correctly model the heat exchange between primary and secondary side, exchange driven from the lowest heat transfer coefficient between the two mentioned.

3. CONSIDERED MODELS FOR CONDENSATION HEAT TRANSFER

To perform studies on the differences in the modeling of condensation phenomenon, 5 different models are implemented in the computer program to evaluate, against experimental results, the differences in the phenomenon representation using different theoretical approaches.

Two of the models considered correlate experimental data as a function of non condensable concentration, in the form of heat transfer coefficient or a correction factor to the pure steam condensation condensate film resistance. The models considered are the UCB correlation (Ref. /8/) and the Coddington correlation (Ref. /9/), a modification of the previous one, where the influence of the shear between the liquid film and the bulk vapor is modeled using a theoretical approach rather than a correlation of experimental data.

The other models used in this study consider separately the local thermal resistance of the condensate film and of the mass diffusion of non-condensable. The mass diffusion problem is solved using an energy balance and the analogy between heat and mass transfer. Generally, an iterative method is needed to evaluate the condensation heat flux matching the energy transfer and the mass transfer across the interface liquid film-gas core.

In the model of Gido-Koestel ^{/10/}, the thermal resistance of the liquid film is considered to be negligible compared with the resistance in the gas-steam mixture; thus the interface temperature is set to be equal of the inner wall temperature of the condensing side. This assumption simplify the model, which does not need of iterative procedures to evaluate the condensation heat transfer coefficient. In the case of the other models, the Colburn-Hougen model /11/ and the Peterson model /12/, an iterative technique is needed to evaluate the heat transfer coefficient, starting from the analogy between mass and heat transfer in the condensation process.

4. COMPARISON OF CONDENSATION MODELS WITH EXPERIMENTAL DATA

4.1 Considered Experiment for condensation model evaluation

J. Kuhn of the University of California at Berkeley set up and ran a series of experiments to measure the heat transfer coefficients under SBWR-PCCs-like conditions. The set up is described in Ref. /13/.

In this work two of them have been considered, named respectively 72.1 and 2.1-3. The geometric and flow parameters are described in Tab. 4.1.

Because the available data for the considered experiments are limited to the fluid and wall temperature of the section components at different elevations, it was chosen to use only the Steam-Air temperature and the pool temperature as an index of the performances of the selected models to represent the condensation phenomenon.

In one of the experiment considered, the 2.1-3 experiment, a full condensation before the end of the condensing tube happens: this phenomenon cannot be handled properly from the simple computer model used, since the model does not consider, in the primary side, any other heat transfer model than condensation. Thus, when all the steam disappear from the mixture, the model simply does not calculate any heat transfer coefficient and set all the temperatures equal to the external coolant temperature.

This means that the model can predict when full condensation take place, but cannot predict any further phenomenon after full condensation. Considering the purpose of the model, this is an acceptable limitation.

4.2 Evaluation of calculated results for local and integral parameters

In the Figs. 4.1 to 4.6 the results for the different condensation models in representing the experimental tests are shown. Considering the test 72.1, it is clear how some of the models predict full condensation before the end of the tube (where occurs in the experiment). The Peterson model and the Colburn models predict full

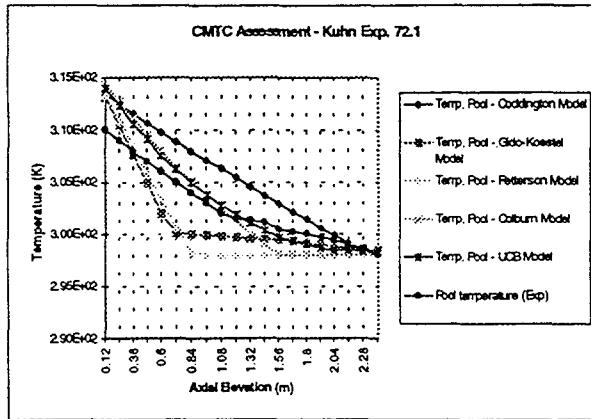


Fig. 4.1: Kuhn Exp. 72.1 - Steam-Air bulk temperature results for the selected models

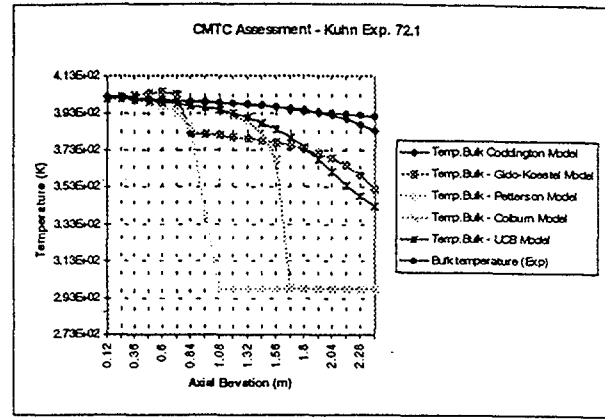


Fig. 4.2: Kuhn Exp. 72.1 - External pool temperature results for the selected models

Tab. 4.1: Kuhn experiments : geometrical and boundary conditions of test section

Parameter	Unit	Exp. 72.1	Exp. 2.1-3
Tube length	m	2.418	
Inner diameter	m	0.0508	
Outer wetted perimeter	m	0.388	
Outer flow area	m ²	0.002124	
Tube thickness	m	0.00165	
Inner pressure	Pa	2.8e5	4.71e5
Steam flow rate	kg/s	0.008	0.014
Air-Steam ratio	-	0.27	0.03
Outer pressure	Pa	1.0e5	1.0e5
Outer flow rate	kg/s	0.27	0.34
Outer coolant inlet temperature	K	298	304

condensation after 1/3 and 2/3 of the tube length, respectively. A small jump is detected in the results using the Gido-Koestel model, and also in this case the final temperature of the steam in the tube is largely underpredicted. A rather good behaviour is shown by the UCB model, at least for the first half of the section, and a good agreement with experimental data are reached by the Coddington model. From these results seems that the code fails in the calculation of the interface temperature, at least following the models as they are described in the literature. This is clearly shown by the fact that the better results are reached through the use of models that does not make use of interface temperature.

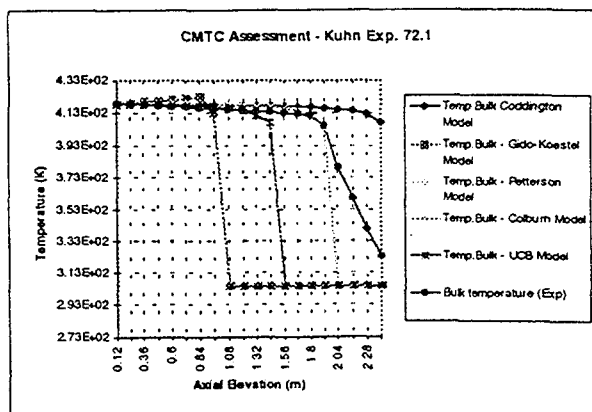


Fig. 4.3: Kuhn Exp. 2.1-3 - Steam-Air bulk temperature results for the selected models

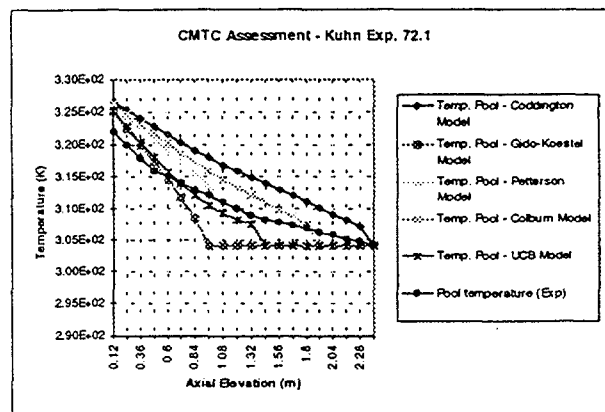


Fig. 4.4: Kuhn Exp. 2.1-3 - External pool temperature results for the selected models

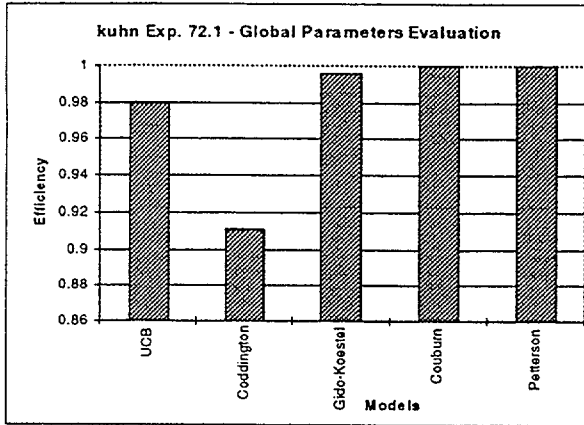


Fig. 4.5: Kuhn Exp. 72.1 - Efficiency results (only calculated) for the selected models

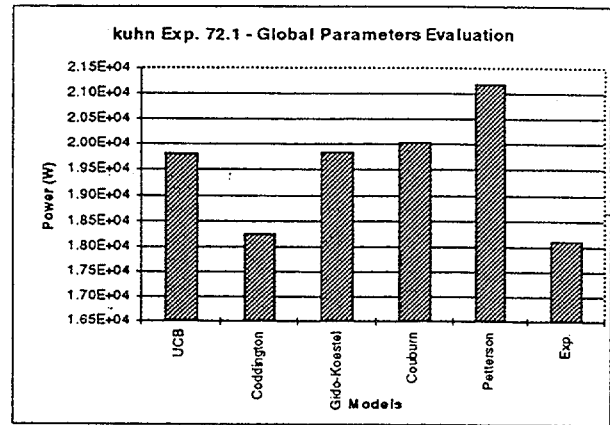


Fig. 4.6: Kuhn Exp. 72.1 - Condensation Power exchanged for the selected models

For the results in calculating the external pool temperature, one can apply the same considerations, even if, in this case, because of the not highly sophisticated model to solve the energy equation in the secondary side, part of the results can be in some cases invalidated by the not perfect convergence of the numerical scheme used.

In the case of the Kuhn Exp. 2.1-3, as previously warned, the results are comparable with experimental data just before full condensation. In this case, differently than in the previous comparison, the better agreement with experimental data is reached by the Colburn model in predicting the steam core temperature in the condensing tube. The Coddington model gives reasonable results, but underestimates the condensation rate and, finally, does not predict full condensation at the end of the test section. It is worth to note that, the UCB model and the Peterson model work, in this case, almost identically, even using a completely different approach for modeling the condensation phenomenon.

In the Figs. 4.5 and 4.6 are represented the results for the integral parameters of 72.1 Exp.: exchanged power and tube efficiency, defined as in Ref. /13/. The results show that, in general terms, the different models can determine the experimental heat exchanged between condensing tube and secondary side of apparatus, though a certain overestimation of the power (about 10%-15%) is predicted by most of the models, excluding the Coddington models, that predict almost the experimental value. This is confirmation of the efficiency results, where most of the models

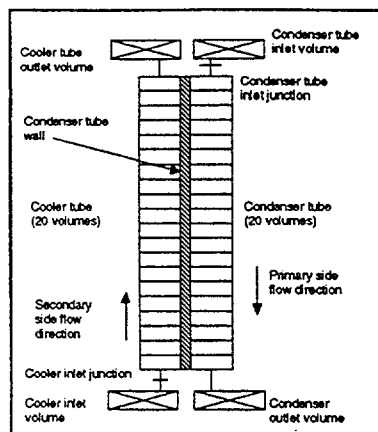


Fig. 5.1: RELAP5/Mod3.2 Input scheme for Kuhn experiments calculation

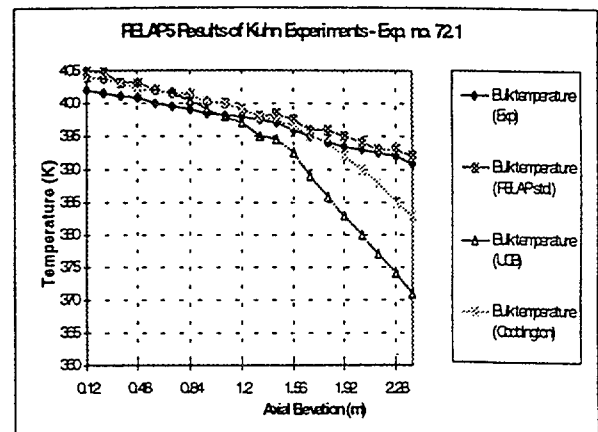


Fig. 5.2: RELAP5 results for Kuhn 72.1 experiment - Steam core temperature

predict nearly full or full condensation of the steam (efficiency equal to one). In the case of 2.1-3 Exp., because full condensation occurs, the values are the same for all the models, so that it was not worth to discuss them.

Considering the limitation of the model above mentioned, the prediction of the coolant temperature distribution is reasonable for all the different models, and the results are in general consistent with those described for the steam core temperature data.

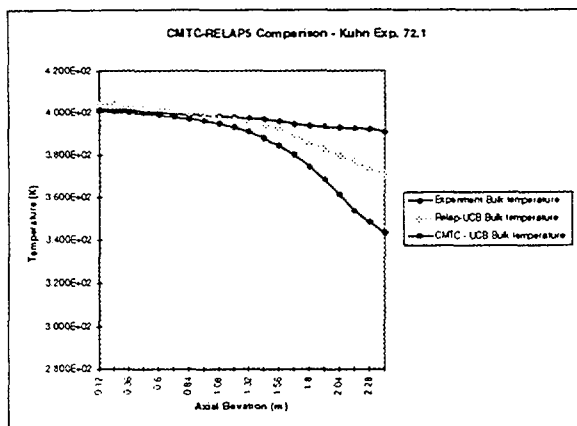


Fig. 5.3: Comparison between RELAP5 and CMTC results for Kuhn 72.1 experiment - Steam temperature

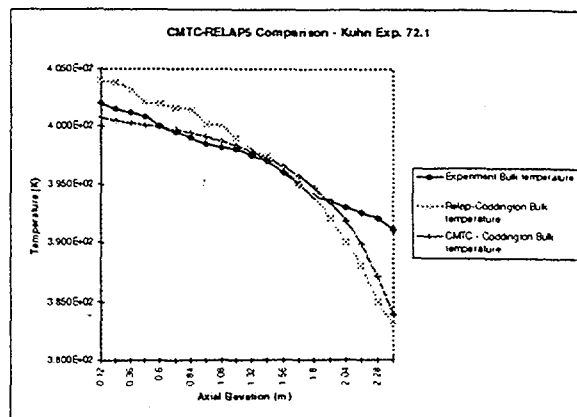


Fig. 5.4: Comparison between RELAP5 and CMTC results for Kuhn 72.1 experiment - Pool temperature

5.COMPARISON WITH RELAP5 CODE CALCULATION

5.1 Model implemented in the RELAP5 thermal-hydraulic code

The main purpose of this section is to examine and analyze the performances of some selected condensation models (among those already analyzed separately) when implemented in the RELAP5/Mod3 code. This is necessary to investigate the impact of a model in a highly sophisticated and complex numerical structure, and the capability for the

RELAP5 code structure to include more advanced model for phenomena description when available. To implement the selected correlations in the RELAP5 code, the following procedure was followed:

1. The structure of the correlations, previously coded in the Fortran77 language, in a form suitable for implementing into the CMTC code, was included in the RELAP5 code as a function call.
2. When a stable and correct form of the coding had been reached, the function representing the correlations was linked to the source code of RELAP5, recompiled and , for each different correlation, a separate version of code was created.

Because time and resource shortage, only two correlations were implemented^{/14/}:

- the UCB model,
- the Coddington model.

In the standard version of the RELAP5/M3.2^{/15/} the Colburn model is included: so that, it was possible to evaluate the performances of three of the five original models when implemented in the code. This procedure results both in a RELAP model qualification and in the evaluation of the CMTC code as a correlation tester for working coupled with a large system code, in the development stage.

5.2 Evaluation of RELAP5 results

In Fig. 5.1 the input scheme used for analyzing the Kuhn experiments with the RELAP5 code is shown. Basically the input consists of 20 hydraulic nodes, which simulate the condensing tube, connected to other 20 nodes, simulating the cooling channel. The connection is realized through 20 heat structures, simulating the tube wall. Four time dependent volumes (two of each side of condenser) and two time dependent junction (to provide the two sides with the correct values of mass flow rate of fluid) completed the input deck elements.

Some of the results are shown in Fig. 5.2: the different code versions with different condensation models predict reasonably well the temperature trend along the condensing tube. To note that, the better behaviour have been obtained with the standard version.

The main discrepancies among code results and experimental data are calculated for the UCB model, because of his simple model to evaluate the stress shear between liquid and steam-air mixture at the interface.

5.3 Impact of the implementation of the models in the code

The main purposes of RELAP calculation of Kuhn experiments are the following:

- to show the capability of the code to predict the condensation phenomenon^{/16/}, statement achieved in the previous section;
- to evaluate the differences in the behaviour of the different condensation models when implemented in a complex system code such as RELAP5, in comparison with the calculations performed with the simplified CMTC code, to investigate the suitability of this simplified model to test correctly the performances of the models selected.

In this paragraph some comments of the investigation in the latter object are given. Looking at the Figs. 5.3 and 5.4 (related to the Kuhn 72.1 experiment) one can see how the results obtained from the RELAP5 and from the CMTC code are substantially in agreement. Especially for the calculations performed using the Coddington model, the steam-

air temperature trend is almost the same for the two cases, with minor differences due to differences in the steam properties, more precise in the case of RELAP5 code. For the calculation performed with the UCB model, some differences in the temperature at the bottom of the tube are present, but both the calculations show an underestimation of temperature, that means overestimation of heat transfer coefficient in the condensing side. Considering the limitation of the CMTC code, one can conclude that the results are acceptable to consider the model suitable to these the general behaviour of a condensation model during the conditions considered.

6. ANALYSIS OF PCC COMPONENT WITH DIFFERENT CONDENSATION MODEL

6.1 Boundary conditions for PCC analysis

The last step in evaluating the selected condensation models is the analysis of PCCs performances, using as boundary conditions typical values of mass flow rate and pressures at PCC inlet that are expected to occur during a postulated loss of coolant accident transient.

In Tab. 6.1 are listed the boundary condition chosen for this analysis; is worth to note that the range of non condensable gas/steam flow ratio ranges from 0.01 to 1.0, to evaluate the models in all the possible conditions occurring during a transient., especially in the regions (startup of the containment transient) where the air content in

Tab. 6.1: Boundary condition for PCC performance analysis

Range Identifier	Core Power (MW)	Steam Flow (kg/s)	Air Flow(kg/s)	Pressure (bar)
Low Power	15 MW	6 kg/s	0.006 - 6 kg/s	1.0 - 3.0
Middle Power	30 MW	12 kg/s	0.012 - 12 kg/s	1.0 - 10.0
High Power	60 MW	24 kg/s	0.024 -24 kg/s	1.0 - 10.0

Tab. 6.2: Main PCC geometrical parameters

Parameter	Unit	Value
Tube length	m	2.4
Tube diameter	m	0.0508
Number of tubes	-	480
Total flow area	m ²	3.5
Total heat transfer area	m ²	184
PCC pool flow area (PCC tube bundle zone)	m ²	2.8

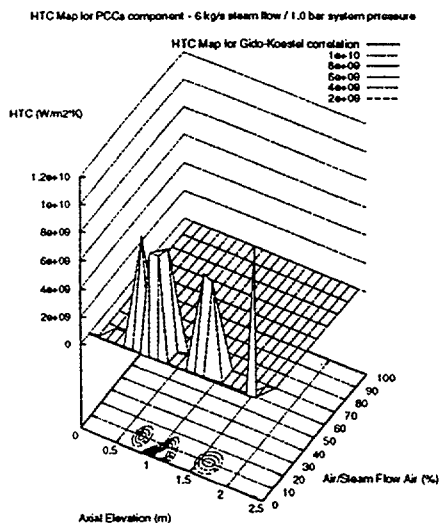


Fig. 6.1: Gido:Koestel Model results for heat transfer coefficient map - Low pressure - Low power conditions

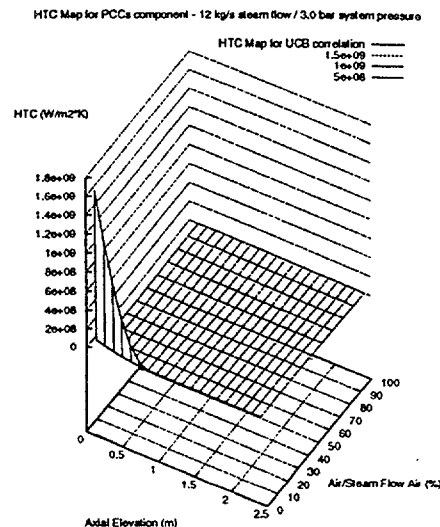


Fig. 6.2: Coddington Model results for heat transfer coefficient map - Low pressure - Low power conditions

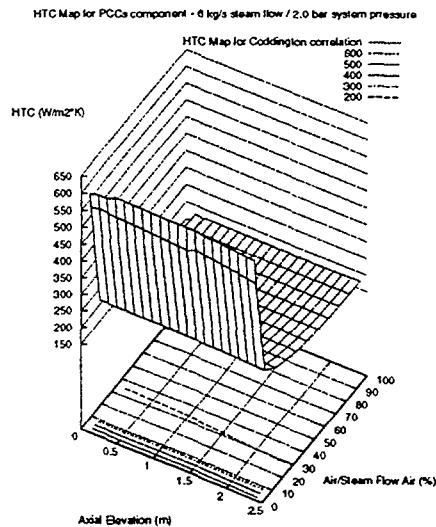


Fig. 6.3: UCB Model results for heat transfer coefficient map - Middle pressure - Middle power conditions

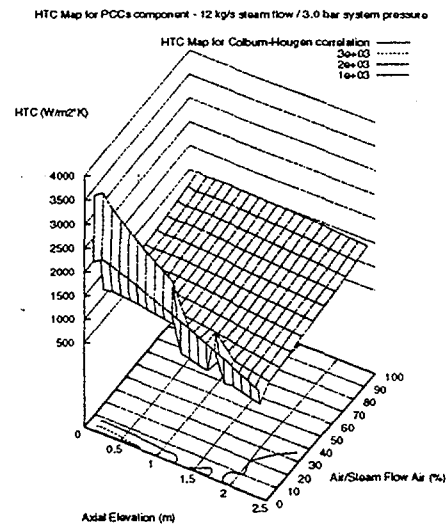


Fig. 6.4 : Colburn Model results for heat transfer coefficient map - middle pressure - middle power conditions

the steam flow is considerably higher, reason due to the nitrogen gas presence in the SBWR containment for inertization purposes. For completeness, in Tab. 6.2 the geometrical values for the PCC component take as reference are listed too.

6.2 Heat transfer coefficient maps for condensation phenomenon

The first analysis of the PCC performances is related to the heat transfer coefficients calculate by the different models in the PCC component. This coefficient is plotted against the measurement level along the tube and against the air content in the mixture incoming in the PCC component. In Figs. 6.1 to 6.6 some of the results for the calculations are shown. In particular, two plots for each power region are shown, and for them some following comments are given:

- for the low power region, the Gido-Koestel model predicts a value of heat transfer coefficient generally near to zero for all the range of parameter consider. Because no range of validity of correlation was indicated in Ref. /10/, it is not possible to say that this behaviour is such because the model is applied beyond its limits. For the Coddington model instead, a low heat transfer coefficient is generally calculated, apart for the low air content zone (< 10%) where is three times higher than for the rest of the range
- In the case of middle power conditions (Fig 6.3 and 6.4) similar behaviour have been calculated both from Colburn Model and UCB model. No special remark has to be made for this case, except that for a certain instability in the

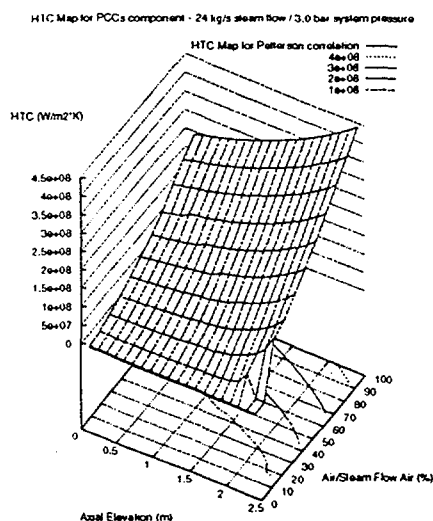


Fig. 6.5: Peterson Model results for heat transfer coefficient map - middle pressure - high power conditions

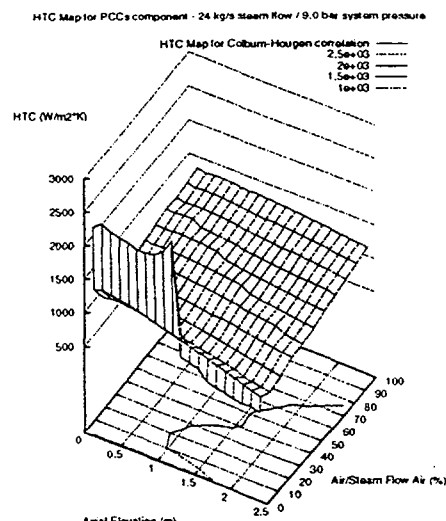


Fig. 6.6: Colburn Model results for heat transfer coefficient map - high pressure - high power conditions

calculation of heat transfer coefficient for the Colburn model, probably due to the iterative method needed to evaluate the heat transfer coefficient.

- For the high power case (Fig.6.5 and Fig. 6.6) the main remark is related to the unphysical behaviour of the Peterson model, that calculates higher values for heat transfer coefficient in correspondence with higher air content. In fact, increasing the air contents, the heat transfer coefficient increases, and also increase along the tube, where, because the air percentage increase along the tube due to the upstream condensation, it should decrease, as shown by the other models. Again, because no range of validity was indicated in Ref. /12/ and Ref. /17/, it could be possible that this behaviour is caused by the use of the correlation beyond their limit, hypothesis supported also by the satisfactory responses of the model in the other analyzed cases. It is also possible that this is caused by the
- influence of the numeric of the computer program in which the model is implemented, being the model more sensitive to this because its scheme (related to other models as UCB or Coddington, where no iterative method is needed to evaluate the heat transfer coefficient for condensation). Whatever the reason is, in any case this behaviour have to be indicated and considered in following analyses, to avoid misunderstanding of model results.

6.3 Efficiency evaluation of PCC component

The evaluation of PCC efficiency is the main issue of this analysis, because can give the PCC responses related to the capabilities to remove the decay heat power produced in the core.

Some of the calculation performed are shown in Fig. 6.7 and Fig. 6.8. In general terms, with the increase of the air content in the flow incoming in the PCC component, the efficiency tend to diminish, till values near to zero (no condensation in the tube). Nevertheless, despite this general behaviour, each model has a different representation of these maps, and noticeable differences among the models are detected. In fact, while for the Coddington model the efficiency is rather linear with the air percentage in the flow and is not much influenced by the pressure of the flow itself, the UCB correlation shows a different behaviour, and, increasing the pressure, the air contents limit under which high condensation is reached is increasing. The Gido-Koestel model show a efficiency map behaviour rather different, but these differences can be also explicated by the fact that, this model, it was not directly defined for tubes but for condensation in large walls. This means that it is not completely optimized for the phenomenology of condensation in tubes, that can be quite different than for walls, especially in the consideration of parameters to identified natural and forced convection.

In all the plots there are some "holes" or "spikes" in the maps, cause by instabilities in the calculation, that have any physical explanation. In particular, if convergence is not reached during a calculation, can happen that the error propagate in the solution and a extremely low or higher heat transfer coefficient in the condensing side was calculated. Most of these cases are eliminated in the computer model used, but still there are situations not handled by these control routines. In any case, these few points are easy to individuate in the plots.

6.4 Condensation Driving force analysis

The last analysis on the PCC performance data is related to the so called "Condensation Driving Maps". These maps are, essentially, representations of the ratio between the primary and the secondary side heat transfer coefficients, against the tube elevation and the air contents in the condensing mixture. To investigate these maps is of fundamental importance to evaluate which are the parameter ranges where the condensation phenomenon (for each selected model) is effectively a limitation and a driver for the condensation phenomenon, and where the phenomenon is merely limited by the secondary side heat transfer coefficient, case that is out of the scope of this study, and not of interest for the investigation of the condensation mechanisms.

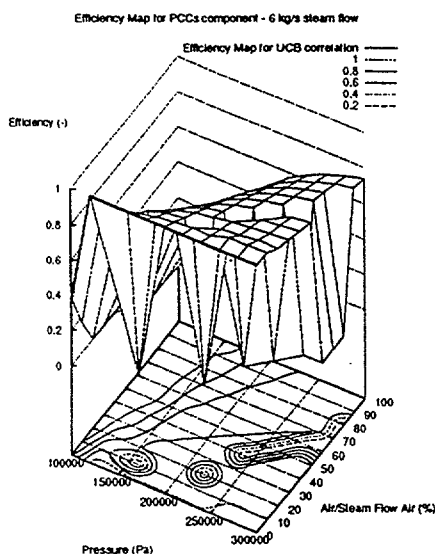


Fig. 6.7: UCB Model efficiency map - low power conditions

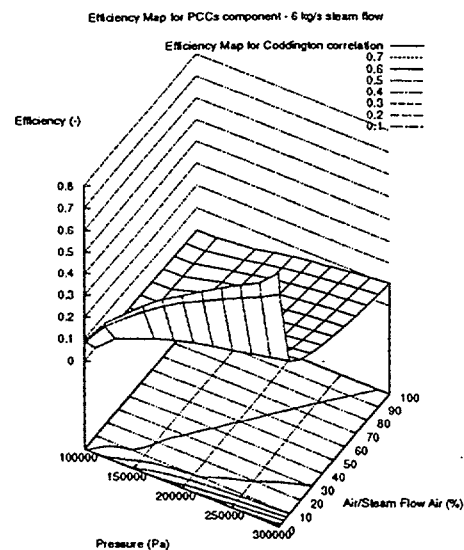


Fig 6.8 : Coddington Model efficiency map - low power conditions

To simplify the interpretation of the results, the ratio between the two coefficients it was plotted in them of 0 and 1, means that 0 was put on the graph when the secondary side heat transfer coefficient drives the condensation phenomenon, 1 otherwise.

In this way, the areas where one or the other heat transfer coefficients are the relevant parameter for condensation are clearly divided, and is easier to get conclusions. This analysis was carried out just for the middle power case (steam flow rate = 12 kg/s). Considering the Figs. 6.9 and 6.10, one can see how, for the same conditions, in the case of UCB model the secondary side heat transfer coefficient plays a more relevant role in the condensation phenomenon description. In fact, just on the bottom of the tube, the outer heat transfer coefficient become larger than the condensation heat transfer coefficient, and this is the only region where the condensation model is relevant to the calculation of the total power exchanged between primary and secondary side. In the case of Peterson model, the area where the condensation model plays a relevant role is much more large, including a wide zone of the considered boundary conditions. This means that, considering the two examples used, for the former model the influence of the model in the condensation phenomenon is relatively small, and this means that no information about the model capabilities can be obtained in this region, because all the key parameters needed to evaluate the model (essentially efficiency and power exchanged) are limited by the secondary side heat transfer coefficient. For the latter model instead, a larger range of parameters where the model is relevant for the condensation phenomenon occurrence is detected, making more meaningful the results on efficiency and heat power exchanged calculated for these regions.

Condensation Driving Map for PCCs component - 12 kg/s steam flow / 3.0 bar system pressure

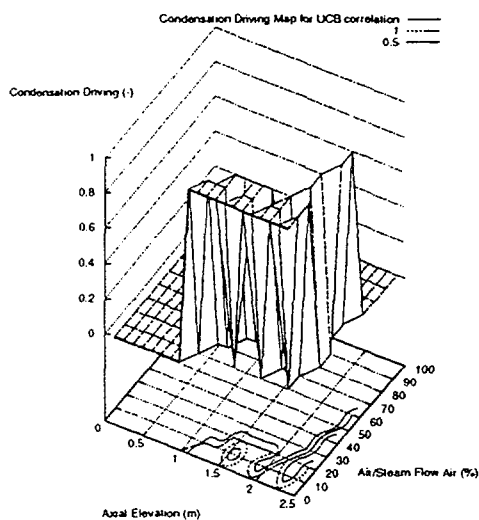


Fig. 6.9: Driving Condensation Map for UCB model - middle power

Condensation Driving Map for PCCs component - 12 kg/s steam flow / 6.0 bar system pressure

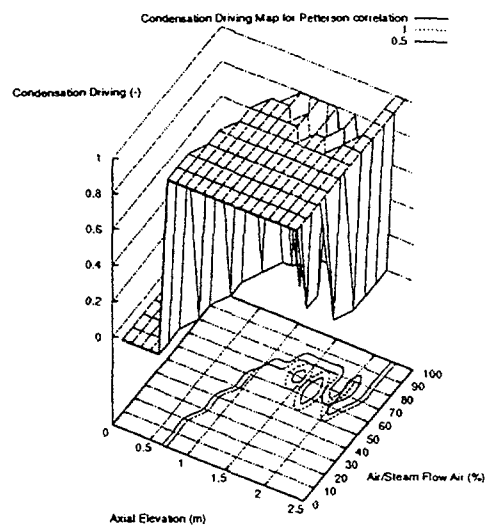


Fig. 6.10: Driving condensation map for Peterson Model - middle pressure

7. CONCLUSIONS

The results presented indicate, in general terms, the different responses of the different models for calculating the condensation phenomenon when non-condensable gases are presented. A comparison with experimental data and RELAP5 code calculations is described. The main results of this study can be summarized as follows:

- In the literature, models for predicting condensation phenomenon in presence of non condensable gases have been derived from a huge amount of experimental data, often taken from different researchers, and covering only a partial spectrum of phenomenon occurrence. Some of the models, because of this, try to interpolate the experimental data and might show unexpected behaviour for conditions not well defined on the experimental side. Some other models try to describe the condensation phenomenon with a more physical approach, but, because of some uncertainties in the mechanisms which drive the exchange of heat and mass at the vapor-liquid interface (which are heavily influenced by the presence of non condensable gases), use numerical models which are somehow source of instabilities in the main phenomenon parameters, which is a main problem during the implementation of a model in the system transient codes. To achieve a reasonable degree of accuracy in the evaluation of different condensation models, a simple code called CMTC was developed, to be able to compare some selected condensation correlations during accident conditions for a simple round tube geometry of a condenser apparatus. The code was considered suitable, after a limited assessment with some experimental results, to be used as a model tester and a tool to predict, in simple geometries and steady state conditions, the behaviour of a PCC-like passive system component, designed to be the main safety system for the new generation of SBWR plants.

- As a second step, the results above mentioned were compared with the results obtained for the same transient using the same models but implemented in a well know thermal-hydraulic system code, the RELAP5/Mod3.2 code. With this step the effect of the model implementation and, mostly, of the large differences in the code structure (much more complex and complete in the case of RELAP5 code) was investigated to evaluate the differences in the phenomenon description using the two different tools. The results showed a reasonable agreement in the phenomenon representation, and, then, the suitability of the CMTC code to be used as a pre-testing tool for a system thermal-hydraulic code to evaluate the suitability of different models to be implemented in the code itself. A further conclusion of this step is related to the limited assessment of the standard condensation model implemented in the code and of the other models tested. In general terms, the code, either with the standard model and with the other selected correlations, is capable to well predict the considered tests. From the results one can see that the better performances are achieved with the standard model for condensation, probably due also to some tuning of the correlation implementation done by the RELAP developers.
- Lastly, the different condensation models have been used to calculate some so called "maps" for the heat transfer coefficient in condensation and condenser efficiency, related to a PCC-like geometry under accident conditions. These maps represent, for each model considered, the expected response of the PCC component for different phases of a postulated loss of coolant accident, and give a general overview how the component behaves under different conditions. In this way it is easy to evaluate some critical combinations for parameters as pressure and air content in the condensing mixture, evaluation that, for a large range of parameters, it is not always easy. Particular importance have to be devoted to the efficiency maps, that give a summary of the capabilities of the PCC component to extract all the decay heat power generated in the core during the accident transient. These maps can show, in a univocal way, the regions where the operation of the safety component is optimal, when the efficiency is equal to 1, and all the power is condensed in the PCC. This is a fundamental issue for safety analyses, because through this analysis one can evaluate the conditions under which the containment conditions are kept controlled by the safety system. These maps show, for almost all the models, a good behaviour of the PCC component, which is capable to remove, for most of the cases analyzed, all the power for air contents less than 40% of the total flow incoming in the condenser. Unfortunately, large scatter of data are detected, and for some model unphysical behaviour is represented, such as large values of efficiency for air contents higher than 80%. The last comment about the results of this part of the work is related to the so called "driving condensation maps", diagrams where is shown which one of the heat transfer coefficients between primary and secondary side is controlling the condensation phenomenon. It is clear that, from engineering point of view, the optimal design of the PCC component is that where is always the primary side heat transfer coefficient which drives the condensation. In fact, comparing different designs of condenser components through the use of these maps, one can find the optimal configuration which use all the capabilities of condenser itself, that is the configuration where is the condensation heat transfer that drives the phenomenon. As previously said for the efficiency and heat transfer coefficient maps, for some models unphysical large values for heat transfer coefficient are calculated, and practically only the secondary side of the condenser drives the condensation phenomenon. This case is useless to understand the capabilities of the condenser itself, because all the component capabilities relies on the boiling heat transfer coefficient in the secondary side, whatever model and condenser configuration is chosen.

REFERENCES

1. M. Siddique, M.W. Golay, M.S. Kazimi: "Theoretical modelling of forced convection condensation of steam in a vertical tube in the presence of a non condensable gas", NURETH-5, Saratoga Springs, 1995
2. M.H. Kim, M.L. Corradini, "Modeling of Condensation heatTransfer in a Reactor Containment", Nuclear Engineering and Design, 118 (1990), pp. 193-212
3. J. Kuhn, P.F. Peterson, V.E. Schrock,: "Experimental Investigation of Downward Condensation in vertical Tubes with Noncondensable Gases", UCB Internal publication, September 1993
4. Carlson K.E., Riemke R.A., Rouhani S.Z., Shumway R.W., Weaver W.L.,1990b: "Relap5/Mod3 Code Manual - Volume II. User Guide and Input Requirements", NUREG/CR-5535
5. Trodeas, N. E., Kazimi, M. S. : "Nucler System I", Hemisphere, New York
6. M. Meier : " SBWR-PCCS Numerical Integration Program and Test Results ", TM-42-94-08/ALPHA 406, Paul Scherrer Institut Internal Report, July 1994.
7. Hewitt, G.F. : "Two Phase Flow in Vertical Pipes", Short Courses in Multiphase flow and Heat Transfer, Zurich, 1993
8. K. M. Vierow, K. E. Shrock: "Condensation in a natural Circulation Loop with Non condensable Gases. Part I - Heat Transfer", Paper presented at the International Conference on Multiphase Flows, Tsukuba, Japan (1991)
9. P. Coddington: "Comments on the analysis of single tube condensation experiments, and the development of the functional form of the heat transfer correlation", PSI Internal report, TM-42-93-07, (1993).
10. R.G. Gido, A. Koestel, " Containment Condensing Heat Transfer", Two Phase Flow and Heat Transfer, HDT-Vol. 197, ASME 1992
11. A. P. Colburn, O. A. Hougen: " Design of Cooler Condensers for Mixture of vapors with non condensing Gases", Industrial and Engineering Chem., Vol. 26, No. 11, 1934.

12. P.F. Peterson, V.E. Schrock, T. Kageyama: "Diffusion Layer Theory for turbulent vapor condensation with non-condensable gases", Two Phase Flow and Heat Transfer, HDT-Vol. 197, ASME 1992
13. V. Faluomi, S.N. Aksan : "Post Tests Calculations of PANDA S1-S6 Steady-State Tests with RELAP5/Mod3.2 Code', PSI internal Report, to appear (1998)
14. G. Th. Analytis, V. Faluomi " Assessment of Condensation Models for the use in the RELAP5/Mod3.2 thermal-hydraulic code ", PSI Internal report, to appear (1998).
15. The RELAP5 Development Team: "RELAP5/MOD3.2 Code Manual Volume IV: Models and correlations (Draft)", INEL, June 1995.
16. V. Faluomi, S.N. Aksan : "Post Tests Calculations of PANDA B Series of Steady-State Tests with RELAP5/Mod3.2 Code', PSI Internal Report, to appear (1998)
17. P.F. Peterson, V.E. Schrock, T. Kageyama: "Diffusion Layer modeling for condensation in vertical tubes with non-condensable gases", Nuclear Engineering and Design, 141 (1993), pp. 289-302

NEXT PAGE(S)
left BLANK



MODELLING CONTAINMENT PASSIVE SAFETY SYSTEMS IN ADVANCED WATER COOLED REACTORS

L.E. HERRANZ

Department of Nuclear Fission,
CIEMAT,
Madrid, Spain

M.H. ANDERSON, M.L. CORRADINI

Department of Nuclear Engineering,
University of Wisconsin,
Madison, Wisconsin,
United States of America

J.L. MUÑOZ-COBO

Department of Chemical and Nuclear Engineering,
Universidad Politecnica de Valencia,
Valencia, Spain

Abstract

Most designs of advanced passive reactors incorporate Passive Containment Cooling Systems (PCCS) relying on steam condensation to cope with possible pressure increase that would result in the case of a postulated accident. As a consequence, experimental and analytical research programmes have been launched worldwide to investigate new configurations and conditions involved in these new scenarios. This paper summarises the major outcomes of the joint research of CIEMAT, UPV, and UW in developing predictive models to address anticipated conditions in the Simplified Boiling Water Reactors (CIEMAT-UPV) and in the AP600 (CIEMAT-UW). Even though both models share some of their fundamental characteristics (such as being mass/heat transfer analogy based), samples of their validation against independent databases illustrate their intrinsic differences in formulation according to the scenarios addressed by each one. Relative importances of condensate film or gas mixture velocity are discussed, and the effect of key factors such as noncondensable gas presence and pressure are stated. Experimental data from University of Berkeley (UCB) and from University of Wisconsin - Madison (UW) will be used to support comparisons and discussions held in the paper. In short, this work demonstrates that heat/mass transfer analogy-based models, particularly those relying on diffusion film modelling to account for noncondensable gas presence, are extremely useful in test interpretation and result in good agreement with reliable databases.

1. INTRODUCTION

Nuclear Energy is one of the options presently available to cope with energy needs along the forthcoming century. This challenge is requiring a tremendous effort to assure nuclear energy competence in terms of economics and safety with respect to other potential sources of energy. In the case of water cooled power reactors, new advanced designs have been proposed of either an evolutionary or a passive type, the latter being particularly appealing for using natural forces to carry out safety functions under the most adverse conditions posed by hypothetical accidents. In this regard, containments of passive reactors are to be equipped with what has been called *Passive Containment Cooling System* (PCCS).

PCCS's features depend upon specific designs. However, most of them share their reliance on steam condensation to mitigate long term pressure rise in containments. New boundary conditions and device geometries prompted renewed interest to investigate steam condensation to eventually demonstrate PCCS's capability to meet their goal. As a result, experimental and analytical programmes were launched worldwide, often on the basis of a fruitful international co-operation.

In-containment condensation scenarios may be characterised, in general terms, by several key features:

- **Heterogeneous filmwise nature.** Steam entering the containment in a postulated accident can condense onto internal structures and surfaces. Even though it could occur in dropwise mode, at least for some time, a conservative approach assuming that condensed steam forms a film is usually taken.
- **Variable gas flow regimes.** Gas flow intensity varies with time during hypothetical accidents as well as with specific PCCS's designs, ranging from natural to forced convection and from laminar to turbulent regime.
- **Condensate film motion.** Condensate film on vertical or inclined surfaces experiences gravity force, so that a downward motion is expected to occur. In the case of horizontal surfaces facing down, droplet detachment is likely to happen.
- **Non-condensable gases presence.** In normal conditions containment atmosphere is usually composed of air or nitrogen which will be heated and influenced to some extent by the steam discharge into containment.
- **Hydrogen injection from primary circuit.** Hydrogen coming from different sources can enter containment during a postulated accident, consequently altering non-condensable gas mixture composition and flow fields.

This paper summarises the major results of the joint research of CIEMAT, UPV and UW in developing predictive models capable of simulating in-tube steam condensation under anticipated conditions in the *Simplified Boiling Water Reactor PCCS* (CIEMAT-UPV) and of reproducing on-plate condensation typical of AP600 PCCS (CIEMAT-UW). A sketch of both containment facilities and PCCS's are given in Figs 1 and 2.

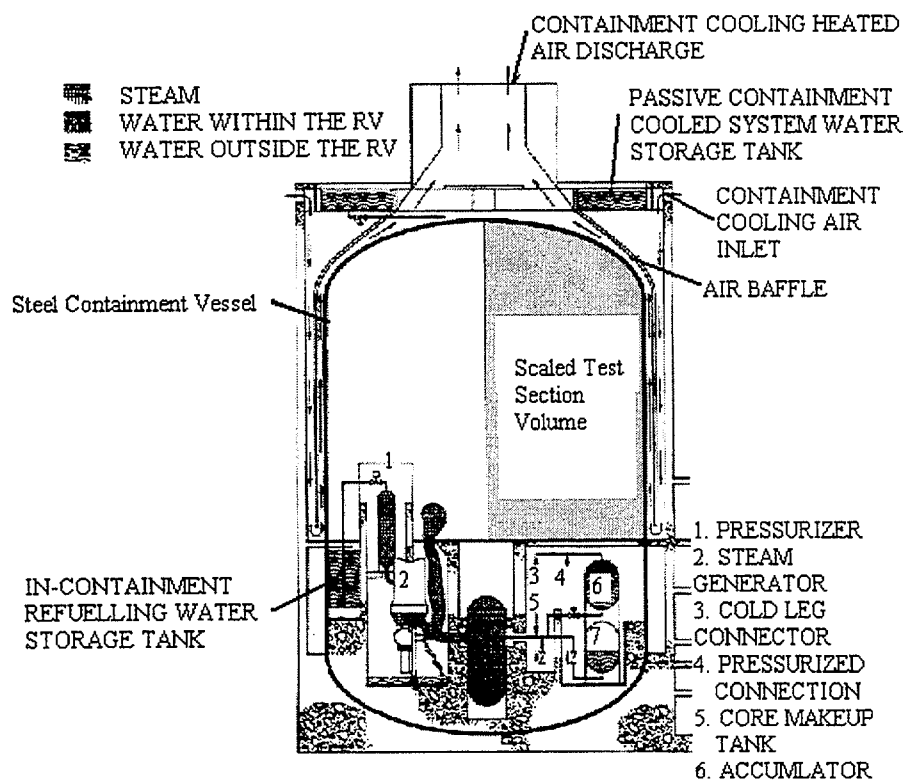


FIG. 1. Simplified Layouts of AP600 Containments.

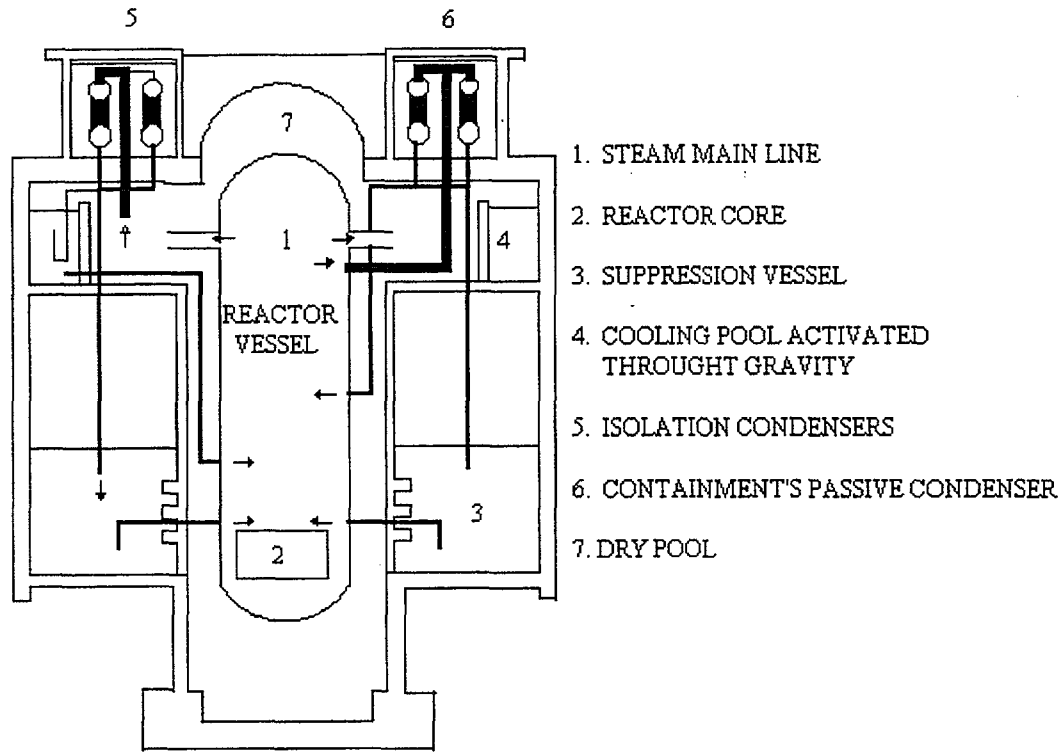


FIG. 2. Simplified Layouts of SBWR Containments.

2. MODELLING FUNDAMENTALS

A very detailed description of the SBWR and AP600 condensation models can be found in Refs. [1, 2]. Below the major common fundamentals as well as some specifics that will be discussed in next sections are summarised.

Newton's law of cooling gives the overall heat flux transferred from the gas mixture to the wall:

$$q_{\text{TOTAL}} = h_{\text{TOTAL}} (T_b - T_w) \quad (1)$$

where h_{TOTAL} is the total heat transfer coefficient and T_b and T_w are the gas bulk and wall surface temperatures, respectively. By assuming that the total thermal resistance is estimated as a combination in series of gas and liquid phases, neglecting radiative contribution to heat transmission, and, summing up the effects of condensation and convection, h_{TOTAL} may be expressed as:

$$h_{\text{TOTAL}} = \frac{k_{\text{film}} (h_{\text{conv}} + h_{\text{cond}})}{k_{\text{film}} + \delta (h_{\text{conv}} + h_{\text{cond}})} \quad (2)$$

so that the condensate thickness (δ), and h_{conv} and h_{cond} have to be determined to calculate the total heat transfer coefficient. The condensate film thickness is calculated by solving the momentum equation of both phases, whereas gaseous heat transfer coefficients are approximated by implementing a diffusion layer approach [3].

2.1. Condensate film thickness (SBWR)

As usually condensate thermal resistance does not have a substantial effect on the overall heat transfer scenario in the case of steam condensation onto plane surfaces, this section is focused on the specific solution of film thickness within vertical tubes (SBWR), where the film can play a more substantial role in the overall heat transfer scenario.

Assuming a heat balance at the interface between gas and condensate, it is found that the film thickness is related to the axial position in the tube (z) through a transcendental equation in which the circumferential mass condensation rate (Γ) is involved:

$$z = \frac{h_{fg}}{k_{film} \Delta T_{iw}} \int_0^\delta \frac{d\Gamma}{d\delta'} \delta' \quad (3)$$

To obtain Γ (directly proportional to the condensate downward velocity), the condensate momentum equation is solved, and the following expression for condensate velocity results:

$$u_z(y) = \frac{g}{2\mu_{film}} \left[ry - \frac{y^2}{2} + (r - \delta)^2 \ln\left(1 - \frac{y}{r}\right) \right] \left(\rho_{film} - \rho_m^* \right) - \frac{\tau_{li}}{\mu_{film}} (r - \delta) \ln\left(1 - \frac{y}{r}\right) \quad (4)$$

where it can be observed that u_z is, in turn, a function of the condensate thickness, so that an exact solution to determine δ would require an iteration process along with numerical techniques to solve integrals involved in the algorithm. Nonetheless, an approximate method based on successive inclusion of major influences, such as cylindrical geometry or interface tension, provided an accurate enough algorithm capable of estimating δ with errors less than 5% with respect to the exact solution [4]. The final equation may be written as:

$$\delta = \frac{1.259 \delta_{Nu}^{*4/3}}{\left[\delta_p A(x) + \ell_i B(x) + m_i \delta_p C(x) \right]^{1/3}} \quad (5)$$

where A , B and C are polynomials of δ_p which is the approximation of film thickness accounting for geometry but without considering interfacial tension; m_i and ℓ_i are functions depending on interfacial shear stress; and, finally, δ_{Nu}^* is the corrected Nusselt expression [5].

In addition to this plain mechanistic formulation, the condensate film thinning caused by waviness and droplet entrainment were also taken into account on a semi-empirical basis. Contrarily to waviness, which was shown to have a significant influence, droplet entrainment had a meaningless impact in the scenarios analysed.

2.2. Gas boundary layer approach (AP600)

As it has been stated above, the boundary layer approach provides expressions for h_{conv} and h_{cond} through Nusselt (Nu) and Sherwood (Sh) dimensionless numbers. Correlations for Nu are available in the literature for a number of conditions. In the case of anticipated accident conditions in the AP600 containment (turbulent natural convection), McAdams correlation seems particularly suitable given its independence of the characteristic length of the system:

$$Nu = 0.13 Gr^{1/3} Pr^{1/3} \quad (6)$$

By applying the heat/mass transfer analogy, Sh can be estimated by substituting the Prandtl nondimensional number (Pr) in Eqn. (6) by the Schmidt number (Sc).

Using Sh to estimate h_{cond} still requires that there exist a “condensation conductivity” that plays the same role as thermal conductivity in h_{conv} and Nu . Peterson’s approach to the diffusion layer theory together with corrections for high temperature differences between gas and wall (characteristic of the external cooling of AP600 containment walls), and high mass fluxes under condensation scenarios (suction effect) has been used to develop an expression of k_{cond} :

$$k_{cond} = \frac{CM_v h_{fg}^2 D}{R_{steam} T_i T_b} \Phi \Theta \quad (7)$$

where Θ is the suction factor and Φ is the ratio between the average molar fractions of steam and noncondensable gases in the boundary layer.

In the case of vertical tubes (SBWR) an additional factor considered was the enhancement of transport process while gas flow is developing. In addition, the suction factor formulae was particularised for the specific geometry and conditions according to the experimental investigation of Aggarwal et al. [6].

3. MODEL PERFORMANCE

Samples of both models validation (SBWR and AP600) against independent data bases show their responses to changes in primary variables, emphasising their consistency at the same time as illustrating intrinsic differences between both models according to the different scenarios addressed.

3.1. Global validation

The PCCS model of the SBWR has been validated against the database set up at the University of California - Berkeley [7]. In the table I the ranges of the major variables are given.

In Fig. 3 heat transfer coefficients calculated with the model (h_{HVTNC}) are compared to measurements. It can be observed that most of the points are within the $\pm 25\%$ band. Major deviations are located in the zone of lower heat transfer; namely, those points correspond to tube locations where only residual heat is to be transferred to tube walls, because most of it has been transmitted in the upper part, where gas flow is richer in steam, its velocity is higher, and the variables profile development enhance condensation heat transfer

TABLE I. RANGES OF MAJOR VARIABLES OF THE EXPERIMENTAL PROGRAMME AT UCB.

Variable	Range
Gas mass flowrate (kg/s)	$10^{-3} - 5 \cdot 10^{-3}$
Molar fraction of non-condensables (%)	0 – 14
Pressure (Pa)	$10^5 - 4.5 \cdot 10^5$
Gas Temperature (K)	343.15 – 423.15

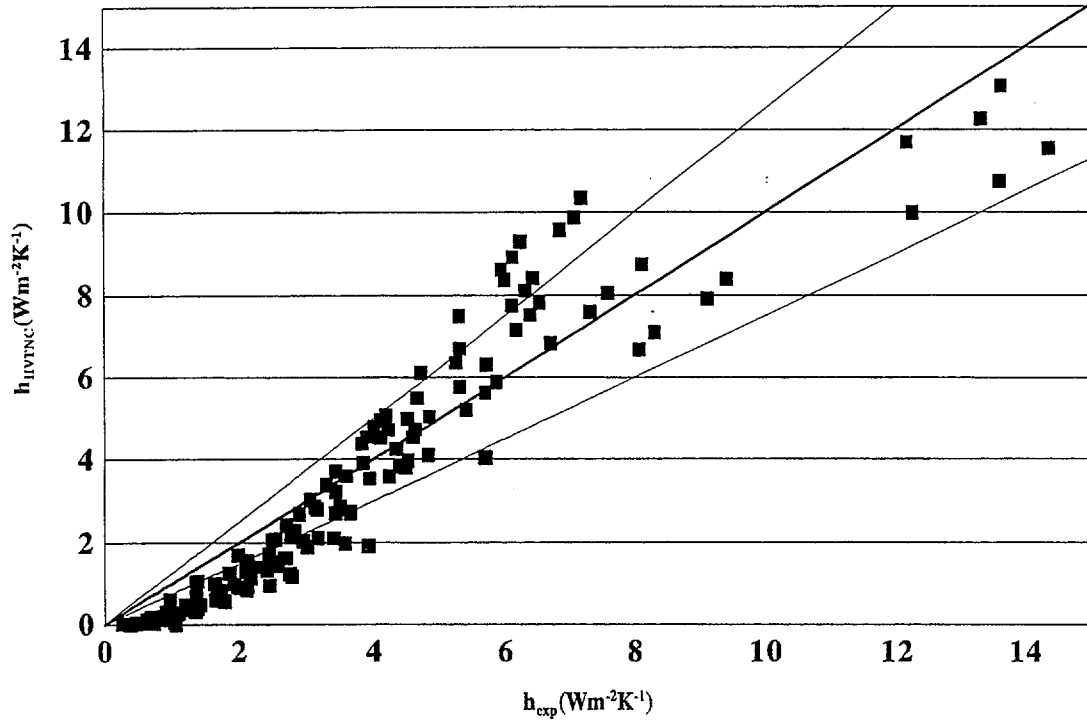


FIG. 3. Comparison of Theoretical Predictions with Data Recorded at UCB.

In the case of vertical tubes the major variables governing condensation heat transfer are non-condensable presence and gas flow regime. In Fig. 4 the similarity of model behaviour and measurements is noticeable, indicating the good qualitative and quantitative performance of the model with respect to these primary variables.

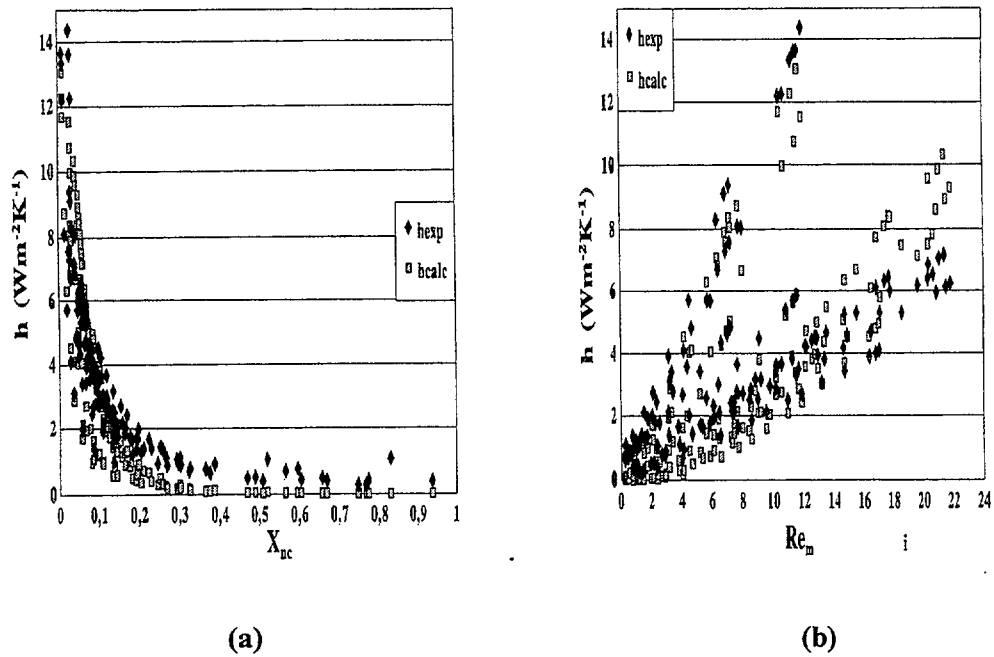


FIG. 4. Measurements and Predictions as a Function of Noncondensable Molar Fraction (UCB Database).

In order to illustrate the usefulness of this modelling approach in test interpretation, Fig. 5 shows two plots where estimates and data are compared (a) and predictions are split into its two components (i.e., h_{film} and h_{gas}) (b). This case is a low noncondensable concentration scenario, so that thermal resistance is mostly determined by condensate. However, this is not always the case as can be seen in Fig. 6 that corresponds to a high noncondensable test and, therefore, the thermal resistance across the gas boundary layer becomes higher than that of the liquid film. In both figures, heat transfer deterioration with z is observed.

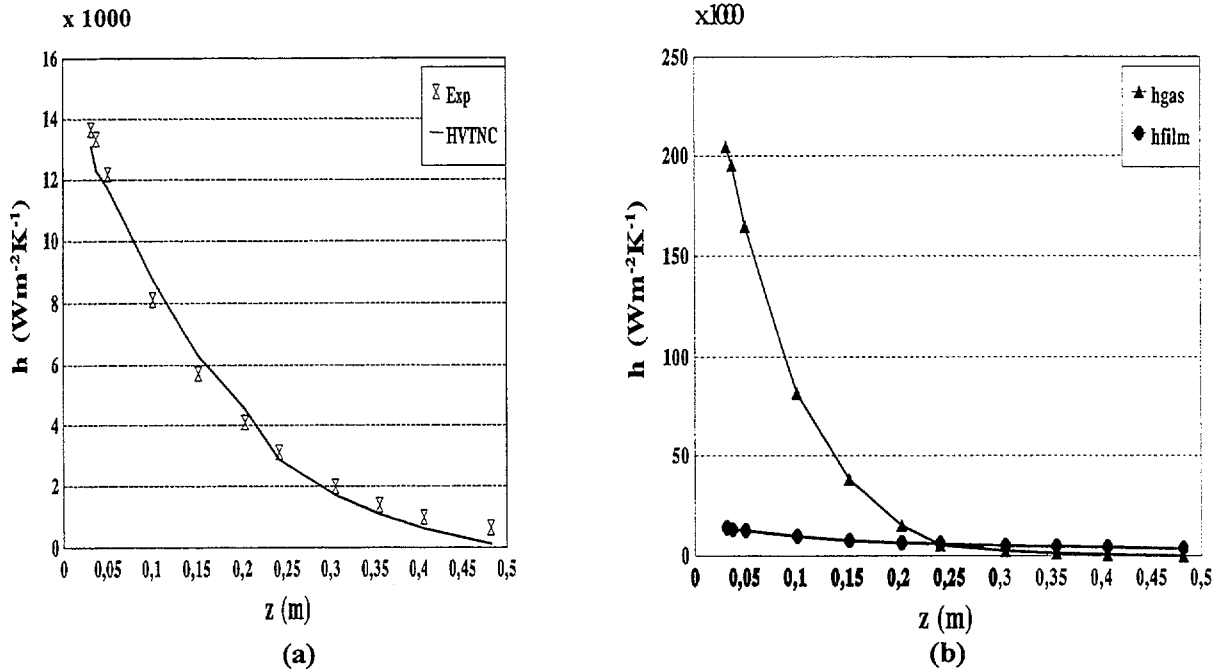


FIG. 5. Total and Partial Heat Transfer Coefficients for a Low Noncondensable Concentration Scenario (UCB Database).

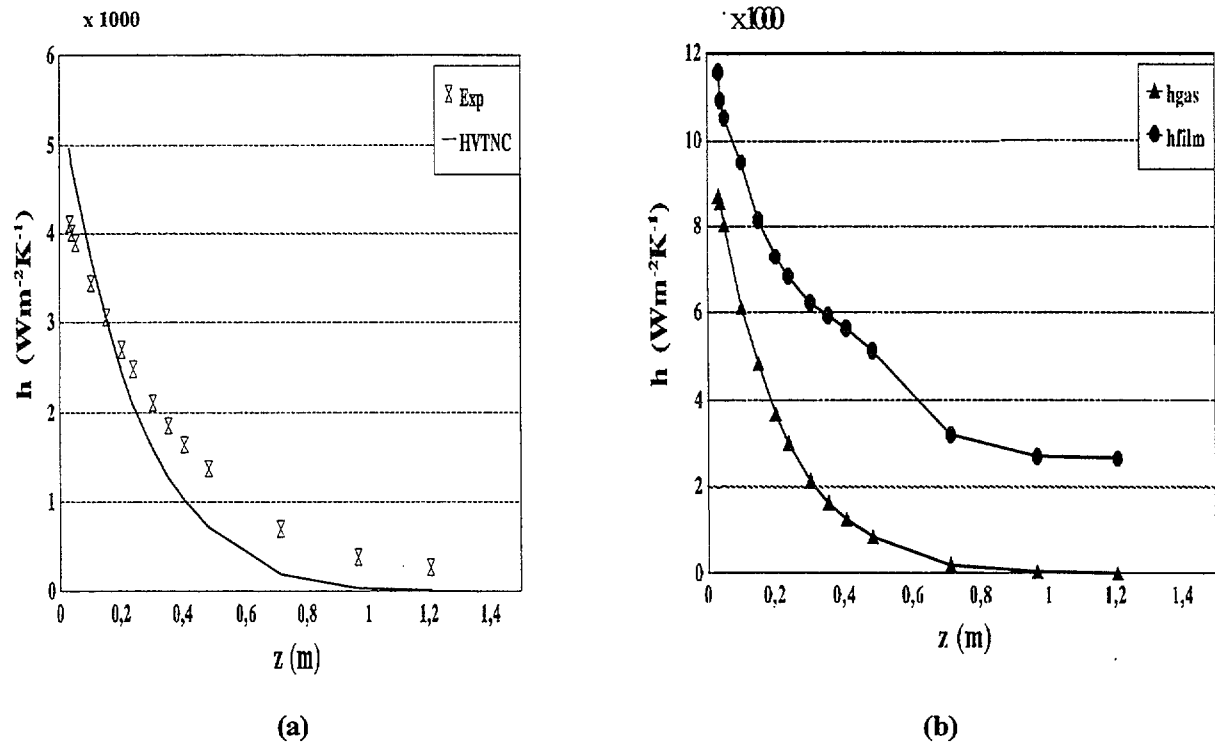


FIG. 6. Total and Partial Heat Transfer Coefficients for A High Noncondensable Concentration Scenario (UCB Database).

TABLE II. RANGES OF MAJOR VARIABLES OF THE EXPERIMENTAL PROGRAMME AT UW

Variable	Range
Molar fraction of helium (%)	0 - 30
Pressure (Pa)	$10^5 - 3.0 \cdot 10^5$
Wall temperature (K)	298.15 - 373.15
Gas Temperature (K)	233.15 - 393.15

The PCCS model of the AP600 has been validated against UW database [8]. The conditions covered by this experimental programme are given in Table II.

In Fig. 7 the comparison between measurements and predictions in terms of heat transfer coefficient is shown. As observed, most of the points are within the $\pm 15\%$ band. In addition, Dehbi's correlation results have been included [9]. Generally speaking, the model accuracy is better than Dehbi's correlations, particularly for those points out of the experimental conditions where the correlation was derived from (pressure higher than 1.5 bar).

Finally, the influence of pressure on heat transfer coefficient was shown to be well reproduced by the model (Fig. 8). Furthermore, by algebraic manipulation it has been demonstrated that the actual pressure effect is rather moderate, most of its influence being linked to variation in gas composition (pressure rise comes from steam injection).

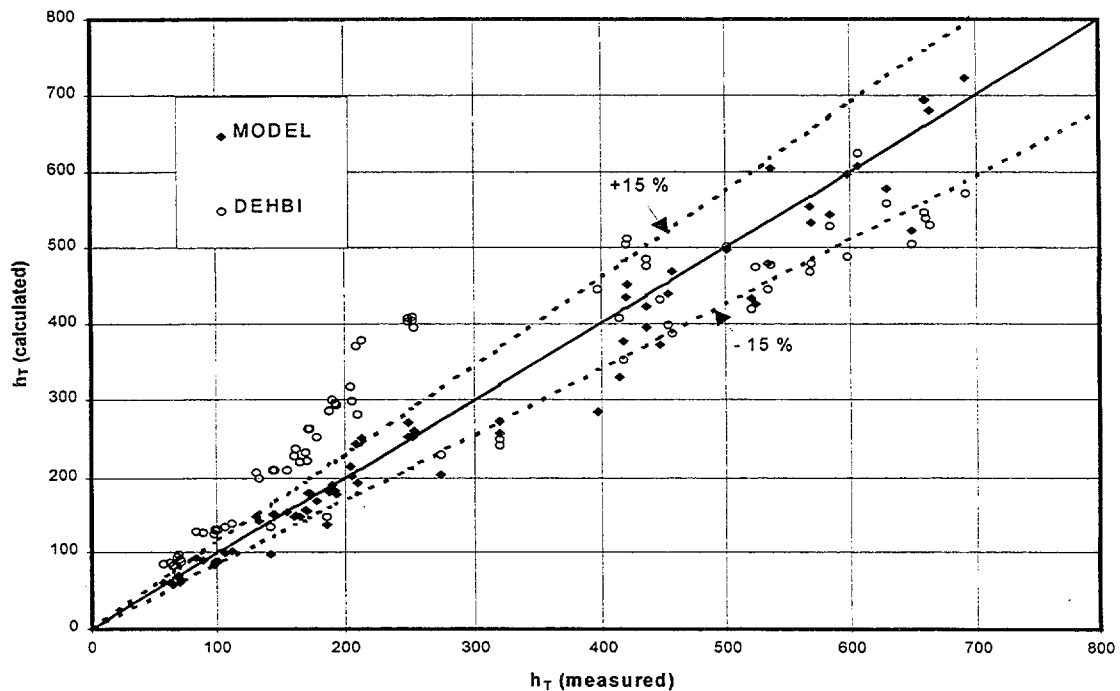


FIG. 7. Comparison of Theoretical Predictions with Data Recorded at UW.

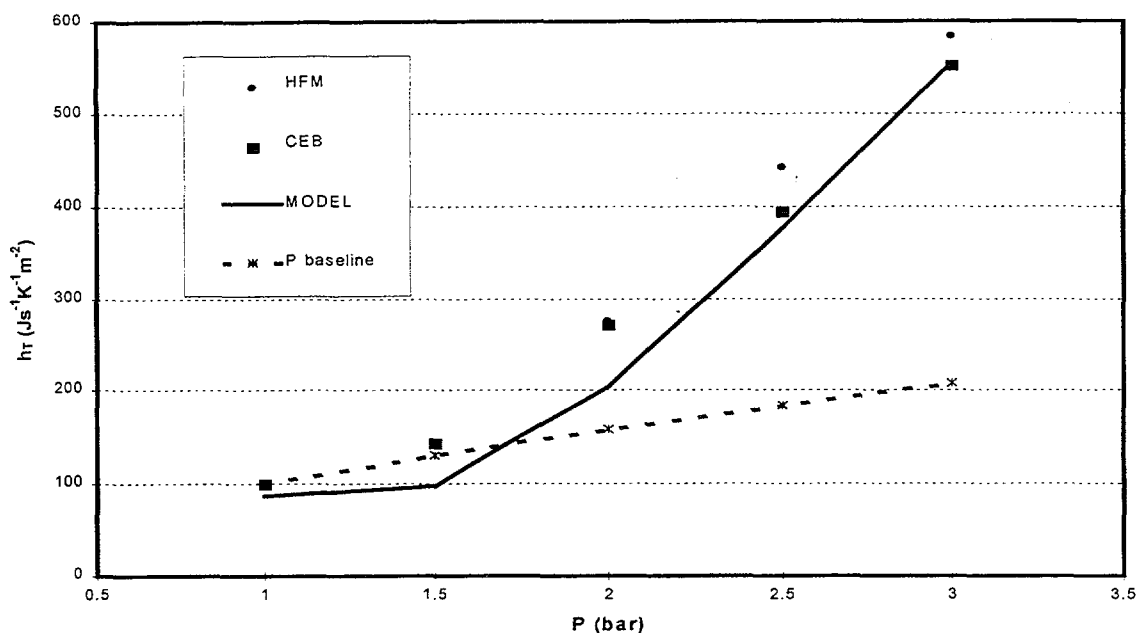


FIG. 8. Pressure Effect on Heat Transfer Coefficient (UW Database).

4. SUMMARY AND FINAL REMARKS

The new condensation scenarios foreseen in case of hypothetical accidents due to the new Passive Containment Cooling Systems used by some new advanced reactors, have renewed the interest on condensation research. The major goal of this investigation is to demonstrate that these systems, in accordance with their anticipated capabilities, can cope with containment overpressure threat at long term. In this paper two models addressing possible conditions in SBWR and AP600 containments are briefly presented and samples of their validation have been given along with specific interpretation of the effect of primary variables. The qualitative and quantitative accuracy of the model is considered good as compared with representative databases, pointing out the suitability of the modelling approach followed in each case. Therefore, a Nusselt type formulation of the condensate film resistance properly modified according to major forces involved in the system, and heat/mass transfer analogy combined with diffusion layer theory to account for thermal resistance across the gaseous boundary layer are considered valuable fundamentals to develop predictive tools capable of estimating heat transfer under conditions posed by these new scenarios.

ACKNOWLEDGEMENTS

The authors gratefully acknowledge CIEMAT, Polytechnical University of Valencia and University of Wisconsin – Madison for their logistic support, without which this work would not have been possible.

REFERENCES

- [1] HERRANZ, L.E. et al., "Heat transfer modeling in the vertical tubes of the passive containment cooling systems of the simplified boiling water reactor", *Nuclear Engineering and Design* 178 (1997), 29-44.
- [2] HERRANZ, L.E. et al., "A diffusion layer model for steam condensation within the AP600 containment", accepted for publication in *Nuclear Engineering and Design* (1998).

- [3] PETERSON, P.F. et al., "Diffusion layer theory for turbulent vapor condensation with noncondensable gases", HTD-197, Two-Phase Flow and Heat Transfer, ASME (1992), 181-188.
- [4] HERRANZ L.E., "Desarrollo y validación de modelos avanzados de transmisión de calor en los condensadores de refrigeración pasiva de la contención SBWR, PhD Thesis (1996), Polytechnical University of Madrid.
- [5] COLLIER J.G., THOME J.R., Convective boiling and condensation, Ch. 10, Oxford Science, London (1994).
- [6] AGGARWAL, J.K., HOLLINGSWORTH, M.A., "Heat transfer for turbulent flow with suction in a porous tube", Journal of Heat Mass Transfer 16 (1973), 591-609.
- [7] VIEROW, K.M., "Behavior of steam-air systems in cocurrent vertical downflow", M.S. Thesis (1990), University of California (Berkeley).
- [8] ANDERSON M.H. et al., "Experimental analysis of heat transfer within the AP600 containment under postulated accident conditions", accepted for publication in Nuclear Engineering and Design (1998).
- [9] DEHBI A.A. et al., "Condensation experiments in steam-air and steam-air-helium mixtures under turbulent natural convection", National Heat Transfer Conference, AIChE Symposium Series (1991), 19-28.

**DATA AND MODELS FOR CRITICAL HEAT FLUX (CHF) AND
POST-CHF HEAT TRANSFER**

(Session 2)

Chairman

P. Kirillov
Russian Federation

**NEXT PAGE(S)
left BLANK**

EXPERIMENTS ON CRITICAL HEAT FLUX FOR CAREM REACTOR

C.M. MAZUFRI
Nuclear Engineering Division,
Investigacion Aplicada SE (INVAP),
San Carlos de Bariloche, Argentina



XA0055007

Abstract

The prediction of critical heat flux (CHF) in rod bundles of light water reactors is basically performed with the aid of empirical correlations derived from experimental data. Many CHF correlations have been proposed and are widely used in the analysis of the thermal margin during normal operation, transient, and accident conditions. Correlations found in the open literature are not sufficiently verified for the thermal-hydraulic conditions that appear in the CAREM core under normal operation: high pressure, low flow, and low qualities. To compensate this deficiency, an experimental investigation on CHF in such thermal-hydraulic conditions is being carried out. The experiments have been performed in the Institute of Physics and Power Engineering of Russian Federation. A short description of facilities, details of the experimental program and some trends in the preliminary results obtained are presented in this work.

1. INTRODUCTION

The CAREM nuclear power plant design [1] is based on a light water reactor, selfpressurized, using several once-through steam generators. The mass flow of the coolant on the primary circuit is achieved by natural circulation. The primary system concept is of the integrated type, where the core, steam generators, and the steam dome are allocated inside the pressure vessel. The fuel element design for CAREM core is of the hexagonal type. The thermal-hydraulic parameters of the core in normal operation are:

<i>Pressure</i>	12.25	MPa
<i>Mass Flux</i>	540	kg/m ² /seg
<i>Inlet Temperature</i>	284	C
<i>Outlet Temperature</i>	326	C

Considering the concept of the reactor, one of the main points to be studied is the core behaviour and its thermal margin to critical phenomenon like the critical heat flux, under normal operation and transients. Typically, in PWR and BWR type reactors the prediction of CHF is made through correlations, developed "ad hoc" for the geometry of the fuel element and for a narrow range of thermal hydraulic conditions. Taking into account that the mass flow rate in the core of the CAREM reactor is rather low than typical light water reactors, due to the natural circulation cooling, most of these correlations must be verified in that range before used. Unfortunately, not many experimental data are available in that range to carry out the verification.

To compensate this deficiency, an experimental investigation on CBF for the particular thermalhydraulic conditions and fuel element geometry of CAREM reactor is being carried out. The main goal of the experimental program is to generate a substantial database to develop

a prediction methodology for CHF that would be applicable to the CAREM core, covering a wide range of thermal-hydraulic parameters around the point of normal operation, i.e.:

<i>Pressure</i>	10-13	MPa
<i>Mass Flux</i>	200-700	kg/m ² /seg
<i>Quality</i>	-0.15 to 0.15	-

In order to minimize the cost of the program, most of the tests were performed using Freon as coolant in a low-pressure thermal-hydraulic facility. These results are extrapolated to water conditions through scaling models. A small quantity of tests in a narrow range was performed using water as coolant in a high-pressure loop facility to verify the scaling model of extrapolation.

The experiments were performed in the thermal-hydraulic facilities of the Institute of Physics and Power Engineering of Russian Federation.

In the present paper a description of the Freon and Water facilities are presented, some details on the design of the experimental program and trends in the preliminary evaluation of the results are also presented.

2. FACILITY DESCRIPTIONS

2.1. Freon test facility-STF

The STF (Freon Thermal-physical Facility "STEND" in Russian) is a loop that involves the following elements: two canned pumps, a preheater, two test channels, six heat exchangers (coolers), an air separator and two Freon tanks. Figure 1 shows a diagram of the facility. The piping, like all other elements of primary circuit, is made of stainless steel tubes of an internal diameter of 50 mm. The designed pressure of the facility is 5.0 MPa.

The pumps can operate either in parallel, in series or independently one from each other. The flow rate is 20 m³/hr each, and the pressure head is of 1.0 MPa. The pumps also provide a sufficiently high head (0.8 MPa) even with a flow of up to 30 m³/hr.

The preheater is manufactured as an electrically heated tube. Its electrical power is 160 kW and in case this power is not enough, hot water from an external circuit is supplied to the secondary side in two heat exchangers. Alternately, if lower temperatures are required, cool water is supplied.

Two places for different test channels are available: one of the channels can be under preparation for testing, whereas the second one is used in tests. The maximum height of test channels is approximately 8 m.

Freon tanks are placed below the level of the test loop and test channel, providing the coolant discharge at the pre-testing stage. These reservoirs are also used as steam pressurizers during the tests, where electrical heaters are located. They are also provided with an exterior annular chamber where hot or cold water can be supplied. The electrical heaters are mainly used to keep the pressure in the loop at the prescribed level, while the hot or cold water fed to the annular chamber provides fast filling of the loop either with coolant or its discharge. The capacity of each reservoir is 0.25 m³.

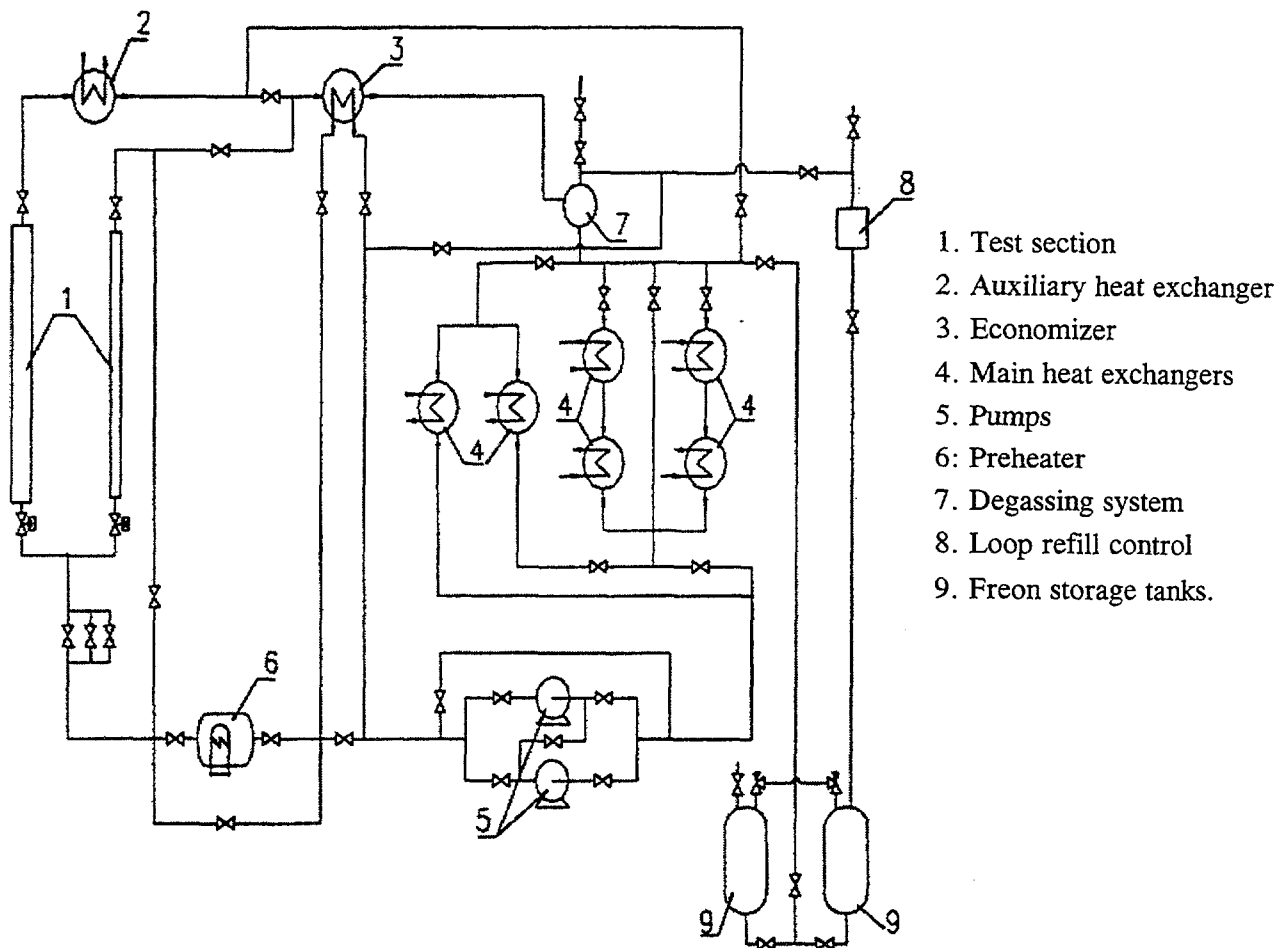


FIG. 1. Scheme of STF Facility.

The power supply of the test channel is provided by a direct current generator of an electric capacity of 540 kW (equivalent to 8 MW for water) driven by a synchronically motor. The power can be changed smoothly from zero to the maximum value (0-6000 A, 0-90V).

To measure the most important parameters of the tests (inlet and outlet temperatures, flow rate, pressure, pressure drop, etc.) two independent devices are used. Usually, the number of measurements used in experiments of critical heat flux, in bundles with 19-25 rods, is approximately 120 to 150. Among them 50-100 are for temperature of rods, and several dozens for electric power, coolant temperatures, pressure and pressure drop measurements. The sampling time of all 150 measurements is about 0.1 sec.

A summary of the main parameters of this facility is presented in the Table I.

2.2. Water test facility W-200

The W-200 facility (Water, 200 bar of pressure) consists of several loops for different purposes (different pressures, different flow rate). In Figure 2 a diagram of the facility is presented. The main loop includes the following elements: main pumps, two high pressure injections pumps, a preheater, two boxes for test channels, twelve heat exchangers (coolers) and three pressurizers. The piping and all other elements of the primary circuit are made of stainless steel. The tube's diameter of main loop is 50 mm. Maximum height of test section is 11 m.

This facility includes several auxiliary systems: high-pressure nitrogen system (for pressurization and for pressure equalization in test section to prevent deformation of heated elements) distilled water supply, electrical power supply and data acquisition system.

TABLE I. MAIN PARAMETERS OF STF FACILITY

<i>Pressure</i>	Up to 5.0 MPa (25.0 MPa for water)
<i>Coolant temperature</i>	Up to 120 C
<i>Maximum Flow rate</i>	40 m ³ /hr
<i>Pump pressure head</i>	2.0 MPa (Max.)
<i>Test section power</i>	540 MW. DC current (8 MW for water)
<i>Test section height</i>	Up to 8 m
<i>Data acquisition system</i>	150 channel. 1.5 Hz

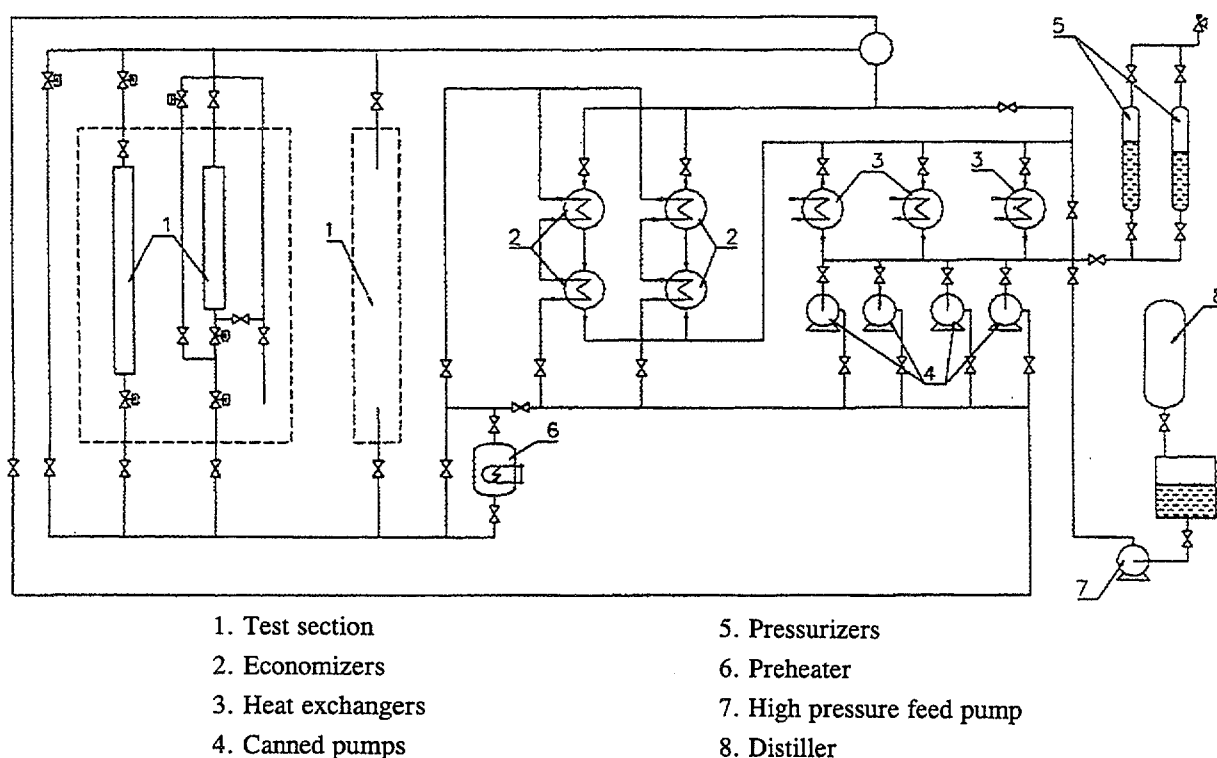


FIG. 2. Scheme of W-200 Facility.

An alternate current from two induction regulators in high voltage level and 20 transformers in low voltage circuit provides the power supply of the test channels. The maximum power is 2 MW.

The preheater is manufactured as electrically heated tubes. Its electrical power is 500 kW.

Two main rotor canned high-pressure (250 bar) pumps can provide 10 m³/hr each, and a pressure head of 2.0 MPa. The low-pressure pump (10 bar) provides up to 15 m³/hr.

The W-200 facility is used to study CHF in high and low-pressure regions, hydraulics water hammer phenomenon and heat transfer under accident condition.

A summary of the main parameters of the water is presented in Table II.

TABLE II. MAIN PARAMETERS OF W-200 FACILITY

<i>Pressure</i>	Up to 20 MPa
<i>Coolant temperature</i>	Up to 370 C
<i>Maximum Flow rate</i>	30 m ³ /hr
<i>Pumps pressure head</i>	2 MPa (max.)
<i>Test section power</i>	2 MWatt (max.)
<i>Test section height</i>	UP to 11 m
<i>Data acquisition system</i>	150 channel 1.5 kHz

3. TEST SECTION DESCRIPTION

The test section consists of a bundle of nineteen rods located in a test channel having hexagonal cross section. The same test channel is used in both facilities. Details of the test channel are presented in Figure 3.

Indirectly electrically heated rods simulators were used in the bundle in the Freon facility while direct electrically heated rods were used for the water facility. These simulators were designed to produce uniform axial heat flux. To detect the CHF occurrence, more than 70 thermocouples were located inside the cladding of simulators at the end of the bundle.

4. DETAILS OF THE EXPERIMENTAL PROGRAM

The main goal of all CHF tests is to obtain the critical phenomena reproducing the same thermal-hydraulic conditions that will occur in every core region. It implies to relate the CHF value obtained under local parameters, in an axial position of a test section to the heat flux in the same position of a real fuel assembly located in the core. Some characteristics of the fuel assembly seem to influence the value of the CHF and must be studied: the presence of unheated rods in the fuel bundle, the non-uniformity in the heat flux and the grid spacers. Beside, there is a fact that in pressurized reactors the quality is negative in the high heat fluxes region, so CHF values for subcooled liquid are necessary.

The best way to analyze the influence of such characteristics is to carry out experiments studying the separate effect of each using a case as reference. The reference case was a test section with 19 rods, with uniform axial and radial heating, using the geometry characteristic of the CAREM fuel assembly, 9-mm rod diameter, 13.8 mm of pitch and 1.4 m of heated length.

Considering that for qualities below 0.15 the local condition hypothesis is valid, it is not necessary to study the influence of non-uniformity in the axial heat flux.

On the other hand, in case of radial non-uniform heat flux, the mixing efficiency between subchannels must be studied. To cover this effect, tests using a bundle with 19 heated rods, where the seven central rods have 15% of power higher than the bundle average, were performed.

To cover the effect of non-heated rods in the CHF, tests using a bundle with 17 heated rods and 2 unheated rods were performed.

A rhomboidal cell grid spacer type was used in all of these tests. The study of the influence of grid spacers over the CHF was not included in this stage of the program.

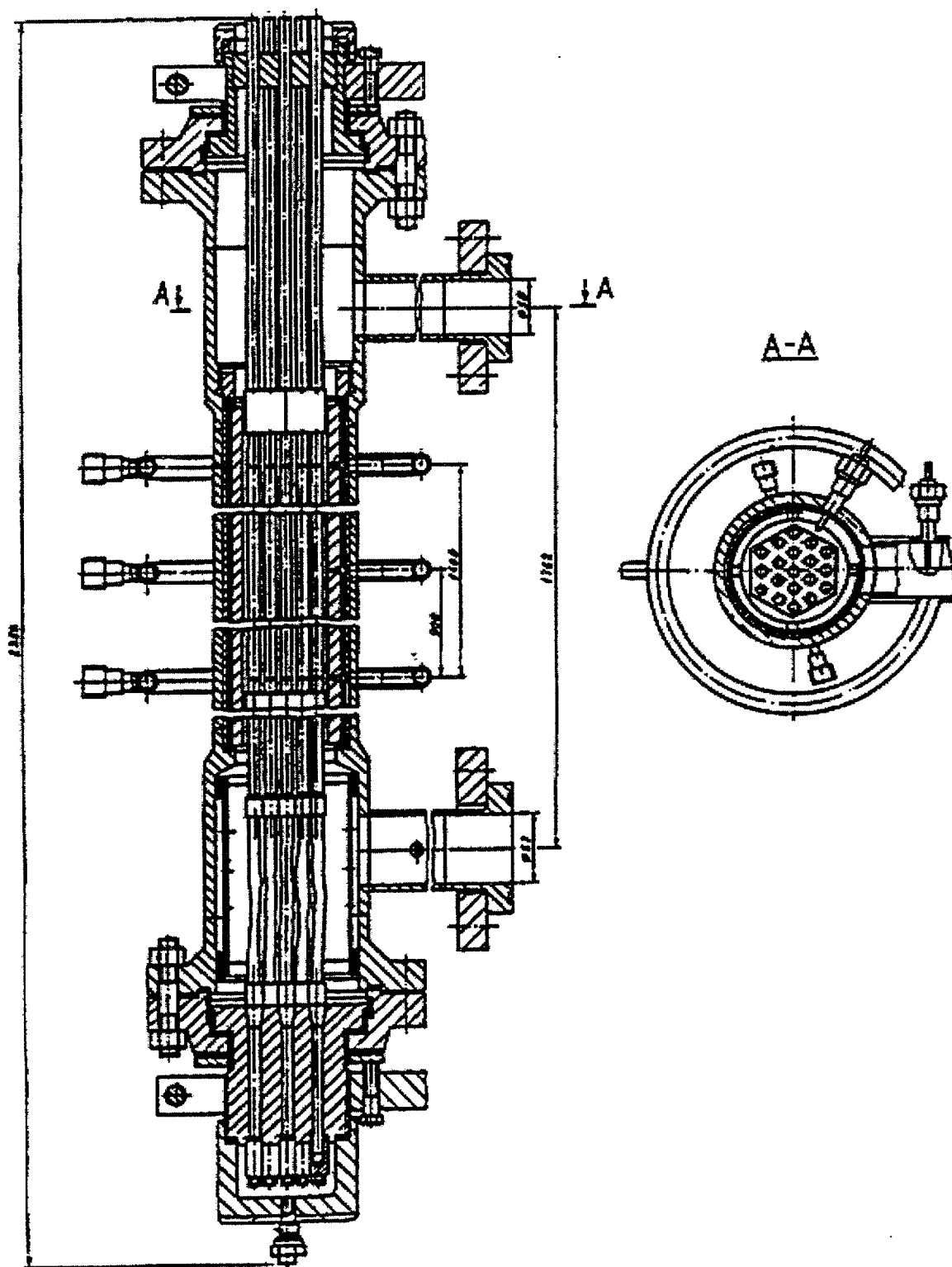


FIG. 3. Test Channel with the 19 Rod Bundle Simulator.

In order to verify the range of outlet qualities that can be obtained with the reference test section under different conditions, preliminary theoretical analyses were performed.

Estimations using typical correlations like EPRI [2], for a heated length of 1.4 m, nominal flow rate and pressure of the CAREM core, show that even under the lowest inlet temperature that can be possibly reached in the loop, the CHF phenomena appears near to the region of positive qualities. It means the requirements to reach negative qualities is not achieved with a test section of only one length. Table III shows these results.

TABLE III. ESTIMATION OF CHF USING A HEATED LENGTH 1.4 m

P	G	T	POW _{EPRI}	X _{EPRI}
MPa	Kg/m ² /s	C	kW	
12.25	540	40	77.6	-0.031
12.25	540	140	63.1	0.119
12.25	540	240	47.6	0.280
12.25	540	284	40.1	0.358
12.25	540	300	37.0	0.391

P- pressure; G-mass flow rate; T-inlet temperature; Pow-power per rod, X-equilibrium mass quality at CHF point

As can be seen, in order to obtain the data in subcooled region $X = -0.15 - 0.0$ it is necessary to reach CHF phenomena in shorter lengths. The simplest way was to use the shorter rod bundle. Preliminary calculations showed that to get CHF with negative qualities using lower inlet temperatures as 50 - 100 C in water, it was necessary to decrease the heated length of the bundle to 0.7 - 1.0 m.

Considering the use of Freon as a coolant, the length of the test section was reduced to 0.5 m, because the minimum lower inlet temperature in the loop that can be reached in normal condition is 25 C, corresponding to 200 C for water. The results of this preliminary estimation are presented in Table IV.

As result of these considerations and analysis, the experimental program was planned. A summary of the performed tests is given in the following sections.

TABLE IV. ESTIMATION OF CHF USING A HEATED LENGTH 0.5m

P	G	T	POW _{EPRI}	X _{EPRI}
MPa	Kg/m ² /s	C	kW	
12.25	540	40	43.9	-0.50
12.25	540	140	35.8	-0.27
12.25	540	240	27.0	-0.01
12.25	540	284	22.8	0.11
12.25	540	300	21.0	0.16

P- pressure; G-mass flow rate; T-inlet temperature; Pow-power per rod, X-equilibrium mass quality at CHF point

4.1. CHF EXPERIMENTS IN FREON TEST FACILITY

The major part of the tests has been carried out in this facility. Freon facility was used within the range of operating parameters meeting the same thermal-hydraulic parameters for CAREM core in water, that is:

<i>Pressure</i>	1.6 - 2.2	MPa
<i>Mass Flux</i>	170 - 600	kg/m ² /s
<i>Inlet Temp.</i>	19 - 57	C

An appropriate distribution of the experimental points was adopted to obtain a correlation covering the range previously specified.

Four bundle configurations have been tested in this facility:

Bundle Configuration No. 1

Tests using a bundle with 19 heated rods, heating length of 1.4 m, uniform radial power distribution and the same quantity, and axial position of grid spacers used in the full scale CAREM fuel element, were performed.

More than 100 CHF points, under different conditions within the range of operating parameters meeting the required thermal-hydraulic parameters for CAREM core in water, were obtained.

Bundle Configuration No. 2

Tests using a bundle similar to bundle No. 1, but with non-uniform radial power distribution to study the mixing effect were performed.

More than 25 CHF points, under different conditions within a reduced range of operating parameters meeting the required thermal-hydraulic parameters for CAREM core in water, were obtained.

Bundle Configuration No. 3

Tests using a bundle with 17 heated rods and 2 unheated rods, heated length of 1.4 m, uniform radial power distribution and the same quantity, type and axial position of grid spacers used in the full-scale CAREM fuel element were performed to study the effect of unheated rods on CHF.

More than 40 CHF points, under different conditions in a reduced range of operating parameters meeting the required thermal-hydraulic parameters for CAREM core in water, were obtained.

Bundle Configuration No. 4

Tests using a bundle with 19 heated rods, heating length of 0.5 m, uniform power distribution and the same type of grid spacer used in the full-scale CAREM fuel element were made to obtain critical heat flux condition with negative local thermodynamic qualities.

More than 100 CHF points under different conditions within the range of operating parameters meeting the required thermal-hydraulic parameters for CAREM core in water were obtained during these tests.

4.2. CHF EXPERIMENTS PERFORMED IN WATER TEST FACILITY

The purpose is to verify the methodology of modeling the conversion factors from Freon conditions to water conditions. The investigations were performed using the bundle configuration No.1 previously used in the Freon facility but using directly heated rods due to the high powers involved.

The tests were carried out within a limited range of thermal-hydraulic parameters using water with pressures up to 13 MPa. More than 25 different points were obtained in these tests.

5. EXPERIMENTAL RESULTS AND DISCUSSION

In this section an evaluation of preliminary results obtained in the Freon loop with bundle No. 1 for the range of positives outlet qualities is presented. Such evaluation is made using a one-dimensional model to obtain the local thermal-hydraulic parameters and two typical methods to predict the CHF: EPRI correlation and CHF Look-up Table [3].

EPRI correlation was derived under the hypothesis of constant inlet condition and uses the "Critical Power Ratio" (CPR) as the figure of merit to predict the power at the CHF point [4]. The Look up table is a methodology that uses as figure of merit the "Departure to nucleate boiling ratio" to predict the CHF. So no direct comparison could be made between them.

Using the method presented in [5] it is possible to use the Look up Table to obtain the "critical power ratio".

In Figure 4, a histogram showing the capability of prediction of EPRI correlation is showed. As can be seen the mean value is a little greater than unity but the standard deviation is acceptably low (approximately less than 10 %)

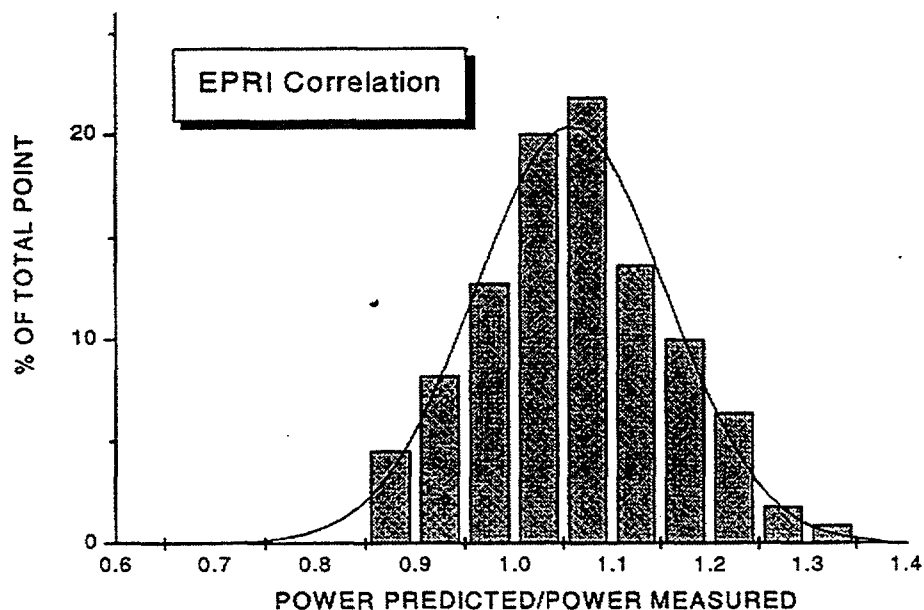


FIG. 4. EPRI Correlation Prediction.

In Figure 5 the same evaluation using the Look up table to get the CPR value is showed. In this case the correction factors used were developed especially for the geometry of a CAREM fuel element and adjusted with experimental data from VVER CHF experiments [6]. The result shows a mean value close to the unit and a standard deviation smaller than EPRI correlation.

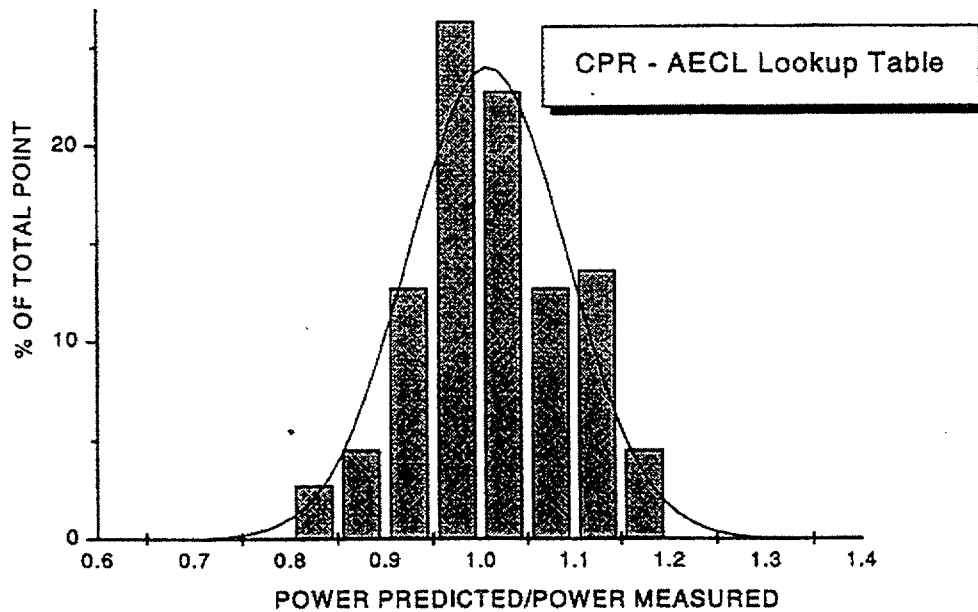


FIG. 5. AECL Look Up Table Correlation using CPR Figure.

Figure 6 shows the prediction of the Look-up table using the figure of DNBR. As can be seen, the mean value is very near to the unit and the standard deviation has an acceptable value according to the figure of DNBR.

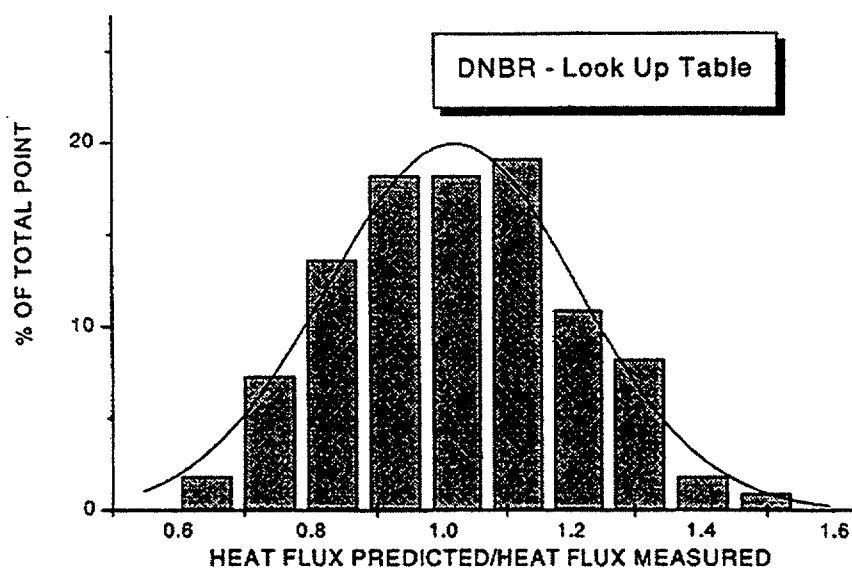


FIG. 6. AECL Look Up Table Correlation Using DNBR Figure.

6. CONCLUSIONS

The experimental program developed to build a database to study the CHF phenomena in the thermal-hydraulic range foreseen in the CAREM core has been presented. Tests at high-pressure, low flows and low qualities, where experimental data are scarce or non-existent have been performed. More than 250 experimental points under different conditions in the Freon loop and more than 25 point in the water loop were obtained in this program.

Different types of test sections were assembled to simulate different geometric regions in the fuel element as well as radial uniform and non-uniform power generations were tested to study the mixing effect in the bundle. Besides this, and to obtain CHF data under average subcooled conditions, a bundle with 35 % of the full length of fuel element was tested.

The preliminary results from Freon loop show that correlations like EPRI present a good agreement, but the mean value is greater than the unity. The Look up Table, with adequate correction factors, shows better prediction and a mean value close to the unity. These results are being verified with the results obtained in the water loop in order to check the scaling model applies.

In the future, additional tests will be carried out to study the influence of different grid spacer designs and the distance between them and the CHF point.

REFERENCES

- [1] ABATTE, P. M.; MAZUFRI, C. M.; "Aspectos Termohidraulicos en el diseno del Reactor CAREM 25", 9th Brazilian Meeting on Reactor Physics and Thermal-hydraulics', Caxambu, Brazil (1993).
- [2] FIGHETTI, C. F.; REDDY, D. G.; "Parametric Study of CHF Data, Volume 2: A Generalized Subchannel CHF Correlation for PWR and BWR Fuel Assembly". Report EPRI NP-2609, Columbia University, New York, (1983).
- [3] GROENEVELD, D. C. et al; "1986 AECL-UO Critical Heat Flux Lookup Table", Heat transfer Engineering, vol. 7, nos. 1-2 (1986).
- [4] NISSLEY, M. E. et al; "Considerations for Comparing CHF correlations", 2nd International Topical Meeting on Nuclear Power Plant Thermal-Hydraulic and Operations. (1986).
- [5] LELLOUCHE, G. S.; "The boiling transition: analysis and data comparisons", Nuclear Engineering and Design; 116 pages 117-133 (1989).
- [6] DUBROVSKY, I. S. et al.; "Investigations of critical heat fluxes in rod bundles at stationary and non-stationary heat transfer conditions", Teplofizika-74, Proc. of Seminar of Countries-Members of SEV, Moscow, 1974.

NEXT PAGE(S)
left BLANK

ENHANCING THE MODERATOR EFFECTIVENESS AS A HEAT SINK DURING LOSS OF COOLANT ACCIDENTS IN CANDU-PHW REACTORS USING GLASS-PEENED SURFACES

T. NITHEANANDAN, R.W. TIEDE, D.B. SANDERSON
Whiteshell Laboratories,
Atomic Energy of Canada Ltd,
Pinawa, Manitoba



R.W.L. FONG, C.E. COLEMAN
Chalk River Laboratories,
Atomic Energy of Canada Ltd,
Chalk River, Ontario

Canada

Abstract

The horizontal fuel channel concept is a distinguishing feature of the CANDU®-PHW reactor. Each fuel channel consists of a Zr-2.5Nb pressure tube and a Zircaloy-2 calandria tube, separated by a gas filled annulus. The calandria tube is surrounded by heavy-water moderator that also provides a backup heat sink for the reactor core. This heat sink (about 10 mm away from the hot pressure tube) ensures adequate cooling of fuel in the unlikely event of a loss-of-coolant accident (LOCA). One of the ways of enhancing the use of the moderator as a heat sink is to improve the heat-transfer characteristics between the calandria tube and the moderator. This enhancement can be achieved through surface modifications to the calandria tube which have been shown to increase the tube's critical heat flux (CHF) value. An increase in CHF could be used to reduce moderator subcooling requirements for CANDU fuel channels or increase the margin to dryout.

A series of experiments was conducted to assess the benefits provided by glass-peening the outside surface of calandria tubes for postulated LOCA conditions. In particular, the ability to increase the tube's CHF, and thereby reduce moderator subcooling requirements was assessed. Results from the experiments confirm that glass-peening the outer surface of a tube increases its CHF value in pool boiling. This increase in CHF could be used to reduce moderator subcooling requirements for CANDU fuel channels by at least 5 °C.

1. INTRODUCTION

There are approximately 400 horizontal fuel channels (Fig. 1) in CANDU-PHW reactors, consisting of Zr-2.5Nb pressure tubes (PT) and concentric Zircaloy-2 calandria tubes (CT), submerged in a large volume (~250,000 liters) of heavy-water moderator at 70 °C. The hot pressure tubes (104-mm ID), operating near 300°C, are insulated from 70 °C calandria tubes (130-mm ID) by a 9-mm thick annulus filled with CO₂. Within each pressure tube are twelve 0.5-m long fuel bundles each consisting of 37 Zr-4 clad fuel elements containing UO₂ pellets (Fig. 2). The thermal energy produced in the UO₂ fuel pellets is removed by heavy water, the heat-transport medium, flowing at about 10-MPa pressure and approximately 300°C under normal operating conditions. The fuel bundles are held off to the pressure tube by 1.1-mm high bearing pads on the outer elements. These bearing pads help maintain uniform flow of heat transport fluid around the bundle and aid movement of the bundles during on-power refueling.

The moderator provides a secondary heat sink in CANDU reactors that helps ensure adequate cooling of fuel in the unlikely event of a LOCA. Numerous studies have confirmed the ability of the moderator, available at a radial distance of 15 mm from the

fuel, as a backup heat sink to remove residual heat during emergencies [1 - 2]. In some postulated LOCA scenarios, for example, the fuel will heatup due to decay power. Fuel-temperature escalation leads to pressure-tube heatup and plastic deformation (ballooning) which starts at approximately 650°C and continues until the calandria tube is contacted. Upon contact, the stored heat in the pressure tube is transferred across the interface to the

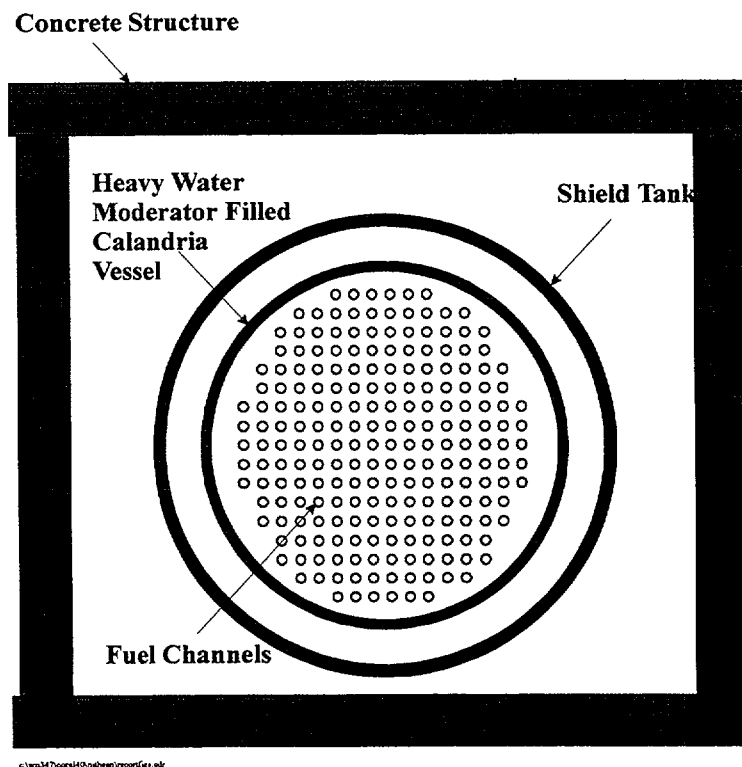


FIG. 1. CANDU reactor core showing fuel channels, calandria vessel, shield tank, and concrete structure.

FUEL CHANNEL ARRANGEMENT

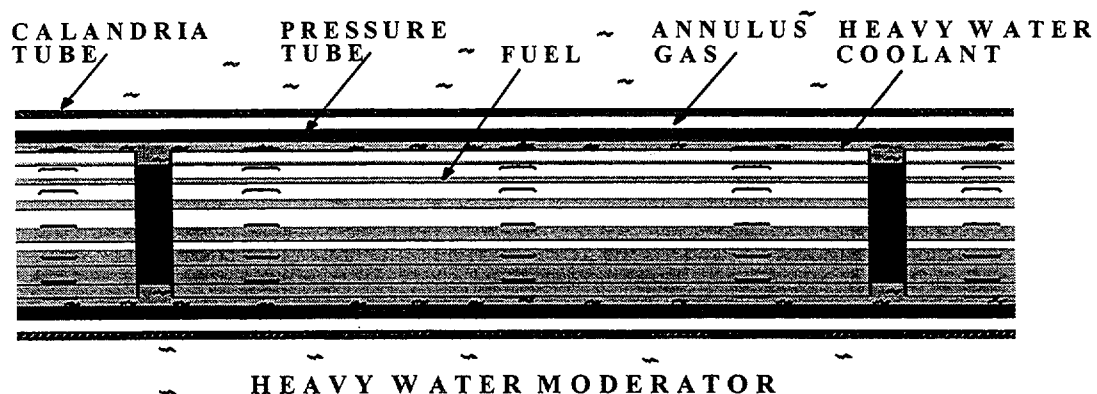


FIG. 2. The proximity of the fuel to the heavy water moderator which acts as a heat sink in postulated accidents.

calandria tube, conducted through the calandria-tube wall and into the surrounding heavy-water moderator.

Moderator temperatures (subcooling) are specified to ensure the transfer of stored heat to the moderator occurs without film boiling on the calandria tube, which could compromise channel integrity [3 - 4]. The subcooling required to minimize the extent of film boiling was determined from a series of experiments where pressure tubes were ballooned into contact with calandria tubes at internal pressures ranging from 0.5 to 10 MPa.

An objective of AECL's ongoing R&D program is to improve safety margins for CANDU reactors and reduce capital costs through component improvement. One of the ways to enhance safety is to improve the effectiveness of the moderator as a heat sink by reducing subcooling requirements. Possible ways to reduce moderator subcooling requirements are to reduce the post-contact heat-transfer coefficient between the pressure tube and the calandria tube or to increase the critical heat flux (CHF) on the outer surface of the calandria tube. Reducing the contact heat-transfer coefficient between the two tubes can be achieved by limiting the metal-to-metal contact area upon ballooning contact, as demonstrated by Sanderson et al. [5]. Increasing the CHF for a given subcooling on the outer surface of the calandria tube can be achieved by surface modifications [6 - 8].

The ability of the new designs to increase the CHF on the outside surface of the calandria tube was demonstrated in a series of small- and large-scale experiments. Analysis of the test results indicated that increasing the tube's CHF using a glass-peening process is a promising option for reducing moderator subcooling requirements. This paper describes small-scale pool boiling tests conducted to establish the CHF enhancement, and large-scale tests conducted to demonstrate the reduction in subcooling requirements.

2. SMALL-SCALE CHF-ENHANCEMENT TESTS

Small-scale pool boiling experiments were conducted to quantify the CHF enhancement provided by roughening the outside surface using a glass-peening process. Glass-peening is a process of impinging spherical glass beads to produce microscopic cavities on the surface. The size and distribution of these cavities can be modified by selecting appropriate glass-peening parameters.

The controllable parameters during glass-peening process are bead size, Almen intensity, and coverage. In our experiments, four ranges of bead diameters were used: (1) 60 - 90 μm , (2) 90 - 125 μm , (3) 125 - 180 μm , and (4) 180 - 210 μm . The deflection caused by beads impinging on steel strips (SAE 1070) is defined as Almen intensity. For these experiments the intensity was kept between 0.23 mm (N9) and 0.28 mm (N11). The coverage is defined as the ability of the glass-peening process to remove a fluorescent dye applied to a sample. When no dye can be detected under ultraviolet light, the coverage is considered to be 100%.

2.1. Small-scale CHF experiments

The test apparatus (Fig. 3) consisted of 450-mm long pieces of Zircaloy-4 (Zr-4) tubing (19.5 mm in diameter) clamped to two power cable leads submerged in a tank of water. The tube ends were sealed using rubber stoppers to prevent water from entering the tube. A 6.4-mm diameter stainless steel vent pipe was attached to one of the rubber stoppers to release the gas expansion from the tube. A 5000 A dc power supply was used

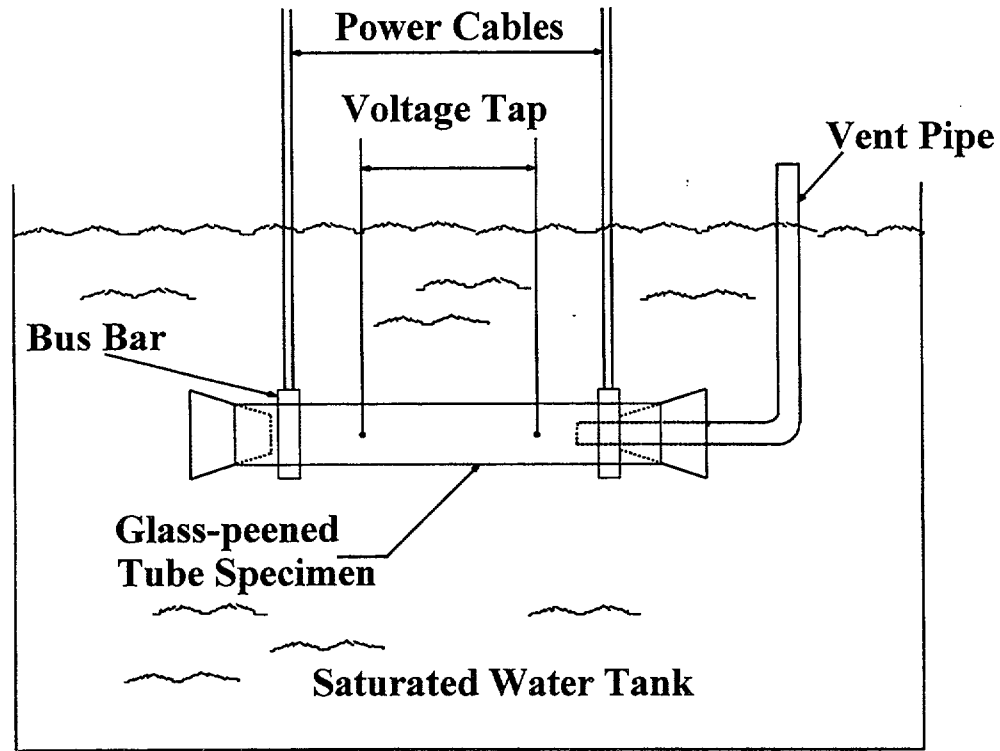


FIG. 3. The schematic diagram of the small-scale CHF test apparatus.

to electrically heat the Zr-4 tube, with the actual power determined by multiplying the circuit current by the voltage drop between voltage taps welded on the surface of the tube. The tests were recorded with a video camera to observe boiling on the tubes to identify the first occurrence of dryout.

Two types of experiments were conducted during this study. The first was a gradual power ramp, where electrical power was increased at 0.2 to 0.6 kW/s until dryout was observed on the tubes. Following the first dryout, the power was turned down to zero until all visible signs of dryout had disappeared. The electrical power was then ramped a second time until another dryout patch became visible. This procedure was repeated three or more times with each tube tested. The second type of experiment was a spiked power ramp test. The spiked power ramp was achieved using a switching circuit to ramp the power at approximately 75 kW/s to a set point and then decrease the power rapidly to 5 kW. The set points for spiked power ramps were gradually increased during successive ramps until dryout was observed on the tube. When dryout became visible, a digital event signal was triggered manually to indicate the dryout condition in the recorded data.

All tests were conducted with water at saturation temperature (approximately 100°C). Steam circulating through a heat exchanger was used to maintain pool temperature. The Zr-4 tube temperatures were not measured, as the use of direct electrical heating interfered with the thermocouple outputs. The critical heat flux was calculated using the measured power at dryout (voltage across the voltage tap times the current) and the wetted outside surface area of the test specimen.

2.2. Experimental results and discussion

The experimental results are summarized in Table I with the uncertainty due to scatter in the data (2 x the standard deviation) provided with mean CHF values. The mean

CHF value of the as-received (un-peened) tube (Table I) was 0.68 MW/m² in the gradual power ramp tests. The CHF increased by 0.45 MW/m² or approximately 66% when glass-peened using 60 – 90 µm beads compared with as-received tubes. The tube glass-peened with 90 – 125 µm beads increased the CHF by 0.48 MW/m² or 71% compared with as-received tubes. In comparison, those tubes glass-peened with 125 – 180 µm and 180 – 210 µm beads only increased the CHF by 0.12 MW/m² (18%) and 0.18 MW/m² (27%), respectively. The coverage appeared to have a weak influence on CHF compared with the influence bead size had on CHF (Table I).

TABLE I. COMPARISON OF CHF VALUES OBTAINED FROM SPIKED AND GRADUAL POWER RAMP TESTS

Bead Size (µm)	Coverage (%)	Gradual power ramp		Spiked power ramp	
		CHF (MW/m ²)	Percent improvement from as- received	CHF (MW/m ²)	Percent improvement from as- received
<i>as-received</i>		0.68 ± 0.20	—	0.86 ± 0.15	—
60 - 90	100	1.12 ± 0.04	66	1.29 ± 0.07	50
90 - 125	100	1.15 ± 0.07	71	1.35 ± 0.08	58
125 - 180	100	0.79 ± 0.23	18	1.32 ± 0.16	54
180 - 210	100	0.86 ± 0.34	27	0.95 ± 0.15	11
125 - 180	80	0.88 ± 0.19	31	0.95 ± 0.10	11
125 - 180	120	0.83 ± 0.02	23	1.14 ± 0.07	33

The second test series using a spiked power ramp was conducted to identify the influence of a sudden power spike on CHF. This type of sudden heat flux release is relevant to the contact boiling scenario for CANDU reactors as contact of an overheated pressure tube rapidly heats a cool calandria tube. The objective of these tests was to explore whether rapid heating changes the CHF on a glass-peened surface compared with the CHF obtained from a gradual power ramp test. The CHF enhancement experienced during spiked power ramp tests were similar to the gradual power ramp tests, Table I. The test results are summarized in Fig. 4. For both series of tests, the 90 – 125 µm beads provided the maximum CHF enhancement. The CHF enhancement observed in the small-scale tests was consistent with the enhancements reported with experiments conducted elsewhere using roughened surfaces [9].

A comparison between the theoretical CHF value and the experimental CHF value obtained from the as-received tubes can be made. The CHF for horizontal cylinders with $R/L_b > 1.2$ [10] is given by:

$$\frac{q_{\max}^*}{q_{\max,Z}^*} = 0.9. \quad (1)$$

Here

q''_{\max} is the CHF in horizontal cylinders (W/m^2),

R is the radius of the cylinder (m),

L_b is the bubble length scale (m) given by:

$$L_b = \sqrt{\frac{\sigma}{g(\rho_l - \rho_v)}} \quad (2)$$

and, $q''_{\max,Z}$ is Zuber's [11] maximum heat flux (W/m^2) given by:

$$q''_{\max,Z} = 0.131 \rho_v h_{lv} \left[\frac{\sigma(\rho_l - \rho_v)g}{\rho_v^2} \right]^{1/4} \quad (3)$$

In Equations 2 and 3 ρ_v is density of vapour phase (0.6 kg/m^3), ρ_l is the density of liquid phase (958 kg/m^3), h_{lv} is the latent heat of evaporation ($2,257,000 \text{ J/kg}$), σ is the surface tension (0.6 N/m), and g is the acceleration due to gravity (m/s^2). For saturated water at 100°C and a tube diameter of 19.5 mm , the theoretical CHF value for the small-scale experiments is 1 MW/m^2 . The tests with as-received tubes had measured CHF values of 0.68 to 0.86 MW/m^2 which are lower than this theoretical value. The CHF observed in the small-diameter glass-peened tube tests occurred in isolated patches of less than 1000 mm^2 . The measured heat flux, however, represented the average heat flux for the entire tube surface between the voltage taps. Although critical heat flux was exceeded in these isolated patches in the small diameter glass-peened tube tests, a large surface area of the tube was not in CHF. Consequently, the measured CHF values in the experiment are lower than the theoretical CHF values derived from equations given in Reference [10]. Similar observations were also reported in References [12-13] where the CHF measured from isolated patches were lower than the theoretical CHF.

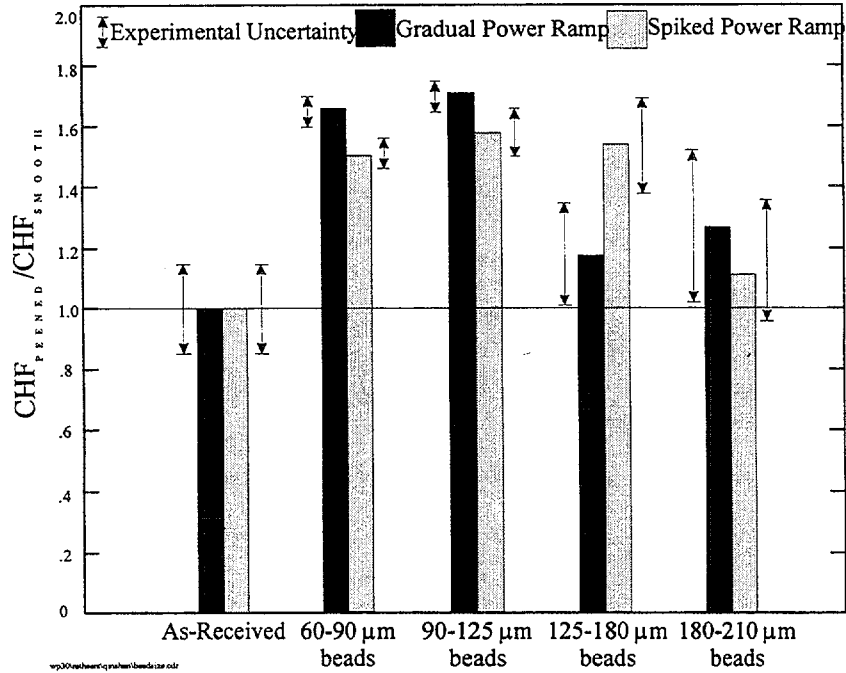


FIG. 4. The influence of bead size on CHF

The purpose of the small-scale tests was to determine the enhancement to pool boiling CHF provided by roughening the outer surface of a tube by glass-peening process. The CHF ratios shown in Table I represent the enhancement produced by glass-peening the tubes. The results show a clear and consistent CHF enhancement for the roughened tube relative to the as-received smooth surfaces.

3. LARGE-SCALE EXPERIMENTS

The efficacy of glass-peened calandria-tube surfaces to minimize the extent of film boiling during pressure-tube ballooning contact was determined in large-scale contact boiling experiments. In these tests, two calandria tube sections, one representing the as-received calandria-tube design and the other representing the glass-peened calandria tube design, were butt welded together as shown in Fig. 5. The inside surface of the calandria tube was left as-fabricated except for one test (PTC3). The outside surface of the calandria tube was glass-peened using the conditions shown to give the largest improvement from the small-scale tests (90 – 125 μm beads at N-9 to N-11 Almen intensity and 100% coverage).

Following three full-scale comparative tests, a series of five calandria tube qualification tests were conducted. The full length of the calandria tubes used in the qualification tests was glass-peened using 90 – 125 μm beads at N-9 to N-11 Almen intensity and 100% coverage. Similar procedures and experimental apparatus were used in the comparative and qualification tests.

3.1. Experimental apparatus

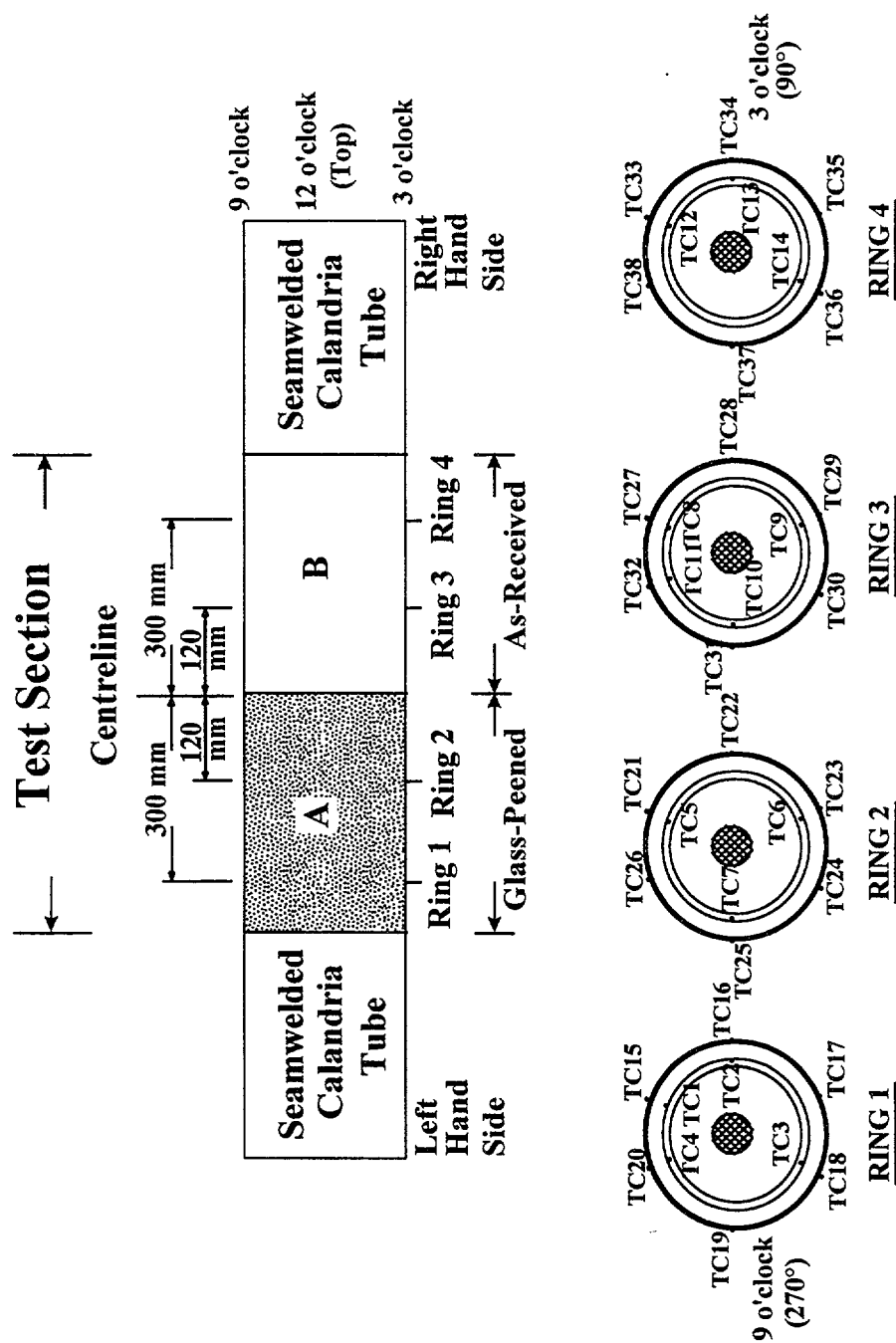
The test apparatus consisted of a 1750-mm long sections of Zr-2.5Nb pressure tube placed concentrically inside 1700-mm long Zircaloy-2 calandria tubes (Fig. 6). The calandria tubes were submerged in an open tank of water simulating the heavy water moderator in a reactor. The top surface of the calandria tube was covered by at least 190 mm of water throughout the experiment. The walls of the open tank were equipped with Lexan windows enabling video taping of boiling patterns on the outside surface of the calandria tube.

A 950-mm long graphite rod heater, 34 mm or 38 mm in diameter, was located inside the test section assembly. Each end of the heater was tapered to a 60 cone, corresponding to receptacles machined into 51-mm diameter water-cooled stainless steel busbars. The busbars were forced into contact with the graphite rod by springs.

The calandria tube for the third comparative test (PTC3) was autoclaved at 500 °C for 3 hours after being glass-peened to produce a uniform oxide on the inner and outer surfaces of the calandria tubes. The black oxide (1- μm thick) increases the tube's coefficient of absorptivity during thermal radiation. This property is being investigated to increase heat removal rates from an overheated pressure tube to the water cooled calandria tube during low pressure (< 0.5 MPa) LOCA scenarios when the pressure tube may not balloon into intimate contact with the calandria tube. The impact of this oxide during the contact boiling experiments reported here is small.

3.2. Instrumentation

Power was supplied by a 5000 A dc power source. The power delivered to the test apparatus was determined by multiplying circuit current by the voltage drop measured between voltage taps on the graphite heater. The inside of the pressure tube was



c:\hp\347mso\office\powerpoint\utility\report\fig5ppt

FIG. 5. A schematic diagram of instrumentation used in full-scale ballooning experiment conducted to compare the efficacy of glass-peened outside surface of the calandria tube with an as-received outside surface of the calandria tube.

pressurized to 1 or 4.3 MPa with argon. The annulus gap between the pressure tube and the calandria tube was filled with CO₂ that remained at essentially atmospheric pressure throughout the experiment (all pressures reported are gauge pressures).

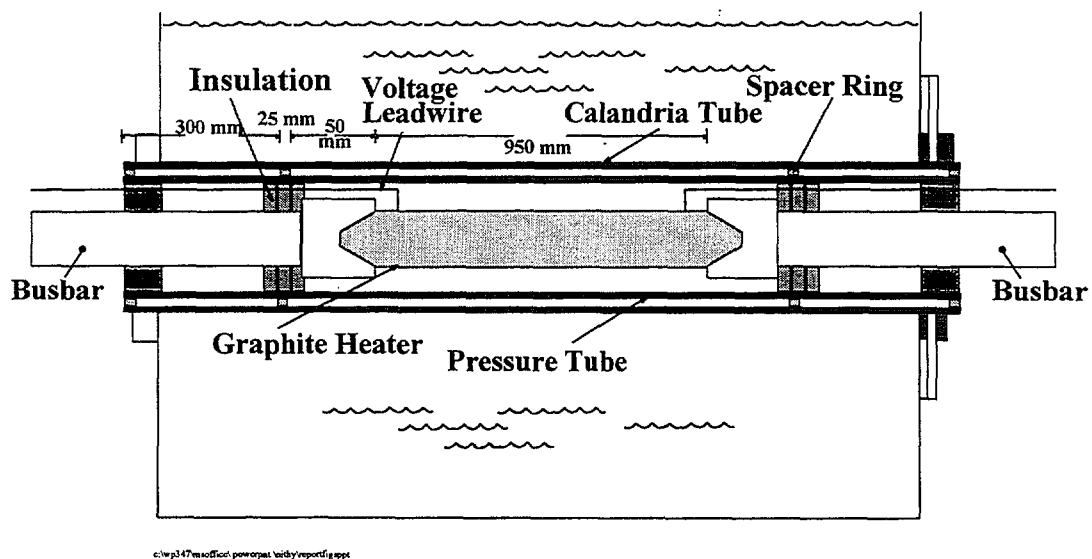


FIG. 6. The test apparatus used in full-scale ballooning experiments.

The pressure tube and calandria tube were instrumented with thermocouples to monitor test-section temperatures. Calandria-tube thermocouples, spot welded on the outside surface at locations shown in Fig. 5, were special grade teflon-insulated Type-K (chromel-alumel) thermocouples with 0.13-mm diameter sensing wires. For the pressure-tube, 1-mm diameter Inconel-clad Type-K thermocouples with magnesium-oxide insulation were used. The junction end of each thermocouple was swaged to 0.5 mm diameter for insertion into small diameter blind holes drilled part way through the pressure-tube inner wall. These holes were slightly larger than the thermocouple diameter and were at a 45° angle to the tube axis to shield them from direct thermal radiation from the heater. Along with the above thermocouples, four platinum resistance temperature detectors (RTDs) were used to measure water temperatures in the tank surrounding the calandria tube. The tests were recorded with three video cameras to observe boiling patterns on the calandria tube following ballooning contact.

Uncertainties in the temperature measurements were ± 2.4 °C at 275 °C and ± 3.8 °C at 800 °C. The measurement uncertainty in the platinum resistance temperature detectors (RTDs) used to measure the tank water was ± 0.75 °C at 80 °C. The uncertainty in pressure measurement was $\pm 0.23\%$. The estimated uncertainty in heater power was $\pm 1.2\%$.

3.3. Experimental procedure

The following generalized procedure was used for all tests:

1. The annulus between the calandria tube and the pressure tube was purged with CO₂.
2. The water surrounding the calandria tube was heated to approximately 10 °C higher than the desired tank water temperature to partially degas the water for better

visibility. The water was then cooled to the desired subcooling (Table II). A small impeller inside the water tank stirred the water throughout the test to maintain uniform water temperatures.

3. The pressure tube was pressurized to the test pressure (Table II).
4. The total power was increased to the test power (Table II) within 50 s.
5. The test was terminated when the pressure-tube ballooned into contact with the calandria tube and the calandria tube rewet or ruptured.

TABLE II. TEST CONDITIONS FOR FULL-SCALE CONTACT BOILING EXPERIMENTS

Test	Pressure (MPa)	Pressure-tube heatup rate (°C/s)	Power (kW/m)	Pressure-tube contact temperature (°C)	Subcooling (°C)
PCT1	1.0	13.5	103	810 — 900	21.0
PCT2	1.0	18.2	132	855 — 910	20.0
PCT3	1.0	17.2	134	840 — 890	19.4
Q1	4.1	24.1	173	755 — 795	26.2
Q2	4.1	24.6	149	785 — 860	28.4
Q3	4.2	10.3	54	745 — 780	25.5
Q4	4.3	10.3	64	740 — 775	22.1
Q5	4.1	23.4	149	800 — 880	26.0

3.4. Experimental results from comparative tests

The detailed experimental results from test PTC3 and a summary of the other tests are presented below.

The pressure tube was pressurized to 1 MPa and the power to the graphite heater was increased from 0 to 120 kW over 25 s, heating the pressure tube at a rate of 16 to 18 °C/s. The pressure tube began to balloon once temperatures exceeded 650°C due to the 1 MPa pressure. The pressure-tube temperatures at contact ranged from 840 to 890 °C (Figs. 7 and 8). Upon contact, the stored energy from the hot pressure tube was rapidly transferred to the water-cooled calandria tube causing temperature escalations as shown in Figs. 9 and 10. The calandria-tube temperatures on the glass-peened side rewet within 18 s whereas on the as-received side extensive film boiling continued until the channel ruptured (Figs. 9 and 10). The test was terminated following channel rupture.

During experiment PCT3 variables such as incident heat flux (on the pressure tube) and water subcooling (outside of the calandria tube) were identical for both sections of the calandria tube (Fig. 5). The only difference between the two calandria-tube sections was the surface treatments for one half of the test section.

The temperature histories recorded by all thermocouples in the glass-peened side of the calandria tube are shown in Fig. 9. Among twelve calandria-tube thermocouples on the glass-peened surface, four were in nucleate boiling (< 135°C), four experienced rapid quench (< 3 s), and the remaining were in film boiling (515 and 645°C) for less than 18 s. The film boiling occurred in isolated patches covering less than 10% of the tube surface. These patches were located in the bottom quadrant of the tube (facing downwards) and were likely due to vapour entrapment.

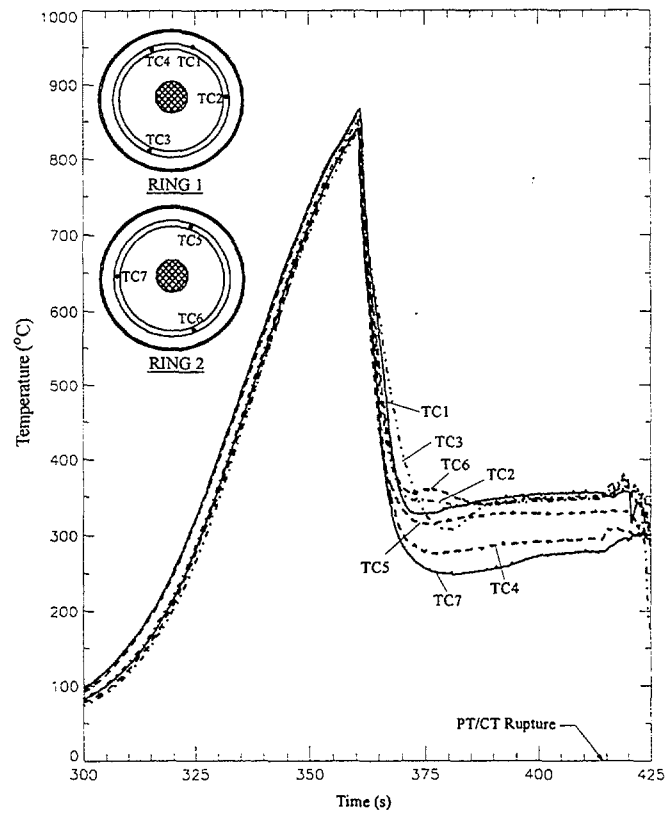


FIG. 7. Pressure-tube temperatures in the glass-peened calandria-tube section of test PCT3.

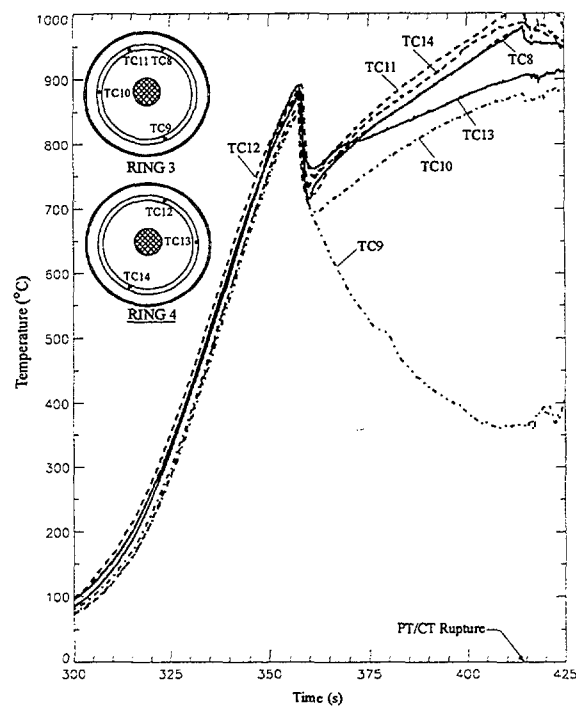


FIG. 8. Pressure-tube temperatures in the as-received calandria-tube section of test PCT3.

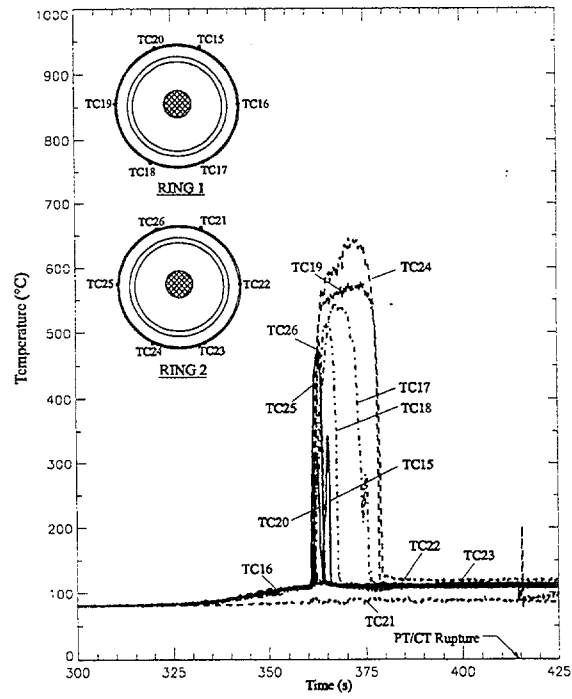


FIG. 9. Calandria-tube temperatures in the glass-peened side of the test section of test PCT3.

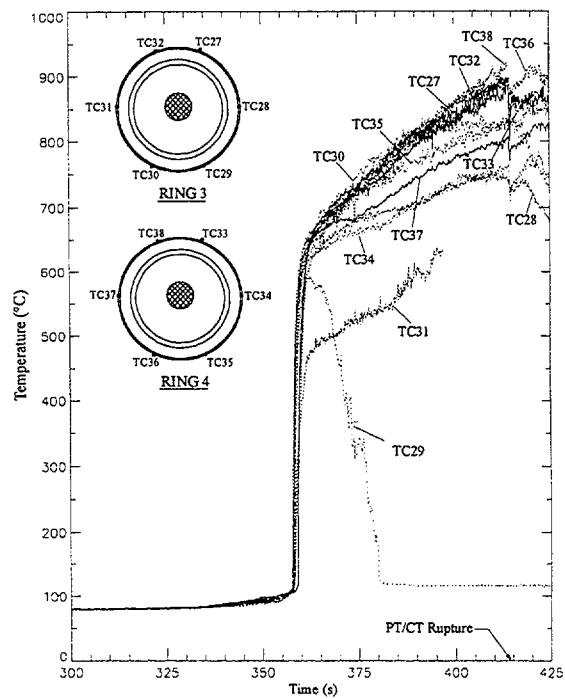


FIG.10. Calandria-tube temperatures in the as-received side of the test section of test PCT3.

For comparison, temperature histories on the as-received side of the calandria tube are shown in Fig. 10. All thermocouples, except two, were in extensive film boiling until the channel ruptured. The maximum temperatures recorded before rupture ranged between 755 and 920 °C.

The efficacy of the glass-peened calandria tube is demonstrated from a comparison of the post-contact calandria-tube temperature histories and visual inspection for extent of dryout on the calandria tubes. The characteristic boiling regime on the outside surface of the calandria tube was determined by visually examining the black oxide patches on the calandria tube, video observations, and calandria-tube temperatures. A post-test representation of the oxidized area observed on the outside surface of the calandria tube is shown in Fig. 11. The severity of calandria-tube temperature escalation can be identified by the extent of oxidation during post-test examination. Less than 10% of the surface area in the glass-peened side of the calandria tube was covered with a thin oxide layer. Negligible oxide discolouration on the glass-peened area indicated that the duration of film boiling (less than 18 s) was not sufficient to cause significant discolouration. More than 80% of the as-received surface area was significantly discoloured. The rupture location on the calandria tube is shown in Fig. 11. The rupture was 128-mm long and up to 22-mm wide. Based on this comparison, we conclude that glass-peening the outside surface of the calandria tube increased the CHF on the outer surface of the calandria tube such that the extent of film boiling was significantly reduced following ballooning contact at 1 MPa internal pressure when the moderator subcooling was 20 °C.

In this experiment, the glass-peened calandria-tube surface augmented the heat flux to the moderator compared with an as-received calandria-tube surface. From a heat transfer point of view, this augmentation amounts to an increase in the CHF in comparison to an as-received surface. For a given pressure-tube contact temperature, the enhancement of the CHF obtained from a glass-peened surface provides a reduction in the

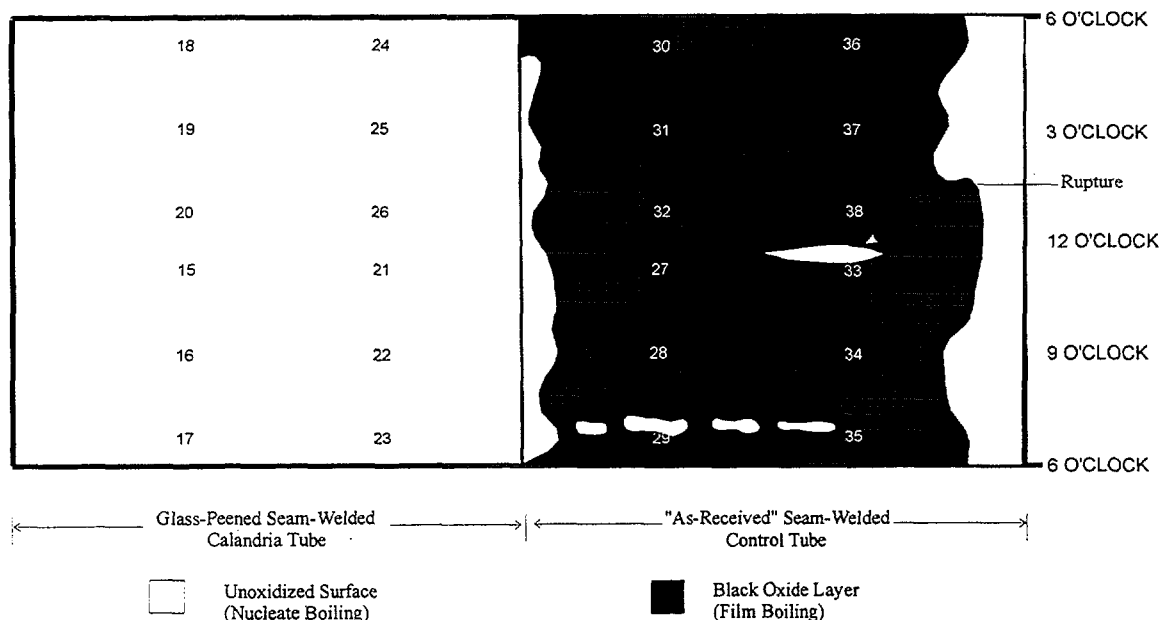


FIG. 11. The post-test oxide pattern on the outside surface of the calandria tube showing the extent of film boiling on the as-received calandria-tube surface while the glass-peened calandria tube surface indicated little oxide for test PCT3.

moderator subcooling requirement (or an increase in the margin to dryout). This enhancement is illustrated in Table III, where the results obtained from three tests with

TABLE III. COMPARISON OF CONTACT BOILING EXPERIMENTS CONDUCTED WITH AS-RECEIVED AND GLASS-PEENED CALANDRIA TUBES AT INTERNAL PRESSURES BETWEEN 0.5 MPa AND 1.1 MPa

Glass-Peened Calandria Tubes					As-Received Calandria Tubes				
Test	PT Contact Temperature °C	Subcooling °C	PT Heatup Rate °C/s	Boiling Regime	Test	PT Contact Temperature °C	Subcooling °C	PT Heatup Rate °C/s	Boiling Regime
PCT1	811-897	21	13.5	☉	FCHT3	840-940	7.2	9.1-17.3	●
PCT2	855-909	20	18.2	☉	S4/T2	895	10.0	7.0	●
PCT3	839-892	19.4	17.8	○	FCHT1	855-955	15.5	14.9-19.7	●
					FCHT2	830-880	15.9	6.9-11.9	☉
					12	905-1010	15.9	9.6-16.3	☉
					9	845-905	21.0	6.3-8.6	☉
					3	825-855	28.0	3.8-4.7	☉
					DELTI	820-890	28.3	6.9-12.3	☉
					19	855-930	28.7	0.1-13.6	○
					18	825-845	28.9	5.5-10.3	○
					4	835-860	33.5	4.5-4.6	○

LEGEND: ○ Immediate quench ☉ Small patches of film boiling ● Patches of film boiling
● Extensive film boiling ● Entire calandria tube in film boiling

glass-peened calandria tubes are compared with contact boiling experiments conducted with as-received calandria tubes.

The boiling regimes observed in the contact boiling experiments are used to determine the subcooling required to minimize the extent of dryout on the calandria tubes. The boiling regimes for the two types of tests are listed in a descending order, namely from “entire calandria tube in film boiling” regime to “immediate quench” regime. Comparing the subcooling and the boiling regime of the eleven as-received calandria-tube tests, approximately 28 °C subcooling is required to reduce the extent of film boiling to preserve fuel channel integrity following ballooning contact. In comparison, the glass-peened calandria tubes show 21 °C is sufficient to ensure the calandria tube rewets. The comparison implies a potential reduction in subcooling requirement of 7 °C. This reduction becomes possible only because of an enhancement to CHF occurring in the glass-peened calandria-tube surface. The enhancement is consistent with the observations from the small-scale CHF experiments discussed in Section 2.2.

3.5. Experimental results from qualification tests

Following these comparative tests, five qualification tests were conducted at internal pressures between 4.1 and 4.3 MPa and at heating rates greater than 10 °C/s (Table II). In these tests the entire length of the calandria tube was glass-peened and none of the tubes were autoclaved.

The measured calandria-tube temperatures following pressure-tube ballooning contact were quite similar in trend to that of the glass-peened side of test PCT3. The maximum calandria-tube temperatures recorded in these tests were less than 505 °C (test Q2). While the majority of thermocouples indicated nucleate boiling during pressure-tube contact, some thermocouples in the bottom quadrants of the calandria tube indicated film boiling by showing temperature excursions. These small dryout patches rewet within 7s.

Table IV compares the contact boiling experiments conducted with as-received calandria tubes and the glass-peened calandria tubes at internal pressure between 4.1 and 4.3 MPa. The as-received calandria tube at 26 °C subcooling indicated extensive film boiling whereas the glass-peened calandria tube is in immediate quench or had only small patches of film boiling. The patchy film boiling observed in the as-received calandria tube was obtained at a pressure-tube heatup rate less than 10 °C/s. In the glass-peened calandria-tube tests, the pressure-tube heatup rates were higher than 10 °C/s. For heatup rates > 10 °C/s the as-received calandria tube required a subcooling >26 °C. In the glass-peened calandria tube, a subcooling closer to 22 °C appears to be adequate to avoid the occurrence of extensive film boiling. Hence, a subcooling reduction of at least 5 °C is available when glass-peened tubes are used. This is in good agreement with the reduction to subcooling requirement determined from the comparative tests. Three different test methods and ten tests (two CHF tests and eight contact boiling tests) were able to show glass-peening the outside surface of a tube increases its CHF value in pool boiling. This increase in CHF has been shown to translate to a reduction in moderator subcooling requirements for CANDU reactors of approximately 5 °C.

TABLE IV. COMPARISON OF CONTACT BOILING EXPERIMENTS CONDUCTED WITH AS-RECEIVED AND GLASS-PEENED CALANDRIA TUBES AT INTERNAL PRESSURES BETWEEN 4.0 MPa AND 4.3 MPa

Glass-Peened Calandria Tubes					As-Received Calandria Tubes				
Test	PT Contact Temperature °C	Subcooling °C	PT Heatup Rate °C/s	Boiling Regime	Test	PT Contact Temperature °C	Subcooling °C	PT Heatup Rate °C/s	Boiling Regime
Q1	755-795	26.2	24.1	☉	HPCB11	740-810	19.3	11.9	☉
Q4	741-776	22.1	10.3	○	HPCB13	750-810	20.0	10.4	☉
Q3	747-782	25.5	10.3	○	QM1	750-850	26.0	17.5	☉
Q5	799-878	26.0	23.4	○	2	710-855	14.9	4.9	☉
Q2	784-858	28.4	24.6	○	10	685-740	14.4	9.5	☉
					6	735-750	19.0	5.0	☉
					1	720-760	33.6	6.3	○

LEGEND: ○ Immediate quench ☉ Small patches of film boiling ☉ Patches of film boiling
 ● Extensive film boiling ● Entire calandria tube in film boiling

4. SUMMARY

A series of experiments were conducted to assess the benefits provided by glass-peening the outside surface of calandria tubes for postulated LOCA conditions. In particular, the ability to increase the tube's CHF value and thereby reduce moderator subcooling requirements was assessed.

Three different test methods and ten tests (two CHF tests and eight contact boiling tests) were able to show glass-peening the outside surface of a tube increases its CHF value in pool boiling. This increase in CHF has been shown to translate to a reduction in moderator subcooling requirements for CANDU reactors of approximately 5°C.

REFERENCES

- [1] SIMPSON, L.A., "Severe Accident Research in Canada", Proc. 9th Pacific Basin Nuclear Conference, Sydney, Australia, Australian Nuclear Association Inc. and Institute of Engineers, Australia, May 1-6, (1994).
- [2] HART, R.S., SNELL, V.G., SIMPSON, L.A., SANDERSON, D.B., "Passive Heat Removal in CANDU", Proc. of the IAEA Advanced Group Meeting on Technical Feasibility and Reliability of Passive Safety Systems, Julich, Germany, November (1994).
- [3] GILLESPIE, G.E., MOYER, R.G., THOMSON, P.D., "Moderator boiling on the external surface of a calandria tube in a CANDU reactor during a loss-of-coolant accident", Proc. of the International Meeting on Thermal Nuclear Reactor Safety, Chicago, IL, Nuclear Regulatory Commission Report, NUREG/CP-0027, 1523-1533, (1982).
- [4] GILLESPIE, G.E., MOYER, R.G., HADALLER, G.I., HILDEBRANDT, J.G., "An experimental investigation into the development of pressure tube/calandria tube contact and associated heat transfer under LOCA conditions", Proc. of the 6th Annual Canadian Nuclear Society Conference, Ottawa, ON, 2.24-2.30, (1985).
- [5] SANDERSON, D.B., MOYER, R.G., LITKE, D.G., ROSINGER, H.E., GIRGIS, S., "Reduction of pressure-tube to calandria-tube contact conductance to enhance the passive safety of a CANDU-PHW reactor", Proc. of the IAEA Technical Committee Meeting on Advances in Heavy Water Reactors, Toronto, ON, Canada, (also available as AECL-10892), (1993).
- [6] DUTTON, R., "Advanced fuel channel concepts", Proc. of the IAEA Technical Committee Meeting on Advances in Heavy Water Reactors, Toronto, 1993 June, International Atomic Energy Agency Technical Document, TECDOC-738, (1994).
- [7] COLEMAN, C.E., FONG, R.W.L., DOUBT, G.L., NITHEANANDAN, T., SANDERSON, D.B., "Improving the calandria tubes for CANDU reactors", Proc. of the 18th Annual Conference of the Canadian Nuclear Society, 1997 June 8-11, Toronto, Canada (also available as AECL-11815), (1997).
- [8] FONG, R.W.L., COLEMAN, C.E., NITHEANANDAN, T., KROEGER, V.D., MOYER, R.G., SANDERSON, D.B., ROOT, J.H., ROGGE, R.B., "External glass peening of Zircaloy calandria tubes to increase the critical heat flux," Proceedings of the 11th Pacific Basin Nuclear Conference, 1998 May 3-7, Banff, Alberta, Canada (also available as AECL-11898), (1997).
- [9] RAMILISON, J.M., SADASIVAN, P., LIENHARD, J.H., "Surface factors influencing burnout on flat heaters", ASME J. Heat Transfer, Vol. 114, pp. 287-290, (1992).
- [10] LIENHARD, J.H., DHIR, V.K., "Hydrodynamic prediction of peak pool-boiling heat fluxes from finite bodies", ASME J. Heat Transfer, Vol. 95, 152-158, (1973).

- [11] ZUBER, N., On the Stability of Boiling Heat Transfer, Trans. ASME, Vol. 80, 711-720, (1958).
- [12] CHOWDHURY, S.K.R, WINTERTON, R.H.S., "Surface effects in pool boiling", Int. J. Heat Mass Transfer, Vol. 28, No.10, 1881-1889, (1985).
- [13] MESLER, R., "Peak heat fluxes in boiling as determined by steady-state and transient experiments", A.I.Ch.E.Jl, Vol.25, 549-551, (1979).

NEXT PAGE(S)
left BLANK



UNCERTAINTY OF EVALUATIONS OF FLOW FILM BOILING HEAT TRANSFER COEFFICIENT

A.A. IVASHKEVITCH, P.L. KIRILLOV, V.V. SERGEEV,
I.P. SMOGALEV, V.N. VINOGRADOV
SSC, Institute of Physics and Power Engineering,
Obninsk, Russian Federation

Abstract

The results of evaluations of the heat transfer coefficient (α_s) for the flow film boiling (FFB) region received by two approaches, which are complemented each other are discussed here. In particular, they are as follows: 1) using empirical or semiempirical correlations, 2) developing the look-up tables (LUT). There is a need to distinguish two FFB heat transfer regime, such as 1) the post-dryout (PDO) heat transfer and 2) before-critical heat flux (CHF) heat transfer. A new version of the LUT for α_s is presented at forced water flow in long tubes uniformly heated. It covers the following range of parameters: pressure 0.1÷20 MPa; mass flux 250÷3000 kg/m²s; quality (-0.2)÷2.2; heat flux 0.2÷1.0 MW/m²; tube diameter 10 mm. The values of the FFB heat transfer coefficient in the LUT are marked by different methods depending on the used calculation method. Four methods were applied to develop the LUT for α_s , namely: 1) averaging experimental data, 2) calculations on the base of the Sergeev model, 3) using data from the LUT developed by Leung L. et al. (1997), 4) using both interpolation and extrapolation beyond the range of experimental data and theoretical evaluations. The calculated errors of the α_s values were obtained by comparison the LUT data with the experimental data stored in the database of the IPPE Thermophysical Data Center.

1. INTRODUCTION

The prediction of the heat transfer coefficient (α_s) for the FFB region is important in such fields as once-through steam generator calculations and an accident analysis for water-cooled reactors. The different versions of the LUT for α_s in tubes were developed by Kirillov et al (1996, 1997), Leung et al (1997). Besides, Chen et al. (1998) supposed the tabular method for the FFB heat transfer calculations. However, these methodologies cannot cover all fields of practical engineering calculations. The aims of this work are as follows: 1) to widen the quality range and 2) to develop the joint international version of the LUT for the FFB heat transfer coefficient and to remedy the shortcomings of previous LUT versions.

2. OUTLINES OF LUT FOR FLOW FILM BOILING

2.1. Previous LUT versions

The first LUT version by Kirillov et al. (1996) includes the mean values of α_s for the PDO heat transfer in tubes averaged over the experimental data. These data were taken from the database of the IPPE Thermophysical Data Center that contains 42800 points (see Table 1). It covers the follow range of parameters: $P = 0.2 \div 21.6$ MPa, $G = 200 \div 3000$ kg/m²s, $X = 0 \div 2.48$; $q = 0.09 \div 1.36$ MW/m²; $d = 8, 10$ mm and $l = 0.9 \div 10$ m. This LUT version is characterized by such deficiencies as 1) presence of empty cells and 2) inaccuracy for the low and negative quality values.

Hereafter, it was updated by Kirillov et al. (1997) on the base of the Sergeev model (1987) within the range of parameters: $P = 4.0 \div 20$ MPa, $G = 250 \div 2000$ kg/m²s, $X = (-0.2) \div 2.2$ and $q = 0.2 \div 1$ MW/m². The substantiation of a model choice is well grounded by data. Moreover in these both LUT versions, the heat transfer coefficient was connected with the difference between a wall temperature and a saturation temperature ($T_w - T_s$). In this way, the LUT empty cells were filled, but the quality range remained narrow because the Sergeev model is valid at the dispersed flow film boiling (DFFB) regime.

Leung et al. (1997) has presented the other LUT version within the parameter range: P - from 0.1 to 20 MPa, G - from 0 to 7000 kg/m²s, X - from -0.2 to 1.2, q - from 0.05 to 3 MW/m². During the LUT development the authors used 21515 data points taken from 17 references. In this table, the values of α_s were connected with the difference ($T_w - T_s$) at $X \leq 1$ and the difference ($T_w - T_f$) at $X > 1$. The following procedures were applied to develop the LUT for the FFB heat transfer:

The calculation of α_s at $X < 0.1$ on the base of the Hammouda model (1995) for the inverted annular film boiling (IAFB) regime.

The calculation of α_s at $X > 0.1$ using the Groeneveld and Delorme correlation (1976).

The selection of the maximum heat transfer coefficient as

$$\alpha_{DFFB} = \max(\alpha_{\text{cond}}, \alpha_{\text{conv}})$$

where

$$\alpha_{\text{cond}} = \max(4.36\lambda/d, \alpha_{\text{pool}}).$$

The values of α_{conv} and α_{pool} are taken from Groeneveld et al. (1976) and Berenson (1961). The radiative heat transfer is relatively small for DFFB at $T_w < 770$ °C.

The heat transfer coefficients approach the values for superheated vapor at $X > 1$.

Using the 14687 data points selected from the initial 21515 ones and the application of the smoothing procedure to reduce the fluctuations of the α_s values in the LUT.

Thus the LUT version recommended for FFB by Leung et al. (1977) contains the 20280 values of the heat transfer coefficient at various flow conditions. It should be noted that it was fulfilled only for the fully developed flow conditions in a tube. It its turn, the FFB heat transfer in a rod bundle is depended on the geometry factors. However, the geometry effect is not systematically investigated until recently. At the same time, most likely the diameter tube effect is insignificant.

Nevertheless, the thermohydraulic analysis of the FBB heat transfer requires a detailed knowledge of the rod bundle geometry features. According to Leung et al. (1997), the Nusselt number at the location of interest in a channel or a subchannel is given as,

$$Nu = Nu_0 \cdot K_{\text{geom}} \cdot K_{\text{sp}} \cdot K_{\text{dev}} \cdot K_{\text{AFD}} \quad (1)$$

where

Nu_0 is the Nusselt number for tube at the same conditions;

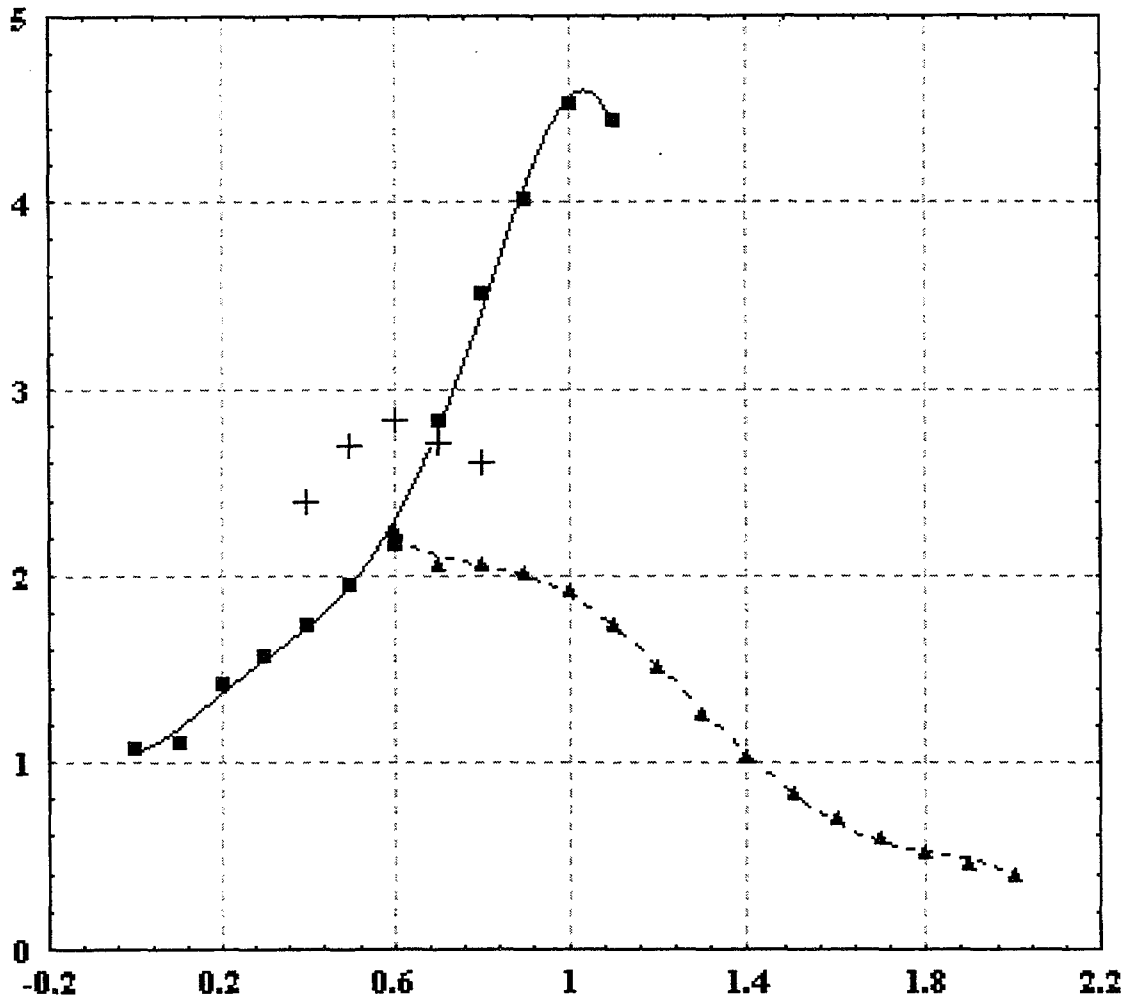
K_{geom} , K_{sp} , K_{dev} and K_{AFD} are the correction factors accounted for the effects of geometry, spacing devices, undeveloped film boiling and axial heat flux distribution.

The imbalance between the local and average qualities has to be taken into account by evaluation of the Nusselt number as $Nu_0 = f(X + \Delta X)$. It is difficult to assume that all separate effects are mutually independent of each other.

The disagreement (see Fig. 1) between the LUTs for α_s developed, respectively by Leung et al. (1997) and Kirillov P. L. et al. (1997, 1998) is caused by following factors:

- using the different experimental data received in short tubes and long tubes, respectively;

$$\frac{\alpha_s}{kW / m^2 K}$$



Legend: + experimental data, "
 ■ taken from Leung et al, 1997,
 ▲ calculated by model of Sergeev, 1987.

FIG. 1. The values OF α_s at $P = 10 \text{ MPa}$, $G = 1000 \text{ kg/m}^2\text{s}$, $q = 0.2 \text{ MW/m}^2$.

- different experimental methods:
 - 1) uniformly heated tubes and
 - 2) hot patch method;
- absence of accurate registration of beginning the FFB regime;
- using the different formulas or methods for calculation of heat transfer coefficient to vapor at the FFB regime;
- inaccurate registration of terminating the non-equilibrium or FFB regime.

The method of α_s calculation in the LUT based on the difference $(T_w - T_s)$ has its own advantages as well as limitations. While it does not permit to reach the limiting value of the heat transfer coefficient in the single-phase region, this method allows simplifying the practical calculations of α_s .

Chen et al. (1998) used the so-called tabular method for the FFB heat transfer prediction. They based on the 2192 data points of CIAE, which were obtained in tubes of diameter 6, 8 and 12 mm by the hot patch method only. The data cover the following parameter range: $P = 0.1 \div 5.8$ MPa, $G = 23 \div 1462$ kg/m²s, $X = (-0.05) \div 1.36$; $q = 0.015 \div 0.488$ MW/m² and $l = 1.2 \div 2.6$ m.

“The experimental data presented by Chen and his coworkers (1984, 1987, 1988) exhibit considerably higher film boiling heat fluxes and show a somewhat peculiar dependence of heat transfer on length near the upstream hot patch compared to other measurements. Definite reasons for this behavior could not be securely identified as the data evaluation procedures applied are not given.” (Johannesen, 1991).

Chen et al. (1979) used the Plummer parameter for processing the data, such as

$$K = \frac{X_a - X_{cr}}{X - X_{cr}} \quad (2)$$

where

X_a, X are the local actual and equilibrium quality,

X_{cr} is the critical quality at the dryout point.

The value K , which is a part of heat spent for liquid vaporization, is a function of pressure, mass flux, inlet and local quality, heat flux and tube diameter,

$$K = K_O \cdot F_q \cdot F_d \cdot F_x \quad (3)$$

where

$K_O = f(P, G, X_{cr})$ that is determined for 8 mm tube on the base of special table drawn up by using both the IAFB model and the DFFB model, Chen et al. (1988) and Chen et al. (1994a, 1994 b) respectively.

Then it is made assumptions: $F_q = 1$, $F_x = 1$ and $F_d = (d/0.08)^{0.26}$. The heat transfer coefficient is defined as,

$$\alpha_s = q/(T_w - T_s) \quad (4)$$

where

$$T_w = T_v + q/(\alpha_v + \alpha_r) \text{ and } \alpha_r < 0.05 \alpha_v \quad (5)$$

$$T_v = T_s + [(X/X_a) - 1]r / \bar{C}_p \quad (6)$$

The value of α_v is evaluated by the following correlation for the convection heat transfer coefficient in pure vapor flow:

$$Nu_v = (Nu_v)_O \cdot F \quad (7)$$

where

$$(Nu_v)_O = 0.0175 Re_v^{0.812} \cdot Pr_v^{0.333} \quad (8)$$

$$F = 1 + 2.32(1 + 0.001P) \exp^{-12Xa} \quad (9)$$

and

P – pressure [bar];

$$T_f = (T_v + T_w)/2.$$

However, it is obtained that $F \approx 1$ since at $X_a = 0.5 \div 1$ the value

$$\exp^{-12Xa} = \exp(-6 \div 12) = 0.$$

2.2. Reference temperature

The reference temperature is one of an important problem at evaluation of the FFB heat transfer. To date, there are at least three possibilities for its determination:

$$\alpha_v = q/(T_w - T_v) \quad (10)$$

$$\alpha_s = q/(T_w - T_s) \quad (11)$$

$$\alpha_b = q/(T_w - T_b) \quad (12)$$

where

$$T_b = T_s \text{ at } X < 1 \text{ and}$$

$$T_b = T_v \text{ at } X > 1.$$

We thoroughly analyzed these correlations and concluded that Eq. 12 is incorrect or at least inaccurate. The practical experience is shown that $T_b \neq T_s$ at $X \leq 1$ because, in this case, vapor is just superheated. Thus we believe that using the different conditions for T_b during the LUT development in the FBB region (T_s and T_v) is doubtful. It is possible to use the value T_v , but its calculation is difficult in engineering practice. Therefore, it is preferred to use only the value T_s as the reference temperature that allows to simplify considerably the engineering calculation methods of the FFB heat transfer coefficient. The convention of this choice is obvious.

Moreover, it should be borne in mind that the recalculation between the values of α_s and α_v

$$\alpha_s/\alpha_v = (T_w - T_v)/(T_w - T_s) \quad (13)$$

gives the incorrect results as well as distorts the function $\alpha_v(G)$. We performed the recalculation $\alpha_s \rightarrow \alpha_v$ and discovered that the effect was being very small and $\alpha_v \neq G^{0.8}$. The calculation was carried out by the Sergeev method based on the Miropolskiy work (1975) where it was found that $Nu \approx Re^{0.8}$.

2.3. Measurement of vapor superheat at FFB

Carrying out the post-CHF experiments provides the direct measurements of such parameters as a wall heat flux, a wall temperature, an inlet water temperature, pressure and mass flux. Then on the base of obtained experimental values of parameters it is possible to calculate the equilibrium quality at the inlet of test section. However, the corresponding measurements of both the actual vapor quality X_a and the average superheated vapor temperature T_b are not generally available. As a result, during the comparison between the correlative models and the experimental data it is occurred an uncertainty, which involves in the prediction of α_v . Besides the values of X and T_v are lumped together, and thus it is not available to isolate the possible sources of error in the proposed phenomenological models.

The measurement of non-equilibrium state is a key to such experimental investigation. In this case, it needs to be carried out the direct measurements of either X_a or T_v . Knowing the one parameter, the other can be calculated by equation:

$$\frac{X_a}{X} = \frac{r}{h_v - h_\ell} = \frac{I}{I + \frac{C_p}{r}(T_v - T_s)} \quad (14)$$

where

$$\overline{C_p} = \frac{I}{T_v - T_s} \int_{T_s}^{T_v} C_p dt \quad (15)$$

There is a very serious problem to measure a vapor temperature at DFFB owing to the effect of entrained liquid droplets [Grachev et al. (1975); Nijhman et al. (1980); Chen et al. (1994a)]. They are occurred essentially at a saturation temperature and tend to quench any temperature sensor, thus do not permit to determine T_v . In addition, the second complication is the walls of test section heated to high temperature since the radiation heat transfer to a temperature sensor can cause the measurement errors. It seems likely that the most precise method of X_a evaluation is the concentration method, which was suggested by Hewitt and realized by Forslund and Rohsenow (1968).

3. THE JOINTED LUT DEVELOPMENT

The values of α_s in the jointed LUT were generated by using three approaches:

- 1) direct analysis of experimental data;
- 2) calculations on the base of the Sergeev model (1987);
- 3) using the values of α_s from the LUT version by Leung et al. (1997).

Application of all these methods allowed to crosscheck each of them and to widen the parameter ranges. The LUT grid values were taken as follows: $P = 0.1 \div 20$ MPa; $G = 250 \div 3000$ kg/m²s; $X = (-0.2) \div 2.2$ and $q = 0.2 \div 3$ MW/m².

All experimental data taken from the database of the IPPE Thermophysical Data Center were grouped around the LUT grid values. The faces of elementary volumes were defined by numbers: for $P - (\pm 1)$ MPa, for $G - (\pm 125, 250)$ kg/m²s, for $X - (\pm 0.05)$, for $q - (0.2 \pm 0.2)$. The data available in these elementary volumes that were analyzed using the statistical criteria and the estimates of means were chosen as the table values.

The calculation scheme on the base of the Sergeev model (1987) was as follows:

- 1) The actual value of relative enthalpy, X_a , is defined after solving the differential equation:

$$\frac{dX_a}{dX} = 1.5 \cdot m \frac{\lambda_v}{\sigma \rho_\ell} \frac{G^2}{q} X_a (1 - X_a) \cdot \left(\frac{X - X_a}{X} \right)^n \quad (16)$$

where

$$n = 0.98 + 0.036P; \quad m = 955 - 54.6P \quad \text{at } 1 \leq P \leq 5 \text{ MPa} \quad (17)$$

$$n = 1.005 + 0.0286P; \quad m = 892 - 42P \quad \text{at } 5 \leq P \leq 18 \text{ MPa} \quad (18)$$

The integration of Eq. 16 starts from the critical quality value, X_{cr} . The following equation was used by Sergeev (1987) to define X_{cr} :

$$X_{Cr} = 1 - 0.86 \exp(-19/W) \quad (19)$$

where

$$W = G \sqrt{[d/(\sigma \rho_\ell)]} \quad (20)$$

It should be noted that the special analysis was performed to define the effect of various X_{cr} calculation methods on the final results i.e. values of α_s . The analysis based on the data of Ivashkevitch (1995) and Groeneveld et al. (1995) has shown that the small effect takes place close to $X_{cr}(X_{cr} + 0.1)$ and, otherwise, it becomes negligible.

2) The overheated steam enthalpy is evaluated,

$$h_v = h + r(X/X_a - 1) \quad (21)$$

and then the average superheated vapor temperature can be calculated

$$T_v = T_s + \frac{r}{C_p} \left(\frac{X}{X_a} - 1 \right) \quad (22)$$

3) The coefficient of heat transfer to vapor m is defined as

$$\alpha_v = Nu_v \frac{\lambda_\ell}{d} \quad (23)$$

where

$$Nu_v = 0.023 Re_v^{0.8} Pr_v^{0.4} (T_v/T_w)^{0.5} \text{ and } Re_v = (G \cdot d \cdot X_a) / \mu_v \quad (24)$$

4) The wall temperature, T_w , is found as,

$$T_w = T_v + q/\alpha_v \quad (25)$$

5) At last, the heat transfer coefficient at the FBB regime is calculated as,

$$\alpha_s = q/(T_w - T_s) \quad (26)$$

The Sergeev method discussed above was verified against the experimental data at conditions:

$$\begin{aligned} 3 \leq P \leq 18 \text{ MPa}; & \quad q < 1 \text{ MW/m}^2; \\ (T_w - T_v) = 500 \text{ }^\circ\text{C}; & \quad X > X_{cr}; \\ 100 \leq G \leq 1000 \text{ kg/m}^2\text{s}; & \quad 5 \leq d \leq 20 \text{ mm}. \end{aligned}$$

To fill the blank table cells at the negative and low positive values of X , the values of α_s generated by Leung et al. (1997) were used. At the final stage, all values were compiled in

TABLE I. THE IPPE EXPERIMENTAL DATA BANK ON PDO HEAT TRANSFER

Reference	Form of channel	d, mm	l, m	P, MPa	G, kg/m ² ·s	X	q, MW/m	n, number of points
Z.L. Miropolsky ^[17]	Tube	8	1.5	3.9 ÷ 21.6	398 ÷ 2100	-2.43 ÷ 3.42	0.07 ÷ 2.33	5500
D. Swinnerton ^[28]	Tube	9.75	0.92	0.2 ÷ 1.92	200 ÷ 1000	0 ÷ 0.46	0.005 ÷ 0.5	273
O.V. Remizov ^[29]	Tube	10	1.5 ÷ 10.2	4.9 ÷ 19.6	350 ÷ 3000	0 ÷ 2.48	0 ÷ 1.28	37298
N.S. Grachev ^[30]	Tube, sodium heated	11; 12	2.1 ÷ 9.0	7 ÷ 14	350 ÷ 1000	0.35 ÷ 1.3	0.05 ÷ 0.3	414
OKB GIDROPRESS Report, No. 213-0-084 ^[32]	Rod bundles	9.1 (7 rods) pitch 1.38	1.75	1 ÷ 6	130 ÷ 700	0.6 ÷ 1.24	0.1 ÷ 0.35	301
OKB GIDROPRESS Report, No. 431-0-047 ^[33]	Annuli	15.5/9.1	3.245	1.5 ÷ 15.9	8.9 ÷ 148	0.5 ÷ 1.96	0.03 ÷ 0.275	1154

one table and analyzed visually on the plots and by statistical methods. The analysis shown that there are regions both of agreement and disagreement between three groups of values. The criterion of final value generating was its closeness to the experimental value of α_s and to reasonable trends. Also, the preference was given to the lower values of α_s to provide the conservative approach. Finally, the procedure of smoothing was applied to the table values of α_s .

4. RESULTS AND DISCUSSION

There are presented four types for values of α_s in the jointed LUT, which was obtained within three methods mentioned and provided by procedure of smoothing, interpolation and extrapolation. The examples of the dependence of α_s on X at various G and q are shown in Fig. 2-4 and Table II. The analysis of the final LUT version shown the following trends:

- At $X < 0$, the value of α_s falls with the growth of X . It appears to be caused by decrease of liquid subcooling and growth of vapor film with vapor overheating in it.

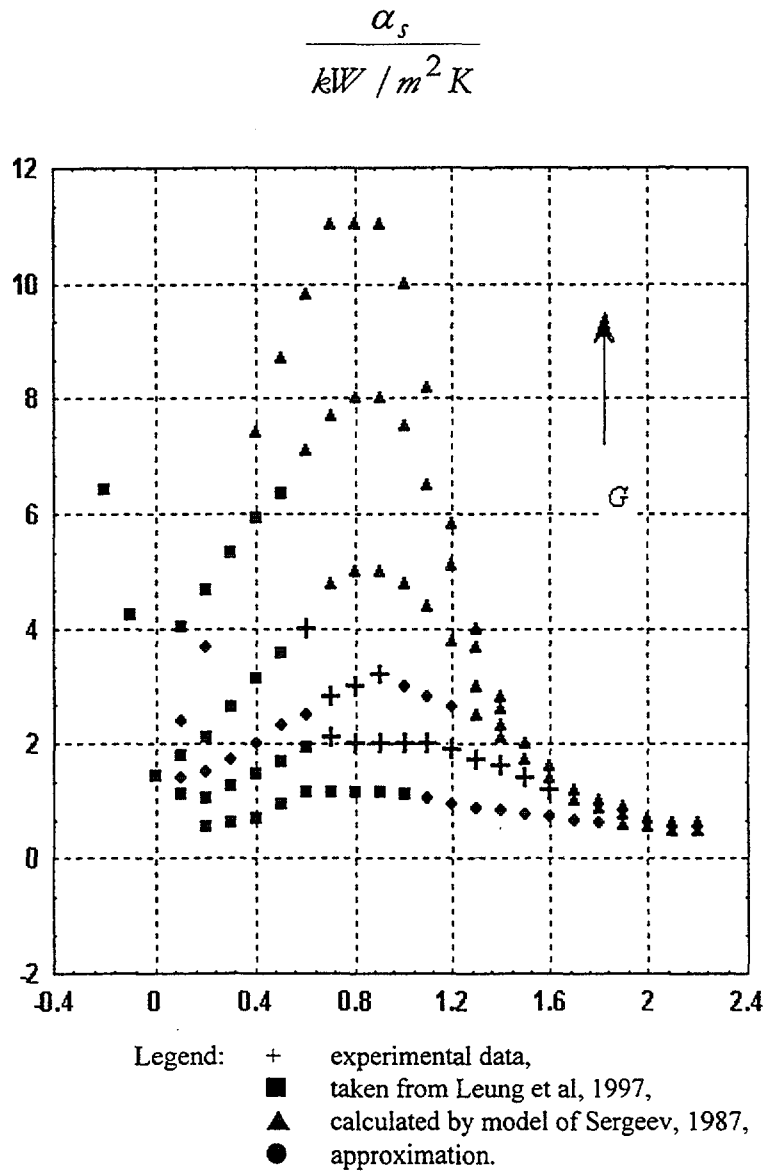


FIG. 2 The dependence of α_s on relative enthalpy at $P = 16$ MPa, $q = 0.2$ MW/m² and $G = 250, 500, 750, 1000, 1500$ and 2000 kg/m²s.

- At $X \approx 0$, the value of α_s takes the minimum value and grows together with increase of X , that can be explained by increase of linear velocity of two-phase flow.
- At $X \approx 0.4 \div 0.8$, the competitive processes of mentioned velocity increasing and of vapor overheating lead to the maximum value of α_s at $X=0.8 \div 1$.
- At higher X (after $X=1$), the value of α_s falls again that can be connected with increase of vapor overheating.

It seems that such complicated dependence of α_s on X and of other parameters (P , G and q) makes it difficult to describe all these trends by a simple equation. It is this fact that forced us to choose a form of the LUT for evaluation of α_s because it helps to avoid such a problem. The jointed LUT presented here should be considered as working material that needs to be verified. Hereafter, we suppose to refine the table values of α_s , to smooth the main trends and to widen the parameter regions. It is desirable also to estimate the heat transfer by radiation.

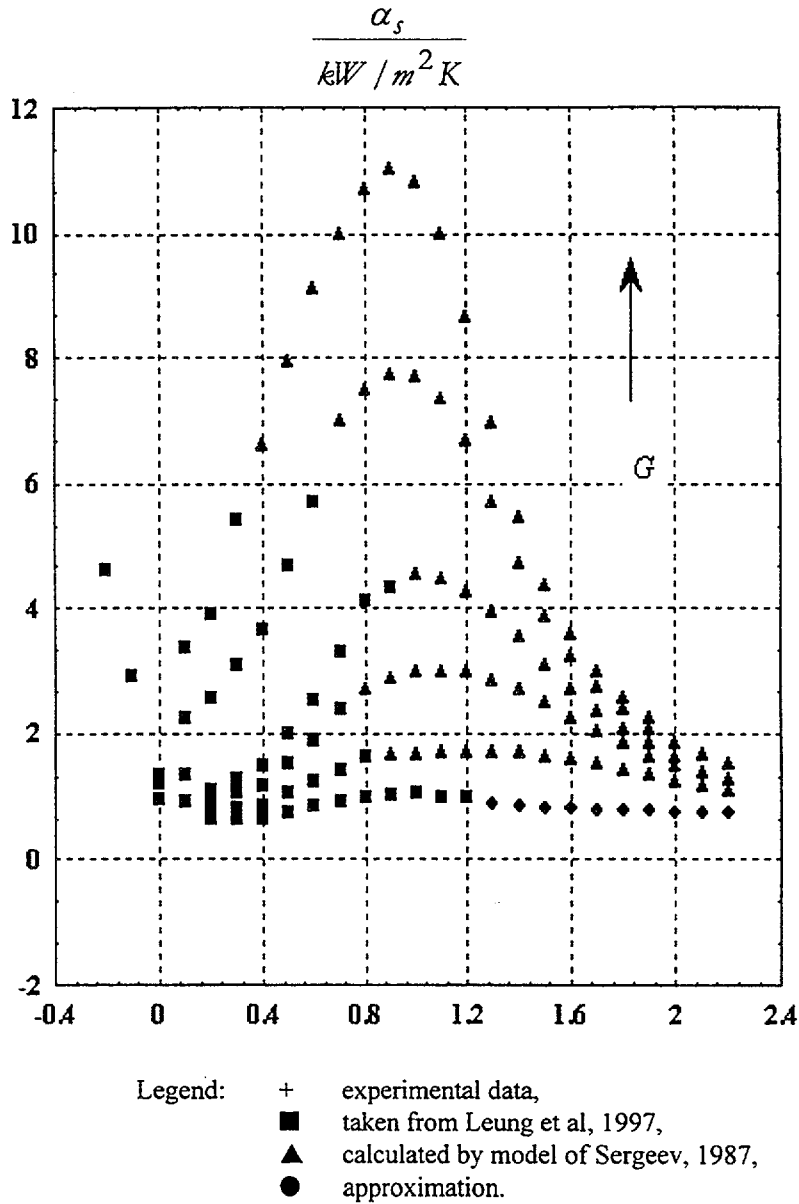


FIG. 3. The dependence of α_s on relative enthalpy at $P = 16 \text{ MPa}$, $q = 0.6 \text{ MW/m}^2$ and $G = 250, 500, 750, 1000, 1500 \text{ and } 2000 \text{ kg/m}^2\text{s}$.

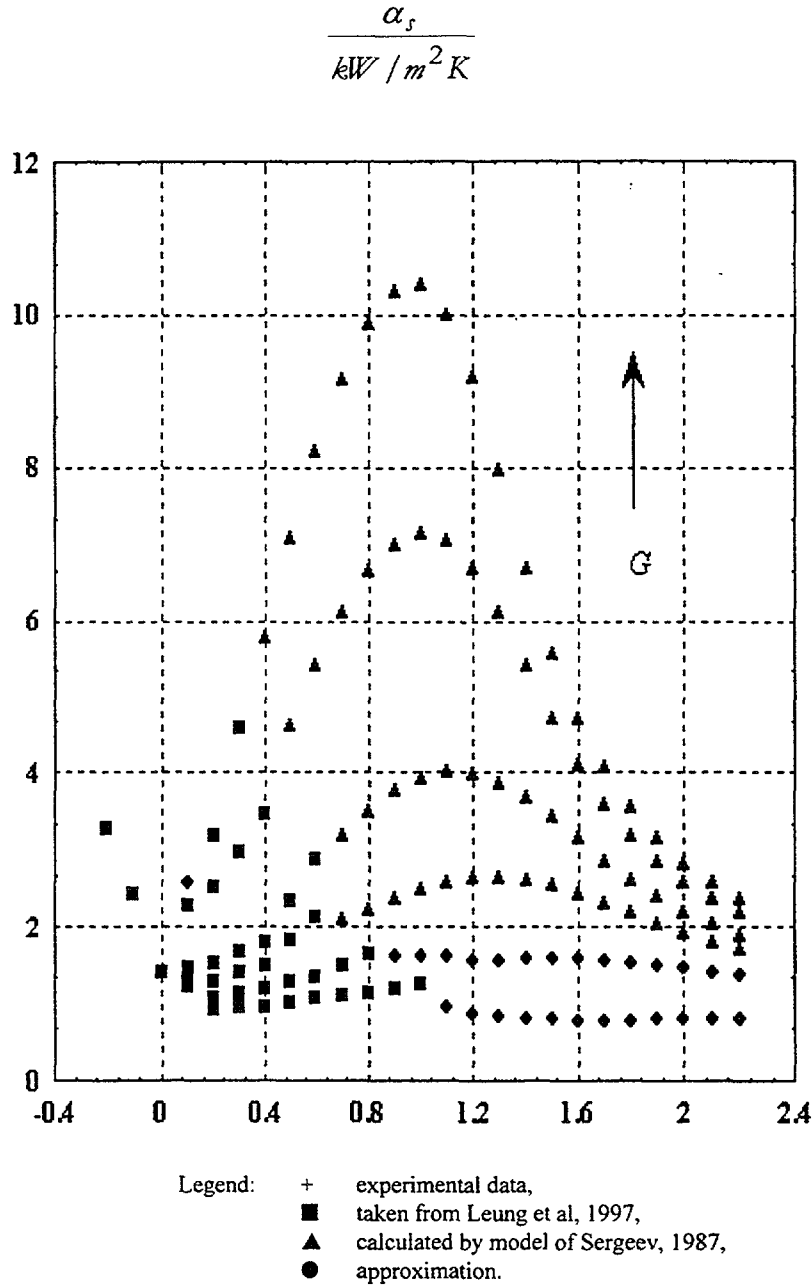


FIG. 4. The dependence of α_s on relative enthalpy at $P = 16$ MPa, $q = 1.0$ MW/m² and $G = 250, 500, 750, 1000, 1500$ and 2000 kg/m²s.

It needs to be added that the Chen methodology takes into account the degree of thermal non-equilibrium defined by Eq. 2, 3, but latter he assumed that $F_q = 1$ and $F_x = 1$. Thus effects of quality, heat flux as well as radiation are ignored. Moreover, Chen writes: "The calculations are made at such a heat flux that the wall temperature of around 600°C is achieved...". As a result, all data in the table for K_o are related only to such heat flux that is typical for $T_w = 600$ °C. From the other hand, the actual quality X_a by the Chen method can get a value of more then 1 that is impossible from physical sense. For example, if the range of parameter will be follows: $X_c \equiv X_o = 0.4 \div 0.6$; $P = 0.1 \div 1.0$ MPa; $G = 1000 \div 1500$ kg/m²s, and $K = K_o = 0.9$ then at $X = X_e = 1.2$ it will be mean that $X_a = X_o + K(X - X_o) \cong 0.5 + 0.9(1.2 - 0.5) = 1.06$.

TABLE II. THE FRAGMENT OF A LOOK-UP TABLE FOR α_g , kW/m²K, FOR $P = 4, 6$ MPa AND $X \leq 1$.

$\frac{P}{\text{MPa}}$	$\frac{G}{\text{kg/m}^2\text{s}}$	$\frac{q}{\text{MW/m}^2}$	X																
			-0.2	-0.1	0.0	0.1	0.2	0.3	0.4	0.5	0.6	0.7	0.8	0.8	0.8	0.8	0.8	0.8	1.0
4	250	0.2	1.08 G	0.92 G	0.63 G	0.50 G	0.36 G	0.40 G	0.43 A	0.43 A	0.44 A	0.55 A	0.69 A	0.72 A	0.72 A	0.72 A	0.72 A	0.72 A	0.75 A
		0.6	1.22 G	0.90 G	0.75 G	0.68 G	0.59 G	0.60 G	0.61 G	0.63 G	0.64 G	0.71 G	0.77 G	0.82 G	0.82 G	0.82 G	0.82 G	0.82 G	0.85 G
		1.0	1.42 G	1.20 G	0.92 G	0.88 G	0.84 G	0.85 G	0.85 G	0.87 G	0.88 G	0.91 G	0.93 G	1.00 G	1.00 G	1.00 G	1.00 G	1.00 G	1.07 G
		0.2	1.10 G	0.96 G	0.65 G	0.53 G	0.50 G	0.58 G	0.66 G	0.77 G	0.87 G	1.15 G	1.35 A	1.35 A	1.35 A	1.35 A	1.35 A	1.35 A	1.30 S
4	500	0.6	1.22 G	0.99 G	0.82 G	0.73 G	0.72 G	0.79 G	0.86 G	0.91 G	0.96 G	1.07 G	1.17 G	1.17 G	1.17 G	1.17 G	1.17 G	1.17 G	1.55 G
		1.0	1.46 G	1.22 G	1.01 G	0.93 G	0.92 G	0.96 G	1.01 G	1.06 G	1.12 G	1.14 G	1.17 A	1.38 A	1.38 A	1.38 A	1.38 A	1.38 A	1.59 G
		0.2	1.20 G	0.99 G	0.68 G	0.61 G	0.66 G	0.76 G	0.87 G	1.07 G	1.28 G	1.25 A	1.22 A	1.20 S	1.20 S	1.20 S	1.20 S	1.20 S	0.91 S
		0.6	1.22 G	0.99 G	0.82 G	0.75 G	0.84 G	1.07 G	1.19 A	1.31 G	1.45 A	1.60 G	1.70 G	1.61 A	1.61 A	1.61 A	1.61 A	1.61 A	1.57 A
4	1000	1.0	1.46 G	1.22 G	1.02 G	0.99 G	1.01 G	1.17 G	1.34 G	1.37 G	1.41 G	1.53 G	1.65 G	1.95 G	1.95 G	1.95 G	1.95 G	1.95 G	2.16 S
		0.2	1.30 G	1.02 G	0.70 G	0.70 G	0.82 G	0.95 G	1.08 G	1.38 G	1.67 G	1.60 A	1.40 S	1.10 S	1.10 S	1.10 S	1.10 S	1.10 S	0.98 S
		0.6	1.22 G	0.99 G	0.82 G	0.78 G	0.96 G	1.34 G	1.52 A	1.71 G	1.68 G	1.95 G	1.90 S	1.85 S	1.85 S	1.85 S	1.85 S	1.85 S	1.58 S
		1.0	1.45 G	1.22 G	1.03 G	1.05 G	1.11 G	1.39 G	1.67 G	1.68 G	1.70 G	1.92 G	2.14 G	2.31 S	2.31 S	2.31 S	2.31 S	2.31 S	1.98 S
4	1500	0.2	1.30 G	1.03 G	0.84 G	0.90 G	1.27 G	1.71 G	2.16 G	2.80 G	2.40 S	2.00 S	1.80 S	1.70 S	1.70 S	1.70 S	1.70 S	1.70 S	1.50 S
		0.6	1.22 G	0.99 G	0.90 G	0.88 G	1.32 G	1.91 G	2.49 G	2.79 G	3.09 G	2.58 S	2.28 S	2.14 S	2.14 S	2.14 S	2.14 S	2.14 S	2.04 S
		1.0	1.46 G	1.22 G	1.04 G	1.04 G	1.36 G	1.77 G	2.19 G	2.49 G	2.78 G	3.02 S	2.62 S	2.44 S	2.44 S	2.44 S	2.44 S	2.44 S	2.33 S
		0.2	1.30 G	1.03 G	0.84 G	1.04 G	1.70 A	2.30 A	2.60 A	2.80 A	2.90 S	2.90 S	2.80 S	2.50 S	2.50 S	2.50 S	2.50 S	2.50 S	2.10 S
4	2000	0.6	1.22 G	0.99 G	0.90 G	1.03 G	1.82 G	2.61 G	3.39 G	3.87 G	3.28 S	3.14 S	3.10 S	3.02 S	3.02 S	3.02 S	3.02 S	3.02 S	2.85 S
		1.0	1.46 G	1.22 G	1.04 G	1.12 G	1.54 G	2.19 G	2.83 G	3.35 G	3.62 S	3.35 S	3.29 S	3.25 S	3.25 S	3.25 S	3.25 S	3.25 S	3.17 S
		0.2	1.56 G	1.15 G	0.77 G	0.71 G	0.48 G	0.50 G	0.53 G	0.55 G	0.58 G	0.70 G	0.82 G	1.03 G	1.03 G	1.03 G	1.03 G	1.03 G	0.97 A
		0.6	1.35 G	1.10 G	0.88 G	0.79 G	0.66 G	0.67 G	0.68 G	0.69 G	0.70 G	0.78 G	0.87 G	0.94 G	0.94 G	0.94 G	0.94 G	0.94 G	1.01 G
6	250	1.0	1.53 G	1.29 G	1.01 G	0.96 G	0.90 G	0.90 G	0.90 G	0.91 G	0.91 G	0.92 G	0.93 G	1.02 G	1.02 G	1.02 G	1.02 G	1.02 G	1.12 G
		0.2	1.57 G	1.18 G	0.81 G	0.72 G	0.64 G	0.71 G	0.78 G	0.87 G	0.96 G	1.20 G	1.42 G	1.40 S	1.40 S	1.40 S	1.40 S	1.40 S	0.95 S
		0.6	1.47 G	1.26 G	0.98 G	0.85 G	0.82 G	0.88 G	0.95 G	1.02 G	1.10 G	1.17 G	1.24 G	1.47 G	1.47 G	1.47 G	1.47 G	1.47 G	1.29 S
		1.0	1.55 G	1.39 G	1.14 G	1.04 G	1.01 G	1.05 G	1.09 G	1.14 G	1.19 G	1.15 G	1.17 A	1.20 A	1.20 A	1.20 A	1.20 A	1.20 A	1.27 A
6	500	0.2	1.62 G	1.21 G	0.85 G	0.78 G	0.80 G	0.91 G	1.02 A	1.10 A	1.20 A	1.30 A	1.20 A	1.00 S	1.00 S	1.00 S	1.00 S	1.00 S	0.87 S
		0.6	1.48 G	1.27 G	1.03 G	0.91 G	0.95 G	1.17 G	1.39 G	1.46 G	1.54 G	1.69 G	1.73 S	1.43 S	1.43 S	1.43 S	1.43 S	1.43 S	1.27 S
		1.0	1.56 G	1.40 G	1.18 G	1.12 G	1.12 G	1.28 G	1.44 G	1.49 G	1.55 G	1.60 G	1.66 G	1.51 S	1.51 S	1.51 S	1.51 S	1.51 S	1.41 S
		0.2	1.66 G	1.25 G	0.89 G	0.85 G	0.96 G	1.11 G	1.26 G	1.59 G	1.93 G	1.58 S	1.27 S	1.16 S	1.16 S	1.16 S	1.16 S	1.16 S	1.08 S
6	1000	0.6	1.49 G	1.28 G	1.07 G	0.97 G	1.08 G	1.45 G	1.83 G	1.90 G	1.98 G	1.94 S	1.61 S	1.47 S	1.47 S	1.47 S	1.47 S	1.47 S	1.39 S
		1.0	1.58 G	1.42 G	1.22 G	1.20 G	1.22 G	1.50 G	1.78 G	1.85 G	1.91 G	1.94 S	1.70 S	1.61 S	1.61 S	1.61 S	1.61 S	1.61 S	1.55 S
		0.2	1.66 G	1.25 G	0.89 G	0.96 G	1.10 G	1.26 G	1.60 G	1.93 G	2.00 S	2.00 S	2.00 S	1.90 S	1.90 S	1.90 S	1.90 S	1.90 S	1.80 S
		0.6	1.49 G	1.28 G	1.10 G	1.02 G	1.44 G	2.02 G	2.59 G	2.40 A	2.18 S	2.04 S	2.04 S	2.06 S	2.06 S	2.06 S	2.06 S	2.06 S	2.04 S
6	1500	1.0	1.58 G	1.42 G	1.22 G	1.20 G	1.49 G	1.90 G	2.32 G	2.28 A	2.23 A	2.18 S	2.07 S	2.10 S	2.10 S	2.10 S	2.10 S	2.10 S	2.13 S
		0.2	1.66 G	1.25 G	0.95 G	1.21 G	1.80 A	2.00 A	2.40 S	2.80 S	3.00 S	3.10 S	3.00 S	2.80 S	2.80 S	2.80 S	2.80 S	2.80 S	2.50 S
		0.6	1.49 G	1.28 G	1.10 G	1.15 G	2.01 G	2.76 G	2.72 A	2.67 A	2.67 A	2.67 A	2.94 A	2.94 A	2.94 A	2.94 A	2.94 A	2.94 A	2.88 A
		1.0	1.58 G	1.42 G	1.22 G	1.25 G	1.74 G	2.38 G	2.50 A	2.60 S	2.56 S	2.70 S	2.84 S	2.94 S	2.94 S	2.94 S	2.94 S	2.94 S	2.97 S

However, the CIAE tabular method together with the correction factor ‘ K ’, which accounts for both history effect and the non-equilibrium degree, appears to be perspective. At the same time, the present verification of this method was carried out only on the base of the CIAE data without inclusion the databases developed by other researchers.

5. CONCLUSIONS

The 1998-version of the LUT for the FFB heat transfer coefficient for water flow in a round tube is presented. This LUT covers the range of parameters:

$$P = 0.1 \div 20 \text{ MPa}, G = 250 \div 3000 \text{ kg/m}^2\text{s},$$

$$X = (-0.2) \div 0.2, q = 0.2 \div 1.0 \text{ MW/m}^2; d = 10 \text{ mm}.$$

The results can be summarized as follows:

There is a need to distinguish two FFB heat transfer regimes, such as the PDO (post-CHF) heat transfer and before-CHF heat transfer. At present time it is not obvious yet that the heat transfer correlations would be the same for the both regimes.

The FFB heat transfer prediction in a rod bundle would be based both on the CHF look-up table for bundles and the LUT for FFB in tubes with appropriate correction factors.

The further research activities on the refinement of the LUT for FFB are to be carried out including:

The table would be widened for the tubes uniformly heated at large mass flux.

The values of parameters, which characterize beginning the FFB regime, would be added into this LUT. In any case, the method of determination of such parameters is to be given. Moreover, it needs to be introduced here the difference between the experimental and calculated values of the FFB heat transfer coefficient.

The values of the experimental data errors on α_s as well as a number of experiments that were the base for their calculation would be presented.

NOMENCLATURE

\bar{C}_p	average heat capacity, [J/kg·K]
d	diameter, [mm]
G	mass flux, [kg/m ² ·s]
h	specific enthalpy, [J/kg]
K	Plummer parameter
l	length, [m]
Nu	Nusselt number
P	pressure, [MPa]
Pr	Prandtl number
q	heat flux, [MW/m ²]
Re	Reinolds number
T	temperature, [K]
T_f	equilibrium flow temperature, [K]

T_v average superheated vapor temperature, [K]
 X quality

Greek symbols

α_s FFB heat transfer coefficient, [W/m²·K]
 λ thermal conductivity, [W/m·K]
 μ dynamic viscosity, [kg/m·s]
 ρ density, [kg/m³]
 σ surface tension, [N/m]

Subscripts

a actual
 b bulk
 cr critical
 l liquid
 r radiation
 s saturation
 v vapor
 w wall

ABBREVIATIONS

AFD Axial Heat Flux Distribution
CHF Critical Heat Flux
DFF Dispersed Flow Film Boiling
B
FFB Flow Film Boiling
IAFB Inverted Annular Film Boiling
LUT Look-Up Table
PDO Post-Dryout

REFERENCES

- [1] BERENSON, P. J., 1961, "Film boiling heat transfer from horizontal surface", *J. Heat Transfer*, vol. 83, pp. 351-358.
- [2] BOBKOV, V. P., BLOKHIN, A. I. et al., 1982, "The heat and mass transfer information center for nuclear technology", *Atomnaja Energija*, vol. 53, ¹ 3, pp. 183-184 (Rus.).

- [3] CHEN, Y. Z. and LI, J. S., 1984, "Subcooled flow film boiling of water at atmospheric pressure in: two-phase flow and heat transfer", China-US Progress, ed. by Chen, X. J. and Veziroglu, N., Washington, Hemisphere, pp. 141-150.
- [4] CHEN, Y. Z. and FU, X. X., 1988, "Experimental and analytical study of inverted annular film boiling of water", *Proc. 1st World Conf. on Experimental Heat-Transfer, Fluid Mechanics and Thermodynamics*, Yugoslavia, pp. 1438-1443.
- [5] CHEN, Y. Z. and CHEN, H. Y., 1994a, "An experimental investigation of thermal nonequilibrium in dispersed flow film boiling of water", *Proc. Int. Conf. on New Trend in Nuclear System Thermohydraulics*, Pisa, vol. 1, pp. 31-38.
- [6] CHEN, Y. Z. and CHEN, H. Y., 1994b, "A model of dispersed flow film boiling heat transfer of water", *Proc. 10th Int. Heat Transfer Conf.*, Brighton, vol. 7, pp. 419-423.
- [7] CHEN, Y. Z. and CHEN, H. Y., 1998, "A tabular method for prediction of the heat transfer during saturated film boiling", *Proc. 11th Int. Heat Transfer Conf.*, Kyongju, vol. 2, pp. 163-168.
- [8] FORSLUND, R. P. and ROHSENOW, W. M., 1968, "Dispersed flow film boiling", *J. Heat Transfer*, vol. 90, ¹ 4.
- [9] GRACHEV, N. S., IVASHKEVITCH, A. A. and SHUMSKIY, R. V., 1975, "Measurements of moisture in superheated vapor (method for actual vapor temperature)", Preprint FEI-509, Obninsk, IPPE, (Rus.).
- [10] GRACHEV, N. S., IVASHKEVITCH, A. A., KIRILLOV P. L. et al., 1974, "DNB in sodium-cooled steam generators and heat transfer in PDO region", *Proc. US/USSR Seminar on Development of Fast Breeder Reactor Steam Generators*, vol. 1, pp. 302-331 (Rus.).
- [11] GROENEVELD, D. C. and DELORME, G. C. I, 1976, "Prediction of thermal non-equilibrium in post-dryout regime", *Nuclear. Engineering and Design*, vol. 36, ¹ 1, pp. 17-26.
- [12] GROENEVELD, D. C., LEUNG, L. K. H. et al., 1996, "The 1995 look-up table for critical heat flux in tubes", *Nuclear. Engineering and Design*, vol. 163, ¹ 1, pp. 1-23.
- [13] HAMMOUDA, N., 1995, "Subcooled film boiling in non aqueous fluids", Ph.D. thesis, University of Ottawa, Canada.
- [14] IVASHKEVITCH, A. A., 1995, "The choice of parameters to describe data on burnout in tubes", Preprint FEI-2424, Obninsk, IPPE (Rus.).
- [15] JOHANNENSEN, K., 1991, "Low quality transition and inverted annular flow film boiling of water: an updated review", *Experim. Therm. and Fluid Science*, ¹ 4, pp. 497-509.
- [16] KIRILLOV, P. L., IVASHKEVITCH, A. A. et al., 1997, "Conceptual problems of heat transfer calculation at post-dryout regime", *Proc. 8th Int. Topic. Meeting NURETH-8*, Kyoto, vol. 3, pp. 1559-1568.
- [17] KIRILLOV, P. L., SMOGALEV, I. P. et al., 1996, "Look-up table for heat transfer coefficient at post-dryout for water flow in tubes (1996-version)", Preprint FEI-2525, Obninsk, IPPE (Rus.).

- [18]KIRILLOV, P. L., SMOGALEV, I. P., IVASHKEVITCH, A. A., VINOGRADOV, V. N., 1997, "The Look-up table for the post-dryout heat transfer prediction", Report CRP Meeting IAEA, Obninsk, Oct. 6-10.
- [19]LEUNG, L. K. H. and GROENEVELD, D. C., 1997, "Recent development of prediction methods for chf, pdo heat transfer", *ibid*.
- [20]LEUNG, L. K. H., HAMMOUDA, N. and GROENEVELD, D. C., 1997, "A look-up table for film-boiling heat-transfer coefficients in tubes with vertical upward flow", *Proc. 8th Int. Topic. Meeting NURETH-8*, Kyoto, vol. 2, pp. 671-678.
- [21]MIROPOSKIY, Z. L., 1975, "Heat transfer to superheated steam at heat supply and heat removal", *Teploenergetika*, ¹ 3, pp. 75-78 (Rus.).
- [22]NIJIHAVAN, b., CHEN, J. C. and SUNDARAM, R. K., 1980, "Measurement of vapor superheated in post-CHF boiling", *J. Heat Transfer*, vol. 102, ¹ 3, pp. 465-470.
- [23]PLUMMER, D. N., GRIFFITH, P. and ROHSENOW, W. M., 1974, "Post-CHF to flowing liquid in a vertical tube", *Trans. CSME*, vol. 4, pp. 151-158.
- [24]REMIZOV, O. V., 1987, "Study of the steam generating surface temperature conditions at CHF", *Teploenergetika*, ¹ 10, pp. 55-56 (Rus.).
- [25]SERGEEV, V. V., 1987, "Calculation of heat transfer in post-dryout zone of vertical tubular channels", Preprint FEI-1836, Obninsk, IPPE (Rus.).
- [26]"Study of heat transfer in rod bundles after CHF", 1976, OKB GIDROPRESS Report, ¹ 213-0-084 (Rus.).
- [27]"Study of heat transfer of wetted and superheated steam at low mass flux", 1980, OKB GIDROPRESS Report, ¹ 431-0-047 (Rus.).
- [28]SWINNERTON, D., MOOD, M. L. and REARSOW, K. G., 1988, "Steady state PDO experiments at low and medium pressure", AEEWR 2267, Winfrith.

DISPERSED FLOW FILM BOILING HEAT TRANSFER OF FLOWING WATER IN VERTICAL TUBES — CIAE STEADY STATE DATA AND PREDICTION METHODS

CHEN YUZHOU, CHEN HAIYAN
China Institute of Atomic Energy,
Beijing, China



XA0055010

Abstract

In CIAE a great number of film boiling experimental data have been obtained at steady state by using directly heated hot patch technique, covering the range of pressure 0.1-6MPa and mass flux of 23-1462 (23-500 mainly) kg/m²s. It is observed that in dispersed flow film boiling significant thermal nonequilibrium exists, and the heat transfer coefficients exhibit strongly history-dependent nature. Based on the experimental results a mechanistic model and a tabular method are proposed, and the assessment of RELAP5/MOD2.5 is made.

1. INTRODUCTION

Film boiling may be encountered during the blowdown and reflood phases in the loss of coolant accident (LOCA) of a nuclear reactor. Precise calculation of the heat transfer of the film boiling is important because the maximum temperature in the fuel elements is primarily determined by the heat transfer in this regime.

Film boiling occurs in dispersed flow purely, or in inverted annular flow over a short length followed by dispersed flow. Therefore, the calculation of the heat transfer in dispersed flow film boiling is particularly interest for the analysis of a reactor accident. In the dispersed flow film boiling the main path for the heat transfer is from the wall to the vapor and then to the liquid droplets, characterized by the thermal nonequilibrium between the vapor and liquid droplets. Especially at lower pressure and/or lower flow, which is typical condition for the reflooding process of a LOCA, the thermal nonequilibrium is significant, presenting a major challenge for the calculation of heat transfer[1]. This is due to the fact that (1) the thermal nonequilibrium is dominated by the interfacial exchanges of the heat, mass and momentum, which are poorly understood and are difficult to measure in experiment at present, and (2) it is difficult to establish the film boiling regime of flowing water at steady-state by using a conventional experimental technique, so that the data are not adequate.

So far great number of correlations and models of the film boiling heat transfer have been available in literature. Significant discrepancies exist among them as to the calculated values and even the parametric trends. A comprehensive review has been given by Groeneveld[2], and it is concluded that "reliable post-CHF correlations are not yet available for low flows and pressure" and "caution should be exerted in using these correlations as here the data base is scarce". Since Groeneveld[3] first applied the hot patch to establish the steady-state film boiling regime, great number of data have been obtained by many researchers with this technique, and the database of the film boiling has been greatly extended[4-6].

Recently, Leung et al.[7] and Efanov et al[8] developed the look-up tables for the film boiling heat transfer coefficients, based on the AECL data bank and IPPE data bank, respectively. Compared to the correlations and models, the table method has advantages of higher accuracy, wide range of validity and convenience for updating. Nevertheless, the table is heavily relied on the database, so that it can not be used with confidence for those ranges where the database is limited, e.g., for lower pressure and/or lower flow conditions.

In 1984 the author successfully applied a modified version of the hot patch technique (so-called directly heated hot patch) to establish the film boiling regime at stable condition in China Institute of Atomic Energy (CIAE)[9]. Since then, a great number of data have been obtained over wide range of conditions with emphasis on lower flow region [10-13]. The effects of various parameters have been systematically studied. In the experiment the vapor superheats have also been obtained, which are important for the development of physical model. Significant thermal nonequilibrium exists in the dispersed flow film boiling (DFFB), associated with extremely complicated parametric trends and strong history-dependence of the heat transfer coefficients. Based on the measurements of both wall and vapor temperatures a mechanistic model and a tabular method have been proposed [14,15], and the assessment of RELAP5/MOD2.5 has been made. This paper presents the typical results, discussions and the comparison of experimental results with some other prediction methods.

2. CIAE STEADY-STATE FILM BOILING EXPERIMENT

2.1 Directly heated hot patch technique

The experiment is performed in vertical tubes with water flowing upward inside. At both ends of the boiling length the local thickness of the tube is reduced with about 1mm in height (Fig.1). When the tube is heated directly by the electric current, a hot patch is created there due to higher local resistance. It catches the quench front there, and the film boiling is stably maintained downstream. The hot patch is very small, so that the axial conduction can prevent it from an excessive temperature rise or burning out. The heat fluxes in the boiling section and preheat section are controlled separately by different supplies. The directly heated hot patch can reach very high heat flux, enabling the experiment to cover a wide range of conditions. The hot patch of the test section associates with the transition from the pre-CHF to post-CHF regime. This is similar with the rewetting front of the fuel element during the reflooding process. Both of them reach the critical heat flux.

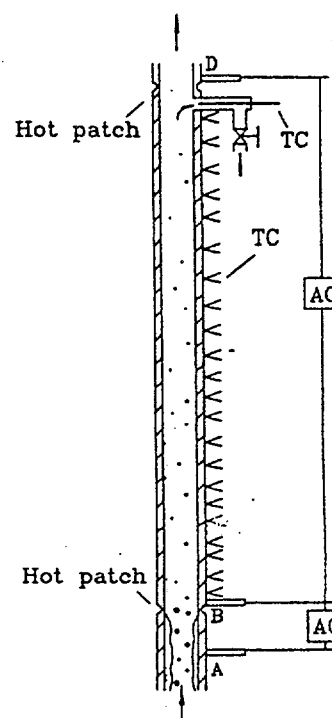


Fig. 1 The test section with the measurement of both wall and vapor temperatures

2.2 Measurement of the vapor superheats

As shown in Fig.1, the vapor is drained in a bypass near the outlet, where the droplets are separated from the vapor due to greater inertia and vapor superheats can be measured. The vapor draining in the bypass is controlled by a valve. At larger draining rate the vapor comes not only from the boundary zone but mainly from the core. The measured value does not vary with the draining rate, representing the mean vapor temperature of the section. At low or medium flow the vapor superheats are successfully obtained, showing significant thermal nonequilibrium. The measurement is failed at higher flow as the droplets are not well separated from the vapor. For this condition the nonequilibrium is expected to be less important.

The measurement of vapor temperatures is verified by two methods: (1) The vapor temperatures are taken near the outlet where the quality is relatively high and the effect of droplet on the vapor convection heat transfer is not important, so the vapor temperature can be reasonably

estimated by a traditional heat transfer correlation for vapor flow. The deviation between the measurement and calculation is comparable with the accuracy of experiment. (2) The vapor temperatures are also measured using another technique [13]. The results obtained with two different techniques agree with each other.

2.3 Experimental results

The experiments are carried out in tubes of 6.8mm and 12mm ID, covering the range of pressure 0.1 - 6.0 MPa, mass flux 23 - 1462 (23-500 mainly) kg/m²s, local quality -0.05 - 1.36 and heat flux 1.5 - 48.8W/cm², as shown in Fig.2. The typical distributions of heat transfer coefficients along the length are exemplified in Fig.3 by plotting the $h (= q / (T_w - T_s))$ against equilibrium quality x_e (x_e increases linearly as the distance increasing for uniform heating). The extremely complicated parametric trends and strong history-dependence of the heat transfer coefficients are observed. The effects of major parameters have been discussed in the previous papers. The history-dependence of the heat transfer coefficients and the entrance effect are discussed hereafter.

2.3.1 History-dependence of the heat transfer coefficients

In Fig.3, the results for the runs with same flow conditions but different inlet qualities are displayed on one figure. As seen, at the same pressure and mass flux a given equilibrium quality generally corresponds to different heat transfer coefficients for different inlet qualities, suggesting the history-dependence of the heat transfer coefficients. This effect is the result of thermal nonequilibrium, and is particularly strong at lower flow condition.

The thermal nonequilibrium is evidenced by the measurement of vapor superheats. At $P = 0.1$ MPa, $G = 25$ kg/m²s and $x_0 = 0-0.8$, for instance, the vapor superheat measured at the position of 2m from the dryout point is generally up to 500K, while the temperature difference between the wall and vapor, $T_w - T_v$, is less than 200K; and at $P = 6$ MPa, $G = 400$ kg/m²s, the vapor superheat there reaches about 250K, and $T_w - T_v$ is around 200K.

In the DFFB the thermal nonequilibrium is controlled by the fractions of the wall heat going to the liquid for evaporating into vapor. This fraction, k , may vary over nearly the whole range of 0 - 1.0 with the flow conditions. At lower flow and higher quality, only small fraction of heat goes to the liquid but most to the vapor, thus, the vapor generation along the length is small and the vapor and wall superheats increase greatly along the length. Therefore, the heat transfer coefficients ($= q / (T_w - T_s)$) decrease steeply and exhibit strong history-dependence. On the contrary, at higher flow and lower quality conditions the major part of heat goes to the liquid and less to the vapor, so the heat transfer coefficients exhibit increase trend, and the history effect is less important.

2.3.2 Entrance effect

In the practical applications the film boiling may occur at different heating condition at the dryout point and upstream. Therefore, over the entrance region the thermohydraulic condition in the flow is not fully developed, and there would be some uncertainty in calculation of the heat transfer. The inverted annular flow generally sustains over a shorter length, so this entrance effect would be appreciable. Nevertheless, the dispersed flow film boiling can sustain over a very long length, and after a distance the hydrodynamic condition is essentially developed and the effect due to the axial heat conduction at the dryout point is diminished, so that the entrance effect becomes not appreciable. It is noted that the stable film boiling experimental data obtained in CIAE, AECL and Winfrith are close to each other except for the entrance region. In the present experiment the hot patch is very small (only about 1mm in height), and the dryout initiates from the upper edge of the hot patch. Therefore, the energy from the hot patch to the dryout side is mainly by axial conduction in the wall, and it only makes a minor contribution for the evolution of thermal nonequilibrium beyond the entrance region.

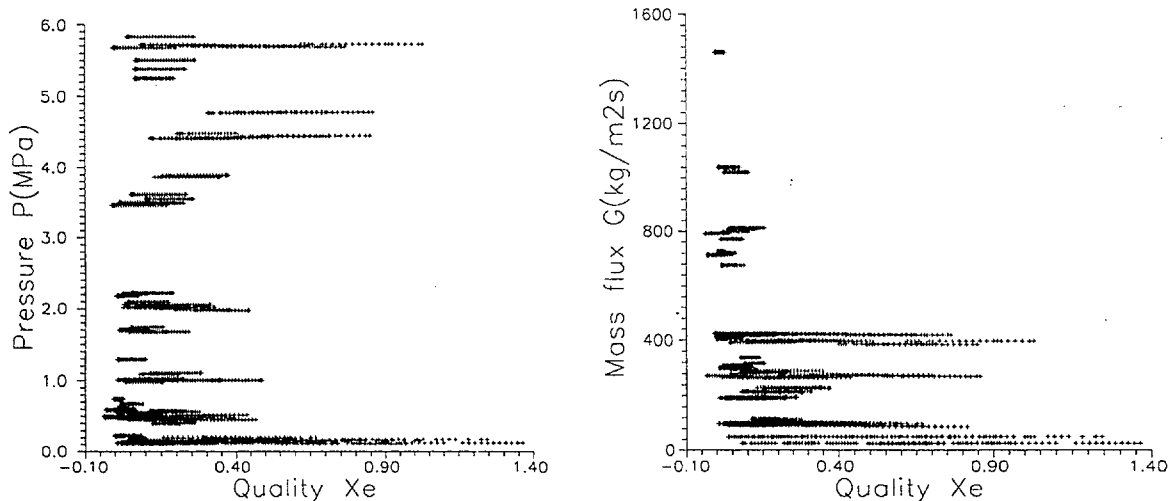


Fig. 2 The range of flow conditions covered by CIAE data bank

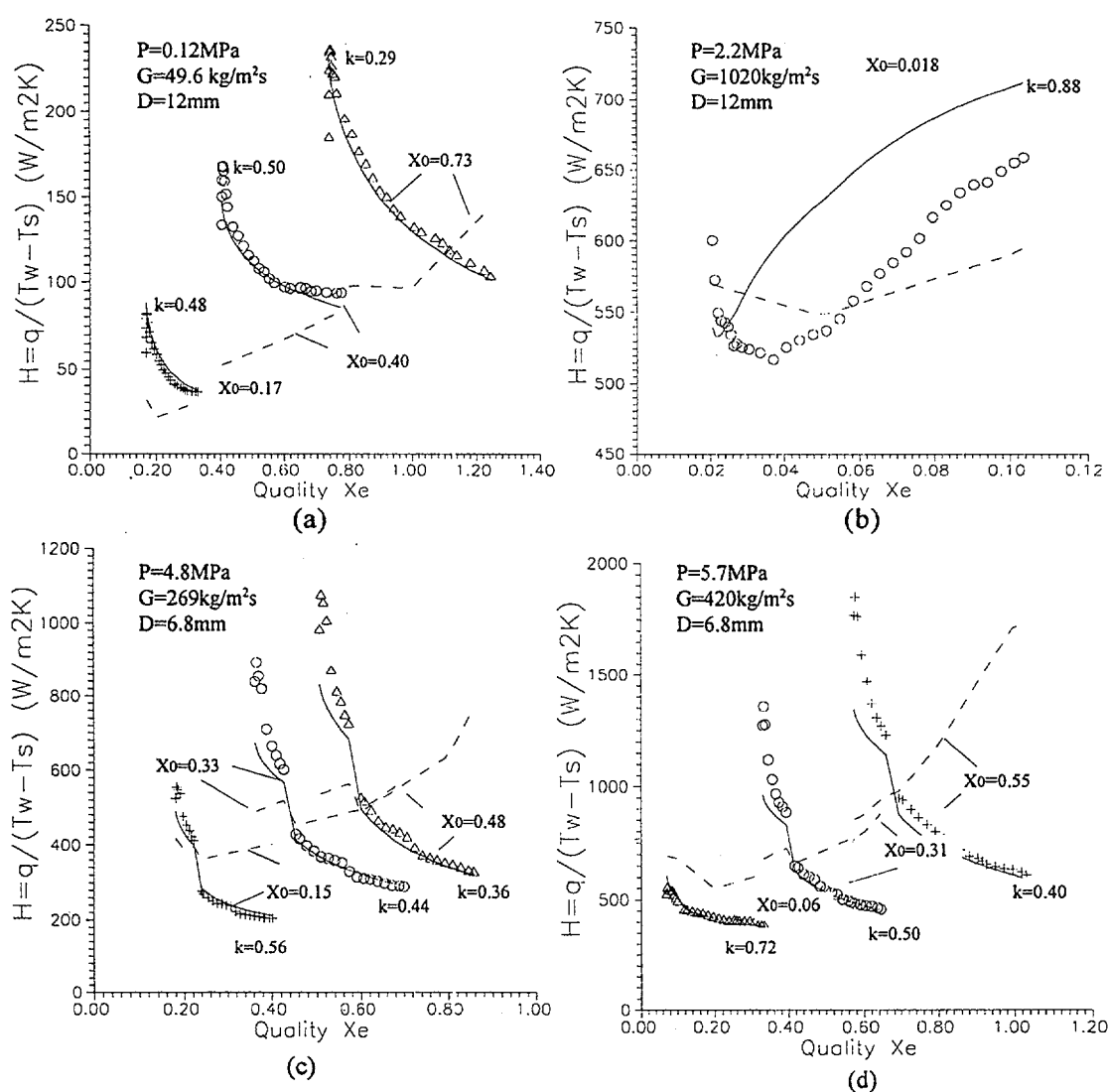


Fig.3 The distribution of the heat transfer coefficient along the length for different conditions
(— present tabular method, ---- Leung's look-up table, Δ \circ + data)

Note: in Fig.2(c,d) two portions of boiling length are at different heat flux

3. PREDICTION METHODS

Based on the steady state data a mechanistic model[14] and a tabular method[15] have been proposed.

3.1 Mechanistic model[14]

The mechanistic model is based on the motion, mass and energy equations for two fluids with the closure laws on the vapor-droplet heat transfer, drag coefficient and droplet diameter. It calculates the vapor and wall temperatures along the length step by step. This model is similar with that developed by Arrieta and Yadigaroglu [16]. Two major modifications are made for its application in wider range of conditions: (1) an enhancement factor F is introduced to account for the effect of the droplets on vapor convection heat transfer, which is important for lower quality condition, and (2) different expressions for the droplet diameter are used for the DFFB initiated from the break-down of IAFB and from the dryout of annular flow, respectively. The present mechanistic model calculates the CIAE DFFB data ($L > 0.1\text{m}$) for the wall temperature with the average error (AVG) of 2.1% and root-mean-square error (RMS) of 8.9%, respectively (Fig.4).

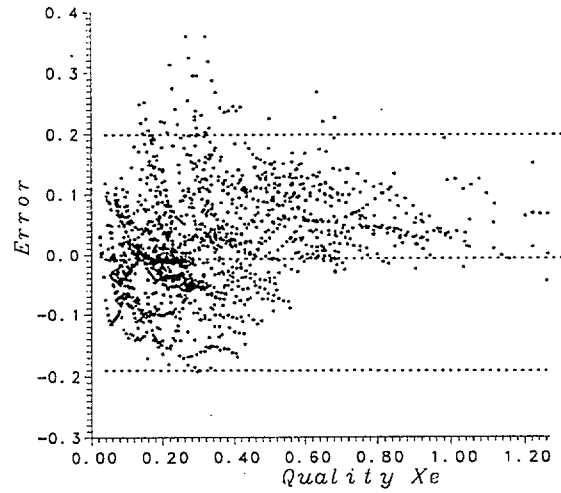


Fig. 4 The error distribution of the calculation of the mechanical model for wall temperature

The mechanistic model can be easily implemented in the two-fluid six-equation system codes, such as RELAP5 and CATHARE. It has sound physical basis and is capable of the calculation of the heat transfer for various complicated conditions of a reactor accident, e.g. transient with non-uniform heating. This has been attempted in RELAP5/MOD2.5 by modifying some constitutive equations[17].

3.2. Tabular method[15]

The nonequilibrium parameter is introduced, which is defined as[18]

$$k = \frac{x_a - x_0}{x_e - x_0} \quad (1)$$

where

- x_a is the local actual quality,
- x_e is the equilibrium quality,
- x_0 is the inlet quality (at the dryout point),

and the k is expressed as

$$k = k_0 \cdot k_q \cdot k_d \cdot k_x \quad (2)$$

where

- k_q is the correction factor for the effect of heat flux,
 - k_d is the correction factor for the effect of diameter,
 - k_x is the correction factor for the effect of local quality,
- and the k_0 is a function of the pressure, mass flux, inlet quality.

The calculation of the mechanistic model shows that over the main portion of the boiling length the k does not vary appreciably, except for the entrance region. In the present method the k is approximated as a constant for the whole length. This treatment is similar with that in the Plummer correlation[18] in which the k is independent of local quality. It does not produce a great difference for the calculation of wall temperature since the vapor superheating over the entrance region is not important, as shown in Fig. 5.

The values of the k_0 are obtained from the calculation of the mechanistic model and are tabulated with three parameters: P, G and x_0 [15].

Having the value of k , the X_a is calculated, and the vapor temperature is then evaluated by the heat balance equation

$$T_v = T_s + \left(\frac{X_e}{X_a} - 1 \right) \frac{H_{fg}}{C_{pg}} \quad (3)$$

where

H_{fg} is the latent heat,
 C_{pg} is the vapor specific heat,
 T_s is the saturation temperature.

Finally, the wall temperature is calculated by

$$T_w = T_v + q / (h_c + h_r) \quad (4)$$

where

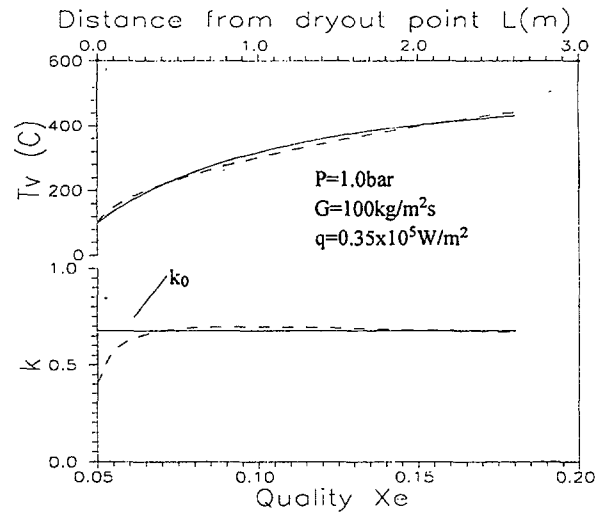
q is the wall heat flux to the coolant,
 h_c is the heat transfer coefficient for the convection,
 h_r is the heat transfer coefficients for the radiation.

and the h_c is evaluated by the correlation for convection heat transfer in pure steam flow (Nu_{f0}), multiplied by an enhancement factor F , i.e.,

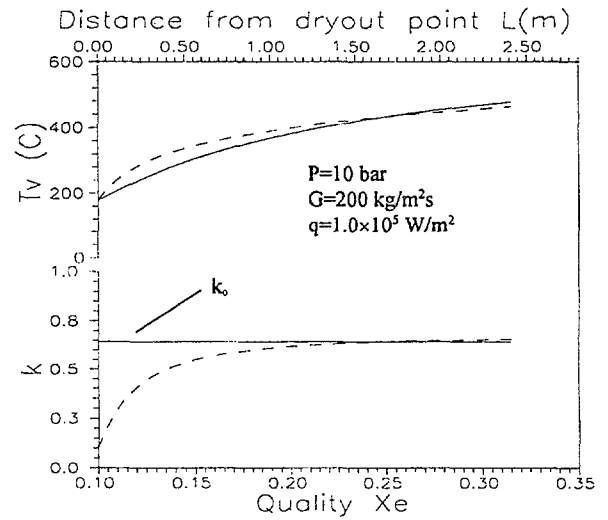
$$Nu_f = Nu_{f0} F \quad (5)$$

The convection heat transfer coefficients for pure steam are calculated with[19]

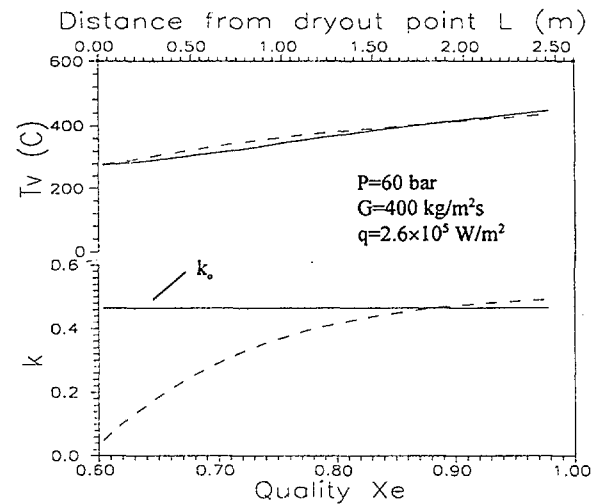
$$Nu_{f0} = 0.0175 Re_f^{0.812} Pr_f^{0.333} \quad (6)$$



(a)



(b)



(c)

Fig.5 The calculation of T_v and k
 (---- with model — with $k=k_0$)

and the enhancement factor F is estimated by[14]

$$F = 1 + 2.32(1 + 0.01P)e^{-12X_a} \quad (7)$$

where

P is the pressure in bar,
 x_a is the actual quality,

For the present conditions, the radiation heat flux is generally less than 5% of the total wall heat flux and is not considered.

The present tabular method has been used to calculate the CIAE data bank for $We > 10$ ($We = (GX)^2 D / (\rho_g \sigma)$) and $L > 0.1m$, which cover basically the dispersed flow and the transition between the dispersed flow and inverted annular flow. In the present calculation the correction factor for the diameter is

$$k_d = \left(\frac{D}{0.008} \right)^{0.26} \quad (8)$$

and the effects of local quality and heat flux are not considered ($k_q=1$ and $k_x=1$).

2192 data points ($L > 0.1m$, $We > 10$) are calculated for the wall temperature with the AVG of 1.4% and RMS of 7.2%, respectively. (Fig. 6).

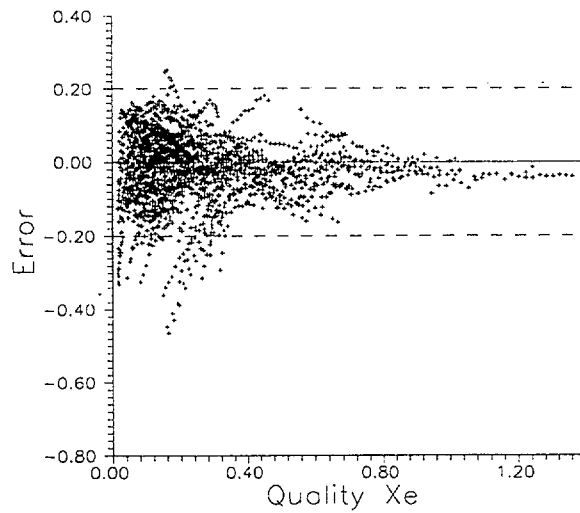


Fig.6 The error distribution of the calculation of present tabular method for the heat transfer coefficient

4. COMPARISON OF CIAE DATA WITH OTHER PREDICTION METHODS

The CIAE data are calculated with the Sergeev correlation[19]. The AVG and RMS are -48.1% and 50.4% for the wall temperatures (Fig.7), and 80.1% and 97.9% for the heat transfer coefficients, respectively. The discrepancy between them would be mainly due to the fact that part of CIAE data are out of range of Sergeev correlation, and also due to the difference in the conditions (at steady state for the CIAE data and at transient for the database of Sergeev correlation)

The CIAE data are calculated with the Leung's look-up table with the AVG of 5.4% and RMS of 30.2% for the wall temperature (Fig.8). The RMS of 30.2% is much greater than that of 6.73% in calculation of the AECL data bank with the same table. This is expectable since the most of CIAE data lie on the region where the leung's table has no database. Especially the Leung's table is based on the local conditions and can not reflect the history effect.

The comparison of the CIAE data with the Plummer correlation is made in Fig.9a. The AVG and RMS are 18.1% and 28.9% respectively, for the calculation of wall temperature. The larger deviation corresponds to low quality region. At this condition the effect of droplets on the convection heat transfer is appreciable, which is not considered in the Plummer correlation. By introducing the enhancement factor, F (Eq.7), to the Plummer correlation the RMS is decreased to 12% (Fig.9b).

5. ASSESSMENT OF RELAP5/MOD2.5 WITH THE CIAE DATA BANK

By setting reflood flag off, the best estimate system code RELAP5/MOD2.5 can calculate the stable film boiling experiment. It has been performed to assess the model based on the CIAE data bank[17]. The comparison of the calculations with the experimental results reveals some shortages in the physical models of the code as follows:

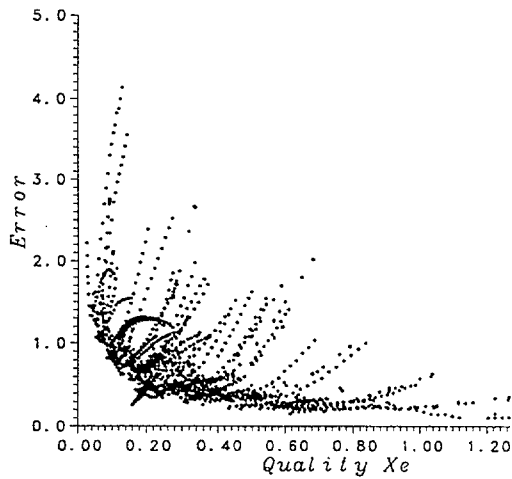


Fig.7 The error distribution of the calculation of Sergeev's correlation for the water temperature.

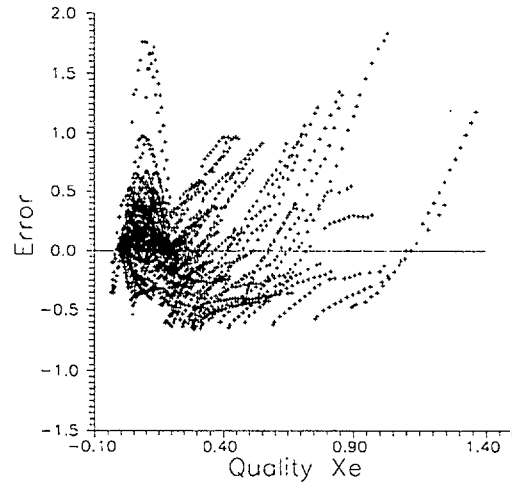
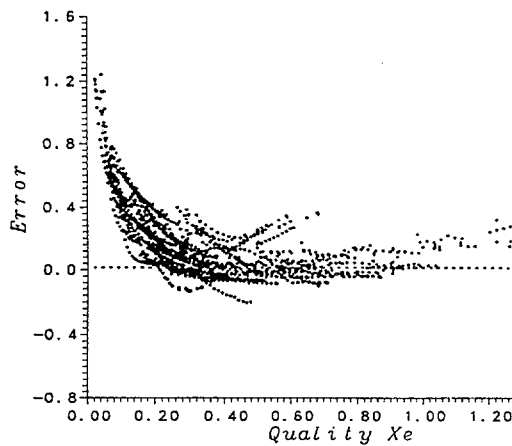
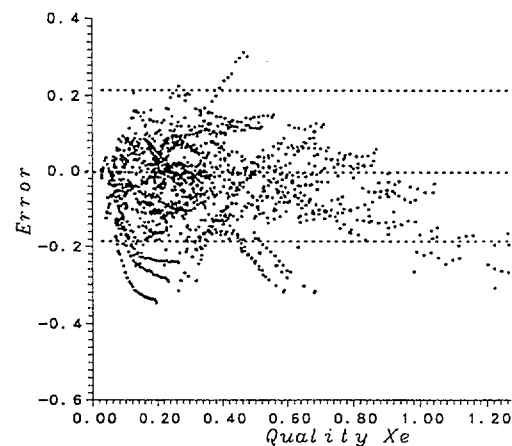


Fig.8 The error distribution of the calculation of Leung's table for the heat transfer coefficient



(a)



(b)

Fig.9 The error distribution of the calculation of Plummer's correlation for the water temperature.

(a) – original (b) – modification with factor F

- At some experimental conditions the post-dryout is not predicted over the test section, which is determined by the criterion of the onset of film boiling.
- The liquid-wall friction (FWALF) is calculated as in the pre-CHF regime. This is not the true in the film boiling, where the FWALF is negligible as the liquid does not contact with the wall. It results in an underprediction of the liquid velocity, V_f , (or an overprediction of $V_g - V_f$) and thus, an overprediction of the interfacial heat transfer.
- In the code the wall heat transfer ($q_w = q_{wl} + q_{wv}$) is essentially accounted by a vapor convection correlation as the calculated q_{wl} is negligible small for the experimental conditions. Therefore, the significant effect of droplets on the heat transfer at low quality condition can not be predicted by the code.
- The droplet diameter is determined by the criterion of the critical Weber number ($WED = 1.5$). This is only the true for the DFFB preceded by the IAFB. While for the DFFB initiated from the dryout of annular flow the droplets are generated upstream of the dryout point by the entrainment from the thin liquid film and are much smaller than those in the previous case.

These models in the RELAP5/MOD2.5 are modified as follows:

- (i) As the criterion for the onset of film boiling the empiric correlation of the minimum film boiling temperature is introduced, which was derived from the CIAE steady-state experiment[21].
- (ii) The FWALF is set to be zero.
- (iii) The convection heat transfer between the wall and vapor is evaluated by the Dittus-Boelter correlation multiplying the enhancement factor, F (Eq.7), to account for the effect of droplets.
- (iv) An expression of the droplet diameter is introduced for the DFFB initiated from the dryout of annular flow, and for the DFFB preceded by the IAFB the WED is increased from 1.5 to 5.0.

With the modified version of the RELAP5/MOD2.5 the calculations of the experimental results are improved substantially. Fig.10 exemplifies the calculation of the vapor temperature along the test section with the modification of these models for the run with $P = 5.62\text{MPa}$, $G = 416.6\text{kg/cm}^2\text{s}$, $X_i = 0.383$ and $q_0 = 20.2\text{W/cm}^2$. The code(O) denotes the original version of the code, the code(M) denotes the code(O) with modification of the model of minimum film boiling temperature.

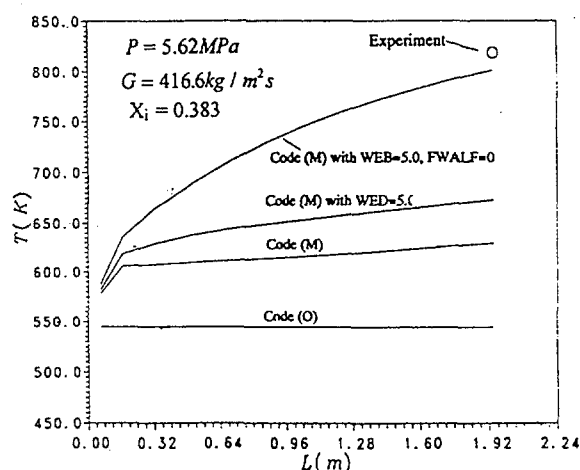


Fig.10 Calculation of the vapor temperature with modified model of RELAP5/MOD2.5

6. CONCLUSIONS

A great number of film boiling experimental data have been obtained at steady-state condition by using the directly heated hot patch technique. They have greatly extended the database and covered the range of interest for the reactor accident. The dispersed flow film boiling exhibits significant thermal nonequilibrium and strong history-dependence of the heat transfer coefficients. Based on the data, the mechanistic model and the tabular method are proposed, and the assessment of RELAP5/MOD2.5 is made. The present methods have provided appropriate approaches for the calculation of such complicated dependence of the heat transfer in dispersed flow film boiling. They will be refined for extended range of conditions.

REFERENCES

1. Yadigaroglu G. and Andreani M., 1989, "Two-Fluid Modeling of Thermal-Hydraulic Phenomena for Best-Estimate LWR Safety Analysis," Proc. 4th Int. Topical Meeting on Nuclear Reactor Thermal-Hydraulics, Vol.2, 980-995
2. Groeneveld D.C. and Snoek C.W., 1984, "A Comprehensive Examination of Heat Transfer Correlations Suitable for Reactor Safety Analysis," Multiphase Science and Technology, Vol.2
3. Groeneveld D.C. and Gardiner S.R.M., 1978, "A Method of Obtaining Flow Film Boiling Data for Subcooled Water," Int. J. Heat and Mass Transfer, Vol. 21, 664-665
4. Stewart J.C. and Groeneveld D.C., 1982, "Low Quality and Subcooled Film Boiling of Water at Elevated Pressure," Nuclear Engineering and Design, Vol. 67, 254-272
5. Gottula R.C. et al., 1985, "Forced Convective Nonequilibrium, Post-CHF Heat Transfer Experiment data and Correlation Comparison Report, NUREG/CR 3193
6. Swinnerton D., Hood M.L. and Pearson K.G., 1988, "Steady State Post-Dryout at Low Quality and Medium Pressure: Data Report," UKAEA Report AEEW-R2267
7. Leung L.K.H., Hammouda N. and Groeneveld D.C., 1997, "A Look-up Table for Film Boiling Heat Transfer Coefficients in Tubes with Vertical Upward Flow," Proc. 8th Int. Topical Meeting on Nuclear Reactor Thermal-Hydraulics, Kyoto, Vol.2, 671-678
8. Efanov A.D. et al., "The General Post-CHF Heat Transfer Prediction Method for Tubes on the

- Bases of the Look-up Table," Proc. 11th Int. Heat Transfer Conf., Korea, Vol.2, 237-242
9. Yuzhou Chen and Jusheng Li, 1984, "Subcooled Flow Film Boiling of Water at Atmospheric Pressure," Two-Phase Flow and Heat Transfer, Xue-jun Chen and T.N.Veziroglu eds. 141-150
 10. Yuzhou Chen P. Cheng et al., 1989, "Experimental Results of Subcooled and Low Quality Film Boiling Heat Treansfer of Water in Vertical Tube at Moderate Pressure," Proc. 4th Int. Topical Meeting on Nuclear Reactor Thermal-Hydraulics, Karlsruhe, Vol.2, 1105-1110
 11. Yuzhou Chen and Haiyan Chen, 1996, "Experimental Results of Steady-State Film Boiling of Forced Flow Water," Presented at 2nd Research Co-ordination Meeting of IAEA CRP on Thermohydraulic Relationships for AWCR, Vienna, 7-11 Oct. 1996
 12. Yuzhou Chen and Haiyan Chen, 1994, "An Experimental Investigation of Thermal Nonequilibrium in Dispersed Flow Film Boiling of Water," Proc. Int. Conf. on New Trends in Nuclear System Thermohydraulics," Pisa, Italy, Vol.1, 31-37
 13. Yuzhou Chen, Hanyan Chen and Z.C. Zhu, 1992, "Post Dryout Droplet Flow Heat Transfer - Measurements of both Wall and Vapor Superheats at Stable Condition, in Transport Phenomena Science and Technology, Wang B.X., eds, 319-324
 14. Yuzhou Chen and Haiyan Chen, 1994, "A Model of Dispersed Flow Film Boiling Heat Transfer of Water," Proc. 10th Int. Heat Transfer Conf., Brighton, UK, Vol.7, 18-FB-3, 419-424
 15. Yuzhou Chen and Haiyan Chen, 1998, "A Tabular Method for Prediction of the Heat Transfer during Saturated Film Boiling of Water in a Vertical Tube," Proc. 11th Int. Heat Transfer Conf., Korea, Vol.2, 163-168
 16. Arrieta L. and Yadigarogru G., 1978, "Analytical Model for Bottom Reflooding Heat Transfer in Light Water Reactor", EPRI NP-756
 17. Yuzhou Chen and Haiyan Chen, 1997, "Assessment of RELAP5/MOD2.5 with Steady-State Dispersed Flow Film Boiling Experiment," Proc. 5th Int. Topical Meeting on Nuclear Thermal Hydraulics, Operations and Safety, kk5
 18. Plummer D.N., Griffith P. and Rohsenow W.M., 1976, "Post-Critical Heat Transfer to Flowing Liquid in a Vertical Tube," 16th National Heat Transfer Conf. 76-CSME/CSChe-13, St Louis
 19. Yuzhou Chen and Haiyan Chen, 1996, "Forced Convection Heaty Transfer to Steam in Tubes with Different Diameters", Chinese J. Engineering Thermophysics, Vol.17. sup. 107-110
 20. Sergeev et al., Thermohydraulic Relationships for Advanced Water Cooled Reactors, IAEA-TECDOC Revision 2
 21. Chen Yuzhou et al., 1989, "Experimental Measurements of the Minimum Film Boiling Temperature for Flowing Water", Multiphase Flow and Heat Transfer, X. J. Chen, T.N.Veziroglu and C. L. Tian, Hemisphere Pub. Co., Vol.1, 393-400.

PASSIVE SYSTEMS FOR FLUID AND HEAT TRANSPORT

(Session 3)

Chairman

J. Lillington
United Kingdom

NEXT PAGE(S)
left BLANK



EFFECTIVENESS OF PASSIVE SYSTEMS TESTED IN THE NOKO FACILITY

E.F. HICKEN, H. JAEGER, M. FETHKE, L. ROSSNER
Institute for Safety Research and Reactor Technology,
Forschungszentrum Jülich GmbH,
Jülich, Germany

Abstract

In the NOKO facility, the components Passive Initiators, Emergency Condensers, Building and Plate Condenser have been studied experimentally. The influential parameters – pressure and concentration of non-condensables – have been varied substantially. In combination with tests of the same components in an other facility (PANDA), tests with other components in other test facilities (PANDA, PANTHERS, SPES-2) and future tests in NOKO, the available data form a good basis for the assessment of the thermal-hydraulic effectiveness of passive decay heat removal from the core region and the containment – mainly of BWRs. In a next step, the structural reliability should be evaluated for the use in Probabilistic Safety Analyses.

1. INTRODUCTION

It is a good demonstration of safety culture if vendor, utilities and licensing authorities equally make an effort to increase the safety level of Nuclear Power Plants—existing and future ones. Recognising that design and main licensing requirements were developed in the sixtieth and seventieth it is appropriate now to develop new solutions as well as new licensing requirements, evaluate the feasibility of these solutions and possibly test their effectiveness.

The goals for new safety systems are evident: effective, simpler, more reliable, cheaper and licensable. Without major efforts, it can be stated that passive safety systems are simpler and are to be expected more reliable [1]. They seem to be also licensable if the remaining uncertainty with respect to requirements for redundancy and diversity have been solved. An assessment of the costs is complex and cannot be discussed here.

During recent years and still ongoing are efforts to experimentally study the effectiveness of passive safety systems and compare the results with code calculations [2,3]; due to the different operating conditions (e.g. small driving forces) as compared with active systems, some models in computer codes have to be improved.

2. TEST FACILITIES

2.1. Overview

In Fig. 1, some European test facilities capable to perform thermal-hydraulic tests with passive safety systems are shown. It is evident that the wide spread of power and pressures will allow the test of the same component in several facilities of different size and thus increasing the confidence in the assessment of the effectiveness of this component. It has to be mentioned that the PANDA test facility has a higher volume than the other test facilities.

2.2. The NOKO facility

In Fig. 2, the layout of the NOKO facility is shown [4]. In principle, the facility consists of three loops:

- 1) The high pressure (< 10 MPa) "primary" loop with the electrical heated boiler (< 4 MW), the recirculation pump, the steam-water separator, the pressure vessel and the test object (passive initiator, emergency condenser, building condenser or plate condenser).

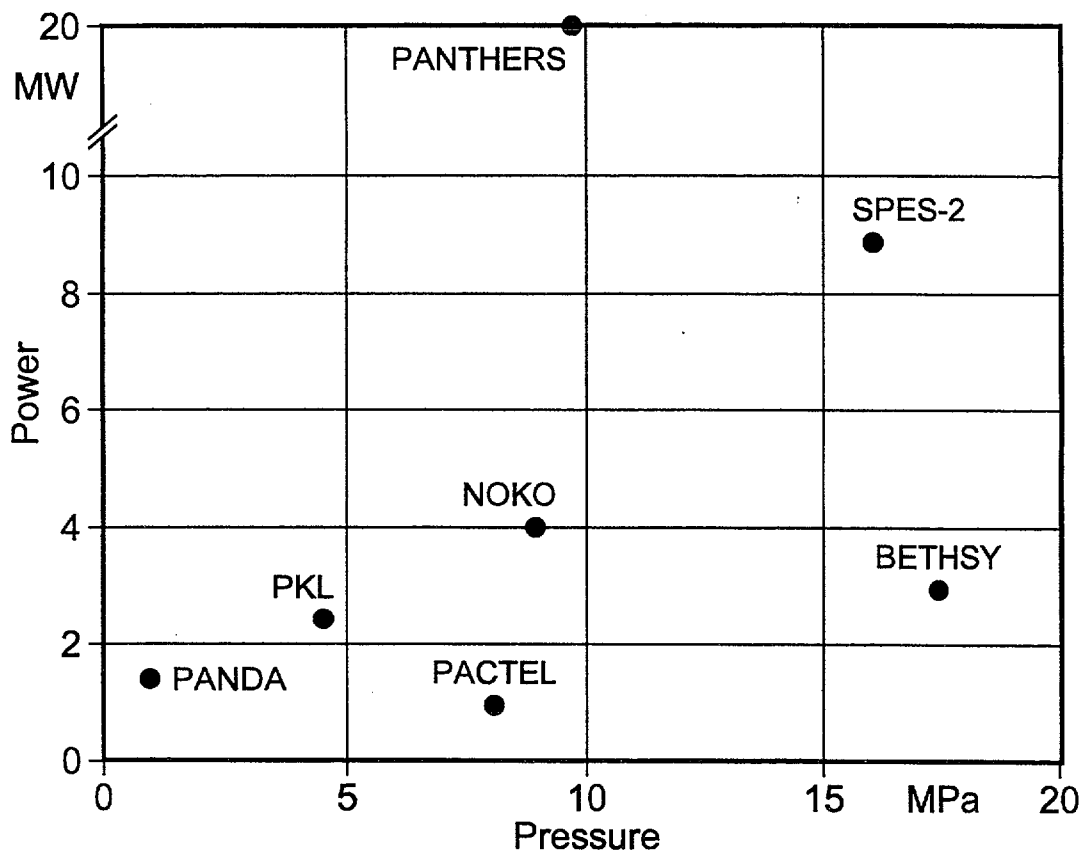


FIG. 1. European test facilities to perform thermal-hydraulic tests with passive safety systems.

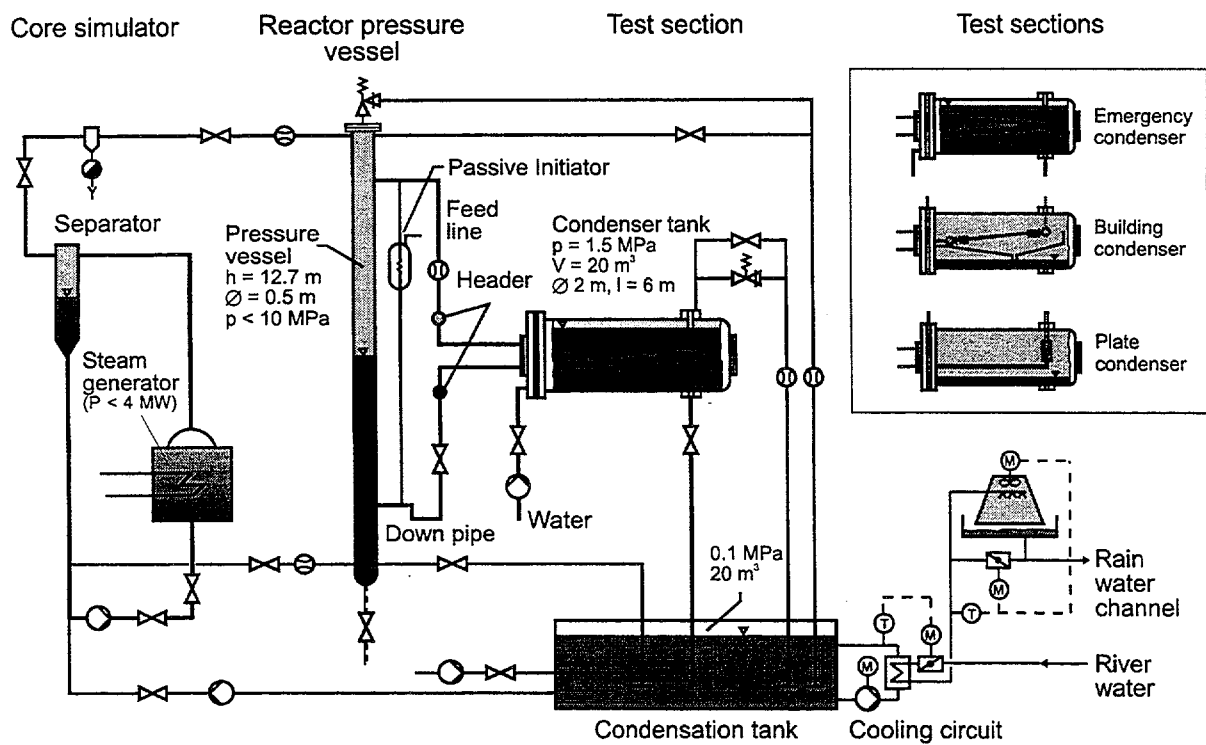


FIG. 2. Schematic of the NOKO test facility.

- 2) The medium pressure ($< 1 - 1.5$ MPa) "secondary" loop with the condenser tank with inlet- and outlet-pipes for the different fluids (water, steam, non-condensables).
- 3) The ambient pressure "auxiliary" loop with relief tank and heat exchanger which is cooled by river water or via a cooling tower.

A commonly used instrumentation is installed; the data are finally available through the Internet—of course protected by a password.

3. SOME PASSIVE SAFETY SYSTEMS FOR SIGNAL CONDITIONING AND DECAY HEAT REMOVAL FROM THE CORE REGION AND FROM THE CONTAINMENT

Multiple designs for passive safety systems have been proposed. Only those have been considered here which are planned to be installed in advanced design, i.e. AP-600(W), SBWR(GE) and SWR 1000 (SIEMENS). In addition, the Thermal Valve (proposed by CEA) and steam-jet-pump-system for decay heat removal (proposed by Soplenkov) are considered. In Fig. 3, an overview is given for those components tested or to be tested in NOKO and tested in other facilities.

4. EXPERIMENTAL RESULTS

4.1. Passive initiator

The Passive Initiators tested are full size and operate with water. Three different designs of the Passive Initiator were tested in NOKO. In Fig. 4, the pressure history for the three Passive Initiators are shown [5]. The specified pressure to be exceeded is 0.6 MPa. It is evident that two Passive Initiators react too slow; the reason is the small heat transfer area/participating mass of steel - ratio. A new design shall avoid this disadvantage. It is also evident that a Passive Initiator can only operate above about 1 MPa. There are plans to study other fluids than water with a lower situation pressure than water. In principle, the tests have demonstrated the effectiveness of the Passive Initiators for signal conditioning.

4.2. The SIEMENS emergency condenser

The emergency condenser tested in NOKO has tubes with original dimensions and material; the reference case was the bundle installed in the NPP Gundremmingen A. Only the number of rods has been reduced in NOKO as compared with the bundle to be installed in a SWR 1000. In Fig. 5, the transferred energy is shown as a function of the water level and the pressure as a parameter [5]. The tests have demonstrated the effectiveness of the emergency condenser if only steam and water are present. A new bundle with an increased tube diameter and the smallest possible wall thickness has just been installed. In addition to tests with the bundle oriented in a vertical position, tests will be performed with the bundle turned to an angle of 40.9° ; this will allow a smaller level change in the pressure vessel between flooded and empty bundle.

4.3. The SIEMENS building condenser

The building condenser tested in NOKO has finned tubes with original dimensions and material [4]. It should be added that the tests in NOKO are separate-effect-tests to study the influence of pressure and non-condensables (oxygen, helium). These tests are complemented by system behaviour tests in PANDA [2].

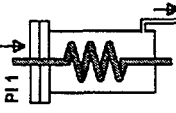
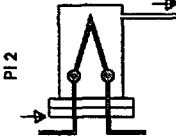
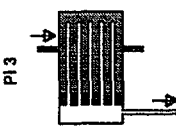
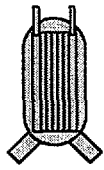
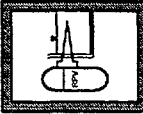
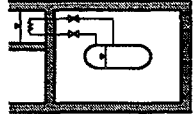
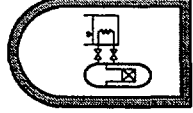
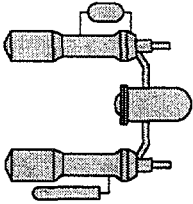
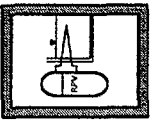
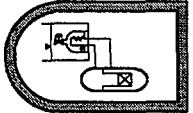
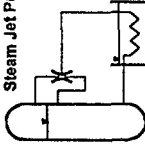
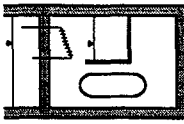
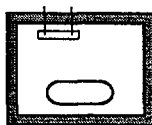
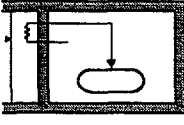
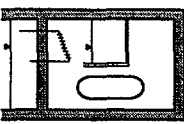
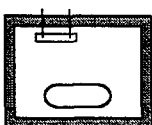
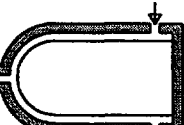
	Tested in NOKO	Tested in other facilities	To be tested in NOKO
Signal Conditioning	<p>PI 1</p>  <p>WAF = 0.35 m² W_{tot} = 45 l</p> <p>PI 2</p>  <p>WAF = 0.44 m² W_{tot} = 44 l</p> <p>PI 3</p>  <p>WAF = 0.7 m² W_{tot} = 4.5 l</p>		<p>PI 4</p> 
Decay Heat Removal from the Core Region	<p>Emergency Condenser</p>  <p>1. bundle</p>	<p>Isolation Condenser</p>  <p>Heat Exchanger</p>  <p>CMT, ACC.</p>  <p>Emergency Condenser</p>  <p>2. bundle</p> <p>Thermal Valve</p>  <p>Steam Jet Pump</p> 	
Decay Heat Removal from the Containment	<p>Building Condenser</p>  <p>Containment Plate Condenser</p> 	<p>Passive Containment Cooler</p>  <p>Building Condenser</p>  <p>Containment Plate Condenser</p>  <p>AP-600 Containment Cooling</p> 	

FIG. 3. Passive safety system for signal conditioning and decay heat removal from the core region and from the containment.

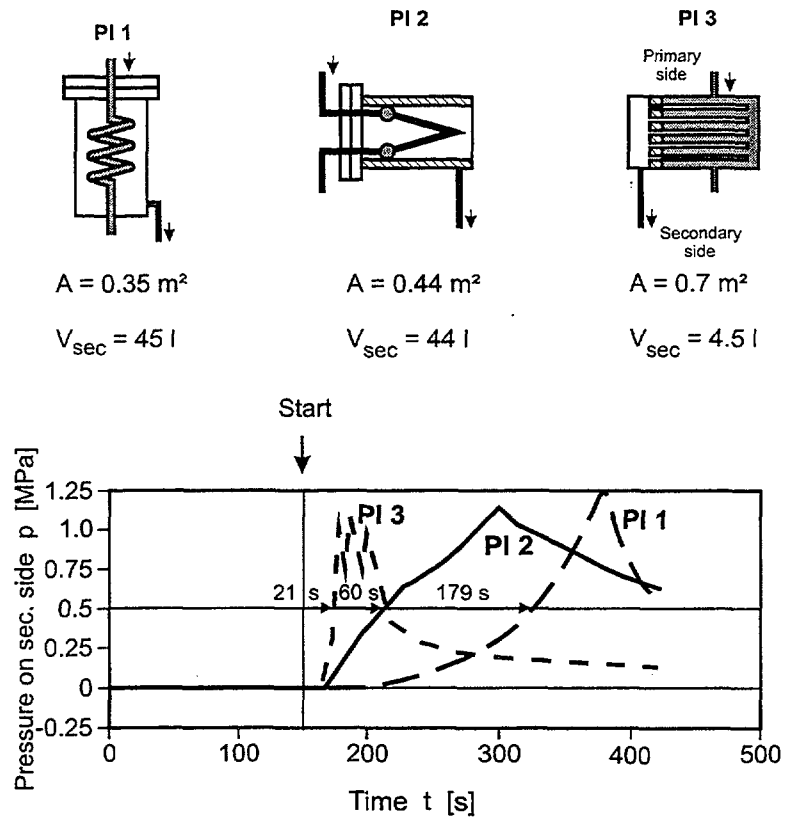


FIG. 4. Pressure build-up of three different designs of passive initiators tested in NOKO.

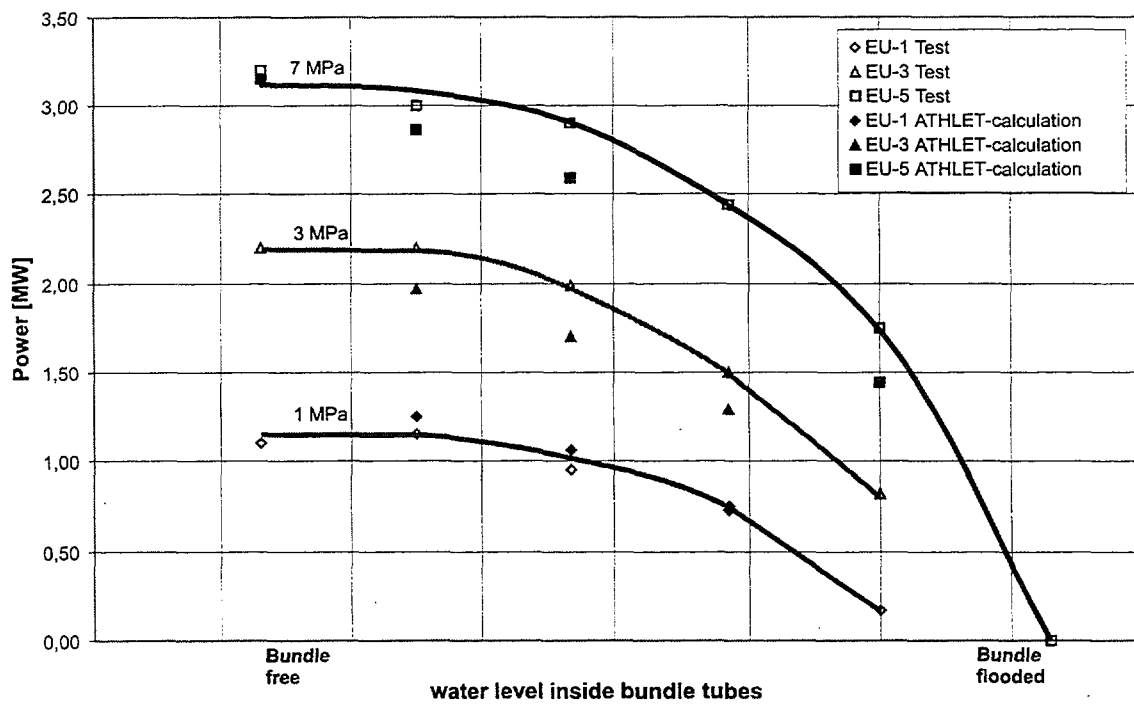


FIG. 5. Capacity of the emergency condenser bundle tested in NOKO as a function of the water level inside the tubes and the pressure as a parameter.

In Fig. 6a and 6b, it is shown that a pronounced stratification develops within the condenser tank. In Fig. 6c to 6f, the heat exchange with the total pressure and different non-condensables as parameter is shown [6].

The tests have demonstrated the effectiveness of the building condenser also if non-condensables are present.

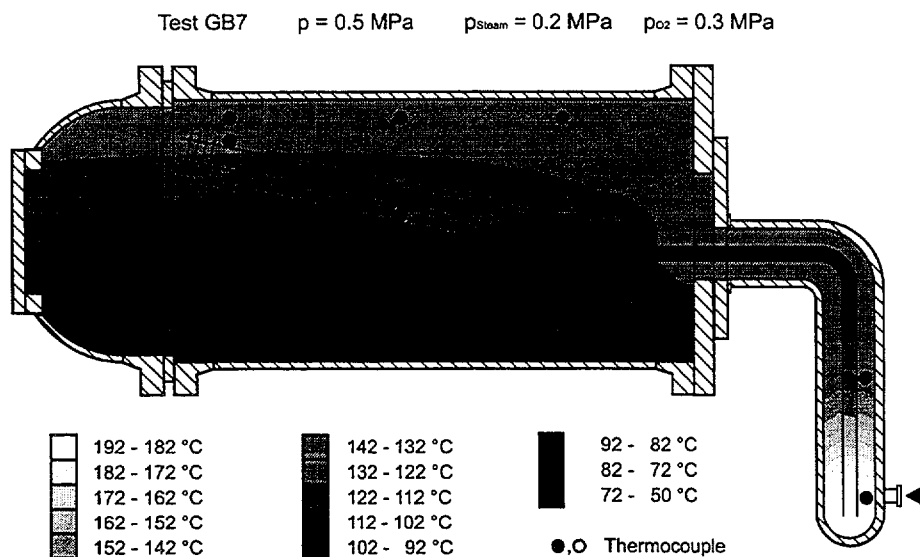


FIG. 6a. Temperature distribution for an experiment with steam and oxygen.

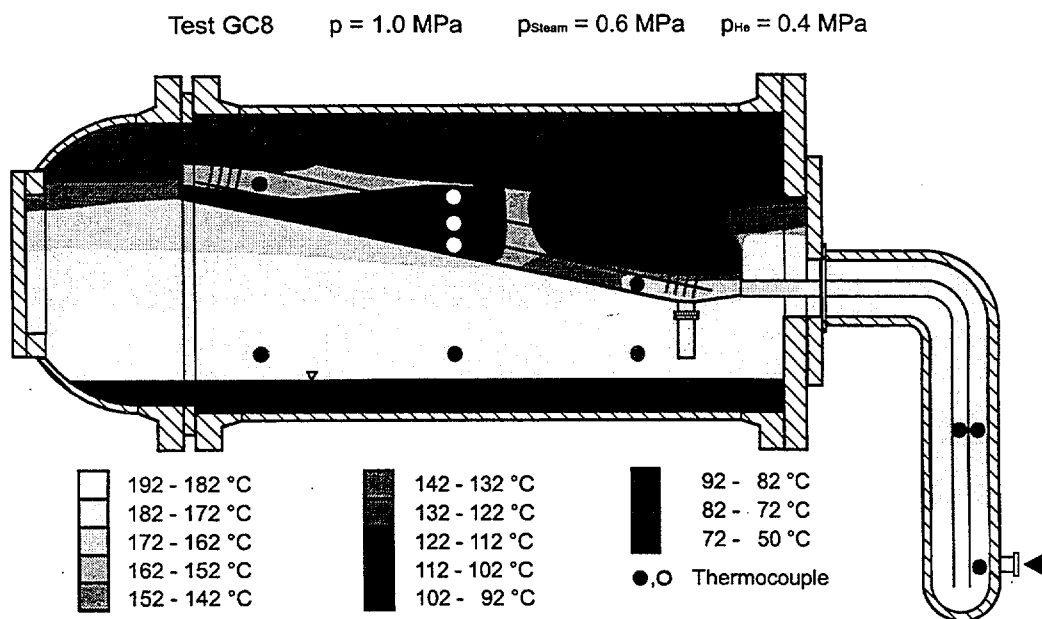


FIG. 6.b. Temperature distribution for an experiment with steam and helium.

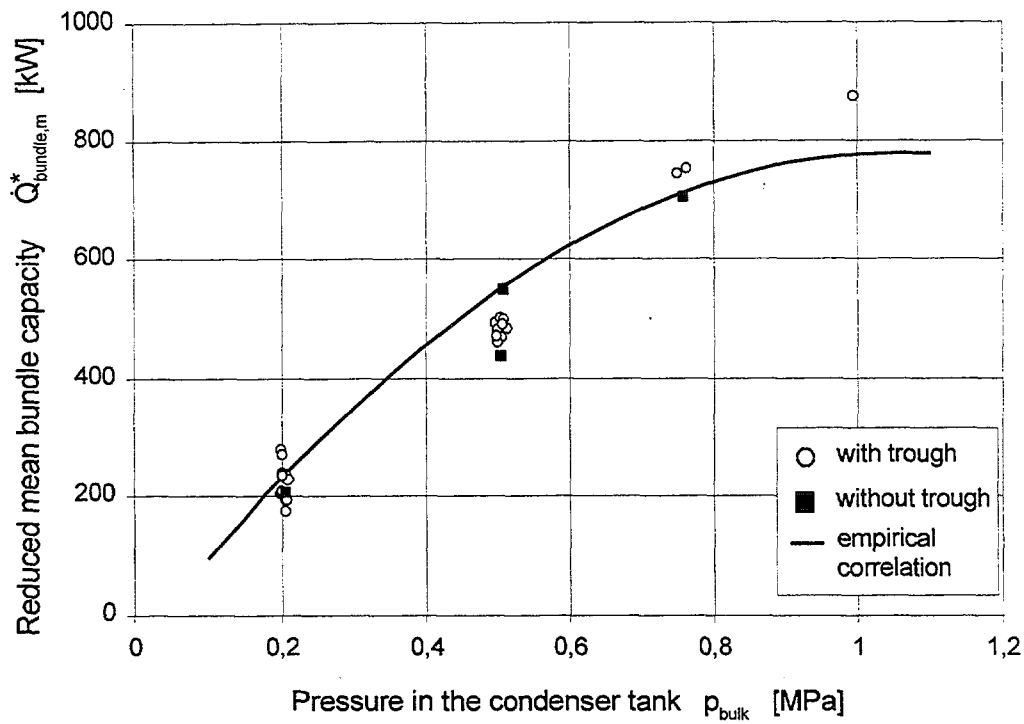


FIG. 6c. Bundle capacity for tests without non-condensable gas.

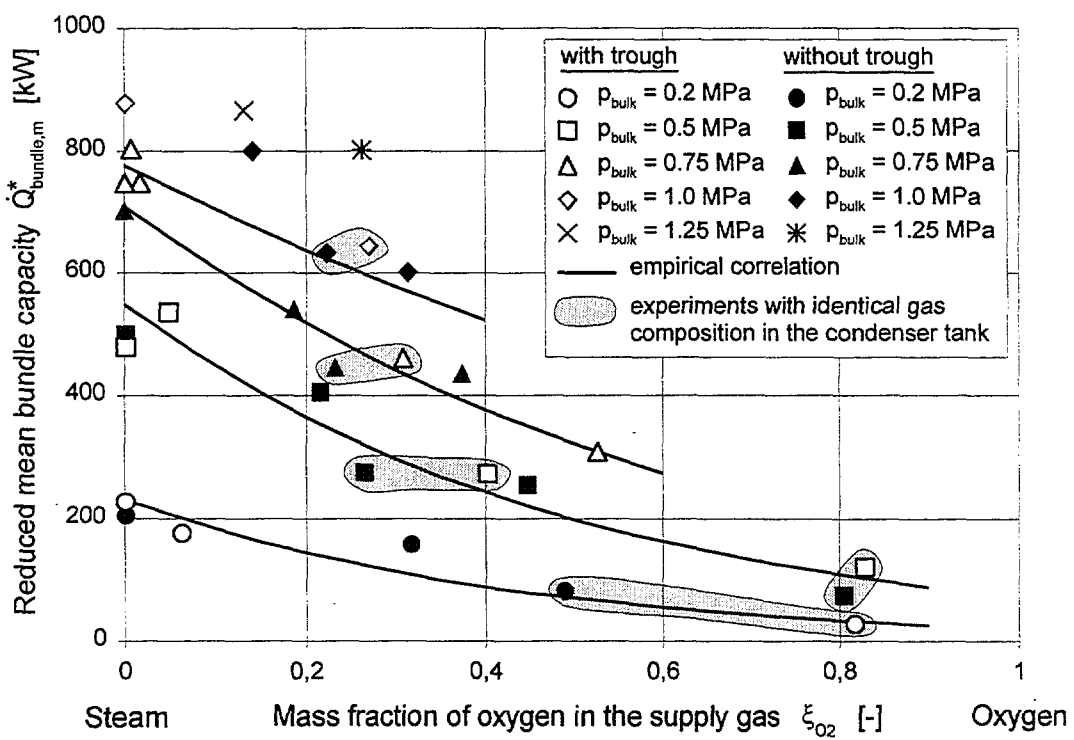


FIG. 6d. Bundle capacity for tests with oxygen as non-condensable gas.

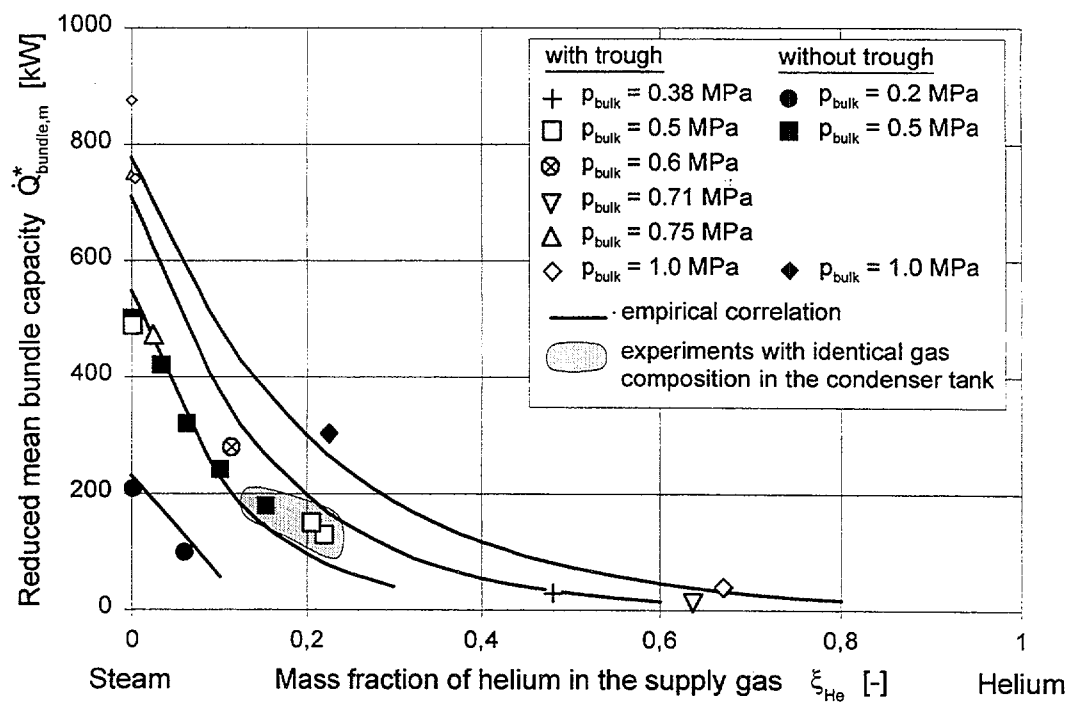


FIG. 6e. Bundle capacity for tests with helium.

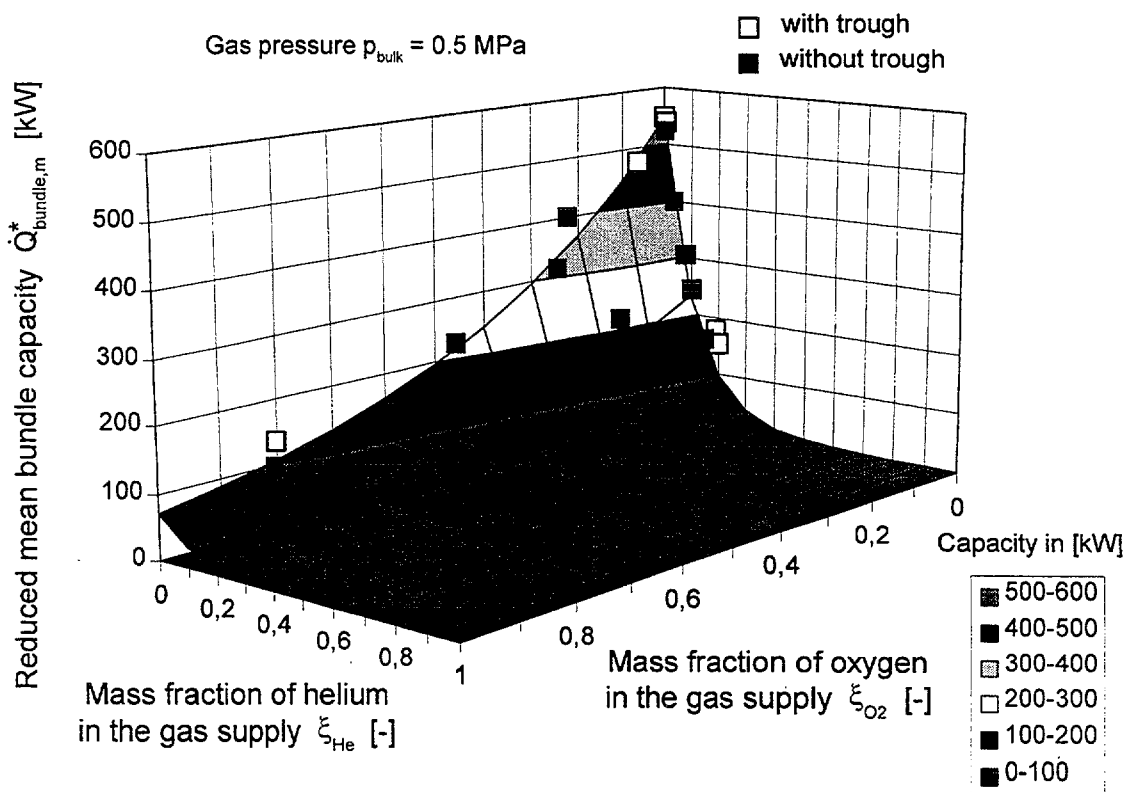


FIG. 6f. Bundle capacity for tests with oxygen and helium as non-condensables.

4.4. The plate condenser

Plate condensers have been proposed to be installed in the containments of PWRs. The plate condenser tested in NOKO has a very rigid structure to cope with loads resulting from severe accident sequences; the same plate condenser has been tested before in the BATTELLE MODEL CONTAINMENT. One first preliminary result of the plate condenser experiments in NOKO is shown in Fig. 7. The temperature distribution of the gas mixture inside the condenser tank is given for a test with steam and oxygen.

5. EXPERIMENTS PLANNED IN THE FUTURE

Besides the results with a second bundle of the Emergency Condenser, which is just being installed, tests for two different systems for Decay Heat Removal from the Core Region are planned in 1999/2000. This is the Thermal Valve as proposed by CEA; the Thermal Valve needs an active activation but this system should be more reliable than a system with valves in a primary loop. The other system focuses on jet-pumps; the driving fluid is steam or saturated water.

6. CODE VALIDATION

The tests performed allow a comparison or an improvement of models which are or have to be implemented in computer codes simulating the system behaviour of BWRs and PWRs.

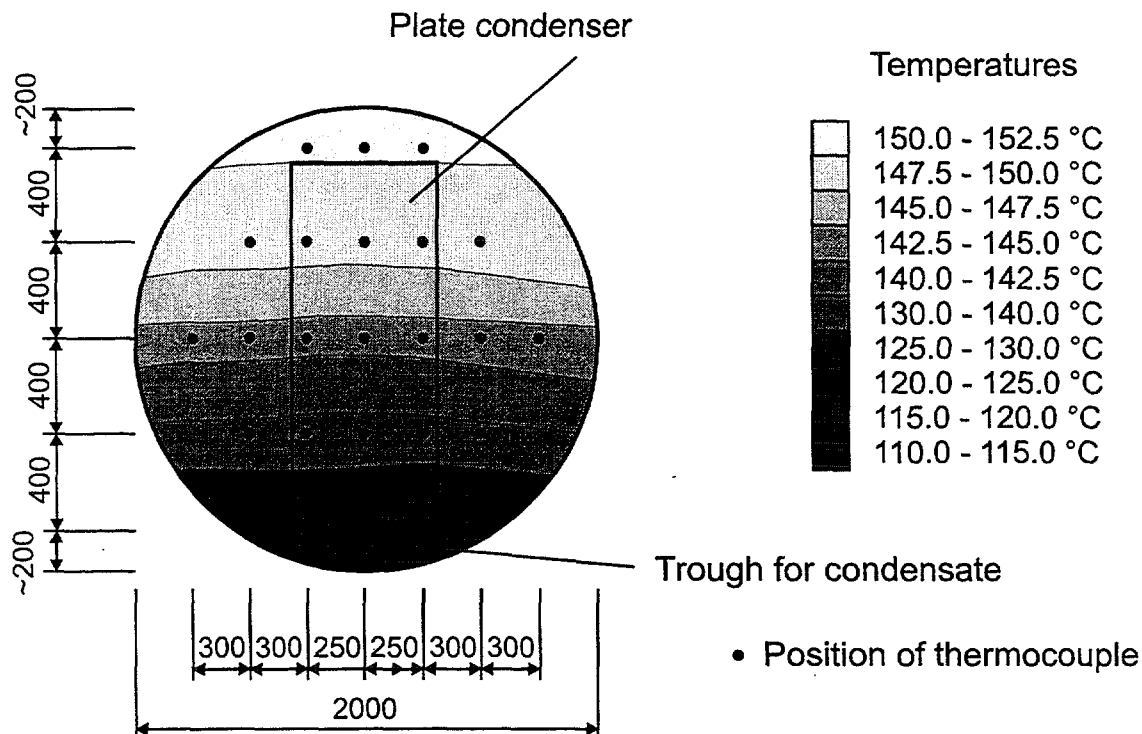


FIG. 7. Temperature distribution of the gas mixture inside the condenser tank for a plate condenser test with steam and oxygen.

For the SIEMENS emergency condenser, the codes RELAP5, TRAC, APROS and ATHLET have been used. In principle, the condensation in horizontal tubes has to be modelled. For ATHLET, this model was improved by implementing a flow regime map. The comparison between the results from the codes and between experimental and analytical results was good. The comparison between ATHLET calculations and experimental data is shown in Fig. 5. A report analysing the results in more detail is under preparation.

Post-test calculations of the building condenser tests have been performed with the lumped-parameter code RALOC. A comparison between RALOC calculations and experimental data is shown in Fig. 8. Although the comparison between experimental and analytical results is satisfactory it is evident that more detailed calculations with modern CFD codes are mandatory.

7. SUMMARY AND OUTLOOK

In NOKO, the effectiveness of components of passive safety systems for decay heat removal from the core region and the containment has been experimentally studied. In specific, three passive initiators, the first bundle of an emergency condenser, the building condenser with an without trough and a plate condenser have been tested within a wide range of parameters. The primary side pressure for the passive initiator and the emergency condenser was varied between 1 and 7 MPa; the pressure on the secondary side was varied between 0.1 and 1 MPa for the emergency condenser. For the tests with the building and plate condenser the total pressure varied between 0.1 and up to 1.5 MPa; and the concentration of oxygen and helium as non-condensables up to 100 %.

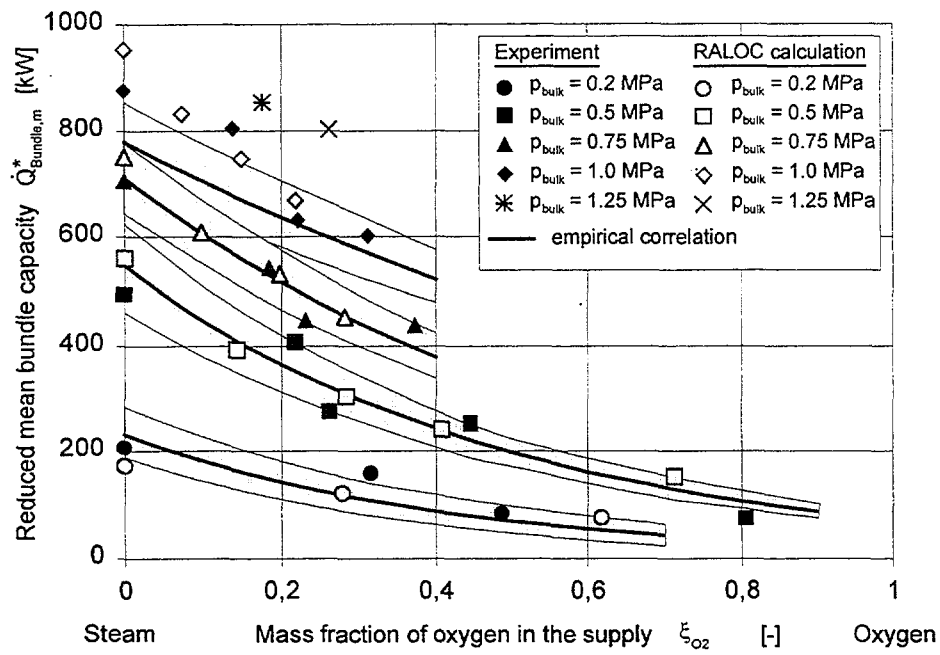
The effectiveness of the components studied could be demonstrated. Due to the geometrical dimensions, the original material and the right thermal-hydraulic conditions, the experimental results could be used directly. However, due to high instrumentation density the experimental data provide a good basis for code validations. Up to now, the codes TRAC, RELAP APROS, ATHLET, RALOC have been used; the analytical data compare well with the experimental data.

A second bundle for the emergency condenser and an optimised passive initiator are just being installed.

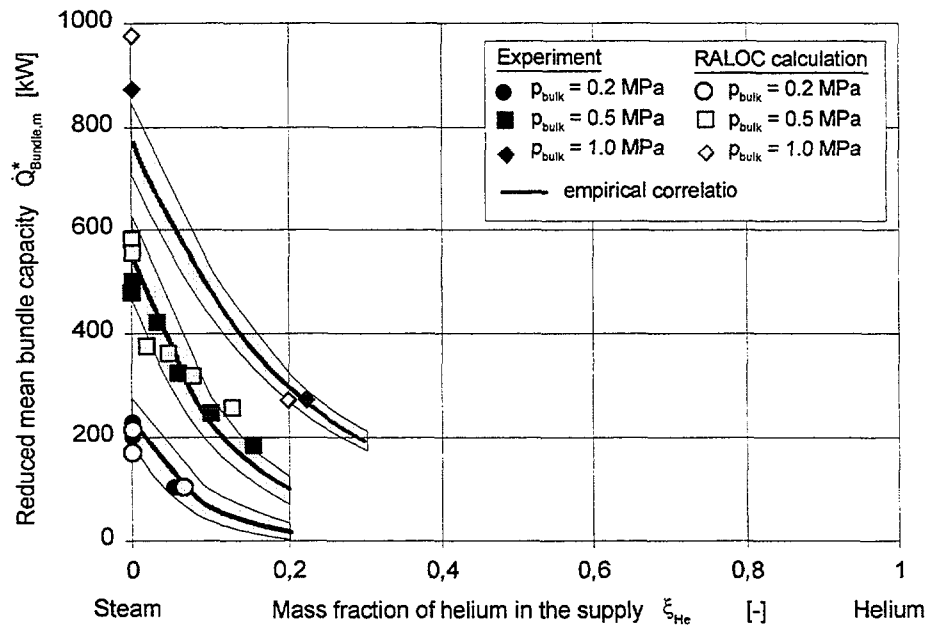
In the years 1999/2000, a jet-pump-system and a so-called thermal valve – both for a decay heat removal from the core region – will be studied.

Having experimentally studied and analytically modelled the thermal-hydraulics of these passive components, a good basis for the comparative thermal-hydraulics is available. To further assess the related thermal-hydraulics, the use of modern CFD-codes is mandatory.

In a next step, the structural reliability should be evaluated to use the quantitative values in Probabilistic Safety Analyses.



a) Bundle capacity for tests with oxygen as non-condensable gas



b) Bundle capacity for tests with helium as non-condensable gas

FIG. 8. Comparison between experimental data of the building condenser experiments without trough in NOKO and post-test calculations using RALOC.

ACKNOWLEDGEMENTS

The experimental and analytical work of this paper was gained within the framework of the "European BWR R&D Cluster for Innovative passive Safety Systems" (IPSS), Contract No. F141-CT95-0005, which is funded by the CEC.

REFERENCES

- [1] HICKEN, E.F., 1996, "Passive safety systems, a possibility of enhancing reactor safety", Kerntechnik 61 (1996) 5-6, Carl Hanser Verlag, Munich, p. 207-209.
- [2] HICKEN, E.F., VON LENSE, W., 1996, "European BWR R&D Cluster for innovative passive safety systems", Kerntechnik 61 (1996) 5-6, Carl Hanser Verlag, Munich, p. 210-213.
- [3] HICKEN, E.F. et al., November 1997, "European BWR R&D Cluster for Innovative Passive Safety Systems", Proc. of the FISA'97 - Symposium on EU Research on Severe Accidents, Luxembourg.
- [4] FETHKE, M., JAEGER, H., Jül-3440, October 1997, "Modification of the NOKO test rig facility for the experimental investigations of the building condenser", Reports of the Forschungszentrum Jülich.
- [5] HICKEN, E.F., JAEGER, H., ROSSNER, L., FETHKE, M., 28.06.-02.07.1998, "The effectiveness of passive decay heat removal systems from advanced water reactors", Proc. of the 9th International Conference on Emerging Nuclear Energy Systems ICENES'98, Tel Aviv, Israel, p. 593-600.
- [6] FETHKE, M., JAEGER, H., HICKEN, E.F., 10.-15.05.1998, "First experiments of the passive safety system building condenser in the NOKO test facility and post-test calculations using the RALOC code", Proc. of the 6th International Conference on Nuclear Engineering ICONE-6, San Diego, USA, Paper No. 6506.

THE DIVA PROGRAMME: GENERAL PRESENTATION AND FIRST RESULTS

P. DUMAZ
DRN/DER/SIS



XA0055012

B. DUC
DRN/DEC/SECA

CEA-Cadarache,
Saint-Paul-lez-Durance, France

Abstract

The French "Commissariat à l'Energie Atomique" (CEA/DRN, Nuclear Reactor Division) is carrying out a new programme devoted to the thermalhydraulics of steam injectors. This programme was called DIVA. Both experimental and theoretical works are planned. Motivations, objectives, test facility and test section dimensioning of this new programme are presented. A first test series was just performed. The validation of the test section dimensioning and experimental procedures was obtained. These first experimental data are presented and preliminary analyses are given.

1. INTRODUCTION

The use of passive systems to remove decay heat in advanced light water reactor is one way to improve significantly safety. Among those systems, Steam injectors (SI) or condensing ejectors seem to have promising capabilities. The principle of these apparatus is to expand pressurised steam through a converging-diverging nozzle. Steam reaching low pressures, cold water is drawn into the SI, then, steam condenses and transmits momentum to water (part called mixing chamber). In a diffuser, pressurised water is obtained, the pressure being recovered in what looks like a straight shock.

During past 3 years, CEA/DRN studied the potential applications of SI and attempted to develop a SI numerical model using the CATHARE computer code [1] [2].

CATHARE is a two-phase flow code devoted to the thermalhydraulics of LWR accidents [3] [4]. The CATHARE standard module is based on the one-dimensional, two-phase, six-equation thermalhydraulic model. The choice of CATHARE was made because :

- CATHARE is a very general and well validated code;
- with CATHARE, integration within a system model (plant) is very easy (system evaluation);
- It is important to extend the range of CATHARE utilisation.

The development of a CATHARE SI model started within the frame of a CEA/DRN-ENEL (Italian Utility) agreement. ENEL and CISE (an Italian engineering company) designed, built and tested a single stage high pressure SI [5]. This apparatus is able to pump cold low pressure water (less than 0.3 MPa) up to pressures about 10% higher than the steam source pressure (This latter varying from 2 MPa to 9 MPa). The analyses of these results using CATHARE have demonstrated the feasibility of a SI CATHARE model [2] [6].

2. MOTIVATIONS AND OBJECTIVES OF THE DIVA PROGRAMME

One of the initial objectives of the CEA/ENEL agreement was to qualify CATHARE for SI thermalhydraulic conditions. This objective was not reached. Actually, the available experiments were not enough instrumented to achieve this objective. This is the first motivation to undertake a new experimental programme.

On the other hand, other important points have to be mentioned :

- Commercially available SI work below 2 MPa. In a pressurised water reactor, a steam pressure up to 15 MPa (pressuriser) could be used.
- More advanced prototypes (regarding LWR applications) have some important disadvantages: the overflows in the ENEL/CISE apparatus, the heat exchanger in the PAHRSEC system [7] (schematised on Figure 1).
- Some basic phenomena controlling the SI behaviour are not actually well understood (liquid film atomisation, abrupt pressure recovery).

From those considerations, CEA/DRN made the decision to undertake new experiments in the frame of its innovative activities. A CEA working group, involving several laboratories, is in charge to define and to manage the programme since the beginning of 1996.

Three main objectives were identified :

- To study thermalhydraulic basic phenomena : shock waves and supersonic flows in two-phase flow, liquid film atomisation, dissipation processes.
- To develop and to qualify a CATHARE SI model.
- To develop a data base and an expertise required to design and to evaluate innovative configurations using SI.

3. THE TEST FACILITY

To perform these experiments, it is necessary to supply several kilograms per second of steam. One looked for available boilers in CEA laboratories and one chose the CLAUDIA facility located on the Cadarache research centre. This facility includes a 30 MW fuel-oil boiler which can supply 11 kg/s of steam up to 3 MPa. This steam pressure is the main disadvantage of CLAUDIA facility but it was thought to be sufficient in the first part of the programme regarding investments required by other facilities.

The steam line coming from the boiler is equipped with an isolating valve and a control valve. The demineralized water supply is made by a 10 m³ tank and a 0.033 m³/s pump. This water can be pressurised up to 3 MPa and heated up to 200°C. A valve controls the water flowrate. Downstream the test section, a control valve regulates the back pressure.

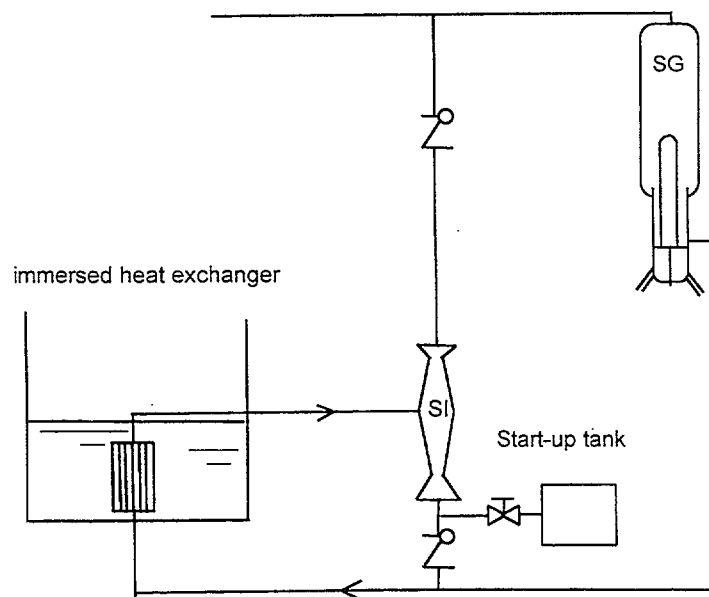


FIG. 1. Recirculation configuration [7].

4. REFERENCE EXPERIMENTAL CONDITIONS

In order to choose, as far as possible, representative experimental conditions, it was decided to choose a reference application, the steam generator auxiliary feedwater system (AFW), and to seek a scaling factor of one (in order to avoid, as far as possible, a scaling analysis). In a 1300 MWe French nuclear reactor, the required flowrate per steam generator is 12.5 kg/s which means a power of 33 MW at 8 MPa. The CLAUDIA facility limitations dictate the choice of the reference steam pressure: 3 MPa.

At least two SI system configurations could carry out the steam generator AFW function :

- the injection configuration (Figure 2).
- the recirculation configuration (Figure 1), mainly developed in Russia [7].

It is intended to study both configurations which will necessitate two different test sections.

For the injection configuration, a reference water flowrate of 12.5 kg/s is chosen, the corresponding steam flowrate being estimated to be about 2 kg/s. In recirculation configuration, 33 MW at 8 MPa means a steam flowrate of 14 kg/s (all the steam produced flows through the SI). At 3 MPa, this gives 5.3 kg/s, the steam flowrate being almost proportional to the pressure. From published data, the water flowrate was estimated to be 70 kg/s. This latter value exceeding the facility capability (see paragraph above), water and steam flowrates had to be reduced. In order to limit the number of parameters, the previous steam flowrate of 2 kg/s was chosen.

Our experimental programme started with a test section devoted to injection configurations. In the following sections, this configuration only will be discussed.

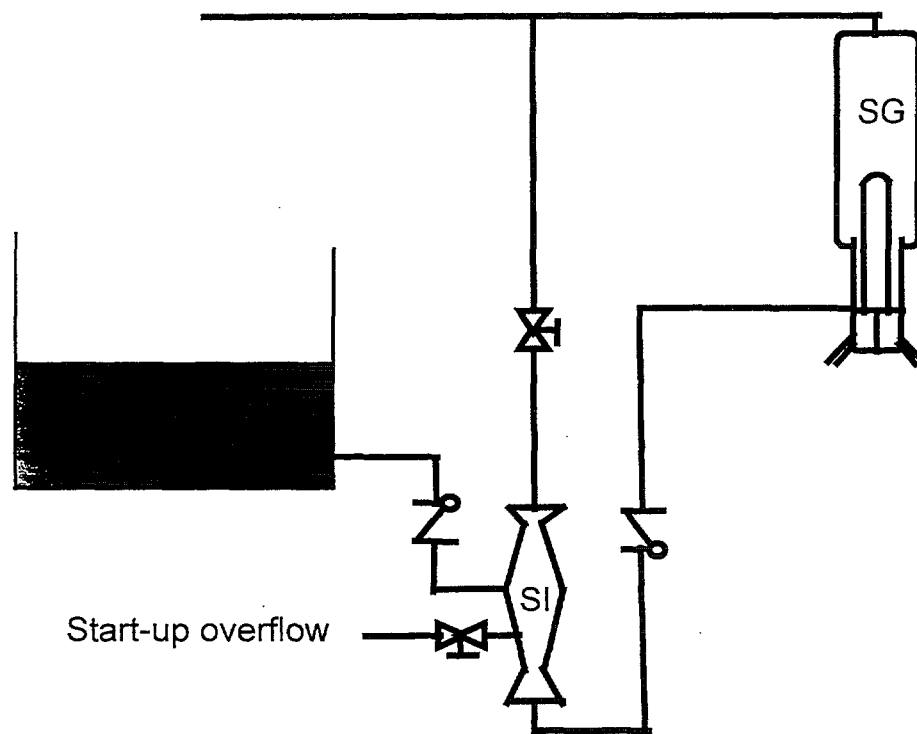


FIG. 2. Injection configuration.

5. TEST SECTION DIMENSIONING

The first choice made was to use a central steam injection with an annular water injection. This was because the high pressure prototypes known [5] [7] use this option.

To have useful data to develop and qualify new models, a regular test section is highly desirable. It was decided to do not use overflow lines (Figure 3). This requires adequate choices of the experimental procedures and the test section dimensions. This means one tolerates a reduction of the test section performance (pressure recovery) which does not matter for basic studies.

For the steam nozzle, the two important dimensions are the throat diameter: D_c and the nozzle outlet diameter: D_s . The former gives the steam flowrate (choked flow) and the latter the nozzle expansion ratio, P_{vo}/P_s (P_{vo} the inlet steam pressure, P_s the steam nozzle outlet pressure). for injection configuration, a ratio of 100 was chosen. Both dimensions were calculated using standard equations of converging-diverging nozzles with an isentropic exponent of 1.2. These gave a throat diameter of 25 mm and an outlet diameter of 90 mm.

For the mixing chamber, the most important parameter is the throat diameter, D_m . A design criterion is derived using the momentum balance.

Upstream the pressure recovery location (called the shock), assuming a constant pressure and neglecting all momentum losses, one has:

$$Q_{vo} \cdot V_s + Q_{lo} \cdot V_{lo} = (Q_{lo} + Q_{vo}) V_l^-$$

and through the shock :

$$(Q_{lo} + Q_{vo}) V_l^- + P^+ \cdot S = (Q_{lo} + Q_{vo}) V_l^+ + P^+ \cdot S$$

where :

Q_{vo} , the inlet steam mass flowrate

Q_{lo} , the inlet water mass flowrate

V_s , the exit velocity of the steam nozzle

V_{lo} , the inlet liquid velocity

V_l^- , P^- are the liquid velocity and the pressure just upstream the shock and

V_l^+ , P^+ just downstream.

S is the "shock" flow area.

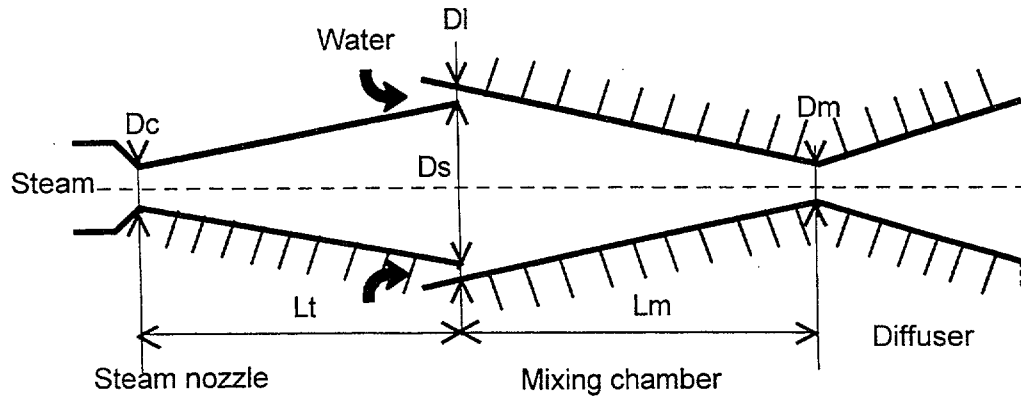


FIG. 3. Schematic of the test section.

Combining these two equations, one finds:

$$P^+ - P^- = \frac{Q_{vo}V_s + Q_{lo}V_{lo}}{S} - \frac{(Q_{vo} + Q_{lo})^2}{\rho_l S^2}$$

$P^+ - P^-$ has a maximum value (Figure 4) for $S = S_o = \frac{2 \cdot (Q_{vo} + Q_{lo})^2}{\rho_l (Q_{vo}V_s + Q_{lo}V_{lo})}$, from stability considerations [8], one must have: $S \geq S_o$. This means $D_m \geq 15$ mm for the injection configuration. To avoid the use of overflow ports and to reduce the stalling risks, it is desirable to have a high value of S (which means a reduction of the apparatus performances). After all, the choice $D_m = 30$ mm was made. Given the significance of this parameter, a second diameter, 20 mm, will be tested.

The length of the apparatus was determined assuming half angles of 3° .

6. INSTRUMENTATION

In these SI experiments, measurements have to be made in difficult conditions : high pressures, temperatures and velocities, vibrations.

In the first test series, the test section dimensioning and the experimental procedure have to be validated. Therefore, conventional measurements are used mainly. These consist in the profiles of pressure and internal wall temperature (steam nozzle, mixing chamber, diffuser, see Figure 5). Of course, standard boundary conditions are also measured. One also used an optical fibre mounted on an axial probe which moves along the diffuser. This fibre should measure the centreline local void fraction

To measure the two-phase flow structure inside the mixing chamber, a multibeam X-ray densitometer is developed [9]. On each axial position, 31 beams will give an accurate determination of the local void fraction. The main drawback of this technique is to require a specific test section (to minimise the wall thickness) which explains that, in first tests, test section dimensioning must be validated.

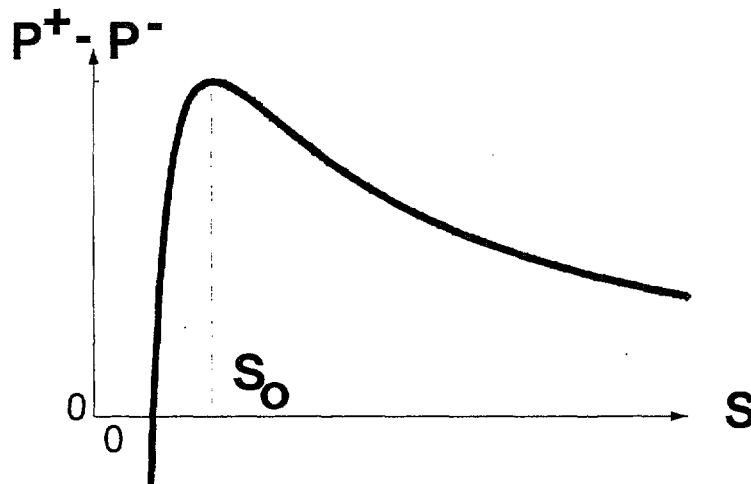


FIG. 4. $P^+ - P^-$ in function of the shock area.

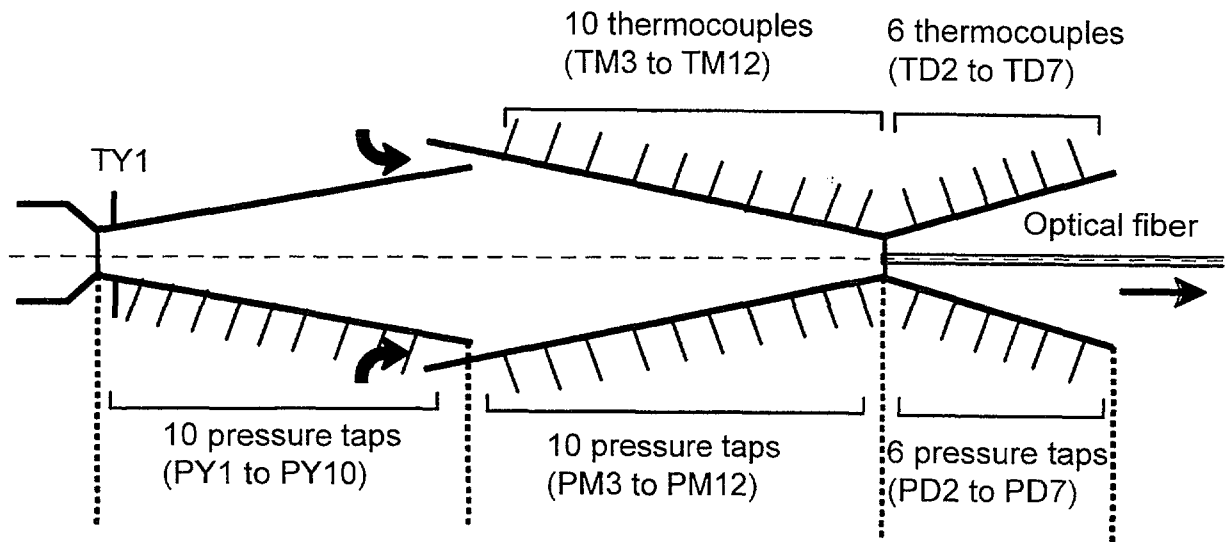


FIG. 5. Instrumentation.

7. TESTS DESCRIPTION AND RESULTS

The boundary conditions which are controlled and which determine the apparatus behaviour are : the steam pressure P_{vo} , the water flowrate Q_{lo} and the back pressure BP . It should be mentioned that in this first test series the steam is saturated and the injected water is at room temperature. At the beginning of the test, the back pressure is always close to the atmospheric pressure and can be increased by a control valve.

Two procedures were tested to start-up the apparatus. The former procedure consists in opening the steam flow first, then to increase the water flowrate and finally the back pressure (see Figure 6, the pressure profiles at different times). By this way, a minimum water flowrate is necessary to obtain a stable behaviour. This stable behaviour appears to be also the limit to have a started SI (with low mixing chamber pressure). The latter procedure consists in opening first the water flow at a value higher than the previous limit and then to open the steam valve. This procedure gives a smooth start-up of the apparatus.

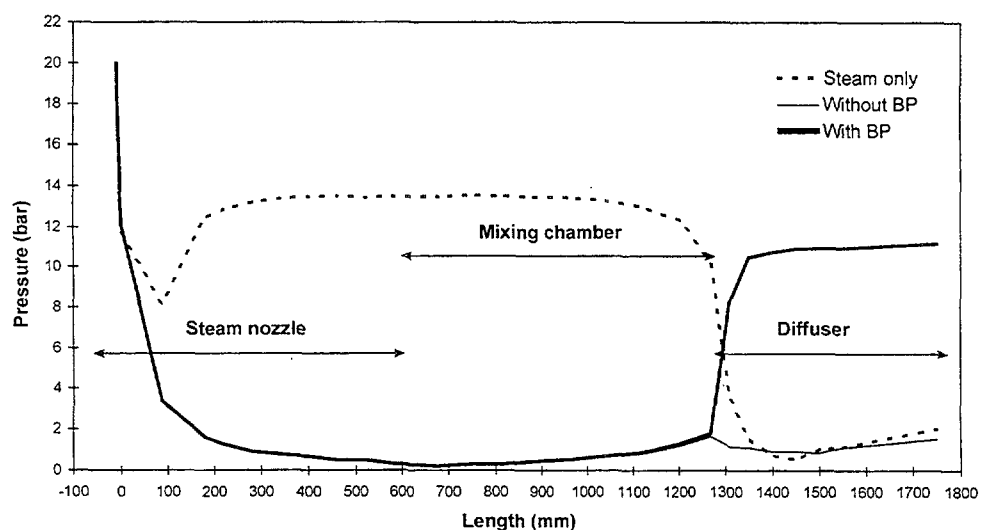


FIG. 6. Pressure profiles for a 2 MPa test.

The test already performed are summarised in the Table I. The start-up procedure is indicated (steam or liquid) as well as the shutdown procedure.

To have a smooth test shutdown, the steam valve is closed first. The other possibilities explored are the back pressure increase and the water flowrate reduction. This leads to a less smooth shutdown (noise and vibrations). Due to an unexpected water flowrate limitation (ongoing analyses), one does not obtain the apparatus shutdown by an increase of the water flow.

The pressure profiles (Figure 6) well illustrate the different test phases. In pure steam flow, one has critical flows at the two throats locations (steam nozzle and mixing chamber). Then, the mixing chamber pressure is high. With a high enough water flowrate, a low mixing chamber pressure is obtained. During this phase, from fluctuating, the pressure measurements become stable (Figure 7). The closure of the back pressure valve causes a pressure increase in the diffuser and the shock appearance. This operation does not modify the mixing chamber pressure. This is an indication of the supersonic nature of the mixing chamber two-phase flow.

We had some problems with the optical fibre (vibration of the mechanical support, leak). Finally, the fibre was broken during the 2 MPa test (back pressure of 0.47 MPa). However, interesting signals were recorded demonstrating the usefulness of this measurement.

8. PRELIMINARY ANALYSES

These analyses are based on energy and momentum balances. Their results are summarised in Table II. Some CATHARE calculations were already run, they require further analyses.

Using the global energy balance, one can calculate the outlet temperature (T_{out} cal) whether the exit flow is a one-phase flow. This is the case when the back pressure is enough high. For the 2 MPa tests, the agreement with the experimental data (T_{out} data) is very good. For the 1 MPa tests, the energy balance gives a slight overestimation of the exit temperature.

TABLE I. MAIN PARAMETERS OF THE PERFORMED TESTS

Pvo (MPa)	Qvo (kg/s)	start-up, Qlo (kg/s)	Qlo (kg/s) nom / max	Shutdown	Back Pressure (MPa)	Optical fibre
1	0.75	Steam, 5.2	6.6	BP	0.1 to 0.59	no
1	0.76	Steam, 6	7	Steam	0.1 to 0.2	yes
1	0.77	Liquid, 7	7	min Qlo, 4.4	0.1 to 0.4	yes
1	0.75	Liquid, 5.6	5 / 12.5	Steam	0.1	no
2	1.38	Steam, 7	10 / 18.4	Steam	0.1	no
2	1.41	Steam, 7.5	8.33	BP	0.1 to 1.14	no
2	1.37	Liquid, 8.5	8.5	Steam	0.1 to 0.47	yes
2.8	2	Liquid, 8.9	8.9	Steam	0.1	no

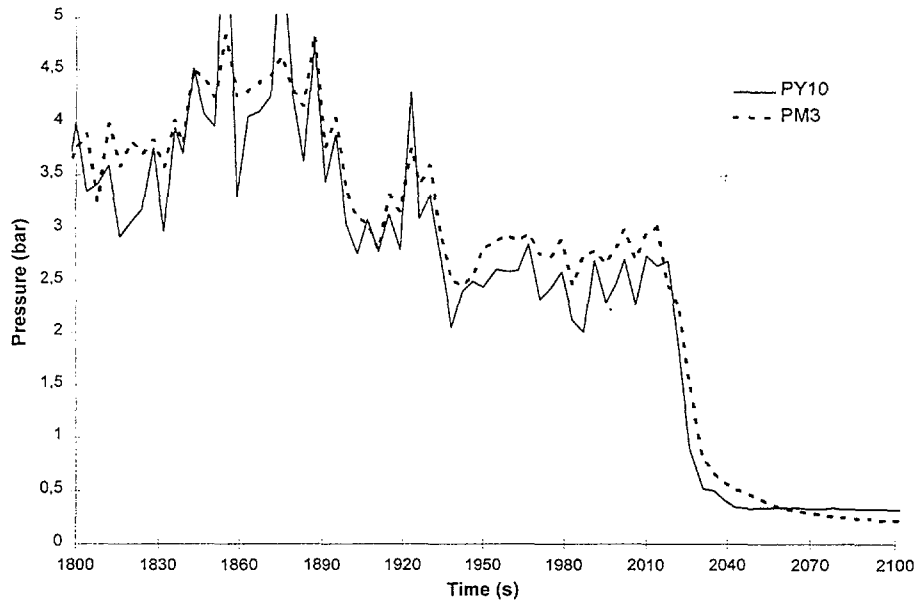


FIG. 7. Pressure variations during SI start-up.

Using a partial energy balance (up to the end of the mixing chamber), one can calculate the mixing chamber condensation rate (Q_c). One has:

$$Q_{vo} \cdot h_{vo} + Q_{lo} \cdot h_{lo} = (Q_{lo} + Q_c) h_{l(TM12)} + (Q_{vo} - Q_c) h_{vsatl(PM12)}$$

where h is the specific enthalpy of steam, subscript v, of liquid, subscript l.

TABLE II. PRELIMINARY ANALYSES

Pvo (MPa)	Qvo (kg/s)	Qlo (kg/s)	Qc cal (kg/s)	ΔT_{sat-12} (°C)	Tout data (°C)	Tout cal (°C)	Pout data (MPa)	Pout cal (MPa)
1	0.75	6.74	0.61	22	89	91	0.59	0.88
1	0.78	6.9	0.64	20	87.5	92		
	0.75	4.7	0.56	17				
1	0.76	9.35	0.65	25.3				
	0.76	12.3	0.67	30.5				
2	1.38	10.3	1.16	22				
	1.39	18.3	1.22	35.5				
2	1.41	8.3	1.1	19	117	117	1.14	1.6
2	1.38	8.45	1.1	18	117	117		
2.8	2	8.9	1.41	19				

PM12 and TM12 are the pressure and temperature measurements at the end of the mixing chamber. This equation means that at the end of the mixing chamber the steam is assumed to be saturated and the water subcooled at the temperature TM12 (this being a questionable assumption). Furthermore, the kinetic energy is assumed to be negligible. The condensation rates obtained appear to be not much dependant of the water flowrate. It seems also that a significant part of steam is not condensed at the end of the mixing chamber (about 20 %). Another interesting result is the increase of the water subcooling (ΔT_{sat} at the location of TM12 and PM12) with the water flowrate. A preliminary conclusion could be that the condensation phenomenon in the mixing chamber is not limited by the liquid side but rather by the vapour side.

Using the momentum balance of the Section 5, the exit theoretical maximum pressure is calculated (Pout cal). It can be noticed that the maximum back pressure obtained is about 70% of this theoretical pressure. This looks quite good since the theoretical calculation assumes no losses at all.

9. CONCLUSIONS

The first tests of the DIVA programme have fulfilled the objectives of dimensioning and test procedures validations. In particular, the choice made to avoid the use of overflows was confirmed. Some interesting features of our apparatus were found out : unstable regime, low momentum losses.

The experimental programme will continue the next two years with the test section devoted to recirculation configuration and with the use of the X ray densitometer. From the modelling point of view, one will have to confirm the CATHARE capabilities regarding the thermalhydraulics of steam injectors.

REFERENCES

- [1] AUJOLLET, P. *et al*, "CATHARE detailed modelling of a steam injector and comparison with experimental data"; European two-phase flow group meeting, Piacenza, June, 1994
- [2] DUMAZ, P.; MAZZOCCHI, L.; VANINI, L.; "Analyses of steam injector experiments" ARS 97 conference, Orlando, 1997
- [3] BARRE, F., *et al*, "New developments in CATHARE2", Nureth 6, Grenoble, Oct 1993
- [4] MICHAELLI, J. C. *et al*, "CATHARE code development and assessment methodologies" ANS Winter Annual meeting, San Fransisco, Oct/Nov, 1995
- [5] CATTADORI, G. *et al*, "A single stage high pressure steam injector for next generation reactors : test results and analysis" Int J Multiphase Flow, vol 21, p591-300, 1993
- [6] DUMAZ, P.; DUC, B., "Status of steam injector studies at CEA" ICONE5 conference, Nice, 1997
- [7] SOPLENKOV, K. I., *et al*, "Design and testing of passive heat removal system with ejector-condensor" IAEA Tech Meeting, Piacenza, May 1995
- [8] IRODOV, V. F.; and ALAD'YEV, T.; "Calculation of the flow in a condensing ejector" Fluid mech, Soviet Res, vol 4, p99, 1975
- [9] JEANDEY, C.; "Multibeam X-ray densitometer for flow pattern and void fraction determination in steam water mixtures" mes in polyphase flow, Edited by TR Heidrick and BR Patel, ASME book nr 100209

NEXT PAGE(S)
left BLANK

A FLASHING DRIVEN MODERATOR COOLING SYSTEM FOR CANDU REACTORS: EXPERIMENTAL AND COMPUTATIONAL RESULTS

H.F. KHARTABIL
Fuel Channel Thermalhydraulics,
Atomic Energy of Canada Ltd,
Chalk River, Ontario, Canada



XA0055013

Abstract

A flashing-driven passive moderator cooling system is being developed at AECL for CANDU reactors. Preliminary simulations and experiments showed that the concept was feasible at normal operating power. However, flow instabilities were observed at low powers under conditions of variable and constant calandria inlet temperatures. This finding contradicted code predictions that suggested the loop should be stable at all powers if the calandria inlet temperature was constant. This paper discusses a series of separate-effects tests that were used to identify the sources of low-power instabilities in the experiments, and it explores methods to avoid them. It concludes that low-power instabilities can be avoided, thereby eliminating the discrepancy between the experimental and code results. Two factors were found to be important for loop stability: (1) oscillations in the calandria outlet temperature, and (2) flashing superheat requirements, and the presence of nucleation sites. By addressing these factors, we could make the loop operate in a stable manner over the whole power range and we could obtain good agreement between the experimental and code results.

1. INTRODUCTION

CANDU® moderator heat-rejection systems normally use pumps to circulate the hot heavy water to heat exchangers where the heat is rejected to pumped service water (Fig. 1). However, heavy-water circulation by natural convection has advantages, and a system to reject heat passively using a flashing-driven natural-circulation loop is being developed at AECL.

The main feature of the flashing-driven concept (Fig. 2) is that vapour is generated by flashing. Preliminary simulations using the CATHENA [1] code have shown that a flashing-driven natural-circulation loop can be used to remove normal moderator heat without any flow instabilities [2]. This concept was verified experimentally using a scaled flashing-driven loop [3]. However, while stable operation was obtained at normal operating power, flow instabilities were observed at low powers (<25% full power).

Separate-effects tests were subsequently conducted to investigate the cause of low-power instabilities. The tests were conducted with a constant cold-leg temperature so that instabilities related to the hot-leg (flashing) part of the loop could be isolated. Two factors were found to be important for loop stability: (1) oscillations in the calandria outlet temperature, and (2) flashing superheat requirements and the presence of nucleation sites.

If the liquid in the calandria is not sufficiently mixed, temperature oscillations can occur at the calandria outlet, and the flow will oscillate because the elevation of the onset of flashing changes with temperature. Temperature oscillations were observed at low powers (<25% full power). The calandria outlet temperature in an actual CANDU reactor can be stabilized with a suitable inlet-outlet configuration. The effect of stabilizing the calandria outlet temperature was investigated by mixing the calandria water in the separate-effects tests. The result was that low-power oscillations were practically eliminated. Residual oscillations remained, but they were finally traced to the lack of sufficient nucleation sites along the glass riser.

CANDU® is a registered trademark of Atomic Energy of Canada Limited.

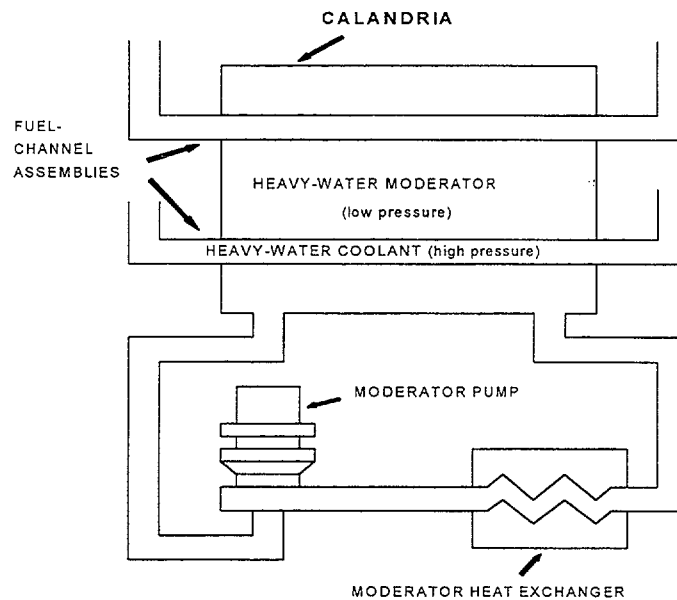


FIG. 1. CANDU calandria schematic.

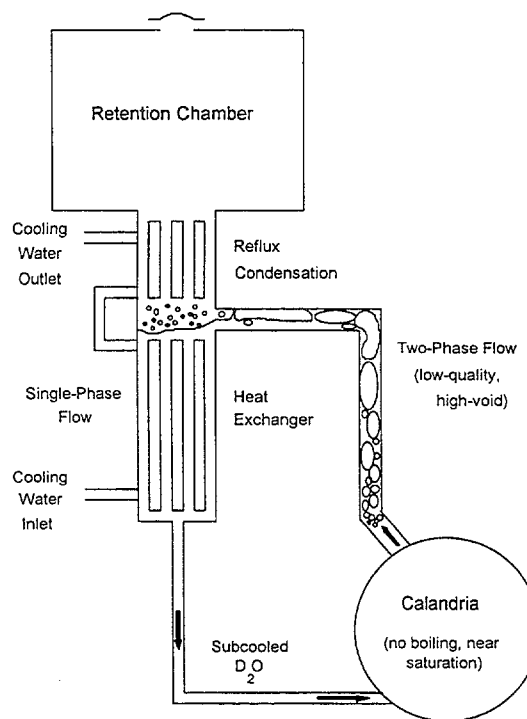


FIG. 2. Flashing-driven concept.

The riser in the experiment was made of glass pipe segments to facilitate flow visualization. Discontinuities existed at the points where the glass pipes were connected. This set-up caused void generation to be non-uniform along the riser because more superheat was required to initiate flashing at the smooth glass surface (which did not have sufficient nucleation sites) than at the points where the glass pipes were connected. This phenomenon caused minor oscillations at low powers, where flashing started in the upper pipe segment. At

higher powers, the oscillations disappeared because void, which acted as further nucleation sites, filled most of the riser. This effect was investigated by introducing an artificial roughness through the insertion of a rough wire in the middle of the top glass riser section. Tests conducted at low powers clearly showed the formation of void on the wire surface but not on the smooth glass surface. This uniform void generation stabilized the flow at powers where unstable operation was observed previously, without the wire insert. In an actual steel riser, void formation should be uniform along the pipe, thereby stabilizing the flow.

Another factor that affects code prediction is the amount of superheat required to initiate flashing. If thermal equilibrium is assumed, the code will predict a longer two-phase region than when a finite amount of superheat is required for flashing. This hypothesis was investigated by artificially lowering the flashing point in the code simulations so that the amount of superheat was equal to that observed in the experiments.

The results (experimental and code predictions) indicated stable loop operation with calandria mixing and improved nucleation. By accounting for these effects, as well as for the amount of superheat required to initiate flashing, good agreement was obtained between the experiments and code simulations.

2. PRE-TEST CATHENA SIMULATIONS

The observed loop behaviour in earlier tests (flow stabilization with increased power) [3] was consistent with the pre-test CATHENA simulations. However, the agreement was only qualitative because of uncertainties in the loop parameters used in pre-test CATHENA simulations. Post-test analyses with more accurate loop parameters did not improve the agreement between the experiments and code simulations.

Closer examination of the experimental results showed that the temperature oscillations were inconsistent with the assumption of a completely mixed calandria. A major assumption in the preceding CATHENA simulations was that the calandria could be modeled as a mixed-volume component. In reality, the flow distribution within the calandria is three-dimensional, and is strongly dependent on the inlet-outlet geometry. Moreover, CATHENA simulations showed that the loop was always stable with a constant calandria inlet temperature.

The preceding results prompted the following modifications to the test loop, which is described in Reference 3:

- (1) Keep the calandria inlet temperature constant throughout the test.
- (2) Reduce the three-dimensional effects of the flow distribution in the calandria to approximate mixed conditions.

3. EXPERIMENTAL SET-UP AND PROCEDURE FOR SEPARATE-EFFECTS TESTS

Scaling of the original test loop [3] was done by keeping the height similar to that of the reactor loop, and by reducing the volume of all pipe components by a factor of 60. The calandria was scaled by a factor of 600 (undersized by a factor of 10).

A schematic of the modified test loop is shown in Fig. 3; it consists of a calandria (with a mixing loop), an 8.5-m-long glass riser (1.0-m-long glass pipe segments with an inner diameter of 10 cm), a condenser and tank, and a steel downcomer. The tests described in

temperature (~ 100 °C). The water volume in the tank below the condenser helped absorb variations in the condensate temperature and ensured that the cold-leg temperature remained constant. The reduction of three-dimensional effects in the calandria was achieved by adding a mixing-loop to the calandria (see Fig. 3).

The measurements consisted of total calandria power, flowrate into the calandria, and temperatures and pressures at various locations (see Fig. 3). The flowrate was measured using a turbine flowmeter. Temperatures were taken using Type K thermocouples, and pressures were measured using Rosemount pressure cells.

A PC-based data-acquisition system was used to scan data at three rates: (1) one scan/10 s (slow), (2) one scan/s (medium), and (3) five scans/s (fast). The experiments were also recorded on video tape, to aid in data analysis.

Before each test, the water in the loop was first heated and degassed for about 3 hours. At the end of the degassing period, the water temperature in the whole loop corresponded to saturation at the condenser pressure ($\cong 100$ °C). The experimental constraint was that the calandria outlet temperature was not to exceed the saturation temperature at the calandria pressure (approximately 117 °C).

4. EXPERIMENTAL RESULTS

4.1. Mixing-loop turned off

This test was first done to provide a reference point for runs with a mixed calandria. The results are shown in Fig. 4, where it can be seen that the flow is unstable up to 112 kW (approximately 25% simulated full power). These oscillations are accompanied by oscillations in the outlet temperature, which cause the flashing point to oscillate. This oscillation, in turn, results in oscillations in the driving head, which result in flow oscillations.

4.2. Tests with calandria mixing

The mixing loop was operated to better simulate a mixed calandria. The results are shown in Fig. 5, where it can be seen that the large-amplitude oscillations associated with the large calandria outlet temperature oscillations have disappeared.

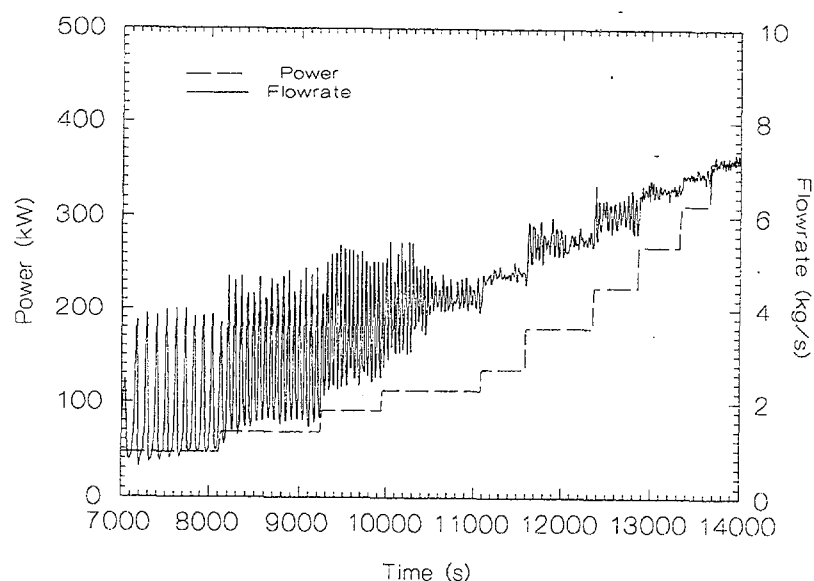


FIG. 4. Results without calandria mixing.

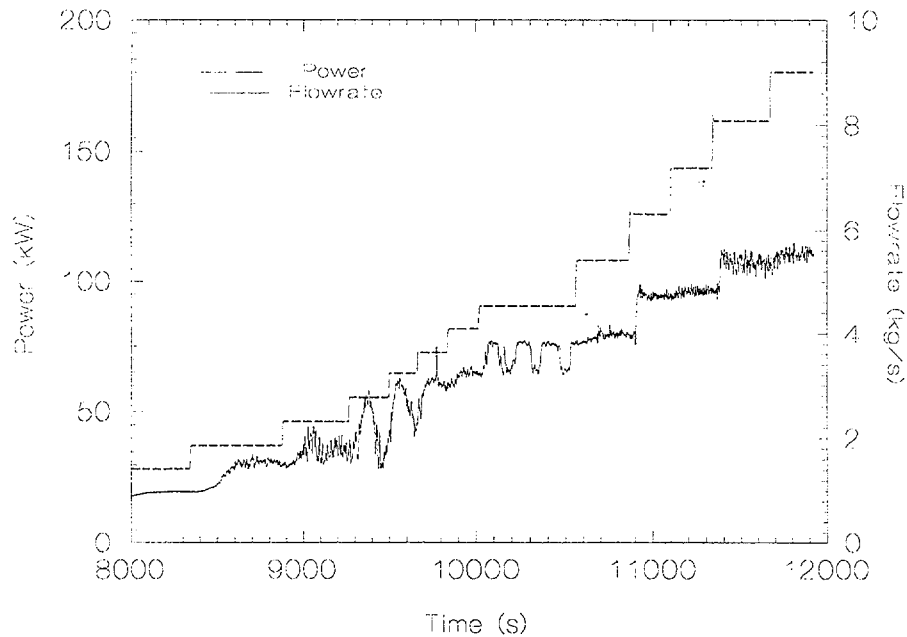


FIG. 5. Results with calandria mixing.

Fig. 5, however, shows that there are still some minor oscillations at some power levels below 108 kW. Visual observations in the top part of the glass riser showed the presence of slug flow when two-phase conditions existed in the riser. Closer examination of the two-phase region showed that discontinuities in the glass riser (at the flanges connecting the 1-m-long glass segments) acted as preferential locations for void generation. This finding is not surprising because the glass surface is very smooth, which means a larger superheat is required for void generation at the continuous glass surface than at the discontinuity between any two glass pipes. This discontinuity in the glass surface caused non-uniform void generation along the pipe (in the direction of decreasing pressure) and resulted in slug flow and minor flow oscillations at low powers.

The above observations were limited to the top 1 m of the glass pipe at low powers. At higher powers, no effect of preferred nucleation sites on stability was observed. The reason is that as the flashing point moves closer to the calandria (at higher powers), the resulting void act as further nucleation sites. This makes the flashing more uniform in the rest of the pipe, and the effect of non-uniform void generation close to the location where flashing begins is swamped by the larger two-phase length where flashing is uniform.

While the oscillations shown in Fig. 5 were minor and occurred at low powers, another test was conducted, to examine the effect of superheat and nucleation sites on flashing and flow stability.

4.3. Effect of superheat and nucleation sites

This phenomenon was investigated experimentally by inserting a rough wire in the middle of the top glass section (~ 1-m long), where the effect of preferred nucleation sites caused slug flow. Tests with the wire insert clearly showed the formation of void on the wire surface, but not on the smooth glass surface. This uniform void generation eliminated slug flow and the associated flow oscillations at low powers. The results are shown in Figure 6,

where it can be seen that the flow is stable at all powers (what appear to be flow oscillations at powers less than 50 kW are flow transients associated with the power increases). A comparison of Figures 5 and 6 at powers less than 100 kW clearly shows the effect of the wire insert on flow stability.

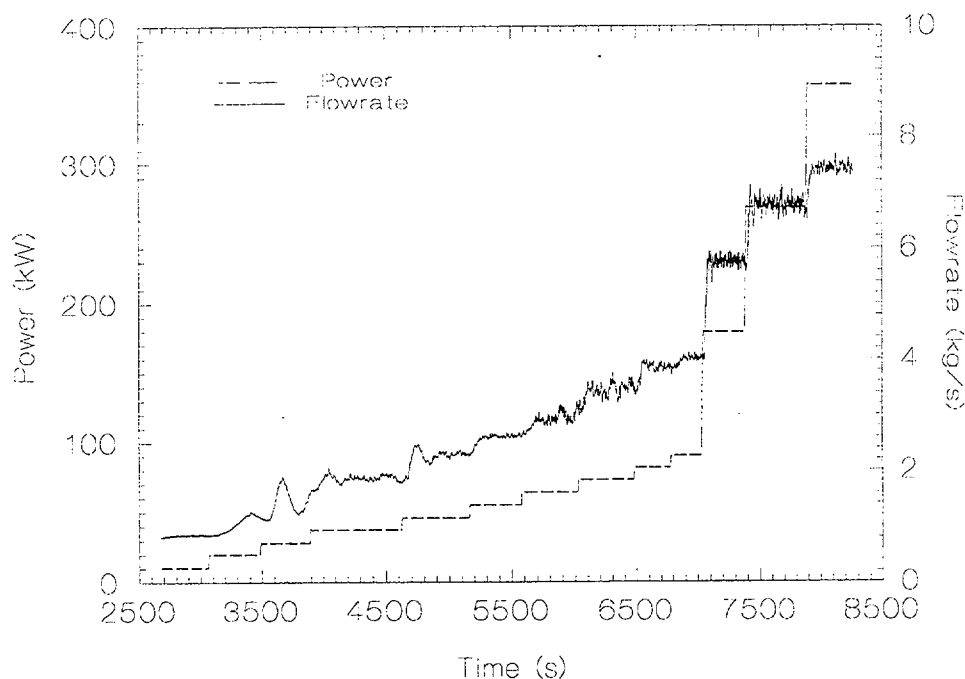


FIG. 6. *Effect of increased nucleation sites.*

The cause of the observed low-power flow oscillations, with the calandria inlet temperature equal to the condenser saturation temperature, was finally traced to insufficient calandria mixing and to the lack of uniform nucleation sites along the smooth glass pipe surface. Accounting for these effects gave experimental results that are in agreement with CATHENA predictions, in that the flow is always stable for the configuration shown in Figure 3.

5. POST-TEST CATHENA SIMULATIONS

Results from the wire-insert experiment (with calandria mixing) were used for comparison with CATHENA. Two cases were simulated: (1) gradual power change, and (2) fast power change.

5.1 Gradual power change (low-power)

These simulations correspond to the test results in Figure 6 where power was increased gradually from 10 kW to 90 kW (~3% to 25% of full power). The experimental results and CATHENA predictions are compared in Figure 7, where it can be seen that CATHENA significantly overpredicted the flowrate. The discrepancy is much greater than the uncertainties in the experimental measurements.

A closer examination of the experimental results showed that relatively high superheat (~2.4 °C) was required to initiate flashing. This conclusion is consistent with studies of

critical two-phase flow [4], which are described in Reference 5; these studies reported that flashing occurred at temperatures higher than the saturation temperature by 2 to 3 °C. CATHENA, on the other hand, predicted a much smaller superheat (a fraction of a degree). This discrepancy caused CATHENA to predict more void in the glass riser which, in turn, caused the flowrate to be overpredicted.

The importance of superheat was investigated by imposing a higher pressure at the condenser and fixing the calandria inlet temperature at 100 °C, to artificially raise the flashing point. A value of 111 kPa was chosen because the saturation temperature at that pressure (102.4 °C) equaled the experimental calandria outlet temperature at 10 kW, where single-phase flow was observed. The CATHENA predictions are shown in Figure 8, where it can be seen that the difference between predicted and measured flow is significantly reduced. Although the imposed pressure did not cause the flashing point to match that of the experiments at all powers, the results showed that the difference between the predicted and measured flowrates in Figure 7 was primarily caused by a large superheat requirement that resulted in delayed flashing.

Despite the improved agreement between CATHENA and the experiments, Figure 8 still shows higher predicted flow at all powers, which cannot be explained by experimental uncertainties alone. The discrepancy can be explained again by the superheat required to initiate flashing, which affects the rate of void increase in the low-quality region just above the onset-of-flashing point. Because these experiments were conducted with a wire insert to provide more nucleation sites, it is not surprising that visual observations clearly showed the presence of void around the wire. However, no void was present in a relatively large portion of the pipe cross-section. This absence of void caused the void fraction, and therefore the driving force, to be less in the experiment than it would be in the ideal case of complete thermal equilibrium.

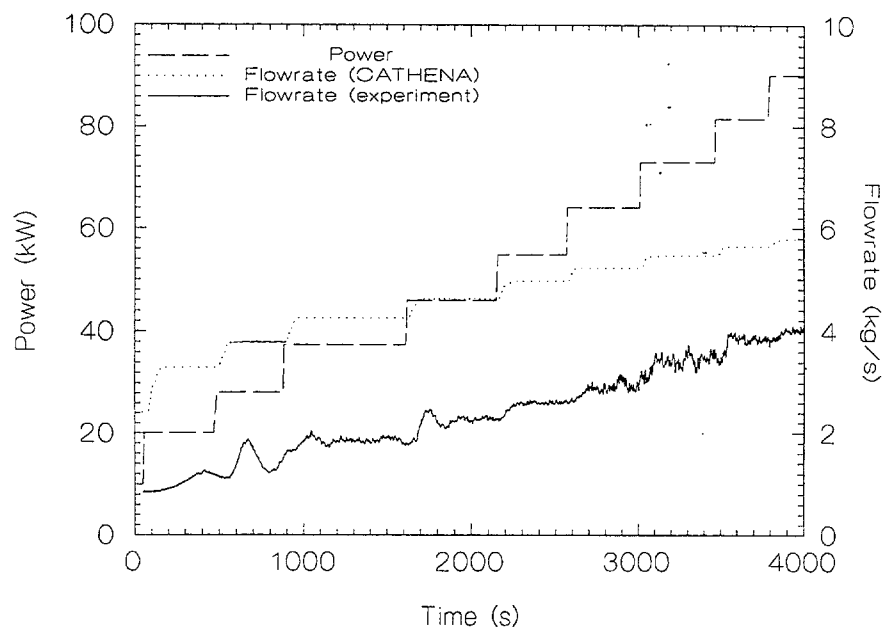


FIG. 7. Low-power comparison with CATHENA using experimental condenser pressure.

Figure 8 also shows some oscillations at very low powers. Both the experimental and CATHENA results suggest that the flow would converge if given sufficient time. No attempt was made to refine the comparison at these powers because the flashing was concentrated in a very small region in the top of the glass riser, which did not include the wire insert.

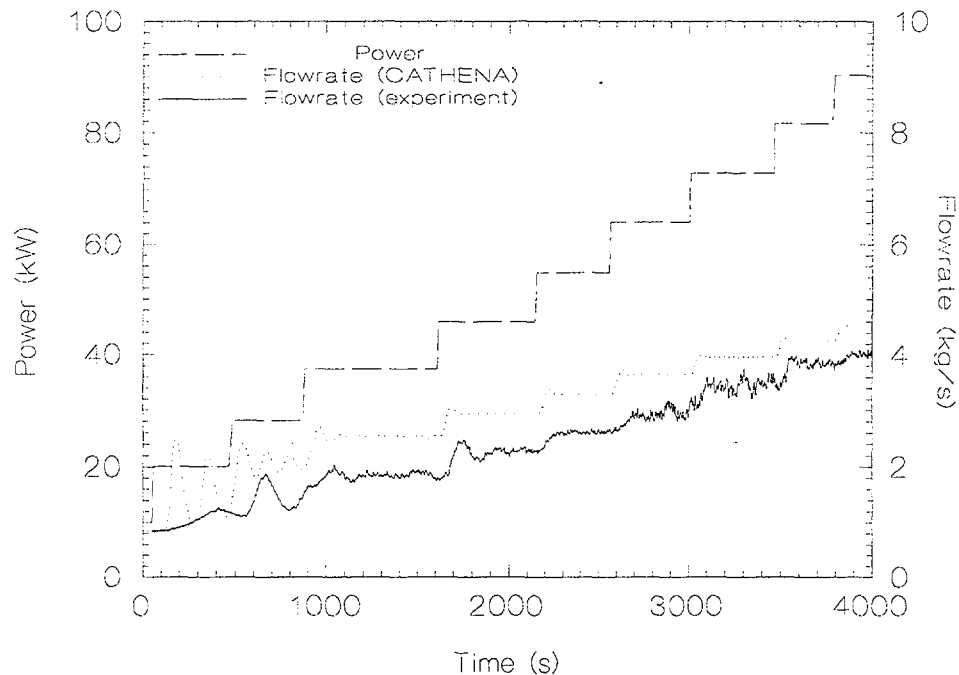


FIG. 8. Low-power comparison with CATHENA using a condenser pressure of 111 kPa.

5.2. Fast power change (high-power)

The test consisted of a fast, three-step power increase from 90 kW to 357 kW, and then a fast power decrease to 82 kW. The results (with atmospheric condenser pressure) are shown in Figure 9, where it can be seen that CATHENA again overpredicts the flow. However, the agreement is better at higher powers, where the two-phase region occupies most of the glass riser.

This better agreement at high powers occurs because the generated void act as nucleation sites that further promote vapour generation. At the point where flashing begins, there is a small amount of void, and thermal non-equilibrium effects cause less void to be generated than when there is complete thermal equilibrium. As the two-phase mixture travels along the glass riser, thermal non-equilibrium effects begin to diminish as more void is generated, creating more nucleation sites. If the two-phase length is long enough (i.e., at high powers), then the void generation in most of the two-phase region will be close to the ideal case of thermal equilibrium between the two phases. This consideration explains the better agreement between CATHENA and the experimental values at the high powers in Figure 11 (>300 kW).

The effect of increasing the condenser pressure to artificially suppress flashing was again simulated for the fast power increases. The results are shown in Figure 10, where it can be seen that the agreement improves, especially at lower powers.

In all cases, CATHENA predicts the loop behaviour well, and discrepancies related to non-equilibrium effects are beyond the capabilities of CATHENA at the present time.

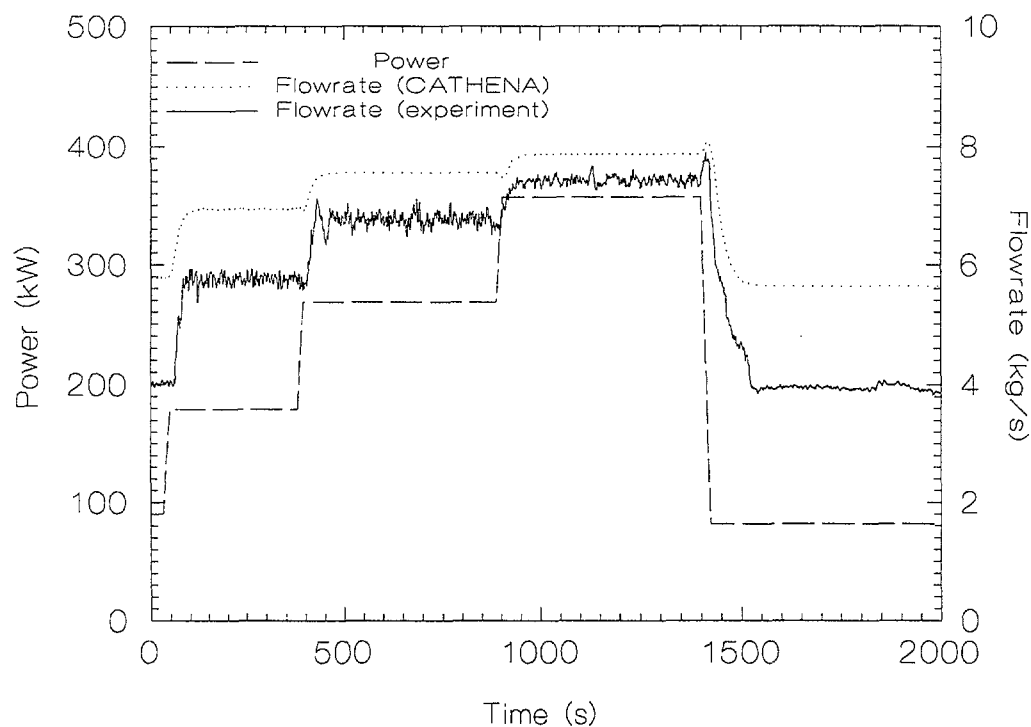


FIG. 9. High-power comparison with CATHENA using experimental condenser pressure.

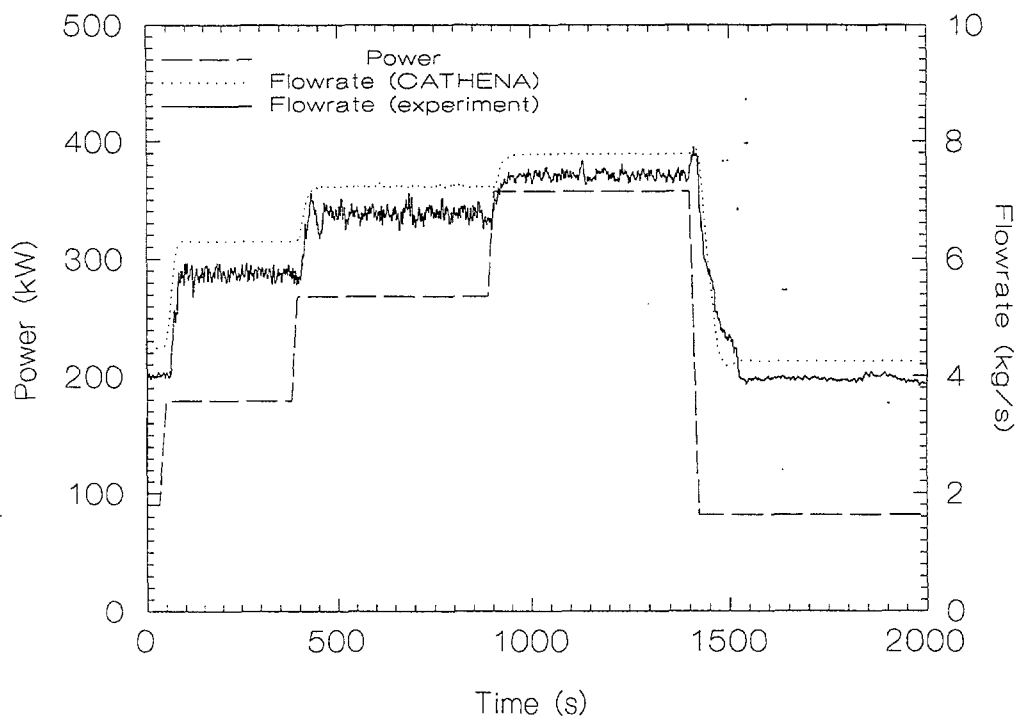


FIG. 10. High-power comparison with CATHENA using a condenser pressure of 111 kPa.

6. DISCUSSION AND CONCLUSIONS

The initial experiments proved that the concept of a flashing-driven natural-circulation loop was feasible. CATHENA pre-test simulations were successful in predicting the loop behaviour and were instrumental in guiding the experimental program.

Post-experiment attempts to refine CATHENA simulations led to a series of special-effects tests to help understand the flashing phenomenon. The special-effects tests demonstrated that two factors were important for flow stability: (1) flow patterns and temperature distribution within the calandria, and (2) flashing superheat requirements and the presence of nucleation sites.

If the temperature distribution within the calandria is within a range where temperature oscillations occur at the calandria outlet, the flow will oscillate because the elevation of the onset of flashing changes with temperature. This problem was dealt with in the test loop by mixing the calandria water, which significantly improved loop stability. The flow and temperature distribution within an actual calandria should be investigated further using a properly sized calandria, and with a suitable inlet-outlet configuration.

The experiments were conducted with the calandria inlet temperature equal to the condenser saturation temperature ($\sim 100^\circ\text{C}$). The results (experimental and CATHENA predictions) indicated stable loop operation with calandria mixing and improved nucleation (wire-insert experiments). By accounting for these effects, we obtained good agreement between the experiments and code simulations.

The case of a variable calandria inlet temperature resulted in flow oscillations at low powers [3]. The results of the separate-effects tests suggest that insufficient mixing in the calandria and non-uniform flashing must have contributed to this instability. However, CATHENA simulations showed that another reason for these oscillations was variations in the outlet temperature that resulted directly from variations in the inlet temperature. This effect was significant in those tests because the calandria was undersized by a factor of 10 [3]. With a properly sized calandria, temperature variations in the cold-leg should be dampened, and the loop behaviour should be similar to that obtained with a constant calandria inlet temperature. This hypothesis was verified using CATHENA, and further tests are planned with a larger calandria.

REFERENCES

- [1] HANNA, B.N., "CATHENA - A thermalhydraulic code for CANDU analysis", Nuclear Engineering & Design, Vol. 180, No. 2 (1998) 113-131.
- [2] BAEK, W.P., SPINKS, N.J., "CANDU passive heat rejection using the moderator", International Conference on New Trends in Nuclear System Thermalhydraulics", Vol. 1, Paper No. C22.1, Pisa, Italy (1994).
- [3] KHARTABIL, H.F., SPINKS, N.J., "An experimental study of a flashing-driven candu moderator cooling system", 16th Annual Conference, Canadian Nuclear Society, Saskatoon, Canada (1995).
- [4] M. Reocreux, "Contribution a l'etude des debits critiques en ecoulement diphasique eauvapeur," Ph.D. thesis, Universite Scientifique et Medicale de Grenoble, France (1974).
- [5] Downar-Zapolski, P., et al. "The non-equilibrium relaxation model for one-dimensional flashing flow," Int. J. Multiphase Flow, Vol. 22, No. 3, (1966) 473-483.



NATURAL CIRCULATION IN AN INTEGRAL CANDU TEST FACILITY*

P.J. INGHAM¹, J.C. LUXAT², A.J. MELNYK³, T.V. SANDERSON¹

¹Safety Thermalhydraulics Branch, AECL Whiteshell Laboratories, Pinawa, Manitoba

²Nuclear Safety Technology, Ontario Hydro Nuclear, Toronto, Ontario

³Emission Management Technology, AECL Chalk River Laboratories, Deep River, Ontario

Canada



XA0055014

Abstract

Over 70 single- and two-phase natural circulation experiments have been completed in the RD-14M facility, an integral CANDU thermalhydraulic test loop. This paper describes the RD-14M facility and provides an overview of the impact of key parameters on the results of natural circulation experiments. Particular emphasis will be on phenomena which led to heat up at high system inventories in a small subset of experiments. Clarification of misunderstandings in a recently published comparison of the effectiveness of natural circulation flows in RD-14M to integral facilities simulating other reactor geometries will also be provided.

1. INTRODUCTION

Under certain postulated accident conditions decay heat is removed from the core of a nuclear reactor by single- or two-phase natural circulation of the primary coolant. An important nuclear safety consideration is to establish that decay heat can be adequately removed in these situations.

Experiments have been conducted in the RD-14M integral test facility located at AECL's Whiteshell Laboratories, Manitoba, Canada, to gain a better understanding of the probable behaviour of natural circulation in a CANDU[®] type heat transport system. The data collected from these tests is used to identify and examine relevant phenomena and assist in model development. An electronic database of all experiments has been developed to aid in the validation of computer models used for safety analysis and licensing.

2. FACILITY DESCRIPTION

Figure 1 shows a simplified schematic of RD-14M, a multiple-heated channel, full-elevation, scaled, integral test facility, possessing most of the key components of a CANDU Primary Heat Transport System (PHTS). The facility is arranged in the standard CANDU two-pass figure-of-eight configuration. The facility is designed to produce similar fluid mass flux, transit time and pressure and enthalpy distributions as those typical of CANDU reactors under both forced and natural circulation conditions [1].

* Funded by the CANDU Owners Group (COG) through the Safety Thermalhydraulics Working Party 5

** Nuclear Safety Technology, Ontario Hydro Nuclear, Toronto, Ontario, Canada, M5G 1X6

*** Emission Management Technology, AECL Chalk River Laboratories, Deep River, Ontario, Canada, KOJ 1J0

® CANDU is a registered trademark of Atomic Energy of Canada Limited (AECL)

The reactor core is simulated by ten, 6 m-long horizontal test sections. Each test section has simulated endfittings and seven electrical heaters, or fuel element simulators (FES), designed to have many of the characteristics of a CANDU fuel bundle. Test sections are connected to headers via full-length insulated feeders. Feeders are equipped with trace heating tapes to minimise heat losses

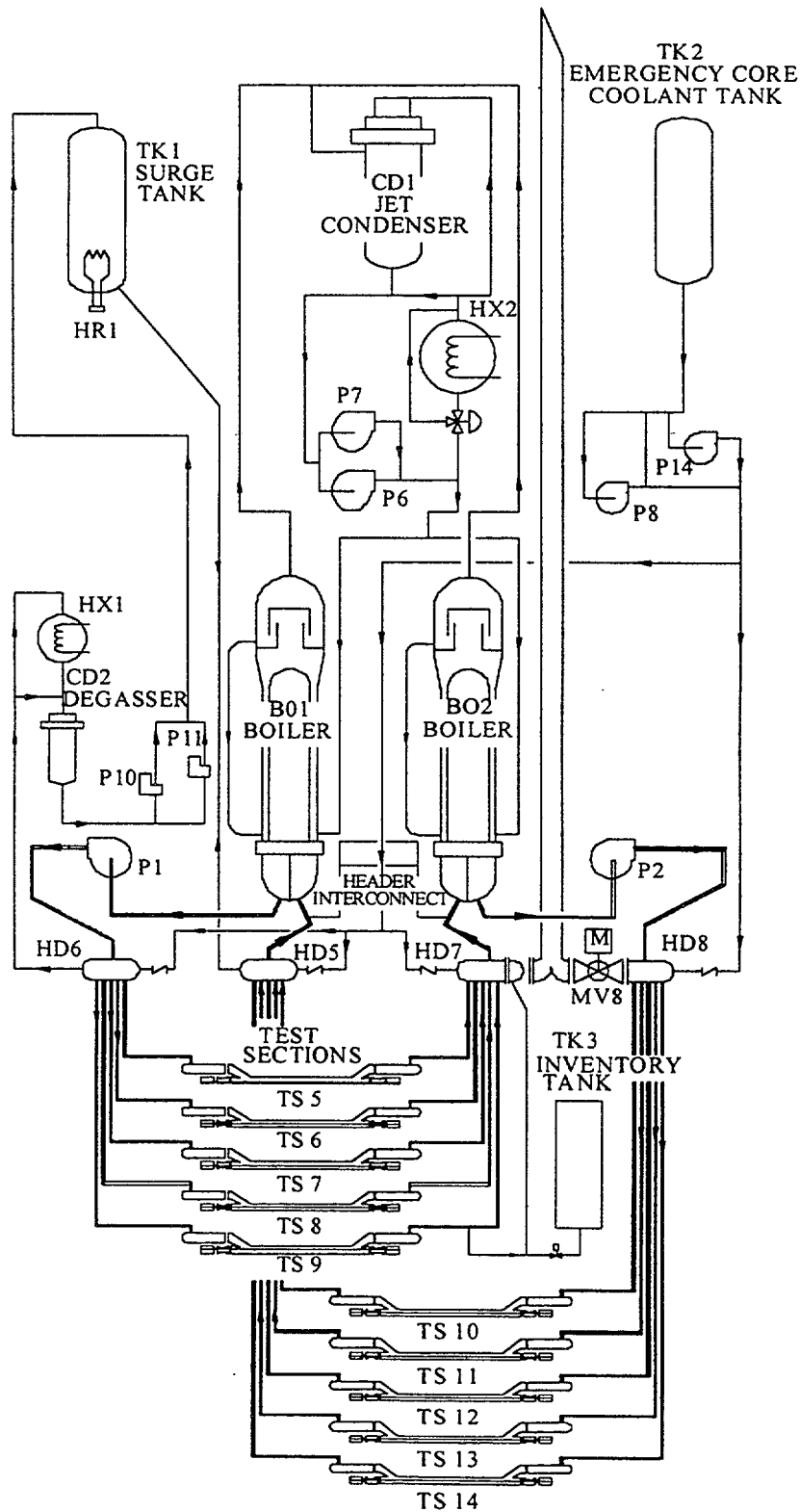


FIG. 1. Schematic of the RD-14M integral CANDU test facility

under natural circulation conditions. Pipework connecting outlet headers can also be valved in to study the effect of outlet header interconnect geometry on mitigating oscillatory behaviour at full and low power conditions.

Above header piping is also CANDU-typical including two full-height, U-tube steam generators or boilers (BO1 and B02) and two bottom-suction centrifugal pumps (P1 and P2). Steam generated in the secondary, or shell, side of the steam generators is condensed in a jet condenser (CD1) and returned as feedwater to the boilers. For natural circulation experiments conducted post 1990 a customised secondary system, designed to operate at reduced power levels typically encountered under natural circulation conditions, was utilised.

The primary-side pressure is controlled by a pressurizer/surge tank (TK1) using a 100-kW electric heater (HR1). The facility operates at typical CANDU primary system pressures and temperatures (typically 10 MPa(g) and 310°C at the outlet header).

For the natural circulation experiments described in this paper, fluid removed from the primary circuit at header 7 (HDR7) is cooled and stored in an inventory tank (TK3). Level monitoring of the inventory tank provides a record of the quantity of primary fluid removed.

The RD-14M facility is extensively instrumented. FES sheath and centre line temperatures up to 1000 °C can be measured axially in five of the seven heaters in each simulated fuel channel to provide a comprehensive picture of the FES temperature distribution. In addition flow, temperature, pressure and the void fraction of the fluid entering and leaving each test section is measured. Gamma densitometers are used to measure the void fraction of fluid at the entrance and exit to both steam generators and at the discharge of both pumps. Fluid temperature, pressure and flow rates are measured at regular intervals throughout the facility. In addition, over 50 differential pressure measurements provide an accurate picture of the pressure distribution throughout the facility. Key secondary-side measurements such as pressure, steam flow rate and temperature, feed water temperature and flow rate and internal shell-side recirculation rate are also recorded. Overall, approximately 600 instruments are scanned and recorded using a dedicated data acquisition system.

3.0. NATURAL CIRCULATION EXPERIMENTS

3.1. Test conditions

To date over 70 natural circulation experiments have been completed in RD-14M. Various parameters have been investigated as summarised in Table I.

TABLE I. RD-14M NATURAL CIRCULATION EXPERIMENTAL TEST CONDITIONS INVESTIGATED

CONDITION VARIED	RANGE INVESTIGATED
POWER	160, 100 and 60 kW/pass
SECONDARY-SIDE PRESSURE	4.5, 4.0, 1.0, and 0.1 MPa(g)
SURGE TANK	on/off
DRAIN RATE	0.03 to 0.2 L/s
SECONDARY-SIDE SYSTEM	High / Low Power
OUTLET HEADER INTERCONNECTS	Dynamic and Geometric Scaled
ECI ADDITION	15-33 L/s
MAKE-UP WATER ADDITION	0.08 kg/s
ECI ISOLATION VALVES	open/closed
TRACE HEATING	on/off

3.2. Test procedure

Prior to the start of each test single-phase natural circulation was established and maintained for several hours at the required test conditions. When steady-state conditions were reached, data collection was initiated and several minutes of steady-state data were collected. The primary inventory was then reduced through a series of discrete drains, from header 7 into the inventory tank. Drains were separated by periods where no perturbations were intentionally introduced to allow steady-state conditions to re-establish. The drains continued until a process protection trip on high FES sheath temperatures, 600°C, was reached terminating the experiment. Slower drain rates with longer periods between drains were used in tests conducted after 1990.

4. NATURAL CIRCULATION BEHAVIOUR

In all RD-14M natural circulation tests the individual channel flows were uni-directional at the start of the test. Once draining started and saturation pressure was reached void was detected in the hot leg regions of the loop. The presence of void increased flow rates throughout the loop due to an increase in the buoyancy driving force. As the primary inventory was further reduced a maximum flow rate through the steam generators was eventually reached. Subsequent reduction in the primary inventory resulted in a decrease in flow rates. In tests conducted at the higher pressures and powers, unidirectional flow was maintained throughout this stage. It is suspected that the reduction of flow resulted from a degradation in the steam generator buoyancy driving force component arising from the penetration of void into the cold leg regions of the steam generators. This phenomenon has also been postulated to explain similar behaviour in integral PWR experiments [2]. In RD-14M high pressure, high power tests (>4 MPa(g) and at 160 kW/pass), further reduction of the primary inventory lead to the establishment of an adverse pressure gradient in the steam generators. This adverse pressure gradient eventually offset the forward buoyancy driving component in the highest elevation feeders resulting in flow reversal in these channels in some tests at about 85% inventory. In all cases, core cooling was maintained even after the onset of bi-directional flow. Tests conducted at these conditions have been captured using existing simple models [3].

In tests carried out at lower secondary-side pressures ($P \leq 1.0$ MPa(g)), flows were highly oscillatory at high primary inventories and exhibited highly dynamic behaviour. Flow reversed preferentially in some channels at primary inventories of 95-90% as a result of statistically characterised lags between steam generator and feeder pressure drop components. Channels having long horizontal feeder sections immediately adjacent the end-fittings generally had the largest lags and were most vulnerable to flow reversal.

In all tests, at high and low pressures, continued reduction in primary inventory was accompanied by additional channel flow reversals. While bi-directional flow in the channels caused a break down in net flow through the loop as measured through the steam generators, it did not cause a simultaneous breakdown in core or channel cooling as shown in Figure 2. This suggests that reflux-condensation in the steam generators became the prime heat rejection mechanism at lower inventories. Similar behaviour is also reported for PWR integral tests [2].

In the overwhelming majority of tests FES heatup did not occur until primary fluid inventories were reduced to less than 70%. A small subset of tests carried out at powers of 160 kW/pass and a secondary-side pressure of 1.0 MPa(g) has been the focus of particular interest as FES heatup occurred at primary fluid inventories greater than 85%.

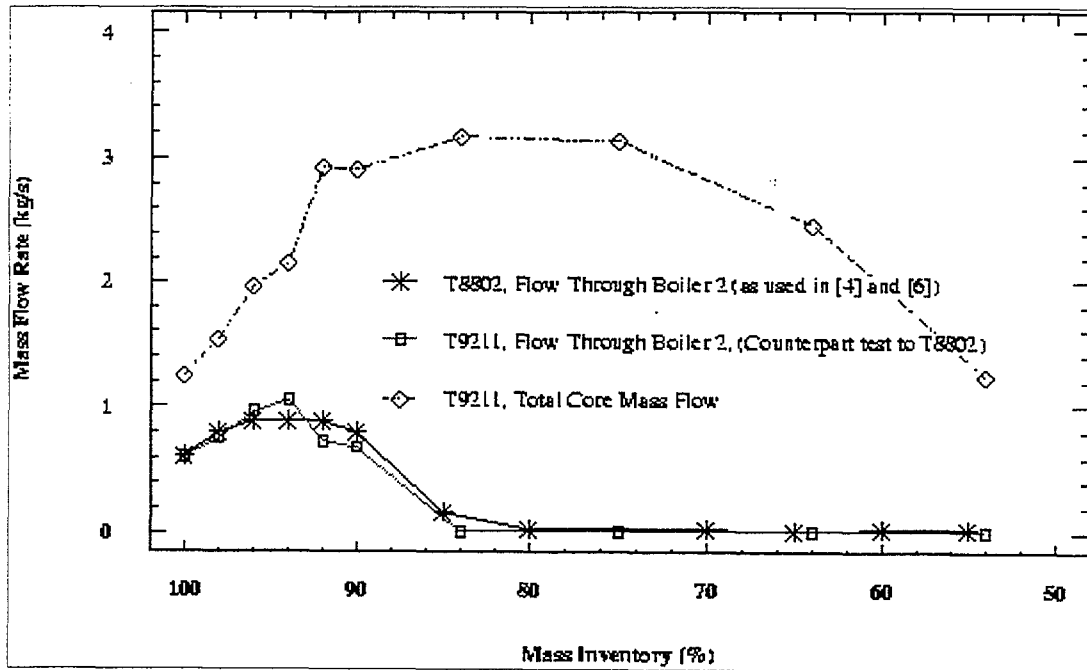


FIG. 2. Comparison of above header and total core flow in RD-14M

4.1. Dryout at high primary fluid inventories

Dryout at primary inventories greater than 85% resulting in FES temperature excursions in excess of 600°C only occurred in 3 natural circulation experiments carried out at primary powers of 160 kW/pass and a secondary side pressure of 1.0 MPa(g). Six other tests conducted under similar conditions did not experience dryout at inventories greater than 70%. In all cases dryout did not occur until the flow in at least 2 of the 5 channels in a pass was reversed.

At these test conditions, the net buoyancy driving force component from the steam generators becomes negligible by about 90% inventory. Individual channel flow is driven by the feeder buoyancy component, which is made up of the liquid filled inflow feeder and a highly voided outflow feeder. In these 3 tests, dryout occurred following a continuous reduction in the pressure drop in the inflow feeder which caused a proportional reduction in the flow through the channel. Inflow feeder gamma densitometer and pressure drop measurements indicate this reduction was caused by void penetration of the inflow feeder (VPIF). Gamma densitometers are located on the feeder piping near the inlet and outlet of each channel. Since void is observed in the feeder, as inferred from pressure drop measurements, prior to being detected by the gamma densitometers, the void does not seem to have originated in the test section (Fig. 3).

All 9 tests showed evidence of void in an inflow feeder at some time following the onset of flow reversal. In fact, a review of natural circulation experiments conducted at other test conditions showed

VPIF to be a common phenomenon. However, in all but these 3 tests the extent of void penetration of the inflow feeder was limited to an intermediate level and only resulted in a partial degradation of channel flow. In some cases, inflow feeders appeared to refill after a period of several minutes, in other cases inflow feeders remained partially voided for several hours. In these latter situations flow through the channels was reduced but did not totally break down. In

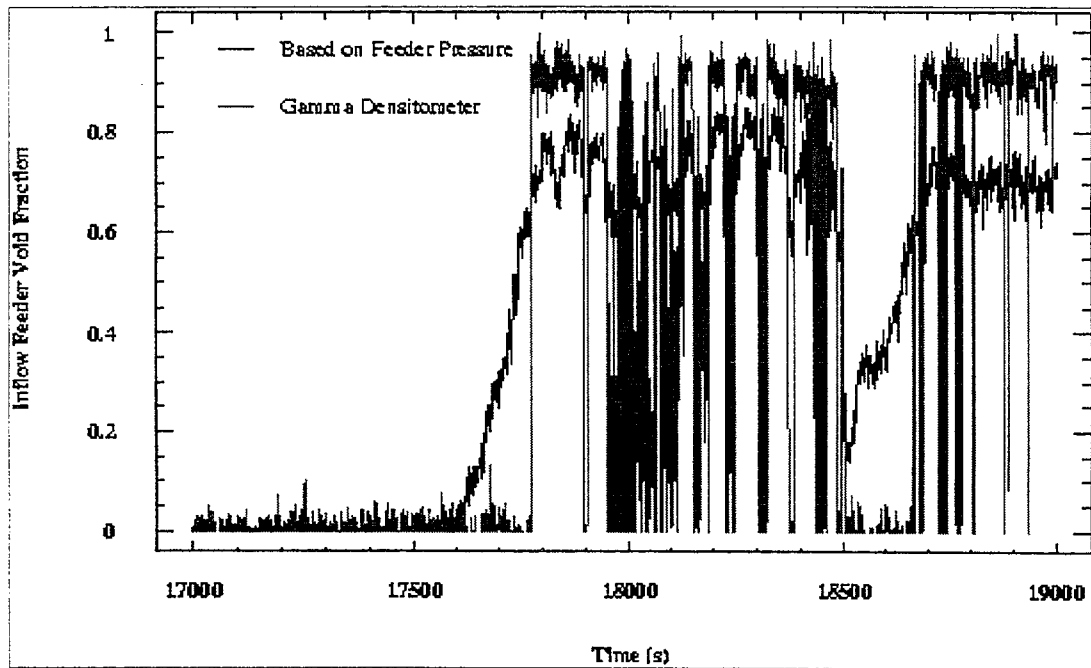


FIG. 3. Appearance of void in the inflow feeder

the three tests experiencing dryout at high inventories, void penetrated the inflow feeder until there was no net buoyancy driving flow in one channel. Flow in all other channels remained sufficient to provide channel cooling. In tests T8809, T8810 and T9308, VPIF, and subsequent dryout, was induced by a depressurization caused by a draining operation as shown in Figure 4.

To obtain more information on conditions leading to dryout at high primary inventories and to establish limits of FES temperature excursions additional tests were carried out. These tests were conducted at power levels of 160 kW/pass and a secondary side pressure of 1.0 MPa(g). FES trips were set at 800 °C as an extrapolation of these earlier results suggested that the FES temperatures would have approached an asymptotic limit close to 700 °C had a process protection trip at 600 °C not occurred. Primary inventories were limited to greater than 80%. Primary coolant draining and/or small changes to the secondary side (10%) were used to induce dryout. Although 69 of the previous 70 natural circulation experiments had trace heating applied to the inlet and outlet feeder piping in these tests feeder trace heating was initially off.

Results from these tests showed that without trace heating only limited VPIF of Test Section 7 (TS7) and TS12 inflow feeders could be induced (Figure 5) and FES temperature excursions were limited to less than 300 °C. Turning on the trace heating resulted in immediate but limited VPIF in some inflow feeders (Figure 5). Further VPIF phenomena were then readily induced by secondary side perturbations (Figure 6). A maximum FES temperature of 675 °C was reached prior to quenching in TS 11 at a primary inventory greater than 85% (Figure 7).

4.2. VPIF mechanisms

It still is not clear why dryout occurred in only T8809, T8810 and T9308. However, it should be noted that T88 tests had a drain rate three times that of subsequent tests and an unplanned secondary side pressure transient during the drain prior to dryout occurred in T9308. It should also be noted that dryout only occurred at these test conditions in a reversed channel

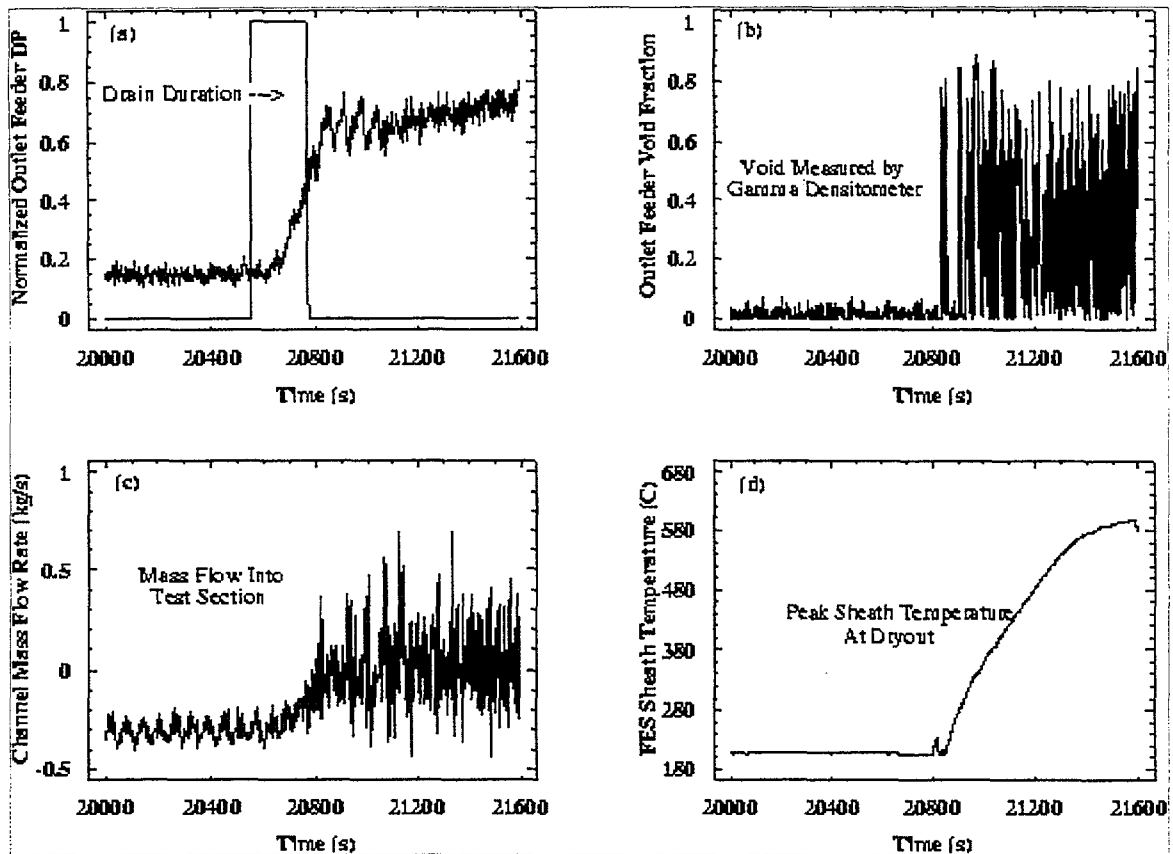


FIG. 4. RD-14M test T9308 (a) VPIF induced by draining, (b) void measured at the inflow of the test section, (c) mass flow through the channel is reduced, (d) dry out occurs at 87% mass inventory

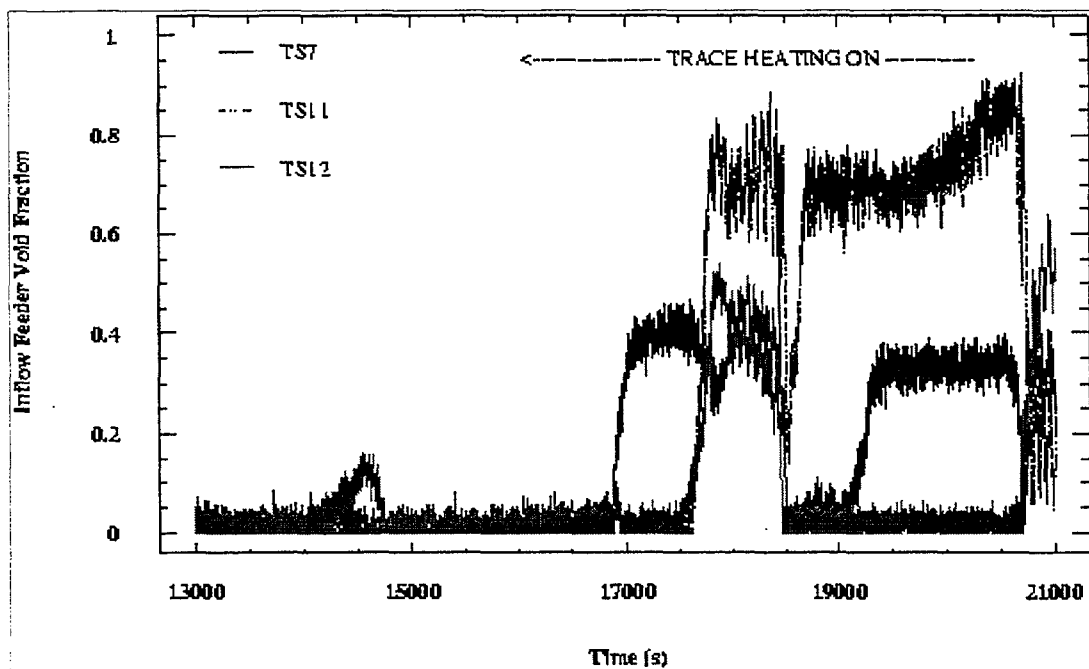


FIG. 5. The effect of feeder trace heating on VPIF

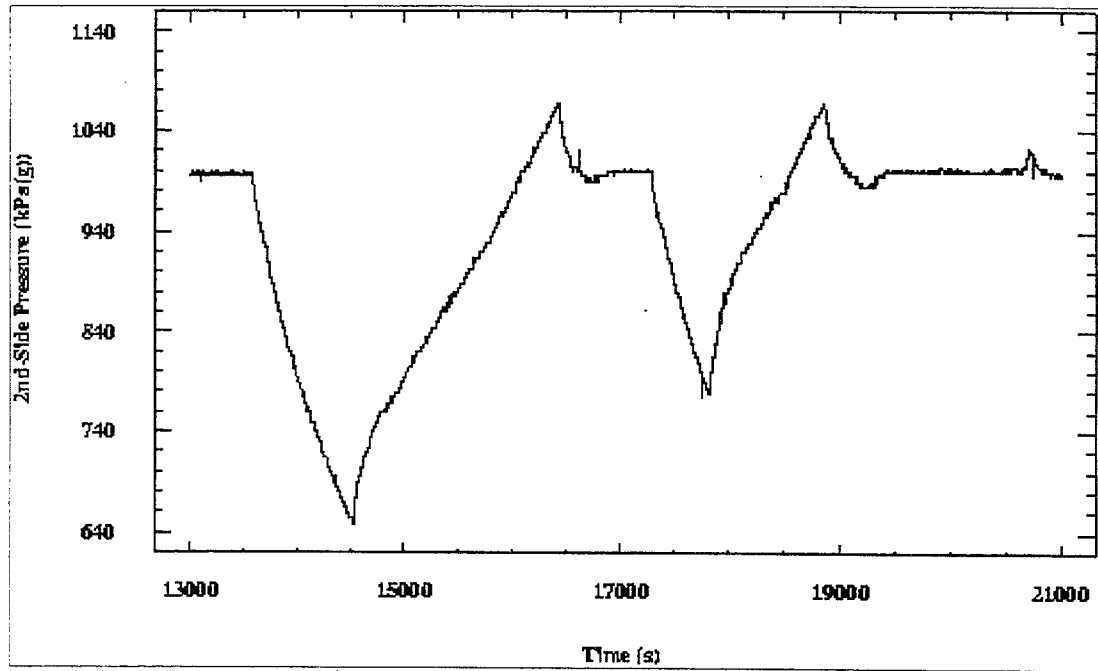


FIG. 6. Secondary side pressure transient

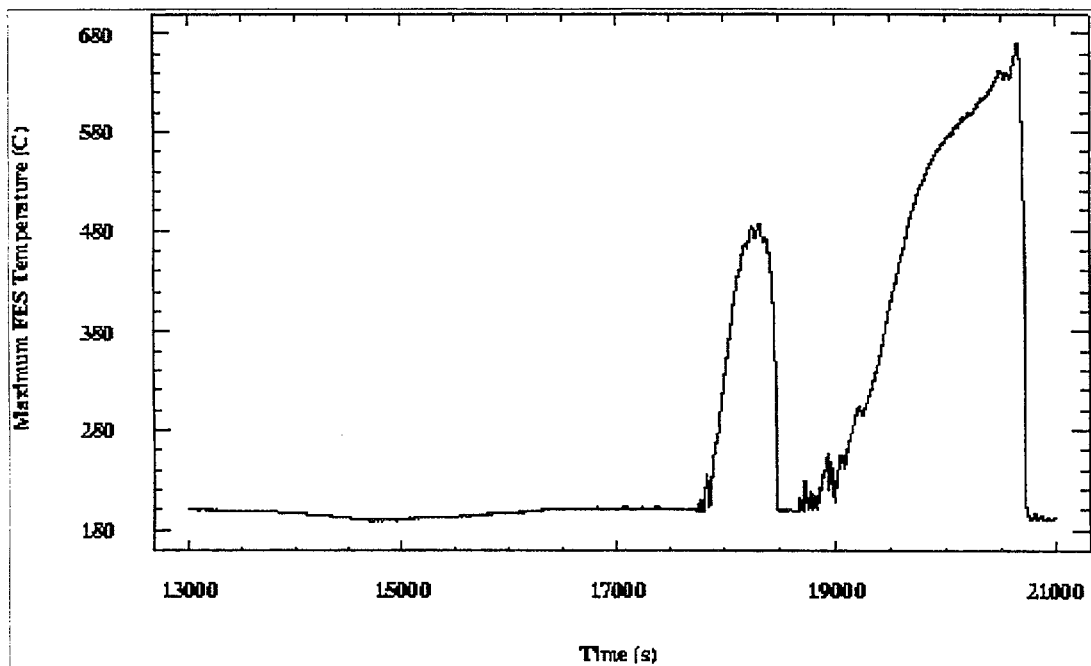


FIG. 7. Test section 11 FES temperature transient

following the second channel flow reversal. Under this circumstance fluid entering the inflow feeder is at saturation temperature. A brief explanation of the various hypotheses as to the cause of VPIF follows.

Steam bubble entrainment and flashing were mechanisms considered. For steam bubble entrainment, the drag forces exceed buoyancy forces causing steam bubbles to be dragged from the header into the feeder. This mechanism should be self limiting and self correcting as a result

of reduction in drag forces caused by flow reduction and bubble coalescence. Flashing would imply that void production is solely due to depressurization. This is highly unlikely since all saturated feeders should be effected instead of only a few. Flow induced flashing was also considered. This is attributable to frictional pressure drop and is highly unlikely due to the very low flow rates. This is a self correcting and non sustainable mechanism.

Liquid starvation is a mechanism where an adverse distribution of void in the headers exists such that insufficient liquid is available at the header/feeder interface to offset the flow from the feeder into the channel. Depending on the availability of liquid from the header, the liquid level in the feeder and consequently the flow into the channel will drop until a new steady-state is reached, or in extreme cases, until total flow breakdown occurs and dryout results.

Test data suggests the void entering the feeders originates from the headers and indicates that the void distribution inside the header is extremely complex. Both axial and radial variations must occur with more void present at lower elevations within the header. No direct measurements of void in the RD-14M headers are currently available. However, recent separate effect tests using an instrumented RD-14M inlet header, although not conducted at conditions expected during natural circulation, confirm these variations are possible. Work is presently continuing to extend the study of the distribution of void in RD-14M headers to conditions more typical of natural circulation.

4.3. Complicating factors affecting VPIF mechanisms

Trace heating has a marked effect on VPIF. The trace heating used for natural circulation tests in RD-14M is fixed at the start of the test and is not controllable. Following the onset of bi-directional flow, the added energy may exceed the actual heat losses and void may be generated in the inflow feeder. Trace heating also inhibits void collapse. Experiments are planned to examine this effect.

Feeder metal mass temperature can also effect VPIF. As the primary pressure drops with each subsequent drain, the saturation temperature of the fluid is reduced, possibly below the temperature of the metal pipe. Additional void production may result as stored energy from the pipe walls is transferred to the fluid. Pressure vessel requirements have resulted in an increase in the relative metal to fluid mass ratio from that expected in typical CANDU headers and feeders. Experiments are planned to study this effect as well.

5. CLARIFICATION OF A RECENT COMPARISON OF NATURAL CIRCULATION FLOWS IN OTHER INTEGRAL FACILITIES

Differences in the geometrical configuration between the CANDU PHTS and other reactor systems make direct comparison of natural circulation results difficult. Although many similarities in natural circulation phenomena between CANDU and PWR's have been identified, the multiple, horizontal-channel reactor core allows phenomena like individual channel flow reversal to occur which do not have a counterpart in other systems.

Recently, a quantitative comparison of the effectiveness of natural circulation flows in the CANDU type RD-14M facility and integral facilities simulating PWR and WWER geometries was published [4]. The RD-14M data presented in this comparison was inappropriately extracted and interpreted from an early paper for test T8802 [5]. The authors of this comparison incorrectly

TABLE II. INITIAL CONDITIONS, BOUNDARY CONDITIONS AND KEY EXPERIMENTAL RESULTS FOR COUNTERPART EXPERIMENTS T8802 AND T9211

PARAMETER / RESULT	T8802	T9211
INITIAL PRIMARY PRESSURE (MPa(g))	8.0	7.0
SECONDARY-SIDE PRESSURE (MPa(g))	4.3	4.0
PASS 1 - TOTAL POWER (kW)	100.0	101.9
PASS 2 - TOTAL POWER (kW)	101.5	101.7
INITIAL HEADER 5 TEMPERATURE (°C)	264.2	259.5
INITIAL HEADER 6 TEMPERATURE (°C)	246.9	242.9
INITIAL HEADER 7 TEMPERATURE (°C)	264.8	260.4
INITIAL HEADER 8 TEMPERATURE (°C)	248.0	244.1
TRACE HEATING (kW)	22.0	22.0
BOILER FEEDWATER TEMPERATURE (°C)	57.1	164.9
% MASS INVENTORY OF FIRST CHANNEL TO REVERSE (CHANNEL NUMBER) - PASS 1	84% (HS5)	91% (HS7)
% MASS INVENTORY OF SECOND CHANNEL TO REVERSE (CHANNEL NUMBER) - PASS 1	84% (HS7)	82% (HS7)
% MASS INVENTORY OF FIRST CHANNEL TO REVERSE (CHANNEL NUMBER) - PASS 2	89% (HS10)	91% (HS12)
% MASS INVENTORY OF SECOND CHANNEL TO REVERSE (CHANNEL NUMBER) - PASS 2	84% (HS11 & HS14)	82% (HS14)
% MASS INVENTORY WHERE FLOW THROUGH BOILERS BREAKS DOWN ^a	84%	82%
% MASS INVENTORY AT DRY OUT ^b (CHANNEL NUMBER)	48% (HS7)	48% (HS8)

^a Breakdown of flow through the boilers based on stalling of above header turbine flow meters. These meters stall at flows below 0.4 L/s.

^b Dry out based on first channel to have at least two fuel element simulator temperatures exceed 600°C.

assumed the core flow for the RD-14M test was equivalent to the reported flow through only one of the steam generators [6]. Because of the figure-of-eight configuration, this assumption is a factor of two too low under strictly unidirectional flow conditions. The error in this assumption becomes even greater following the onset of channel flow reversal. The RD-14M experimental data used is not consistent with the author's analysis methodology. As a consequence, the magnitudes of RD-14M natural circulation flows are severely underestimated.

Core mass flow rates for the RD-14M test used in this comparison, T8802, cannot be calculated due to insufficient instrumentation in this early test. However, a more recent, better instrumented test, T9211, was conducted at the same nominal conditions as T8802. Test T9211 was the only test conducted using similar conditions and test procedure. Experimental results for T9211 are comparable to T8802 as shown in Figure 2. The similarity between these two tests is also illustrated in Table II where initial conditions, boundary conditions and key experimental results are compared. Important results to note include the similarity of inventory for the first and second flow reversals, breakdown of flow through the boilers and break down of flow in one of the channels (dry out).

The core mass flow rate is obtained by adding the mass flow rate through each channel. Individual channel mass flows are determined by correcting single-phase inflow feeder flow rate measurements made at steady-state conditions at each inventory for density.

To make an accurate comparison of RD-14M with other facilities, the total core mass flow as shown in Figure 2 should have been used in Ref. [4] instead of the flow through only one of the steam generators. As illustrated in Figure 2, both the effective range and the magnitude of the core mass flow rates are significantly larger than the values used in assessing RD-14M results. The referenced comparison implies significant core flow rates only occur over a narrow range of primary inventories (82 to 100%), whereas in reality effective core flow rates were measured at inventories as low as 48%. Similarly, the actual maximum core mass flow rate is a factor of three higher than that in the data used in the referenced comparison. It is unfortunate that the differences in facility configurations and the nature of the data used in this comparison were misunderstood. The impact of these oversights is a gross underestimation of the core cooling effectiveness of natural circulation in CANDU geometries. Superimposition of the correct data on the published comparison clearly demonstrates that natural circulation flows in a CANDU type facility are quantitatively as high, if not higher, than flows encountered in integral facilities representing PWR and WWER geometries.

6. SUMMARY

The key features of RD-14M, an integral CANDU test facility, have been described. An overview of the general behaviour observed in RD-14M natural circulation experiments has been discussed. Void penetration of inflow feeders (VPIF) has been identified as the mechanism responsible for early heatup in a small subset of tests. For these tests, heatup is limited to FES temperatures less than 700 °C and is followed by quenching. VPIF probably originates in the RD-14M headers and is strongly coupled with both header conditions and feeder trace heating.

Natural circulation flows in RD-14M, when accurately compared on a quantitative basis to those found in integral facilities representing PWR and WWER geometries, are as good if not better.

In essence, RD-14M natural circulation results are understood and explainable. They provide a valuable experimental data base for development and validation of physical models.

REFERENCES

- [1] INGHAM, P.J., et al, "Scaling laws for simulating the CANDU heat transport system", Proc. 2nd Intern. Conf. Sim. Meth in Nucl. Engrg., Montreal, Canada (1986)
- [2] DUFFEY, R.B., SURSOCK, J.P., "Natural circulation phenomena relevant to small breaks and transients", Nucl. Engrg. Des., 102,115-128. (1987)
- [3] WAN, P. T., et al, "Modelling of RD-14M partial-inventory thermosiphoning tests using the OHAT code", 4th Intern. Sim. Meth. Conf., Montreal, Canada, (1993)
- [4] D'AURIA, F. and GALASSI, G.M., "Code validation and uncertainties in system thermalhydraulics", Progress In Nuclear Energy, Vol. 33. No.1/2. Pp175-216, (1998)
- [5] MELNYK, A.J., AECL, D'AURIA, F., University of Pisa, personal communication, 1997 February 20
- [6] INGHAM, P.J., et al., "Natural circulation experiments in RD-14M with emergency coolant injection", ANS Intern. Top. Meetg.-Safety of Thermal Reactors, Portland, Oregon, USA (1991)

NATURAL CIRCULATION PERFORMANCE IN NUCLEAR POWER PLANTS

F. D'AURIA, G.M. GALASSI
Dipt. di Costruzioni Meccaniche e Nucleari,
University of Pisa,
Pisa



XA0055015

M. FROGHERI
DITEC,
University of Genoa,
Genoa

Italy

ABSTRACT

The present paper deals with a study of natural circulation in PWR systems.

The study consists of two parts: in the first one, natural circulation in experimental facilities simulating PWR plants was analyzed. This made it possible to gather a broad data base which was assumed as a reference for the subsequent part of the research. Seven Nuclear Power Plants nodalizations and additional experimental data from "non-PWR" facilities have been considered in the second part of the paper.

Conclusions are drawn about natural circulation capabilities derived for the seven Nuclear Power Plants nodalizations and from data base pertinent to three "non-PWR" facilities.

1. INTRODUCTION

Natural circulation is an important mechanism in several industrial systems and the knowledge of its behavior is of interest to nuclear reactor design, operation and safety. This is especially true for the new reactor concepts which largely exploit the heat removal capabilities of natural circulation.

The evaluation of natural circulation performances (NCP) in experimental facilities has been the object of previous works. In that frame, the natural circulation scenarios occurring at different values of the primary mass inventory were considered making reference to the data measured in the PWR simulators Semiscale, Spes, Lobi, Bethsy, Pkl and Lstf /1/, /2/, /3/.

In order to evaluate the NCP of these facilities, significant information comes from the comparison of the trend of core flow rate versus primary loop mass inventory. In the present study the flow rate and the residual mass have been normalized, taking into account the volume of each facility and the level of power utilized in the experiment. The obtained natural circulation map has been used in the evaluation of the NCP of the Pactel (two configurations) and the RD-14M facilities, simulators of WWER and CANDU reactors, respectively; the two configurations of Pactel make reference to WWER-440 and to the same reactor equipped with a passive safety system.

The enlargement of the natural circulation data base to the Nuclear Power Plants (NPP) was achieved through the application of thermalhydraulic codes. The Relap5/Mod3.2 code is suitable for the simulation of natural circulation transients and the nodalizations of seven reactors of different type are available: two PWR - Westinghouse (built), one PWR - Babcock & Wilcox (built), WWER-1000 (built), EPR (designed by NPI), AP-600 (designed by Westinghouse) and EP-1000 (in design phase by a consortium led by Westinghouse).

The objectives of the present paper can be summarized as follows:

- qualification of the NPP nodalizations;
- demonstration of the quality level of the old and new generation plants design, as far as natural circulation is concerned.

2. DERIVATION OF REFERENCE NATURAL CIRCULATION FLOW MAP

2.1 Reference facilities

The considered test facilities (Lobi, Spes, Bethsy, Semiscale, Pkl and Lstf) reproduce the primary circuit of a PWR plant equipped with U-tubes steam generators. Relevant general data related to the facilities hardware are summarized in Tab. 1. Additional information is provided hereafter.

Lobi-Mod2 facility /4/ was installed at the Ispra Research Centre and simulated a four-loop 1300 MWe PWR (the reference reactor was the KWU plant of Biblis). The primary circuit was constituted by an "intact loop" (simulating 3 loops of the reference plant) and a "broken loop" in which pipe ruptures of different sizes could be mounted. The core was simulated with a heated bundle with 64 electrically heated rods, arranged in a 8x8 matrix. Volume and power were scaled down by a factor of 712, while the elevations of all the components (with the exception of the pressurizer) were preserved.

Spes /5/ was a simulator of the Italian Standard Nuclear power plant (PWR-PUN, Westinghouse 312 type, 3 loops), with a volume and a power scaling ratio equal to 1:427 and the elevations preserved. The power channel was heated with 97 rods for a maximum power corresponding to about 140 % of the reactor nominal power.

Bethsy /6/ is located in Grenoble and simulates a 3 loops, 900 MWe, Framatome PWR. It is a full pressure facility with an overall volume scaling factor equal to 1:100. The core is simulated with 428 electrically heated rods with a power that is 10 % of the scaled value.

Semiscale Mod-2A /7/ is the simulator of a 4 loops PWR, with a volume scaling ratio equal to 1:1700. It is constituted by two circuits: the intact loop, representing three loops of the reference plant and a broken loop, where different types of break can be simulated. The core is simulated with a 5x5 matrix of electrically heated rods, with a scaled nominal power of 3 MW.

Pkl-III /8/ represents a typical KWU-PWR of 1300 MW. It simulates, with a volume scaling ratio 1:145, the 4 loops of the reference plant with a maximum pressure of 40 bar. The core is constituted by 314 electrically heated rods for a total power of 2.5 MW, corresponding to 10% of the nominal power.

Lstf /9/ is a scale model of a Westinghouse type PWR (4 loops and 3423 MWth) with a volume scaling ratio of 1/48. The four loops of the reference plant are represented by two equal volume loops and the core power is 14 % of the scaled value.

Tab. 1: Relevant hardware characteristics of the PWR simulators

Quantity	Semiscale Mod 2A	Lobi Mod 2	Spes	Pkl-III	Bethsy	Lstf
Reference reactor and power (MW)	W-PWR 3411	KWU-PWR 3900	W-PWR 2775	KWU-PWR 3900	FRA-PWR 3423	W-PWR 3423
Number of rods	25	64	97	340	428	1064
Number of U-tubes per steam generators	2/6	8/24	13/13/13	30/30/60	34/34/34	141/141
Internal diameter of U-tubes (mm)	19.7	19.6	15.4	10.0	19.7	19.6
Actual Kv	1/1957	1/589	1/611	1/159	1/132	1/48

2.2 Reference experiments

Natural circulation in a PWR occurs due to the presence of a heat source (core) and sinks (steam generators), which, in a gravity environment, create driving forces leading to flow rates in the loops and core cooling. Four main patterns were identified at different values of the mass inventory in the primary loop:

- single-phase natural circulation with no void present in the primary system excluding the pressurizer;
- stable co-current two-phase natural circulation with increasing mass flow rate;
- unstable two-phase natural circulation-siphon condensation;

- (d) stable reflux condensation with condensed liquid flowing back to the core through the hot legs. Natural circulation experiments have been performed in all the considered facilities /1/.

2.3 Natural circulation flow map

A typical natural circulation transient can be represented through the trend of core mass flow rate versus primary loop inventory.

The measured tests in the above facilities are qualitatively similar: the core flow rate shows a maximum in the two-phase regime and becomes equal to zero in the reflux condensation zone.

In order to have a homogeneous representation of the data, the values of core flow rate and residual mass have been normalized, adopting the test power level (MW) and the facility volume (m^3), respectively. The resulting curves are reported in Fig. 1.

These data allowed the achievement of upper and lower boundaries for natural circulation, assumed as reference in evaluating the NCP in PWR systems (Fig. 2).

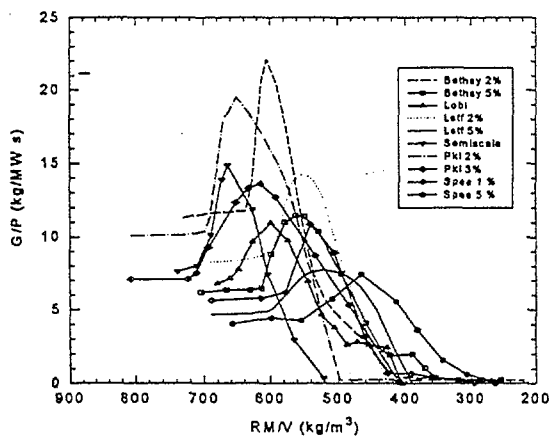


Fig. 1: Natural circulation curves for PWR simulators

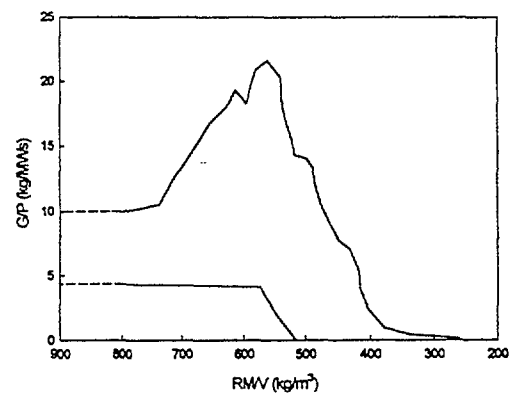


Fig. 2: Upper and lower boundaries for NCP evaluation in PWR systems

3. EVALUATION OF NATURAL CIRCULATION IN PWR SYSTEMS

3.1 Considered Nuclear Power Plants and nodalizations

Seven commercial NPP systems have been considered in the present study, as listed in the first row of Tab. 2.

Reactors 1 to 4 have been built and are in operation. Reactors 5 to 7 are in a more or less advanced design stage.

Tab. 2: Relevant characteristics of the considered NPP

	1 PWR	2 PWR	3 PWR	4 WWER 1000	5 EPR	6 AP-600	7 EP-1000
Nominal power (MW)	1877	870	2773	3000	4250	1972	2958
PS volume* (m^3)	167	150	330	359	459	211	339
SG type	U-tubes	U-tubes	Once-Through	Horizontal	U-tubes	U-tubes	U-tubes
N. of loops	2	4	2	4	4	2	3
N. of pumps	2	4	4	4	4	4	6
Nominal mass (kg)	108350	107620	224150	239810	306726	145160	226830
Nominal core flow rate (kg/s)	9037	315	17138	15281	20713	8264	14507
PRZ pressure/SG pressure (MPa)	15.6 6	14 3.1	15 6.4	15.7 6.3	15.5 7.2	15.5 5.5	15.8 6.4

- * excluding ECCS and related connecting lines

Nodalizations for each system have been set up at DCMN of Pisa University, adopting standard procedures for the development and the qualification. In such a way, reference nodes dimensions of about 0.5 m have been fixed along the flow path. The number of nodes for each nodalization is strongly a function of the steam generators geometry and the number of loops: the resulting total number of nodes ranges between 250 (case of Krsko) and more than 1400 (case of EPR). In the same way, the number of mesh points for conduction heat transfer ranges from 1000 to more than 10000. The nodalizations have been qualified, as far as possible, adopting the procedure reported in ref. /10/.

3.2 Considered facilities

Pactel is a Russian WWER-440 simulator (volume scaling ratio 1:305) available in Finland. The reference reactor design has several features differing from the Western PWR typical one; such as six primary loops with horizontal steam generators, loop seal in both hot and cold legs, a shorter core in comparison with most PWRs.

The six loops of the reference WWER are simulated by three coolant loops with double capacity steam generators. The reactor vessel is simulated with a U-tube construction, being the core section connected to the external downcomer by means of an inverted U-tube pipe. The core consists of 144 electrically heated fuel rods, with a chopped cosine axial power distribution; the heated length and the other dimensions of the rods are identical to the reference reactor ones /11/. In this configuration (without primary pumps), Pactel was utilized for an OECD CSNI International Standard Problem (ISP 33).

The facility was then modified in the steam generators design and by adding the main recirculation pumps and a passive safety injection system. This mainly consists of a Core Make up Tank (CMT), a Pressure Balancing Line (PBL) connecting the CMT with one of the cold leg and an Injection Line (IL) connecting it with the downcomer.

RD-14M is a Candu simulator located in Manitoba (Canada). Its primary heat transport system contains ten 6-m-long horizontal heated channels which represent CANDU fuel channels, connected to end-fitting simulators, representing two symmetrical passes through a reactor core. Each channel contains seven electrically heated fuel-element simulators. The channels are arranged to cover the elevation difference present in a Candu reactor core.

Primary fluid circulation is provided by two centrifugal pumps. Heat is removed from the primary circuit through two full-height, recirculating U-tube steam generators. The heated channels are connected to flow distribution manifold, or headers, by pipework (feeders). The channels, feeders, headers, pumps and steam generators are arranged in a full elevation (25 m) figure-of-eight in a Candu primary coolant circuit. The Emergency Coolant Injection (ECI) system consists of a tank pressurized to high pressures using nitrogen. Coolant supplied by the ECI system can be directed to all, or any, of the headers /12/.

Relevant features of both systems are given in Tab. 3.

Tab. 3: Relevant hardware characteristics of the Pactel and RD-14M

Quantity	Pactel (original design)	Pactel (with CMT)	RD14M
Reference reactor and power (MW)	VVER-440 1375	VVER-440 1375	CANDU 1800
Number of rods	144	144	70
Number of U-tubes per steam generators	38/38/38	118/118/118	44/44
Internal diameter of U-tubes (mm)	13	13	15.9
Actual Kv	1/433	1/462	1/378

3.3 Natural circulation performances

The evaluation of the NCP of the mentioned NPP and facilities, has been finalized by the use of the reference flow map derived above. The idea is, essentially, to compare measured (case of the facilities) and calculated by qualified system codes (case of the NPP) NCP with the data in the reference flow map.

The following procedure has been adopting for evaluating NCP:

- a) Case of NPP. Following the achievement of steady state at decay power (calculated by the standard ANS 1973 curve), assuming the feed water flow consistent with this, draining of primary side mass inventory has been imposed. The drained flow rate versus time reproduces the steps of the Lobi test A2-77A (adopted for deriving the boundary curves); the values of mass flow have been derived by multiplying the Lobi related quantities by the ratio $NPP_{vol}/Lobi_{vol}$. The case of advanced reactors requires additional comments: both AP-600 and EP-1000 are continuously connected with safety systems, so it seemed worthwhile to allow the intervention of these systems, although loosing the possibility of a direct comparison of the overall scenario with the present generation reactors (this would imply the activation of High Pressure Injection Systems).
- b) Case of facilities. Natural circulation experiments have been performed with modalities similar to the above, in the case of Pactel (original design) and RD-14M, as from refs. /13/ and /12/. A Small Break LOCA experiment without HPIS (i.e. continuous draining of primary side mass) has been used in the case of Pactel with CMT /14/.

The achieved results can be subdivided into two groups: time trends relevant only to NPP (Figs. 3 to 6) and use of reference flow maps for NPP (Figs. 7 and 8) and facilities (Fig. 9).

3.3.1 Analysis of results

Specific mass inventories start from similar values in all the considered cases (Figs. 3 and 4). Differences are attributable to slight differences in the average temperature. It may be noted that the pressurizer volume has been included in the data; a contribution of this to the mentioned discrepancy can be envisaged. The transient evolution is also similar in all the cases, with the exception of the passive advanced reactors (AP-600 and EP-1000). In the case of AP-600, removed mass is replaced by mass delivered by passive ECCS, essentially CMT and PRHR connected to the primary loop. This happens to a lower extent in the case of EP-1000.

Three parameters have been chosen to evaluate the NCP:

- good performance in single-phase condition = high value of the initial flow rate;
- good performance in two-phase condition = high value of the flow rate maximum;
- good performance at low primary system inventory = low value of residual mass at which flow rate becomes equal to zero.

Owing to a number of uncertainties characterizing the comparison, other significant aspects of the transient, e.g. the minimum mass at which dry out occurs, occurrence of instabilities soon after the flow rate peak /3/, have not been considered.

Core flow over core power transient trends (Figs. 5 and 6) reflect the similarity, as far as the initial values are concerned, a noticeable exception being represented by the low power PWR (PWR-2). In this case, the presence of four loops, coupled with a low pressure at the secondary side, largely improves the core cooling capabilities. Additional notes from Figs. 5 and 6 are as follows:

- U-tubes PWR, WWER and EPR behave very similarly during the entire transient. Again, the better performance of PWR-2 can be noted;
- the Once-Through steam generators PWR shows an early flow rate decrease and early stop of natural circulation flow;
- natural circulation flow rate in AP-600, as expected, is not affected by draining because of passive ECCS supplied liquid. This behavior does not show up in the case of EP-1000.

The use of flow maps (Figs. 7 to 9) allows a quantitative judgment of the calculated or measured values.

The conclusions reached when analyzing Figs. 5 and 6 are substantially confirmed by the analysis of Figs. 7 and 8: NCP of PWR-1, WWER and EPR are qualitatively and quantitatively similar to the trends gathered from facilities. The PWR-2 confirms the large value of mass flow rate at different

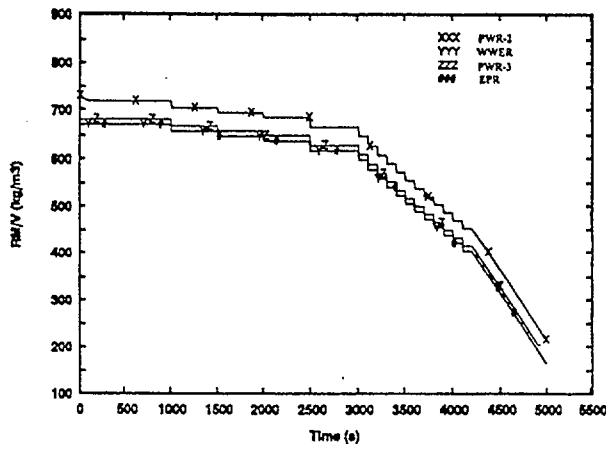


Fig. 3: Specific mass inventory trends for PWR-2, PWR-3, WWER and EPR

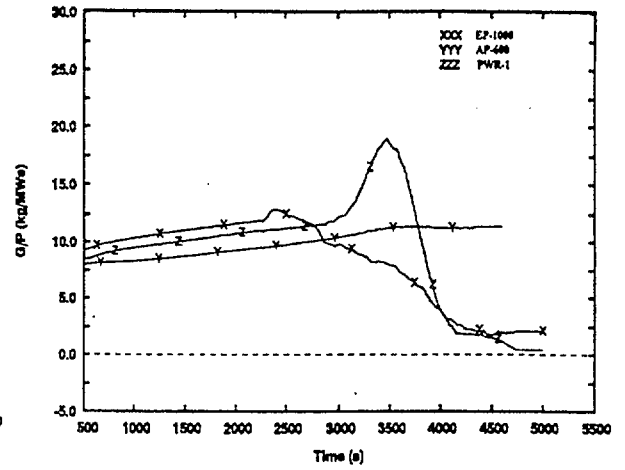


Fig. 6: Core flow rate over core power trends for PWR-1, AP-600 and EP-1000

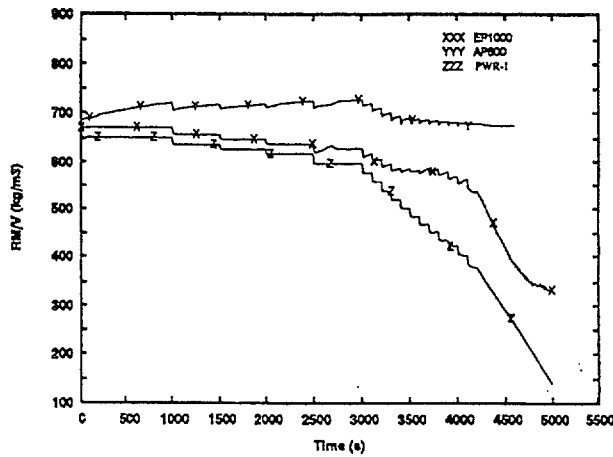


Fig. 4: Specific mass inventory trends for PWR-1, AP-600 and EP-1000

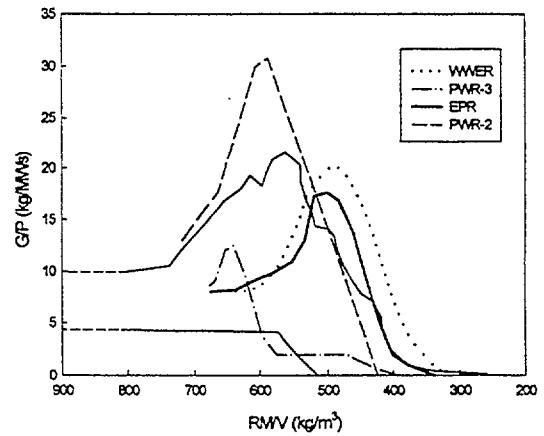


Fig. 7: Evaluation of NCP for PWR-1, PWR-2, WWER and EPR (use of nat. circ. flow map)

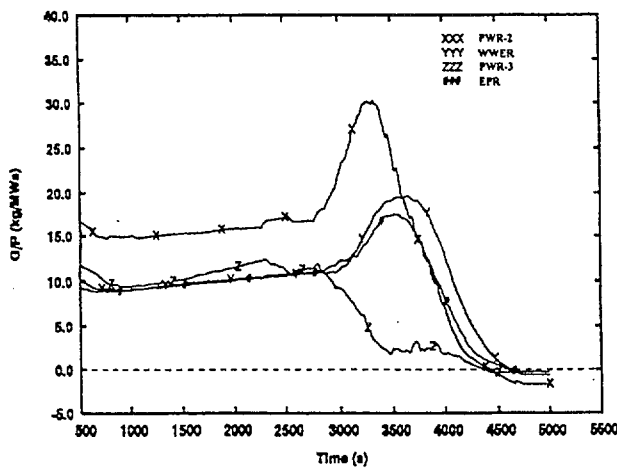


Fig. 5: Core flow rate over core power trends for PWR-2, PWR-3, WWER and EPR

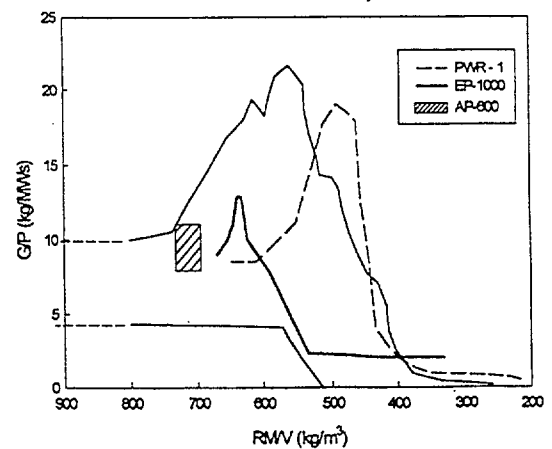


Fig. 8: Evaluation of NCP for PWR-3, AP-600 and EP-1000 (use of natural circulation flow map)

values of mass inventories. The performances of PWR equipped with O-T SG appears poorer than U-tubes PWR, as far as natural circulation in the selected conditions is concerned. Again, AP-600 exhibits an expected behavior, i.e. nearly constant core flow notwithstanding draining; this can not be repeated in the case of EP-1000.

The evaluation of data from "non-PWR" facilities (Fig. 9), brings to the following conclusions:

- WWER-440 simulator (Pactel) exhibits a decrease in the cooling capabilities, at a relatively high mass inventory, owing to the flow stagnation originated by the presence of hot leg loop seal. The problem is removed by introducing a passive system (at least making reference to the considered experiment).
- The Candu simulator exhibits two different trends, depending from the considered test; this simply shows the need of a deeper investigation before drawing conclusions (see also ref. /15/).

A summary of the evaluation of NCP of the various systems is given in Tab. 4.

The second column deals with the demonstration of the data base quality achieved with activities not connected with the present one. In the case of nodalizations, the answer NO or YES depends upon the fulfillment of requirements defined in ref. /10/. In the case of facilities, the qualification is related to the availability of data (e.g. measurements in other test facilities or qualified computer codes calculations) confirming the considered results.

Two levels of evaluation are included in the third column, the first one being connected with the nodalization and the second one with the NCP, only the latter being applicable to the facilities. The NO for PWR-3 comes from the poor NCP at low values of mass inventories depending upon the long ascending siphon leg constituted by the hot leg. The NO in the case of EP-1000 is mostly connected with nodalization qualification level and causes the n.a. evaluation for the second level of judgment. The n.a. in the case of RD-14M is consequence of the contradictory data available at the moment.

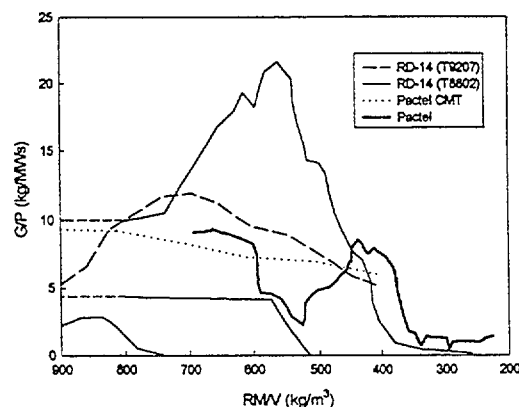


Fig. 9: Evaluation of NCP for WWER and Candu simulators (use of nat. circ. flow map)

NPP / non-PWR facility	Demonstration of data base quality independently from the present work	Demonstration of quality from the present work
Krsko	*YES /16/	YES/YES
TMI	*YES /17/	YES/NO
WWER-1000	*YES /18/	YES/YES
Trino	*NO	YES/YES
EPR	*NO /19/	YES/YES
AP-600	*YES /20/	YES/YES
EP-1000	*NO /21/	NO/ n.a.
Pactel (WWER-440)	YES /13/	YES
Pactel (with CMT)	YES /14/	YES
RD-14M (Candu)	n.av.	n.a.

* related to nodalization

n.av. = not available

n.a. = not applicable

Tab. 4: Summary of the NCP evaluation for NPP systems and facilities

4. CONCLUSIONS

The performed research constitutes the end-point of a long lasting activity, started from gathering of experimental data from PWR simulators. This allowed the availability of a tool for judging NCP in PWR systems.

The activity documented in this paper consisted in comparing predicted NCP of PWR and "non-PWR" systems with the available data base.

The results can be summarized as follows (Tab. 4):

- qualified nodalizations of PWR-1, PWR-3, WWER and AP-600 confirmed the qualification judgment, thus producing a reasonable prediction for system NCP;
- unqualified nodalization of PWR-2 and EPR demonstrate a quality level, again connected with a reasonable prediction for system NCP;

- the unqualified EP-1000 nodalization did not achieve qualified results;
- WWER-440 simulator confirmed the suitable NCP for this kind of reactor, in the situation with passive safety system;
- data from Candu simulator are contradictory and did not allow a definitive judgment;
- a worse performance of OTSG PWR in comparison with U-tubes PWR was demonstrated, while horizontal tubes SGs exhibit NCP comparable or even better than what shown in PWR (see also first item of the list);
- suitability of passive safety systems, as far as NCP is concerned, is demonstrated in the case of AP-600 and Pactel, facility equipped with CMT.

REFERENCES

- /1/ D'Auria F., Galassi G.M., Vigni P., Calastri A., 1991, "Scaling of natural circulation in PWR systems" *Nuclear Engineering and Design* 132, pp. 187-205.
- /2/ D'Auria F., Frogheri M., Leonardi M., 1994, "Natural circulation performance in Western type and Eastern Type PWR". *Proc. of the Simulator Multiconference*, San Diego, 11-13 April 1994.
- /3/ D'Auria F., Galassi G.M., 1990, "Characterization of instabilities during two-phase natural circulation in PWR typical conditions", *J. Experimental Thermal and Fluid Science* Vol. 3
- /4/ Ohlmer E., Addabbo C., Piplies L., Riebold W., 1985, "The Lobi-Mod2 integral system test facility", *Spec. Meet. on Small Break LOCA analyses in LWR's*, Pisa (I).
- /5/ Cattadori G. and Rigamonti M., 1987, "Spes facility description and specification for OECD/CSNI Int. Standard Problem No. 22, Vol. 1: Spes system description", ENEA TERM-RISIL NFAGITP4B 87073.
- /6/ Bethsy Team, 1990, "Bethsy general description", Note Seth/LES/90-57, Grenoble (F).
- /7/ Loomis G.G., Soda K., 1981, "Quick look report for Semiscale Mod-2A, test S-NC-3", EGG-SEMI-5522.
- /8/ Siemens UB KWU, 1989, "Versuch PKL-III AC1", U9312/88/33.
- /9/ The Rosa-IV Group, 1985, "Rosa-IV: Large Scale Test Facility (LSTF) system description", JAERI report, M84-237.
- /10/ Bonuccelli M., D'Auria F., Debrecin N. and Galassi G.M., 1993, "A methodology for the qualification of thermalhydraulic codes nodalizations", *6th Int. Top. Meet. on Nuclear Reactors Thermalhydraulics*, Grenoble (F).
- /11/ Purhonen H., Miettinen J., 1991 "Pactel-parallel channel test loop-general description for ISP 33". Technical Research Center of Finland, Nuclear Eng. Laboratory, Lappeenranta, Finland
- /12/ Ingham P.J., Melnyk A.J., Murray T.V., 1990 "Natural circulation experiment in RD-14M with Emergency Coolant Injection". AECL Research Whiteshell Laboratories. Pinawa, Canada.
- /13/ Purhonen H., Kouhia J., 1993, "OECD/NEACSNI ISP 33: Pactel natural circulation stepwise coolant inventory reduction experiment. Preliminary comparison report". Technical Research Center of Finland, Nuclear Engineering Laboratory, Lappeenranta, Finland.
- /14/ Tuunanen J., 1996, "Quick look report passive safety injection experiments GDE-21, GDE-22, GDE-23, GDE-24 and GDE-25", VTT Technical Report, PAHKO 2/96.
- /15/ D'Auria F., Frogheri M., Vigni P., 1995, "Natural circulation in Candu, VVER and PWR type nuclear plants" *Proc. of XIII UIT National Heat Transfer Conference*, Bologna (I), June 22-23.
- /16/ Bajs T., Debrecin N., D'Auria F., Galassi G.M., 1993, "Uncertainty evaluation for Relap5/Mod2 code calculations of the NPP Krsko Small Break LOCA scenario", University of Pisa Report, DCMN NT 209 (93).
- /17/ Cappariello A., 1997, "Thesis in Nuclear Engineering", University of Pisa.
- /18/ D'Auria F., Galassi G.M., Mastrantonio L., 1997, "Accident management studies in the WWER-1000 plant", *The 5th Int. Conf. on Nuclear Engineering ICONE5*, Nice (F), May 26-30, 1997.
- /19/ D'Auria F., Galassi G.M., Giannotti W. (Authors), Fruttuoso G., Oriolo F. (Approval), 1996, "Nodalization and calculation by Relap/Scdap code of steady state conditions in EPR plant", University of Pisa Report, DCMN NT 302(96), Pisa (I), Nov. 1996.
- /20/ D'Auria F., Fruttuoso G., Galassi G.M., Oriolo F., 1993, "Analysis by Relap5/Mod2 code of a SGTR in the AP-600: effects of reverse flow in PRHR", University of Pisa Report, DCMN NT 215(93), Pisa (I), Sept. 1993.
- /21/ D'Auria F., Galassi G.M., Pellicoro V., Fruttuoso G., Oriolo F., 1995, "Calculation by Relap5/Mod3.1 code of steady state conditions in the EP-1000 plant", University of Pisa Report, DCMN NT 270(95), Pisa (I), Dec. 1995.

BOILING INDUCED MIXED CONVECTION IN COOLING LOOPS

J.U. KNEBEL, G. JANSSENS-MAENHOUT, U. MÜLLER
 Institut für Angewandte Thermo-und Fluidodynamik,
 Forschungszentrum Karlsruhe — Technik und Umwelt,
 Karlsruhe, Germany



XA0055016

ABSTRACT

This article describes the SUCO program performed at the Forschungszentrum Karlsruhe. The SUCO program is a three-step series of scaled model experiments investigating the possibility of a sump cooling concept for future light water reactors. In case of a core melt accident, the sump cooling concept realises a decay heat removal system that is based on passive safety features within the containment. The article gives, first, results of the experiments in the 1:20 linearly scaled SUCOS-2D test facility. The experimental results are scaled-up to the conditions in the prototype, allowing a statement with regard to the feasibility of the sump cooling concept. Second, the real height SUCOT test facility with a volume and power scale of 1:356 that is aimed at investigating the mixed single-phase and two-phase natural circulation flow in the reactor sump, together with first measurement results, are discussed. Finally, a numerical approach to model the subcooled nucleate boiling phenomena in the test facility SUCOT is presented. Physical models describing interfacial mass, momentum and heat transfer are developed and implemented in the commercial software package CFX4.1. The models are validated for an isothermal air-water bubbly flow experiment and a subcooled boiling experiment in vertical annular water flow.

1. INTRODUCTION

Supposing a core melt down accident and considering the problem of melt stabilization and decay heat removal, these requirements can be achieved by an initially dry spreading of the core melt on the containment basemat in combination with a passive sump water flooding and passive cooling from above. This sump cooling concept is sketched in Knebel and Müller (1997). After the flooding of the core melt, the decay heat is transferred from the core melt to the sump water by evaporation, convection and conduction. Condensers are provided to recondense the evaporating sump water. In addition, a natural sump water circulation transports the decay heat to water cooled heat exchangers. Considering the decrease of the decay heat with time, two characteristic mechanisms of decay heat removal can be distinguished: the short-term behaviour that is characterized by mixed single-phase and two-phase natural circulation phenomena due to the high local heat fluxes along the core melt surface, and the long-term behaviour that shows single-phase natural circulation phenomena.

At the Forschungszentrum Karlsruhe the feasibility of the sump cooling concept is investigated by the SUCO program that consists of scaled model experiments and numerical calculations, table 1. Here, the experiments in the SUCOS-2D test facility and first measurement results from the SUCOT test facility are discussed.

The objectives of the SUCOS test facilities are integral phenomenological thermo- and fluiddynamic investigations for the long-term single-phase behaviour. The dominating fluiddynamic process, the pool mixing, is scaled correctly as the Richardson number ratio is equal to unity, Knebel and Müller (1997).

Table 1: SUCO program at the Forschungszentrum Karlsruhe.

Parameters	Future LWR 1300 MW Scale 1:1	SUCOT Volume 1:356 Power 1:356 Heights 1:1	SUCOS-3D Lengths 1:20 Power 1:20 ³ Heights 1:20	SUCOS-2D Lengths 1:20 Power 1:20 ^{3/4} Heights 1:20
Working fluid	<i>water</i>	<i>water</i>	<i>water</i>	<i>water</i>
Spreading area, <i>m</i> ²	<i>160</i>	<i>0.45</i>	<i>0.4</i>	<i>0.4/4</i>
Water height, <i>m</i>	<i>5.5</i>	<i>5.5</i>	<i>0.275</i>	<i>0.275</i>
Initial decay heat, <i>MW</i>	<i>25</i>	<i>0.07</i>	<i>0.003125</i>	<i>0.003125/4</i>
Initial heat flux, <i>W/cm</i> ²	<i>15.6</i>	<i>15.6</i>	<i>0.783</i>	<i>0.783</i>
Investigated behaviour		<i>short-term two-phase</i>	<i>long-term single-phase</i>	
Code		<i>CFX4.1</i>	<i>FLUENT</i>	

Altogether, 140 different parameter variations are investigated, the parameters are heating power, distribution of heating power, heat exchanger configuration, heat exchanger inlet temperature, flow resistances, sump water height, three-dimensional effects. The nomenclature of the heat exchangers is given in fig. 1, being a sketch of the SUCOS-2D test facility. The experiments are performed as steady-state and transient experiments according to the heating power.

The objectives of the SUCOT test facility are two-phase natural circulation flow phenomenology such as a) subcooled and saturated pool boiling and flow boiling, b) flow pattern and flow instabilities, c) formation, rise and collapse of steam bubbles and d) influence of heated plate surface structure on boiling.

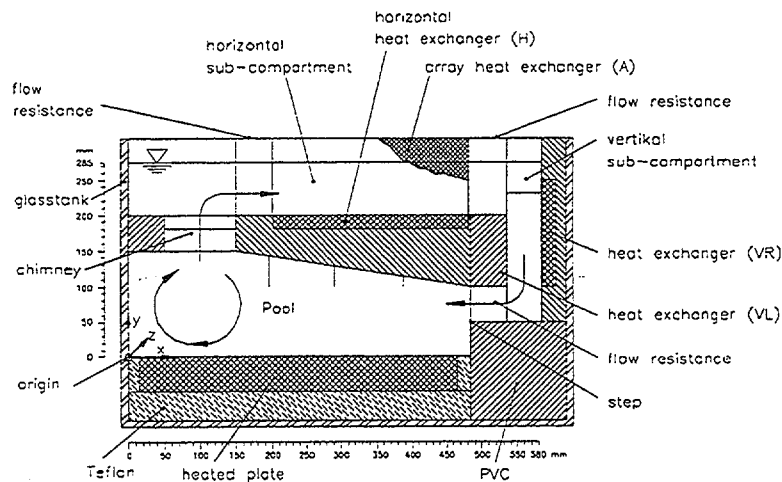


FIG. 1. Sketch of the SUCOS-2D test facility.

2. TEST FACILITY SUCOS-2D

Generally, a stable clockwise natural circulation flow is observed for all heat exchanger configurations investigated. Above the heated plate a well-defined mixing zone with high horizontal velocities establishes. The pool above is isothermal and stagnant and acts as an intermediate and homogeneous heat storage. Below the chimney a large eddy is observed. Along the heat exchangers thin boundary layers are found. The pool temperature is proportional to the heat exchanger inlet temperature. A non-uniform distribution of the heating power does not influence the mean pool temperature in the 2D case, however, in the three-dimensional test facility changes in the thermal stratification in the sump area are observed. Increasing flow resistances lead to increasing pool temperatures due to a decrease in natural circulation.

Steady-State Experiments

The optimisation of the heat exchanger arrangement in the small-scale test facilities SUCOS is done with respect to minimising both the surface area of the heat exchangers and the mean pool temperature. The results are given in table 2. The heating power is 40% of the initial decay heat. The surface area of the heat exchangers A_{HX} and the mean pool temperature ΔT_{Pool} are normalised by the values of the original arrangement H+VR from Weisshäupl and Bittermann (1993). The pool temperature is taken relative to the heat exchanger inlet temperature. The stable stratification above the horizontal heat exchanger H results in a very inefficient heat transfer characteristic. A replacement of the horizontal heat exchanger by a second vertical heat exchanger VL and two array heat exchangers 2A results in a value of 0.66 for the normalised pool temperature that is considerably lower than the one in the original arrangement. At the same time, the heat transfer area and thus the technical equipment used can be kept the same. The array heat exchangers are installed along both sides of vertical concrete walls of one meter thickness in order to prevent them from damage due to shock waves. As a result, the optimum heat exchanger arrangement is VR+VL+2A.

Table 2: Surface area of the heat exchangers and pool temperature of test facility SUCOS for different heat exchanger arrangements. The heating power is 40% of the initial decay heat. Reference arrangement is H+VR from Weisshäupl & Bittermann (1993).

Heat exchanger arrangement	chimney blockage	$A_{HX} / A_{HX,Ref}$	$\Delta T_{Pool} / \Delta T_{Ref}$	heat exchanger arrangement	chimney blockage	$A_{HX} / A_{HX,Ref}$	$\Delta T_{Pool} / \Delta T_{Ref}$
H	0%	0.66	1.66	VR+VL	67%	0.56	1.02
VR	0%	0.35	1.38	H+VR+VL	67%	1.22	0.82
H+VR	0%	1.00	0.94	2A	67%	0.44	1.09
VR+VL	0%	0.56	0.99	H+2A	67%	0.94	0.85
H+VR+VL	0%	1.22	0.77	VR+VL+2A	67%	1.00	0.66
H+VR+VL+4A	0%	1.94	0.51	H+VR+2A	67%	1.29	0.63
H	67%	0.66	1.82	H+VR+VL+2A	67%	1.50	0.56
VR	67%	0.35	1.40	H+VR+VL+4A	67%	1.94	0.53
H+VR (Ref.)	67%	1.00	1.00	VR+VL	200 mm	0.44	1.27

Transient Experiments

Figure 2 gives typical results of transient experiments in the SUCOS-2D test facility for three characteristic heat exchanger configurations, the pool temperature T_{pool} and the heating power Q being plotted versus the scaled time t . The index M denotes model findings. The pool temperature is taken relative to the heat exchanger inlet temperature T_{HX} . Both the heating power and the pool temperature are normalized by the initial values at $t = 0$ for steady-state conditions.

The heating power is reduced according to $Q \propto t^{-0.18}$. Using the local one-dimensional balance equations along the natural circulation loop one can derive a proportionality between the pool temperature and the heating power of $T_{pool} \propto Q^{1/3}$. Thus, the pool temperature decay can be described by $T_{pool} \propto t^{-0.11}$. The pool temperature decay curves in fig. 2 fall perfectly together in one curve showing self-similar behaviour. The experiments give an exponent of -0.18 , thus reproducing the physics of the relationship from above well.

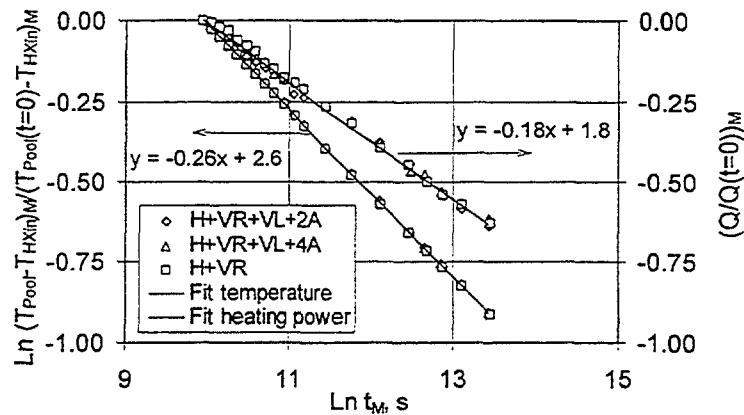


FIG. 2. Pool temperature and heating power versus time for the SUCOS-2D test facility. Nomenclature see fig. 1.

In order to scale-up the model findings (index M) to prototypic conditions (index P), the integral heat transfer characteristics of the natural circulation system has to be known. For the scaled SUCOS-2D test facility, the integral heat transfer characteristic can be described by a laminar heat transfer correlation of the form $Nu \propto Gr^{1/4}$, see Knebel and Müller (1997). The Rayleigh number for the model is in the order of $Ra = 5 \cdot 10^9$. As for the prototype a Rayleigh number in the order of $Ra = 2 \cdot 10^{14}$ is expected, a turbulent heat transfer correlation of the form $Nu \propto Gr^{1/3}$ is chosen.

Considering the transient experiments of figure 2 with a secondary side temperature of $20^\circ C$, one can scale-up to the prototype pool temperatures in the long-term behaviour given in figure 3. A well subcooled pool is found for the heat exchanger configurations that operate two or four of the array heat exchangers (H+VR+VL+2A and H+VR+VL+4A). The temperatures above saturation temperature for heat exchanger configuration H+VR indicate pool boiling conditions. The pool temperature in the prototype is calculated by

$$T_{Pool P} = T_{HX, in P} + 2.7(T_{Pool} - T_{HX, in})_M + (c_T - 2.7)(a \cdot T_{HX, in} + b)_M \quad (1)$$

The coefficient c_T is a characteristic value for the heat exchanger configuration, a and b are geometric parameters, equ. (1) being corrected in comparison to a misprint in Knebel and Müller (1997). The transformation of the velocity is done according to

$$u_P = 7.37 u_M \quad (2)$$

which results in maximum values of 0.2 m/s in the prototype.

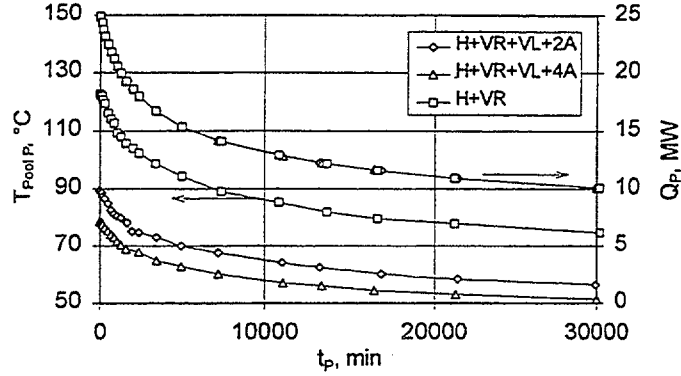


FIG. 3. Pool temperature and decay heat versus time for a prototype geometry.

3. TEST FACILITY SUCOT

The SUCOT test facility is a real height model experiment with a power and volume scale of 1:356, see fig. 4. The local heat flux ratio is kept equal to unity. The heated bottom plate is divided into seven section which can be controlled individually. The front and the back wall of the test facility are made of large glass windows allowing for flow visualization (shadow graph, laser light sheet). Various flanges are provided to introduce traversable instrumentation, such as thermocouple rakes for temperature and twin-fiber optic probes for void measurement. In addition, the void is measured using a gamma-densitometer (Caesium 137). A Laser Doppler anemometer LDA for the measurement of the liquid velocity in the single-phase regions is provided, the bubble velocity will be measured using particle image velocimetry PIV. The system pressure is limited to ambient conditions.

Using the same working fluid as in a real reactor, this test facility preserves the phase change number N_{PCh} and the subcooling number N_{Sub} correctly. The phase change number has recently been renamed as Zuber number N_{Zu} in recognition of Zuber's most significant contributions to the field. The phase change number and the subcooling number are the control parameters of the test facility.

Phase change or Zuber number:

$$N_{PCh} = N_{Zu} = \frac{\Delta h}{\Delta h_{LG}} \frac{\Delta \rho}{\rho_G} = \frac{\dot{Q} / \dot{m}}{\Delta h_{LG}} \frac{\Delta \rho}{\rho_G} = \frac{\text{mass flux due phase change}}{\text{inlet mass flux}} \quad (3)$$

Subcooling number:

$$N_{Sub} = \frac{\Delta h_{sub}}{\Delta h_{LG}} \cdot \frac{\Delta \rho}{\rho_G} = \frac{\text{subcooling}}{\text{latent heat}} \quad (4)$$

The phase change number N_{PCh} takes into account the change of phase due to heat transfer to the sump water. The subcooling number N_{Sub} scales the subcooling of the sump water entering the heated section and, thus, the dimension of the purely liquid region along the core melt. These two numbers are important for the scaling of both the dynamic and the steady-state conditions of a natural circulation system.

In fig. 5 characteristic temperature profiles above the heated plate are given. The subcooled fluid heats up in a thin mixing layer, the pool above being isothermal. The thickness of the boundary layer increases with decreasing x . This is in perfect agreement with the findings in the small-scale test facilities SUCOS, see Knebel and Müller (1997). At $x = 1400 \text{ mm}$ the fluid in the mixing layer has reached a value that is above pool temperature, however, still being single-phase flow.

In the chimney, at an elevation of $y > 3 \text{ m}$, the fluid reaches saturation conditions due to geodesic pressure relief. Vapour bubbles are generated. The flow regime is bubbly flow. At a frequency of $1/60 \text{ Hz}$ the phenomenon of geysering is observed, which results in a violent vapour production. During geysering, the fluid surface is elevated by about 0.5 m . The flow regime is observed to be churn turbulent.

The next set of experiments will aim at reaching saturation conditions and a net vapour production at the downstream end of the heated plate.

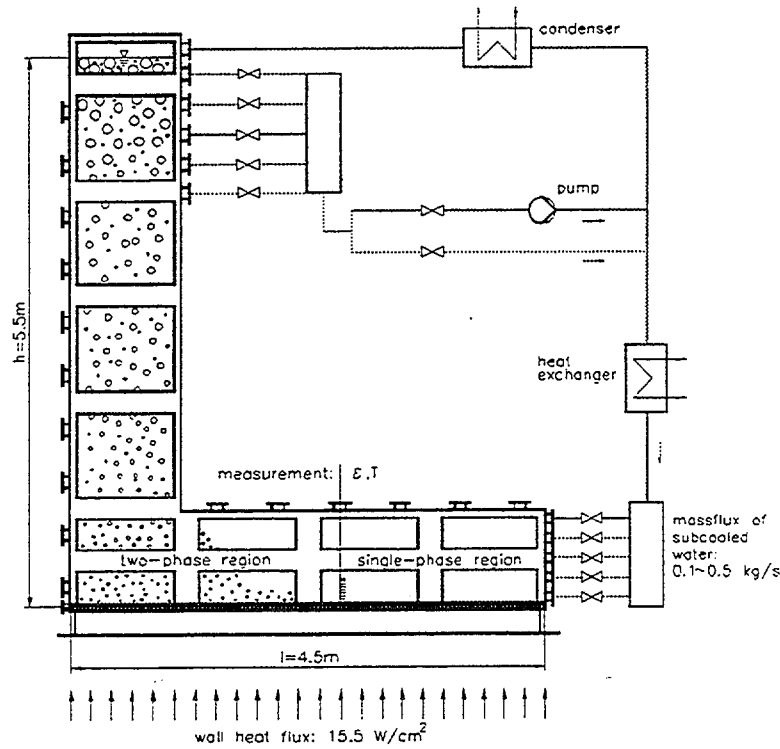


FIG. 4. Sketch of the SUCOT test facility at the Forschungszentrum Karlsruhe.

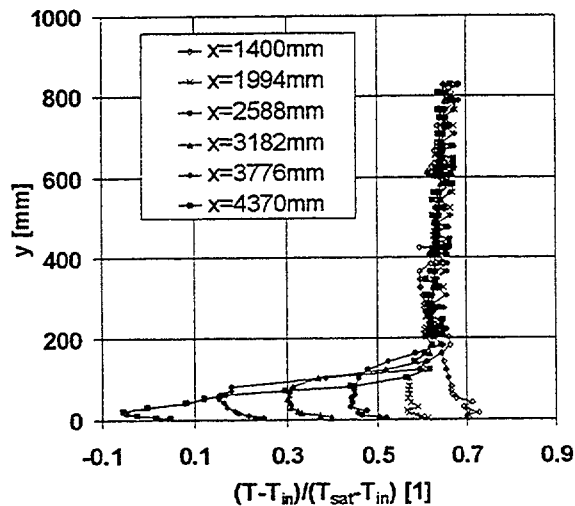


FIG. 5. Temperature profiles above the heated plate for the SUCOT test facility.

First local void measurements are made using a fibre-optic probe. The probe has an outer diameter of 0.6 mm , the tip being of conical shape with an internal angle of 90° . The surface is polished. The fibre is loaded with 850 nm light of an LED. The probe is used as a phase identifier: The light is not reflected or reflected from the tip depending on whether the probe is in contact with the liquid phase or the gas phase. The reflected light is detected by a photo-diode. Figure 6a gives the typical signal of a fibre-optic probe, the signal being from bubbles of about 5 mm diameter that are ejected through a nozzle in stagnant water at a volume flux of 8 l/h . The sampling frequency is 10 kHz . The signal shows a very sharp rise both as the bubble hits the probe and as the probe is re-wetted again. Thus, the threshold above which the signal is considered a bubble is a level just above the noise level. A typical threshold is 10% of the difference between the gas phase level and the liquid phase level. Plotting the cumulative probability density function, fig. 6b, the local void of the above signal is found to be 12% , the threshold being 10% .

The next step will be the utilisation of a twin fibre-optic probe to measure the interfacial velocity, the interfacial area concentration and the mean Sauter diameter, as described in Hibiki, Hogsett and Ishii (1997).

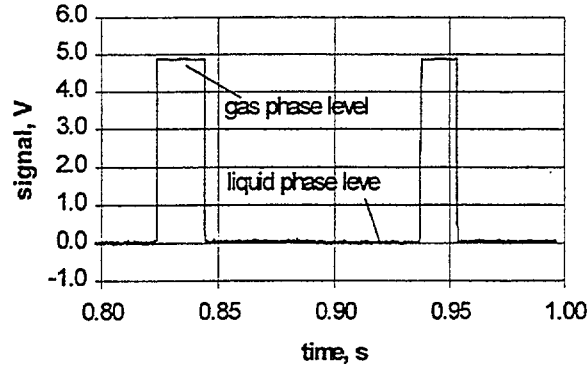


FIG. 6a. Typical signal of fibre-optic probe (recording window of 0.2 s).

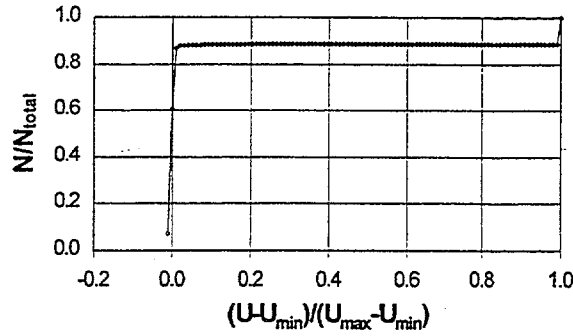


FIG. 6b. Cumulative probability density function.

4. PHYSICAL MODEL DESCRIPTION

The model of interfacial mass, momentum and heat transfer originates with the two-fluid model for disperse flow. Both phases the continuous water and the disperse vapour phase are described by the ensemble-averaged mass, momentum and energy transport equations.

Mass conservation equation:

$$\frac{\partial(\varepsilon_k \rho_k)}{\partial t} + \nabla \cdot (\varepsilon_k \rho_k \langle \tilde{u}_k \rangle_k) = \underbrace{\langle \Gamma_k \rangle_k}_{\text{Vapour-Source}} \quad (5)$$

Momentum conservation equation:

$$\begin{aligned} & \frac{\partial(\varepsilon_k \rho_k \langle \tilde{u}_k \rangle_k)}{\partial t} + \nabla \cdot (\varepsilon_k \rho_k \langle \tilde{u}_k \rangle_k \langle \tilde{u}_k \rangle_k) \\ &= -\nabla(\varepsilon_k p_k) + \varepsilon_k \rho_k \bar{g} + \nabla \cdot \varepsilon_k \left(\langle \overline{\tau}_k \rangle_k + \langle \overline{\tau}_k^{re} \rangle_k \right) + \underbrace{\langle \bar{I}_k \rangle_k}_{\text{Interfacial Forces}} + \langle \bar{f}''_k \rangle_k \end{aligned} \quad (6)$$

Energy conservation equation:

$$\begin{aligned} & \frac{\partial(\varepsilon_k \rho_k \langle h_k \rangle_k)}{\partial t} + \nabla \cdot (\varepsilon_k \rho_k \langle \tilde{u}_k \rangle_k \langle h_k \rangle_k) \\ &= \varepsilon_k \lambda_k \Delta \langle T_k \rangle_k + \underbrace{\nabla \cdot \langle \bar{q}''_k \rangle_k}_{\text{Interfacial Heat Flux}} + \langle h''_{rk} \rangle_k \end{aligned} \quad (7)$$

The modelling of the interphase transport phenomena is done for dilute bubbly flow, with air bubbles as small spherical particles. The momentum exchange is described in equ. (2) by a summation of the interfacial forces $\langle \bar{I}_k \rangle_k$. This results in equ. (4) from an averaging of the forces on a particle volume, induced by the surrounding fluid, derived under Lagrangian approach.

$$\begin{aligned}
\langle \underline{L}_t \rangle_t = & \underbrace{-C_d \frac{3 \varepsilon_G}{4 D_B} \rho_L \langle \underline{u}_G \rangle_G - \langle \underline{u}_L \rangle_L \langle \langle \underline{u}_G \rangle_G - \langle \underline{u}_L \rangle_L \rangle}_\text{Drag Force} - \underbrace{C_{TD} \rho_L k_L \nabla \varepsilon_G}_\text{Turbulent Diffusion} \\
& - \underbrace{C_L \rho_L \varepsilon_G \langle \underline{u}_G \rangle_G - \langle \underline{u}_L \rangle_L \times \langle \nabla \times \underline{u}_L \rangle_L}_\text{Lift Force} - \underbrace{C_{VM} \rho_L \varepsilon_G \left(\left\langle \frac{D \underline{u}_G}{D t} \right\rangle_G - \left\langle \frac{D \underline{u}_L}{D t} \right\rangle_L \right)}_\text{Virtual Mass}
\end{aligned} \quad (8)$$

The first term in equ. (4) represents the drag force. This friction force is modelled with the projected interfacial flow area and the drag coefficient C_d , which is in the turbulent Newton regime $C_d = 0.44$. The second term is the turbulent diffusion force, which represents the local changes in dynamic pressure at the interface. This term is modelled with the turbulent kinetic energy and with a turbulent diffusion coefficient $C_{TD} = 0.1$ for a disperse bubbly flow. The third term is the lift force, acting on bubbles which are unequally surrounded by the fluid flow. The lift term is modelled with a lift coefficient $C_L = 0.5$ for weakly viscous flows. The last term represents the virtual mass, which is implemented for steady state flows and is modelled with a virtual mass coefficient $C_{VM} = 0.5$ as analytically derived for an isolated bubble.

The modelling of the vapour source is done for subcooled nucleate boiling under low pressure with models valid only for water as fluid and for moderate wall heat fluxes. The vapour generation model is based on bubble formation and detachment mechanisms, the condensation model on bubble growth and shrinking mechanisms. The vapour inside the bubble and the bubble surface are assumed to remain at saturation temperature, modelled as a function of the pressure in the bubble. The vapour generation rate Γ_G at the wall is determined under a mechanistic approach as a function of the bubble release frequency f which depends on the given wall heat flux \dot{q}_w , of the bubble departure diameter D_D , and of the active nucleation site density N , which depends on the calculated wall temperature T_w .

$$\Gamma_G = \frac{\pi D_D^3}{6} \rho_G \cdot \underbrace{f(\dot{q}_w)}_\text{Detachment frequency} \cdot \underbrace{N(T_w)}_\text{Nucleation site density} \quad (9)$$

The mechanism of bubble formation is described with the active nucleation site density N given by an empirical correlation of Dhira and Wang (1993),

$$N = 5.8 \cdot 10^{-23.4} \cdot \frac{1 - \cos \phi}{D_c^{5.4}}, \quad (10)$$

as a function of the surface wetting angle ϕ and of the critical bubble diameter D_c , which is approximately inversely proportional to the wall superheat

$$D_c = \frac{4 \sigma T_{sat}}{\rho_G \Delta h_{LG} (T_w - T_{sat})}. \quad (11)$$

The mechanism of bubble detachment is described with the detachment frequency f and the bubble detachment diameter D_D . The major parameter in literature characterising heat transfer in boiling is the product $f \cdot D_D^a$. D_D^a with the power $a = 1$ for the system water/vapour under atmospheric conditions. This product $f \cdot D_D$ is given as "bubble departure velocity", depending on the wall heat flux \dot{q}_w by a correlation of Malenkov (1973).

$$f \cdot D_D = \frac{u_B}{\pi} \left(1 - \frac{1}{1 + u_B \Delta h_{LG} \rho_G / \dot{q}_w} \right)^{-1}; \quad u_B = \left(\frac{D_D g \Delta \rho}{2(\rho_G + \rho_L)} + \frac{2\sigma}{D_D(\rho_G + \rho_L)} \right)^{1/2} \quad (12)$$

The bubble departure diameter D_D is expressed by a correlation of Cole and Rohsenow, see Dhira (1990) using a dimensionless Laplace length and a Jakob number Ja .

$$D_D = 1.5 \cdot 10^{-4} \left(\frac{\sigma}{g \Delta \rho} \right)^{1/2} Ja^{5/4}; \quad Ja = \frac{\rho_L c_p \Delta T_{sat}}{\Delta h_{LG} \rho_G} \quad (13)$$

In the condensation model no coalescence or fragmentation is assumed for the dilute bubbly flow in the subcooled region. The bubble size variations are coupled to changes in void fraction. During condensation the bubble diameter change rate obeys the following energy balance

$$\Delta h_{LG} \frac{d}{dt} \left(\rho_G \frac{\pi}{6} D_B^3 \right) = \alpha_B (T_{sat} - T_L) \pi D_B^2. \quad (14)$$

The heat transfer coefficient α_B in equ. (10) is defined by the Nusselt number Nu , given by a correlation of Ranz and Marshall (1952).

$$Nu_B = 2 + 0.6 Re_B^{0.5} Pr_L^{0.3} \quad \text{with} \quad Nu_B = \frac{\alpha_B D_B}{\lambda_L} \quad (15)$$

Solving equ. (10) yields the typical relation between the bubble diameter D_b and the time $t^{2/3}$, which is in agreement with literature on bubble growth.

5. VALIDATION OF THE PHYSICAL MODELS

Isothermal Air-Water Bubbly Flow Experiment

At the Forschungszentrum Karlsruhe an isothermal air-water bubbly flow experiment has been performed by Samstag (1996). In a vertical pipe of 5000 mm length and internal diameter $D = 70.34$ mm the axial development and the radial redistribution of air bubbles have been measured for symmetric and non-symmetric air injection types. The water was injected at the entrance section with a superficial fluid velocity of $J_L = 1.08$ m/s. The water flow is turbulent, the Reynolds number being in the range of $0.25E5 < Re_L < 1.E5$. Air with a superficial velocity of $J_G = 0.12$ m/s could be injected through the central nozzle and 6 surrounding concentric nozzles. The bubbles generated by the nozzles could be characterised as spherical particles with a diameter mainly varying from 2 mm to 4 mm. Four different types of air injection have been analysed: through all nozzles, through the central nozzle, through 1 eccentric nozzle and through 2 opposite nozzles. The spatial bubble distribution is measured in distinct horizontal sections by Röntgen-Tomography, hot wire probes and resistance probes.

The simulation of the flow using CFX4.1 is done within a three-dimensional geometry. Starting from the measured profiles for the void, the velocity and the turbulent kinetic energy at the entrance section at $5D$ ($= 35$ mm) height, the profiles at the section at $10D$ ($= 700$ mm) height and $63D$ ($= 4430$ mm) height have been calculated for the 4 different types of air injection. The bubbles are simulated as small spherical particles with a mean diameter $D_B = 3$ mm. Different classes of bubble sizes were not simulated, as the present models are not sensitive to bubble size and bubble interactions.

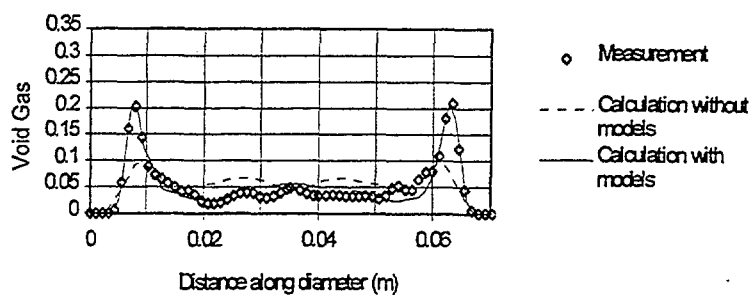
Figures 7a and 7b show the measured and calculated void profiles across the tube diameter at $10D$ ($= 700$ mm) height and at $63D$ ($= 4430$ mm) height respectively, for the symmetric case of air injection through all nozzles. The formation of a lubricated ring profile for the void and the azimuthal redistribution of the bubbles around the wall, mainly caused by the lift force in the non-developed flow region remain recognisable for all heights investigated. The calculations, with the additional models for the interfacial forces included, reproduce the void profile well. Without these additional models, the calculation shows a void profile with decreased peaks around the wall and the creation of a high void in the centre of the tube. Thus, a calculation without the additional models is not applicable for this non-developed bubbly flow.

Similar results for the other symmetric case with air injection through the central nozzle are given in Figs. 8a and 8b. In the subsequent presentation of the simulation results, the calculations without additional models have been omitted as no additional information can be gained. For the non-symmetric case of air injection through one eccentric nozzle the Figs. 9a and 9b show the measured and calculated void profiles across the middle of the open eccentric nozzle. Here a turbulent bubble transport along the wall can be observed by the decrease of bubble concentration above the eccentric nozzle and by the build-up of a bubble concentration along the wall. In this case the turbulent diffusion causes mainly the dispersion of the bubbles in the radial void profiles. For the case of air injection through two opposite nozzles, Figs. 10a and 10b, the void profiles are almost the same as in Figs. 7a and 7b, as they are again affected by the lift force and the turbulent diffusion force.

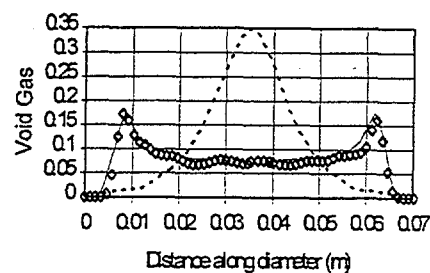
In general, the experimental and the numerical results are in good agreement and show a bubble transport towards the wall for the axial positions measured. This emphasises the importance of the lift force, partially counteracted by the turbulent diffusion force. Comparing different cases of air injection with the same global void fraction of 0.10, a difference in void profile at 63 diameters height was still present, varying from double peaked, as expected for a non-developed two-phase flow to single peaked, as expected for a developed two-phase flow. This shows that the length of flow establishment for turbulent multi-phase flows is significantly longer than for turbulent single-phase flows.

Subcooled Boiling Experiment In Vertical Annular Water Flow

The implemented boiling model is validated against the experiment of Bibeau and Salcudean (1994), investigating subcooled boiling in vertical annular water flow. Along the symmetry axes of a vertical pipe of 600 mm length and with internal diameter $D = 17.0$ mm, an internal heater of 9 mm diameter is placed, acting as a variable heat source. Water is injected at the entrance section with a superficial fluid velocity of $J_L = 0.134$ m/s, performing a laminar annular water flow. The inlet temperature of the subcooled water could be varied as $T_{L,in} = 45^\circ\text{C}$, $T_{L,in} = 60^\circ\text{C}$ and $T_{L,in} = 75^\circ\text{C}$ and the pressure at the outlet section at $35D$ ($= 600$ mm) could be varied as $p = 1$ bar, $p = 2$ bar and $p = 3$ bar. The heat source Q is varied between 0 kW and 60 kW, generating vapour bubbles along the heater surface after the point of onset of nucleate boiling. At

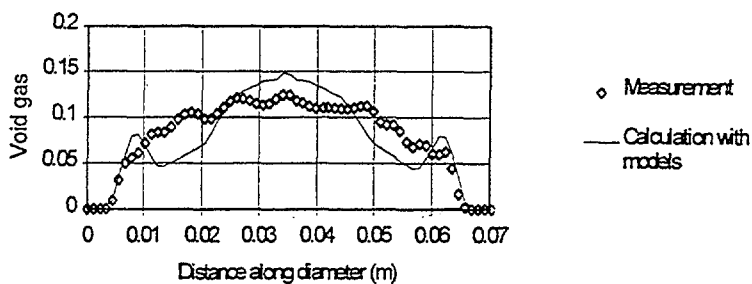


Void profile at 10 D height

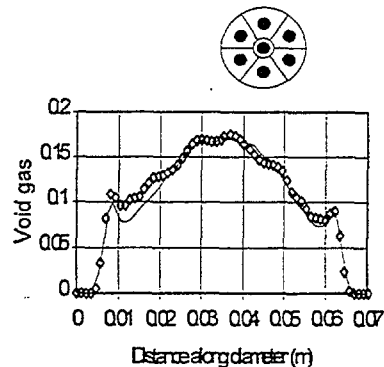


Void profile at 63 D height

FIG. 7. Air injection through all nozzles.

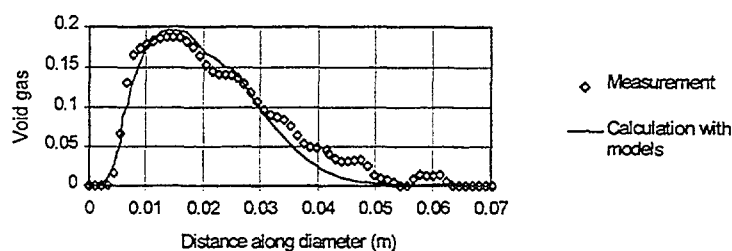


Void profile at 10 D height

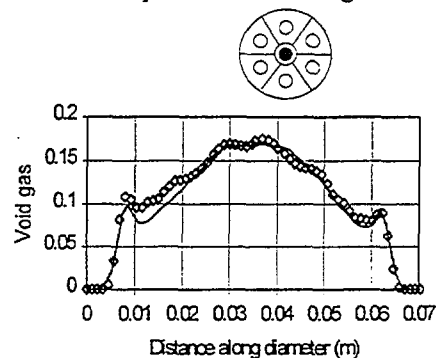


Void profile at 63 D height

FIG. 8. Air injection through the central nozzle.

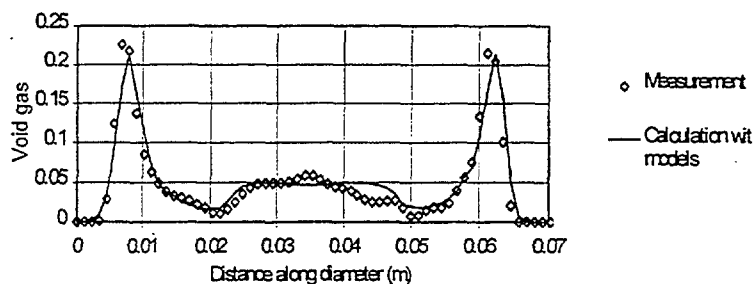


Void profile through the middle of the nozzle at 10 D height

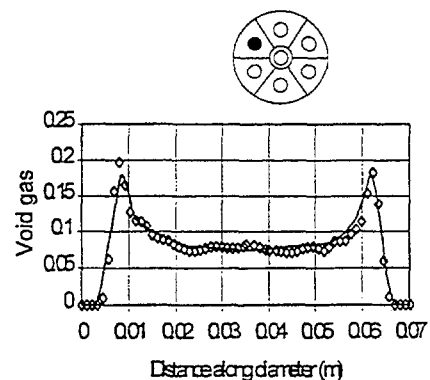


Void profile through the middle of the nozzle at 63 D height

FIG. 9. Air injection through one eccentric nozzle.



Void profile through the middle of two nozzles at 10 D height



Void profile through the middle of two nozzles at 63 D height

FIG. 10. Air injection through two opposite nozzles.

the measurement section at $32D$ ($= 550 \text{ mm}$) height the vapour volume fraction has been measured by Gamma-Densitometry for different heat sources. For steady state conditions with a given liquid flow rate each measured volume fraction thus corresponds to one imposed heat flux.

The geometry is simulated in two dimensions. The vapour generation source is additionally implemented in CFX4.1 using the models from before. Each measurement point is simulated separately. As the wall temperature is the important parameter in the vapour generation model, the temperature profile along the wall has to be calculated using a time-marching method. When steady-state conditions are reached the vapour generated at the measurement section could be integrated over the cross-section.

In Fig. 11 the integral void generated and the wall temperature achieved at the measurement section are presented versus the equilibrium quality of the mixture x_{eq} , for the case of an inlet temperature of $T_{L,in} = 60^\circ\text{C}$ and an outlet pressure of $p = 2 \text{ bar}$. The equilibrium quality x_{eq} is defined as the ratio of the enthalpy consumed by the mixture to evaporate to the latent heat.

$$x_{eq} = \frac{\Delta h_L - \Delta h_{Sub}}{\Delta h_{LG}} = \frac{\dot{Q} / \dot{M} - c_{pL}(T_{sat} - T_{L,in})}{\Delta h_{LG}} \quad (16)$$

Six cases of imposed heat source \dot{Q} , corresponding to $x_{eq} = -11.6\%$, -10.5% , -10.1% , -7.9% , -5.5% and -4.0% , have been chosen to cover the single phase flow regime, to reach the onset of nucleate boiling and to finally cover the fully established nucleate boiling regime. Each of them are calculated with the extended two-fluid-model. Both the onset of nucleate boiling and the total void are in good agreement with the experimental data, the experimental error bashing given in the diagram. The corresponding increasing wall temperatures are also shown. As long as no void is generated the calculated wall temperature increases with a slope as found in single-phase calculations. The difference in the calculated and experimental wall superheated temperature is within the range of standard deviations in the measured data.

The influence of the outlet pressure p and the water inlet subcooling $T_{sub} = T_{sat} - T_L$ on the void generated at a certain equilibrium quality x_{eq} has also been checked. With increasing pressure, the saturation temperature increases and the enthalpy of the mixture at the inlet is further removed from the saturation point. The onset of nucleate boiling is therefore moved to a lower equilibrium quality. With decreasing water inlet subcooling, the enthalpy of the mixture at the inlet is closer to saturation. The onset of nucleate boiling occurs at higher equilibrium qualities. These physical behaviours are also found in the numerical results, indicating the correct physical behaviour of the vapour generation model.

In general, the vapour generation at the heated wire in the annular flow is in good qualitative agreement with the experimental results for the onset of nucleate boiling as well as for the amount of vapour generated.

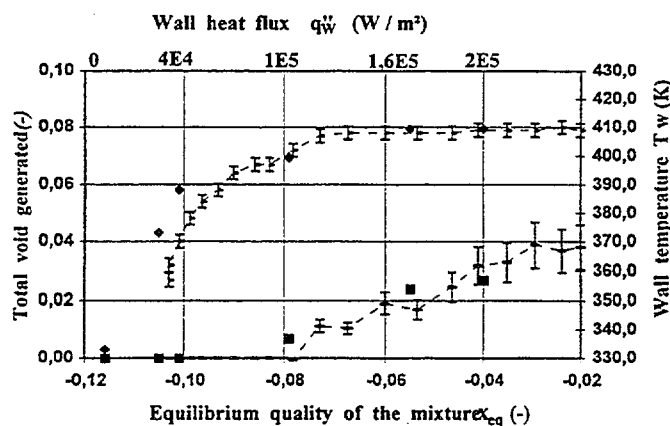


FIG. 11. Void and temperature profile versus the equilibrium quality for subcooled boiling mixture. $P=2\text{bar}$. Void: ■ CFX, — experiment; wall temperature: ♦ CFX, — experiment.

SUMMARY

The sump cooling concept for future LWR that realises a passive decay heat removal system in case of a core melt accident, could be significantly improved by substituting the horizontal heat exchanger by several vertical heat exchangers. Providing the same heat transfer area, the pool temperature can be lowered by 44% relative to the first proposal by Weisshäupl and Bittermann (1993). The temperature decay of the transient experiments in SUCOS-2D shows self-similar behaviour and can be described by $T_{pool} \propto t^{-0.17}$. A scale-up of

the model pool temperatures to prototypic conditions demonstrates that the long-term decay heat can be removed from the containment having a well subcooled reactor sump. However, subcooled boiling will be observed in the short-term along the core melt surface. The sump cooling concept realizes a long-term decay heat removal system.

The test facility SUCOT is in operation. First experiments show a boundary layer flow above the heated plate and an isothermal pool above. Due to a geodesic pressure relief, violent geysering is observed in the chimney. The fibre-optic probe shows a good performance according to phase identification.

The two-fluid-model of the software package CFX4.1 is extended by physical models to describe interfacial mass, momentum and heat transfer in flows with subcooled nucleate boiling. The models are thoroughly validated against two experiments, an isothermal air-water bubbly flow experiment and a subcooled boiling experiment, which represent good benchmarks to test both the fluiddynamic and the thermodynamic behaviour of the extended two-fluid-model. Now, a validated numerical tool is available to calculate the subcooled nucleate boiling phenomena observed in the test facility SUCOT.

The next step of the present work will be experiments in the SUCOT test facility with net vapour production at the heated plate, and the numerical simulation using CFX4.1.

REFERENCES

Knebel, J.U., Müller, U., Scaling of Passive Decay Heat Removal by Sump Cooling, Jahrestagung Kerntechnik 1997, Aachen, pp. 144-147, 1997.

Bibeau, E.L., Salcudean, M., Subcooled Void Growth Mechanisms and Prediction at Low Pressure and Low Velocity, Int. Journal of Multiphase Flow, 20, pp. 837-863, 1994.

Cole, R., Rohsenow, W., Correlations of Bubble Diameter for Saturated Liquids, Chem. Eng. Prog. 65, pp. 211-213, 1969.

Dhir, V. K., Nucleate and Transition Boiling Heat Transfer under Pool and External Flow Conditions, Proc. 9th Int. Heat Transfer Conf., vol. 1, Jerusalem, Israel, pp. 129-155, 1990.

Dhir, V. K. and Wang, C. H., Effect of Surface Wettability on Active Nucleation Site Density During Pool Boiling of Water on a Vertical Surface, Trans. ASME Journal of Heat Transfer, vol. 115, pp. 659-669, 1993.

Hibiki, T., Hogsett, S., Ishii, M., Local Measurement of Interfacial Area, Interfacial Velocity and Liquid Turbulence in Two-Phase Flow, Proc. OECD/CSNI Spec. Meeting on Advanced Instrumentation and Measurement Techniques, Santa Barbara, USA, March 17-20, 1997.

Malenkov, I. G., Detachment Frequency as a Function of Size for Vapor Bubbles, translated from Inzhenerno-Fizicheskii Zhurnal at the Academy of Sciences of the USSR, vol. 20, pp. 988-994, 1973.

Ranz, W. E. and Marshall, W. R., Experimental Correlation for Heat Transfer Between Particle and Fluid, Chemical Engineering Prog., vol. 48, pp. 141, 1952.

Samstag, M., Experimental Investigations on Transport Phenomena in Vertical, Turbulent Air-Water Bubbly Flow, Ph.D. Thesis, Mechanical Eng. Dept., Karlsruhe University, 1996.

Weisshäupl, H. A., Bittermann, D., Large Spreading of Core Melt for Melt Retention/Stabilization, Proc. 5th Int. Seminar on Containment of Nuclear Reactors, August 23-24, Karlsruhe, FR Germany, pp. 347-355, 1993.

NEXT PAGE(S)
left BLANK



THERMAL HYDRAULIC RESEARCH ON NEXT GENERATION PWRs USING ROSA/LSTF

T. YONOMOTO, Y. ANODA

Department of Reactor Safety Research,
Japan Atomic Energy Research Institute,
Tokai, Ibaraki, Japan

Abstract

A thermal-hydraulic research on next generation PWRs has been conducted at JAERI using the ROSA-V/ Large Scale Test Facility (LSTF), focusing on phenomena related to passive safety systems. This paper describes two test results conducted for this research: a small break loss-of-coolant accident (SBLOCA) test and a low pressure steady-state natural circulation (NC) test. The former test investigated a combined use of a SG secondary-side automatic depressurization system (SADS) and a gravity-driven injection system (GDIS) to mitigate a SBLOCA. The results have shown that the primary loop can be depressurized to the GDIS actuation pressure of 0.2 MPa by the SADS alone, and then the stable long-term core cooling can be established by NC.

Results of both tests showed a complicated nonuniform flow behavior among SG U-tubes during NC, which was characterized by the coexistence of concurrent condensing two-phase flow in some tubes and stagnant two-phase stratification in the others. The mechanism for the stratification was understood from the measured secondary side temperature distribution showing the lowest temperature at the top and bottom regions and the highest around the midplane. This was caused by the saturation temperature difference corresponding to the static pressure difference, and the recirculation in the secondary. This secondary side temperature distribution enabled the condensation occurring around the tube top to be balanced with evaporation occurring around the midplane in the U-tube with the stratification. Since the heat transfer occurs primarily through tubes with the concurrent flow, the nonuniform behavior directly affects the effective heat transfer area at SG. When the SG primary side was modeled with one lumped flow channel, the RELAP5 significantly over predicted the primary depressurization rate, and could not predict the stable long-term core cooling behavior at low pressure. In order to understand the mechanism of the nonuniform behavior, the RELAP5 analysis was conducted using a partial SG model. The analysis results have revealed that 1) the fraction of tubes with the concurrent two-phase flow is affected by the flow stability, and 2) the balance of evaporation and condensation is possible in a U-tube under the measured secondary side temperature condition. Based on this analysis result, a simplified tentative procedure using RELAP5 was proposed to predict the system behavior taking into account the nonuniform behavior.

1. INTRODUCTION

Next-generation pressurized-water-reactors (PWRs) are currently developed worldwide. Many of these designs rely on passive safety systems for mitigation of consequences of accidents. Such designs include the Westinghouse AP600 [1], Mitsubishi New PWR-21 (NP-21) [2], the Japan Atomic Energy Research Institute's JPSR [3], and the Russian V-407 (or VVER 640) [4].

All these reactor designs rely on a gravity-driven safety injection system (GDIS) for the long-term core cooling following a loss-of-coolant accident (LOCA). Because the gravity injection can occur only after the reactor primary-side pressure is lowered nearly to the containment atmospheric pressure, all these reactor designs are provided with means to depressurize automatically the primary loop. The depressurization of the primary loop is achieved generally by relieving steam directly from the primary loop and/or cooling the primary coolant using a dedicated heat exchanger or steam generators (SGs). These reactor designs also have a medium-pressure range safety injection system similar to or the same as the existing accumulator injection system (AIS), to maintain the core cooling during the depressurization phase, and quickly provide coolant to the core in case of a large break LOCA.

To assess and optimize such passive safety system designs, their performance should be evaluated against various accident scenarios. The current computer codes for doing this job, however, have large uncertainties in predicting phenomena occurring in new components which the current PWRs do not have, and those occurring under the thermal-hydraulic conditions which the current PWRs never experience. For example, the long-term core cooling relies on the pump-driven cooling system for the current-generation PWRs, which are operable when the pressure is lower than 1 MPa. Therefore, the low pressure natural circulation (NC) behavior has not been sufficiently investigated.

Motivated by this background, a thermal-hydraulic research program has been conducted on next-generation PWR designs using the ROSA-V/Large Scale Test Facility (LSTF) [5]. This research aims to improve the understanding on the passive safety system related thermal hydraulics and contribute the advancement of a safety assessment technique, the development of a reactor design, and the decision making for the selection of a next-generation reactor.

So far, four small break LOCA (SBLOCA) tests have been conducted for this test program [6, 7, 8]. These tests focused on the combined use of a secondary-side automatic depressurization system (SADS) and a GDIS for the long-term core cooling. The primary loop is depressurized to the GDIS actuation pressure by the SG secondary side depressurization. This combination is adopted in the design of NP-21, for which horizontal SGs are used instead of vertical SGs [2]. Several important phenomena were identified through the analysis of the tests, including nonuniform flow behavior among U-tubes during the NC at low pressure. It was found that the primary depressurization rate was overpredicted and the NC flow was unrealistically oscillatory when the nonuniform behavior was not taken into account in the RELAP5 calculation [8]. In order to investigate the NC behavior under more clearly specified boundary conditions, a steady-state NC test was conducted.

In this paper, the results of these SBLOCA tests using the SADS and GDIS will be summarized after a short description of the test facility. Then the results of the NC test and the RELAP5 analysis, will be presented focusing on the nonuniform flow behavior among U-tubes and its mechanism.

2. TEST FACILITY

The LSTF was originally built as a 1/48 volumetrically-scaled, full-height, full-pressure simulator of the current-generation Westinghouse-type four-loop (3 423 MW the thermal power) PWR [5]. The core is simulated by a 10 MW electric heater rod assembly which consists of 1000 heater rods. The four loops of the reference PWR are lumped into two model loops (Fig. 1). Each loop has a SG consisting of 141 full-size (19.6 mm id.) inverted-U-tubes, a reactor coolant pump, a hot leg and a cold leg.

The passive safety injection systems, currently available in the LSTF, include the GDIS, the conventional nitrogen gas-driven AIS, and a flashing-driven safety injection system (FDIS) [6].

The GDIS consists of a tank holding water of ambient temperature and pressure. An injection line connects the bottom of each tank to the cold leg, or to the vessel down comer. The line includes a check valve so that the liquid injection automatically initiates when the system pressure sufficiently decreases. The LSTF has two tanks designed to simulate the AIS in the current-generation PWR. One of the two tanks has the design pressure of 11.7 MPa. This high-pressure accumulator tank can be used for the FDIS, which is a medium-pressure

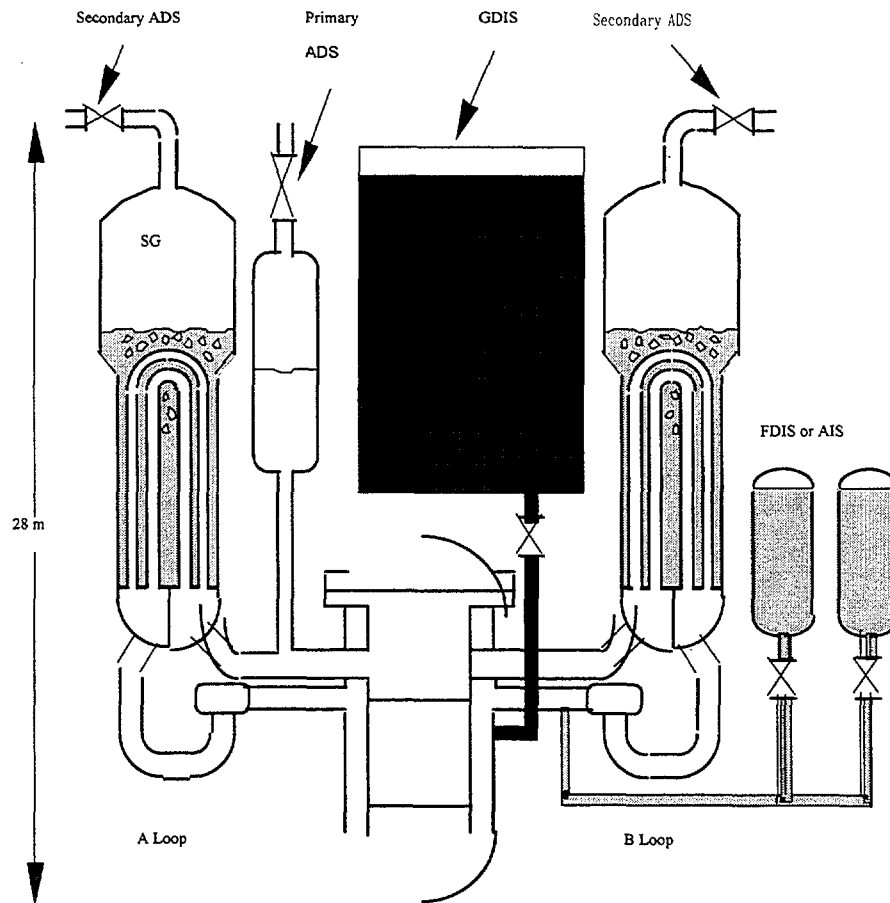


FIG. 1. Geometry of LSTF.

safety injection system proposed by the authors [6]. It utilizes steam, generated by flashing, to pressurize the coolant for injection. An apparent advantage of the FDIS over the current nitrogen-driven accumulator design is that it would not bring any noncondensable gases into the primary system. Such gases would degrade the performance of a primary-side heat exchanger. Thus, this advantage would be significant for reactor designs which rely on heat exchangers or SGs for the system depressurization and core decay heat removal.

An automatic depressurization system (ADS) for the primary system is simulated using valves connected to the pressurizer top. The SADS is also simulated using valves connected to each SG steam dome.

3. SUMMARY OF A SBLOCA TEST

3.1. Test conditions and results

A system break was simulated in the cold leg of the loop without the pressurizer (loop B). The break diameter was 16 mm, corresponding to 4.4 inch-diameter break in the reference reactor. The test simulated a two-step SADS, roughly using the tentative setpoints for the Mitsubishi NP-21 in a crude manner. The FDIS with the initial pressure of 5.5 MPa and the GDIS with the constant liquid level of 12.5 m above the cold leg elevation were used.

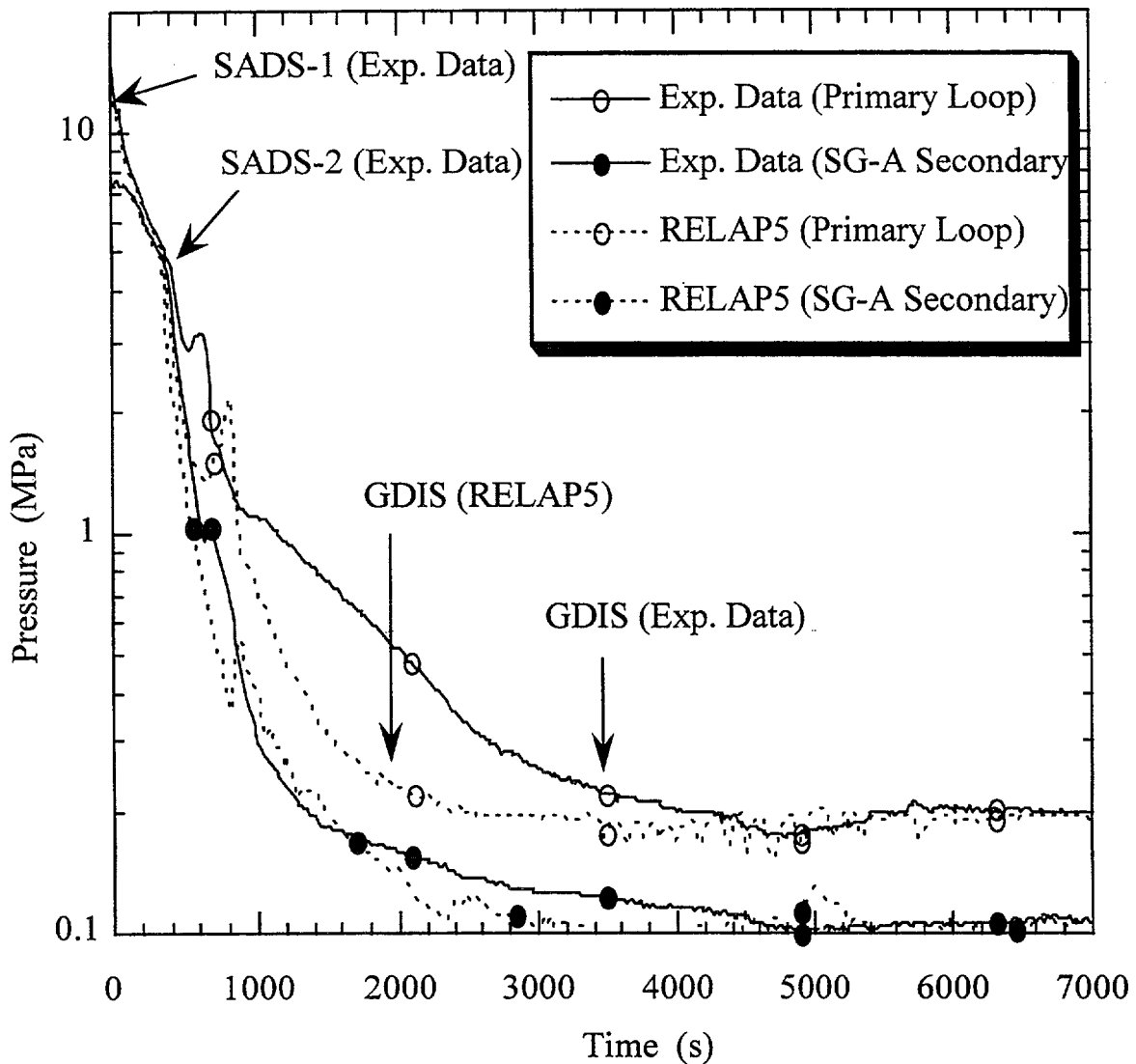


FIG. 2. Comparison Of Primary And Secondary Pressures Between Experiments and Relap5.

The primary loop was depressurized quickly toward the SG secondary-side pressure immediately after the break at time zero, as shown in Fig.2. During this initial depressurization, several trip-initiated events occurred, including the core power decay, pump coastdown, isolation of the SG secondary sides, and actuation of the first stage of SADS (SADS-1). The primary-side depressurization was arrested for a while at a pressure slightly higher than the secondary-side pressure. The depressurization resumed, however, immediately after the second stage of SADS (SADS-2) was actuated at 407 s. Liquid injection from the FDIS occurred between 331 and 387 s, when the primary-side pressure decreased below the FDIS initial pressure of 5.5 MPa. Immediately after this, the two-phase NC resumed due to the increase of the primary coolant inventory. As the primary pressure decreased further, the GDIS injection started at 3435 s. After the GDIS actuation, a stable long-term cooling condition was established; the primary pressure at the upper plenum was almost constant at 0.2 MPa, the decay heat was transferred to SGs by NC, and the break flowrate was balanced with the GDIS injection flowrate. The core was always covered with liquid water or two-phase mixture through the experiment, which ended at 14 000 s.

Nonuniform flow behavior among parallel U-tubes was observed both during the blowdown phase and low pressure long-term core cooling phase. The behavior was characterized by the coexistence of concurrent condensing flow in some tubes and stagnant two-phase stratification in the other tubes as shown in Fig.3.

The stable two-phase stratification in U-tubes during the blowdown phase was caused mainly by the temporal liquid level drop in the secondary side. The secondary side liquid level temporarily decreased down to 40% of the U-tube height due to the coolant loss from the SADS valves [7, 8]. This decreased the condensation in the U-tube top region and resulted in the stable existence of vapor space above liquid columns in there.

On the other hand, the two-phase stratification during the long-term core cooling phase occurred when entire U-tubes were covered with the two-phase mixture in the secondary side. This stratification was caused by the secondary side temperature distribution as will be discussed in the next section describing the NC test.

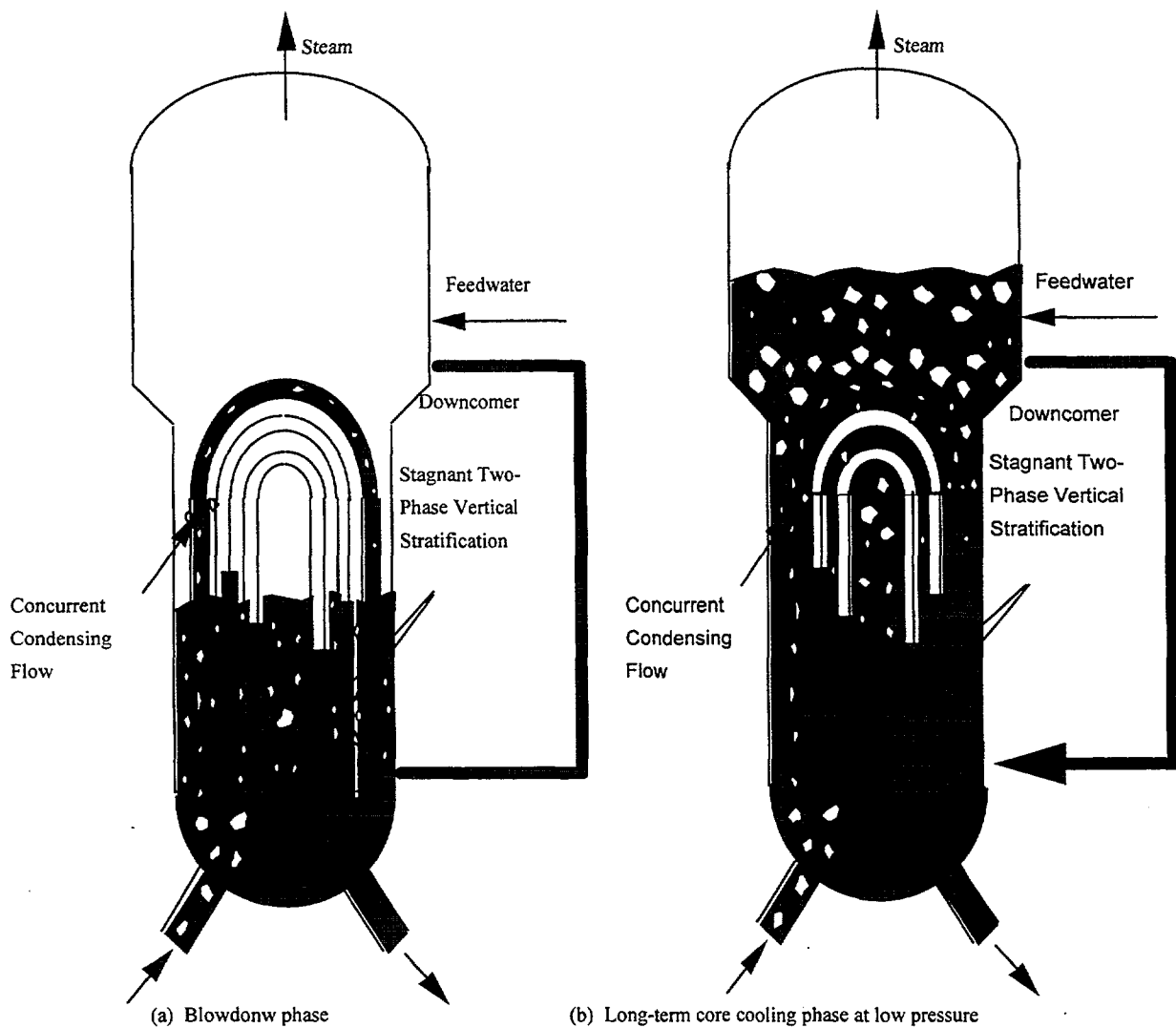


FIG. 3. Nonuniform Flow Behavior Observed Among U-Tubes.

3.2. RELAP5/MOD3 ANALYSIS

The test was analyzed using the RELAP5/MOD3/V5M5 [9]. The primary and secondary loops were modeled using 235 volumes and 204 heat structures. The measured data were used for the temperature and flowrate of the feedwater. The primary side of the SG was modeled with a single flow channel. This is because the nonuniform behavior was not reproduced just by putting two flow channels for the SG primary side as will be discussed in the next section.

The primary depressurization caused by the SADS actuation was relatively well predicted before the SADS-2 actuation, as shown in Fig. 2. The depressurization rate was, however, overpredicted at lower pressure. Because of the overpredicted depressurization, the GDIS actuation was predicted to occur about 1500 s earlier than the experiment as shown in Fig. 2. Since the pressure and mixture level in the SG secondary side were predicted well, the overprediction of the primary depressurization was caused by the overprediction of the effective heat transfer area at SG and/or the heat transfer coefficients for condensing flow. Note that the effective heat transfer area was smaller than the total geometrical surface area of U-tubes due to the stagnant two-phase stratification. Since the code does not have a model to take into account this effect, the overprediction of the heat transfer may be inevitable. The overprediction of the heat transfer coefficient can be a cause because the RELAP5 code does not have appropriate heat transfer models for vertical concurrent condensing flows [7, 8].

The inability of the code to deal with the nonuniform U-tube flow also resulted in a very oscillatory NC flow compared with the experimental data as shown in Fig. 4. The overestimated heat transfer area caused excess condensation in the U-tube, which resulted in the flow oscillation including the flow reversal. The exaggerated oscillation of the NC flow affected the prediction of the core cooling. Although the core fluid changed to single-phase liquid from two-phase mixture after 4500 s in the test, such transition was not predicted at all.

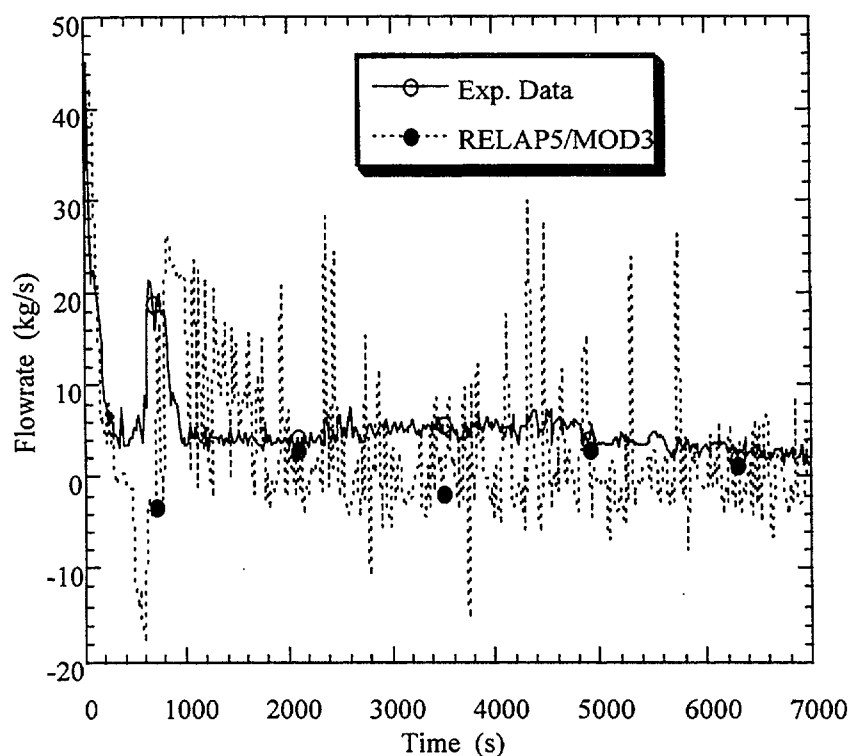


FIG. 4. Comparison of Loop Flowrates Between Experimental Data and RELAP5/MOD3.

The inability of the code to predict the NC behavior is noteworthy when compared with the code assessment results using the high pressure NC data. Even using a lumped flow channel for U-tubes, the loop flow rate under various two-phase flow modes, including a fill and dump mode, was somehow calculated [10, 11]. These results stress the importance of a calculation model for the nonuniform behavior in order for the prediction of the low pressure NC.

4. LOW-PRESSURE NATURAL CIRCULATION TEST AND ANALYSIS

4.1. Test conditions and results

A steady-state NC test was conducted by decreasing a primary mass inventory stepwisely as a test parameter, and controlling the core power at 0.94 MW (1.3% of the nominal core power) and the SG secondary pressure at 0.14 MPa.

Figure 5 shows the loop flowrate vs. the primary mass inventory observed in the test. With decreasing the mass inventory, the loop flowrate increased due to the transition from the single-phase NC to the two-phase NC, peaked at 90%, and then decreased. The reflux condensation was observed for the mass inventory below 40%.

The nonuniform two-phase flow behavior similar to that observed in the SBLOCA test was observed when the primary mass inventory was between 70 and 91%. Among six instrumented SGU-tubes in the loop-A, the stagnant two-phase stratification was observed in five U-tubes, while the concurrent condensing flow was observed only in one U-tube.

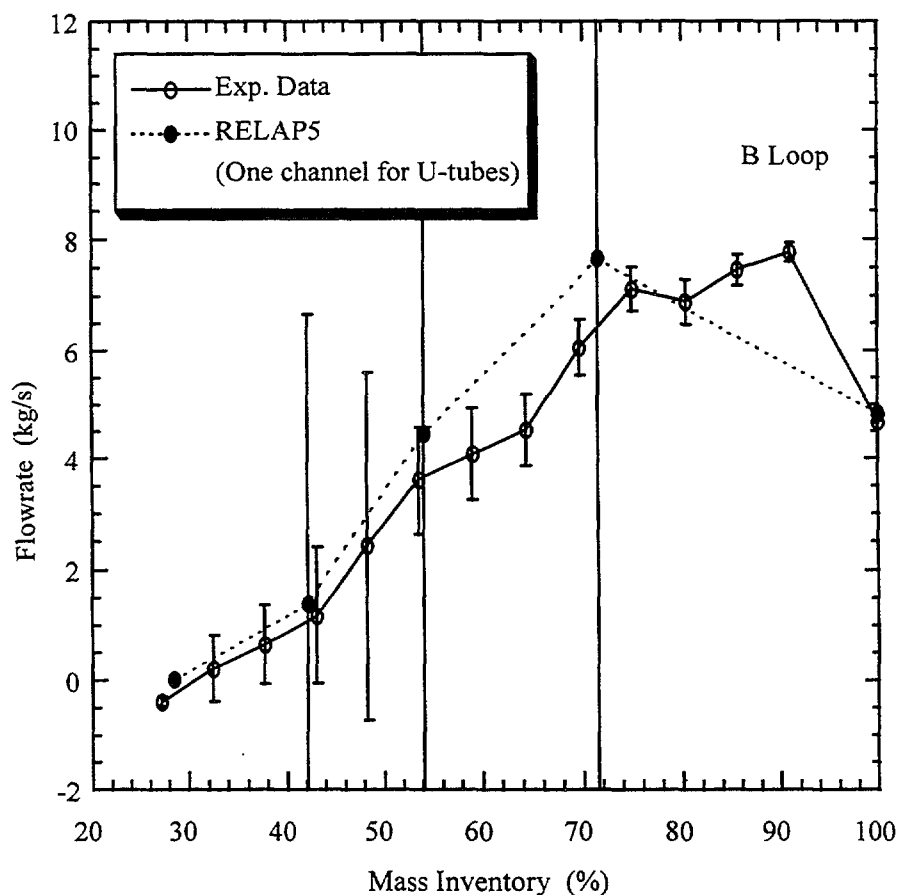


FIG. 5. Loop Flowrate at Cold Leg vs. Primary Mass Inventory for NC Test and RELAP5 Analysis.

The existence of the two-phase stratification suggests that the vapor mass does not change with time in the vapor continuous regions above the liquid levels in such U-tubes. Note that all the core power was transferred to the SG secondary sides during the test, that is, the average primary temperature was higher than that in the secondary side. Only condensation was seemingly possible in U-tubes under this condition.

The mechanism for the stagnant stratification can be understood from the measured secondary side temperature distribution showing the lowest temperature at the top and bottom regions and the highest around the midplane as shown in Fig. 6. This was caused by the saturation temperature difference corresponding to the static pressure difference, and the recirculation in the SG secondary side. The condensation occurring around the tube top was balanced with the evaporation occurring around the midplane in the U-tube with the stratification. This enabled the stable existence of vapor space above the liquid levels in the U-tube. This behavior is one of characteristic behaviors at low pressure where the pressure is comparable to the water head. On the other hand, such coexistence of evaporation and condensation in a tube is impossible to occur at high pressure where the secondary side temperature is generally uniform [11].

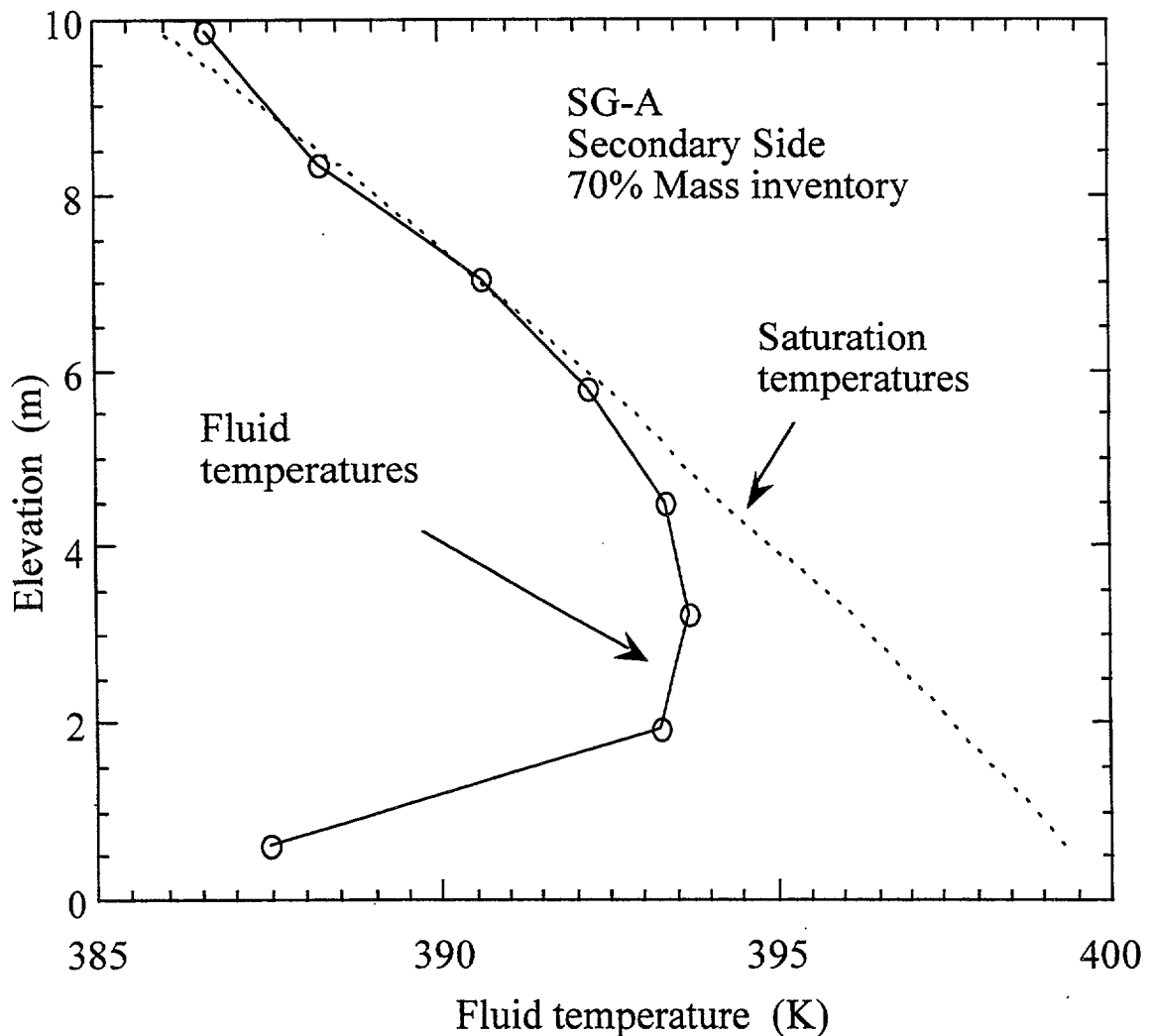


FIG. 6. Comparison of SG-A Secondary Side Fluid And Saturation Temperatures at 70% Mass Inventory for NC Test.

4.2. ANALYSIS

4.2.1. RELAP5 analysis using a partial SG model

Flow characteristics for a U-tube were analyzed using the RELAP5/MOD3.2.1.2 code to better understand the mechanism of the nonuniform behavior. One U-tube was modeled using the pipe component with 32 cells. For the analysis of the two-phase concurrent flow, the inlet flowrate, inlet quality, and outlet pressure were imposed. For the analysis of the two-phase stratification, the measured pressure and quality were imposed both for the inlet and outlet. For both analyses, measured secondary side fluid temperatures were given as the outer surface temperatures of the tube wall heat structure components. Although this procedure neglects the heat transfer resistance on the tube wall outer surface, it was used to keep the secondary side conditions to be constant without being affected by the primary side calculation results. Note that it is impossible for the current RELAP5 code to impose the secondary fluid temperatures and calculate the heat resistance at the same time.

A calculated flow characteristic curve for the SG primary side is shown in Fig. 7, in which the pressure difference between the tube inlet and outlet, an indicator of the SG flow resistance, is plotted against the inlet flowrate. Here the flowrate is normalized by that obtained assuming the uniform flow distribution among U-tubes. That is, the normalized flowrates of 1 and 4, for examples, mean the fraction of tubes with the concurrent condensing flow of 100 and 25%, respectively. The error bar attached to each point in Fig. 7 represents the standard deviation to indicate the magnitude of the fluctuation.

The calculated flow behavior was very oscillatory for the normalized flow of 1, showing a cyclic reverse flow from the outlet. The oscillation occurred because the vapor inlet flowrate was so small, compared to the condensation rate, that the pressure could not maintain at a sufficiently high level to prevent the reverse flow. This oscillatory behavior was similar to the RELAP5 results for the NC flowrate at low pressure shown in Fig. 4. This analysis, thus, confirms that the stable NC behavior at low pressure can not be predicted by the RELAP5 code when the nonuniform behavior is not take into account.

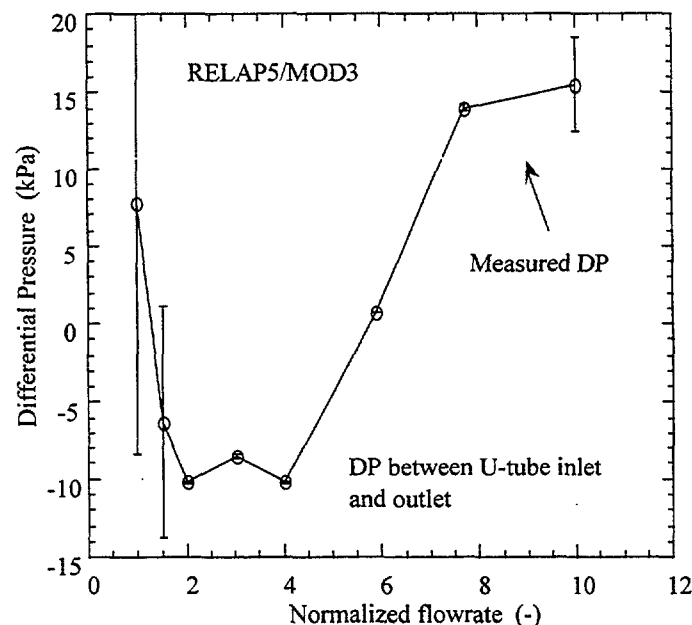


FIG. 7. Differential Pressure Between U-Tube Inlet and Outlet vs. Normalized Flowrate where Flowrate is Normalized by that Assuming Aniform Flow Distribution.

With increasing the flowrate from 1, the differential pressure first decreased showing a negative slope in the flow characteristic curve. The negative slope was caused by that the void fraction in the upflow side increased with increasing the mass flowrate. It is known that the negative slope causes the flow excursion type instability. The flow behavior was relatively stable for the normalized flowrate between 4 and 8, in which the slope was positive because the upflow side became fully voided and the effect of the flow resistance increased with increasing the flowrate. Above the normalized flowrate of 9, all the vapor did not condense in the U-tube.

The measured differential pressure of 11 kPa corresponded to the normalized flowrate of 1 and 7, as shown in Fig.7, or the fraction of tubes with the concurrent condensing flow of 100 and 14%, respectively. Since the unstable flow tends to be avoided, this analysis may indicate that the fraction of the U-tubes with the condensing flow was 14% during the test at 70% mass inventory. It should, however, be noted that the calculated results have large uncertainties because the RELAP5 code does not have appropriate heat transfer models for vertical condensing flows, and the outer surface heat transfer resistance was not taken into account in this analysis as mentioned before.

Since the crosssection of the SG inlet plenum of the LSTF is almost a semi-circle having a relatively large diameter of 0.73 m, the inlet quality is expected to be nonuniform for each U-tube. Indeed, fluid saturation caused by the vapor ingress was observed in the bottom part of the upflow side of some U-tubes with the stratification, while the subcooling was observed in the other tubes with the stratification during the test. The inlet quality was, therefore, changed as a parameter in the stagnant two-phase stratification analysis. Figure 8 shows a volumetric vapor generation rate in a tube as a function of the elevation for the inlet quality of 0.0 and 0.018. The inlet quality of 0.018 corresponds to the core outlet quality. For both quality conditions, calculated liquid levels in the upflow and downflow sides of tubes were stable except for the initial transient condition. This confirms that the balance of the condensation and evaporation is possible under the measured secondary side temperatures and estimated inlet quality conditions.

The above two analyses have made clear that the fraction of tubes with the concurrent condensing flow is determined so that the stable flow can exist while all the vapor is condensed in tubes. The flow behavior in the other tubes can be stable with the two-phase stratification.

4.2.2. Simplified system analysis procedure taking into account the nonuniform behavior

From the discussions above, it has been made clear that the nonuniform behavior should be taken into account in the system analysis using the RELAP5 to realistically predict the low pressure NC behavior. This is clearly indicated in Fig. 5, where the loop flowrates calculated by the RELAP5 using one channel U-tube model are compared with the experimental data. Although the average flow rate is somehow predicted, the calculated flow was significantly oscillatory as indicated by the error bar in Fig. 5. A trial analysis was made just by putting two parallel channels to represent the SG primary side assuming the fraction of tubes with the concurrent condensing flow. The result was completely the same as the result using the one channel U-tube model, that is, the calculated behavior in the two channels were both oscillatory.

It is expected that the stagnant two-phase stratification may be predicted by imposing very high flow resistance for the flow channel representing the two-phase stratification. Such

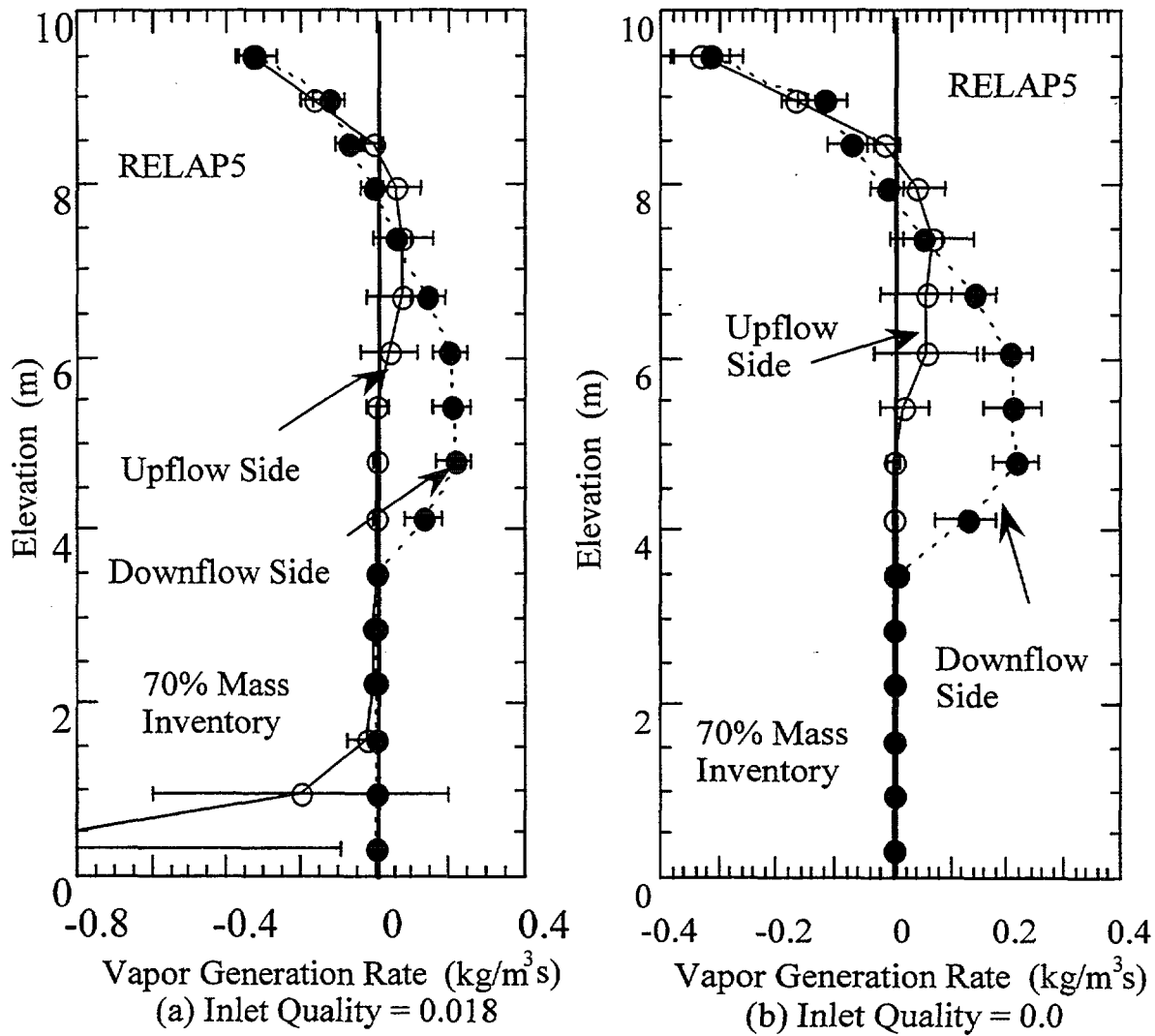


FIG. 8. Calculated Vapor Generation Rate in U-Tube.

an artificial adjustment may be justified because it does not affect the calculation results if the flow velocity is small enough, that is, the resistance coefficient has an influence on the result only when the flow exists.

The effectiveness of this simple procedure were investigated by analyzing the NC behavior at the 70% mass inventory using the RELAP5. The used nodding was the same as that used for the SBLOCA analysis except for the SG primary side that was modeled with two parallel channels. The secondary-side pressure, collapsed liquid level, and feedwater temperature were forced to match the experimental data. Each U-tube channel was modeled with a pipe component with eight calculation cells. The fraction of tubes with the condensing flow was assumed to be 25%. The imposed flow resistance for all the junctions in the component representing the two-phase stratification was 105.

Figure 9 shows the comparison of loop flowrates between the test and analyses using one or two channel model for the SG primary side. The oscillation was suppressed significantly for the two channel analysis, although there still exists disagreements between the data and calculation. For more reliable prediction of the low pressure NC behavior, the

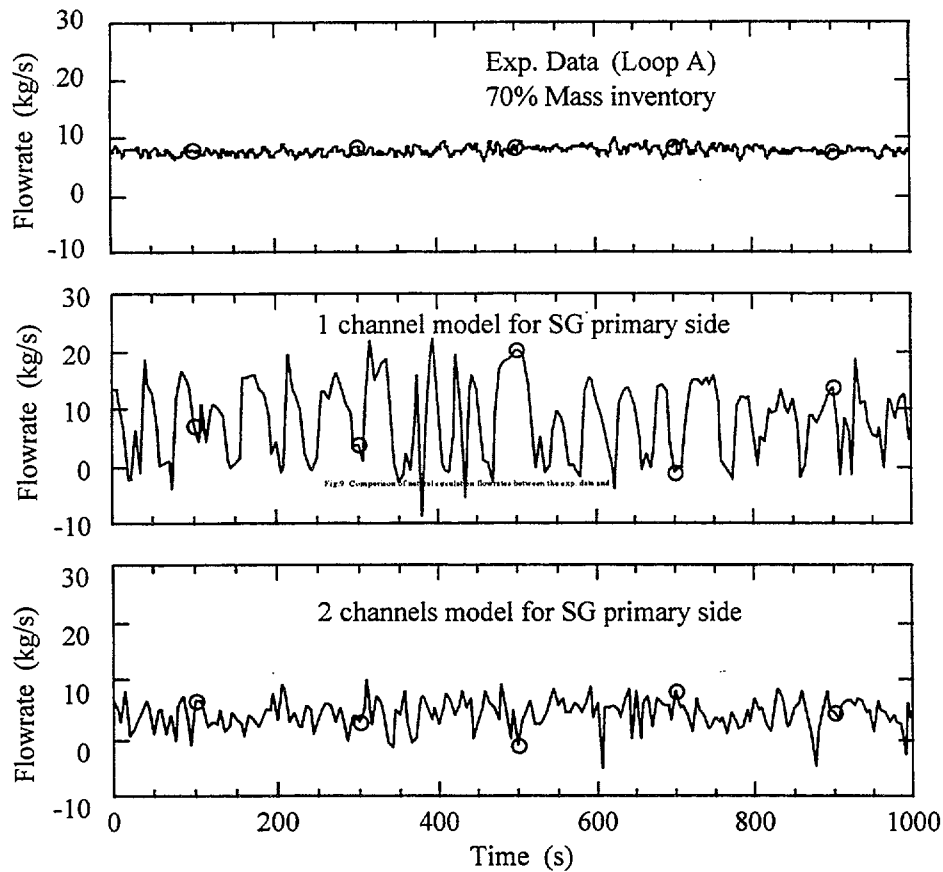


FIG. 9. Comparison of Natural Circulation Flowrates Between the Experimental Data and RELAP5 Using One or Two Channel Model for SG Primary Side.

heat transfer correlations for the condensing flow should be investigated. At the present time, the low pressure NC behavior may be investigated, at least qualitatively, by using this procedure and changing the fraction as a calculation parameter.

5. CONCLUSIONS

Thermal-hydraulic safety research program is currently being conducted by using the ROSA-V/LSTF, to better understand the phenomena associated with passive safety systems for the next generation PWRs. The test data also are useful for assessment and improvement of computer codes. This paper describes the two test results: one small-break LOCA test for the investigation of the combined use of a gravity-driven injection system (GDIS) and a SG secondary-side automatic depressurization system (SADS), and one low-pressure steady-state natural circulation test. The results of the tests and RELAP5/MOD3 analysis can be summarized as follows.

1. The primary system was depressurized, by means of the SADS, successfully to the GDIS injection pressure of 0.2 MPa, even when the primary ADS was not used. Long-term passive core cooling by the natural circulation flow, with the GDIS injection flow balanced with the break flow, was established at low pressure. These results confirm the effectiveness of the combined use of the SADS and GDIS.

2. Nonuniform flow behavior was observed among SG U-tubes during the low-pressure natural circulation core cooling phase in the two tests, that is, the heat transfer occurred primarily in U-tubes with the two-phase concurrent condensing flow, while the stagnant two-phase stratification was observed in the others. This causes the reduction of the effective heat transfer area in the SG.
3. The primary depressurization was overpredicted by the RELAP5/MOD3 code using one lumped U-tube after the SADS-2 actuation. The natural circulation flow was excessively oscillatory, and the observed stable core cooling by a single-phase liquid flow was not predicted. These are caused mainly by the inability of the code to simulate the nonuniform behavior among U-tubes.
4. The RELAP5 analysis using a partial SG model have indicated that U-tube flow is stable and all the vapor inflow is condensed in the tube in a certain flowrate range. This suggests that one of the main factors to determine the number of the U-tubes with the concurrent flow is the flow stability in a U-tube.
5. The stagnant two-phase stratification occurred in a U-tube when the average temperature is higher in the primary than in the secondary because the condensation occurring in the top part of the U-tube was balanced with the evaporation occurring around the midplane of the tube. These were caused by the secondary side temperature distribution which is a characteristic at low pressure where the static head is comparable with the system pressure. The RELAP5 analysis using a partial SG model have confirmed the balance of the evaporation and condensation.
6. A simple analysis procedure was proposed to take into account the effect of the nonuniform behavior. In this procedure, the fraction of the tubes with concurrent flow is changed as a parameter, and the very large flow resistance is imposed on junctions for the pipe components representing U-tubes with the stagnant two-phase flow stratification. One example have clearly demonstrated the effectiveness of this procedure, although further research is required for more accurate prediction.

ACKNOWLEDGEMENTS

The authors express their thanks to Mr. Etsuo Ohtani of Nihon Computer Bureau and Ms. Kazue Toyoda of Information Technologies Japan Inc. for their contribution to the RELAP5 analysis.

NOMENCLATURE

ADS : Automatic Depressurization System
 AIS : Accumulator Injection System
 FDIS : Flashing-Driven Injection System
 GDIS : Gravity-Driven Injection System
 LOCA : Loss-Of-Coolant Accident
 NC : Natural Circulation
 SADS : Secondary Side Automatic Depressurization System
 SADS-1 : First Stage of SADS
 SADS-2 : Second Stage of SADS
 SBLOCA : Small Break Loss-Of-Coolant Accident

REFERENCES

- [1]TOWER, S. N., SCHULZ, T. L. AND VIJUK, R. P., "Passive and simplified system features for the advanced Westinghouse 600 MWe PWR", Nucl. Eng. Des. 109 (1988) 147-154.
- [2]MATSUOKA, T. et al., "Safety features of the simplified Mitsubishi pressurized reactor", Nuclear Safety, 33 (1992) 196-208.
- [3]MURAO, Y., ARAYA, F. AND IWAMURA, T., "A concept of JAERI passive safety light water reactor system (JPSR)", Proc. of the 7th Int. Mtg. on Nucl. Reac. Thermal-Hydraulics NURETH-7, NUREG/CP--0142-Vol.2 (1995) 1169-1195.
- [4]INTERNATIONAL ATOMIC ENERGY AGENCY, Review of design approaches of advanced pressurized LWRs, IAEA-TECDOC-861, Vienna (1996).
- [5]ROSA-IV GROUP, "ROSA-IV Large Scale Test Facility (LSTF) System Description for Second simulated fuel assembly", JAERI-M90-176 (1990).
- [6]YONOMOTO, T., KONDO, M. AND KUKITA, Y., "PWR small break loss-of-coolant-accident experiment at ROSA-V/LSTF with a combination of secondary-side depressurization and gravity-driven safety injection", Nucl. Sci. Tech., 34 (1997) 571-581.
- [7]YONOMOTO, T. et al., "Small break LOCA tests at ROSA-IV/LSTF on next generation PWR designs", Proc. of Eighth International Topical Meeting on Nuclear Reactor Thermal-Hydraulics (NURETH-8), Kyoto, Japan, 1 (1997) 535-542.
- [8]YONOMOTO, T., OHTSU I., AND ANODA, Y., "Thermal-hydraulic characteristics of a next-generation reactor relying on steam generator secondary side cooling for primary depressurization and long-term passive core cooling", To be published in Nuclear Engineering and Design (1998).
- [9]RELAP5 DEVELOPMENT TEAM, "RELAP5/MOD3 code manual", NUREG/CR-5535, INEL-95/0174, 1~4 (1995).
- [10]SCHULTZ, R. R., CHAPMAN, J.C., KUKITA, Y., et al., "Single and two-phase natural circulation in Westinghouse pressurized water reactor simulators: phenomena, analysis and scaling", Proc. of the Winter Annual Meeting of ASME, Boston, MA, FED-Vol. 6 1, HTD-Vol. 92 (1987) 59-70.
- [11]KUKITA, Y., NAKAMURA, H. AND TASAKA, K., "Nonuniform steam generator U-tube flow distribution during natural circulation tests in ROSA-IV Large scale test facility", Nucl. Sci. Eng., 99 (1988) 289-298.

EXPERIMENTS AND ANALYSIS OF PASSIVE SAFETY SYSTEMS

(Session 4)

Chairman

A. Rao

United States of America

**NEXT PAGE(S)
left BLANK**



EC-SPONSORED RESEARCH ACTIVITIES ON INNOVATIVE PASSIVE SAFETY SYSTEMS

J. MARTIN BERMEJO, G. VAN GOETHEM

Reactor Safety Research Programme,
European Commission,
Brussels, Belgium

Abstract

On April 26th 1994, the European Union (EU) adopted via a Council Decision a EURATOM Multiannual Programme for community activities in the field of Nuclear Fission Safety (NFS) Research for the period 1994 to 1998. An area of work having, as an objective, to "explore innovative approaches" to improve the safety of future and existing reactors, was introduced in this programme. Most of the projects selected in this area, which have been grouped under a common cluster known as "INNO", are currently being carried out on a "cost-shared" basis, i.e. contribution of the European Commission is up to 50% of the total cost. At present, the "INNO" cluster is composed of 10 projects in which 25 different organisations, representing research centres, universities, regulators, utilities and vendors from 7 EU member states and Switzerland, are involved. These projects are proving to be an efficient means to gain the necessary phenomenological knowledge and to solve the challenging problems, many times of generic nature, posed among others by the characteristically small driving forces of the systems studied and by the lack of really prototypical test facilities.

1. INTRODUCTION

During the last ten years considerable activity has been developed by the main actors of the nuclear power plant business, namely the research organisations, the suppliers, the regulatory authorities and the electrical utilities, in their attempts to design the next generation of commercial reactors. The concepts being studied span the technological range from "evolutionary" type (i.e., many of the new design features are simplifications and improvements in safety systems of currently operating power reactors) through "innovative" type (i.e. radical conceptual changes in design approaches or system configuration are incorporated).

In the European Union (EU), these designs share two basic common goals: (i) to demonstrate that the cost of generating power from the future nuclear power plants will be competitive with alternative electricity sources, and (ii) to enhance the safety of the plants such that the chances of an accident are further reduced and that no stringent off-site emergency response actions (i.e. prompt evacuation, resettlement, etc.) will be necessary.

Some of these new designs include the use of "passive" systems which rely on immutable natural forces (e.g. gravity, natural circulation, etc.) for the essential safety functions. The characteristically small driving forces of some of these safety features as well as the long-duration, slowly-developing transients compared to current reactor designs, pose challenging problems from both experimental and analytical points of view, which often require complex and expensive research activities. Considering the large experimental facilities usually needed to test these systems as well as the substantial effort necessary to improve the existing numerical thermal-hydraulics systems analysis codes, co-ordinated international research programmes are nowadays the most cost effective way to investigate such problems.

2. THE 1994-1998 EU RESEARCH PROGRAMME ON NUCLEAR FISSION SAFETY

The European Union (EU), via a Council Decision of April 26th 1994, adopted a EURATOM Multiannual Programme for Community activities in the field of Nuclear Fission Safety (NFS) Research and Technological Development (RTD) for the period 1994 to 1998. This programme consists of *five* main activity areas:

Area A.	Exploring Innovative Approaches
Area B.	Reactor Safety
Area C.	Radioactive Waste Management, Disposal and Decommissioning
Area D.	Radiological Impact on Man and Environment
Area E.	Mastering Events of the Past

This Programme is being implemented either via direct actions under the responsibility of the Joint Research Centre (JRC) of the EC, or via indirect actions co-ordinated by units F-5 and F-6 of Directorate General XII of the European Commission (EC). The latter are structured around a limited number of significant projects which were selected by the EC and a group of independent experts with the aim to stimulate co-operation among public and private organisations of different Member States, to avoid unnecessary duplication efforts and to use the available resources in an efficient way. Notice that through a special association agreement Switzerland is also allowed to participate in the NFS programme without financial contribution from the EC.

Most of these projects are essentially carried out through “*shared cost*” actions, for which EC contribution is up to 50% of the total project costs. A small part of the programme though, is carried out through “*concerted*” actions whose objectives are the exchange of information, on some critical R&D issues or the development of a consensus on specific problems of common interest. For the concerted actions the EC reimburses only co-ordination costs, such as travel and living expenses, meetings, etc.

In both cases, “cost-shared” or “concerted” actions, there is a “*Project Co-ordinator*” who is responsible for the management, technical direction of the project and production of the deliverables committed in the Work Programme. The co-ordinator’s responsibilities also include administrative tasks, such as general liaison with the EC, the submission of all required documents (e.g. periodic progress reports, minutes of meeting, specific technical reports, etc.) and the distribution of the financial support paid by the EC.

For Areas A and B, one of the most important events was the EC-sponsored symposium “FISA-97” (about 300 participants), which was a kind of mid-term review of all the on-going projects in the areas A and B mentioned above. This symposium took place in Luxembourg from 17 to 19 November 1997 and was open to scientists and technical experts from the European Union and abroad. The proceedings have been published as an “EUR” document by the EC Office for Official Publications [1].

3. EU-SPONSORED RESEARCH ON INNOVATIVE APPROACHES

The activities in the above mentioned area A should contribute to the development of new (mainly “passive”) concepts for improving the safety of nuclear reactors and fuel cycle, giving priority to problems of generic nature. They should also provide a data base from

which industry can choose features that respond best to the development trends of future nuclear power plants in the EU and world-wide. "Active" concepts and systems for the mitigation of severe accidents, are considered under Area B, of the 1994-1998 Nuclear Fission Safety RTD Programme. The area A has been further broken down in two sub-areas:

A.1. Conceptual reactor safety features

Assessment of new, especially passive and inherent conceptual safety features with regard to their feasibility and their contribution to the overall safety of a nuclear plant. Emphasis is made on generic problems related to techniques for passive decay heat removal from both the core region and the containment building, as well as for other passive safety measures (e.g. initiation, depressurization, injection).

A.2. Fuel cycle concepts

Alternative fuel cycle concepts are under consideration, mainly from the point of view of safeguards and minimisation of the long-lived radioisotope inventory. Partitioning and Transmutation offers the possibility to reduce the content of long-lived radioisotopes of the high level waste. It implies the application of sophisticated separation techniques and adequate methods of transmutation of actinides.

The projects which were accepted in Area A.1 have been grouped under a common cluster known as "INNO". The "INNO" cluster is composed of ten projects (7 "shared-cost" and 3 "concerted" actions) in which 25 different organisations, representing research centres, universities, regulators, utilities and vendors from 7 EU member states and Switzerland, are involved. Table I shows the most relevant details (e.g., duration, co-ordinator, partners involved, facilities, codes) of the projects presented in this paper.

These projects include both experimental and analytical activities directed mainly to study the phenomena associated with the use of passive systems for decay heat removal (both from the core region and the containment building) and for safety measures (e.g. initiation, depressurization, injection), as well as to demonstrate their feasibility for different types of advanced Light Water Reactor (LWR) designs. The experiments are being performed in some of the most important European thermal-hydraulics facilities in Europe covering : (i) large-scale integral (e.g. PANDA, PACTEL), (ii) large-scale separate-effect (e.g. NOKO) and (iii) small-scale separate-effect (e.g. LINX, EPICE, SUCOT, MUCON, STORM, AIDA, PECA, etc.) tests. The use of different neutronics and thermal-hydraulic computer codes (ATHLET, CATHARE, TRAC, RELAP5, etc.) for pre and post-test calculations is an important part of the work programmes of these projects, as it will enable to define better the test configuration and parameter range extensions and to extrapolate the results of the small scale experiments towards full scale reactor applications.

4. PROJECTS OF THE "INNO" CLUSTER

This section briefly describes the objectives as well as the main activities foreseen within 8 of the "INNO" cluster projects whose experimental and analytical activities are relevant to this Technical Committee Meeting, and also presents the results obtained up to date.

TABLE I. PROJECTS SUMMARY INFORMATION

Acronym	Duration (months)	Co- ordinator	Partners	Facilities	Computer Codes
SYNTHE SIS	27	ENEL	SIEMENS, CISE	CISE (IT), SIET (IT)	RELAP 5
POOLT HY	36	CEA-DTP	FZK, Univ. Manchester, Univ. "La Sapienza"	EPICE (FR), SUCOT (DE), NUCON (UK), QUSCOCS (IT)	CATHARE, CFX
APSI	33	VTT- Energy	AEA Tech., Univ. Pisa, Univ. Lappeenranta	PACTEL (FI)	CATHARE, RELAP5 APROS
TEPSS	36	ECN	CIEMAT, NUCON, KEMA, niversities of. Catalonya and Valencia	PANDA, LYNX and AIDA (CH)	GOTHIC, MELCOR, RELAP5, TRAC, CFX
IPSS	36	FZJ (Jülich)	ECN, GRS, KEMA, NUCON, SIET, PSI, VTT	Dodewaard Reactor (NL), NOKO (DE), PANDA (CH),	APROS, PHOENICS, ATHLET, MELCOR, RELAP5, RALOC, TRAC
BWRCA	12	CEA-DRN	SIEMENS, CIEMAT, ENEA, Univ. Delft, FZ Rossendorf	DESIRE (NL)	ATHLET, CATHARE, DYN3D- ATHLET, RELAP5, TUBEX RAMONA3, HELIOS, APOLLO, CRONOS,
INCON	26	ENEL	ANSALDO, CIRTEN, EdF, PSI, Empresarios Agrupados,	CISE (IT), LINX (CH)	GOTHIC, LEGO, RELAP5
CONGA	24	SIEMENS	ENEL, CIEMAT, JRC-Ispra, PSI	CISE (IT), DRAGON (CH), STORM (CH), PECA (ES)	SPARC, CONTAIN

4.1. Project “System for Emergency Core Cooling through High Performance Steam Injector” (SYNTHESIS)

This project is a “shared-cost” action which started in January 1996, and was carried out by a consortium of 3 organisations (ENEL, CISE and Siemens) under the co-ordination of ENEL. The project was completed on 31 March 1998.

The main objective of the project was to demonstrate the feasibility of an injection system (SYNTHESIS), based on a passive device named High Performance Steam Injector (HPSI). The system should be able to pump water into a Reactor Coolant System (RCS) at high pressure, taking water from an atmospheric tank, without requiring any human intervention. The key component of the system, the HPSI, is a single-stage steam injector able to operate at the required pressure conditions, which has already been developed, patented and successfully tested by ENEL and CISE for industrial applications.

The SYNTHESIS functional requirements for a reference (the German SWR 1000 concept) and an alternative application (secondary side of a PWR) were first defined, including system interfaces, preliminary layout, operating conditions and required performances. The system to be investigated was equipped with active components, i.e. automatic actuators (valves), for start-up and for keeping the optimum operating conditions during transients. This was followed by a design optimisation process for the HPSI prototype to meet these requirements. An HPSI prototype was manufactured and the modifications to the existing test loop (located at the SIET facilities near Piacenza [2]) needed to perform the experimental programme were implemented. Once the Test Matrices as well as the specification for the active components were defined, the experimental activities started.

The test programme was performed in three phases. Phase I consisted in a series of tests using different nozzles and nozzles positions, various combinations of internal parts and hardware modifications, until the measured performance met or exceeded the requirements. When a successful configuration was determined, additional tests were performed in order to develop the best procedure for the automatic start-up sequence (phase II). Finally, in phase III, a number of tests were carried out using a modified HPSI and a wider range of operating steam pressures in order to obtain the optimal performance configuration. Additional tests to investigate the effect of non-condensable gases (using Helium) showed a negligible impact on the HPSI performance.

The analytical activities included a benefit evaluation of the SYNTHESIS application to both the SWR 1000 and the secondary side of a PWR. Transient and accident analysis using RELAP5-MOD3.1 (for the SWR 1000) and RELAP5-MOD3.2 (for the PWR) were performed to that end. The main results of these analyses are that although the optimal HPSI configuration seems adequate to avoid the ADS actuation for all SB-LOCAs (depending on the setpoint selected), a reduction of the initial water inventory in the RPV, and consequently a reduction of the RPV height of the SWR1000, seems not feasible.

4.2. Project “Thermal-hydraulics of Large Pools with Immersed Heat Exchangers and Natural Convection Heat Transfer” (POOLTHY)

This project is a “shared-cost” Action which started in January 1996, and is being carried out by a consortium of 4 organisations (CEA-DRN, FZK, University “Victoria” of Manchester and University “La Sapienza” of Rome) under the co-ordination of CEA-DRN. The duration of the project is 36 months.

The main objective of this project is to provide a bank of experimental data about different phenomena related to the removal of decay heat by means of passive systems. These data could then be used to improve and validate the numerical models of existing thermal-hydraulic codes. The project consists in different separate effect tests to be performed at four independent experimental facilities.

The *EPICE* test loop (see page 503 of reference [1]) is located at the CEA-DRN facilities in Grenoble, and is being used to study the performance of immersed vertical tubes heat exchangers operating with pool boiling at low pressure. The investigation of the thermal-hydraulic behaviour of such components needs an specific experimental validation of the following aspects: (i) two-phase heat transfer correlations along the tubes at low pressure, (ii) critical heat flux for various flow conditions (i.e. natural circulation, forced convection) and different bulk temperatures, and (iii) occurrence of instabilities. Three test campaigns have been designed: EPICE1-FC (forced convection using an electrically heated tube), EPICE1-NC (natural circulation using also an electrically heated tube) and EPICE2-NC (natural circulation using a tube heated with a primary fluid). The test series with the EPICE1-FC and EPICE1-NC configurations have already been completed, while the tube for the tests on EPICE2-NC is still being manufactured.

The *MUCON* (see page 507 of ref. [1]) experiments are being conducted by the University "Victoria" of Manchester. They are specifically concerned with the efficiency of condensers handling flowing steam and non-condensable gas mixtures. The general aim of these experiments is to produce correlations of condensation heat transfer data with various geometrical arrangements of condensing surface. Specific aims are : to examine the effect of steam flow rate and non-condensable gas concentration for three configurations of condensing plate (vertical, horizontal and inclined) and to investigate means of enhancing the condensation process by using extended surfaces and mixing devices. During the course of the first tests, some limitations of the original copper condensing plate became apparent (e.g. non-uniformity of plate temperature, deterioration of plate surface). After several tests with modified plates and some modelling studies, a completely new condensing plate was manufactured. Again copper was used, but this time the surface was plated with a thick layer of nickel followed by a thin layer of chromium.

The main aim of the *QUSCOCS* experimental facility (see page 504 of ref. [1]) run by University "La Sapienza" is to identify the optimal configuration of a pool - immersed heat exchanger, coupled with a natural circulation system, and to gather data on different phenomena, like natural convection in pools, nucleate pool boiling, effects of tube characteristics (e.g. materials, lay-out, inclination) on the system performance, and thermal-hydraulic transients. The results will be useful to optimise the full scale design of the MARS nuclear plant emergency decay heat removal. The experiments performed so far have shown very large heat losses in spite of the thermal insulation of the test loop which prevented to reach a steady boiling during tests with low power supply. New tests sections had to be manufactured using different surface finishing and materials.

The *SUCOT* test facility (see page 505 of ref. [1]) is installed at the "Forschungszentrum Karlsruhe" (FZK), and is being used to investigate the short term two-phase phenomenology of the natural circulation within a flooded spreading compartment of a future light water reactor containment. Several separate effect tests under steady state and transient conditions will be performed to investigate: subcooled and saturated pool boiling, flow aspects (pattern, flashing, instabilities), formation, rise and collapse of bubbles and

influence of non-condensable gases on boiling behaviour. The first steady-state experiments have been performed showing a stable natural circulation for all operational conditions investigated. A physical model to describe the momentum and heat exchange between the phases and to describe subcooled boiling phenomena has been developed. These models have been implemented in the commercial software package CFX4.1.

4.3. Project “Assessment of Passive Safety Injection Systems of Advanced Light Power Reactors - Passive Safety Injection Tests” (APSI)

This project [3] is a “shared-cost” action which started in January 1996, and is being carried out by a consortium of 4 organisations (VTT Energy, University of Lappeenranta, AEA Technology and University of Pisa) under the co-ordination of VTT-Energy. The duration of the project is 33 months.

The main objective of the project is to investigate the performance of the gravity driven passive safety injection systems developed for new Advanced Light Water Reactors (ALWRs), under accidental conditions, particularly the Loss of Coolant Accident (LOCA). These passive systems are intended to replace the current pump driven Emergency Core Cooling Systems (ECCS) and therefore it must be assured that they will achieve the desired functions.

This project is based on experiments carried out in the *PACTEL* integral test facility [4] on the performance of a passive core make-up tank (CMT). Of particular interest are the phenomena occurring in the CMT, such as possible rapid condensation and temperature stratification of water. The first activity of the project was to carry out a review of thermal-hydraulic phenomena and an evaluation of current system code capabilities important in the modelling of passive safety injection systems. The results have served as a basis for the specification of the test parameters.

The experimental part of the project is being performed at the *PACTEL* facility located in Lappeenranta (Finland) and run by VTT-Energy. Since *PACTEL* does not model any of the proposed passive ALWR designs, the investigation has focused on phenomenology, and the CMT has been used to simulate the gravity driven flow to the primary system. Three series of tests have been performed to investigate the effects of break sizes and location, the CMT size, and the CMT elevation.

In general the first two series of experiments have shown that the CMT performed basically as it was planned. The use of a flow distributor (sparger) in the CMT was decisive to avoid the problems of rapid condensation experienced in the past. The tests were very useful to assess the effect of different break sizes (1st series) and smaller CMT sizes (2nd series) on the CMT behaviour during recirculation and injection phases. Valuable data about CMT temperature distribution, heat transfer to the CMT walls, and injection mass flow rates, have been collected for their interpretation. For the third experiment series, the CMT was moved 1 meter higher (compared to the second series) in order to increase the driving head for the Passive Safety Injection System (PSIS). With the CMT in this position, the effect of miscellaneous factors was investigated: increased flow resistance of the PSIS line, very small break sizes, CMT and injection lines full of cold water and a different PSIS configuration.

After each series of experiments, selected tests were analysed with three computer codes: APROS, CATHARE and RELAP5. The main phenomena investigated were:

- a) thermal stratification of liquid in the CMT (temperature profile; formation of hot liquid layer),
- b) condensation in the CMT (wall condensation; condensation to water),
- c) heat transfer from hot liquid to the CMT wall,
- d) CMT injection flow (possible oscillations), and
- e) influences of CMT behaviour in the overall system behaviour (core heat-up; primary pressure)

During the numerical analyses, several and different problems (depending on the code) were encountered (e.g. numerical diffusion, parameter oscillations, large computing time, etc.) and, although the overall behaviour was well simulated, there were considerable differences between the measured and the calculated values, which highlights some inadequacy in the existing models.

4.4. Project “Technology Enhancement for Passive Safety Systems” (TEPSS)

This project [5] is a “shared-cost” action which started in January 1996, and is being carried out by a consortium of 7 organisations (ECN, Stork Nukon, KEMA, CIEMAT, Universities of Barcelona and Valencia, and the Paul Scherrer Institute) under the co-ordination of ECN. The duration of the project is 36 months.

The objective of this project is to undertake research needed to support further development of the technology base related to Advanced Boiling Water Reactors (BWR) of passive-type design. The research focus mainly on mixing and stratification phenomena in large water pools, passive decay heat removal, and effects of aerosol deposition inside heat exchangers tubes. The experimental work is being performed in three existing Swiss facilities run by the Paul Scherrer Institute: *LINX-2*, *PANDA*, and *AIDA*. It will be supported by analytical work to identify and understand the governing phenomena, and to produce useful correlations and reliable physical models. Different computer codes (RELAP5, GOTHIC, TRAC/BF1, MELCOR) will be used. The work programme consists of the following activities :

4.4.1. Suppression pool mixing and stratification

Two series of tests will be performed at the LINX-2 experimental facility [6]. In the first series, mixing and condensation phenomena that are induced by steam/nitrogen venting in a suppression pool will be investigated in a global manner using both a single vent and a six-side arms sparger. In the second test series, experiments will be performed to provide a database for three dimensional code development and validation. In particular, the objective is to improve the physical models for bubble plumes in water pools existing in the CFX-F3D code.

4.4.2. Passive decay heat removal

A series of eight tests have been conducted at the PANDA facility [7] in order to investigate the performance of the Passive Containment Cooling System (PCCS) of the reference design (i.e. the European SBWR) to remove decay heat from the containment after a loss of coolant accident. In the PCCS, steam from the drywell is condensed inside the tubes of

the heat exchangers immersed in a water pool outside containment. Scaling analyses were performed to assure that the experimental observations will be in known relationship to the phenomena in the reference design. The preliminary conclusions of the test programme can be summarised as follows:

- The PCCS showed a favourable and robust long term post-accident behaviour;
- There is a wide margin in the PCCS;
- The PCSS started under extreme conditions without problems;
- The injection phase of the Gravity Driven Cooling System (GDCCS) was successfully demonstrated
- Trapped air released from the drywell slightly reduced the PCC heat removal capacity
- Helium injected to the drywell later in the transient adversely affected the PCCS performance

For each test run, pre-test analyses have been performed with RELAP5/MOD3, in order to better define the test configuration and parameter range extensions. In addition, post-test analyses for each test run are being performed with RELAP5/MOD3, GOTHIC, TRAC/BF1, and MELCOR to benchmark the codes against the experimental data. A realistic PCC model (accounting for both primary and secondary side heat transfer) has been developed by the University of Valencia and incorporated in TRAC-BF. The RELAP5 results obtained so far are generally in good agreement with the experimental data of the PANDA tests, although some phenomena (e.g. recirculation in the PCC pools, mixing of gas and liquid spaces, tracking of more than one non-condensable gas, etc.) cannot be predicted due to the one-dimensional nature of the code.

4.4.3. Passive aerosol removal

The AIDA-PCCS experimental facility [8] was used to investigate the degradation of decay heat removal due to the fission product aerosols which might deposit on the inside surfaces of the heat exchanger tubes. One experiment using SnO_2 aerosol as simulant has been performed showing a decrease of the condenser efficiency of about 20%. This has been explained by a significant, but abnormal, aerosol deposition in the upper plenum of the heat exchanger. Pre- and post- test analyses have been performed using the MELCOR code, and the results show no degradation in the heat transfer. The conclusion is that the modelling in MELCOR is not adequate to simulate the experiment. Additional experiments (not foreseen in this project) would be necessary in order to develop and validate an improved model.

4.5. Project “European BWR-R&D-Cluster for Innovative Passive Safety Systems (IPSS)”

This project [9] is a “shared-cost” action which started in January 1996, and is being carried out by a consortium of 8 organisations (FZJ, ECN, GRS, KEMA, Stork Nukon, SIET, VTT, and the Paul Scherrer Institute) under the co-ordination of FZJ. The duration of the project is 36 months.

The objective of the project is to use the existing large scale test facilities *NOKO* (Germany) [11] and *PANDA* (Switzerland) [7] as well as the past experience of the *Dodewaard* reactor (Netherlands) for a co-ordinated experimental research programme on the reliability and features of selected passive safety systems for innovative BWRs (particularly Siemens’ SWR 1000). The project will also contribute to validating and improving thermal-

hydraulic computer codes with regard to natural convection of the coolant and passive decay heat removal both from the core region and from the containment. The R&D activities have been grouped in five Work Packages:

4.5.1. Natural convection in the reactor coolant system

Until its closure, the Dodewaard reactor was the only power reactor in the western world that demonstrated the characteristics and feasibility of coolant recirculation by natural convection without pumps even under full power. Data from steady-state and transient conditions of this reactor have been compared with the results obtained by different computer codes (ATHLET, TRAC-BF, RELAP).

4.5.2. Passive decay heat removal from the core region

Two types of passive decay heat removal systems are being tested and analysed: (i) Isolation Condensers (IC) and (ii) Emergency Condensers (EC). In the first case, the steam produced in the core region is condensed in heat exchangers placed outside the containment (e.g. SBWR) while in the second case they are located inside (e.g. SWR 1000, Dodewaard). In particular, the following aspects are being investigated: heat transfer in the condenser, influence of pressure, influence of water levels, condenser geometry variation, heat conductivity of materials, influence of non-condensable gases, heat transfer in the pools, start-up behaviour, function of siphons, and accident response.

The IC experimental programme, already completed, consisted in a series of tests which have been performed at the PANDA facilities using different flow rates of pure steam as well as steam-air and a steam-helium mixtures. Post-test calculations with RELAP5 have shown a good agreement with the experimental results, the maximum deviations being between -23% and + 25%. In overall, the code can be suitable to evaluate condensation phenomena with and without the presence of non-condensable gases, especially at low pressure (~3 bar). However the prediction accuracy decreases with increasing pressure.

The EC experimental programme, still on-going, consists in a series of tests performed at the NOKO facility. Two test bundles have been used. The first one (4 tubes) had been previously tested in a German-sponsored programme. The test matrix included a range of primary pressures between 1 to 7 MPa, and different water levels and temperatures in the secondary side (i.e. the condenser tank). In some of the experiments, a specially instrumented tube was installed in parallel to the four tubes of the NOKO bundle in order to study the two-phase flow patterns in a single tube. The experimental results of individual tests have been compared with calculated values obtained from several computer codes (APROS, ATHLET, CATHARE, RELAP5, TRAC) showing a fair agreement. A second optimised EC bundle, with thinner wall thickness to reduce the thermal resistance, will be tested during 1998.

Finally, the heat transfer from the condenser to the water side as well as the possible stratification in the pool area of both the NOKO EC and the PANDA IC have been analysed using the PHOENICS CFD code and the experimental results.

4.5.3. Application of steam jet pumps for passive safety systems

A study has been performed to identify potential safety-related applications of steam jet pumps in the nuclear industry (e.g. depressurization by water injection, decay heat

removal, shut-down). The experience from countries like Russia, US, Japan and Italy has been taken into account.

4.5.4. Passive initiators

Passive initiators can perform safety related functions without relying on external power and safety-grade control systems. The concept is based on the heating up of a fluid within the passive initiator which produces a pressure build-up. A number of tests has been performed at the NOKO facility in order to study the behaviour and feasibility of three different types of passive initiators. It is foreseen to enhance the operation regime by the use of alternative fluids with lower saturation temperatures. The results have led to recommendations of possible improvements and applications.

4.5.5. Passive decay heat removal from containment

Components for different versions of passive containment cooling are being studied within this Work Package: the Building Condenser (BC) with condensation outside the heat exchanger tubes (concept proposed in the SWR 1000), the Passive Containment Cooler (PCC) with condensation inside the heat exchanger tubes (concept proposed in the SBWR), and a Containment Plate Condenser (CPC) with surface condensation. The main R&D areas concentrate on heat transfer in the condensers, influence of non-condensable gases, pressure dependence, start-up behaviour and heat transfer in pools.

The BC experimental programme was carried out both at the PANDA and at the NOKO facilities. The test matrix of PANDA BC consisted of six system behaviour experiments simulating different loss of coolant accidents using prototypical fluids at prototypical conditions. Nitrogen and hydrogen were simulated by air and helium respectively. The experiments have shown that the BC behaves as expected under the range of conditions simulated. At the NOKO facility, more than 40 parametric tests with trough and a similar number without trough have been performed in a wide range of experimental conditions. These tests complemented those performed in PANDA and have produced a broad data base which will be used for code assessment and validation. In particular, the comparison of results from ATHLET, CFX-F3D, RALOC and RELAP/MELCOR calculations will indicate needs for further improvement.

The PCC experimental programme was carried out at the PANDA facility and consisted in a test simulating a main steam line break (base case) and several tests simulating extreme asymmetric break flow conditions coupled to reduced PCC capacity. Post-test calculations were performed using RELAP/MOD3.2, showing a good agreement with the experimental results.

The CPC experimental programme consists of two series of tests: one at the NOKO facility (already performed) and another (on-going) at the PANDA facility, using the same test objects. The analytical activities include calculations using the RALOC and the CFX-F3D computer codes.

4.6. Project “BWR Physics and Thermal-hydraulics Complementary Actions to the BWR R&D Cluster” (BWRCA)

The BWRCA project is a “Concerted Action” which started in January 1997, and was completed on 31 December 1997. It was carried out by a consortium of 6 organisations (CEA-

DRN, Siemens, ENEA, CIEMAT, University of Delft and FZ Rossendorf) under the co-ordination of CEA-DRN.

The work Programme of this “Concerted Action” can be considered as a natural complement of the activities developed in project “IPSS” described above. In fact, a co-operation scheme was agreed between both projects in order to define the contents of the work packages, exchange information and assign responsibilities. Four work packages were defined:

4.6.1. Thermal valve modelization and assessment

The feasibility and behaviour of a so called “thermal valve” [13], which may achieve smooth and passive activation of isolation condensers (IC) was investigated, and a conceptual design resulted from it. Two computer codes, CATHARE and RELAP5, were used to model and perform calculations for steady state and transient conditions. These calculations have confirmed the effectiveness of the preliminary design of the “thermal valve”. The results though were not completely conclusive and some code weaknesses have been detected.

4.6.2. Theoretical support to NOKO-EC experiments

Selected NOKO-EC experiments of the “IPSS” project were analysed using two computer codes (CATHARE, ATHLET). The comparison of global calculated values with the experimental results showed good agreement for high and medium steam pressures, but not for small steam pressures. In addition to these post-test analyses, support to the NOKO experiments on two-phase flow instrumentation, test preparation, and optimisation of passive components was provided by the project partners. An State of the Art on condensation phenomena within tubes (vertical and horizontal), with and without non-condensable gases, was also produced.

4.6.3. Modelisation and assessment of the building condenser (BC)

Post-test analyses on selected BC experiments carried out in NOKO within the “IPSS” project were performed using TUBEX. The CEA’s TUBEX software has been developed to evaluate the condensation efficiency for a transversal flow through a bundle of smooth tubes. The results on the exchanged power show a good agreement with the experimental data.

4.6.4. BWR core dynamics and thermal-hydraulic

The 3D power distribution and neutronic characteristics of the Dodewaard core have been investigated using different computer codes: APOLLO1, HELIOS, RAMONA, CRONOS, DYN3D. The neutron cross-section libraries for the Dodewaard fuel assemblies were generated from raw data of the reactor’s operating cycle 26. A substantial effort was necessary to elaborate the input decks of these codes, to couple them to thermal-hydraulics codes (ATHLET, FLICA-4) and to validate all the tools in order to simulate the complex dynamics of BWRs natural circulation.

Results from measurements taken at the *DESIRE* loop of the University of Delft [14] as well as from the Dodewaard reactor have been used to conduct an experimental and theoretical research on natural circulation for BWR static and dynamic conditions, in particular to study the relationship between the core and riser void fraction and the natural circulation flow rate.

4.7. Project “Innovative-containment Cooling for Double Concrete Containment” (INCON)

This project is a “shared-cost” action which started in January 1996, and was carried out by a consortium of 6 organisations (ENEL, ANSALDO, CIRTEN, Empresarios Agrupados, EdF-SEPTEN, and the Paul Scherrer Institute) under the co-ordination of ENEL. The project was completed on 30 April 1998.

The objective of this project was to study the phenomenological aspects of innovative containment cooling for a rugged double concrete containment, which meets the European Utility Requirements (EUR Document). The proposed experiments were to be carried out at the CISE (Italy) and LINX (Switzerland) facilities, and were based on some alternative solutions, which had been screened out as results of a previous extensive research programme performed by ENEL together with ANSALDO and CISE in the last five years. The design to be used consist basically of three components : an inner heat exchanger located in the “inside” containment, an outer heat exchanger immersed in an external pool, both located in the “outside” containment, and an intermediate circuit connecting the inner and the outer heat exchangers. Two alternative solutions for the inner heat exchanger will be assessed in this project : (i) a “compact” device consisting of straight finned tubes, and (ii) a plate-type device. Three main work packages have been defined in this project :

4.7.1. Inner finned tube heat exchanger tests

The experimental activities consisted of a series of functional and characterisation tests of single and bundle finned tube heat exchangers in both natural and forced circulation conditions for different containment atmosphere compositions and tube geometries. The functional tests were performed at CISE while the characterisation tests were carried out at PSI. The results have showed that the heat transfer of the tested concept is efficient even in the presence of high non-condensable gas concentrations. The analytical activities focused on the assessment and development of correlations and physical models as well as extrapolation of test results to the full scale system. The basic models for predicting heat transfer on finned tubes under natural and forced convection developed by CIRTEN, CISE, and PSI have shown in general good agreement with the experimental results.

4.7.2. Inner Plate Type Heat Exchanger Tests

This alternative solution uses a plate type internal heat exchanger in which two metal liners conforming a “water jacket” are anchored to the inner surface of the primary (i.e. “inside”) containment. The heat from the containment atmosphere is transferred to the water jacket. Then the water boils and the steam produced is condensed on an external heat exchanger connected to it. The water jacket mock-up as well as its supporting structure were designed and constructed by Ansaldo. The main objective was to evaluate the thermomechanical stresses of both heat exchanger and structure under the most challenging conditions. Pre-test analyses were performed using the GOTHIC code coupled to the LEGO code for the mock-up sizing. Four tests at different conditions (i.e. pressure, temperature, and temperature gradient) were performed. The main conclusion was that the real displacements are higher than expected due to the flexibility of the structure. Therefore lower tolerances would be necessary if the real system is manufactured.

4.7.3. Intermediate loop and integrated systems tests

The thermal-hydraulic behaviour of the intermediate loop was studied through an experimental test programme covering a wide range of steady state and transient conditions and configurations (e.g. presence of non-condensable gases, hydrogen deflagration). From the analysis of experimental results, the optimum water inventory and tube slope were determined. A model of the test facility was built using the RELAP5 code in order to perform pre and post-test analyses.

The interactions among the different natural circulation loops (containment atmosphere, intermediate two phase fluid, pool water and external air flow after the pool water level decreases) as well as the system response time have been investigated using a dedicated facility built at CISE. Both transient and steady state conditions tests have basically confirmed the design assumptions and performances, and a data base has been elaborated. The integral system has been simulated by means of the LEGO computer code library modules, and the validation of the model successfully achieved for steady state conditions.

4.8. Project “Containment Behaviour in the Event of Core Melting with Large Gaseous and Aerosol Releases” (CONGA)

This project is a “shared-cost” action which started in January 1997, and is being carried out by a consortium of 5 organisations (Siemens, ENEL, CIEMAT, JRC-ISIS and the Paul Scherrer Institute) under the co-ordination of Siemens. The duration of the project is 24 months.

The main objective of this project is to investigate the phenomena and processes occurring inside different types of containments for some new reactor concepts (e.g., EPP with double containment for PWRs and SWR 1000 for BWRs) in the event of core melt accompanied by the release of large quantities of non-condensable gases (particularly hydrogen) and aerosols. These new containment designs foresee the use of passive systems consisting of several units of quasi-horizontal finned tubes bundles. Steam released into the containment atmosphere condenses onto these tubes which are internally cooled by water under natural circulation regime. The energy absorbed by the coolant is then discharged into a pool which acts as a heat sink for at least three days. The experiments are being performed at four different facilities: *DRAGON* (PSI, Switzerland), *STORM* (JRC/ISIS, Italy), *CISE* (Italy) and *PECA* (CIEMAT, Spain). Emphasis will be put on the following aspects :

4.8.1. The effect of aerosol deposition on heat-exchange surfaces in the containment atmosphere.

This will be investigated at the *DRAGON* and *STORM* [10] facilities using two different test objects: (i) an arrangement of five finned tubes in two layers with different tube geometries (i.e. PWR and BWR), and (ii) a mock-up of a real heat exchanger consisting of several layers of inclined tubes with only one tube geometry (PWR type). Two pressure vessels, one for each object, will be required to perform the scheduled tests. The reference accident scenarios for the reference plants (i.e. Italian PUN design for PWR and German SWR 1000 design for BWR) to establish the initial and boundary conditions required for the experimental work were firstly defined.

Most of the tests will be performed using insoluble solid SnO_2 particles to simulate aerosols; however some tests have been foreseen with a mixture of soluble and insoluble

aerosols (i.e. CsOH/SnO₂) in order to reproduce prototypical accident scenario conditions. The range of the most relevant test parameters will be: pressures between 1 bar to 3 bar absolute, gas temperatures between 120 to 150 ° C, gas mass flow rate between 230 Kg/h (DRAGON) and 750 Kg/h (STORM), and aerosol mass concentrations between 1 and 5 g/m³. The experimental results will be used to define a theoretical correlation for a single tube which accounts for the aerosols deposition. The basic models for predicting heat transfer on finned tubes under natural and forced convection developed by CIRTEN, CISE, and PSI in the INCON project (see section 4.7) will be used to establish a preliminary correlation.

4.8.2. The effect of large hydrogen concentrations on heat transfer (and thus on containment pressure).

This has been investigated at the CISE facilities using two different heat exchangers mock-ups, one typical for PWRs (identical to the mock-up used in the INCON project mentioned above) and another typical for BWRs which was manufactured especially for this project. The hydrogen (simulated by Helium) concentrations studied ranged between 20 % by volume (maximum value tested in the INCON project) and 80 % by volume (maximum possible value for the SWR1000 containment). The tests have shown that the measured heat flux is scarcely influenced by the coolant temperature whereas it is mainly dependant on steam partial pressure in the gas mixture, and that the heat transfer reduction is very steep when injecting helium at low helium/steam mass ratios and smooth at higher helium/steam mass ratios.

4.8.3. The effect of large aerosols releases into typical BWR plants with pressure suppression type containment.

The main objective is to investigate the potential reduction of containment pressure in BWR plants by using the existing plant gaseous waste treatment ("off-gas") systems for exhausting the non-condensable gases (H₂, N₂, air) to the atmosphere. This off-gas system consists mainly of a catalytic recombiner for hydrogen removal, a condenser and a charcoal filter system. The presence of large quantities of aerosols could degrade the functional capability of the recombiner line.

Two series of tests were planned to be performed at the CIEMAT's PECA facility [12] in order to study: (i) the aerosol retention and concentration in the suppression chamber on the long term, and (ii) the aerosol and hydrogen behaviour in the recombiner line of the "off-gas" systems in order to determine the aerosol deposition and the potential degradation of the catalytic material. The first series of experiments has already been completed. The SPARC and CONTAIN codes were used to calculate the preliminary decontamination factors associated to the injection of a mixture of aerosols-gas in the suppression pool. The preliminary results have shown that (i) the presence of steam produces agglomeration of the aerosols and, thus, the particle size grows and its shape becomes more irregular than in absence of steam; (ii) the aerosol concentration in the vessel gas space is 10 times lower than the one injected, and (iii) the bubble size when injecting the aerosol-gas mixture is smaller than when injecting only steam.

5. CONCLUSIONS

International research programmes can offer a cost effective opportunity to investigate multidisciplinary and complex problems like those encountered in the development of Innovative Passive Safety Systems for the next-generation reactors. Although, relatively

recent, the EC-sponsored projects on this area are proving to be an efficient means to gain the necessary phenomenological knowledge and solve the challenging problems, many times of generic nature, posed by the characteristically small driving forces of these systems. In all these projects the collaboration of organisations of different EU member states is enforced. This has contributed to stimulate co-operation among public and private organisations, to avoid duplication efforts and to use the available resources in an efficient way.

The projects of Area A.1 of the EU 1994-1998 Nuclear Fission Safety R&D Programme, "Exploring Innovative Approaches/Conceptual Reactor Safety Features" have been grouped under a common cluster known as "INNO". At present there are 10 projects in this INNO cluster which involve 25 different organisations from 7 EU State Members. In 5 of these projects there is also an important participation of the Paul Scherrer Institute (PSI) from Switzerland. Most of these projects include both experimental and analytical activities directed mainly to study the phenomena and issues associated with the use of innovative systems for decay heat removal from both the core region and the containment building of Light Water Reactors (LWRs).

The experiments are being performed in some of the most important large-scale (e.g. PANDA, NOKO, PACTEL) and separate-effect (e.g. LINX, EPICE, SUCOT, MUCON, STORM, AIDA, PECA, etc.) thermal-hydraulic test facilities in Europe. The use of different neutronics and thermal-hydraulic computer codes (ATHLET, CATHARE, TRAC, RELAP5, etc.) is an important part of the work programmes of these projects, as it enables to define better the test configuration and parameter range extensions, to benchmark the codes against experimental data, and to extrapolate the results of the small scale experiments towards full scale reactor applications.

REFERENCES

- [1] "FISA-97 - EU Research on Severe Accidents". Mid-term review symposium on shared-cost and concerted actions in reactor safety, EUR 18258 EN, Office for Official Publications of the European Communities, 1998.
- [2] CATTADORI, G., GALBIATI, L., MAZZOCCHI, L. VANINI, P., 1995, "A Single-Stage High Pressure Steam Injector for Next Generation Reactors : Tests, Results and Analysis"; *Int. J. Multiphase Flow*, 21, 4, pp. 591-606.
- [3] TUUNANEN, J., VIHAVAINEN, J., 25-27 August 1997, "PACTEL experiment programme for the investigation of passive safety injection systems of advanced light water reactors". Post-SMIRT 14 Seminar, Pisa, Italy.
- [4] VIRTANEN, E., HAAPALEHTO, T., KOUHIA, J., September 10-15, 1995, "Analysis of steam generator loss of feed later experiments with APROS and RELAP5/MOD3.1 codes"; Seventh International Topical Meeting on Nuclear Reactor Thermal Hydraulics (NURETH-7), , Saratoga Springs, USA.
- [5] STOOP, P.M., SPOELSTRA, S., HUGGENBERGER, M., YADIGAROGLU, G., May 26-30, 1997, "TEPSS - Technology Enhancement of Passive Safety Systems" I CONES-2172, Proceedings of ICONE5, Nice, France.

- [6] DE CACHARD, F. et al., May 26-30, 1997, "The first LINX-2 Tests", Proceedings of ICONE 5: 5th International Conference on Nuclear Engineering, Nice, France.
- [7] FISCHER, O., et al., June 1-4, 1997, "PANDA asymmetric-configuration passive decay heat removal test results", Proceedings of the 2nd International Conference on Advanced Reactor Safety (ARS497), Orlando, Florida (USA)
- [8] GÜNTAY, S., VARADI, G., DREIER, J., November 21-24, 1994, "Advanced Light Water Reactor Passive Heat Removal and Aerosol Program", IAEA Advisory Group Meeting on Technical Feasibility of Passive Safety Systems, Jülich, Germany, IAEA TECDOC 920, p 231-251.
- [9] HICKEN, E.F. and VON LENSE, W., November 1996, "European BWR R&D Cluster for innovative passive safety systems", Kerntechnik, Carl Hauser Verlag, Vol. 61, N° 5-6.
- [10] KRASENBRINK, A., HUMMEL, R., HAUTOJÄRVI, A., AREIA CAPITÃO, J., DE SANTI, G., 4-6 June, 1996, "Simplified Tests On Resuspension Mechanisms. The STORM Project". Proceedings of an ENS Class 1 Topical Meeting on "Research Facilities for the Future of Nuclear Energy", Brussels, Belgium. p 414-422
- [11] HICKEN, E.F., JAEGER, H., SCHAFFRATH, A., 16-19 May, 1995, "The Study of Effectiveness of the Emergency Condenser of the BWR 600/1000 in the NOKO Test Facility", IAEA Technical Committee Meeting, Progress in Design, Research and Development for Advanced Water Cooled Reactors; Piacenza, Italy.
- [12] MARCOS CRESPO, M.J., GÓMEZ MORENO, F.J., MELCHES SERRANO, I., MARTÍN ESPIGARES, M., LÓPEZ JIMÉNEZ, J., 1993; "LACE-ESPAÑA Experimental Programme on the retention of aerosols in water pools", EUR-15455EN.
- [13] BIANCHI, F., MELONI, P., GAUTHIER, G.M., PIGNATEL, J.F., 25-27 August 1997, "Thermal Valve System for LWR applications", Post-SMIRT 14 Seminar, Pisa, Italy.
- [14] VAN DER HAGEN, T.H.J.J., VAN DAM, H. AND KOK, H.V. 1996; "The Delft DESIRE facility for studies on (natural circulation) BWR primary system statics & dynamics", Proceedings of an ENS Class 1 Topical Meeting on Research Facilities for the Future of Nuclear Energy, June 4-6, Brussels, Belgium, p 365-371.

<p>NEXT PAGE(S) left BLANK</p>



TEPSS RELATED PANDA TESTS (ESBWR)

M. HUGGENBERGER, C. AUBERT, T. BANDURSKI,
J. DREIER, O. FISCHER, H.J. STRASSBERGER
Thermal-Hydraulics Laboratory,
Paul Scherrer Institute,
Villigen

G. YADIGAROGLU
Swiss Federal Institute of Technology,
ETH-Zentrum/ CLT,
Zurich

Switzerland

Abstract

A number of test series to investigate passive safety systems for the next generation of Light Water Reactors have been performed in the PANDA facility at the Paul Scherrer Institute (PSI). The large scale thermal-hydraulic test facility allows to investigate Passive Containment Cooling Systems (PCCS) and the long-term containment behaviour after a Loss of Coolant Accident (LOCA). After successful completion of the ALPHA phase-I test series, where the PCCS performance of the Simplified Boiling Water Reactor (SBWR) was examined, phase-II was initiated in 1996 with new projects, all with international participation (EC Fourth Framework Programme on Nuclear Fission Safety). One of these projects is entitled „Technology Enhancement for Passive Safety Systems" (TEPSS). TEPSS is focused on the European Simplified Boiling Water Reactor (ESBWR). Several new containment features and PCCS long-term response under different LOCA scenarios were investigated in PANDA. The PCCS start-up was demonstrated under challenging conditions. The effect of nitrogen hidden somewhere in the drywell and released later in the transient was simulated by injecting air for a certain period into the drywell. The effect of light gases on the PCCS performance was investigated by helium injection to the drywell. Finally, the influence of low PCC pool levels on PCCS and containment performance was examined. The main findings were that the PCCS works as intended and shows generally a favourable and robust long-term post LOCA behaviour. The system starts working even under extreme conditions and trapped air released from the drywell later in the transient does only temporarily reduce the PCCS performance. The new PANDA test series provided an extensive data base which will contribute to further improve containment design of passive plants and allow for system code assessment in a wide parameter range.

1. INTRODUCTION

The Paul Scherrer Institute initiated in 1991 the experimental and analytical program ALPHA (Advanced Light Water Reactor Passive Heat Removal and Aerosol Retention Program) [1]. The objectives of this program are to investigate long-term decay heat removal and aerosol transport for the next generation of passive light water reactors. During phase I of this program the long-term LOCA response and performance of the Passive Containment Cooling System (PCCS) of the General Electric (GE) Simplified Boiling Water Reactor (SBWR) were investigated. The ALPHA I program included four major parts: the large scale, integral system behaviour test facility PANDA; an investigation of natural convection and mixing in pools and large volumes (LINX Experiment); a separate-effect study of aerosol transport and deposition in headers and tubes of passive containment coolers (AIDA Experiment); finally, the data from the PANDA facility and supporting separate effects tests were used to develop and qualify models and provide validation of relevant system codes. After completion of ALPHA I, phase II was initiated in 1996 with three new projects, all with international participation (European Commission, Fourth Framework Programme on Nuclear Fission Safety). Different types of passive containment cooling systems for different advanced light water reactor concepts were investigated in the existing facilities PANDA, LINX and AIDA. One of these new projects is

entitled "Technology Enhancement for Passive Safety Systems" (TEPSS) [2]. TEPSS is focused on the European Simplified Boiling Water Reactor (ESBWR). The project has three Work Packages (WP). In WP1 suppression pool mixing and stratification phenomena in large pools are investigated in LINX. The innovative passive decay heat removal system was tested in PANDA (WP2). The deposition of aerosols in condensers was investigated in AIDA (WP3). The project is being conducted by partners from the Netherlands (ECN, Stork NUCON BV, KEMA), Spain (CIEMAT, Universities of Valencia and Catalonia) and Switzerland (PSI). The 1190 MWe ESBWR is a design evolution of the 670 MWe SBWR and utilizes the modular design of passive safety systems. Because of the power up-rate, several technology enhancements became necessary. In order to simulate the ESBWR configuration the PANDA facility was modified accordingly. A test matrix has been defined and ESBWR system calculations were performed by the project partners to establish the test initial conditions. Pre-test calculations were done with different system analysis codes. The PANDA test series started in December 1997 and was completed in March 1998. The main objectives of the tests were the experimental investigation of the new containment features and to provide a data base for system code assessment and analysis of particular phenomena. Post-test calculations with different computer codes (RELAP5, TRAC-BF, MELCOR and GOTHIC) were performed by the project partners.

2. ESBWR CONTAINMENT CONFIGURATION AND PASSIVE SAFETY SYSTEMS

The ESBWR is being developed by an international team of utilities, designers and researchers. The plant is designed to meet the requirements formulated in the European Utility Requirements Document for future light water reactor power plants. The plant uses the modular design of the SBWR passive safety system [3] and takes advantage of the economy of scale. As can be seen from Figure 1, the advanced containment system has several new features. A major change is related to the passive emergency core cooling system. The gas space above the Gravity Driven Cooling System (GDCS) water pool is now connected to the wetwell gas space instead of the drywell. As a consequence, the wetwell gas space volume increases during the GDCS injection phase, as water drains from the GDCS pools to the reactor pressure vessel. The increasing wetwell (WW) volume provides more pressure margin for a given WW size. This also allows for more efficient use of the GDCS pool and WW gas space volumes, leading to a more compact containment design and improvement of overall plant economics. Another design change has been made to the PCCS. Because the GDCS pool is now part of the wetwell, it was necessary to reroute the PCC condensate flow. The drain flow now goes directly from the PCC lower headers to the reactor pressure vessel. This new arrangement is also shown in Figure 1.

3. PANDA - AN INTEGRAL CONTAINMENT TEST FACILITY

PANDA is a scaled thermal-hydraulic test facility for investigating passive decay heat removal systems for the next generation of Light Water Reactors (LWR). The PANDA facility was first used to investigate the LOCA containment response of the Simplified Boiling Water Reactor (SBWR). As shown in Figure 1, PANDA has a modular structure. The relevant LWR containment volumes are simulated by six cylindrical pressure vessels representing the Reactor Pressure Vessel (RPV), Drywell (DW), Wetwell (WW) and Gravity Driven Cooling System (GDCS) pool. Four rectangular pools open to the atmosphere contain three Passive Containment Coolers (PCC) and one Isolation Condenser (IC). One PCC is connected to DW1 and two units are connected to DW2. The Isolation Condenser (IC) is connected to the RPV. Both the drywell and wetwell are simulated by two vessels. The two drywell vessels are interconnected by a large diameter pipe. The wetwell has two large interconnecting lines: one in the gas space and the second connecting the two suppression pools. This arrangement allows for investigation of three dimensional effects, such as the distribution of steam and non-condensable gases and mixing

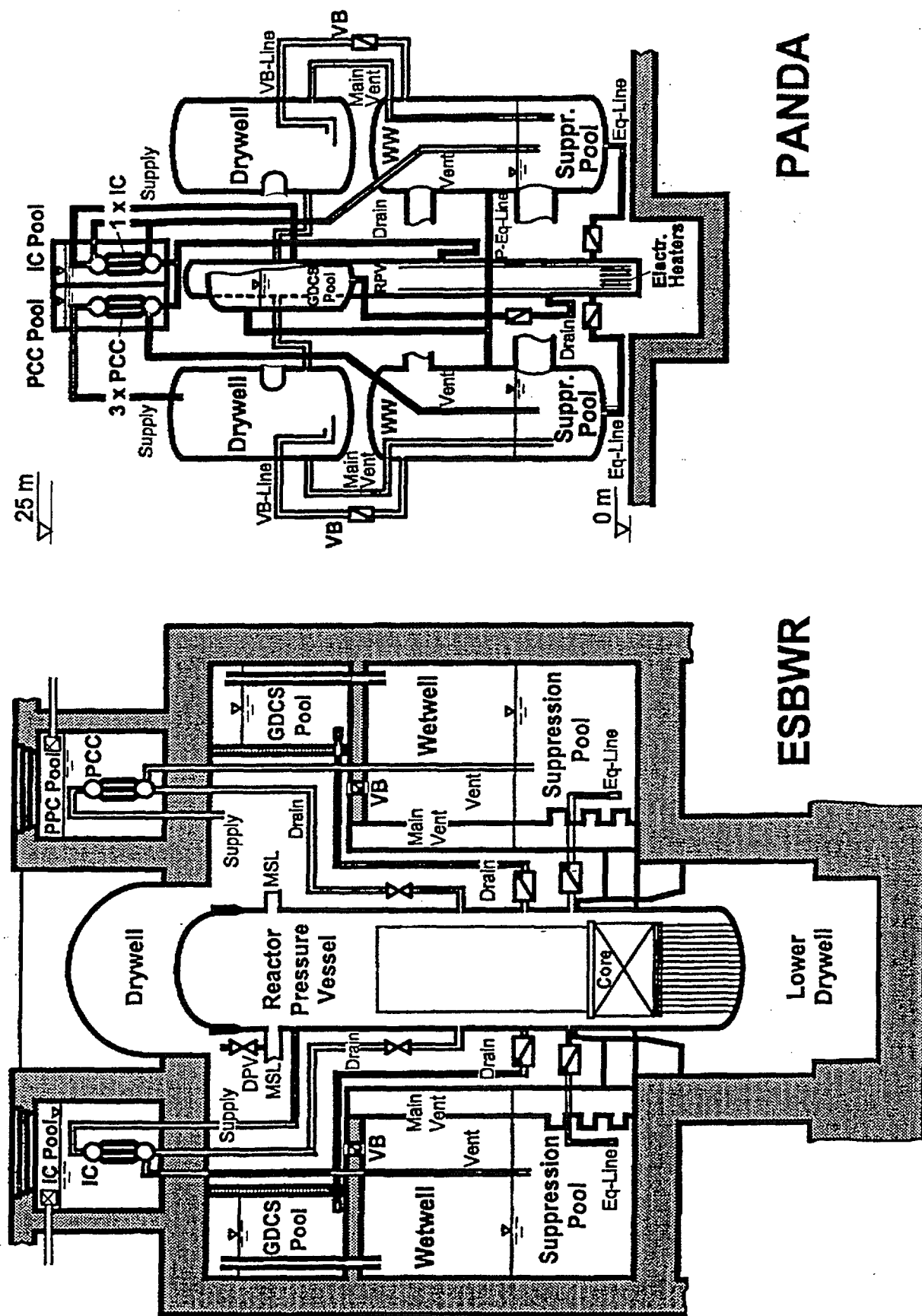


FIG. 1. ESBWR versus PANDA, schematic view of ESBWR containment and PANDA facility, including PCCS and ICS.

within the containment. The vessels, pools and condensers are interconnected by system lines. The pressure loss characteristics of these lines can be adjusted to the required values by exchangeable orifice plates. This arrangement provides flexibility to investigate a variety of containment designs and passive decay heat removal concepts. The total volume of the vessels is about 515 M³ and the height of the facility is 25 m. The installed heater power in the reactor pressure vessel is 1.5 MW and the facility is designed for 10 bar and 180 °C maximum operating conditions. Auxiliary systems can supply water, steam, and gas to any vessel. The primary purpose of these systems is to establish the proper test initial conditions (temperature, pressure, gas concentration and water inventories). Experience from the previous test series has demonstrated that the specified initial conditions can be matched very precisely (e.g. temperatures better than ± 2 K). Under certain circumstances, auxiliary systems may also be used during a test. The facility is controlled with a Programmable Logic Controller (PLC) system, which is governed by a work station-based graphical display Man/Machine Interface with online data visualization. More than 600 sensors are installed in the facility for measuring temperatures, pressures, pressure differences, pool levels, flow rates, gas concentrations, fluid phases and electrical heater power. The measurements are sampled with an integrated data acquisition system, which includes data conversion to engineering units. The data are forwarded to a work station based storage system, which provides capabilities for on-line and off-line time history representation of measurements. The data are finally transferred to the PANDA experimental data base.

A detailed scaling analysis was performed for the PANDA SBWR-related test program. This scaling study has been updated by Stork NUCON for the new ESBWR test series relating to a higher power level reactor plant design with its slightly altered passive decay heat rejection systems. The main results of the study were: The ratio between the corresponding scales of prototype and PANDA is $\sim 1:40$ for power and volume. The relevant heights are $\sim 1:1$. Prototypical fluids under prototypical thermodynamic conditions were used in PANDA; the nitrogen initially filling the containment was, however, replaced by air. The hydrogen released in case of a severe accident was simulated by helium. A number of facility characterisation tests were performed to obtain data about mass leak rates, heat losses and system line pressure losses [4].

4. TRANSIENT SYSTEM TEST MATRIX

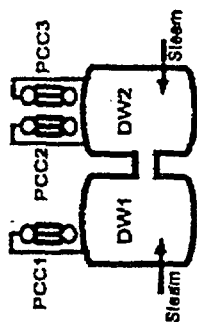
The main objective of the PANDA test program was to make a significant contribution to the technology enhancement of passive safety systems by experimentally investigating the new containment features of the ESBWR design. The first test (P1) represents the “Base Case Test” which is a simulation of the long-term PCCS cooling phase following a LOCA caused by a Main Steam Line Break (MSLB). Perturbations are made to this basic test to assess the effect of specific systems, PCCS start-up, system interactions, and to investigate three-dimensional effects such as the distribution of steam and noncondensable gases (air and helium) within the containment. The test matrix includes eight transient system tests (P1 to P8). The main characteristics and the facility configurations for the individual tests are given in Figure 2.

5. TEST RESULTS

The “Base Case Test” P1 started with initial conditions which correspond to the status of the system at one hour after main steam line break initiation. At that time the RPV was depressurized, the GDACS injection phase was over and steam production caused by decay heat in the RPV had resumed. The initial system pressure was roughly 2.5 bar. The facility configuration (Figure 2) was as follows: The break flow from the RPV was directed equally to both drywells

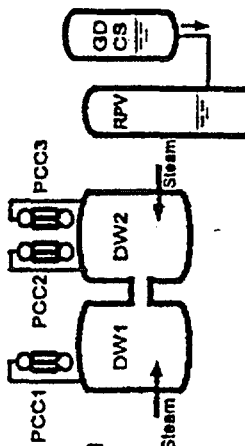
P1: Base Case

MSL break LOCA + 1 hr
(long-term PCCS cooling phase)



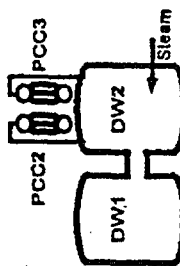
P2: Early Start

MSL break LOCA + 20 min
(transition from GD/CS
injection to long-term
PCCS cooling phase)



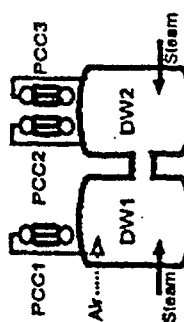
P3: PCCS Start-up

DW initially filled with air
(demonstrate PCCS start-up
under challenging conditions)



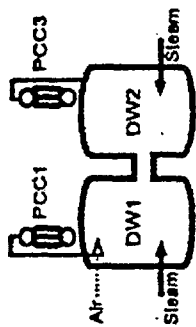
P4: Trapped Air In DW:

Air released during transient
(investigation of how n/c gas
affects PCCS performance)



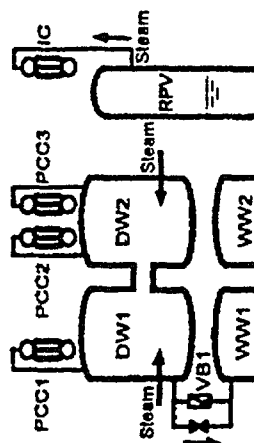
P5: Symmetric Case

PCC2 isolated,
air supply to DW later in transient
(MV clearing phase, caused by
reduced PCC capacity)



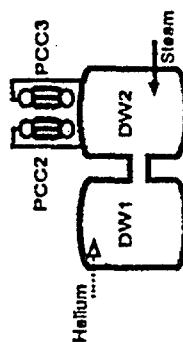
P6: Systems Interaction

ICS and PCCS in parallel,
DW1 to WW1 leakage
(is PCCS performance
adversely affected?)



P7: Severe Accident

All break flow to DW2,
PCC1 isolated,
He supply to DW later in transient
(simulation of hydrogen release
and reduced PCC capacity)



P8: PCC Pool Boil Down

Extension of Base Case P1,
(how do low PCC pool levels affect
containment performance?)

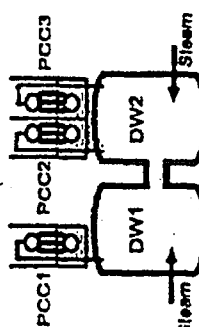


FIG. 2. PANDA facility configurations and main characteristics for the P-series transient system tests.

and all three PCC units were connected to the DWs. The RPV heater power followed the scaled decay heat curve. The test duration was 20 hours. The "PCC Pool Boil Down Test" P8 was performed as an extension of P1. The objective was to investigate the effect of low PCC pool levels on the PCCS performance and containment behaviour in the case where the PCC pools would not be refilled after the "no operator action" period and the pools would boil off further.

The PCCS started working immediately after test P1 was initiated. The main vents cleared during the first 20 minutes into the test. After that the PCCS removed all decay heat. The PCC vent lines cleared during the first half hour after test initiation. There was no significant energy addition to the suppression pool over the duration of test P1. Figure 3 shows the RPV, DW and WW pressure responses. About 3.5 hours after test start the DW pressure had dropped below WW pressure and the vacuum breaker between DW1 and WW1 opened for a short time. The air content of the drywell increased momentarily and the condensation rate of the PCCs were temporarily reduced because of air accumulation in the PCC tubes. Consequently, the DW pressure rose to the initial value and then remained almost constant for the first 15 hours into the test. Later on, the pressure slightly decreased until the end of test P1. Figure 4 shows the water levels in the hydraulically isolated PCC pools. At about 10 hours into the test the PCC tubes started to be partially uncovered (top of PCC tube bundle is at 2.8 m). At the end of test P1 only 0.60 m of the 1.75 m long PCC tubes were covered with water. The partially uncovered tubes to the end of P1 did not adversely impact the overall system performance, because there was still more than enough heat transfer area available to condense all the steam. The water levels in all three PCC pools dropped fairly equal, indicating that each PCC took roughly the same load. This

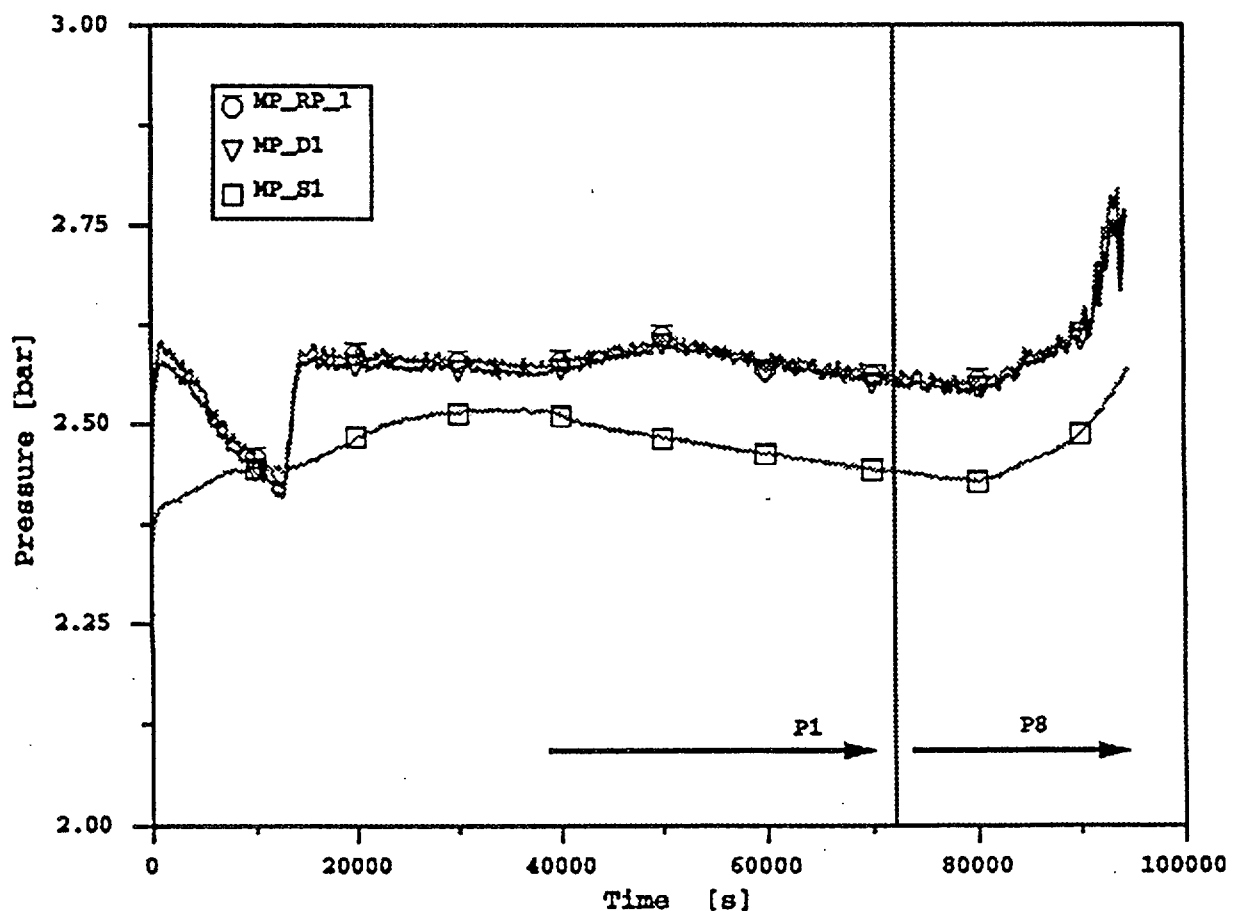


FIG. 3. RPV (MP-RP-1), DW (MP-D 1) and WW (MP-S1) pressures.

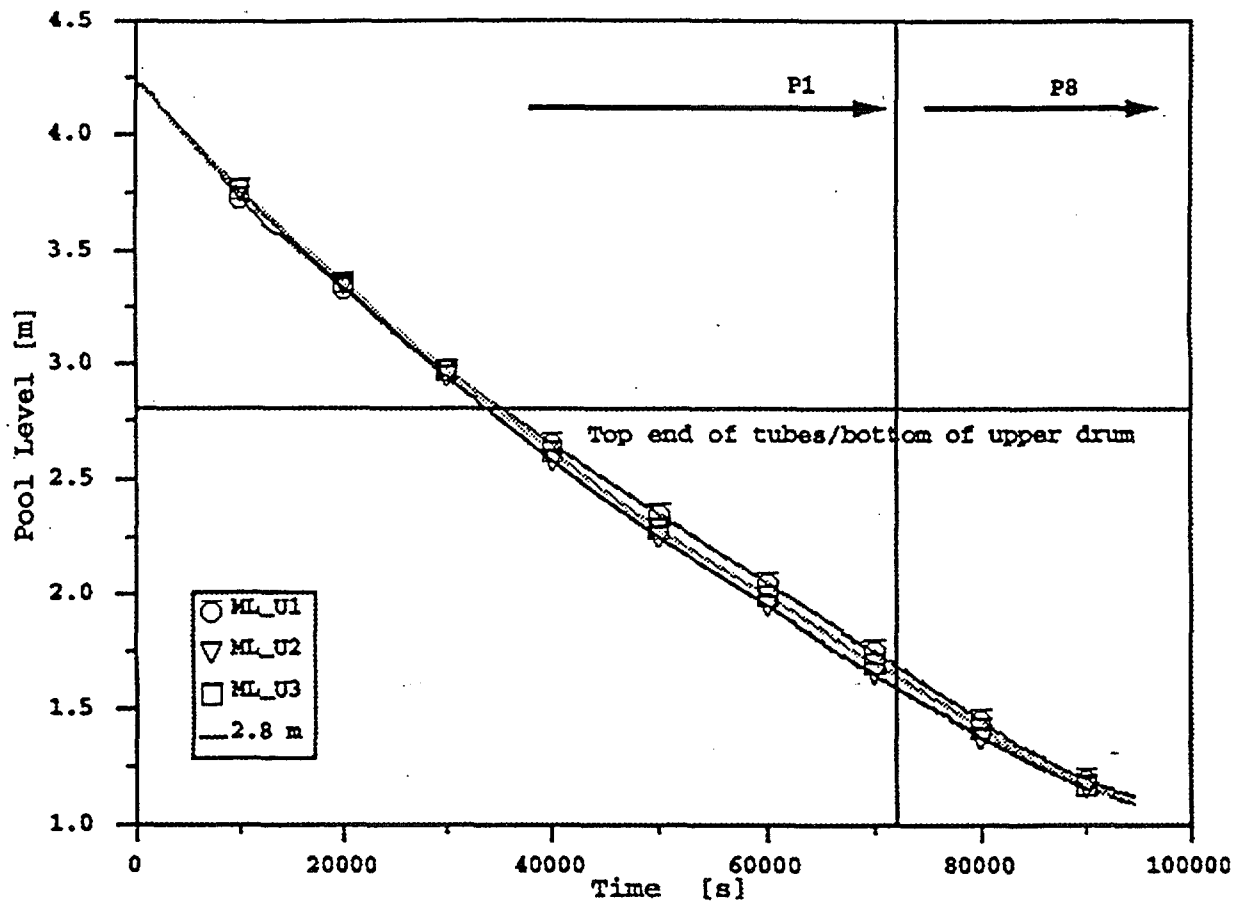


FIG. 4. PCC pool levels (ML-U1... 3).

is also confirmed by the measured feed flows to the individual PCC units. The “Base Case Test” P1 has demonstrated a favourable and robust long-term PCCS and containment behaviour.

The “PCC Pool Boil Down Test” P8 was run as an extension of P1. During test P8 the RPV heater power was kept constant at the scaled decay heat level reached at the end of P1 (570 kW). The initial PCC pool levels were roughly 1.65 m. For the first 2 hours into test P8, the PCCS was able to condense all the steam from the containment. At the end of this period the PCC pool levels had dropped to 1.45 m and only 0.4 m of the PCC tubes were still covered with water. That means that 23% of the 1.75 m long PCC tube bundles were sufficient to remove 570 kW from the containment. Two hours into test P8, the RPV water level started to drop significantly faster than before, indicating that less condensate from the PCCs returned to the RPV. The PCC vent phase detectors indicated frequent flow from the PCC lower drums through the PCC vent lines down to the suppression chamber. As a consequence of the excess steam vented to the suppression pool, the water temperatures in the upper pool region and the WW gas space temperatures started to rise. This finally resulted in an increasing system pressure (Figure 3). The test was completed after the PCC pool levels reached the top of the PCC lower drums. The “PCC Pool Boil Down Test” demonstrated that the PCCs are able to take a significant amount of decay heat from the containment, even at very low PCC pool levels.

Test P2 is the “Early Start Test”. The test objective was to provide data for the transition period from the GDCS injection phase to the long-term PCCS cooling phase of the post-LOCA transient. The test initial conditions for P2 were established based on the predicted state of the ESBWR at 20 minutes into the LOCA. At that time the water level in the RPV was low and

subcooled water from the GDCS pool was draining to the RPV, suppressing steam production in the RPV. Immediately after test initiation the pressure in the drywell dropped below wetwell pressure and the vacuum breakers opened. After GDCS flow to the RPV had stopped, the steam production finally recovered and the PCCS started to operate. After a short period with main vent clearing, all decay heat was removed equally by the three PCC units. The biased open check valve in the GDCS drain line allowed some back flow from RPV to the GDCS pool. Later, this water was drained back to the RPV, causing an other vacuum breaker opening at 7000 seconds into the transient. The overall system behaviour was not affected by the vacuum breaker opening and there was no significant energy deposition in the wetwell. Test P2 has successfully demonstrated the transition period from the GDCS injection phase to the long-term PCCS cooling phase.

Test P3 is the “PCCS Startup Test”. The test initial conditions were quite different from the other P-series tests. The drywell and the condensers were initially filled with air. The system pressure was roughly 1.3 bar (instead of 2.5 bar) and the DW temperature was about 30 °C (instead of 130 °C). The RPV heater power remained constant throughout the test (0.85 MW). Immediately after test initiation the PCCS started purging the air from the drywell to the wetwell. The drywell was heated up and pressurized to the “normal” post LOCA conditions within the first 5000 seconds. Then the main vents started to clear because only two PCCs were not sufficient to take the whole heat load. Because of this continues energy transfer to the wetwell, the system pressure increased slightly until the end of test. Test P3 successfully demonstrated the PCCS start-up under extremely difficult conditions.

The “Trapped Air Test” P4 investigated how trapped air somewhere in the DW and released later in the transient does affect the PCCS performance. The release of non-condensable gas was simulated by injecting air to the top of DW1 for a period of 30 minutes. The initial conditions and the facility configuration were the same as for the “Base Case Test”. The test duration was 8 hours. Before air injection was initiated the test showed the same system behaviour as the “Base Case Test”. At four hours into the test, system pressure started to increase, caused by the injected air. The PCCS heat removal capability was slightly reduced by the non-condensable gas. After the injection phase was completed the air was purged from DW to WW and the system showed again normal long-term PCCS operation. Trapped air, released from DW later in the transient, only temporarily affected the PCCS performance.

Test P5 is the “Symmetric Case with Two PCCs only”. As shown in Figure 2, each DW had one PCC connected and the break flow was directed equally to both drywells. The initial conditions for this test were the same as for the “Base Case Test”. During the first 4 hours of test, two PCCs were not able to remove all decay heat from the drywell, therefore, the main vents to the suppression pool cleared and energy was transferred to the WW. Consequently, the WW pressure slightly rised. Like in test P4, air was injected to DW1, starting at 4 hours into the transient for a period of 30 minutes. As could be expected the PCCS heat removal capability was temporarily reduced until the injected air was transferred from DW to the WW gas space.

The objective of test P6 was to examine the interaction between the IC operating in parallel with all PCC units. In addition, the effect of drywell to wetwell bypass leakage on containment performance was investigated. The facility configuration is shown in Figure 2. The steam produced in the RPV was directed to the IC and via the drywells to the three PCC units. Four hours after test initiation the vacuum breaker bypass leakage path was opened. The IC was shut off 7 hours after test start. The duration of the “Systems Interaction Test” was 12 hours. During test phase 1 when the IC was operational and there was no DW to WW leakage, the IC took roughly one third of the total decay heat load. The DW to WW pressure difference was continuously reduced. During phase 2 the IC was in operation and DW to WW leakage path was

open. Because of the small DW to WW pressure difference there was no relevant leakage flow and the system pressure remained almost constant. At the beginning of phase 3 the IC was shut off. The three PCC units immediately took over the additional load and the DW to WW pressure difference rised (to approximately the PCC vent line submergence head). As a consequence the DW to WW leakage flow first increased, causing a continuous drop in DW pressure and accordingly decreasing DW to WW pressure difference. To the end of the test, both, pressure difference and bypass flow vent to zero. The PCCS removed all decay heat under these conditions. In summary the ICS operation in parallel with the PCCS had positive effect on overall system behaviour and DW to WW leakage did not cause a relevant system pressure increase.

P7 is the "Severe Accident Test". The objective was to investigate the PCCS performance under a severe accident scenario where one PCC unit was not operable and considerable quantities of hydrogen were released. The hydrogen release was simulated by injecting helium to the drywell later in the transient. Only the two PCCs connected to DW2 were available for decay heat removal and all break flow was directed to DW2. As can be seen from Figure 2, P7 had extremely asymmetric conditions. The PCC units started working just after test initiation. For the first two hours only two PCCs were not able to take the whole heat load. Consequently, the DW to WW pressure difference increased until the main vent lines began to clear. About 3 hours into the test, the DW pressure started to drop because of decreasing decay heat power and PCC over capacity. The first phase of test P7 (before helium injection) demonstrated that only two out of three PCC units in operation cause an extended main vent clearing period with accordingly higher energy transfer to the wetwell. Consequently, the temperatures in the wetwell increased and with it also the WW pressure continuously rised. Four hours after test start the helium injection phase was initiated. Cold helium (at room temperature) was injected with a flow rate of 4 g/s to the top of DW1 for a time period of 2 hours. Immediately after helium injection was initiated the topmost thermocouple in DW1 gas space showed a sharp drop in temperature by more than 20 °C. The "cold" helium front moved downwards in DW1. About 1 hour after helium injection started the region between DW top and the connecting line between the two DW vessels was filled with helium. Then the helium began to flow from DW1 to DW2 through the connecting line. The temperatures in the lower region of DW1 remained roughly at saturation temperature. The gas temperatures in DW2 indicated that DW2 was well mixed all the time. From the measured PCC tube gas temperatures it was clear that the PCC performance was negatively affected once the steam/helium mixture reached the condensers. This was also confirmed by the reduced PCC condensate flow rates. The pressure difference between DW and WW increased continuously. About 50 minutes after helium injection was initiated the main vent lines began to clear for a period of roughly 30 minutes. After the helium injection phase was completed, there was still some helium flow from DW1 to DW2 and the system pressure increased slightly until the end of test. From the measured PCC fluid temperature distribution it was concluded that the helium accumulated in mid to upper region of the PCC units. This is because the upward buoyant forces overcome the downward flow forces. All the steam/air tests showed a different behaviour. The air accumulated in the PCC lower region and the steam/air interface moved in a self adjusting process, in order to maintain always sufficient heat transfer area. Test P7 demonstrated that helium injected to the drywell later in the transient affected the performance of PCCS and containment. The test also showed that the PCCS behaves slightly different depending if a light or heavier gas than steam is entering the condensers. Additional investigations would be necessary to come up with final conclusions.

6. CONCLUSIONS

A series of eight transient system tests were performed in the PANDA facility to investigate the performance of the passive containment cooling system of the European Simplified Boiling Water Reactor. The main findings are summarized as follows. The PCCS showed generally a favourable and robust long-term post LOCA behaviour. The PCCs started working even under extreme conditions. Also, the transition period from the GDCS injection phase to the PCCS long-term operation phase has been successfully demonstrated. Trapped air somewhere in the drywell and released later in the transient did only temporarily reduce the PCCS performance. Helium injected to the drywell later in the transient did adversely affect the PCCS performance. This is an issue which would need more detailed investigation. The effect of drywell to wetwell leakage on system behaviour was moderate (at least in the investigated parameter range). The operation of the isolation condenser system in parallel with the passive containment cooling system had positive effect on the overall system behaviour. Finally, it was demonstrated that the PCCS was still able to remove a remarkable amount of decay heat from the containment after the PCC pool boil-off exceeded the expected inventory loss over the „no operator action period“. In summary, the test series successfully demonstrated that the passive decay heat removal systems operate as intended under different accident scenarios. The extensive data base will contribute to further improve containment cooling systems and containment design of passive plants and allow for system code assessment in a wide parameter range.

ACKNOWLEDGEMENTS

The work reported in this paper was supported by the European Commission (Fourth Framework Programme on Nuclear Fission Safety) and the Swiss Federal Office for Education and Science. These financial contributions are gratefully acknowledged.

REFERENCES

- [1] YADIGAROGLU, G.; and DREIER, J.; "Passive Advanced Light Water Reactor designs and the ALPHA program at the Paul Scherrer Institute", *Kerntechnik* 63 (1998) 1-2 pp. 39-46.
- [2] STOOP, P.M.; SPOELSTRA, S.; HUGGENBERGER, M.; YADIGAROGLU, G.; "TEPSS-Technology Enhancement for Passive Safety Systems", ICONE-5, Nice, France, May 26-30, 1997.
- [3] UPTON, H.A.; COOKE, F.E.; SAWABE, J.K.; "Simplified Boiling Water Reactor Passive Safety Features", ASME JSME Joint Int. Conf. On Nuclear Engineering, San Francisco, California, March 21-24, 1993.
- [4] FISCHER, O. et. al., "PANDA Asymmetric-Configuration Passive Decay Heat Removal Test Results", ARS'97, Orlando, Florida, USA, June 1-4, 1997.

SWR 1000 RELATED CONTAINMENT COOLING SYSTEM TESTS IN PANDA

J. DREIER, C. AUBERT, M. HUGGENBERGER, H.J. STRASSBERGER
Thermal-Hydraulics Laboratory,
Paul Scherrer Institute,
Villigen



G. YADIGAROGLU
Swiss Federal Institute of Technology,
ETH-Zentrum/ CLT,
Zurich

Switzerland

Abstract

Since 1991 the Paul Scherrer Institute has participated in the investigations of several of the new passive Advanced Light Water Reactor designs proposed world-wide. The current phase of the project, ALPHA-II, is focused on both the boiling water and the pressurized water reactor passive designs and consists of three projects under the sponsorship of the European Commission. The paper describes the performed PANDA transient system tests related to one of these projects, called "BWR R&D Cluster for Innovative Passive Safety Systems (IPSS)", and details the PSI contribution to the experimental investigation of passive containment cooling by a Building Condenser system which is part of the advanced Boiling Water Reactor SWR 1000 designed by Siemens. First, a short description of the relevant systems of the SWR 1000 design and its simulation in the PANDA facility are presented. After the description of the experimental programme for the large-scale integral system test investigations in the PANDA facility, the main results of the performed tests are also given. Finally, the main conclusions, based on the to date available experimental results and their analysis, are summarised.

1. INTRODUCTION

In 1991, the Paul Scherrer Institute (PSI) in Switzerland initiated a new project aimed at the experimental and analytical investigation of long-term containment decay heat removal and aerosol retention for the next-generation of passive Advanced Light Water Reactors (ALWR). During the first phase of this project, called ALPHA (Advanced Light Water Reactor Passive Heat Removal and Aerosol Programme [1]), three medium and large-scale facilities were designed and built: The large-scale integral system test facility PANDA, LINX-2 for separate-effects investigations of condensation and mixing phenomena, and AIDA for aerosol retention experiments.

In its first phase, the ALPHA project focused on investigation of the General Electric Simplified Boiling Water Reactor (SBWR) Passive Containment Cooling System and related phenomena [2,3]. This first phase of the project was successfully closed at the end of 1995 with the completion of the SBWR related tests.

At the beginning of 1996, the second, ALPHA-II phase of the project started consisting of three projects within the 4th Framework Programme on Nuclear Fission Safety of the European Union (EU). PSI has a major role in all three projects and, with PANDA, LINX-2 and AIDA, provides some of the essential large experimental facilities. The first project, *TEPSS* [4] is related to the European Simplified Boiling Water Reactor [5], which is based on the technology demonstrated at a large scale in the PANDA facility during the first phase of the ALPHA project, and on other tests. The *INCON* [6] is aimed at the development of solutions for passive cooling of double concrete containment's.

Finally, the *IPSS* project ("BWR R&D Cluster for Innovative Passive Safety Systems") [7] is focused on the most important innovations for the safety systems of Boiling Water Reactors (BWRs). The main tasks of the project are related to natural convection in the Reactor Coolant System (RCS), passive Decay Heat Removal (DHR) from the RCS, DHR from the RCS with steam jet pumps, the development of passive initiators for safety functions and the DHR from the reactor containment. The general objective of this project is detailed investigation of passive safety systems in order to rate their effectiveness experimentally, to improve models, validate computer codes and assess uncertainties with regard to such systems, and also to evaluate the possibility of using passive safety systems for existing reactors. For that purpose, existing large-scale test facilities are used in a co-ordinated experimental research programme that will deliver the experimental data base which is also used as a basis for the analytical work. An important part of the activities of the *IPSS* project is related to an innovative BWR design by Siemens in Germany (SWR 1000, [8]). The present paper refers to the experimental large-scale transient system investigation of the containment decay heat removal system of the SWR 1000 design. Besides, complementary separate-effect tests with the specific SWR 1000 DHR component were performed in the NOKO facility at the Research Center Jülich (FZJ), Germany [9]. The results of both experimental investigations yield a rather complete data base; the various related analytical activities will demonstrate the capability of the various computer codes used within the *IPSS* project to predict the behaviour of the specific containment DHR system.

2. THE SWR 1000 REFERENCE DESIGN

Since 1992 Siemens, in close co-operation with the German nuclear utilities and with support from various European partners, has been developing the SWR 1000, a new boiling water reactor with passive safety features and an electrical output of about 1000 MW [8]. Reduction of the probability of occurrence of a severe accident involving core melt and restriction of the consequences of such an accident to the plant itself have been defined as the main development goals related to plant safety. As a consequence three special design features have been identified: low core power density and large water inventories within the Reactor Pressure Vessel (RPV) as well as inside and outside the containment; passive systems together with a reduced number of active systems for accident control; and additional passive features for controlling a core melt in order to ensure retention of the molten core inside the RPV.

The actual SWR 1000 design is presented in Figure 1 and its most important passive safety systems are described briefly in the following. The operation of the passive systems relies solely on basic physical phenomena, such as gravity or heat transfer induced by temperature differences, and therefore neither activation of the reactor protection system nor a supply of electric power is needed to initiate their function.

For the initiation of several important safety functions (such as reactor scram, containment isolation and RPV depressurization), so-called *passive pressure pulse transmitters* are being considered. The passive pressure pulse transmitters are permanently connected to the RPV and their initiation function is controlled only by the water level in the. The *gravity core flooding* system prevents core uncover during accidental transients. In the event of a Loss of Coolant Accident (LOCA), steam or flashing water is discharged in the containment atmosphere and subsequently automatic depressurization of the RPV takes place. The large RPV water inventory prevents core uncover during depressurization. After RPV depressurization, water from the elevated core flooding pool is discharged to the RPV, assuring water coverage of the core throughout the rest of the transient. In each of the four core flooding pools, an *emergency condenser* is installed. Like the passive pressure pulse transmitters, the emergency condensers are connected to the RPV by non-isolatable steam discharge and condensate return lines. During normal operation, the emergency condenser is filled with water and only after a level drop in the RPV does the emergency condenser start removing heat from the primary system to the core flooding pool. Experimental and/or analytical investigations of several of these systems are being performed in the *IPSS* project [7].

For the long-term decay heat removal from the containment, so-called Building Condensers are provided above each of the four core flooding pools. The operating principle of the Building Condenser is shown in Figure 2. At later stages in an accident transient, generation of steam can lead to a rise in temperature and pressure inside the drywell, thus leading to a temperature difference between the primary (containment) and the secondary side of the Building Condenser. Steam then starts condensing which limits the containment pressure and temperature. The secondary side of the Building Condenser is permanently connected to the

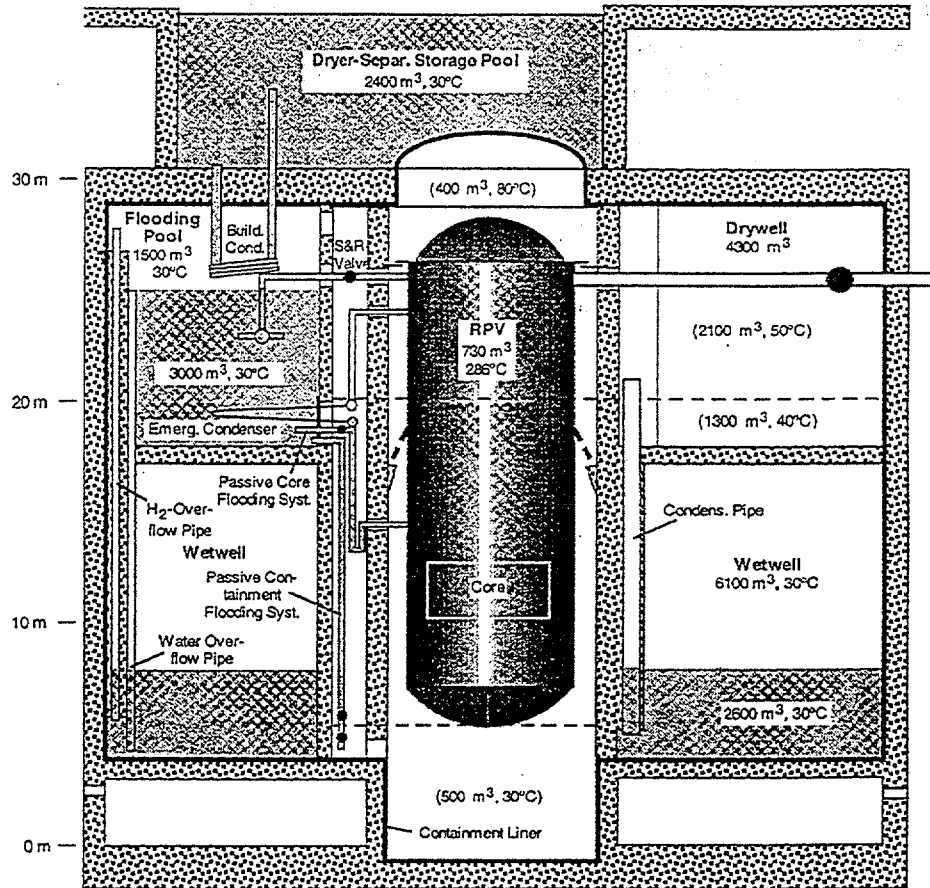


Figure 1: Sketch of the SWR 1000 Containment with Passive Safety Systems

dryer/separator storage pool situated above the containment by feed and return lines. Consequently, the primary side steam condensation initiates the development of the secondary side natural circulation. The start-up of the Building Condenser system is therefore fully passive and controlled only by the difference between the drywell and secondary-side-water temperatures.

3. THE SWR 1000 CONTAINMENT COOLING SYSTEM SIMULATION IN PANDA

PANDA is a large-scale thermal-hydraulic test facility for the investigation of passive ALWR containment phenomena and simulation of system response [2]. PANDA has a modular structure of six cylindrical vessels, representing the various containment volumes, interconnected by piping. Four rectangular pools open to the atmosphere are located on top of the facility. These pools may be equipped with immersed heat exchangers and used as heat sinks outside the containment, or as cooling water storage pools in other configurations. The facility, which has a total height of 25 m, offers a broad flexibility and allows investigation of a variety of containment designs with different passive decay heat removal concepts after a minimum of modifications.

For preconditioning the various system components in advance of a test, the PANDA facility is equipped with several auxiliary systems, like air, helium, and demineralized water supplies, and auxiliary steam and vent systems. The facility is heavily instrumented with some 600 sensors for temperature, pressure, pressure difference, level or void fraction, flow rate, electrical power, and valve position measurements. In addition to the classical instruments, the instrumentation includes non-condensable fraction (oxygen) sensors, phase detectors, and floating thermocouples which measure the surface temperature of pools. The facility is operated and controlled remotely and interactively by a computer-screen-based system.

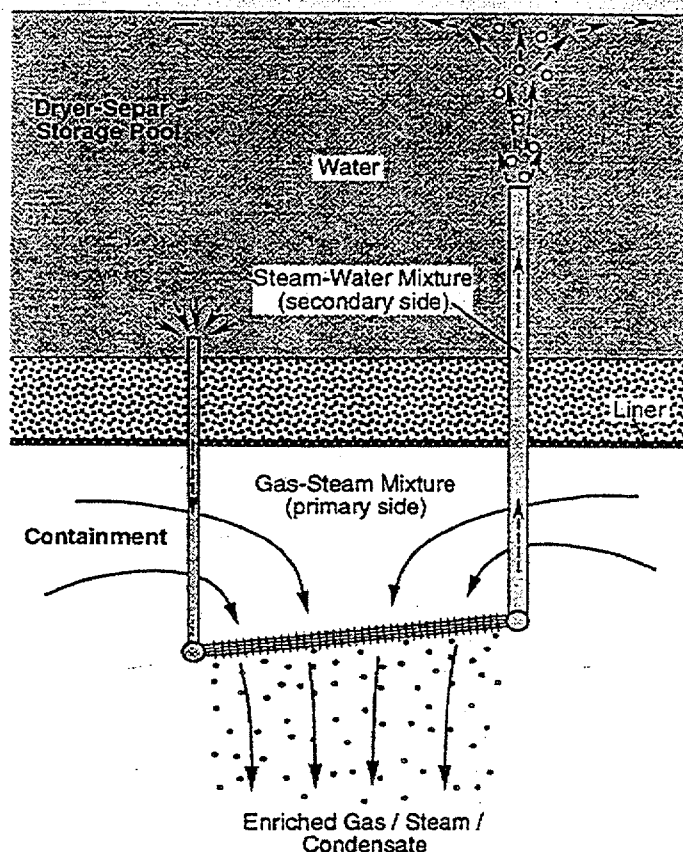


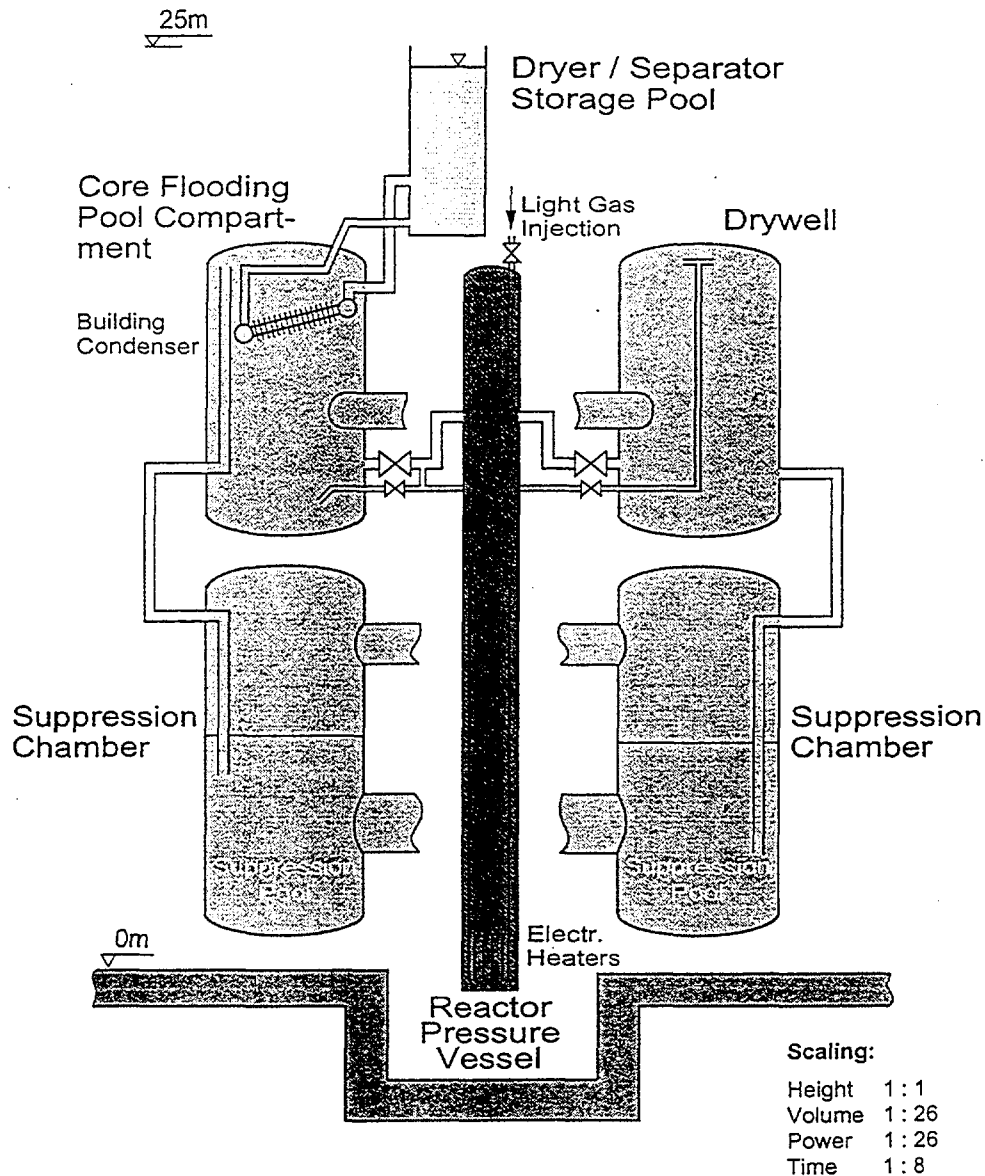
Figure 2: Operating principle of the SWR 1000 Building Condenser

After PANDA was constructed, a number of facility characterisation tests were performed to obtain information about mass leak rates (especially for helium), vessel and line heat losses as a function of temperature, and connecting-line pressure loss characteristics. This facility characterisation information is used both to estimate the system simulation quality and for the analytical and code assessment work.

Figure 3 shows the PANDA facility configuration for the investigation of the passive decay heat removal from the containment by the Building Condenser (BC) system of the SWR 1000 design. The Reactor Pressure Vessel (RPV) of the SWR 1000 is simulated by the PANDA RPV (1.25 m diameter, 20 m high) which is equipped with programmable 1.5 MW electrical heaters simulating the history of core decay heat generation. One PANDA Drywell (4 m diameter, 8 m high) simulates a Building Condenser compartment and the second one (same size) a SWR 1000 Drywell compartment. The two PANDA Drywells are interconnected by a large (1 m diameter) pipe. The two PANDA Wetwells (each 4 m diameter and 10 m high) are simulating the suppression chamber including the pressure suppression pool. They have two interconnections, one in the gas space (1 m diameter) and one in the pool region (1.5 m diameter). The dryer-Separator Storage Pool is represented by one of the PANDA pools (1.5 m by 2 m, 5 m high) on top of the facility.

For the simulation of the SWR 1000 pipes and postulated breaks, the following PANDA system lines are used (cf. Figure 3):

- Main Steam Line 1& 2 and part of the auxiliary steam system with two discharge locations in the core flooding pool compartment (Drywell 1) for the simulation of breaks and steam sources
- and with two discharge locations in Drywell 2 for the simulation of different types of breaks
- Main Vent Line 1 for the simulation of the Hydrogen Overflow Pipe (starting inside Drywell 1 just above the BC and ending inside Wetwell 1 about 1 m below the pressure suppression pool water surface)



PANDA Facility Building Condenser Configuration

Figure 3: PANDA Facility Configuration for Building Condenser System Tests

Drywell 1 contains a scaled model (i.e. a reduced number of prototypical finned tubes with a slightly shorter length) of an SWR 1000 Building Condenser (Figure 3). The BC secondary side water loop consists of the Dryer-Separator Storage Pool, the BC Feed Line, which connects the pool with the lower collector pipe of the BC, the inside of the condenser tubes, and the BC Return Line, which connects the upper collector of the BC with the Storage Pool. In addition to the general PANDA instrumentation available during the BC tests, specific Building Condenser instrumentation has been added. The new instruments are mainly temperature measurements on the primary and secondary side of the Building Condenser and in the Dryer-Separator Storage Pool. Both the primary side condensate drain and the secondary side natural circulation flow are measured.

Because the main focus of these first BC system investigations is the BC behaviour, the influence of the BC on the containment, and the behaviour of the secondary-side natural circulation loop, not all of the passive safety features of the SWR 1000 design have been simulated. Simulation of the core flooding pools, including the emergency condensers, would have been a major effort, but with negligible benefit for the main goals of the BC system investigations. Therefore, they were not modelled for the investigations presented in this paper.

Based on the actual SWR 1000 design and the size of the PANDA components, the configuration described above represents the SWR 1000 at a scale of 1:26 with respect to volumes and power (including the BC) and about prototypically with respect to important heights. The only relevant scaling distortion results from the volume of the PANDA Storage Pool, which, at the above mentioned scale, is 7.8 times too small. Nevertheless, by accelerating the simulated transients in PANDA by a factor of 7.8, the heat-up of the PANDA Storage Pool can be simulated properly and therefore the BC secondary side conditions as well. For the simulations in PANDA, prototypical fluids at prototypical thermodynamic conditions are used. However, nitrogen and hydrogen are replaced by air and helium, respectively.

4. BC TRANSIENT SYSTEM TESTS

For the design of the containment, the heat removal efficiency of the Building Condenser is important, because it controls the long-term containment pressure. Depending on the type of accidental transient, the BC's primary side is exposed to different and/or varying conditions, i.e. steam/non-condensable gas mixtures at different pressures, depending on how mixing and stratification develop in the Drywell during the transient. Because of its realistic BC configuration (cf. Section 3) and large scale, the PANDA facility is very well qualified to simulate the range of conditions expected for the various types of accident transients, including the relevant three-dimensional effects. The main objectives of the PANDA Building Condenser transient system test programme are to investigate the following:

- Containment behaviour in the presence of a heat sink inside the Drywell: *concept demonstration*
- Building Condenser behaviour under different conditions in the Drywell
- Influence of a large amount of light non-condensable gas on system behaviour and BC heat removal performance
- Influence of secondary side natural convection on the BC heat removal performance
- Generation of an experimental data base for model development and computer code validation

These objectives, together with a first analysis of different accident transients, has led to the PANDA BC transient system test matrix of Table I.

Test BC1 is the simulation of a transient without loss of coolant, i.e. the transient starts from cold conditions and with mainly air present in the containment. For this transient, there are two phases, each characterised by a different main heat sink. During the first phase, the decay heat and the energy released by coolant depressurization are transferred mainly to the core flooding pool. The dryer/separator storage pool, and also the Wetwell, if the BC heat removal performance is too low, are the main heat sinks for the second

Table I: PANDA Building Condenser Transient System Test Matrix

Test No.	Test Characterization
BC1	Transient without loss of coolant
BC2	Small break without core overheating, little stratification
BC3	Small break without core overheating, strong stratification
BC4	Small break with core overheating, strong stratification
BC5	Medium break with core overheating, little stratification
BC6	Large break without core overheating

phase. During the second phase, decay heat is the only heat source and the emergency condenser transfers this heat to the core flooding pool. Steam generated in that pool is released in the BC compartment. This situation is simulated in PANDA by the steam discharge in the lower part of Drywell 1, while Drywell 2 acts as a stand-by vessel. The experimental results (cf. Figure 4) demonstrate the self-adjusting behaviour of the BC system: if the heat removal performance of the Building Condenser is poor, the Drywell pressure increases and Hydrogen Overflow pipe clearing occurs. By that, air and/or steam is vented from the Core Flooding Pool Compartment to the Wetwell, leading, if air is present, to a lower air concentration around the BC, and to a higher system pressure with corresponding temperature increase. Both effects are improving the BC heat removal performance. When the BC performance finally matches the actual decay heat level, the system pressure stops increasing. The air initially present above the large connection pipe in Drywell 2, is, mainly during the first phase of the transient, transferred to Drywell 1 and vented to the Wetwell. But the air below the connection pipe stays in the lower part of Drywell 2 throughout the end of the test. Hence, a clear steam/air stratification is established in Drywell 2 during the test and a corresponding amount of almost pure air is accumulated in the lower part of this Drywell.

A small leak at the bottom of the RPV was simulated in Test BC2. At the beginning of this transient, hot pressurized water is discharged into the Drywell generating a large amount of steam. The simulation of the transient in the PANDA facility starts near the end of the RPV depressurization with a short first phase (cf. Figure 5). At that time, a significant part of the initial air content in the Drywell is already purged to the Wetwell and the containment pressure is about 2 bar. During this first test phase, the leak is simulated by injecting steam at the bottom of Drywell 2. Due to the low air concentration and a higher temperature of about 110 °C (compared to the beginning of Test BC1), there is already significant BC heat removal which exceeds the RPV steam release and leads to depressurization of the Drywell. In a second test phase, the core flooding pool heat-up is simulated by injecting steam also at the bottom of Drywell 1. During this phase the Drywell is repressurized following the flooding pool water temperature increase. Finally, the core flooding pool starts boiling and the steam release into the Drywell (simulated by steam injection at the bottom of PANDA Drywell 1) corresponds to the actual decay heat power. During this last test phase, the BC heat removal capability is less than the decay heat power and, according to the self-adjusting behaviour of the BC system described above, the system pressure is still slightly increasing. The air distribution at the end of Test BC2, in comparison with Test BC1, shows that, due to the presence of a leak at the bottom of Drywell 2 during the first and the second test phases, there was no air accumulation in Drywell 2. Instead, almost all the Drywell air was vented to the Wetwell, leading to a higher Wetwell and consequently system pressure.

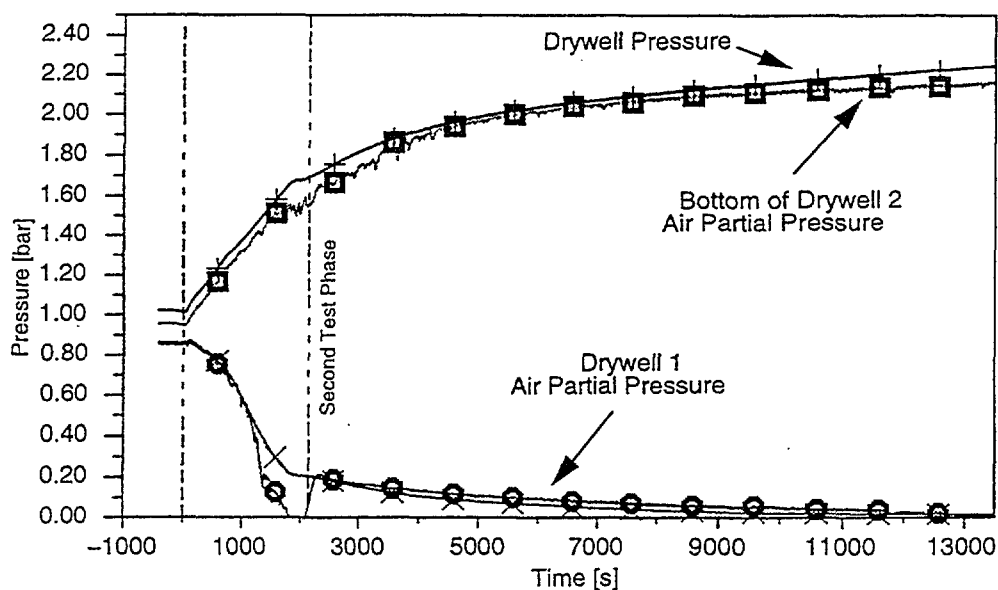


Figure 4: PANDA Test BC1: Drywell Pressure and Air Partial Pressures

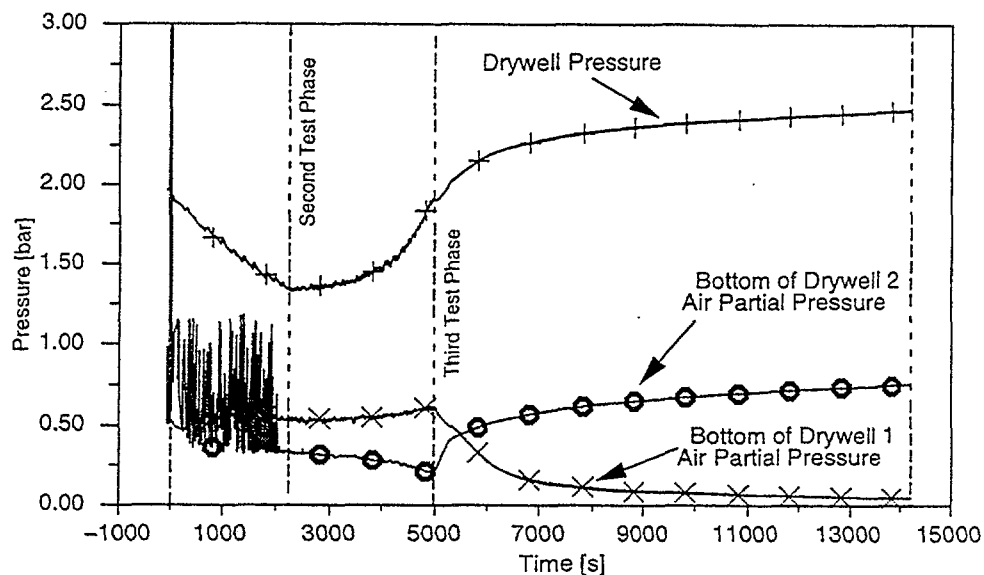


Figure 5: PANDA Test BC2: Drywell Pressure and Air Partial Pressures

PANDA Test BC3 was aimed at the simulation of a small-break loss of coolant accident at a high elevation in the Drywell. This transient has a very similar sequence of phases as described for Test BC2. The experimental results of Test BC3 confirmed mainly the findings of Tests BC1 & BC2, but at slightly different conditions related to air concentrations and pressure levels: the high-elevation leak simulated in PANDA Drywell 2 confirmed the stratification and air accumulation at the bottom of Drywell 2 and the self-adjusting BC behaviour was demonstrated once again.

A SWR 1000 double-ended Main Steam Line break was the reference transient for the PANDA Test BC6. According to the evaluated SWR 1000 transient scenario, the simulation in PANDA was composed of five different test phases. The simulation started with the first phase just before the end of the RPV depressurization, i.e. at pressures of about 5 and 3 bar in the RPV and the containment, respectively (cf. Figure 6). Caused by the violent steam release into the Drywell, especially during the very first phase of the SWR 1000 transient, all the air and a significant amount of steam have already been vented to the Wetwell at this time. Accordingly, from the very beginning of the transient simulation in the PANDA facility, the pure steam and high temperature conditions in the Drywell result in very favourable heat removal performance of

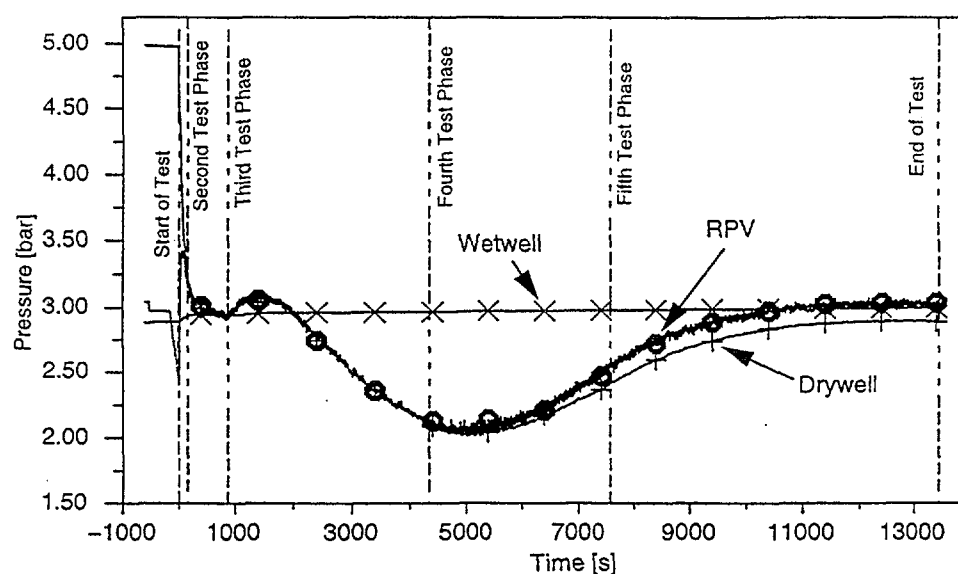


Figure 6: PANDA Test BC6: RPV, Drywell and Wetwell Pressure

the Building Condenser. Therefore, the three following test phases which simulate the containment structures and core flooding pool heat-up and the cooling of the RPV structure are characterised by an over-capacity of the BC, resulting in a Drywell pressure decrease of roughly 1 bar. The last test phase simulates the boiling of the core flooding pool and the steam release into the Drywell corresponds to the decay heat power. During this phase the Drywell pressure is increasing to about 3 bar and at that pressure the BC performance just matches the decay heat power.

PANDA Test BC4 is again a simulation of a small break loss of coolant accident at a high elevation in the Drywell, hence very similar to Test BC3. However, for Test BC4 the malfunction of the core flooding system is postulated, leading to a core overheat. Both, the additional heat production by the strongly exothermic zirconium-water reaction as well as the corresponding hydrogen production (by injecting a large amount of helium into the PANDA RPV) have been simulated during the corresponding phase of Test BC4. Through helium injection into the Reactor Pressure Vessel the whole system is immediately pressurized and about half of the steam/helium mixture flows through the Hydrogen Overflow Pipe to the Wetwell. After the helium injection stops, stratification starts developing in Drywell 1 and 2 according to the steam injection location near the bottom of Drywell 1 (simulating the boiling core flooding pool). Because helium is lighter than steam, it tends to accumulate in the upper part of the Drywells, i.e. above the large Drywell connection line in Drywell 2 and in the upper part of Drywell 1. The helium present around the BC, reduces the BC heat removal. Therefore the Drywell becomes further pressurized and the steam/helium vent flow to the Wetwell continues. This removes helium from the BC region and the BC heat removal performance increases again. The system pressure increase finally stops when the BC heat removal performance corresponds to the actual decay heat.

Test BC5 is the simulation of a feed-water line break with a postulated core overheat. Related to the transient scenario after the core overheat phase, the steam discharge location into the Drywell is the main difference between the Tests BC4 and BC5. In fact, the steam release at top of Drywell 2 prevents helium accumulation in the upper part of Drywell 2. Consequently, much more helium, compared to Test BC4, is vented to the Wetwell which results in a significant higher containment pressure at the end of Test BC5.

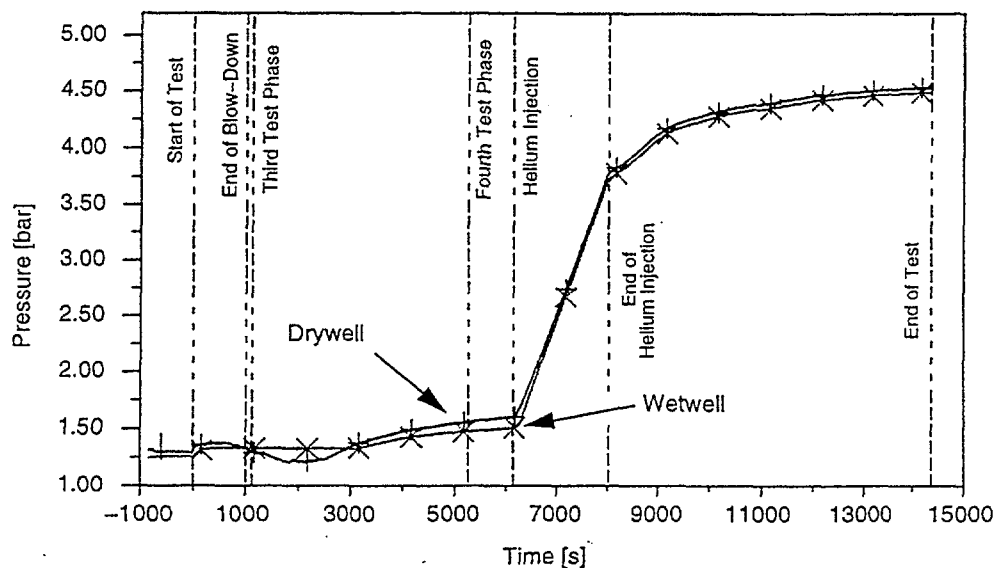


Figure 7: PANDA Test BC4: Drywell and Wetwell Pressure

5. CONCLUSIONS

Based on the experimental results available to date the following conclusions can be drawn:

- The Building Condenser behaves as expected under the range of conditions simulated in the different tests.

- The Building Condenser Decay Heat Removal System always generates favourable (i.e. pure steam) conditions on the Building Condenser primary (i.e. containment) side.
- Temperature/non-condensable gas stratification is a key issue in the concept investigated and was demonstrated very well throughout the tests.
- Operation of the *Building Condenser Concept* for Decay Heat Removal from a BWR containment was successfully demonstrated for a variety of accident scenarios, including a postulated core overheat.

ACKNOWLEDGEMENTS

The work reported in this paper was supported by the European Commission (Fourth Framework Programme on Nuclear Fission Safety), the Swiss Federal Office for Education and Science and the Siemens company. These contributions are gratefully acknowledged.

REFERENCES

- [1] G. Yadigaroglu and J. Dreier, „Passive Advanced Light Water Reactor designs and the ALPHA program at the Paul Scherrer Institut“, *Kerntechnik* 63 (1998) 1-2, pp. 39-46.
- [2] J. Dreier, M. Huggenberger, C. Aubert, T. Bandurski, O. Fischer, J. Heizer, S. Lomperski, H.-J. Strassberger, G. Varadi, G. Yadigaroglu, „The PANDA Facility and First Test Results“, *Kerntechnik* 61 (1996) 5-6, pp. 214-222.
- [3] G. Yadigaroglu, J. Dreier, M. Huggenberger, C. Aubert, T. Bandurski, O. Fischer, S. Lomperski, H.-J. Strassberger, G. Varadi[†], „The PANDA Tests for the SBWR“, 25th Water Reactor Safety Information Meeting, Bethesda, Maryland, October 20-22, 1997
- [4] S. Spoelstra/J. Hart, A.B. van Dijk, J. Talens, M. Huggenberger, J. Polo, J.L. Munoz-Cobo Gonzalez, F. Reventos Puigjaner, „TEPSS - Technology Enhancement of Passive Safety Systems“, FISA-97 EU Research on Severe Accidents, EC Luxembourg, 17 to 19 November 1997 (EUR 18258 EN), pp. 511-520.
- [5] H. Arnold, G. Yadigaroglu, P.M. Stoop, A. Gonzales, A.S. Rao, „From Dodewaard to a Modern Economic Passive Plant - ESBWR“, *Proc. TOPNEX 96*, Paris, Vol. 2, pp. 382-392, September 30 - October 2, 1996.
- [6] L. Brusa, L. Cinotti, F. de Cachard, G. Forasassi, L. Mazzocchi, P. Perezagua, F. Oriolo, M. Vidard, „Innovative Containment Cooling for Double Concrete Containment (INCON)“, FISA-97 EU Research on Severe Accidents, EC Luxembourg, 17 to 19 November 1997 (EUR 18258 EN), pp. 541-550.
- [7] E.F. Hicken, J. Hart, B. Schwinges, W.J.M. Slegers, J. Dreier, G. Cattadori, A.B. van Dijk, P.H. Ludwig, H. Holmström, „European BWR R&D Cluster for Innovative Passive Safety Systems“, FISA-97 EU Research on Severe Accidents, EC Luxembourg, 17 to 19 November 1997 (EUR 18258 EN), pp. 481-490.
- [8] K. Wagner, W. Bretschuh, „SWR 1000, a German Innovative Development of a Boiling Water Reactor“, *Proc. 6th Int. Conf. on Nucl. Eng.*, May 10-14, 1998, San Diego CA, ICONE-6389.
- [9] M. Fethke, H. Jaegers, E.F. Hicken, „Experiments of the Passive Safety System Building Condenser in the NOKO Test Facility and Post Test Calculations Using the RALOC Code“, *Proc. 6th Int. Conf. on Nucl. Eng.*, May 10-14, 1998, San Diego CA, ICONE-6506.
- [10] J. Dreier, C. Aubert, M. Huggenberger, H.-J. Strassberger, J. Meseth, G. Yadigaroglu, „PANDA Transient System Test Results for Investigations of Passive Decay Heat Removal from the Containment of a BWR“, *Proc. 6th Int. Conf. on Nucl. Eng.*, May 10-14, 1998, San Diego CA, ICONE-6483.



MODELLING OF PARTICULAR PHENOMENA OBSERVED IN PANDA WITH GOTHIC

Th. BANDURSKI, F. PUTZ, M. ANDREANI, M. ANALYTIS
Thermal-Hydraulics Laboratory,
Paul Scherrer Institute,
Villigen, Switzerland

Abstract

PANDA is a large scale facility for investigating the long-term decay heat removal from the containment of a next generation "passive" Advanced Light Water Reactor (ALWR). The first test series was aimed at the investigation of the long-term LOCA response of the Passive Containment Cooling System (PCCS) for the General Electric (GE) Simplified Boiling Water Reactor (SBWR). Recently, the facility is used in the framework of two European projects for investigating the performance of four passive cooling systems, i.e. the Building Condenser (BC) designed by Siemens for the SWR-1000 long-term containment cooling, the Passive Containment Cooling System for the European Simplified Boiling Water Reactor (ESBWR), the Containment Plate Condenser (CPC) and the Isolation Condenser (IC) for cooling of a BWR core. The PANDA tests have the dual objectives of improving confidence in the performance of the passive heat removal mechanisms underlying the design of the tested safety systems and extending the data base available for containment analysis code qualification. Among others, the containment analysis code Gothic was chosen for the analysis of particular phenomena observed during the PANDA tests. This paper presents selected safety relevant phenomena observed in the PANDA tests and identified for the analyses and possible approaches for their modeling with Gothic.

1. INTRODUCTION

1.1. The ALPHA-1 project

The ALPHA project was initiated at PSI in 1991 for investigating the long-term decay heat removal from the containment of a next generation "passive" Advanced Light Water Reactor [1]. During its first phase the ALPHA project focused on the examination of the Passive Containment Cooling System for the General Electric Simplified Boiling Water Reactor (SBWR) as required part of its certification by the US NRC (United States Nuclear Regulatory Commission) [2]. The project comprised PANDA system behaviour tests, separate effects test specific to passive decay heat removal systems and analytical work aimed at containment analysis codes assessment. The data of the first PANDA test series was used for the qualification of TRACG for the SBWR [3,4]. TRACG is the GE version of the Transient Reactor Analysis Code (TRAC) developed originally by the Los Alamos National Laboratory. TRACG has been extensively assessed for operating BWRs. The applicability of TRACG with respect to the containment pressure and temperature response of a passively cooled SBWR was not obvious at the beginning of the project. However, the comparison between test data and predictions showed that TRACG was able to predict the integral system behaviour of the PANDA facility over a wide range of conditions. On the other hand, mixing and stratification were not always predicted correctly, mainly, because these phenomena could not be adequately described with the relatively coarse nodalization of the vessels in the TRACG PANDA model.

1.2. The ALPHA-II project

Since 1996 the ALPHA project contributes to three European projects [1]. These are, in particular, "BWR R&D Cluster for Innovative Passive Safety Systems (IPSS)", "Technology Enhancement of Passive Safety Systems (TEPSS)" and "Innovative Double Concrete Containment Cooling (INCON)". The scope of the project was extended and covers now the experimental and analytical investigation of several passive containment and core cooling systems as well as single component and basic phenomena with respect to ALWR containment behaviour, in particular, the

Building Condenser of the SWR-1000 designed by Siemens, the Passive Containment Cooling System of the European Simplified Boiling Water Reactor, the Containment Plate Condenser, the Isolation Condenser, condenser/heat exchanger arrangements for passive PWR dual concrete containments proposed by ENEL. Most of the system analysis tests in PANDA were done and the data is available [5, 6, 7, 8]. Detailed measurements at clearly defined boundary conditions for investigating the vent behaviour and bubble plumes in a pool (LINX) as well as the CPC tests are in progress.

In the recent European projects different kind of analytical tools are employed for different purposes. System analysis codes like RELAP5, TRAC-BF, APROS, RALOC, MELCOR and WAVCO are used by some of the European partners to predict the overall transient system behaviour for selected tests. Codes providing 3D modeling capabilities like CFX [9] and Gothic [10] are used to gain a better understanding of particular phenomena, i.e. spatial velocity fields, gas component distributions and temperature stratification in water pools. Based on the experience obtained during the first project phase with regard to some modeling limitations using system analysis codes, Gothic was selected at the Paul Scherrer Institute (PSI) for the analysis of particular phenomena observed in the PANDA tests, in addition to RELAP5 and CFX.

Taking, in particular, advantage of the 3D modeling capabilities of the code, Gothic is applied for modeling test phases where

- a) the spatial distribution of the noncondensibles is affecting the passive condenser performance,
- b) the accumulation of noncondensibles in certain regions of the PANDA vessels significantly influences the system pressure,
- c) pool stratification has an impact on the system behaviour; and
- d) d) heat exchangers cause natural circulation loops in large volumes.

2. THE CONTAINMENT ANALYSIS CODE GOTHIC

Gothic (Generation of Thermal-Hydraulic Information for Containments) is a general purpose thermal-hydraulics computer code developed for design, licensing, safety and operating analysis of nuclear power plant containments [10]. Gothic solves the conservation equations for mass, momentum and energy for multi-component multi-phase flow, i.e. for steam/noncondensable gas mixture, continuous liquid and liquid droplets. In addition a mass balance is solved for a solid ice phase. The steam/noncondensable mixture can optionally comprise up to eight different noncondensibles at a time. The gases included in a specific analysis are defined by the user. A library of properties for about 50 different gases is available, however, the gas properties can be also specified by user input. Mechanistic models describe the interface mass, energy and momentum transport for the entire flow map from bubbly flow to film/drop flow, as well as single phase flows. The models consider possible thermal and mechanical nonequilibrium between the phases. Gothic provides optional models for turbulent shear as well as turbulent mass and energy diffusion. Any combination of connected lumped parameter volumes and one-, two- and three-dimensional grids can be supplied to the solver. Mass, momentum and energy can be added or removed by means of boundary conditions.

Solid structures are represented in Gothic by thermal conductors. A general model is included for heat transfer between thermal conductors and the steam/gas mixture or liquid. In addition, Gothic includes a set of component models as e.g. pumps, fans, valves, doors, heat exchangers, fan coolers, vacuum breakers, spray nozzles, hydrogen recombiners and ignitors. User-defined control variables can be applied for calculating specific boundary conditions. Hydrogen burn models as well as radioactive isotope decay and transport models are available in Gothic. And last but not least Gothic comprises graphical pre- and post-processors which help significantly to shorten the time for input preparation and analysis of the results.

3. THE PANDA FACILITY CONFIGURATIONS

One of the basic design ideas for PANDA was, instead of linear scaling, to represent the containment compartments by pairs of large connected vessels to allow multidimensional effects to take place[11]. Symmetric and asymmetric test configurations are possible as well as parallel operation of system devices like condensers and vent lines. The flexibility of the facility was further improved by adding the possibility of imposing a variety of controlled boundary conditions during the tests. Therefore, the facility could be employed for testing different concepts of passive containment cooling. Four PANDA test series are part of ALPHA-II addressing the Building Condenser, the Passive Containment Cooling System, the Containment Plate Condenser and the Isolation Condenser. In all tests steam is produced by electrical heaters modeling the core in the lower part of the reactor pressure vessel (RPV). Since in PANDA in first order the long-term decay heat removal is of interest, the maximum heater power of 1.5 MW was sufficient to follow the decay power curve in accordance to the scaling ratios used. Essentially prototypical fluids under prototypical thermodynamic conditions are used in PANDA. However, the noncondensibles nitrogen and hydrogen, heavier and lighter than steam, are replaced by air and helium, respectively.

The PANDA-BC consists of a bundle of 25 tubes in two layers with fins on the gas side located at a small angle to the horizontal in the upper part of a large PANDA-vessel (DW1 as part of the "Drywell" compartment), simulating actually the SWR-1000 flooding pool compartment (Fig. 1) [5]. The investigation of the emergency condensers immersed in the flooding pool and the flooding pool itself are not part of the PANDA testing and, therefore, these components were not modeled in PANDA. The BC is cooled by natural circulation of water taken from the bottom of a pool on top of the DW-vessels and returned to this pool at a higher elevation. Initially, the pool is filled with cold water and the hot return flow is expected to cause thermal stratification in the pool. In the BC tests, breaks and leaks of different size and location were simulated by selecting the appropriate discharge location and geometry for the break flow in the DW vessels (see location A, B and C on Fig. 1). In case of insufficient condenser performance noncondensibles and/or steam can be vented to the Suppression Chamber (SC).

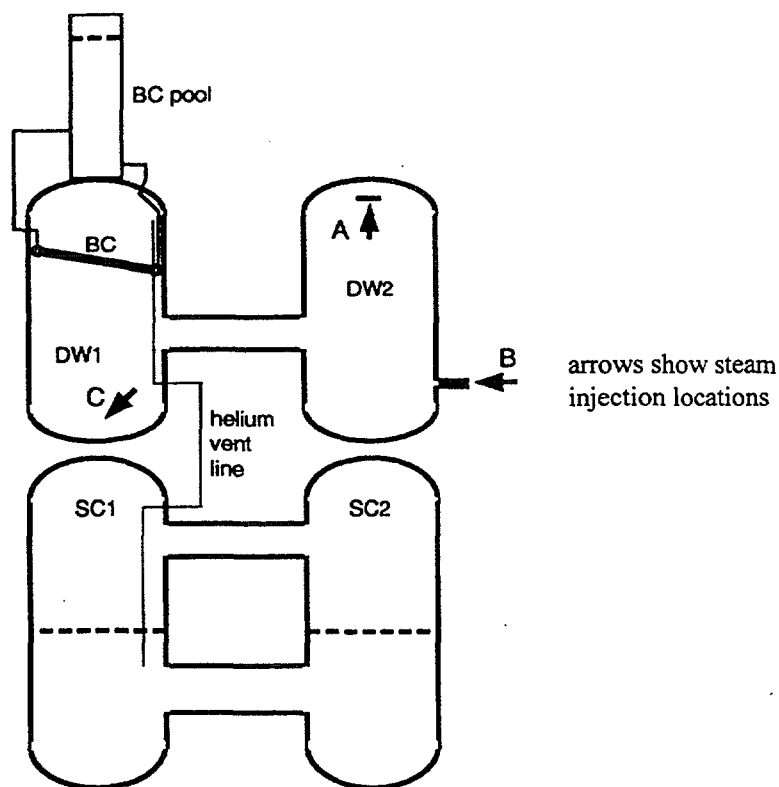


Fig. 1. PANDA BC test facility configurations.

The CPC and BC facility configurations as well as the test matrices are similar to each other. The plate condenser is located vertically in the upper part of the DW1 and is connected by a circulation loop to a water pool on top of the DW vessels.

The condensers of the PCCS are located in pools on top of the DW-vessels, open to the atmosphere (Fig. 2). They are fed with steam or steam/noncondensable mixture from the DW vessels through the feed lines. The condensate is returned from the lower header to the RPV through drain lines, whereas noncondensable gases can be vented from the lower header through the PCCS vent lines to the SC pools. The main vent lines are present but would not open under normal long-term decay heat removal conditions, since their submergence depth in the SC pool is accordingly higher in comparison to the PCCS vents. Vacuum Breakers (VB) make sure that the SC pressure cannot significantly exceed the DW pressure. A variety of asymmetric facility configurations can be easily established by discharging the break flow through one or either blowdown lines and by connecting or disconnecting PCCS condensers and the IC [12]. The IC has been used for a long time for passive core cooling in BWRs. Though it is a passive component, it has to be initiated by opening a valve. The IC can be considered as the prototype for the PCCS condensers. The PANDA IC consists of 20 vertical tubes located in a pool. The performance of this condenser type, in particular in the presence of noncondensibles, was investigated in a separate test series.

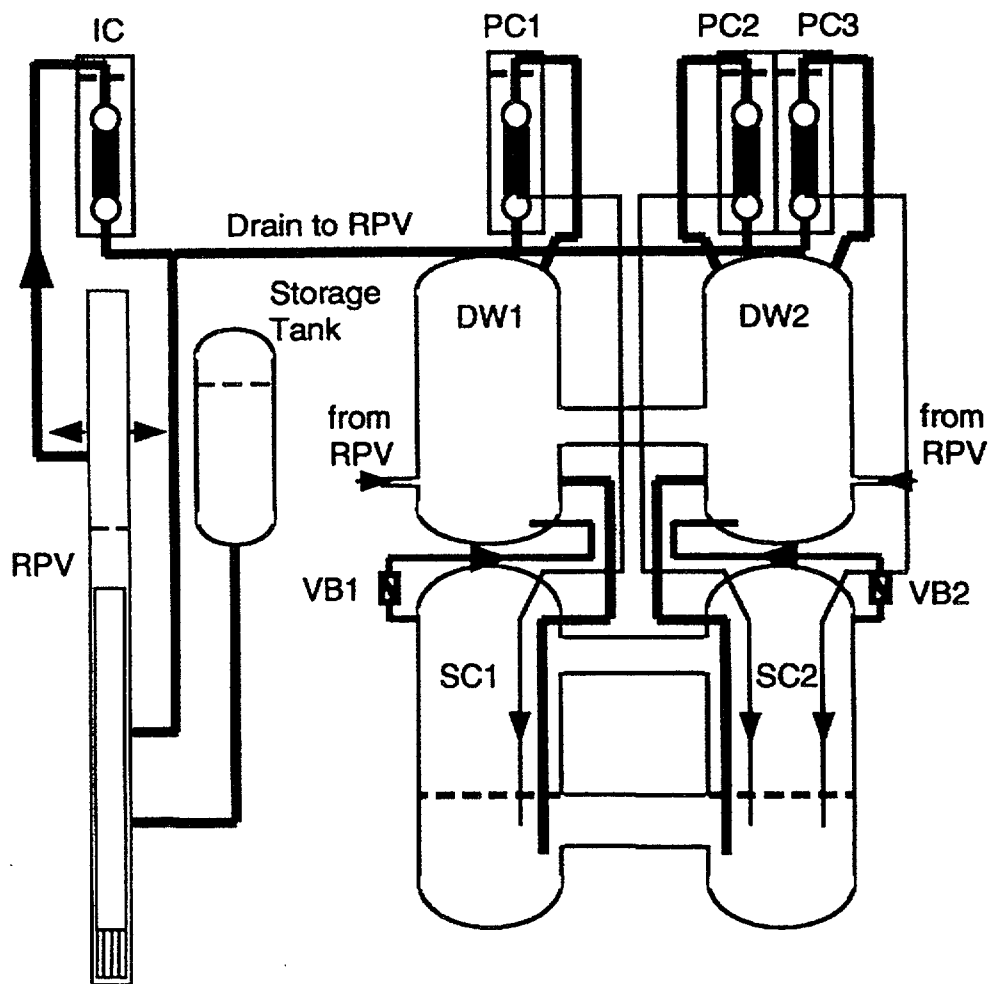


Fig. 2. PANDA ESBWR Facility Configuration.

A detailed description of the passive cooling concepts investigated in PANDA, the facility scaling, underlying accident scenarios, the test philosophy, test matrices and test results can be found in the literature [1, 2, 3, 4, 5, 6, 7, 8, 11, 12, 13].

4. IDENTIFICATION OF CHARACTERISTIC PHENOMENA IN PANDA AND MODELING WITH GOTHIC

The analysis of PANDA tests with known system analysis codes revealed some modeling deficiencies mainly with respect to mixing and stratification driven by density differences (buoyancy forces) in mixtures of steam/noncondensibles and in water pools, but also in processes where natural circulation loops are formed by heat exchangers in large volumes. In this chapter some characteristic phenomena observed during the PANDA tests, as well as the according modeling approaches with Gothic are presented.

4. 1. Heated jet and plume behaviour

Jets, in particular steam jets into a gas filled vessel, were present in all PANDA system tests. Plumes occurred, e.g., due to gas overflow through the DW connecting pipe in asymmetric facility configurations and in the BC pool due to the BC return flow. Steam jets discharged from the blow-down lines into the DW, but also plumes were mixing with noncondensibles. The correct modeling of gas mixing is important since it affects the time dependent noncondensable concentration at the condenser surface and, consequently, the condenser performance, the vent flow rate from the DW to the SC and the pressure in the SC which essentially determines the overall system pressure. On the other hand, plume mixing influences the accumulation of noncondensibles in vessel regions not affected by the main gas flow path. Therefore, preliminary studies were performed with Gothic to obtain experience with respect to heated jet and plume modeling.

Ale amount of air, contained in the DW vessels at test begin was varying over a large range. Typically, the DW air content was very small in tests starting the investigation of the long-term PCCS performance one hour after the initiation of the transient, i.e. a main steam line break in a BWR. However, a PCCS start-up test as well as some BC tests were started with air filled DW vessels. In some cases noncondensibles were added in the course of the test, e.g. hydrogen release simulated by helium injection or hidden air release.

To investigate the heated jet a simplified problem was defined for Gothic. Considering the PANDA vessel dimensions, grids of different size were created for a box of 4 m length, 3.2 m height and 1.2 m depth, assuming symmetry about a vertical plane in the direction of the jet injection. Hot air was injected into cold air at different velocities and temperature differences. The jet was horizontally injected 1 m above the bottom of the box through an area of $1/2 \times 0.16 \times 0.16$ m². On top of the box pressure boundary conditions were connected to a number of cells. The grid dimension made possible jet spreading with an angle of 11° with respect to the centerline. Both the k-ε, and the mixing length turbulence models available in Gothic as well as the laminar flow option were applied. In addition, a special option available in Gothic was used: the calculation was done for the gas phase only neglecting the water and droplet phases to economize computing time.

All calculations show reasonable results for the finer grid (cells of size $0.2 \times 0.04 \times 0.04$ m³) (Fig. 3), but non-physical behaviour in some cases with the coarser grid ($0.4 \times 0.08 \times 0.08$ m³). In particular, the jet behaviour can be completely lost in the calculation with the coarse nodalisation. The predicted declination of the heated jet centerline is in satisfactory agreement with measured data [14] obtained for a free jet over a gas velocity range between 2 and 7 m/s and discharge areas similar to those used in PANDA. For comparison, the velocity of the gas at the blow-down line exit in PANDA is in the range between 20 and 30 m/s. The gas jet will hit the opposite vessel wall and the mixing process starts essentially from there. The differences in the behaviour of round (experimental data) and square jet (Gothic model) were neglected. However, we are aware of the fact that we modelled our jet in a confined volume and the comparison with data of a free jet makes sense in a sufficient distance from the walls only. On the other hand, a detailed test procedure for the free jet experiments [14] is not available what makes possible slightly different interpretations of the centerline definition. Furthermore, there is a lack of experimental data on spreading of heated jets.

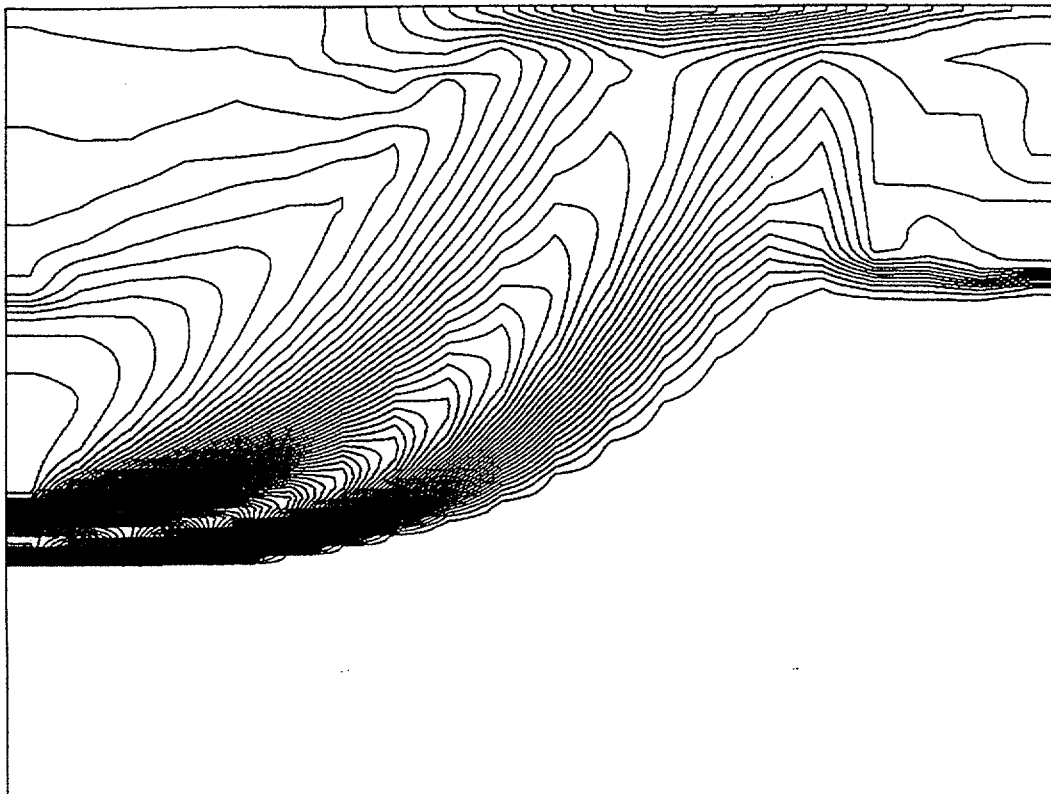


Fig. 3. Heated Gas Jet Modeling.

Fig. 3 shows isotherms calculated with Gothic for a heated air jet into cold air. The inlet velocity amounts to 2 m/s and the temperature difference between the hot and cold air amounts to 40 K.

Regardless of these uncertainties, the correct modeling of the jet behaviour requires fine grids what is seriously limiting with respect to the available computer performance. In addition, with the recent Gothic release grids are created in Cartesian co-ordinates and a fine grid in one region has to be continued throughout the whole vessel volume, what is also disadvantageous regarding computing resources.

Another issue of the gas jet modeling with Gothic was e.g. the improvement of the code with regard to the boundary conditions for the k - ϵ turbulence model [15]. In addition, gas jet mixing calculations were performed for comparing Gothic results with those obtained from CFX. A 2D problem was investigated applying the k - ϵ model in both codes. In general, the results were in good agreement, except the transition from wall plume to jet behaviour.

Single phase gas plumes modeled with Gothic did not show the spreading behaviour reported in the literature [16]. The reason for this could be the limited applicability of the available turbulence models to plume spreading. However, Gothic can predict the gas motion due to very small density differences between the cells of a subdivided volume what is necessary to achieve stratification in regions not affected by the main gas flow path.

4.2. Modeling of the helium injection phase in the PANDA building condenser tests

The BC condenser was located in the gas space of one DW vessel. The BC performance was strongly affected by the composition of the surrounding gas. If noncondensibles were present, their concentration increased at the BC tube bundle due to steam condensation, i.e. the temperature of the gas mixture decreased. In dependence on the density of the noncondensibles in comparison to the

steam density the gas mixture left the BC at the bottom or at the top. It has to be noted here, that below the BC, in parallel to the tubes, a plate was installed for conveying the condensate to a flow measurement device. Therefore, the gas flow needed to follow the plate at the lower side of the bundle.

After leaving the BC due to buoyancy forces the noncondensibles either mixed again with the gas surrounding the BC or accumulated in the lower or upper vessel region, dependent on the gas inlet momentum and density. In case the BC performance was insufficient, part of the gas was vented to the SC and the system pressure increased. However, stratification of a steam/helium mixture made possible the adjustment of the active condenser surface, i.e. the fraction of the BC not blanketed with noncondensibles was controlled by the system's energy balance. Pressure increase and venting of noncondensibles from a location above the BC continued unless the BC performance did match the decay power. Air was collected in the bottom regions of both DW vessels. Of course, the BC performance did also depend on the BC/pool water loop conditions.

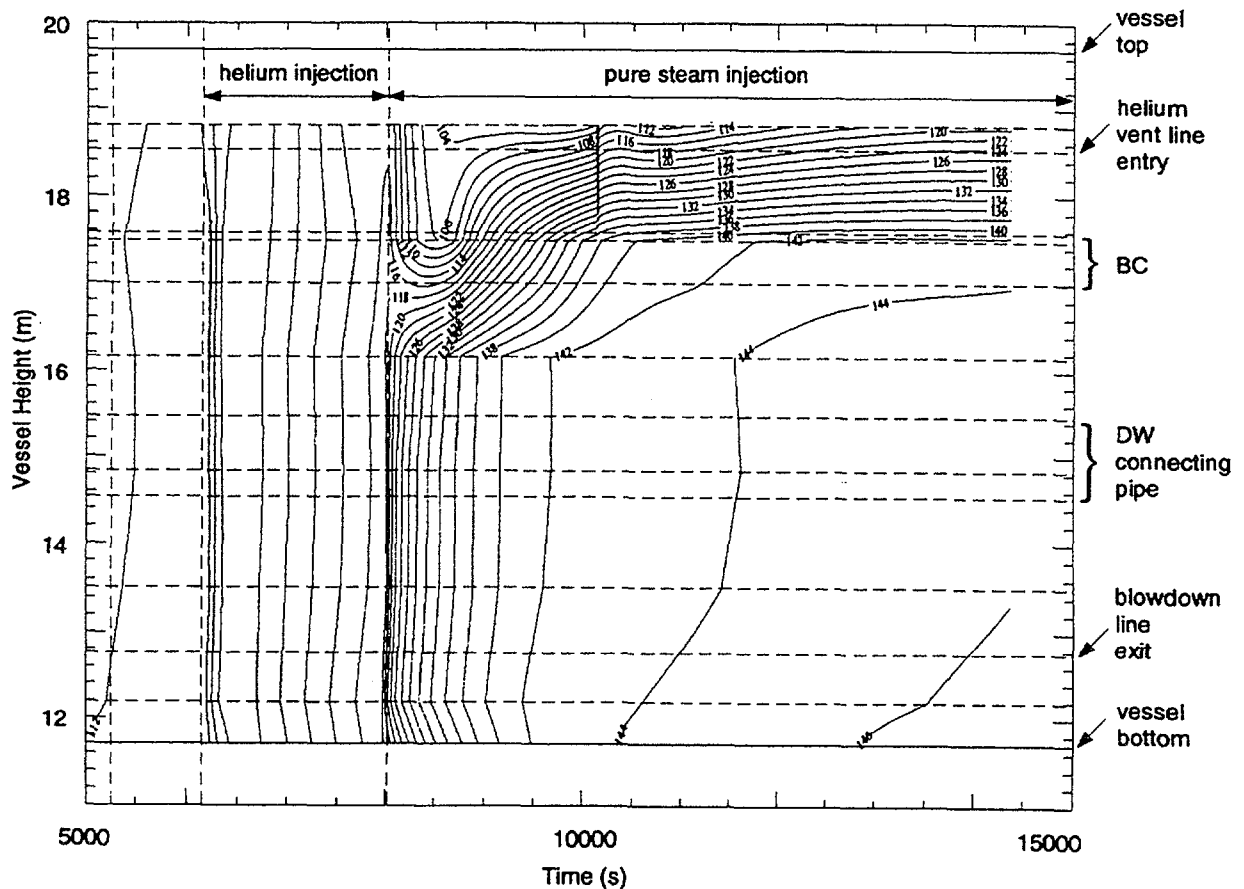
Gothic modeling is challenged by the 3D nature of the noncondensible distribution and the interaction between the BC performance and the noncondensible concentration at the condenser surface. A characteristic test sequence was selected for modeling with Gothic, where a rapid change from homogeneously mixed gas to stable stratification accompanied by large changes in the BC performance was observed. A short description of the particular observation in test BC4 is given below.

Two PANDA BC tests (BC4 and BC5) were partly dedicated to the investigation of the influence of a large amount of noncondensibles lighter than steam on the system behaviour and the BC performance. In both tests helium was added to the system on top of the RPV over a period of time preceded and followed by pure steam injection. In test BC4 the break was located inside of DW1 (high momentum injection, position C on Fig. 1). The blowdown line was directed to the vessel bottom with an angle of 45°. In test BC5 the steam/helium mixture was injected at the top of DW2 through a radial diffuser (low momentum injection, position A on Fig. 1). In these tests, the injection location affected significantly the transient system behaviour.

The helium and subsequent pure steam injection phases can be shortly characterized as follows. In test BC4, the steam/helium mixture fills very soon DW1. At the beginning of the helium injection phase, the BC performance decreased by approximately one third. During the helium injection phase the DW1 gas and wall temperature measurements indicated good mixing in the whole vessel (Fig. 4). At the same time, steam/helium mixture was replacing the pure steam filling initially the DW connecting pipe and the DW2 volume above the lower edge of the connecting pipe. Some steam/air mixture was retained from former test phases in the lower part of DW2. As soon as the helium injection was stopped, a strong stratification was observed in DW1 (Fig. 4). The volume below the BC was filled up with pure steam. Above the BC the gas temperatures decreased significantly due to the accumulation of helium/steam mixture released from the BC. Actually, part of the steam could condense on the BC feed line passing through the gas space in DW1 above the BC. While during the helium injection phase steam/helium mixture was conveyed to the SC through the helium vent line, the injection of pure steam improved the BC operating conditions and less steam was vented to the SC. However, the steam/helium mixture in the upper part of DW2 remained unaffected during the pure steam injection phase.

In test BC5 steam/helium mixture is injected in the upper region of DW2 through a radial diffuser. The relatively light gas mixture filled the DW2 vessel above the connecting pipe, before the gas could flow over to DW1, where it approached the BC. Strong temperature stratification was observed above the BC, where steam/helium mixture with higher helium content could be accumulated. After the helium injection was terminated, the helium was completely purged from the upper region of DW2, obviously being diluted by the incoming steam. Finally, all helium was

vented to the SC except a small amount in a cold gas layer above the helium vent line entry elevation in DW1. As a consequence, the SC pressure and accordingly the DW pressure rose to a much higher value in test BC5 in comparison to test BC4. In test BC4, the DW2 region above the connecting pipe served as an additional volume for noncondensable gas storage.



The predicted mixing and stratification behaviour were qualitatively in good agreement with the test observations (Fig. 5). The BC performance was not predicted adequately, because the correlations for condensation heat transfer implemented in Gothic were not developed for condensation on (almost) horizontal finned tube bundles. This kind of condensers are not available in existing containments. Therefore, in the future, it will be unavoidable to include appropriate condensation heat transfer models in Gothic for correctly predicting the BC heat transfer.

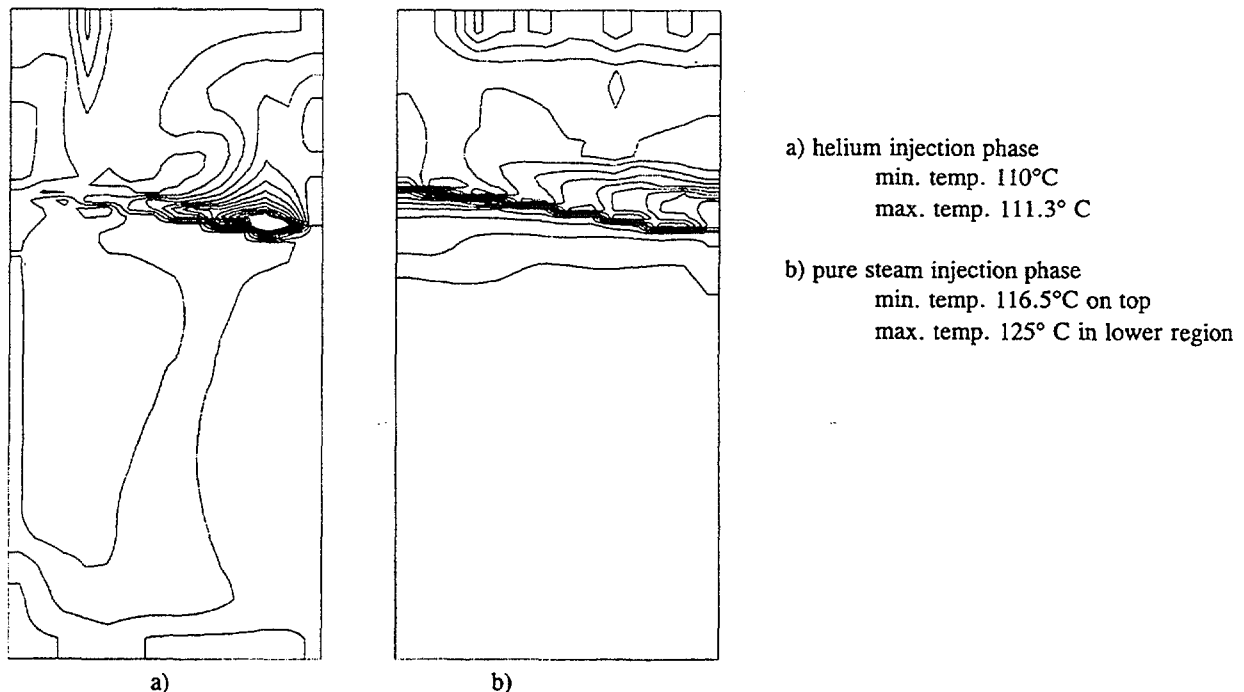


Fig. 5. Test BC4 - DW1 Isotherms Predicted by Gothic.

4.3. Building condenser pool mixing/stratification

The BC was fed with water taken from bottom of the BC-pool and returned to the pool at an elevation higher than the feed line entry. The pool water was expected to stratify in order to feed the BC with water at the lowest possible temperature. The fluid velocity at the return line outlet was rather low and the hot water from the return line was mixed with the pool water and no stratification above the injection point was observed in the tests. This phenomenon could be well predicted with Gothic (Fig. 6). In particular, the calculations showed, that the plume was just passing the thermocouple installed in a small distance from the return line exit. This is exactly what has been observed in the tests. For comparison the problem was run with CFX, which provided practically identical results.

4.4. Heat transfer in the PCCS condensers

Condensation in the PCCS condensers occurred in vertical tubes, but also in the upper and lower headers. Only noncondensibles heavier than steam, i.e. air, will be considered in this paper. In case the condenser heat removal capability was exceeded steam/noncondensable mixture was vented to the SC. In particular steam venting is disadvantageous, since the energy transferred to the SC would cause system pressure increase. On the other hand, in case of excess condensation capability air was accumulated in the lower part of the condenser tubes, where it was mixed with saturated steam at a temperature approximately equal to the pool side temperature (100° C). This way the lower region of the tubes was practically blanketed. With decreasing decay power the blanketed

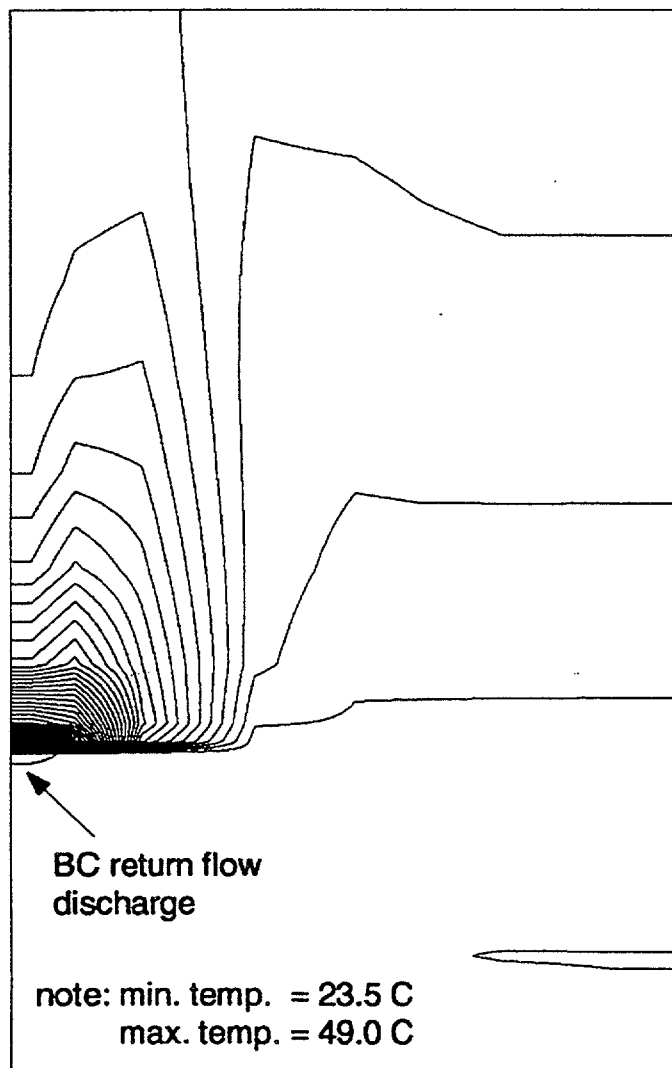


Fig. 6. BC Pools Isotherms in the Plane of the Return Flow Injection.

region was extended (Fig. 7). Unlike the BC, a relative small amount of noncondensibles is sufficient to control the active condenser length.

On the pool side a natural circulation loop was formed by the water heated and rising between the condenser tubes. The pool side heat transfer was accomplished by single phase and boiling heat transfer modes. Approaching the pool surface, the water temperature achieved saturation temperature at atmospheric pressure. Under normal operation conditions, this was also the temperature at which the water was entering the tube bundle.

Single component tests were performed in PANDA to obtain data on the maximum condenser performance for pure steam conditions at different pressure levels and, after adding noncondensibles, on the decreasing efficiency in dependency on the noncondensible fraction at the condenser inlet. However, in scaled long-term decay heat removal tests the condenser heat removal capability was essentially not exceeded and the condensers were operating with partly blanketed tubes.

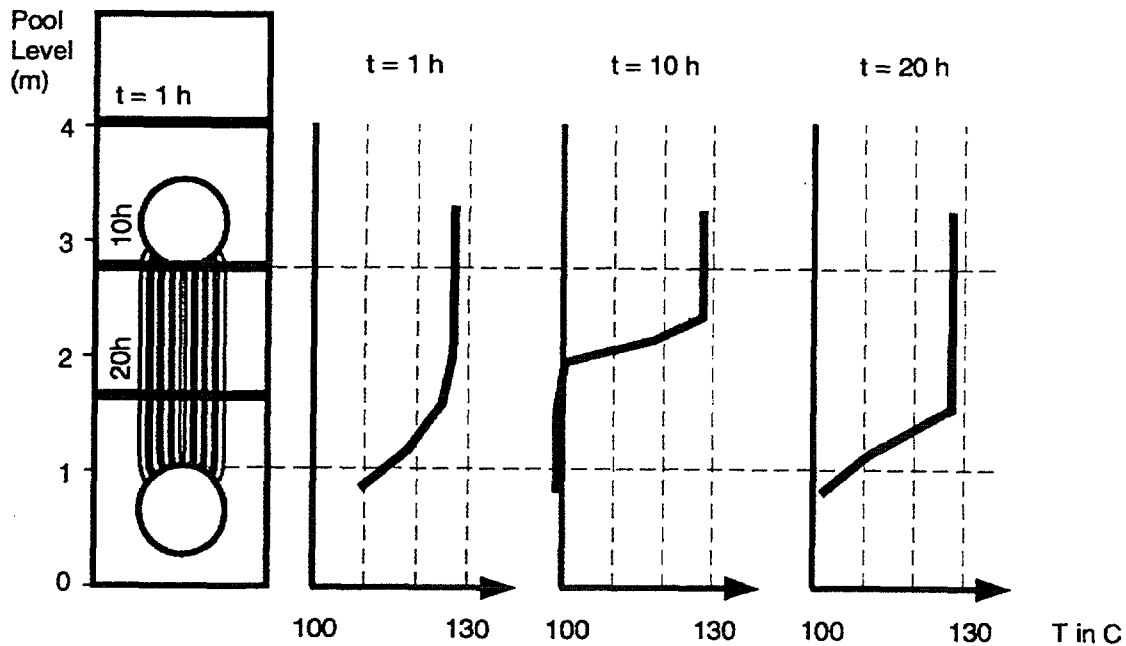


Fig. 7. Typical Axial Gas Temperature Profiles in a PCCS Condenser.

A post-test analysis of the single component tests was performed with Gothic. The condenser tubes as well as the pool were modeled with ID components. Both Gido-Koestel and film condensation models were applied for calculating the condensation heat transfer in the presence of noncondensibles inside the tubes [10, 17]. The applicability of the Gido-Koestel model was questionable at the beginning, since it was developed for condensation on containment walls in large compartments. However, the calculations were in good agreement with the measurements at lower pressures and lower noncondensable fractions, whereas with increasing pressure and noncondensable fraction the inaccuracy of the calculations increased. Comparing the predicted and measured wall temperatures revealed that the condensation heat transfer coefficient was in general overpredicted, whereas the pool side heat transfer coefficient was underdetermined. The reason for this disagreement has to be further investigated.

Another problem arose modeling the pool during condenser uncover, i.e. pool boil-off. Using ID pool components disables the pool water recirculation and provides practically stagnant boiling water between the condenser tubes. As a consequence, the condenser efficiency decreased and steam was vented. Test data and visual observations showed that the water recirculation was always covering the active condenser tube region, but not the passive region. 3D pool modeling helped to overcome part of the problem, i.e. the recirculation was predicted correctly. However, the pool side heat transfer coefficient is underestimated by the code as described above.

5. CONCLUSIONS

Gothic assessment using PANDA data is in progress at PSI. Gothic is a suitable tool for modeling 3D phenomena observed in PANDA tests which could not be adequately modeled with lumped parameter and ID system analysis codes. Further assessment work and code improvements are required, in particular with regard to jet and plume mixing and heat transfer in passive condensers components for ALWRs.

ACKNOWLEDGMENTS

The work reported in this paper was financially supported by the Swiss Federal Office for Education and Science and by the European Commission in the Fourth Framework Programme on Nuclear Fission Safety. This support is gratefully acknowledged.

REFERENCES

- [1] YADIGAROGLU, G.; DREIER, J.; "Passive Advanced Light Water Reactor Designs and the ALPHA Program at the Paul Scherrer Institute", *Kerntechnik* 63 (1998) 1-2 pp. 39-46.
- [2] SHIRALKAR, B. S.; et al; "SBWR Testing and Analysis Program Description (TAJPD)", GE Report NEDC-32391 rev. C, Aug. 1996
- [3] FITCH, J.R.; BANDURSKI, TH.; HEALZER, J.M.; "TRACG Post-Test Analysis of PANDA Tests M3 and M2", Proc. of NUTHOS-5, Beijing, China, (April 1997)
- [4] BANDURSKI, TH.; FITCH, J.R.; HEALZER, J.M.; "TRACG Post-Test Analysis of the Asymmetric PANDA Tests", Proc. of ICONE-V, Nice, France, (May 1997)
- [5] DREIER, J.; AUBERT, C.; HUGGENBERGER, M.; STRASSBERGER, H.-J.; MESETH, J.; YADIGAROGLU, G.; "PANDA Transient System Test Results for Investigations of Passive Decay Heat Removal from the Containment of a BWR", Proc. of ICONE-VI, San Diego, USA, (May 1998)
- [6] HUGGENBERGER, M.; AUBERT, C.; DREIER, J.; FISCHER, O.; STRASSBERGER, H.-J.; YADIGAROGLU, G.; "New Passive Decay Heat Removal Tests in PANDA", Proc. of ICONE-VI, San Diego, USA, (May 1998)
- [7] HUGGENBERGER, M.; AUBERT, C.; BANDURSKI, TH.; DREIER, J.; FISCHER, O.; STRASSBERGER, H.-J.; "TEPSS Related PANDA Tests (ESBWR)", these proceedings.
- [8] DREIER, J.; AUBERT, C.; HUGGENBERGER, M.; STRASSBERGER, H.-J.; YADIGAROGLU, G.; "IPSS Test Results (SWR-1000)", these proceedings.
- [9] CFX 4.2 Documentation, AEA Technology, Oxfordshire, UK, Dec. 97
- [10] GEORGE, TH.L.; CLAYBROOK, S.W.; MCELROY, J.D.; WHEELER, C.L.; WILES, L.E.; SINGH, A.; "Gothic Containment Analysis Package, Technical Manual, Version 6.0" Numerical Application, Inc., NAI 8907-06 Rev 7, prepared for EPRI, (RP4444-1), Dec. 1997
- [11] YADIGAROGLU, G.; "Derivation of General Scaling Criteria for BWR Containment Tests", Proc. of ICONE-IV, New Orleans, LA, USA, (March 1996)
- [12] BANDURSKI, TH.; DREIER, J.; HUGGENBERGER, M.; AUBERT, C.; FISCHER, O.; HEALZER, J.; LOMPERSKI, S.; STRASSBERGER, H.-J.; VARADI, G.; YADIGAROGLU, G.; "PANDA Passive Decay Heat Removal Transient Test Results", Proc. of NURETH-8, Vol 1, Kyoto, Japan, (Oct 1997)
- [13] SHIRALKAR, B.S.; GAMBLE, R.E.; YADIGAROGLU, G.; "SBWR Containment Response to LOCA: Passive Heat Removal System Performance", Proc. of NUTHOS-5, Beijing, (April 1997)
- [14] ABRAMOVICH, G.N. "The Theory of Turbulent Jets", Massachusetts Institute of Technology, USA, 1963.
- [15] ANALYTIS, M.; ANDREANI, M.; "A Simplified Treatment of the Boundary Conditions of the $k-\epsilon$ model in CFD-Type Codes like Gothic", these proceedings
- [16] GEBHART, B.; JALURIA, Y.; MAHAJAN, R.L.; SAMMAKIA, B. "Buoyancy-Induced Flows and Transport", Hemisphere Publishing, New York, 1988
- [17] GEORGES, TH.L.; SINGH, A.; "Separate Effects Tests for Gothic Condensation and Evaporative Heat Transfer Models", *Nuclear Engineering and Design* 166 (1996) 403-411.



MODIFICATIONS OF THE κ - ϵ MODEL IN GOTHIC NEAR PHYSICAL BOUNDARIES

G.Th. ANALYTIS, M. ANDREANI
Thermal-Hydraulics Laboratory,
Paul Scherrer Institute,
Villigen, Switzerland

Abstract

In CFD-type codes like the containment analysis code GOTHIC, one of the options that can be used for modelling of turbulence is the $k - \epsilon$ model. Though, in contrast to other CFD codes which are tailored for performing detailed CFD calculations with a large number of spatial meshes, in codes like GOTHIC which are primarily aiming at calculating transients in reactor containments, one generally uses coarse meshes. The solution of the two parabolic $k - \epsilon$ model equations requires the definition of boundary conditions at physical boundaries and this, in turn, requires very small spatial meshes near these boundaries. Hence, while in codes like CFX this is properly done, in codes like GOTHIC, this is done in an indirect and non-rigorous fashion, exactly due to the fact that the spatial meshes are usually large; this can have catastrophic consequences during the calculation of a transient and in this work, we shall give some examples of this and outline a method by which this problem can be by-passed.

1. INTRODUCTION

In the context of the EURATOM fourth Framework Programme in which the Paul Scherrer Institute (PSI) has a major participation in the Technology Enhancement of Passive Safety Systems (TEPPS) project [1]. The project aims to make significant additions to the technology base related to advanced passive-type Boiling Water Reactors (BWRs). An important part of this project is the analytical work aiming to understand the specific phenomena which control the performance of the Passive Safety systems. Among these phenomena, the occurrence of mixing or stratification (thermal or of gas species) in large volumes is of great interest. In this framework, calculations addressing the phenomena observed in tests carried-out in the PANDA facility [2] are performed and a number of detailed studies are under way for a better understanding of phenomena taking place in different parts of the facility.

For this analysis, one of the tools used is the code GOTHIC [3] which is in principle a 3D, 3-fields (vapour, liquid and droplets) code specially developed for containment analysis, and has the additional capability of modelling a number of different gases as well as air. Furthermore, the user can decide whether to use a laminar flow model or one of two turbulence models, the mixing-length model or the more sophisticated $\kappa - \epsilon$ model. Finally, the code has a pre-processor which greatly simplifies the task of building an input deck as well as a post-processor which can be used interactively for plotting a number of requested variables during the course of a transient.

As part of the effort to analyse and understand a variety of mixing phenomena important in advanced reactor technology, we would be interested in a better description and understanding of the way that a jet of steam injected in a vessel filled with air will eventually purge the air from the vessel. In particular, we are interested in the time taken for the air to be purged by the steam, but also in the time evolution of the spatial distribution of temperature and air concentration in the vessel. In order to have the possibility to compare the results obtained by GOTHIC with CFD calculations (by means of the CFX-4 code [4]) and assess some basic features of the code, the calculations were carried-out for a simpler geometry than PANDA and neglecting wall heat transfer and condensation effects. When the laminar or

mixing-length options were used, the simulation seemed to go through without any noticeable problem. However, when the $\kappa - \varepsilon$ model which is the one that should be used for turbulent flows in large volumes was activated, a number of problems were encountered. In particular, after some time in the transient, the turbulent kinetic energy at some computational volumes was increasing to values much higher than the average kinetic energy of the flow. The result of this unphysical increase of turbulence was that, within a very short time, the turbulent diffusivity was increasing to unacceptably high values and the steam and the air were completely mixed. Furthermore, as expected, the time-step was reduced to unacceptably low values.

In this work we shall report on the actual modelling of some transients similar to the one we mentioned above using GOTHIC and we shall discuss the results obtained by the standard version of the code. As a matter of fact, it was through the analysis of some simple "thought-off" transients that the problems we shall discuss in this report were revealed. In what follows, we shall report the results obtained by the version 6.0(QA) of the code. Similar results had been obtained with version 5. However, the recent interim version of the code released after the version 6.0(QA), includes modifications of the treatment of the wall boundary conditions which seem to solve the problems reported in this paper. The recent modifications produce the same result as the "fix" which we proposed in a previous report [5], i.e., the turbulent kinetic energy at the wall remains bounded, which seems to be a key issue for any coarse mesh description of bounded turbulent flows.

In Section 2, we shall outline the way that the $\kappa - \varepsilon$ turbulence model equations are coupled with the phasic momentum equations in GOTHIC, the way that they are numerically solved and the incorrect way that the boundary conditions of these equations *at the walls* are defined, which is in fact the root of the problem. In Section 3, we shall present the results obtained for some simple transients by using the standard version of the code and discuss all the problems encountered, the origin of which is the aforementioned inappropriate boundary conditions at the walls. Finally, in Section 4, we shall report on the way that we by-passed these problems by imposing a limit on the turbulent kinetic energy at computational cells which include a physical boundary. As a result of this modification, a number of other similar cases which were giving unphysical results when analysed with the standard version of the code due to the same reason (abnormal increase of the κ term) were re-analysed successfully, giving us confidence on the code modifications introduced.

2. THE $\kappa - \varepsilon$ EQUATIONS AND THEIR NUMERICAL SOLUTIONS IN GOTHIC

In GOTHIC, there are two different turbulence models, the rather simple mixing-length model, and the more sophisticated $\kappa - \varepsilon$ model which is now days the generally accepted model for this kind of engineering applications. This can be summarised as follows: The phasic momentum equations for phase f in GOTHIC include the turbulence stress term which must be separately modelled; these equations can be written as:

$$\frac{d}{dt}(\alpha_f \rho_f \underline{v}_f) + \nabla \alpha_f (\rho_f \underline{v}_f \underline{v}_f - \underline{\tau}_f - \underline{\tau}'_f) = -\alpha_f \nabla I p + \alpha_f \rho_f \underline{g} + \langle \underline{v}_i \rangle \Gamma_f + F_f + F_{wk} \quad (2.1)$$

where

τ_f is due to turbulation

$F_f + F_{wf}$ is shared

The turbulence stress tensor τ_f can be modelled (as already noted) by using the $\kappa - \varepsilon$ model.

The turbulent kinetic energy of phase f is defined by

$$\kappa_f = \frac{1}{2} \overline{v_i v_i} \quad (2.2a)$$

while the dissipation tensor $(\varepsilon_{ij})_f$ by

$$(\varepsilon_{ij})_f = \mu \frac{dv'_{ij}}{dx_k} \frac{dv'_{ij}}{dx_k} \quad (2.2b)$$

and the corresponding energy dissipation $(\varepsilon)_f = (\varepsilon_{ii})_f$. A set of time-dependent differential equations including a number of empirical constants can be written down for κ and ε_f which are solved in the code; subsequently, κ and ε_f are used to define the turbulent viscosity μ' by

$$\mu' = C_\mu \rho_f \frac{\kappa^2}{\varepsilon} \quad (2.3)$$

where C_μ is also an empirical constant. This quantity which for highly turbulent flows is 2 - 4 orders of magnitude larger than the molecular viscosity μ is used in the phasic momentum equations for modelling the term τ_f [3]. One should notice that these two differential equations are not implicitly coupled with the rest of the code and hence, situations may arise during which a sudden increase in the value of, say, κ may result in numerical problems. Furthermore, as we shall discuss in this work, the fact that in the version of GOTHIC used in this work the boundary conditions for the solution of the two $\kappa - \varepsilon$ model equations are formulated in an indirect (and not physically sound) fashion, may result in many cases in an unbounded growth of the turbulent kinetic energy κ and the turbulent viscosity μ' . As already noted, the direct consequence of this unphysical behaviour is that since the level of turbulence greatly increases, mixing is predicted to occur very quickly in all computational cells.

The two $\kappa - \varepsilon$ model equations can be written as (without the index f which denotes the phase)

$$\begin{aligned} \rho_f \alpha_f \frac{d\kappa}{dt} + \rho_f \alpha_f \frac{d(\overline{v_i \kappa})}{dx_i} &= \frac{\mu'}{C_k} \alpha_f \rho_f \frac{d^2 \kappa}{dx_i^2} - \alpha_f \rho_f \varepsilon - \\ \alpha_f \mu' [\overline{v_{i,j}} + \overline{v_{j,i}}] \overline{v_j} + g_i \alpha_f \frac{\mu'}{\rho_f Sc^i} \rho_{f,i} &= \frac{\alpha_f \rho_f}{C_k} \frac{d^2 \kappa}{dx_i^2} \left(\frac{\kappa^2}{\varepsilon} \right) + \\ \left[g_i \alpha_f \frac{C_\mu}{Sc^i} \rho_{f,i} - \alpha_f C_\mu \rho_f (\overline{v_{i,j}} + \overline{v_{j,i}}) \overline{v_j} \right] \left(\frac{\kappa^2}{\varepsilon} \right) &- \alpha_f \rho_f \varepsilon \end{aligned} \quad (2.4a)$$

where

$$\frac{d(\overline{v_i \kappa})}{dx_i} = C_k = \text{CONVECTION}$$

$$\frac{\mu'}{C_k} \alpha_f \rho_f \frac{d^2 \kappa}{dx_i^2} = D_k = \text{DIFFUSION}$$

$$\frac{\alpha_f \rho_f}{C_k} \frac{d^2 k}{dx_i^2} \left(\frac{\kappa^2}{\varepsilon} \right) = D_k = \text{DIFFUSION}$$

$$\left[g_i \alpha_f \frac{C_\mu}{Sc'} \rho_{f,i} - \alpha_f C_\mu \rho_f (\overline{v_{i,j}} + \overline{v_{j,i}}) \overline{v_j} \right] = h_c$$

$$\alpha_f \rho_f = \nu_c$$

for the κ term (where Sc' is the turbulent Schmidt number) and

$$\begin{aligned} \rho_f \alpha_f \frac{d\varepsilon}{dt} + \rho_f \alpha_f \frac{d(\overline{v_i \varepsilon})}{dx_i} = \\ \frac{\mu' \alpha_f}{C_\varepsilon} \frac{d^2 \varepsilon}{dx_i^2} + \alpha_f \left[C_{1\varepsilon} (S_s + S_b) (1 + C_{3\varepsilon} R_f) \right] \frac{\varepsilon}{\kappa} - C_{2\varepsilon} \alpha_f \rho_f \frac{\varepsilon^2}{\kappa} = \end{aligned} \quad (2.4b)$$

$$\frac{C_\mu}{C_\varepsilon} \rho_f \alpha_f \frac{d^2 \varepsilon}{dx_i^2} \left(\frac{k^2}{\varepsilon} \right) + \alpha_f \rho_f C_\mu \left[C_{1\varepsilon} (S'_s + S'_b) (1 + C_{3\varepsilon} R_f) \right] \kappa - C_{2\varepsilon} \alpha_f \rho_f \left(\frac{\varepsilon^2}{\kappa} \right)$$

where

$$\frac{d(\overline{v_i \varepsilon})}{dx_i} = C_\varepsilon = \text{CONVECTION}$$

$$\frac{\mu' \alpha_f}{C_\varepsilon} \frac{d^2 \varepsilon}{dx_i^2} = D_\varepsilon = \text{DIFFUSION}$$

$$\frac{C_\mu}{C_\varepsilon} \rho_f \alpha_f \frac{d^2 \varepsilon}{dx_i^2} \left(\frac{k^2}{\varepsilon} \right) = D_\varepsilon = \text{DIFFUSION}$$

$$C_\mu \left[C_{1\varepsilon} (S'_s + S'_b) (1 + C_{3\varepsilon} R_f) \right] = h_{ce}$$

for the ε term. $C_{1\varepsilon}$, C_ε , $C_{2\varepsilon}$ and $C_{3\varepsilon}$ are empirical constants, $C_k = 1$ and S_s , and S_b are the production by shear and buoyant production terms from the turbulent kinetic energy equation given by

$$S_s = \alpha_f \mu' \left[\overline{v_{i,j}} + \overline{v_{j,i}} \right] \overline{v_j} = \alpha_f C_\mu \rho_f \left[\overline{v_{i,j}} + \overline{v_{j,i}} \right] \overline{v_j} \left(\frac{\kappa^2}{\varepsilon} \right) = S'_s \left(\frac{\kappa^2}{\varepsilon} \right) \quad (2.5a)$$

and

$$S_b = g_i \alpha_f \frac{\mu'}{\rho_f Sc'} \rho_{f,i} \left(\frac{\kappa^2}{\varepsilon} \right) = S'_b \left(\frac{\kappa^2}{\varepsilon} \right) \quad (2.5b)$$

respectively, and R_f is the flux Richardson number given by

$$R_f = -\frac{1}{2} \frac{S_b}{S_s + S_b}$$

Equations (2.4a) and (2.4b) are solved numerically and we shall briefly outline the way this is done; in the process of doing this, we shall also indicate the way that the boundary conditions for these equations are taken into account in GOTHIC, this being the reason of the problems reported in this work. The "new-time" values of κ and ε , k^{n+1} and ε^{n+1} , and obtained after finite-differencing these equations in space and time; we shall have:

$$k^{n+1} = k^n + \Delta t (C_k^n + D_k^n) + \left[(h_c) \frac{k^{n+1/2}}{\varepsilon^{n+1}} - (v_c) \varepsilon^{n+1} + (b_c) (k_w - k^{n+1}) \right] \Delta t \quad (2.6a)$$

where

$$k^n + \Delta t (C_k^n + D_k^n) = \text{"SOURCE"} \cdot (q_k)^n$$

and

$$\varepsilon^{n+1} = \varepsilon^n + \Delta t (C_\varepsilon^n + D_\varepsilon^n) + \left[(h_{ce}) k^{n+1} - C_{2\varepsilon} (v_c) \left(\frac{\varepsilon^{n+1/2}}{k^{n+1}} \right) + (b_c) (\varepsilon_w - \varepsilon^{n+1}) \right] \Delta t \quad (2.6b)$$

where

$$\varepsilon^n + \Delta t (C_\varepsilon^n + D_\varepsilon^n) = \text{"SOURCE"} \cdot (q_\varepsilon)^n$$

where h_c , h_{ce} and v_c are defined in Equations (2.4a) and (2.4b).

Notice that the last term in each of the two finite-difference equations above is introduced in order to take into account the boundary conditions and k_w , and ε_w are the turbulent kinetic energy and dissipation at the wall, respectively. These are defined as follows: One defines the turbulent kinetic energy k_w "at the wall" by (5, 6)

$$k_w = \frac{v_{fr}^2}{\sqrt{C_m}} \quad (2.7)$$

where $C_m = 0.09$ is one of the constants of the $k - \varepsilon$ model; v_{fr} is the phasic friction phasic speed, which results from the universal velocity profile for the velocity parallel to the wall.

However, in GOTHIC, v_{fr} , is defined by

$$v_{fr} = |\underline{v}_{fr}| = \sqrt{v_{fr,x} v_{fr,x} + v_{fr,y} v_{fr,y} + v_{fr,z} v_{fr,z}} \quad (2.8a)$$

with its three different components given by

$$\begin{aligned}
v_{fr,x} &= v_x \sqrt{\frac{f}{8}} \\
v_{fr,y} &= v_y \sqrt{\frac{f}{8}} \\
v_{fr,z} &= v_z \sqrt{\frac{f}{8}}
\end{aligned} \tag{2.8b}$$

where v_x , v_y and v_z , are the three components of the phasic velocity vector and f is the friction factor as calculated from an empirical correlation for a smooth pipe. Also, one defines the dissipation at the wall ε_w , by (5, 6)

$$\varepsilon_w = \frac{v_{fr}^2}{0.4 \cdot y_c} \tag{2.9}$$

where y_c , is in fact the *real* distance from the wall. However, in GOTHIC, y_c is defined by

$$y_c = \frac{50 \cdot \mu}{\rho_f \cdot \max(v_{fr}, 0.01)} \tag{2.10}$$

μ being the molecular viscosity. As we have already discussed before, during the iterations for solving the two discretised, finite-differenced non-linear κ - ε model equations, κ and ε are forced to attain the values κ_w and ε_w at the wall. In other CFD codes (e.g. CFX, ASTEC etc), the boundary conditions at the walls (i.e. Eqs. (2.7) and (2.9)) are treated properly; though, this requires using a very fine mesh near the wall, something which is against the philosophy of GOTHIC which is a containment analysis code. In these two terms, *bc* is a rather complicated “smoothing” function.

The two non-linear algebraic equations above are solved iteratively for κ^{n+1} and ε^{n+1} using Newton's method, and at the end of each iteration (a maximum number of 20 iterations is allowed) one updates the values from the previous iteration with the ones obtained from the current one. Finally, apart from the usual restrictions based on mass-error and other convergence considerations, when the κ - ε model is used, the time-step is also limited by

$$\Delta t \leq \text{Min}_{all-cells} \left(\frac{\rho \cdot z^2}{5(\mu + \mu^t)} \right) \tag{2.11}$$

where z is a length-scale, ρ the corresponding phasic density and Min is referring to the minimum for all computational cells.

3 SIMULATIONS AND CODE PREDICTIONS

In the course of the effort to assess the applicability of GOTHIC for the analysis of some specific phenomena like gas mixing in the drywell of the PANDA facility, a number of attempts were first made to understand the way the code would predict some relatively simple transients. Hence, different cases of injection of hot air or steam in a vessel containing cold air were analysed, the aim of this being to investigate the mixing phenomena occurring in such cases as well as the capability of the code to capture the physics of these processes. Clearly, for such transients, turbulence plays a very important role and hence, in order to be able to successfully analyse them, one has to use some kind of turbulence model.

In this work, we shall report on the analysis of two relatively simple transients using a 2-dimensional nodalisation.

(a) *Box test-case*

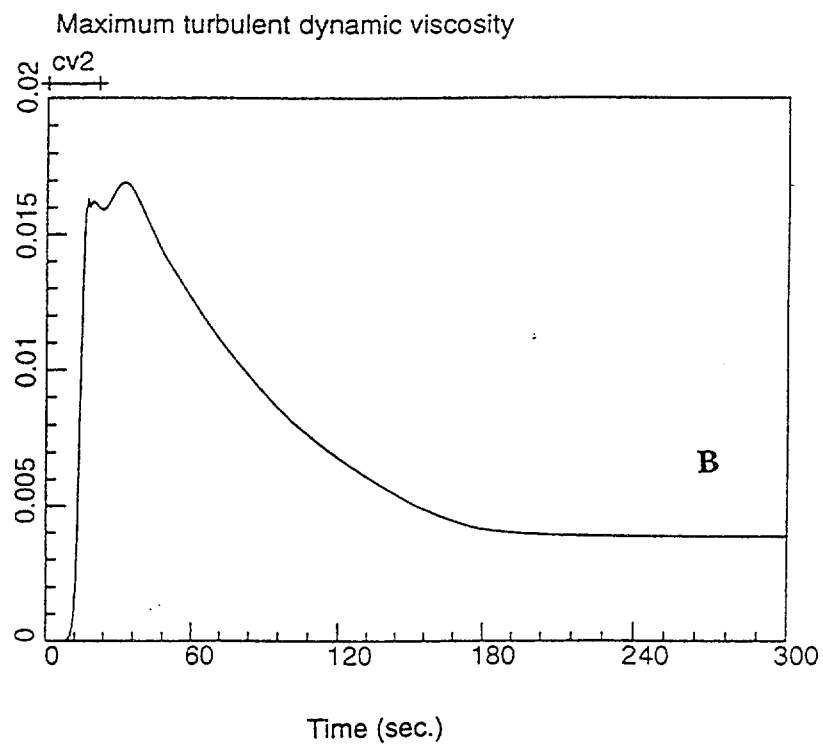
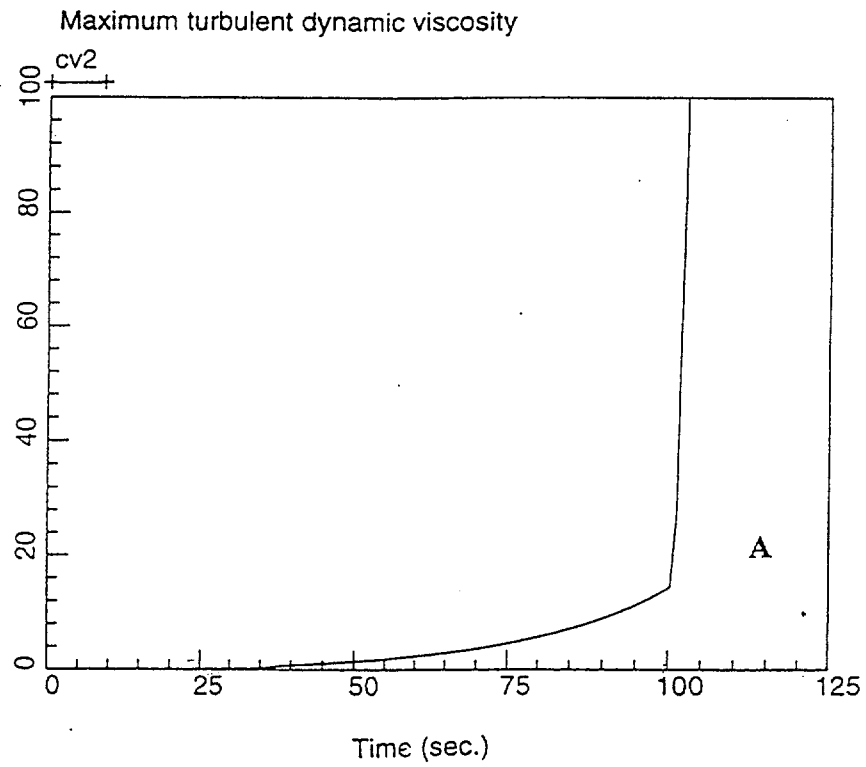
In this transient, air at a temperature of 100 °C and with a speed of 0.5 m/s is injected into a vessel filled with air at a temperature of 25 °C. The air is injected from the centre of the bottom of the vessel while at the centre of the top, there is an outlet. The pressure was 1 bar. The width of the vessel was 1 m while its height is 4 m. The mesh size in the lateral direction is 0.2 m and axially, 0.5 m. In Fig. 1A, we show the maximum turbulent viscosity μ' . One can see that μ' increases to unacceptably high values until at around 100 s, μ' exhibits a further sudden increase and reaches a value of around 1000 (in SI units) at approximately 112 s. Here, we should point out that the molecular viscosity of the air is about $1.8 \cdot 10^{-5}$; hence, the value above indicates that the code predicts that the turbulent viscosity is 8 orders of magnitude higher than the molecular one. The consequence of this is that during the whole transient, the time-step decreases gradually while the run terminates at around 112 s having reached the minimum time-step. The reason for this time-step decrease is that as we mentioned before, when the $\kappa - \varepsilon$ model is used, the time-step is also limited by the condition imposed by Eq. (2.11). The consequence of the aforementioned unphysical increase of μ' can be seen in Fig. 2A, where the temperature histories at 4 different locations are shown. After approximately 80 s, the four temperature histories coincide and at around 100 s (when it exhibits the additional sudden increase), there is a sudden drop in all four temperatures.

(b) *PANDA drywell test-case*

In this transient (which was in fact the transient which originally revealed the problems discussed in this work), steam is injected from the side at a speed of 1 m/s into the drywell of the PANDA facility which is filled with air, at a pressure of 1.32 bar. An outlet (feedline to the PCC condenser) is modelled at the top of the vessel. Again, since at this stage, the aim is only to assess the capabilities of the code in as far as mixing and stratification is concerned, no condensation is allowed. The code predictions for this transient obtained using the standard version of GOTHIC were unphysical due to the same reasons discussed above. Three different modellings of the PANDA drywell were used, a very detailed using a 2D representation, a more coarse one and finally, a coarse one using a 3D model. Here, we shall only discuss the results obtained using the 2D fine mesh nodalisation.

Due to the unphysical increase of the turbulence kinetic energy, we decided not to continue running the 2D fine nodalisation case for more than 50 s transient time since the time-step was already 0.2 ms. In Fig. 3A, we show the maximum turbulent viscosity and turbulent viscosity at the outlet of the PANDA drywell until $t = 50$ s. Clearly, μ' is still bounded during the time period of the calculation, its value has already reached unacceptably high levels which are not physical. As a consequence of this, as can be seen in Fig. 4A where the temperature histories at 5 different elevations are shown, complete mixing occurs at around 50 s. This can also be seen in Fig. 5A, where we show the predicted velocity vectors in the PANDA drywell at $t = 50$ s. Problems similar to the ones reported here were encountered during the analysis of an AP600 reactor containment transient.

Being faced with all the aforementioned problems, we tried to investigate the reasons for this unphysical behaviour. Originally, due to the large values attained by κ and μ' in the cells near the "ceiling" where large density and velocity gradients were observed, two features



[10] FIG. 1. Maximum turbulent viscosity μ' for the box test-case with the standard (A) and modified (B) code.

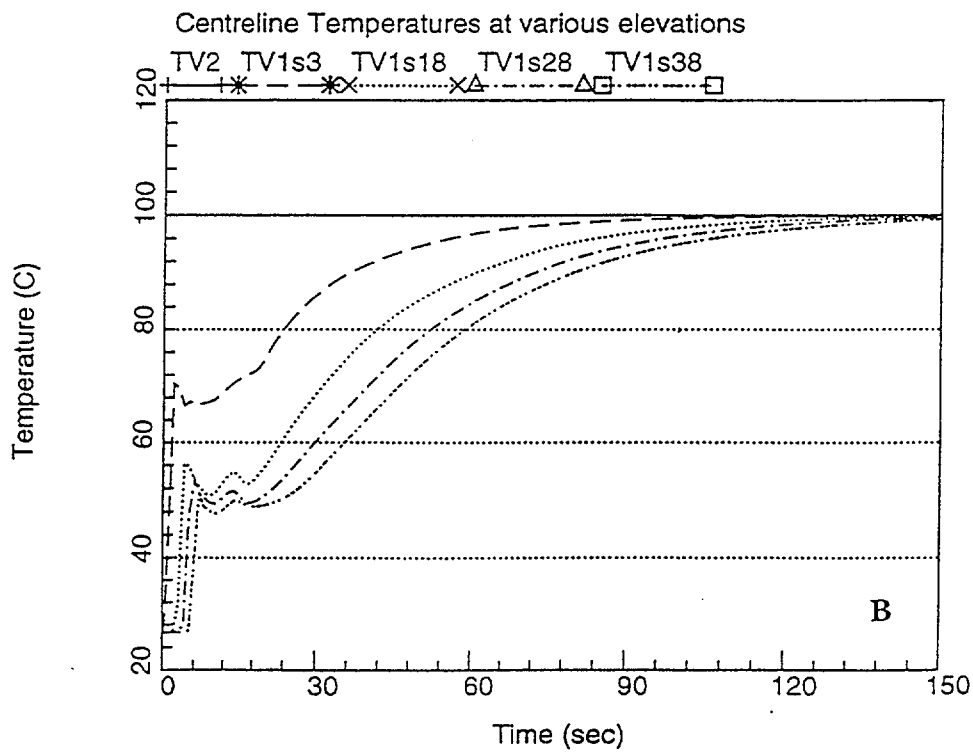
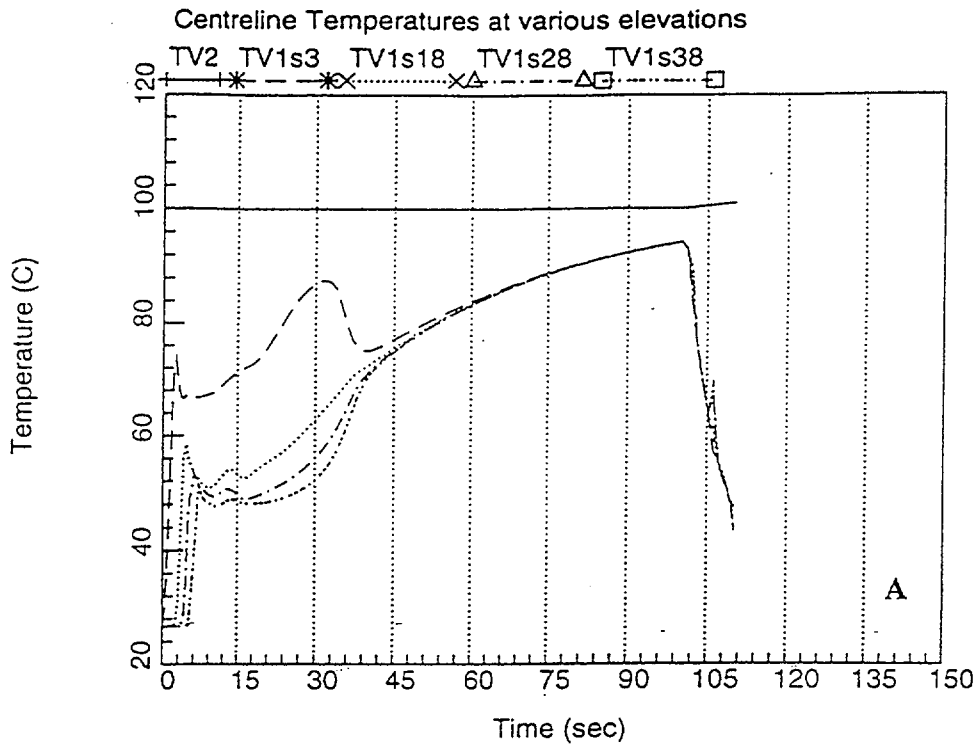


FIG. 2. Temperature histories at 4 differential axial locations along the central line for the box test-case with the standard (A) and modified (B) code.

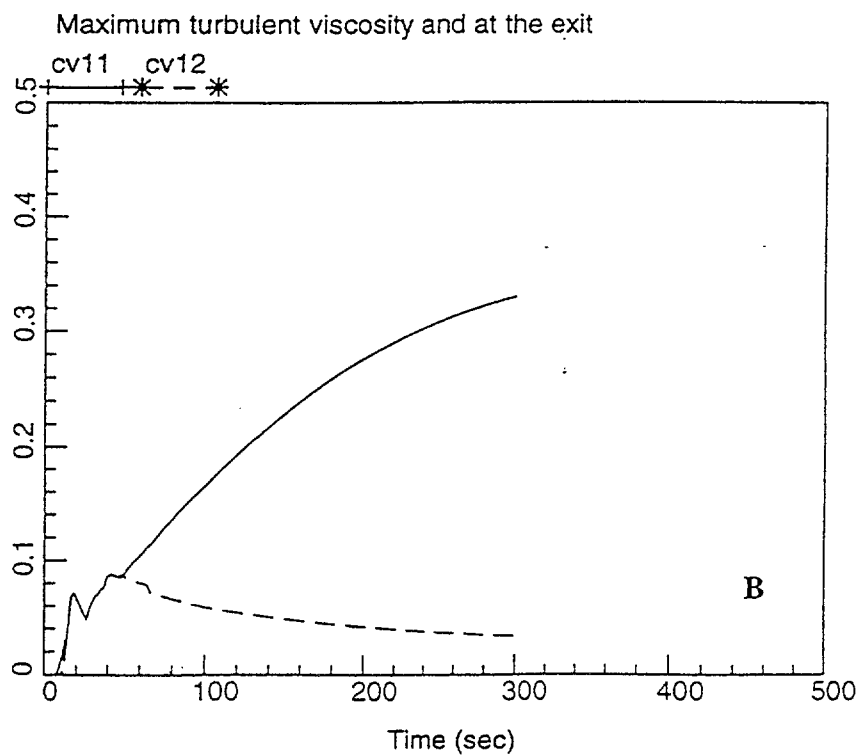
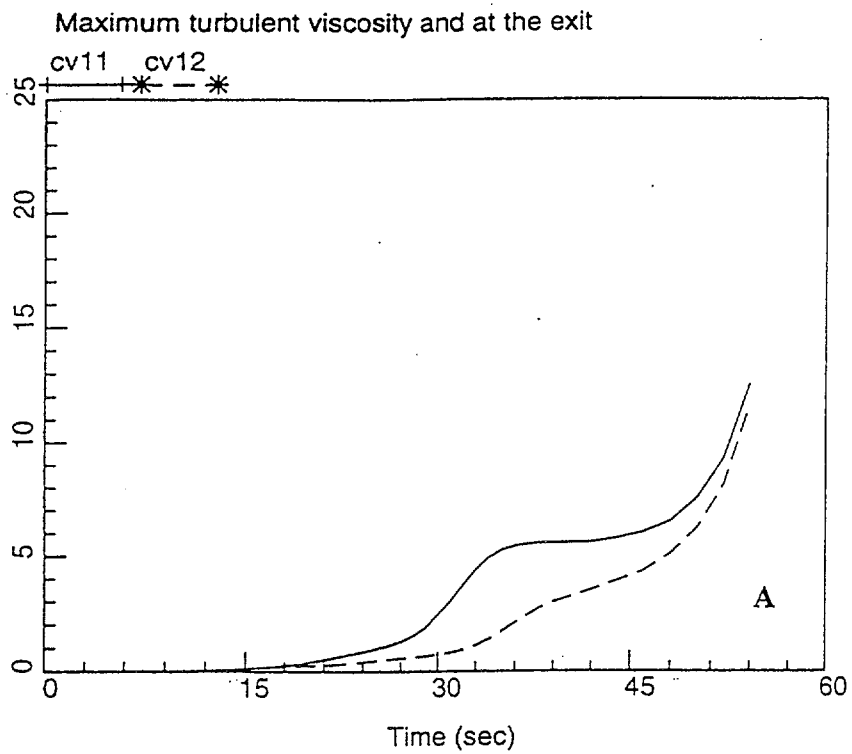


FIG. 3. Maximum turbulent viscosity (—) and turbulent viscosity at the outlet (.....) of the PANDA drywell with the standard (A) and modified (B) code.

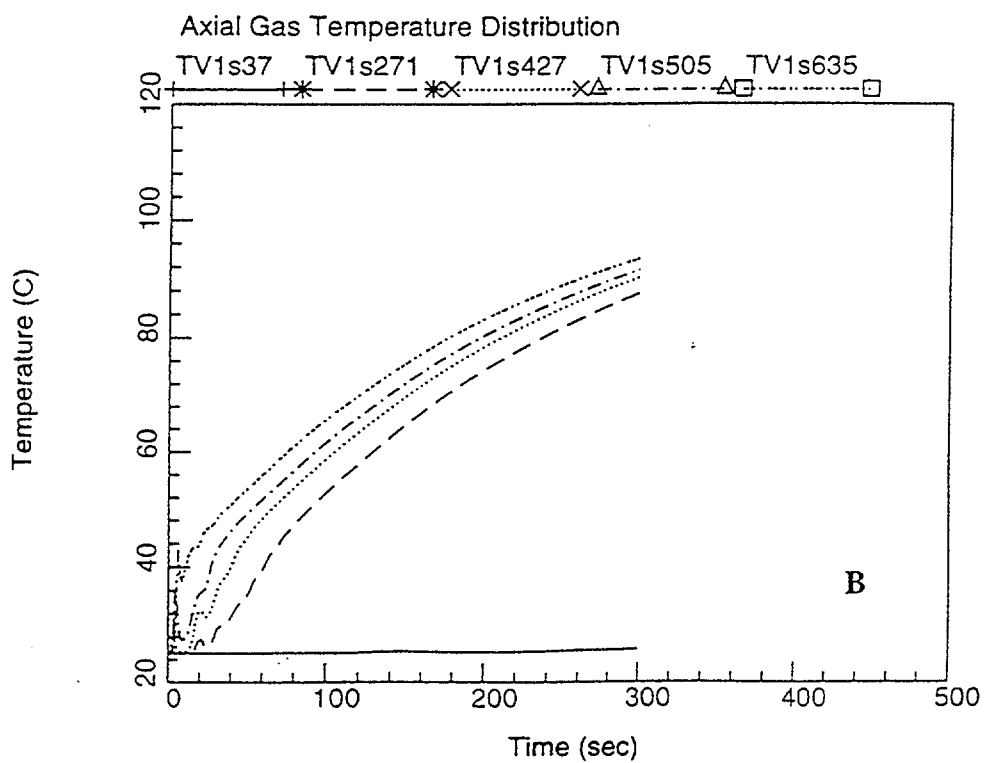
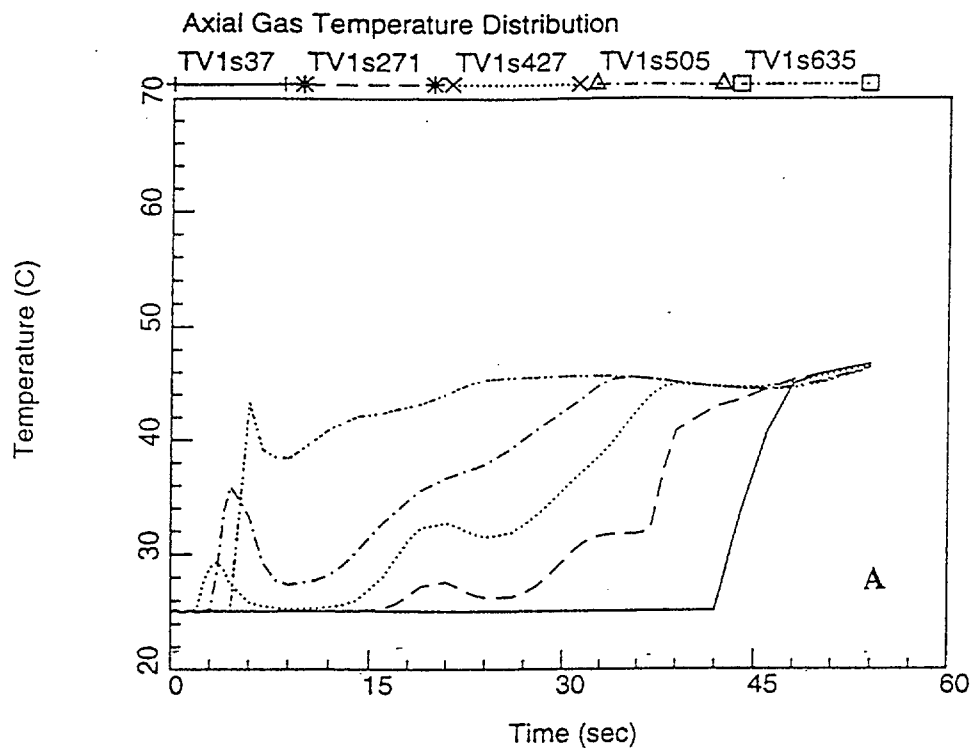


FIG. 4. Temperature histories at 5 differential elevations for the PANDA test-case with the standard (A) and modified (B) code.

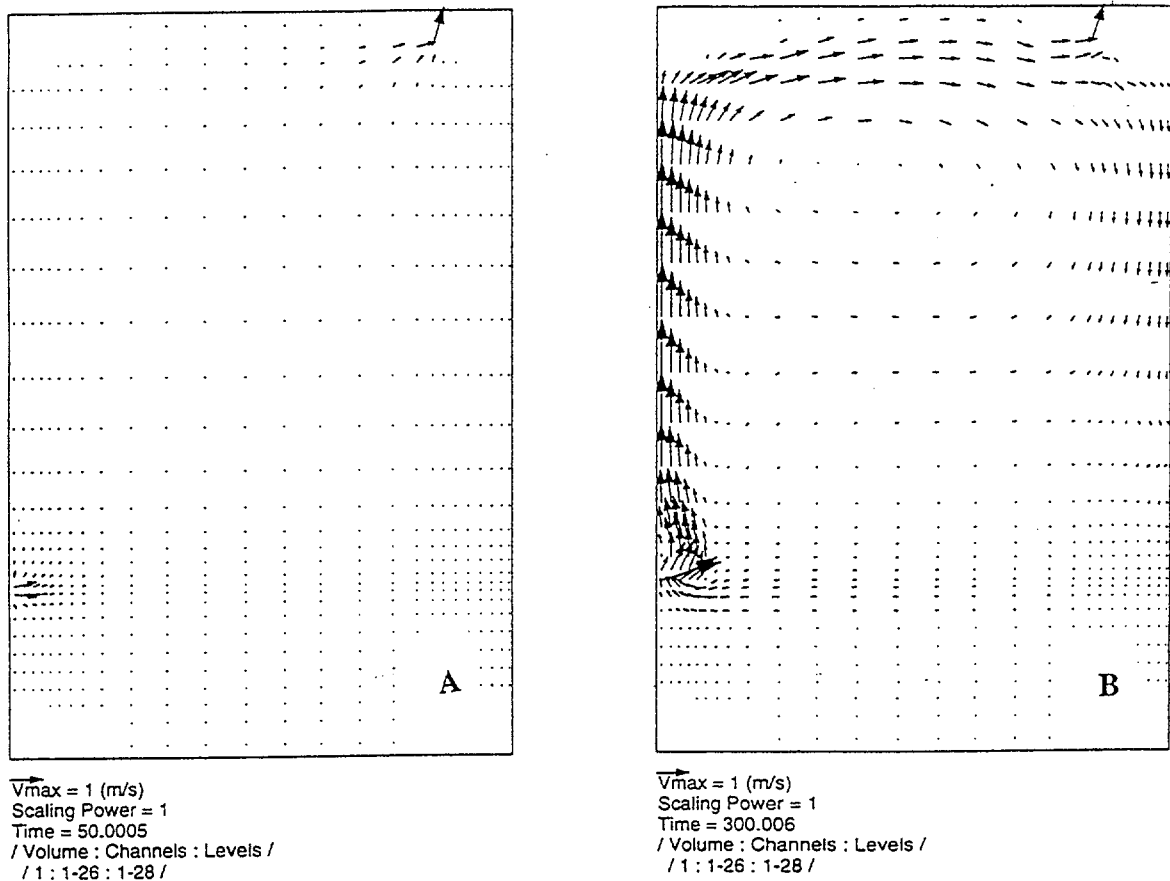


FIG. 5. Velocity vectors in the PANDA drywell at time $t = 50$ s with the standard code (A) and at time $t = 300$ s with the modified (B) code.

of the κ and ε model in GOTHIC were suspected as being the cause: (1) The production due to buoyancy and (2). The wall boundary conditions during the solution of the two κ and ε model equations. We showed that (1) was not the cause of the problem by running a simple test in which two parallel stream of different density were flowing in a plane horizontal channel. Hence, we focused our attention on (2).

4 CODE MODIFICATIONS AND PREDICTIONS

As we already mentioned before, in contrast to CFD codes which are aiming at looking at the very fine detail of the flow, in GOTHIC (version 6.0), the two κ and ε model differential equations are solved without properly taking into account the boundary conditions at physical boundaries like walls. After looking at the subroutine *turb.c* in which the κ and ε equations are solved, it was noticed that the necessary boundary conditions were actually enforced in a rather unusual and indirect fashion, quite differently to the way they are treated in other CFD codes. This we described in the previous section. In fact, in other CFD codes, the values of κ and ε at the centre of a near-wall cell are related to the mean velocity which is given by the universal logarithmic profile and the length scale which is the actual distance of the centre of the cell from the physical wall. The shear at the wall and the friction velocity are consistently calculated from the resulting values of κ . Though, the fact that the actual velocity must be equal to that given from the imposed velocity profile requires the usage of rather fine meshes close to the wall, so that the near-wall node is within the wall layer [6]. Instead, in

GOTHIC where for practical reasons, coarse nodding has to be used, the wall shear stress is calculated from an empirical correlation which relates the friction coefficient to the “free stream velocity”. Since such a velocity is taken to be equal to the average velocity in the near-wall cell (whatever the size of this cell may be), the information on the appropriate velocity, velocity gradients and length scales which relate κ and ε to the wall shear stress is not available. The boundary value of ε is thus (empirically) fixed at a distance of 50 non-dimensional wall units (see previous section), hence not directly related to the actual distance of the near-wall node from the wall. Although this approach seems to be a compromise between the required accuracy in the calculation of the turbulence quantities at the wall and the large meshes usually used for practical containment calculations, it is bound to fail under certain circumstances, since only one mesh size of the cell close to the wall can rigorously produce the desired consistency between κ and ε velocity and shear stresses. For any other mesh size, the calculation can result in large deviations from the equilibrium between turbulence production and dissipation and, in the worst cases like those reported in this work, in unbounded and unphysical large values of the turbulent kinetic energy κ and turbulent viscosity μ' . Nevertheless, this code logic must be retained independently of the modifications we made by restricting the value that κ can attain. Physically, the reason for the problems reported in the previous section are quite clear: At the wall, the turbulence kinetic energy κ should become zero while the dissipation ε should tend to infinity. Actually, what was happening during the analysis of some transients reported in this work was that the turbulence kinetic energy generated at different locations in the flow was reaching the walls and there, due to the lack of proper boundary conditions, was not dissipated. This together with the fact that κ was not equal to zero at the walls, led to a sudden and unbounded increase of κ . Clearly, as we discussed before, the proper way to handle this problem would be to introduce proper physical boundary conditions for the differential equations of the κ - ε model at the walls. Nevertheless, in line with the philosophy of GOTHIC which is a large-scale containment analysis code rather than one that should be able to model fine details like velocity profiles near the walls, we decided to deal with this problem in a simpler and indirect fashion. In particular, if one of the faces of a computational volume was closed by a physical boundary, in this volume, we restricted the turbulent kinetic energy of the gas by not allowing κ to exceed the average kinetic energy of the flow, i.e.,

$$\kappa = \frac{1}{2}(\overline{v_i v_i}) \leq \frac{1}{2}(\overline{v_i v_i})_g \quad (4.12)$$

where $\overline{v_i}$, is the average velocity and the subscript "g" is now used to denote that we are referring to the gas. Our restriction was imposed within this iteration scheme and in fact, we imposed this restriction for all iterations. Hence, if p is the iteration index ($1 < p < 20$), we set

$$\forall p: \quad \kappa^{n+1,p} = \text{Max}\left(\kappa^{n+1,p}, \frac{1}{2}(\overline{v} \cdot \overline{v})\right) \quad (4.13)$$

For most cases of interest, the turbulence kinetic energy κ should only be a percentage of the average kinetic energy of the flow unless there is strong circulation. Should this be the case near the wall (e.g., colliding jets), the average kinetic energy at a certain location could be nearly zero, while κ could be rather large. Hence, by imposing the aforementioned restriction on the magnitude of the turbulence kinetic energy κ , one cannot properly take into account this situation which, however, is beyond the capabilities of the κ - ε model. The way we implemented this logic in GOTHIC is explained in the Ref. 7. At this point, it is worth mentioning that there are three different places at which one can put this restriction: Just before the iterative solution of the κ - ε equations starts, within the iteration loop or after the

iteration loop. Experiments with all three methods revealed that although, for the transients analysed, the predictions obtained by these three methods were not very different, the best is if one imposes this restriction either within the iteration loop or after. Here, we should also mention that during our analysis by GOTHIC of transients of air bubbles injected from the bottom of a stagnant pool filled with waters, at a certain time, GOTHIC was terminating with a minimum time-step and negative pressures. To overcome this problem, we also restricted the liquid turbulent kinetic energy in all computational volumes and did not allow it to exceed the average liquid kinetic energy. This solved this problem and the runs were successfully completed, but only if the restriction of the liquid turbulence kinetic energy was imposed within the iteration loop.

By activating the aforementioned modification, we re-analysed the cases reported in the previous section which were exhibiting an unphysical behaviour. Furthermore, for the PANDA drywell case, even before κ started increasing to unacceptably high values making it impossible to continue the calculation, there were already a number of noticeable unphysical effects observed like the existence of recirculations at locations where there should not be any. With the modified code, the transients were successfully analysed and all the predictions were physically realistic. We shall now proceed and discuss the results obtained using the modified version of the code.

(a) *Box test-case*

In contrast to the unphysical predictions obtained when the standard version of the code was used for this very simple but highly instructive transient, when the modified code was used, all the variables predicted were physically sound and free of the problems encountered earlier. In particular, in Fig. 1B we show the maximum turbulent viscosity μ' as a function of time. As can be seen, μ' is now bounded and does not exhibit the unphysical behaviour exhibited when the standard code was used. In Fig. 2B, we show the temperatures at four different elevations; this is an indication of the time at which there is perfect mixing. For this case, it is clear that at $t = 250$ s, there is complete mixing.

(b) *PANDA drywell test-case*

In contrast to the "predictions" obtained by the standard version of the code and the different problems encountered, the modified version resulted in predictions which were absolutely physical and in agreement with the predictions of CFX [9]. Furthermore, even with the very detailed nodalisation, the code was running very fast, with a time-step in the range of 30 ms. As we already mentioned before, the reason for this is that κ is now restricted by a condition which is forcing it to attain physical values, hence not allowing a degradation of the time-step. This is a very clear indication that usually, small time-steps and hence, long running times are usually due to reasons other than the actual solution scheme used in the code.

Starting with the case of the fine nodalisation, in Fig. 3B we show the maximum turbulent viscosity and turbulent viscosity at the outlet until 300 s. Clearly, there is now nothing unphysical or peculiar about the behaviour of this quantity. In Fig. 4B, we show the temperature histories at five different elevations. Clearly, there is a gradual convergence of the temperatures at locations above the injection point while the zone below remains cold. In Figs 5B, we show the predicted velocity vectors in the PANDA drywell at $t = 300$ s. All velocity distributions are absolutely realistic, something which was not the case when the transient was analysed using the standard version 6.0 of GOTHIC.

Concluding, we should add that we also increased the time-step used by the code by changing in Eq. (2.11) the factor 5 to 2; by doing this, we relaxed the limitation on the time-step size when the $\kappa - \varepsilon$ model is used, hence achieving faster running times.

5 CONCLUSIONS

Different transients involving injection of hot air or steam into a vessel filled with cold air were analysed using the version 6.0 of GOTHIC, the aim of this work being to assess the code and investigate its limitations for modelling mixing phenomena. When the $\kappa - \varepsilon$ model was used (which is the appropriate model for such situations), for some of these problems, it was noticed that the turbulence kinetic energy κ was growing to unphysically high values. This was due to the lack of proper boundary conditions at closed boundaries when the two differential equations of the $\kappa - \varepsilon$ model are solved (i.e. a zero turbulent kinetic energy κ and a dissipation ε tending to infinity). Apart from the fact that the excessive increase of κ (and hence, of the turbulent viscosity μ') was resulting in an inevitable time-step reduction, the ultimate physical consequence of this abnormal and unphysical increase of κ was that within a very short time, there was perfect mixing in the vessel.

In order to by-pass this problem, we restricted the turbulent kinetic energy κ so that near a closed physical boundary, it could not increase above the value of the average kinetic energy of the flow at this volume. For most cases, this is a realistic restriction. Clearly, physically, this restriction which bounds the maximum turbulence kinetic energy to the one of the average flow is not always satisfied, and one can envisage situations in which if there is a circulation present, the turbulence kinetic energy can be larger than the average one.

Concluding this work, we would like to say that although the "fix" reported here helped us by-pass the unphysical increase of κ , one should in principle try to impose the boundary conditions on the $\kappa - \varepsilon$ differential equations in a way similar to codes like ASTEC or CFX. The modifications of the wall boundary conditions in the recent interim version 6.0a(QA) certainly address better the physical considerations above, though still in an empirical fashion, and produce naturally the same result which was the aim of our approach, i.e., to limit the turbulent kinetic energy at the wall. A fully consistent approach, however, cannot avoid the employment of fine meshes. Through, GOTHIC which is a large-scale reactor containment analysis code with aims radically different to the ones of other very detailed CFD code. Consequently, we think that a more pragmatic approach aimed at keeping the parameters of turbulence within physical bounds, such as the one suggested in this paper, should be followed, unless one is really interested in what is happening very near the walls, something which is clearly outside the scope of GOTHIC.

ACKNOWLEDGEMENTS

This work was supported by the European Commission (4th Framework Programme on Nuclear Fission Safety) and the Swiss Federal Office for Education and Science. These contributions are greatly acknowledged. The authors would also like to acknowledge a number of interesting discussions and information exchange with Tom George of Numerical Applications, Inc. and also thank G. Yadigaroglu for critically reading the manuscript.

REFERENCES

- [1] M. STOOP et al., "TEPPS - Technology Enhancement of Passive Safety Systems", Proc. 5th International Conference on Nuclear Engineering (ICONE 5), Nice, France, May 26-30, 1997.
- [2] DREIER et al., "The PANDA facility and first test results", Kerntechnik, 61, 214-222 (1996).
- [3] L. GEORGE, et al., "GOTHIC Containment Analysis Package Technical Manual." Report NAI 8907-06 Rev 5 (1995).
- [4] "CFX-4, AEA Technology, Harwell, Oxford OXI I ORA", U.K. (December 1997).
- [5] SMITH, "On Boundary Layer Modelling Using the ASTEC Code", PSI-Bericht Nr. 101, July 1991.
- [6] RODI, "Turbulence models and their application in hydraulics - A state of the art review" (1984).
- [7] TH. ANALYTIS and M. ANDREANI, "Modifications of the $\kappa - \varepsilon$ Model in GOTHIC Near Physical Boundaries", PSI Internal report TM-42-98-15, ALPHA-814-0 (1998).
- [8] G.TH.ANALYMS, "Modelling of Bubble and Thermal Plumes by GOTHIC", PSI Internal report TM-42-97-09 (1997).
- [9] SMITH AND M. ANDREANI, PSI Internal Report, to appear (1998).



RELAP5 CAPABILITIES IN THERMAL-HYDRAULIC PREDICTION OF SBWR CONTAINMENT BEHAVIOUR: PANDA STEADY STATE AND TRANSIENT TESTS EVALUATION

V. FALUOMI

Dipartimento di Costruzioni Meccaniche
e Nucleari,
University of Pisa,
Pisa, Italy

S.N. AKSAN

Thermal-Hydraulics Department,
Paul Scherrer Institute,
Villigen, Switzerland

ABSTRACT

This paper summarizes the results of the qualification activity of RELAP5/Mod 3.2 code performed using PANDA steady state and integral test experimental data. The steady state tests evaluate the PCC performances in removing decay heat power in presence and in absence of non-condensable gases, while the considered integral test (M3) simulates the transient following a break in the main steam line of the SBWR, using, as nominal initial conditions, those calculated for the SBWR under SSAR assumptions at one hour into the LOCA.

The results obtained simulating both types of tests show a rather good and robust overall code behavior both in the simulation of steady state test and in the representation of the integral test considered: most of the main experimental results (WW/DW pressures, PCC heat exchange) were well represented by the code.

The different studies performed indicated that:

- Different models of PCC pool lead a different trend of system pressure, and sometimes to an opening of vacuum breaker valves, that does not occur in the transient;
- The code underestimate the heat exchanged between PCC pool and tubes: in the considered test the system pressure is slightly overestimated (maximum 2% more than the experimental value). This fact is also proved by the differences in the temperature of the condensing mixture in the PCC, quite large in all the performed studies;
- The treatment of the non condensable gases, as implemented in the code, lead some errors in the calculation of the heat transfer coefficient in the PCC components and generally slow down the overall calculation.

In general terms, the RELAP5/Mod3.2 was found to be suitable to represent the SBWR containment behavior under the conditions specified in the experimental side.

1. INTRODUCTION

The considered steady state tests (B serie)^{11,12} have been performed to evaluate the PCC performances in removing the decay heat for different conditions of pressure, related to different level of power provided. These tests were also performed to provide a set of experimental data with well defined boundary conditions needed to assess the system codes used for safety analyses. Test M3³ is the base case for the PANDA transient integral systems test program for M series. It is a simulation of a break in the main steam line of the SBWR. The nominal initial containment conditions were similar to those calculated for the SBWR under SSAR assumptions at one hour into the LOCA. The initial drywell pressure was approximately 300 kPa. One-half of the steam from the RPV was directed to DW1, which feeds one PCC condenser, and the other one-half of the steam was directed to DW2 with two PCC condensers connected. This was achieved with separate blowdown lines from the RPV to each of the two drywells. The two blowdown lines have essentially equal flow resistances. These test conditions represent a symmetrical situation in the PANDA facility. The M3 test provides a base case for comparison to all the other M series transient tests.

2. TEST FACILITY CONFIGURATION AND INITIAL CONDITIONS

2.1 Steady State Tests

A series of steady state tests have been conducted using one of the PANDA PCC condensers. In total, the B serie of steady state tests includes three pure vapour tests, 6 air-vapour tests and three helium-vapour tests, for

different values of system pressure and gas contents. In Tabs. 2.1 the main boundary conditions identifying the different tests are given.

To run the above mentioned tests, the facility has been configured to inject known flowrates of saturated steam and air directly to the PCC3 heat exchanger. For the pure steam tests the condenser pressure was left to reach the equilibrium for a certain value of inlet vapor. The steam flow to the heat exchanger was controlled and measured. In addition, the condenser drain flow and vent flow was measured. For these tests with no air flow, the PCC3 vent was closed. The PCC non-condensable contents were discharging on the Wetwell through the vent line, open in these tests.

2.2 M3 Integral Tests

The PANDA test facility is described in detail in ref. [4] . For test M3 the PANDA facility was configured to simulate the SBWR post-LOCA configuration as follows^{[5],[6],[7]}:

- The RPV supplies steam to each drywell with two steam lines (one to each drywell). These two steam lines have the same pressure loss characteristics and, therefore, allow for symmetric injection of steam into the two drywells.
- The RPV heater power is controlled as a function of time to simulate the scaled decay heat and stored energy release (as specified in ref. [4]).
- All three PCC units are lined-up to take feedflow from the drywells, to vent non-condensables and steam into the water volume of the suppression pool, and drain condensate to the GDSCS volume.
- The three PCC pools are filled and interconnected at the bottom. During the test, no water is added or drained from the pools. The IC pool is isolated from the PCC pools.
- The only direct lines of communication between the drywell and wetwell are through the vacuum breakers (when the wetwell pressure exceeds drywell pressure sufficiently to open the vacuum breaker) and the main vent lines (which are submerged within the wetwells).

The test initial conditions represent the state of the system one hour after scram. These conditions are presented in Tables 2.2 and 2.3. Those are the average values measured just before connecting the drywells to the RPV, and are the values used to set-up the initial conditions for the code calculations.

Tab. 2.1: Initial conditions for Helium-Vapour Steady State Tests

PANDA Test No.	System Pressure (bar)	Steam Flow (kg/s)	Core Power (kW)
B1	3.07	0.222	432
B2	6.25	0.495	1050
B3	8.99	0.675	1350
B4	3.07	0.222	0.0003
B5	3.07	0.222	0.003
B6	3.07	0.222	0.028
B7	6.19	0.495	0.0003
B8	6.19	0.495	0.003
B9	6.19	0.495	0.028
B10	8.98	0.675	0.0003
B11	8.98	0.675	0.003
B12	8.98	0.675	0.028
B13	8.98	0.675	0.000041
B14	8.98	0.675	0.00041
B15	8.98	0.675	0.00387

Table 2.2: Test M3 Initial Conditions

COMPONENT	Pressure (Pa)	Temperature (K)	Air Partial Pressure (Pa)	Level (m)	Mass Flow (Kg/s)
RPV	2.99e+5	406.5	-	12.63	-
WW	2.87e+5	Gas:350 Water :351	2.45e+5	3.88	-
DW	2.87e+5	402	0.19e+5	0.13	-
GDSCS	2.90e+5	333	2.9e+5*	0.0	-
PCC	2.87e+5	406.5	-	0.0	-
POOLS	1.0e+5	370	-	4.49	-

PARAMETER	Unit	Value
Test Duration	(s)	60000
Start Power	(W)	1.12e+6
Pool Connections	-	open at 0.0 s.
Total Heat Losses	(W)	2.0e4

Table 2.3: Test M3 Boundary Conditions

3.SOME RESULTS OF STEADY STATE AND M3 INTEGRAL TEST

3.1 Steady State Experimental Results^{2/}

In Fig. 3.1 are summarized the main results obtained analyzing the PCC performances for different decay power level, corresponding to three different level of inlet pressure. The PCC performances are evaluated using the efficiency parameter, measuring the ratio between the amount of flow condensed in the PCC and the total inlet flow. The experimental results for steady state tests show a large impact of non-condensable gases in the PCC performances for low pressure conditions (3 bar, tests B4,B4 and B6). Increasing the air quality at PCC inlet from 0.1% to 12% the PCC efficiency drops down from 99% to 59% . This behaviour is less pronounced for the tests performed at 6 bar (tests B7,B8 and B9), where the efficiency drops from 99% to 78%, and the PCC performances reach a near linear behaviour for the tests performed at high pressure (9 bar, tests B10,B11 and B12).

3.2 M3 Integral Test Experimental Results^{2/}

The test M3 showed a favorable and robust overall PCC system performance. The pressure response shown in Fig 3.1 (RPV, WW and DW components) was as expected. The drywell pressure reached the peak value of 3.27 bar approximately 2.4 hours after test initiation. Then the pressure slightly decreased until the end of the test. After the startup transient the drywell/wetwell pressure difference is determined mainly by the PCC vent hydrostatic head (submergence in the suppression pool) and to a small amount by the PCC feed line pressure drop. The drywell/wetwell pressure curves also show that there was no vacuum breaker opening, and was far from taking place, throughout the test period. As can be seen from Fig. 3.3 which shows the PCC feed inlet mass flow rate, the three PCC units shared the load among themselves as needed. About 10 hours after test initiation PCC2 got less steam to the end of test. Small amounts of air have an effect on the individual PCC performance, but do not affect the overall system behavior. The PCC feed flows were apparently measured adequately, for PCC1 and PCC3 for the entire test, and up to time $t = 40000$ seconds for PCC2. At that time the PCC2 instrument fell below its lower range (Fig. 3.3). However, the value of the PCC2 feed can be estimate from the difference between the RPV steaming rate and the mass flows in the other two PCCs.

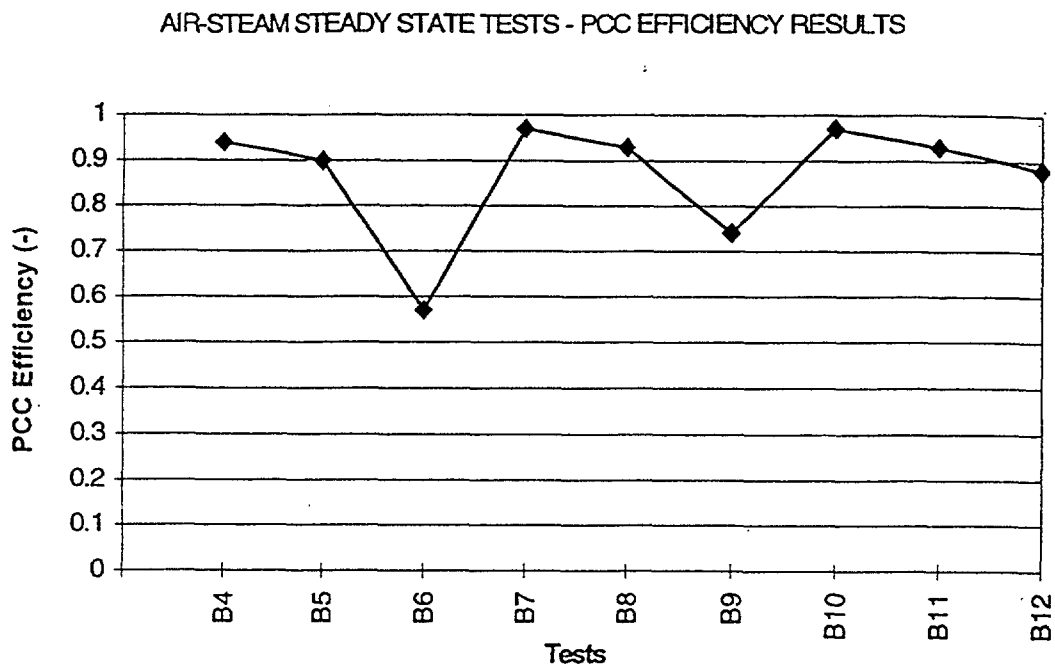


Fig. 3.1: PCC3 Efficiency for Air-Steam Steady state Tests

The estimated PCC2 feed becomes lower than the other two at about 40000 seconds. The corresponding PCC2 pool temperature dropped (at lower pool levels) to about 95 C (with possibly hotter water above and some stratification). The PCC2 wall and gas temperature distributions were different from those of the other two PCCs.

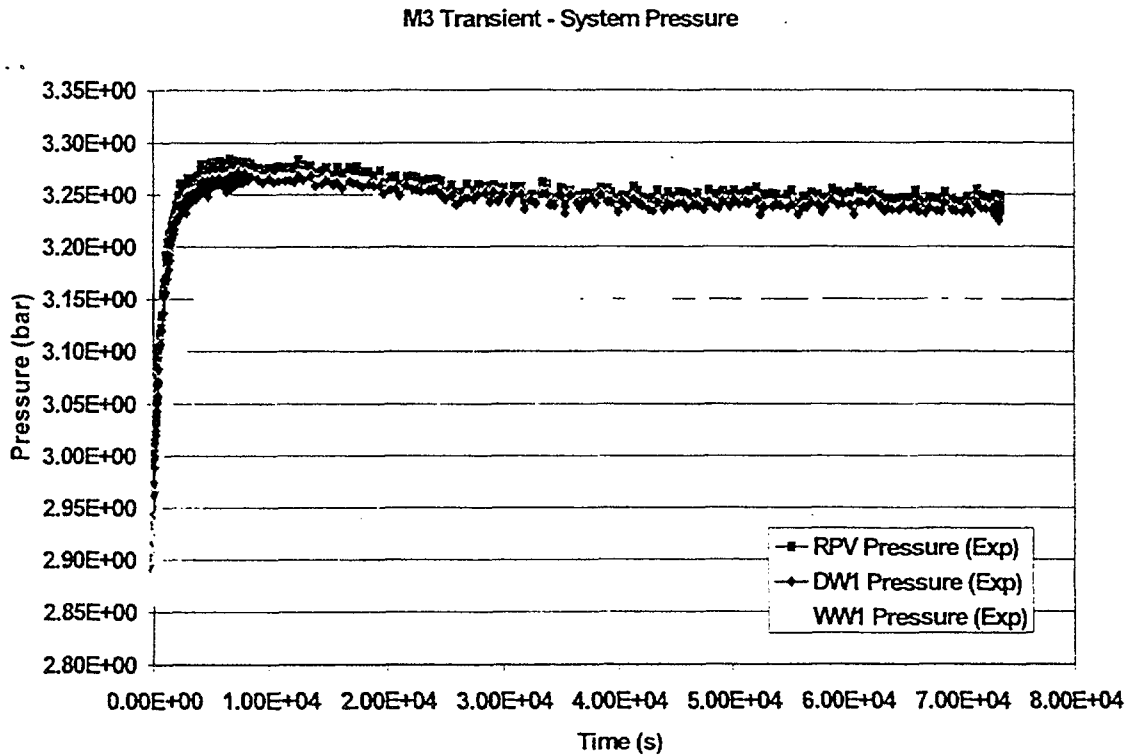


Fig. 3.2: RPV, drywell and wetwell Pressures

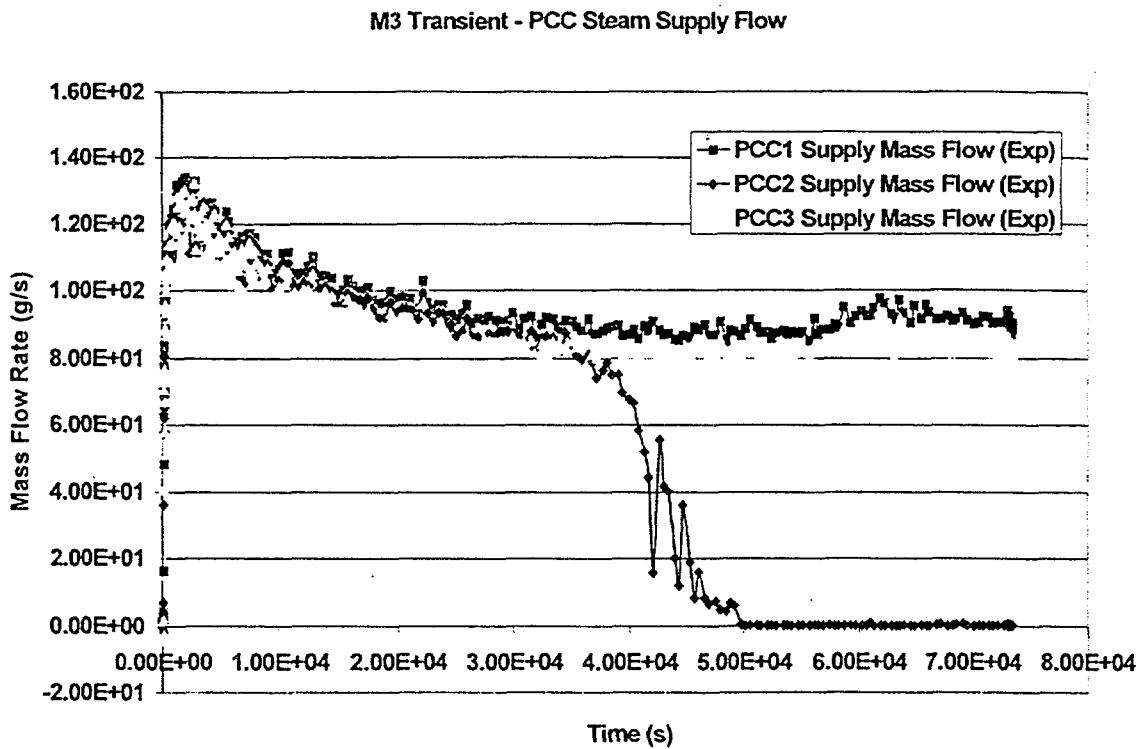


Fig. 3.3: PCC Feed Mass Flow Rates

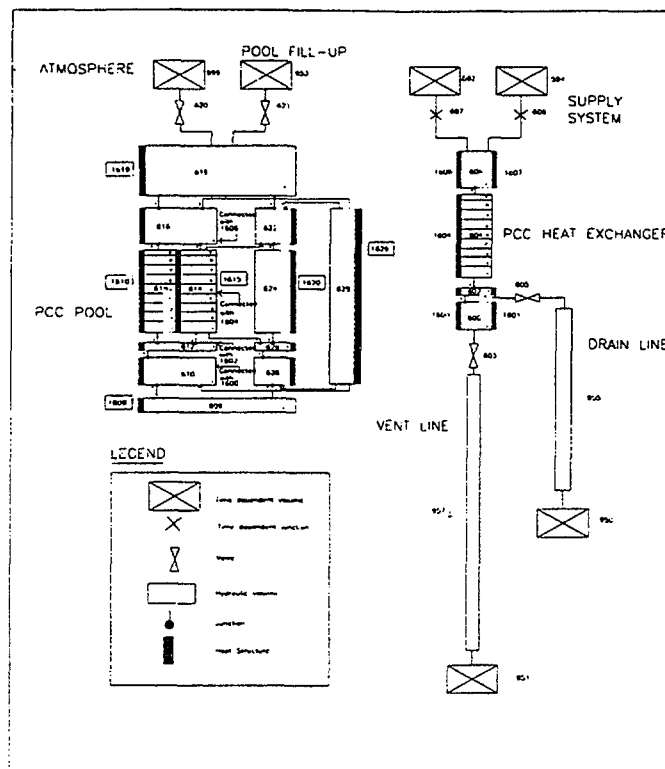
4.THE USED COMPUTER CODE AND SIMULATION SCHEME

The standard frozen version of the RELAP5/Mod 3.2^{8/} has been used as basis of the computer code calculation and analysis in the present study. None of the possible user selected options has been activated when performing the reference calculation; necessary adjustments of initial and boundary conditions, within the experimental uncertainty bands, have been done with this frozen code version ("reference" code version) aiming at getting the "base calculation. The following tasks provided input to the overall strategy of the analysis performed for the PANDA-M3 test:

- transient qualification of the PANDA input deck, as indicated, in detail, in ref. [9] ;
- assessing the capabilities of the "reference" code version used and identifying possible improvements with respect to "reference" code version, in a limited way;
- investigation of nodalization by effects performing calculations with different nodalization schemes of the facility;

An additional objective of the analysis was to confirm the overdesign of the PCCs in removing heat removing and the related capability to maintain most of the core stack covered.

The PANDA PCC nodalization used to simulate the steady state tests is shown in Fig. 4.1, while in Fig. 4.2 the sketch of the nodalization used to simulate the M3 integral test is reported. This nodalization model has been developed as the base nodalization to perform post-test analyses of M-Series of PANDA tests within ALPHA-1 program. Naturally, this base nodalization model can also be used with necessary modifications for the ALPHA-2 program which includes European Community supported projects, e.g., BWR Cluster (IPPS) and TEPPS.



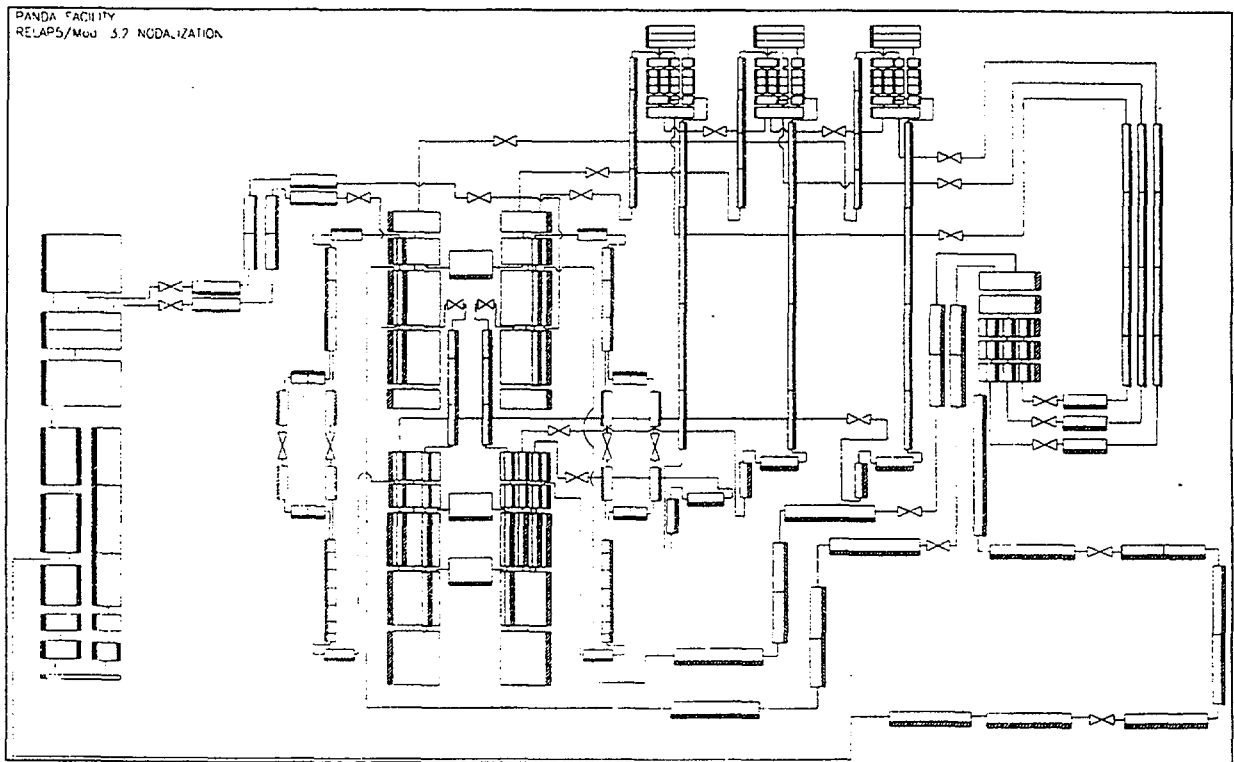


Fig. 4.2 : The PANDA base "reference nodalization" scheme for RELAP5/Mod3.2

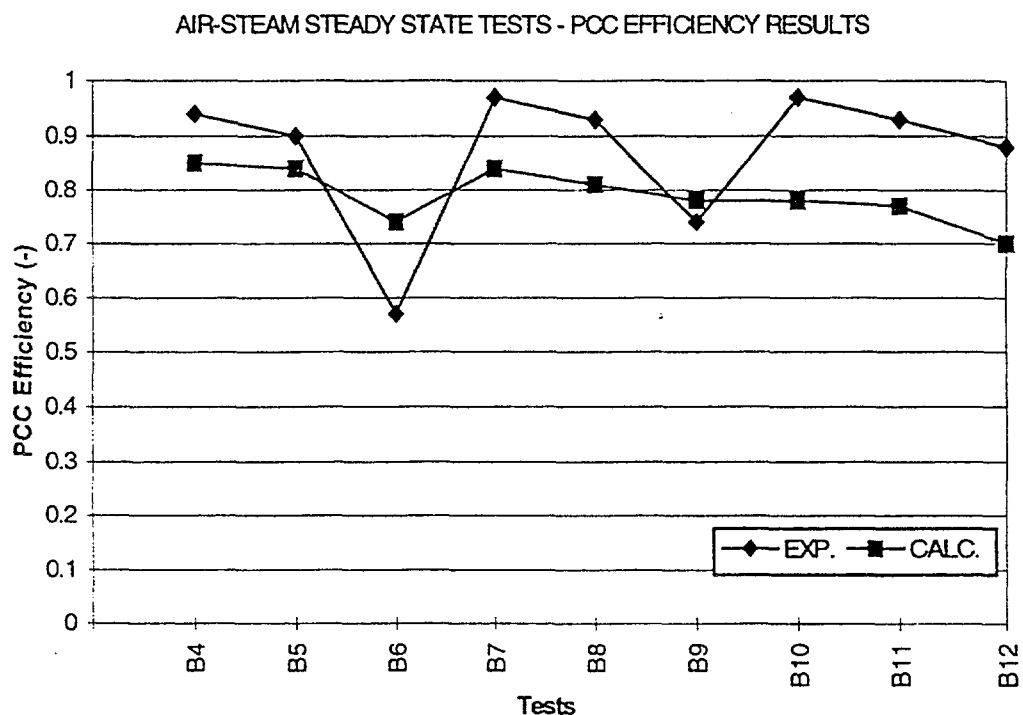


Fig. 5.1 : Experimental and Calculated Efficiency for Steady State Tests (Air-Vapour Tests)

For air-steam tests (Fig. 5.2), there is a general tendency from the code to underestimate the PCC efficiency. This is related to the underestimation of heat transfer coefficient in condensation, and partially can be addressed in the same way as in the last section.

Concerning the impact of non-condensable gases in the code calculation, it seems that the non-condensable effect is underestimate for higher concentrations of gas in the vapor, and overestimate in the case of low

concentration of non-condensable gases. Any conclusion, anyway, should take in account also the behaviour of the code during pure steam calculations, where a noticeable impact of the system pressure in the code accuracy has been identified.

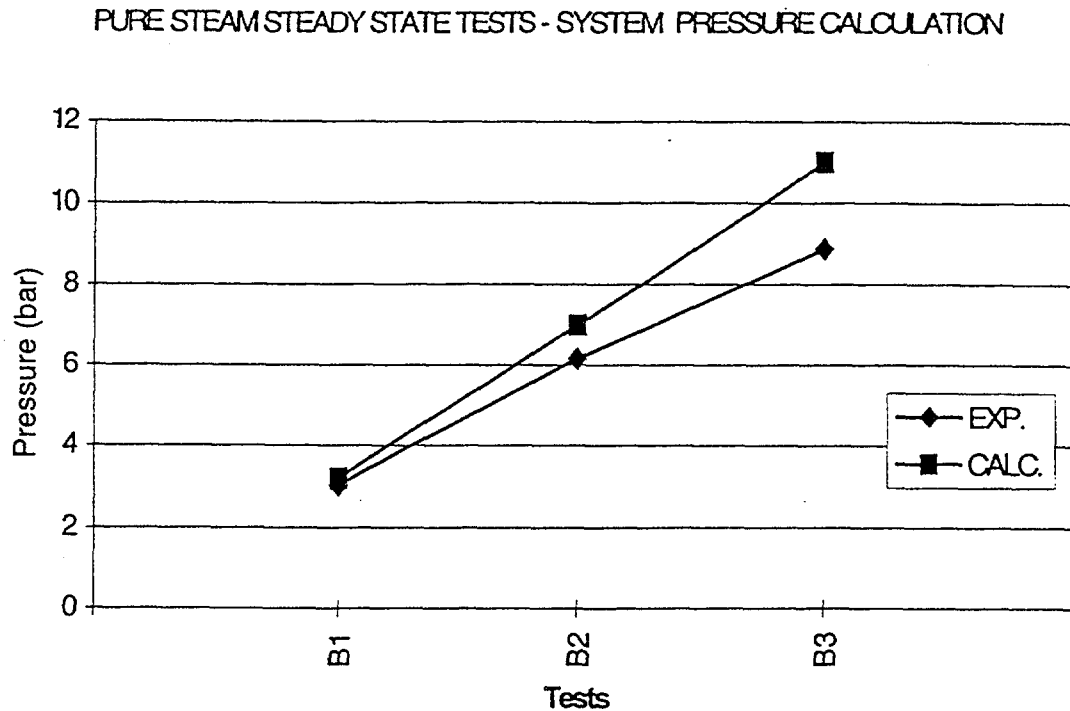


Fig. 5.2 : Experimental and Calculated Pressure for Steady State Tests (Steam Only Tests)

5.2 M3 Integral Test^{/12/}

Concerning the evaluation of the base calculation of PANDA M3 experiment, the following results were achieved:

System pressure behaviour: In order to better address the comparison between measured and calculated trends, three main regions can be distinguished looking at the system pressure (Figs 5.3 and 5.4):

- **Region A** from transient begin till about 1000 s: This region is characterised by a sharp increment of system pressure, up to 3.3 bars. This is the effect of imbalance between the heat produced in the core and the heat exchanged in the PCCs. In this region the code predicts for the RPV and the DW a smooth pressure trend, compared with the experimental one. This is mainly due to the early start of the PCCs, the calculated final pressure in this region is slightly lower than that of the experiment (about 0.05 bar). For the WW pressure, due to the large discharge of the PCC vent line the code overestimates slightly the pressure.
- **Region B** from 1000 s till 10000 s: In this region, the system pressure increases smoothly, till an equilibrium value is reached (at about 9000 s), which will be (more or less) maintained during the rest of the transient. In the region the code overpredicts the system pressure, but represent almost the trend. Towards the end of this region, the pressure continues to decrease slightly instead of staying constant as in the experiment case. The reason of this slight pressure decrease is due to the PCCs behaviour; in fact, the PCCs performances are under the experimental value till 6000 s, while their efficiency increase after this time period. The amount of non-condensables in the PCC tubes and the behaviour of the condensation model of the code may explain the differences detected among experimental and calculated data. Due to the continuous discharging from the PCCs vents, the WW pressure increases and the maximum overestimation is around 0.1 bar at 5000 s. Then the pressure start to decrease, because of the increase of the PCC efficiency.
- **Region C** from 10000 s till the end of the transient: In the experiment during this phase not much happens, except the decrease of PCC2 performance. The system pressure stays constant, while in the code calculation it continues to decrease till the end, reaching roughly the experimental value at 59000 s. This drop of the system pressure in the code calculation is mainly due to the overestimation of the heat exchanged in the PCCs. This affect also the WW pressure, and consequently the calculated WW pressure approaches that experimental one (the overestimation at the end of transient is about 0.005 bar).

M3 DryWell Pressure

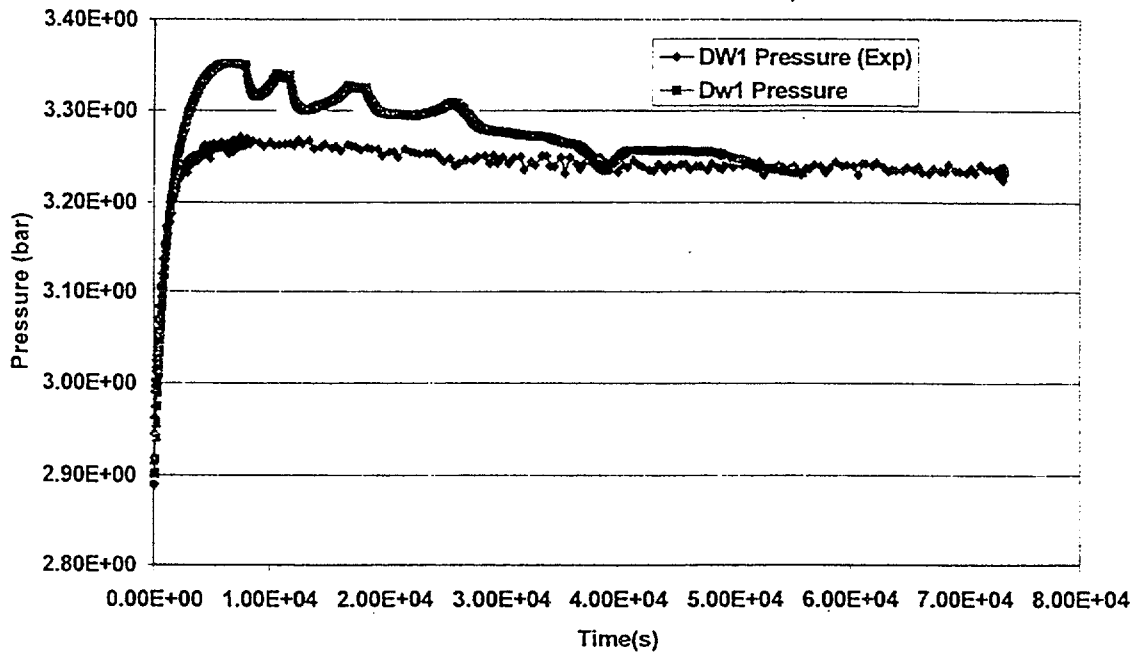


Fig. 5.3 : DW pressure

M3 WetWell Liquid and Gas Temperature

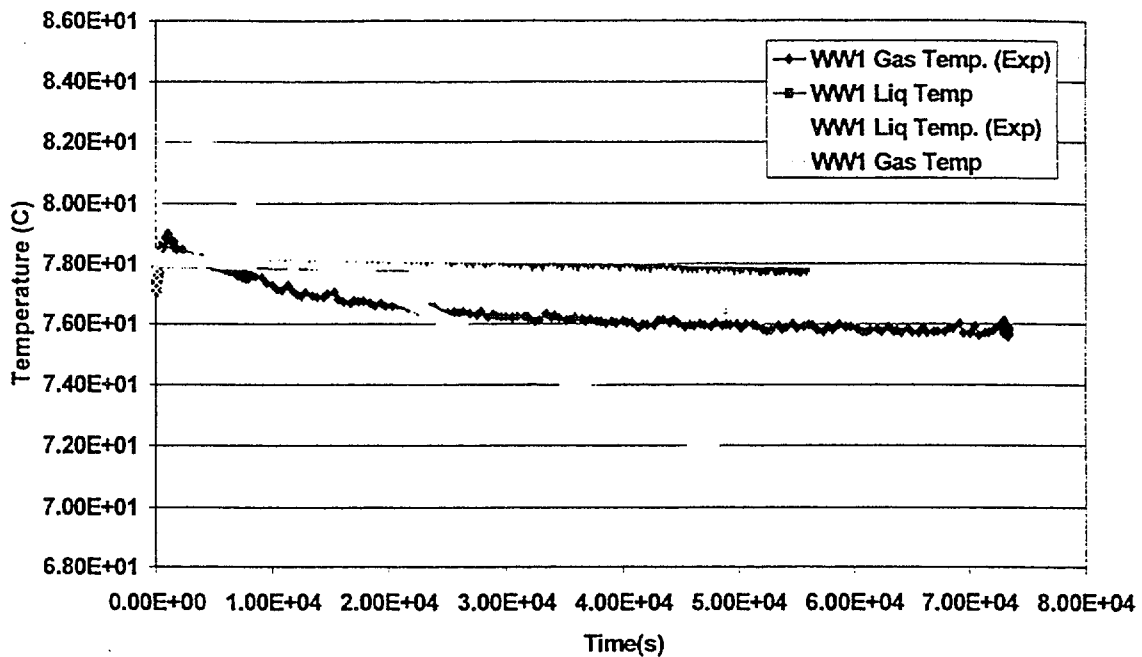


Fig. 5.4 : WW pressure

PCC Tubes Temperatures and levels: The fluid temperatures in the PCCs tubes are influenced by the distribution of the non-condensables in the tubes of PCCs (Figs. 5. 5 and 5.6). In the experiment, at the tube mid-height and at the bottom, the temperature drops to the outside pool temperature during early phase of the transient, but in the calculation the temperature stays around 385 K, without reaching to pool temperature. This is probably due to the different concentration of the non-condensables among experimental and the calculated data. In fact, in the experiment, the derived quality of PCCs air concentration is roughly 0.75, when in the calculation is not more than 0.6. The temperature trend is anyway similar between experimental and calculated data.

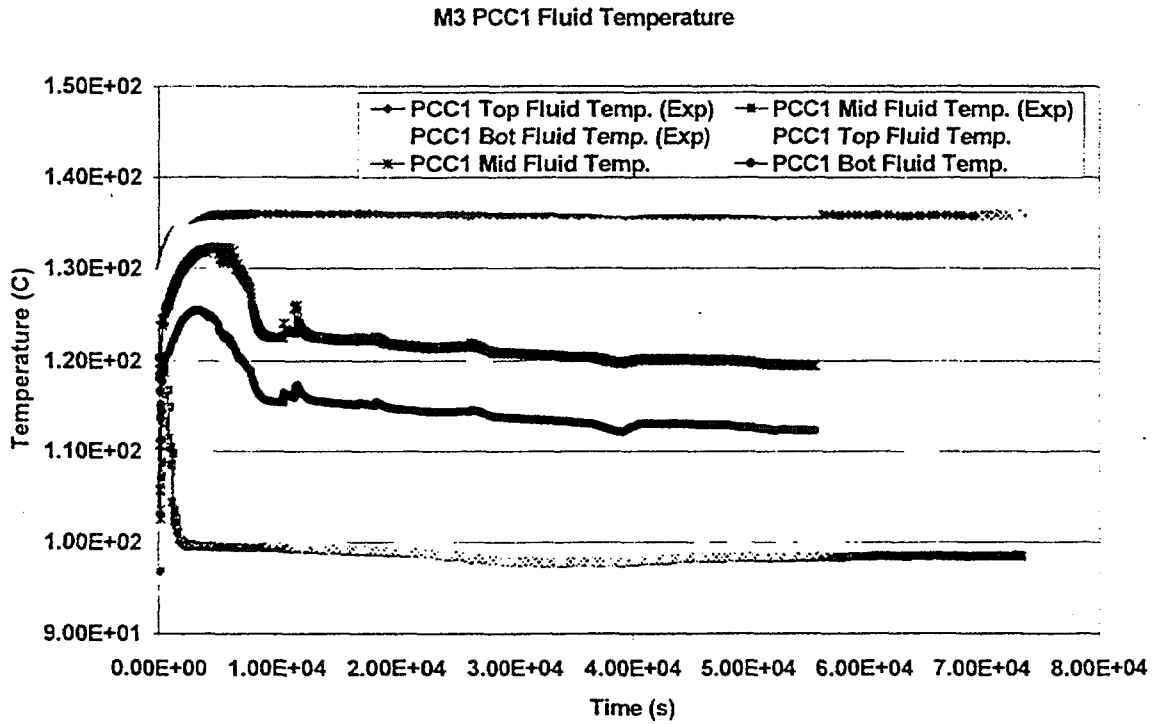


Fig. 5.5: PCC1 fluid temperatures along the bundle

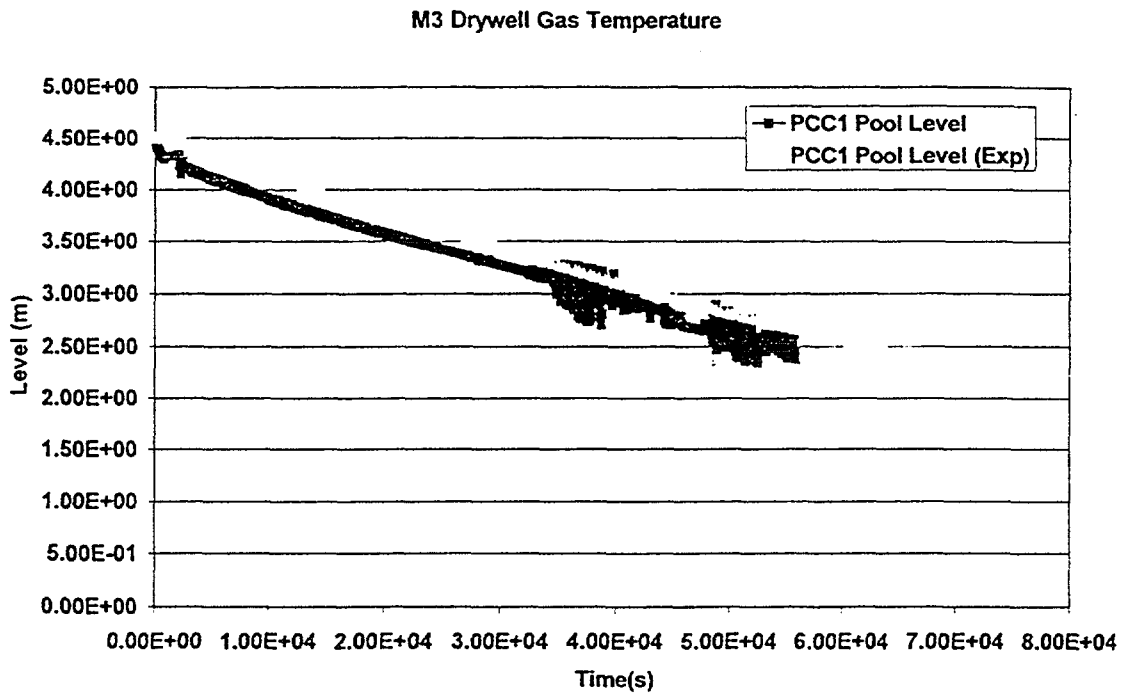


Fig. 5.6: PCC1 pool liquid level

The PCCs pool liquid levels are reasonably well represented. Some remarks can be noted as below:

- there are some jumps in the calculated liquid level, especially at the beginning of the transient. These are corresponding to the crossing of the level from one volume boundary to another volume, on the top of the pool. With the present nodalization of the PCC pool, in this version of the code it was not possible to avoid this type of level jumps, even using special models as the level tracking option, that seems not working in this release of the code.

- After 35000 s., the pool level starts to heavily oscillate. This is mainly due to the upper drum becoming uncovered and the recirculation of the fluid taking place only locally near to the tube bundle, and not involving anymore the bulk of the pool fluids. These oscillations are mainly due by the change of the flow regimes, with related changes in the calculated heat transfer coefficients. These oscillations are also responsible for the major part of the mass error seen at end of the calculation. In terms of calculation stability, however, these oscillations do not affect too much the calculation, and, in particular, the calculated heat exchanged.
- In absolute values, the pool level are generally underestimated about 0.15 m, and the experimental trend is overall conserved, showing a consistent calculation of the total heat exchanged from PCC tubes and pools.

PCC non-condensable accumulation: As mentioned in the previous section, the quality of non-condensables in the PCC tubes is between 0.5 and 0.6, during the transient (Fig. 5.7). These values are lower than the estimated experimental value for the quality of non-condensables in PCCs (about 0.75) and can be explained with the underestimation of the condensate liquid in the tubes. Further analyses showed that, in effect, part of the steam flow coming from the DW is condensed in the drain line, and this lead a low concentration of non-condensables gases in the PCC tubes.

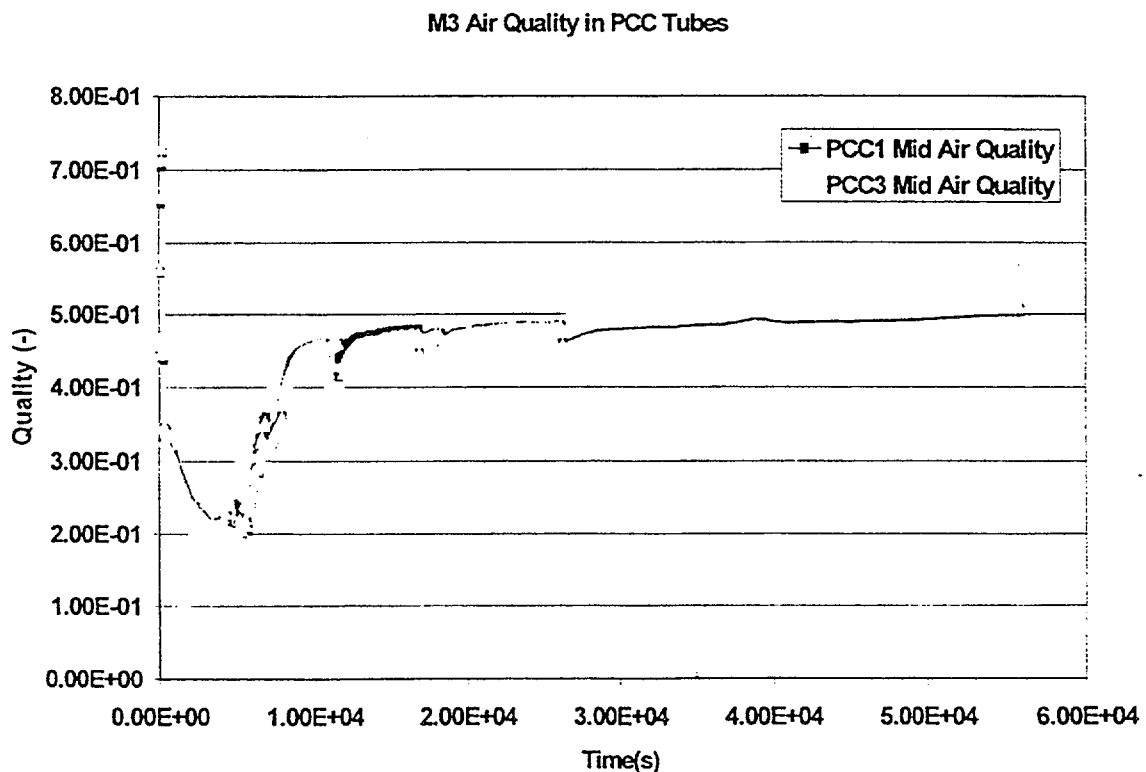


Fig. 5.7 : Non-condensables gases in the PCC tubes

6.CONCLUSIONS

In the frame of the research activities aiming at the evaluation of the capabilities of RELAP5/MOD3.2 system thermalhydraulic code to analyse the performances of SBWR containment component, the steady state tests, together with the M3 test performed in the PANDA facility have been analysed. This suppose to simulate both the PCC behaviour under accident conditions and, in the case of integral test M3, a transient starting one hour after a Main Steam Line Break in the SBWR plant. The results achieved from the activity are:

- the qualification of the PANDA model for the RELAP5/MOD3.2 code;
- the evaluation of the code suitability to be used for these transients;
- the evaluation of some relevant parameter impact in the code results.

In the following, some relevant conclusions about code capabilities in simulating the main thermalhydraulic phenomena taking place in the SBWR containment have been summarised.

About steady state tests these conclusions can be drawn:

- During the simulation of pure steam steady state tests performed in the PANDA facility, the code RELAP5/Mod3.2 shows general overprediction of the system pressure, especially for high pressure conditions. The main reason is the underestimation of the heat transfer coefficient of primary and secondary side;
- For the air-steam tests, and for the helium-steam tests, this underestimation affects strongly the results, because the heat transfer coefficient calculated in absence of non-condensable is still partially used in the determination of the heat transfer coefficient in presence of non condensable gases. Nevertheless, from these tests one can identify that the code overestimates the non-condensable effects for low concentrations of gases, while this effect is underestimated for high concentrations of non-condensable gases.

Concerning the activity involving the integral test analysis, these conclusion that can be summarised about code results:

- The distribution of non-condensables on the system was partially wrong calculated: in particular, low values of non-condensables were calculated in the PCCs, keeping the heat transfer coefficient higher than in the experimental test. The PCCs temperature along the tubes show a final difference about 15 K (among experimental and calculated values), meaning that, at least in the lower part of the PCCs, the accumulation of non-condensables is largely underestimated;
- The heat transfer coefficient among tubes and pool is overestimated: it is not completely clear if it is just a effect of non-condensable distribution , or this distribution is given by the overestimation, by the code, of the heat flux exchanged between tubes and pool. Some results obtained from steady state calculations shown that, in general term, the code tends to overestimate the heat transfer coefficient for the condensation side. So that, this might be another case where this overestimation take place;
- The last item bring the attention to one of the major lack of code model identified from the analysis: a proper model for simulating large and nearly steady state boiling pools. The code, at this stage, need to have some circulation on the pool loop to better calculate the heat transfer coefficient. In this way, the code provide the correct mass flow rate to be used in the heat transfer model. When the level drop down, this recirculation is stopped and the code cannot anymore calculate an appropriate liquid mass flow, because the upper part of the pool is already empty. This effect is what, probably, excites the pool level oscillations and the secondary side pool heat exchange.

As a final comment, the code showed a reasonable good behavior for the transient considered, and the nodalization used has been considered suitable to represent the facility, considering the good accuracy of which the main transient parameters are represented, and considering also the acceptable numerical stability both of the base calculation and the sensitivity analyses performed. Some enhancements of the code models, related to the model of large pools where pool boiling take place, and a better method to track the level of these pools, for reducing the overall mass errors, are the main issues of the present analysis, in relation to the code structure.

REFERENCES

- [1] Dreier J., Torbeck J., Lomperski, S, Aubert C., Huggenberger M., Fisher O., "PANDA Steady-State Tests : PCC Performance Test Plan and Procedures", PSI Report ALPHA 410-0, May 16, 1995
- [2] Fischer, O.: "PANDA Steady-State Tests : PCC Performance Test Procedures" PSI Report TM-42-97-03/ALPHA 701-0, May 2, 1997
- [3] Huggenberger M., Dreier J., Lomperski S., Aubert C, O., Fisher O., Strassberger H.J.: "PANDA Transient Tests: M3 Integral System Test Data Trasmittal Report", PSI Internal Report ALPHA-613-0, June 18, 1996, Proprietary Information.
- [4] "PANDA Facility, Test Program and Data Base General Description (DTR Umbrella Report) ", PSI Internal Report ALPHA-606-0, May 31, 1996, Proprietary Information.
- [5] "SBWR Test and Analysis Program Description" (TAPD, Licensing Topical Report), GE Report NEDC-32391P Rev. C, August 1995, GE Proprietary Information.
- [6] "PANDA Test-Plan, Tests M3, M4, M7" (Specification), GE Document 25A5764 Rev. 1, Sep 18, 1995.
- [7] "PANDA Transient Tests: M3 & M4 Integral System Test Procedure", PSI Internal Report ALPHA-520-0, Sep 22, 1995.
- [8] The RELAP5 Development Team: "RELAP5/MOD3 Code Manual: User Guide and Input Requirements" - NUREG/CR-5535 INEL-95/0174, Idaho (US), March 1995

- [9] V. Faluomi, S.N. Aksan: "RELAP5/Mod3.2 Model of PANDA Facility : General Description and steady state qualification" PSI Internal Report TM 42-98-01 - ALPHA 801-0, February 1998 (Proprietary)
- [10] V. Faluomi, S.N. Aksan: "Post Tests Calculations of PANDA S1-S6 Steady-State Tests with RELAP5/Mod3.2 Code", PSI Internal Report, to be issued (Proprietary)
- [11] Hart J. , 'Status of Panda Relap5 Analyses", SBWR Panda Meeting, Villigen, PSI, September, 1994.
- [12] Faluomi V., Aksan S.N.: "PANDA M3 Integral Test: RELAP5/Mod3.2 Post-Test Results and sensitivity analyses ", " PSI Internal Report TM 42-98-02 - ALPHA 802-0, February 1998 (Proprietary).

TEPSS — TECHNOLOGY ENHANCEMENT FOR PASSIVE SAFETY SYSTEMS

J. HART¹, W.J.M. SLEGGERS² (†), S.L. DE BOER³, M. HUGGENBERGER⁴, J. LÓPEZ JIMENEZ⁵, J.L. MUÑOZ-COBO GONZALEZ⁶, F. REVENTÓS PUIGJANER⁷

¹NRG Petten, Netherlands

²NRG Arnhem, Netherlands

³Stork Nucon B.V., Nuclear Technology, Amsterdam, Netherlands

⁴Paul Scherrer Institute, Villigen, Switzerland

⁵Centro Investigaciones Energeticas, Medioambientales, Technologicas, Madrid, Spain

⁶Universidad Politécnica de Valencia, Valencia, Spain

⁷Universitat Politècnica de Catalunya, Barcelona, Spain



XA0055024

Abstract

The objective of the TEPSS project [1,2] was to make significant additions to the technology base of the European Simplified Boiling Water Reactor (ESBWR). The project focused on mixing and stratification phenomena in large water pools, passive decay heat removal from containments, and effects of aerosol deposition inside a passive heat exchanger.

The PSI experimental facility LINX (Large-scale Investigation of Natural Circulation and Mixing) has been used to investigate venting of steam and steam-noncondensable gas mixtures into water pools. The test revealed that no significant steam bypass could be detected when injecting a mixture of steam or air and that mixing was very efficient. In addition to the tests, 3-D numerical computations and initial model development have been performed to study the behaviour of bubble plumes in water pools.

The major part of the TEPSS project studied selective aspects of the response technology of modern pressure-suppression type containment designs and of passive-type decay heat removal systems. The work included an experimental phase using the large-scale experimental facility PANDA (Passive Nachwärmeabfuhr und Druckabbau), operated by PSI, where eight experiments successfully have been executed to test the performance of the ESBWR containment configuration. The PANDA tests have been analysed successfully using thermalhydraulic system analysis codes and 3-D CFD codes.

The AIDA (Aerosol Impaction and Deposition Analysis) experimental facility of PSI has been used to investigate the degradation of passive decay heat removal due to fission product aerosols deposited on the inside surfaces of the PCC (Passive Containment Cooler) heat exchanger tubes. The one test performed revealed that the degradation of the heat transfer in the PCC tubes due to the deposition of aerosols reached about 20 %. The test has been analysed using the MELCOR severe accident analysis code.

1 Introduction

The objective of the TEPSS project was to make significant additions to the technology base of the ESBWR which offers enhanced safety and improved public acceptance through product design simplicity and increased safety margins. The TEPSS project has performed both experimental and analytical research needed to support advances in the areas of:

- Improved countermeasures against pool stratification, including studies of thermal plumes and testing of concepts to avoid or minimize hot, stratified pool regions (Work Package 1);
- Improved designs of containments, including tests on the passive decay heat removal in a model of the ESBWR containment (Work Package 2);
- Enhanced aerosol removal features, including a test demonstrating that passive heat removal systems can act as an effective aerosol filter and that heat removal capacity is not endangered by aerosol deposition in the containment cooler condenser tubes (Work Package 3).

The TEPSS project has been executed from 1 January 1995 to 31 December 1998 as a Shared Cost Action within the INNO Cluster, "Exploring Innovative Approaches/Conceptual Reactor Safety Features", under contract number FI4I-CT95-0008.

2 Work Programme

The TEPSS project was structured in three separate Work Packages. Descriptions of the three facilities that have been used for the tests can be found in [1].

2.1 Suppression Pool Mixing and Stratification

The motivation of this work, came from the need to confirm the success of passive safety systems over long periods of time after an accident. Therefore, more detailed knowledge seemed necessary with respect to the mixing and stratification behaviour of large water pools. The PSI experimental facility LINX has been used to screen and optimise venting of steam and steam/noncondensable gas mixtures into a large water pool. The aim of this work was to investigate suspected tendencies by hot gas mixture releases to cause stratified heating of a thin topmost layer of a BWR suppression pool, which would impose added vapour pressure loading onto the Wetwell (WW) gas space.

Relevant phenomena that needed further investigation related to the condensation within the steam/air bubbles, mixing and stratification in the pool itself, and the interaction between these two processes. Measurements, including visual methods, have provided a database for the assessment of mixing models included in containment analytical codes.

2.2 Passive Decay Heat Removal

Within this work package, selective aspects have been studied of the response technology of modern pressure-suppression-type containment designs and of passive-type decay heat removal systems. An important goal of the study was to both better understand and predict relevant phenomena that occur in these systems by the use of various existing computer codes. Apart from directly aiming at mitigation of severe accident effects, application of the new features and systems in modern containment designs yielded improved pressure margins under hypothetical loss-of-coolant accidents (LOCAs).

The work package included an experimental phase and an analytical phase encompassing the PANDA facility at PSI. With reference to the ESBWR, the PANDA facility has been modified to reflect the design changes with respect to the formerly investigated SBWR configuration. One important modification of the ESBWR containment design compared to the SBWR is that the gravity-driven cooling system (GDSCS) is made topologically part of the WW gas space. This has the advantage that the WW gas space volume is increased when the GDSCS pools are drained, resulting in a lower pressure build-up in the containment. Because of the higher power output of the ESBWR, the scaling ratio of the PANDA facility has changed to 1:40. Scaling analysis has been applied to assure that the observations in PANDA would be in known relationship to the phenomena in the ESBWR.

In the modified PANDA facility, eight experiments have been executed to test the performance of the ESBWR-like containment configuration. For each of the PANDA tests, pre- and post-test analyses have been performed. The pre-test predictions using RELAP5/MOD3 provided valuable insights in the phenomena that could occur during the test runs. Post-test analyses using RELAP5/MOD3, TRAC-BF1, MELCOR, and GOTHIC have been performed for the purpose of code qualification.

2.3 Passive Aerosol Removal

The AIDA PCCS experimental facility has been used to investigate the degradation of passive decay heat removal due to fission product aerosols deposited on the inside surfaces of the PCC heat exchanger tubes. The experimental work consisted of the execution of one

experiment using tin oxide aerosol as a simulant. Both pre-test and post-test analyses of the experiment have been performed using the integrated accident analysis code MELCOR.

3 Main Results Obtained

3.1 Suppression Pool Mixing and Stratification

In the ESBWR, the primary system depressurization following a LOCA leads to air and steam flowing into the WW through the main vents and the PCC vents (see also Fig.2). In the long term, air and any uncondensed steam are vented only through the PCC vents. The efficiency of the condensation and mixing processes inside Suppression Pool (SP) of the WWs affects the pressure of the entire building containment. For the pressure to be as low as possible the system should condense a maximum amount of steam in the PCCs and in the SP. Moreover, at equilibrium the steam partial pressure in the WW is directly related to the saturation temperature at the pool surface temperature, which means that a good mixing in the water pool must be achieved to involve a maximum amount of water and mitigate the temperature increase.

For a single pipe PCC vent line however, steam by-pass, consisting of uncondensed steam passing through the SP to the WW gas space, could be a concern since it could lead to a thermal stratification in the SP and an increased pressure in the wetwell.

To investigate any steam by-pass from a vertical vent line as well as mixing and stratification in a large water pool, two test series have been executed in the LINX facility (see Fig.1). The first test series investigated steam condensation in the water pool. The purpose of the second test series was to visualize and characterize the flow resulting from gas venting into the ESBWR suppression pool for a wide range of configurations. The following paragraphs contain a summarized overview of the results.

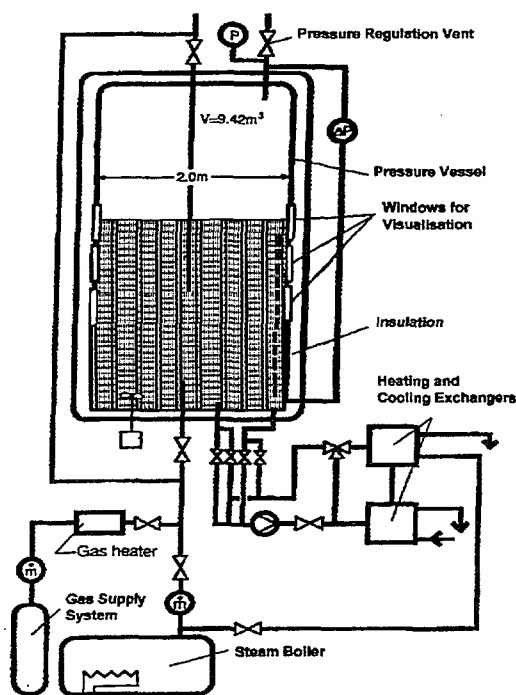


Fig.1 LINX Experimental Facility

reached equilibrium with the bulk water and steam condensation was complete before the gas reached the water surface, even for low submergence depths.

3.1.2 Pool Stratification Tests

For all the tests, pool mixing was found to be very efficient. The pool mixing is greatly enhanced by the presence of air in the injected gas. In the mixing process, geometry may play an important role, so the results of the LINX tests should be handled with care to extend the results to the ESBWR case where the distance from the vent to the wall is much larger than in the LINX vessel.

3.1.3 Visualisation Tests

The visualization test series lead to a better characterization of the flow resulting from venting and of the bubble fragmentation that was found to play a major role in condensation.

The distance necessary for the bubbles to break up has been systematically evaluated and general trends have been detected. Further analysis of the results is however required.

3.1.4 Modeling of Confined Bubble Plumes

In parallel with the LINX experimental programme, 3-D numerical computations have been carried out by PSI. In lieu of data from the LINX tests, which were not available in time for the assessment of the TEPSS analytical work, initial model development has been undertaken and compared with published bubble-plume experiments.

3.2 Passive Decay Heat Removal

The work performed for this Work Package consisted of a scaling analysis of the PANDA facility with respect to the ESBWR (see also Fig.2), the subsequent modification of PANDA, the execution of eight integrated system tests in the PANDA facility, and analytical activities which included both pre- and post-test analyses of the tests using different codes.

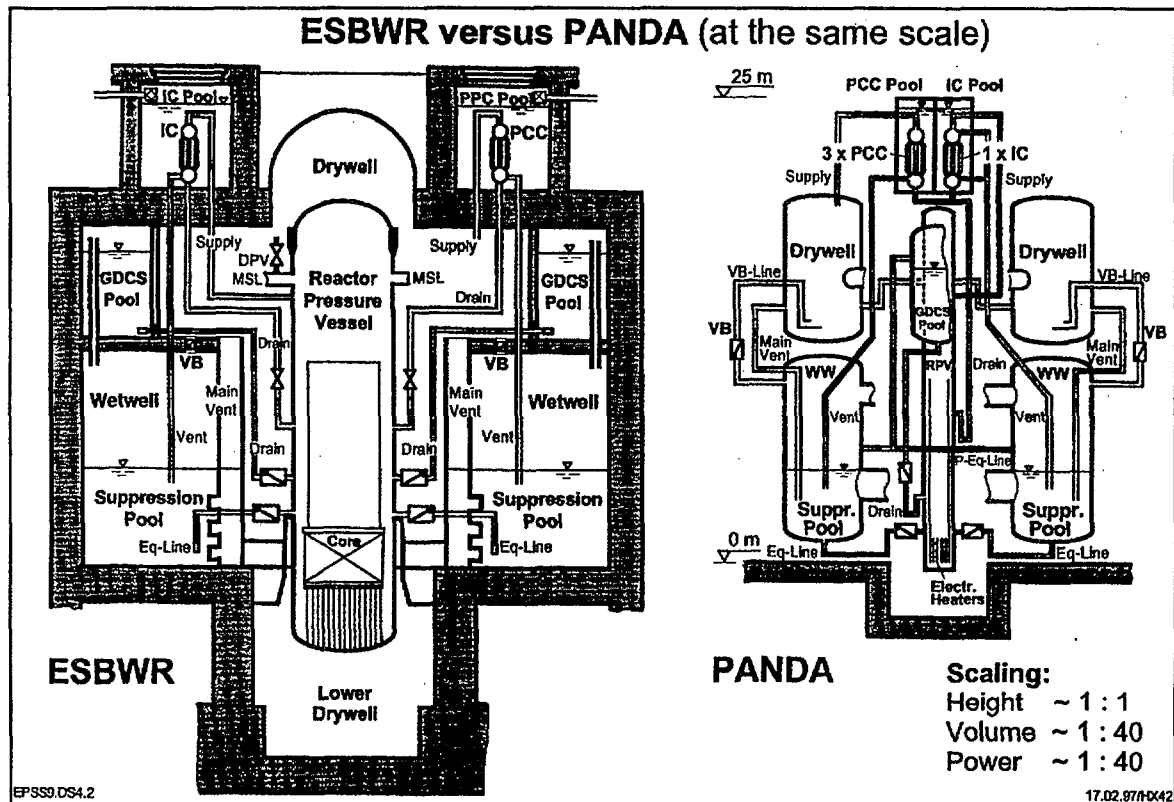


Fig.2 Schematic of the ESBWR design and the PANDA facility

3.2.1 Scaling Analysis

In reduced scale facilities such as PANDA, exact similitude with the reference design such as the ESBWR cannot completely be achieved. Therefore, a scaling analysis has been performed to design the PANDA facility and to determine initial and boundary conditions so that any distortion would not affect significantly the evolution of the physical processes to be investigated. The main conclusions of the scaling analysis were that all major processes have been scaled properly and that the PANDA tests form a good benchmark for pressure response of the ESBWR containment.

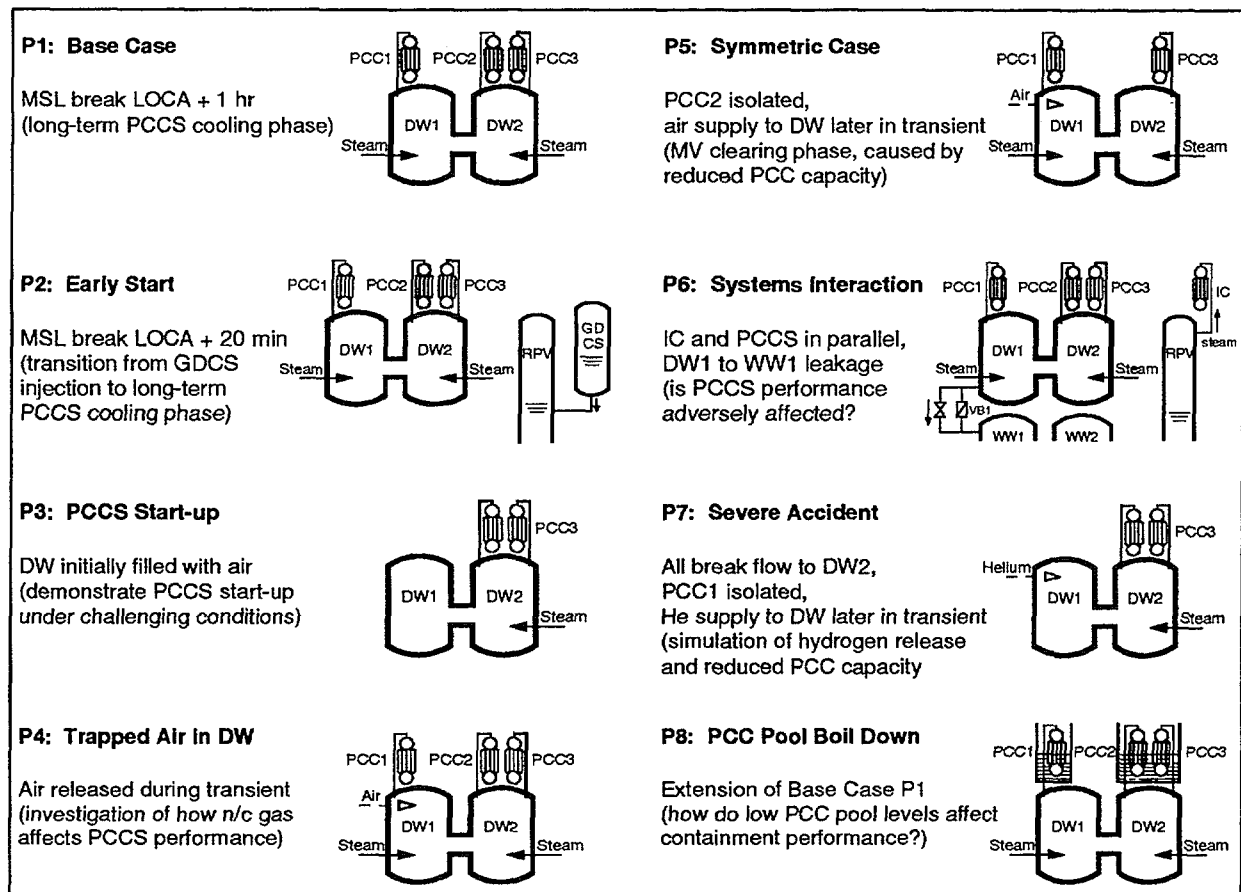


Fig.3 Schematic of the PANDA P-Test series

3.2.2 Experiments and Analytical Support

The work performed for this work package consisted of the execution of eight tests, P1 to P8, in the PANDA facility at PSI, and the analytical support by all partners. The main characteristics and the facility configurations for the individual tests are shown in Fig.3. The codes that have been used for the overall analysis of the P-series tests were RELAP5/MOD3, TRAC-BF, and MELCOR, whereas the 3D code GOTHIC has been used to provide detailed information on phenomena like mixing and stratification in the containment vessels.

Test P1/8: The P1/8 test was actually a combination of two separate tests, the P1 “Base Case” test, and the P8 “PCC Pool Boil Down” test. Test P1 simulated the long-term cooling phase starting 1 hour after a Main Steam Line Break (MSLB) LOCA. Test P8 was executed as an extension of P1 and provided information about how the passive decay heat removal and containment performance are affected by low PCC pool levels. In general, the P1 test showed a favorable and robust overall PCC system behaviour. The global DW (Drywell) and WW (Wetwell) pressure responses as shown in Fig.5 and Fig.4 were expected from the pre-test calculations. From the results of test P8, it appeared that the PCCs are well capable to remove all the decay heat from the PANDA containment up to the point where about 75% of the PCC tubes are uncovered, which occurred at 22 hours for the P1/8 test. An important outcome of the P8 test is that PCC pool level, up to a limit, has no effect on the containment heat removal and containment pressure.

The analysis of the P1/8 test results using RELAP5 and MELCOR showed that the overall behaviour of the test has been calculated quite well with regards to pressure, mass flow rates, and pool boil-off. However, due to the one-dimensional, stacked-volume modeling of the PANDA DW, WW, and GDCS vessels, 3-D-effects such as in-vessel mixing, recirculation and stratification could not be calculated. This did however not significantly affect the overall

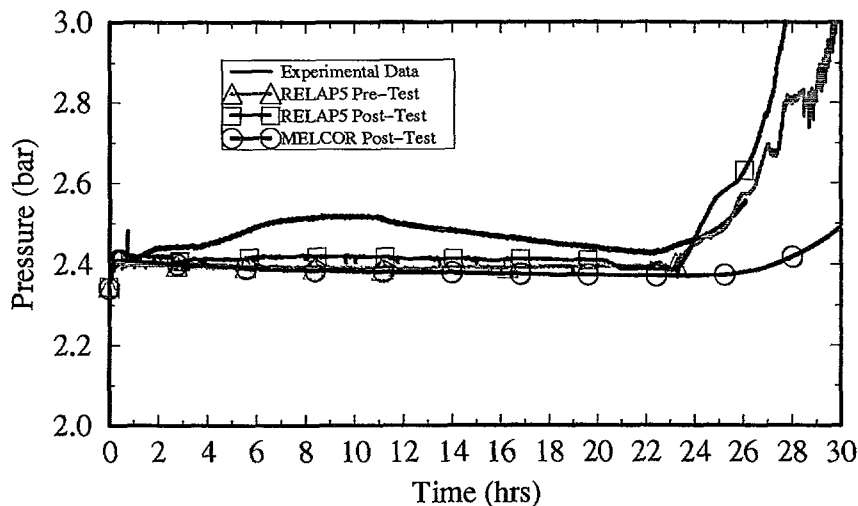


Fig.4 WW1 Pressures of PANDA Test P1/8

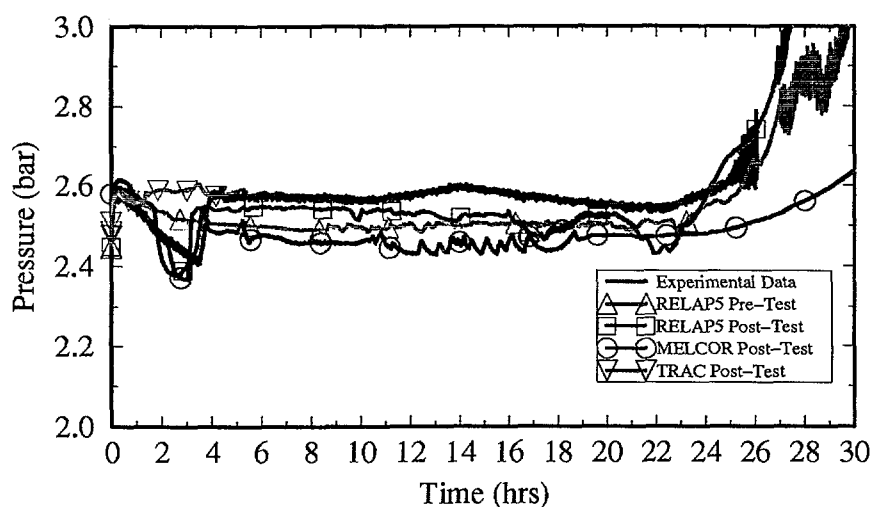


Fig.5 DW1 Pressures of PANDA Test P1/8

Other improvements on the TRAC-BF1 code that were implemented by UPV concerned a model for the steam condensation phenomena in the presence of non-condensable gases and a model for the secondary side heat transfer during natural convection flow outside vertical cylinders immersed in a pool.

Test P2 The "Early Start" P2 test provided data for the transition period from the GDCS injection phase to the long-term PCC cooling phase of the post-LOCA transient. After the start-up, all decay heat was removed equally by the three PCC units. There was no significant energy deposition in the WW.

Generally, the RELAP5 and MELCOR simulations matched quite well the P2 transient. In spite of the large efforts made trying to run TRAC-BF1 code for the P2 test, the code suffered from shortcomings in the level tracking model as a result of which no results have been obtained for this case.

Test P3 The "PCCS Start-Up" P3 test demonstrated the PCC system start-up with the condensers and DW initially filled with non-condensable gas, which represented the most challenging condition for PCC start-up. During the test, air accumulated in the lower region of the "dead end" volume DW1. After the system start-up, the two PCC units operable were not

calculated results. Similar trends for both codes were found for the simulations of the other tests.

The TRAC-BF1 calculations show a reasonable agreement with the P1 test, but only a part of the transient as well as part of the system have been analyzed with the code. This also accounts for the simulations of the other tests. The code suffered from numerical problems that relate to the modeling of three-dimensional volumes that contain air. To solve this problem, additional development of the code is necessary. Similar problems with the one-dimensional level tracking model components were solved by UPV, which provided a significant update of the code when applied to low-pressure, low driving force situations.

sufficient to condense all steam from the DW which lead to a continuous energy transfer from DW to WW. This occurred asymmetrically, in accordance with the asymmetric test conditions.

In general, the applied RELAP5 input model was suitable for calculating the general behaviour of the facility (pressure, mass flow rates). MELCOR overestimated the PCC performance due to air trapped in the dead-end DW1. The TRAC-BF1 estimates showed a reasonable agreement with the experimental values, but the WWs were not simulated.

Test P4 The P4 test investigated how trapped air in a DW, released later in the transient, affected the PCCS performance. The air release has been simulated by injecting air into DW1, 4 hours after test initiation for a period of 30 minutes. The initial conditions and the facility configuration were nearly identical to Test P1. Before the start of the air injection phase, the system behaviour was similar to that of Test P1, which demonstrated the excellent reproducibility of the PANDA tests. Upon the injection of cold air into DW1, the system pressure immediately started to increase. After termination of the air injection, it took about 1.5 hours to vent the air from the DW through the PCCs down to the WW gas space. During the last phase of the test, the system showed normal PCCS operation.

RELAP5 calculated the P4 DW and WW pressures well. MELCOR calculated almost no air trapping in the PCC tubes that could hinder the steam condensation rate, which resulted in lower calculated pressure values. The TRAC-BF1 code was able to simulate the asymmetric DW behaviour upon air injection and the behaviour of air inside the PCCs.

Test P5 In the “Symmetric Case, Two PCCs Only” P5 test, each DW had one PCC connected. After the test start, the PCCs were not able to take the whole load. Upon the air injection, PCC1 was more affected than PCC3, that was connected to DW2. After the air injection, it took 1.5 hours to vent the air to the WW gas space, which is comparable to the P4 test. After the removal of air from the DWs, the system showed normal PCCS operation.

The RELAP5 and MELCOR results showed a rather good agreement with the test results. As the main vent lines and the WWs were not modeled in the TRAC-BF1 model, all mass was vented through the PCC vents during the air release phase resulting in higher calculated PCC feed flows and DW pressures compared to the test.

Test P6 The objective of the “Systems Interaction” P6 Test was to examine the interaction of the IC in parallel with the PCC units. In addition, the effect of DW to WW leakage on the containment performance has been investigated. After 4 hours, the leakage path was opened, whereas the IC operated for the first 7 hours only. No relevant leakage occurred from DW to WW because the pressures were almost equal on that time. An important finding of the P6 test was that operation of the IC in parallel with the PCCs has a positive effect on the system performance due to the enhanced steam condensing capacity.

RELAP5 and MELCOR performed well for calculating the general behaviour of the P6 test. The major discrepancy was the reduced (compared to the experiment) relative load of the IC, likely caused by the pressure loss characteristics of the IC/PCC inlet lines. Discrepancies found between TRAC-BF1 results and experimental data could be explained by the shortcoming of TRAC-BF1 in the handling of 3D scenarios with air present.

Test P7 The objective of the “Severe Accident” P7 test was to investigate the PCC performance under the conditions of a severe accident, where hydrogen may be released to the containment due to the steam oxidation of Zircaloy cladding. Between 4 and 6 hours, helium as a simulant of hydrogen was injected into the top of the “dead end” volume DW1. The first phase of the test demonstrated that, the heat removal through the two PCCs was insufficient. The injection of the cold helium caused a relatively fast pressure rise, starting only at about 5 hours, i.e. 1 hour after the injection started. This delay was caused by initial accumulation of

helium in the upper part of DW1. The pressure started to rise when helium “overflowed” from DW1 to DW2, entered the PCC2/3 units, and degraded the performance of those PCCs.

In the case of the P7 test, both helium and air were present. However, both RELAP5 and TRAC-BF1 are not capable to track more than one non-condensable gas in a system. This shortcoming of the codes complicated a comparison with the experimental results. MELCOR overestimated the capacity of PCC units. The reason for this is the experimentally observed slow release of helium, trapped in the DW1 dead-end volume, into DW2 as a result of the mixing and counter-current gas flows in the DW1-DW2 connection pipe. The slow flow of helium into DW2 degraded the performance of the PCC units. With the applied nodalization, the computer codes could not predict this flow pattern.

3.2.3 Specific Phenomena

The analysis of PANDA tests revealed that the applied system analysis codes were not capable to model mixing and stratification as well as natural circulation loops in gas spaces and in water pools. Therefore, PSI successfully simulated some characteristic phenomena observed during the PANDA tests using the state-of-the-art 3-D CFD codes GOTHIC and CFX, viz. heated jet and plume behavior, and heat transfer in the PCC condensers. The calculated results could however not be verified by experiments due to the lack of detailed data.

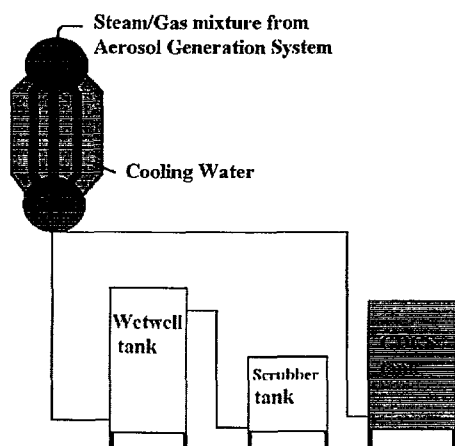


Fig.6 AIDA experimental facility

3.3 Passive Aerosol Removal

The AIDA facility at PSI (see Fig.6) is aimed to study the effects of aerosols on the behaviour of passive decay heat removal equipment (isolation condensers; passive containment cooling system condensers). In Work Package 3 of the TEPSS project one key benchmarking experiment has been performed to investigate the change in the overall PCC condenser heat transfer capability when subjected to SnO_2 aerosol particles. The experiment consisted of two phases. The first phase, Phase A, lasted 100 minutes and determined the condensation behaviour of the condenser at the specified thermal-hydraulic boundary conditions (without aerosol particles). The second phase, Phase B,

lasted 85 minutes and determined the condensation behaviour of the condenser at the specified thermal-hydraulic conditions of the first phase and in addition, at the specified aerosol boundary conditions.

The experimental work has been supported by analyses with the MELCOR 1.8.3 code, including several sensitivity calculations. The main conclusions of this work were that the degradation of the heat transfer in the PCC tubes due to the deposition of aerosols (see Fig.7) reached about 20 % and that the pre- and post-test simulations of the AIDA test using MELCOR 1.8.3 indicated that the code was not well capable to calculate the experimentally observed degradation of the condenser efficiency through the deposition of aerosols

4 Conclusions

The close cooperation between organisations that operate major BWR-related research facilities in Europe and those with additional activities on innovative LWRs turned out to be very beneficial for the course of the project and is strongly recommended for future programmes.



Fig.7 Deposition traces in one of the AIDA condenser tubes

The standard of the experimental and analytical work performed for the TEPSS project was very high. The well-defined measurements have been processed in such a manner that the results are well accessible. The results are a significant addition to the data base for the assessment of thermohydraulic system analysis codes, especially for conditions that could be met in passively operated advanced reactors, i.e. low pressure and small driving forces.

One important design feature in the ESBWR that enhances the economy of scale and that was successfully tested in the TEPSS project concerned the inclusion of the GDCS gas space in the WW gas space. This has the advantage that the WW gas space volume is increased when the GDCS pools are drained, resulting in a lower pressure build-up in the containment.

Work Package 1 of the TEPSS project generated knowledge on the mixing and stratification behaviour of large water pools. From the results obtained in the LINX facility, no significant steam bypass could be detected when injecting a mixture of steam and air into a water pool. For all tests, mixing was found to be very efficient, both in the pool and in the gas space. The LINX tests also revealed that steam vented from a single vertical pipe condenses very efficiently in a subcooled water pool, also when non-condensables are present.

The PANDA tests, performed for Work Package 2, successfully demonstrated a favourable and robust performance of the ESBWR PCC under different challenging conditions. The tests provided detailed data about the PCC start-up, the long-term PCC and containment performance, the interaction of the different systems under "normal" accident scenarios, and about conditions that could be met during severe accidents. Moreover, the tests showed an excellent reproducibility.

The eight PANDA tests have been analyzed with the system analysis codes RELAP5, TRAC-BF1 and MELCOR. The analyses revealed that these codes are well capable to simulate the overall behaviour of the PANDA P-series with regards to pressure, mass flow rates, and pool boil-off. RELAP5 and MELCOR however could not calculate 3-D-effects such as in-vessel mixing and recirculation due to the 1-D, stacked-volume modeling of the PANDA vessels. On the other hand, this did however not significantly affect the calculated results.

Although TRAC-BF1 is able to model 3-D scenarios in general, the code could only analyze part of the PANDA P-series transients as well as part of the PANDA facility due to several numerical problems. These problems relate to the modeling in the code of 3-D-volumes that contain air under thermodynamic conditions that are near saturation. Similar problems with the 1-D level tracking model have been solved by ÜPV, which provides a significant update of the code when applied to low-pressure, low driving forces situations.

The test that has been executed in the AIDA facility under Work Package 3 of the project, showed that the deposition of aerosols in a model of the ESBWR PCC resulted in a 20% degradation of the heat transfer. The MELCOR 1.8.3 simulations of the AIDA test indicated that the code was not well capable to calculate this degradation of the condenser efficiency.

REFERENCES

- [1] Hart, J. et al., "Technology Enhancement for Passive Safety Systems - TEPSS Final Report", INNO-TEPSS(99)-D20, NRG Petten, February 1999.
- [2] Hart, J. et al., "Technology Enhancement for Passive Safety Systems - TEPSS Final Summary Report", INNO-TEPSS(99)-D21, NRG Petten, March 1999.

NEXT PAGE(S)
left BLANK



POST TEST ANALYSIS OF TEPSS TESTS -P2-, -P3-, -P5- AND -P7 USING THE SYSTEM CODE RELAP5/MOD 3.2

D. LUEBBESMEYER
Thermal-Hydraulics Laboratory,
Paul Scherrer Institute,
Villigen, Switzerland

Abstract

For the PANDA- Test- Facility (TEPSS configuration) post-test calculations and analyses have been performed for experiment -P2- (Early Start), -P3- (PCC start up), -P5- (Symmetric case, Two PCCs only) and -P7- (Severe Accident). Post test calculations have been performed with the system code RELAP5/Mod 3.2 using two different nodalisation of the PANDA facility namely a basis nodalisation and a much reduced one.

The general trend of the calculations can be summarised :

- RELAP5/Mod 3.2 calculated the general trends of the experiments sufficiently accurate
- Using the reduced nodalisation the results seem to be slightly more accurate than for the basic nodalisation.
- On the other hand, calculations based on the reduced nodalisation are not significantly faster than those with basic nodalisation.
- The mass error is in the order of 200 to 900 kg

1. NODALISATION OF THE PANDA TEST FACILITY AND DESCRIPTION OF THE TRANSIENT

PSI has performed post-test analyses for test -P2-, (-P3-), -P5- and -P7- using the thermo-hydraulic system analysis code RELAP5/Mod 3.2 [1]. A sketch of the basic nodalisation used for these calculations is shown in Fig. 1.

The PANDA test facility mainly consists of 6 large vessels (shades grey), namely the RPV, the two dry-wells (DW- 1 - and DW-2-), the two wet-wells (WW- 1 - and WW-2-) and the GDSC tank. Pipes connect the vessels to each other and to the three passive containment coolers (PCC- 1 - to PCC-3-) on top of the sketch consisting of primary sides (upper and lower collector drums and the condenser tubes) and secondary sides (pools). Because the fourth condenser, the isolation condenser (IC), was not used for all the tests analysed within this paper, it is not present in Fig. 1). A similar nodalisation has been used by Faluomi and Aksan [2] for the earlier PANDA tests (e.g. M2- test). In contrast to latter nodalisation, here the boundaries of the three PCC pools to the atmosphere have been modelled by RELAP 5 specific separator models thus allowing only pure steam to leave the pools (volumes 518, -548 and -578). The liquid fractions out of these separators are recirculated to the bottom of the pools (volumes 519, -549 and -579).

As an alternative to this basic nodalisation, a much reduced one has been investigated as shown in Fig. 2. Here, the gas spaces of the main vessels are modelled by only very few volumes, i.e. both dry-wells one volume, the gas space of the two wet-wells one volume each, the GDSC two volumes and the gas space of the RPV three volumes. The PCCs remained unchanged.

The two nodalised versions typically consist of :

			basic	reduced
number of	volumes	=	295	205
	junctions	=	325	235
	heat slabs	=	318	228
	valves	=	10	10
	separators	=	3	3
	control variables	=	157	141

For all the for TEPSS experiments, RELAP5/Mod 3.2 calculations have been performed both using the basic nodalisation (RELAP5-basic) and the simplified nodalisation (RELAP5-simple, appended "s" on the curve identifiers in the plots).

2. TEST -P2- (EARLY START)

Test -P2- is an early start up test. It simulates the transition from GDSCS injection to the long-term PCCs cooling phase (a condition which is anticipated to occur in ESBWR approximately 20 min after the LOCA), i.e. the liquid level in the RPV is still rather low (below 4m) and the GDSCS tank half filled with water.

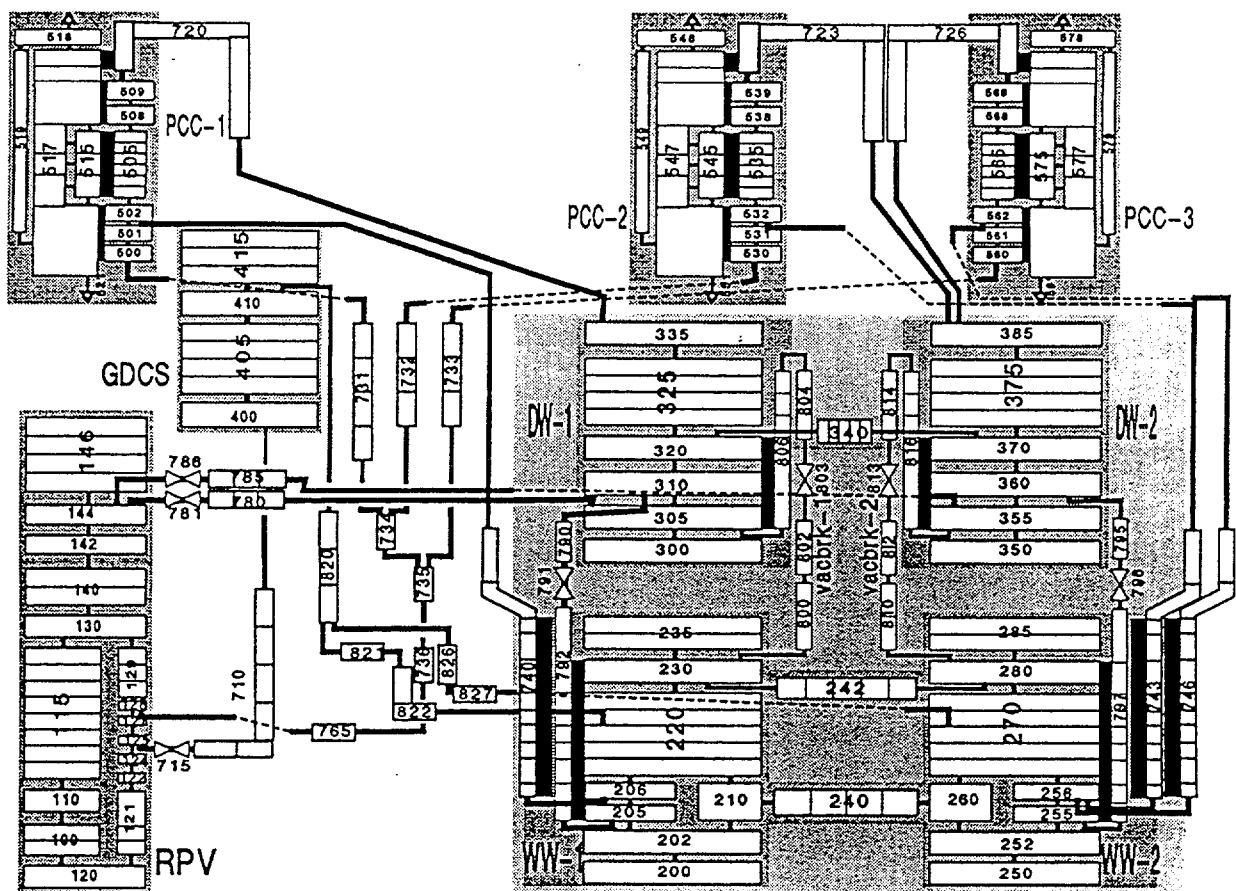


FIG. 1. Basic nodalisation scheme of the PANDA test facility.

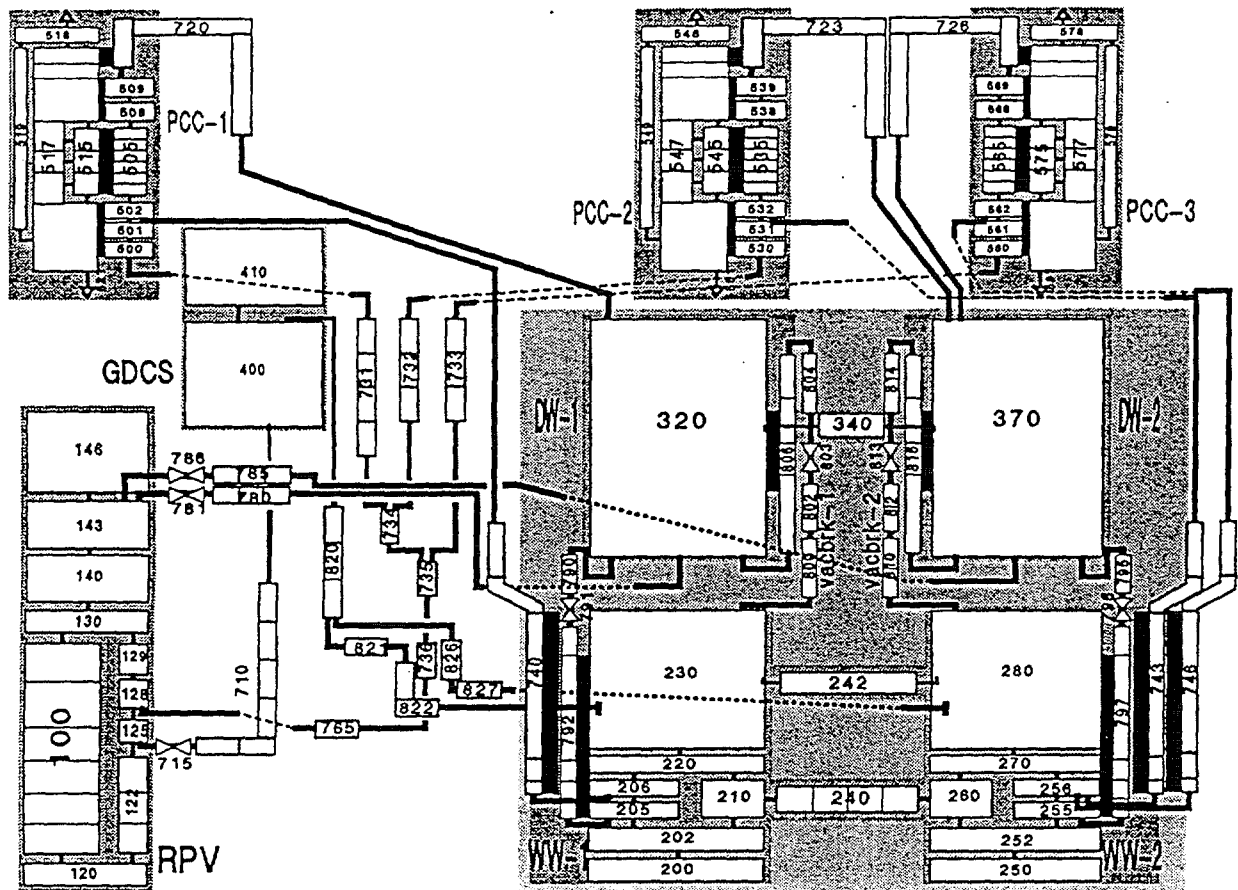


FIG. 2. Reduced nodalisation of the PANDA test facility.

A sketch of the set-up used for this test is shown in Fig. 3. Here, the parts of the system filled with water are slightly darker than those filled with steam, air or a mixture of both. As can be seen from Fig. 3, all three PCCs are operational but there is no interconnection between the different PCC pools. Detailed information on the P2 test procedure and initial conditions can be obtained from Ref. [3] and [4].

The main objective of the test was the "Investigation of the transition period from the GDCS injection phase to the PCC long-term cooling phase". This is expressed by the filling of the RPV out of the GDCS tank, the heat removal by the PCCs and the pressure histories inside all the vessels.

Fig. 4 shows the collapsed liquid levels in the RPV (top) and the GDCS tank (bottom) as calculated by RELAP5-basic (thick curve) and RELAP5-simple compared to the experimental results (dotted curve). For the RELAP5-basic - calculation, the deviations between calculation and experimental results are small but are slightly higher for the RELAP5-simple - results.

Fig. 6 left shows the history of core power and the power dumped into the three PCC pools. Whereas the heater power could be measured experimentally, the power of the PCCs (experimental values) has been derived from the gradient of the PCC pool levels which includes some delay between power deposition into the water and falling of the pool level due to evaporation. Heat removal of the PCCs seems to be slightly over-predicted by the RELAP5-basic - calculation. The results of the RELAP5-simple - calculations exhibit some oscillations during the first hours and after four hours.

On Fig. 6 right, the general system behaviour of test -P2- can be illustrated. Here, the pressures inside the different vessels of the PANDA facility as calculated by RELAP5-basic (thick lines) and RELAP5-simple together with the equivalent experimental results (dotted lines) are plotted as a function of time. After a general pressure drop within the first half hour of the transient which is due to the refill of the RPV with relatively cold water out of the GDCS pool, system pressures recover and then remain nearly constant for the rest of the transient. Compared to the experimental results, both RELAP5-basic and RELAP5-simple calculated a much higher pressure drop for the first half hour. In addition, RELAP5-simple - results exhibited some strong pressure oscillations after 4 hours which can be attributed to numerical instabilities because they decreased with lowering of the maximum time-step (30 ms to 18 ms).

Because during the first hundred seconds of the transient dry-wells pressures significantly fall below wetwells pressures, both vacuum breakers open for some time as can be seen from Fig. 5 where the open times of the vacuum breakers have been plotted as a function of time. Generally, compared to the measurements (dotted line) RELAP5-basic (thick curve) calculated a longer open time of vacuum breaker - 1 - (38 s instead of 18 s) and a shorter for vacuum breaker -2- (4 s instead of 18 s). It failed to predict a second vacuum breaker opening two hours in the transient. With respect to vacuum breaker opening times, the RELAP5-simple results seem to be in a somehow better agreement with the experimental data. However, due to the strong, numerically induced pressure oscillations of the RELAP5-simple - calculation, some more short openings of vacuum breaker occurred after four hours of the transient.

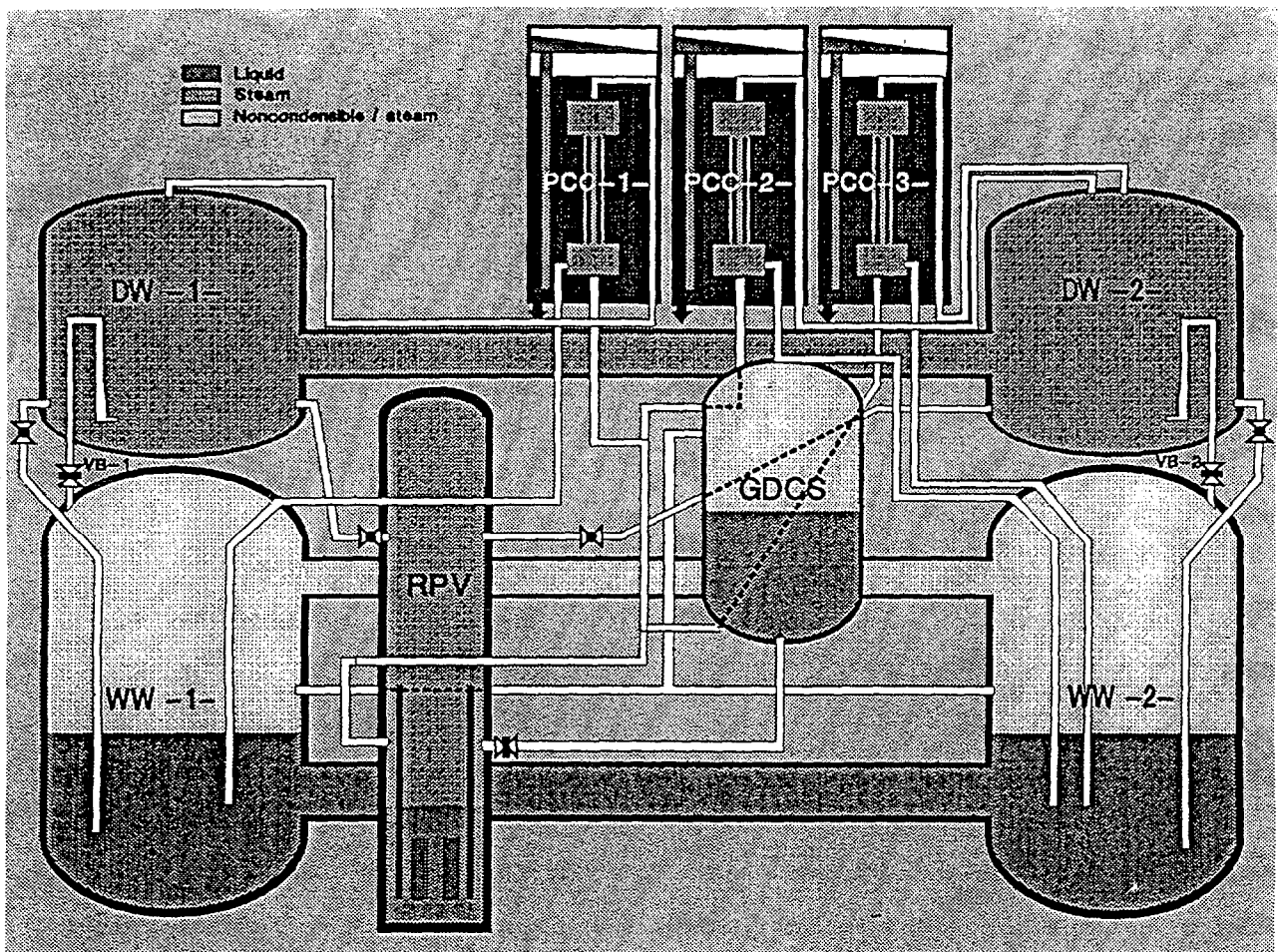


FIG. 3. Scheme of the PANDA test facility as used for test -P2-.

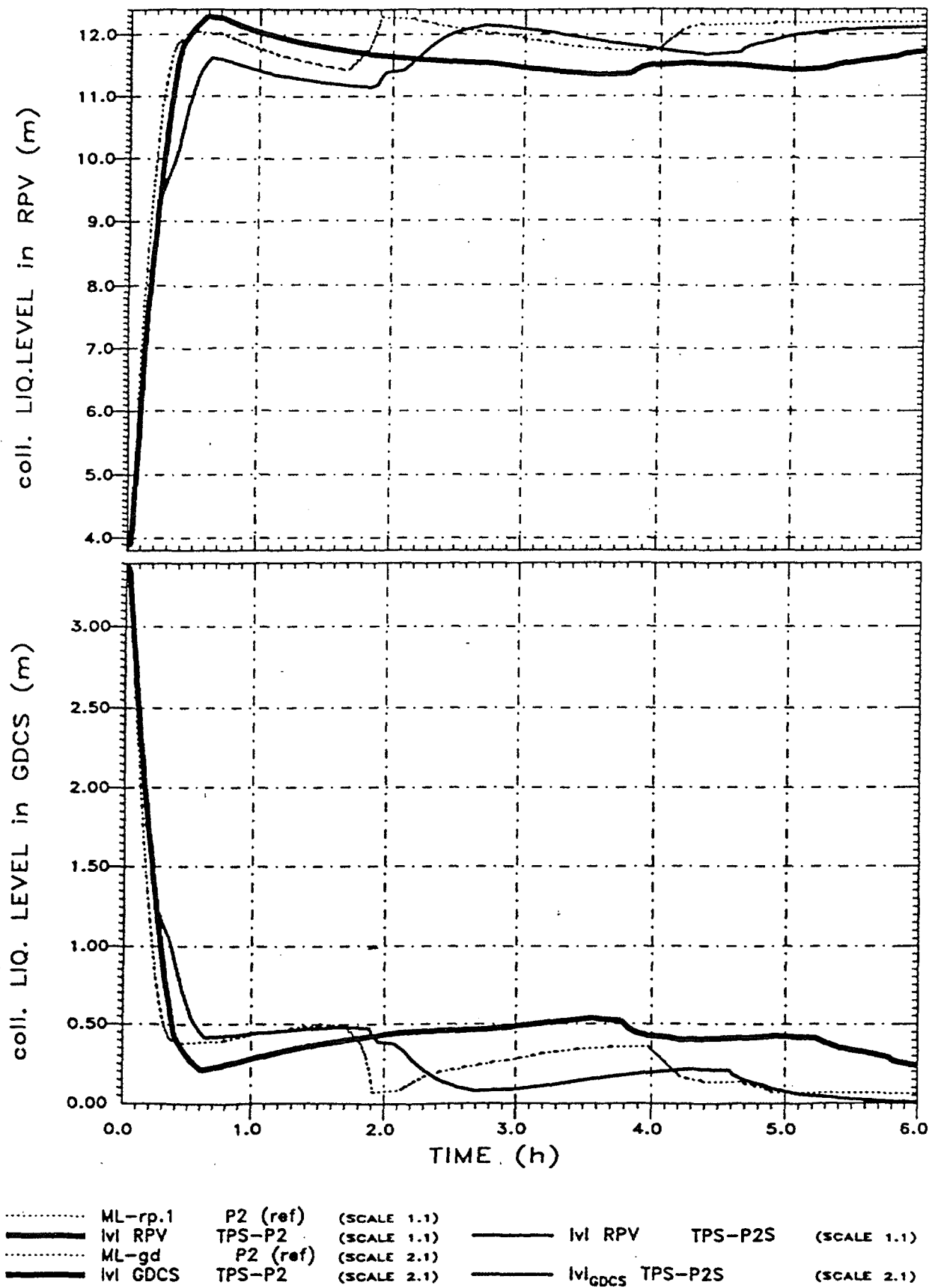


FIG. 4. Calculated and measured (dotted) collapsed liquid levels in RPV (top) and GDCS tank (bottom).

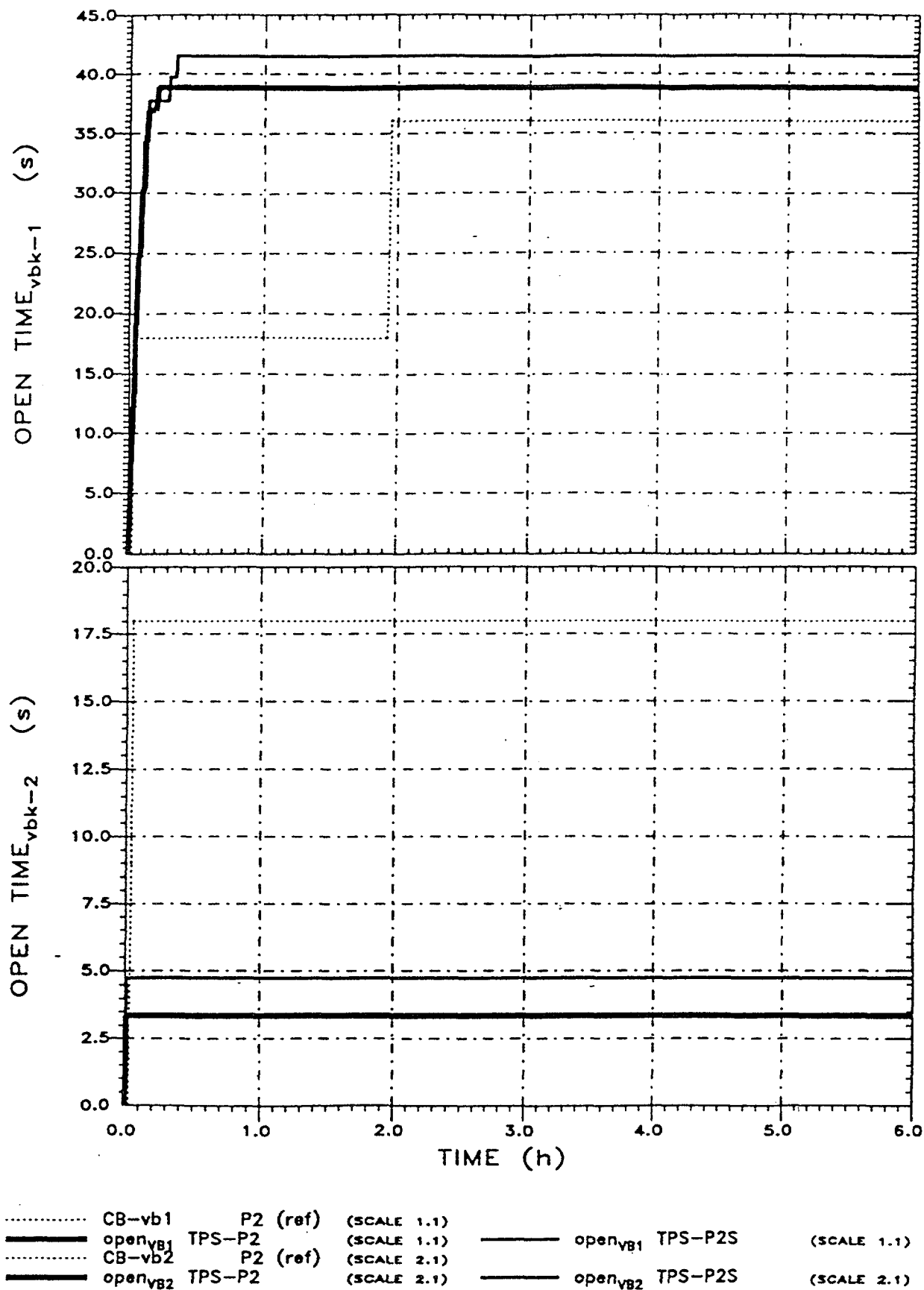


FIG. 5. Open time of vacuum breaker -1- (top) and -2- (bottom) as a function of time for test -P2-

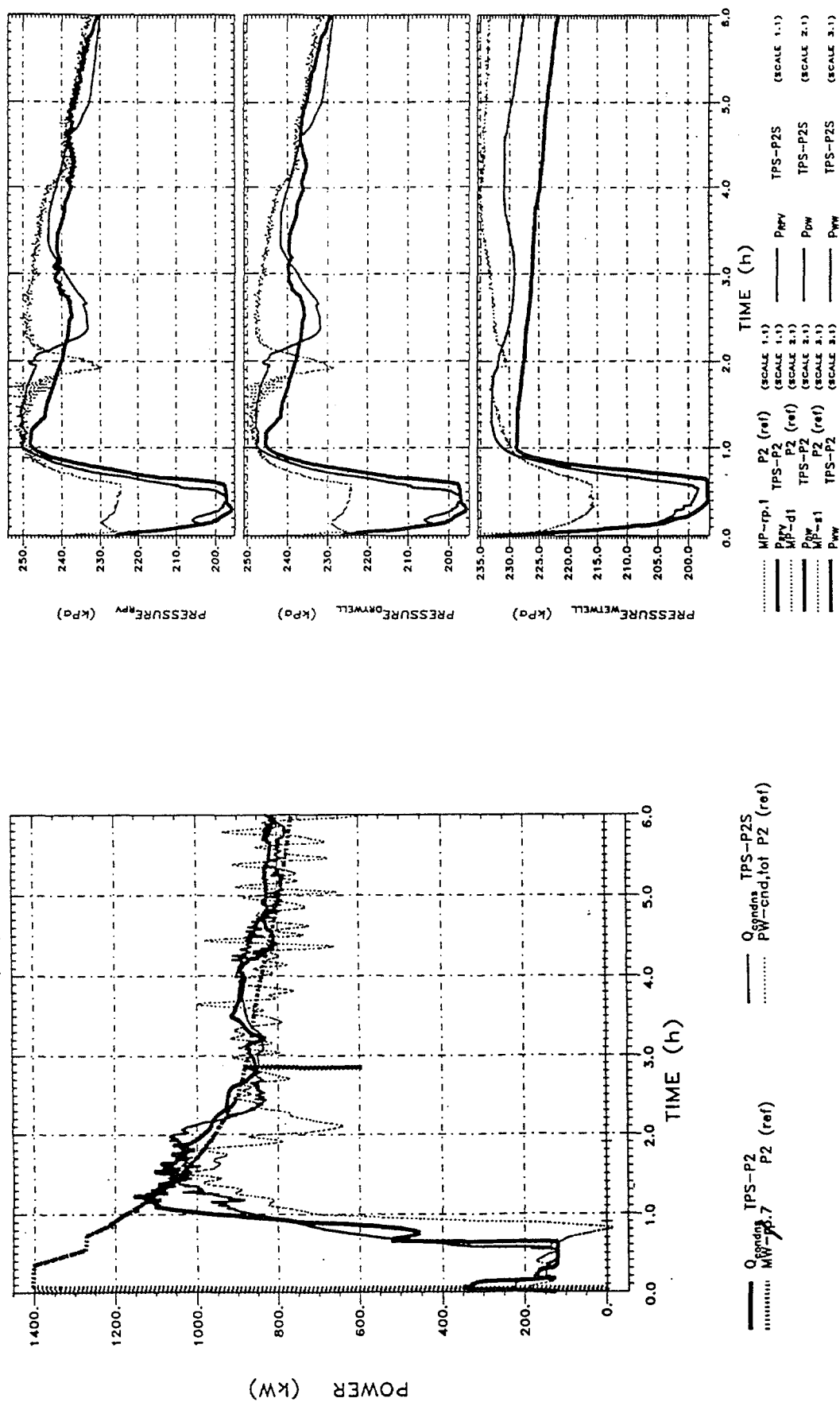


FIG. 6. Experimental core power and calculated as well as experimental total power of the condensers (left) and calculated and measured pressures in RPV (right top), dry-wells (right middle) and wet-wells (right bottom) as a function of time for test -P2-.

The mass error for the RELAP5-basic - calculation was 197 kg and for the RELAP5-simple - case 180 kg. The cpu time to real time ratio was 7.9 and 9.7 using a CRAY-J90.

A more detailed analysis of experiment -P2- can be found in Ref. [5].

3. TEST -P3- (PCCS START-UP)

Test -P3- investigated the PCCs start-up performance under asymmetric conditions, which are shown in the sketch of Fig. 7. Starting from conditions where both dry-wells are filled with air, steam has been injected only into dry-well -2- which is connected to PCCs -2- and -3- leaving dry-well -1- as a dummy volume. Detailed information on the P3 test procedure and initial conditions can be obtained from Ref. [31 and [6].

The objective of the test was the demonstration of the PCC start-up under these extreme conditions.

Fig. 8 left shows the history of power dumped into the two remaining PCC pools (core power remains constant and equals 0.85 MW during the whole transient). Even if one takes into account that the experimental values of the PCC power has been derived from the gradient of the PCC pool levels which includes some delay between power deposition into the water and falling of the pool level due to evaporation (dotted lines), both RELAP5 basic (thick lines) and RELAP5-simple seem to- predict PCC start-up too early. Afterwards, no significant differences can be found between the RELAP5-basic and RELAP5-simple results.

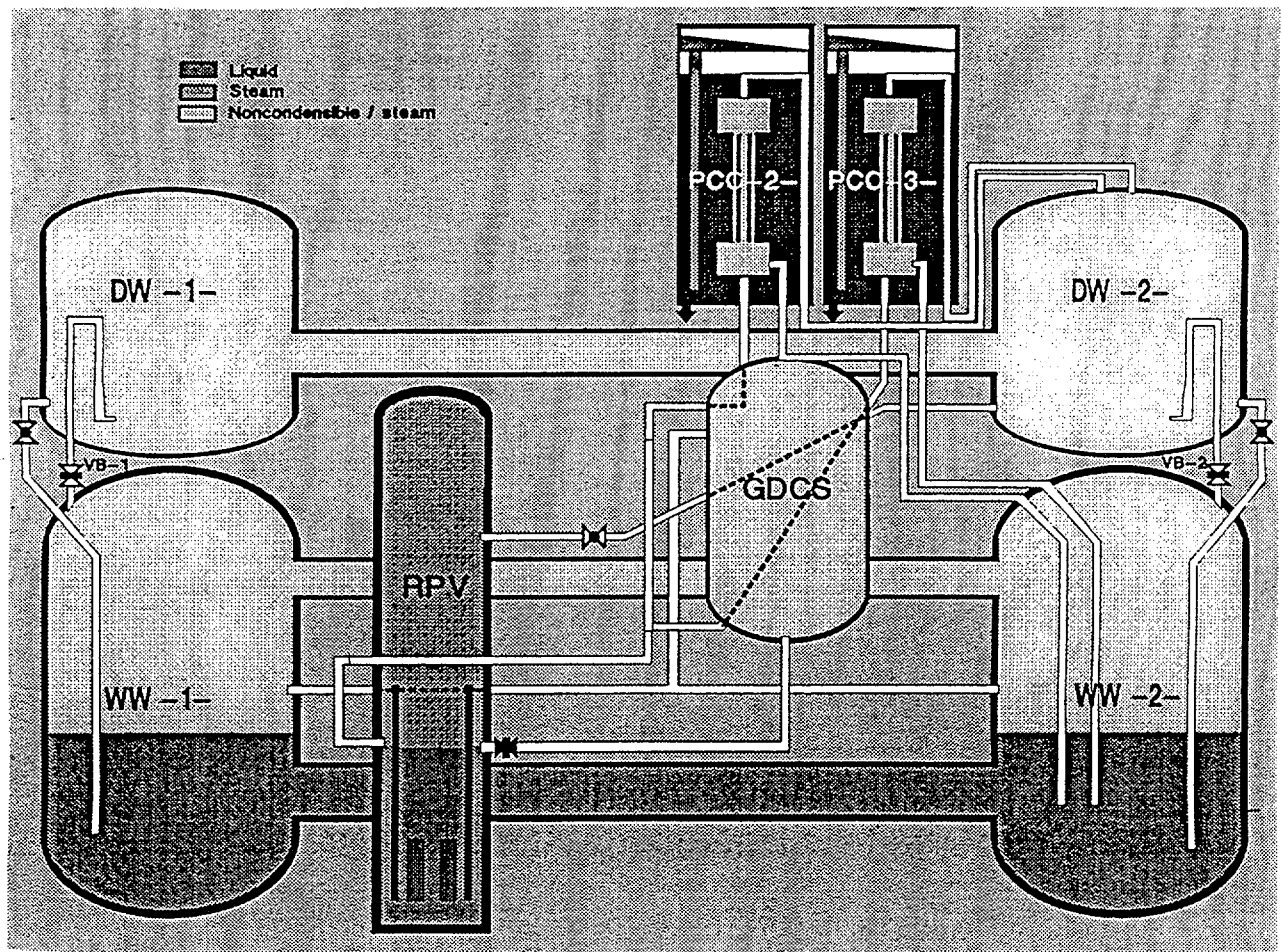


FIG. 7. Scheme of the PANDA test facility as used for test -P3-.

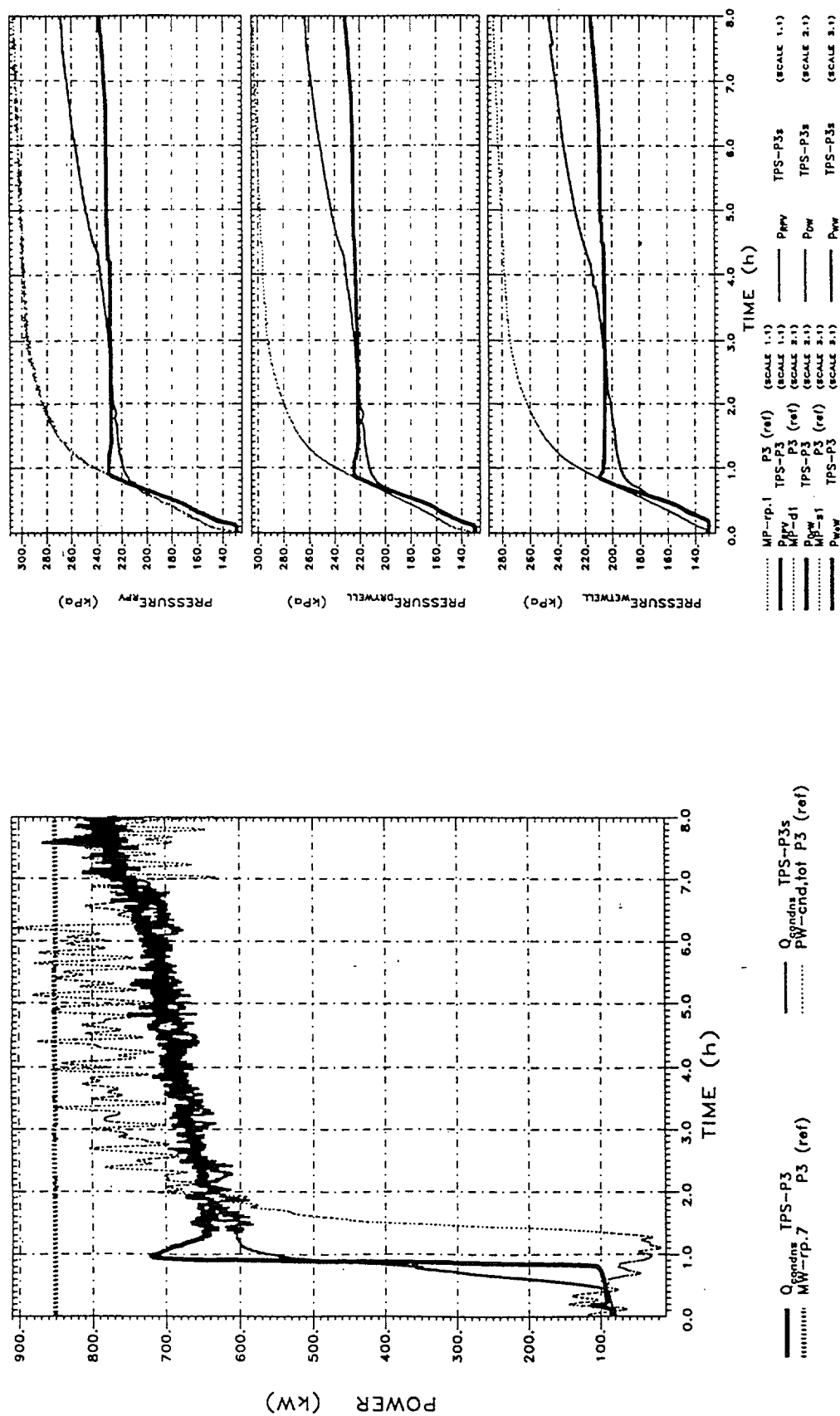


FIG. 8. Calculated as well as experimental total power of the condensers (left) and calculated and measured pressure in RPV (right top), dry-wells (right middle) and wet-wells (right bottom) as a function of time for test -P-3.

The general system behaviour of test -P3- can be illustrated in Fig. 8 right, where the pressures inside the different vessels of the PANDA facility together with the equivalent experimental results are plotted as a function of time. The main deviations occur after PCC start-up. Whereas the experimental results (dotted lines) still rise for another 60 kPa, RELAP5-basic predicted nearly constant pressures for the rest of the transient(thick lines). RELAP5-simple (thin lines) made a slightly better job.

An explanation for the fact that RELAP5/Mod 3.2 predicted PCC start-up to early in the transient may be found in Fig. 9, where the air fractions in the two dry-wells as calculated by

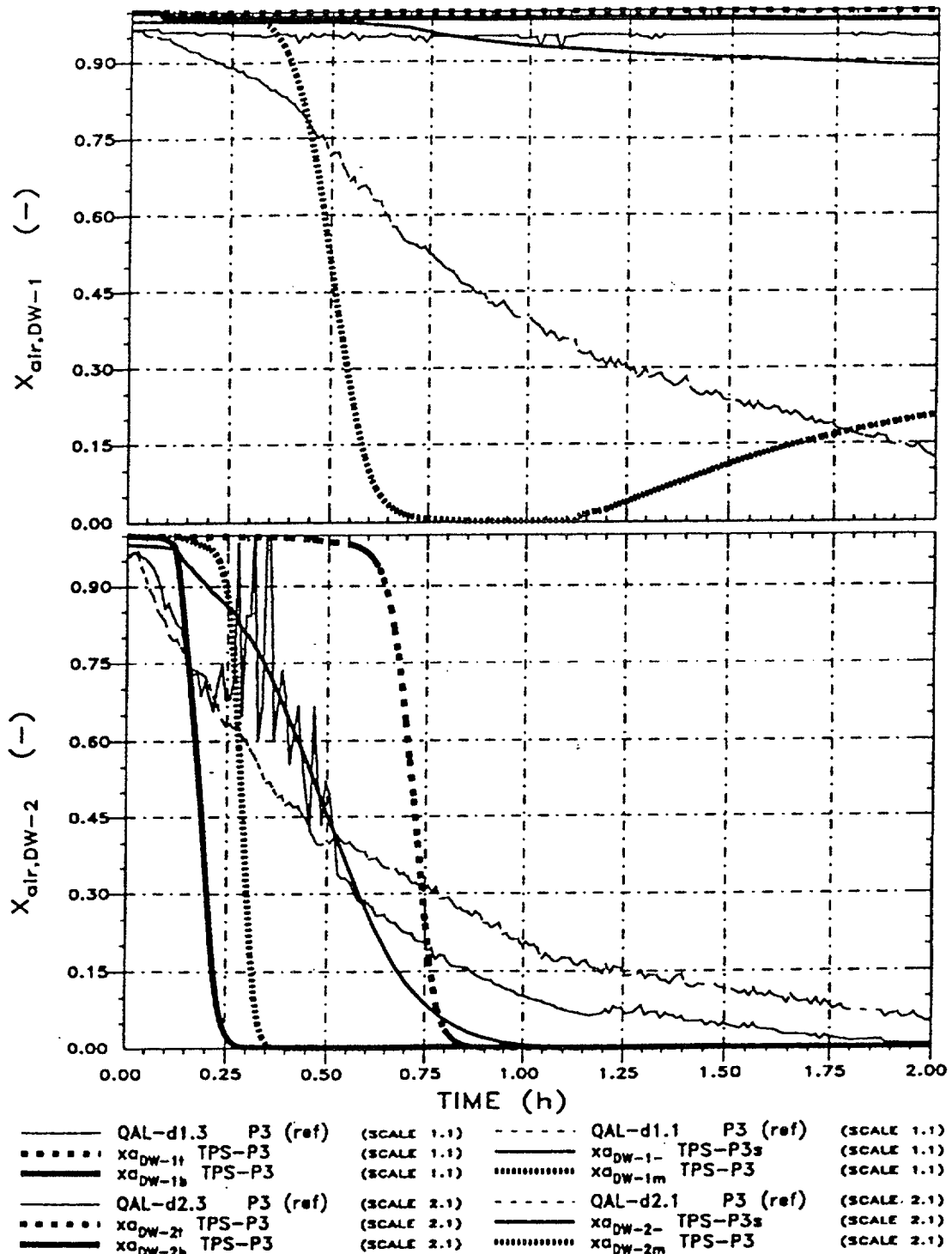


FIG. 9. Calculated and measured air fraction in dry-well-1-(top) and dry-well-2-(bottom) as a function of time for test -P3-.

RELAP5/Mod 3.2 have been compared to the experimental findings. Because only dry-well -2- is connected to the two operating PCCS, the air fraction in this dry-well (lower plot) directly will influence the start-up of the PCCs (dry-well -1- acts as an dummy volume). Contrary to the experimental findings, which indicated a more or less simultaneous purging of the air in the whole dry-well (thin lines in Fig. 9 bottom), RELAP5-basic calculated a stepwise purging beginning at the bottom (thick solid line, identification " $x_{a_{DW-1b}}$ ") over the centre of the volume (thick dotted line, " $x_{a_{DW-1m}}$ ") to the top of the vessel (dashed thick line, " $x_{a_{DW-1t}}$ "). After 0.75h, calculated air fraction are nearly zero at the top of the vessel allowing pure steam to enter the PCCS. Consequently, RELAP5-basic calculated PCC start-up occurred at 0.8 h compared to 1.2 h as found during the experiment. For the RELAP5-simple - calculation, air fraction in the volume (medium thick line, " $x_{a_{DW-1-}}$ ") decreases in a similar manner as do the experimental data but the decrease is still too rapid allowing the entrance of pure steam into the PCCs too early as well. The mass error for the RELAP5-basic - calculation was 617 kg and for the RELAP5-simple - case 304 kg. The cpu time to real time ratio was 6.8 and 6.5 using a CRAY-J90.

4. TEST -PS- (SYMMETRIC CASE, TWO PCCS ONLY)

Test -P5- is a symmetric test, i.e. one PCC was connected to each dry-well which is shown in Fig. 10. In addition, the effect of a release of trapped air into dry-well -1- has been investigated. At the start of the test, both dry-wells are filled with steam. Detailed information on the P5 test procedure and initial conditions can be obtained from Ref. [3] and [7].

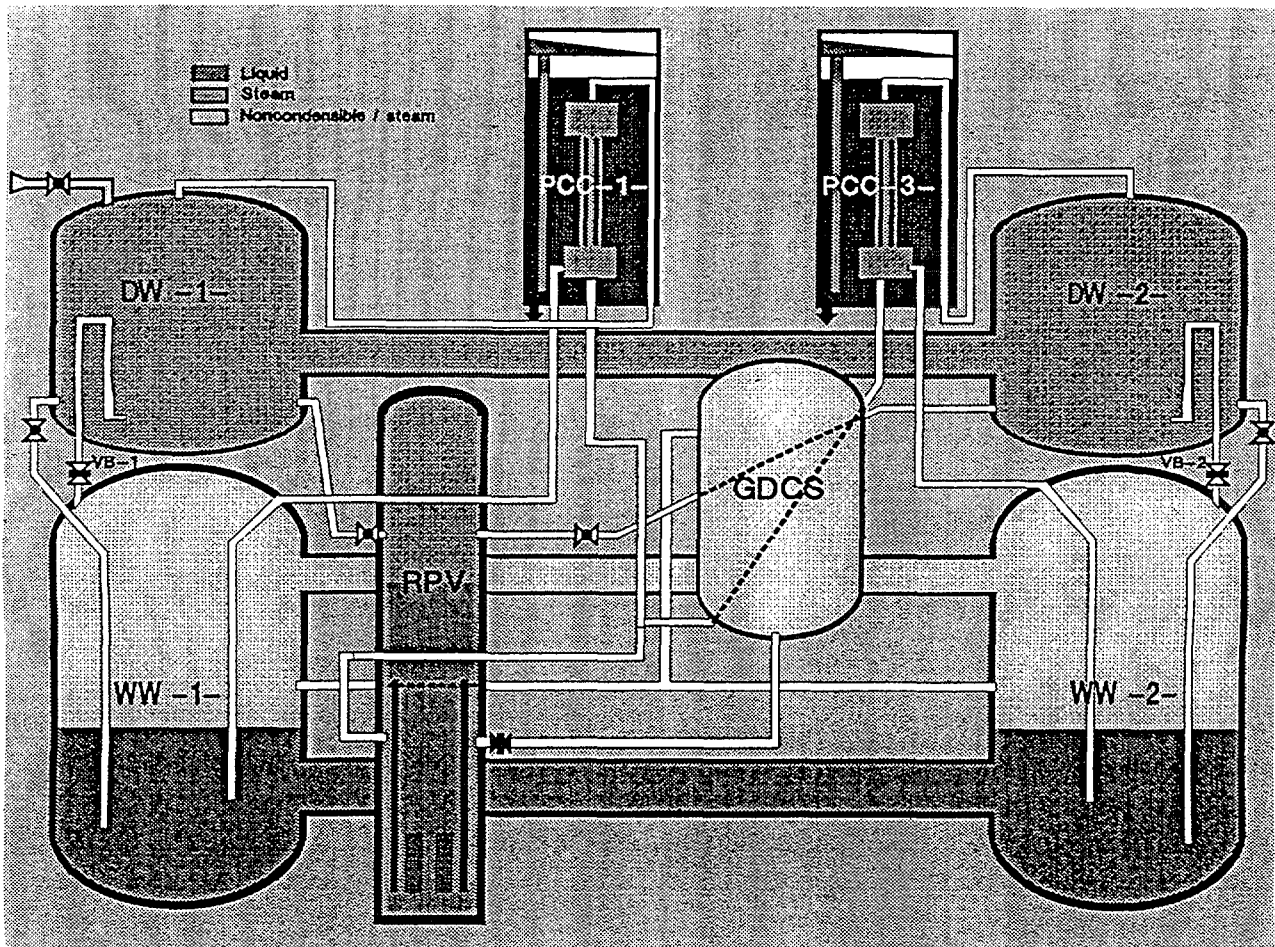


Figure 10. Scheme of the PANDA test facility as used for test -P5-.

The system behaviour of test -P5- has been plotted in Fig. 11. The left plot shows the history of the power both produced in the core (thick dotted line, experimental data "MW-rp.7") and dumped into the two remaining PCC pools (other three curves). PCC power drops from 650 KW to 450 KW when air is released into dry-well -1 - one. This is due to the fact that the power of PCC- 1 - which is connected to dry-well -1 - for half an hour falls to nearly zero because of the appearance of non-condensable on its primary side; PCC-2- is nearly unaffected. Whereas RELAP5-basic (thick solid line) slightly under-predicted the experimental results (thin dotted curve) RELAP5-simple made a quite good job.

On the right side of Fig. 11, the pressures inside the different vessels of the PANDA facility as calculated by RELAP5-basic and RELAP5-simple are plotted as a function of time together with the equivalent experimental results (thin dotted lines). The effect of the inflow of trapped air (28 g/s of air between 4h and 4.5h) at the top of dry-well -1 - has been well calculated by the code although the final pressure level has been slightly underpredicted (10 kPa). The differences between the results of RELAP5-basic and RELAP5-simple calculations remained small. The mass error for the RELAP5-basic - calculation was 820 kg and for the RELAP5-simple case 508 kg. The cpu time to real time ratio was 12.8 and 6.3 using a CRAY-J90.

A more detailed analysis of experiment -P5- can be found in Ref. [8].

5. TEST -P7- (SEVERE ACCIDENT)

Test -P7- is an asymmetric test, i.e. both operational PCCs were connected to dry-well -2- as it is shown in Fig. 12. In addition, the effect of a release of hydrogen (simulated by helium) into dry-well -1 - has been investigated (severe accident condition). At the start of the test, both dry-wells are filled with steam. Detailed information on the P7 test procedure and initial conditions can be obtained from Ref. [3] and [9].

RELAP5/Mod 3.2 cannot track two individual non-condensibles as it is necessary for test -P7-, where helium has been injected into the steam/air atmosphere of the system. For the simulation by RELAP5/Mod 3.2, only one non-condensable in the whole facility could be used which in our case was helium. Consequently, a comparison between calculated and the equivalent measured data can have only limited value. Surprisingly enough, for a lot of parameters the comparison showed sufficient agreement between calculated and measured values.

The system behaviour of test -P7- has been plotted in Fig. 13. On the left hand-side, the history of the power both produced in the core and dumped into the two remaining PCC pools has been plotted. Because both operational PCCs are connected to dry-well -2- which is not affected by the inflow of non-condensibles, the effect of the release of helium on the PCC performance is rather small and the equivalent for both PCCs. From zero to six hours, RELAP5-basic (thick line) has slightly over-predicted the experimental results (dotted line) whereas RELAP5-simple under-predicted them. From six hours to the end of the transient, this observation has reversed.

Fig. 13 right shows the pressures inside the different vessels of the PANDA facility together with the equivalent experimental results as a function of time. The effect of the inflow of helium (4 g/s of helium between 4h and 6h) at the top of dry-well -1- has been registered by RELAP5/Mod 3.2 although the final pressure level has been under-predicted by approximately 55 kPa (RELAP5-basic) and 40 kPa (RELAP5-simple). Compared to the experimental data (dotted line), RELAP5-simple has made a slightly better job in calculating the pressure histories.

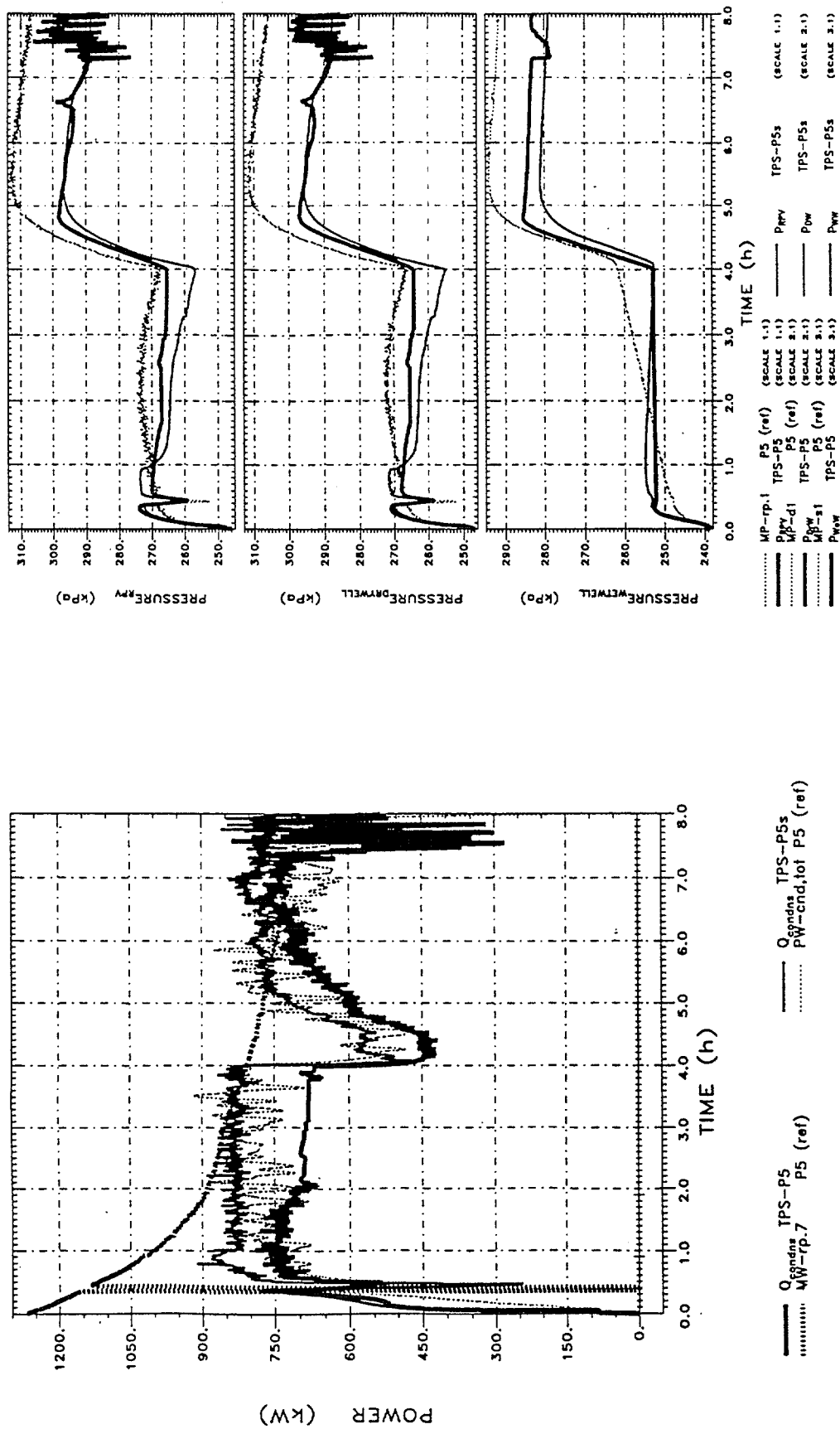


Figure 11. Calculated as well as experimental total power of the condensers (left) and calculated and measured pressures in RPV (right top), dry-wells (right middle) and wet-wells (right bottom) as a function of time for test -P5-.

The mass error for the RELAP5-basic - calculation was 361 kg and for the RELAP5-simple - case 178 kg. The cpu time to real time ratio was 6.7 and 6.3 using a CRAY-J90.

A more detailed analysis of experiment -P7- can be found in Ref [10].

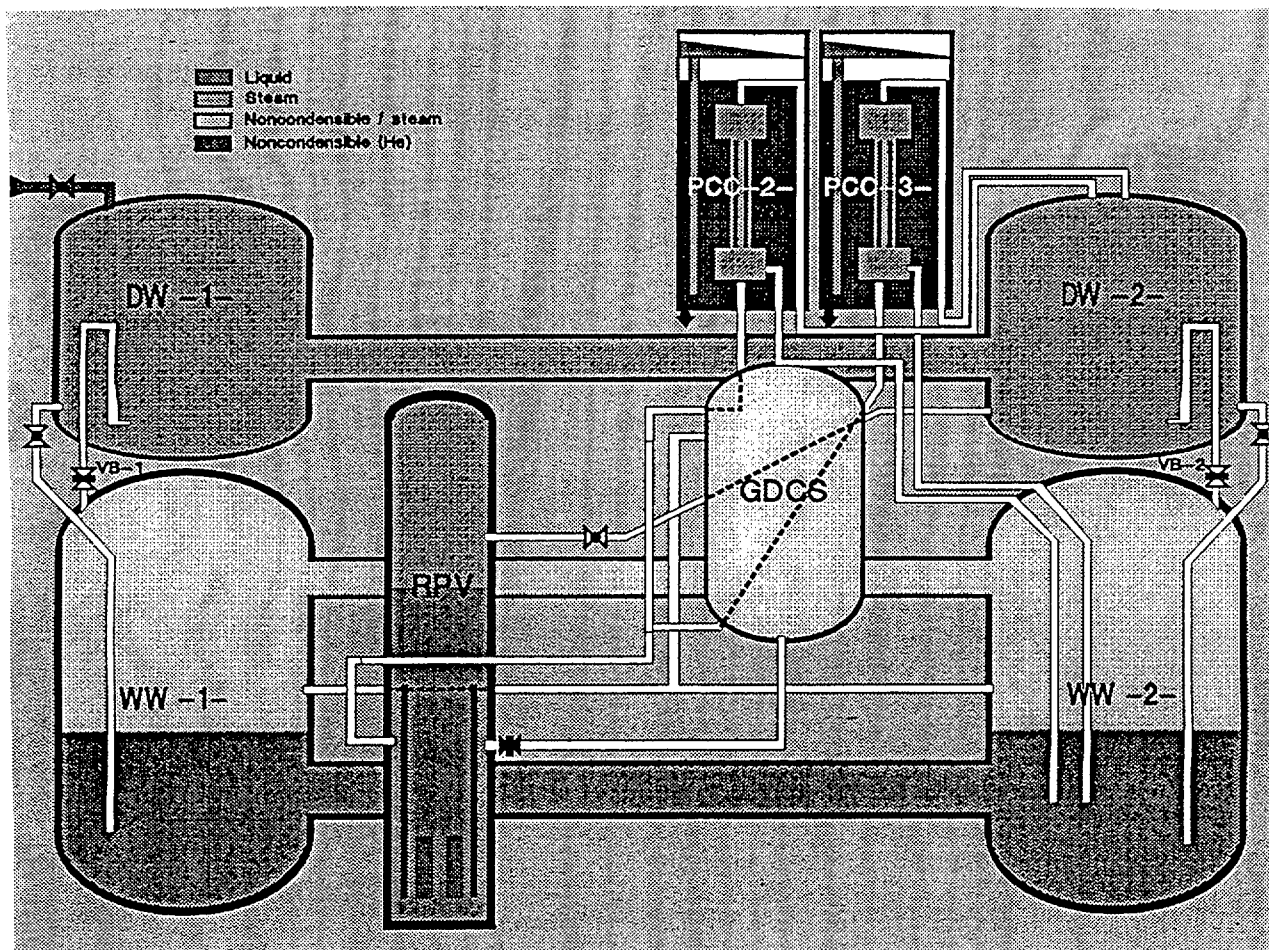


Figure 12. Scheme of the PANDA test facility as used for test -P7-.

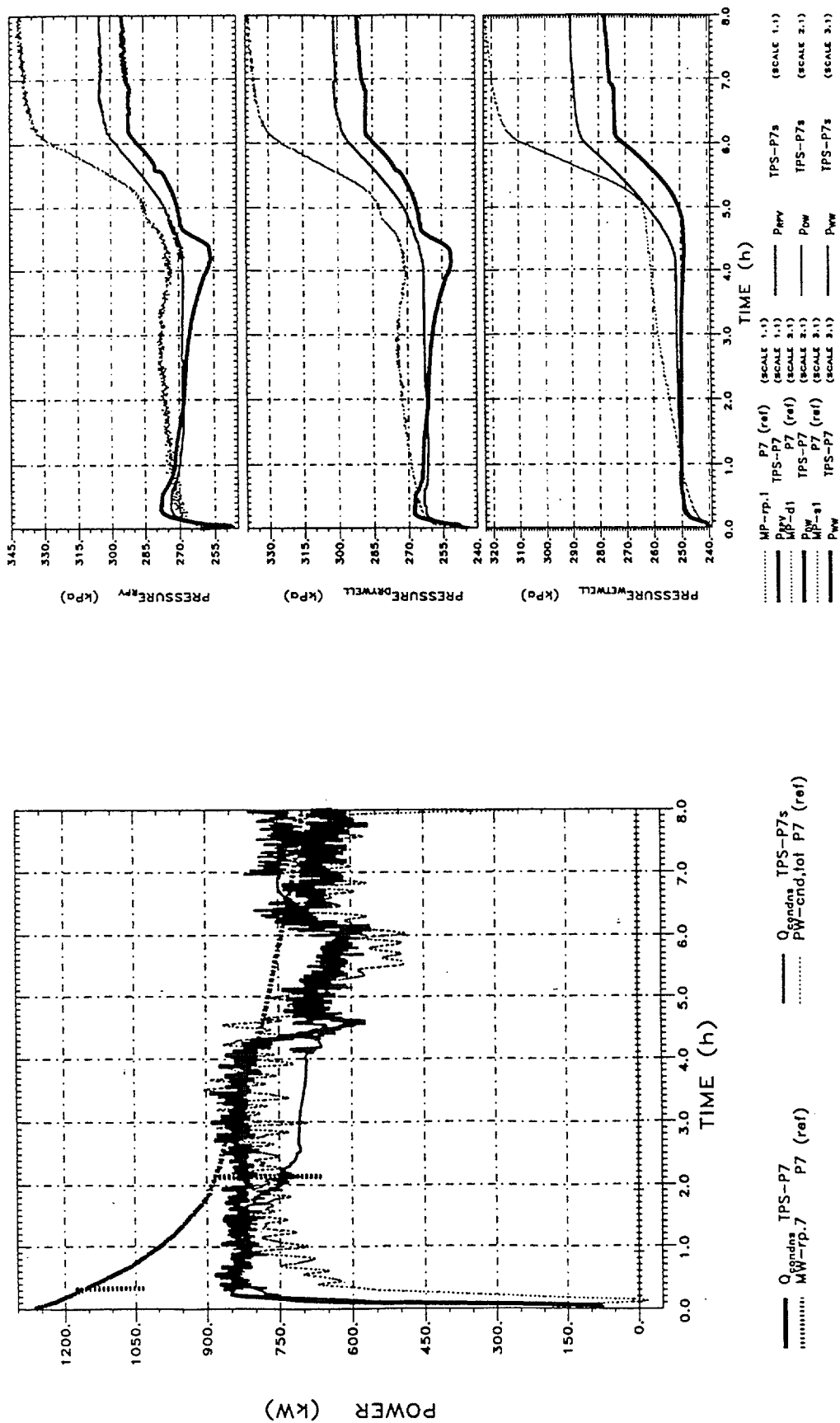


Figure 13. Calculated as well as experimental total power of the condensers (left) and calculated and measured pressures in RPV (right top), dry-wells (right middle) and wet-wells (right bottom) as a function of time for test -P7-.

6. CONCLUSIONS

The general results of these post test analyses of TEPSS tests -P2-, -P3-, -P5- and -P7- can be summarised as follows :

- RELAP5/Mod 3.2 calculated the general trends of the analysed experiments sufficiently accurate.
- Using the reduced nodalisation did not reduce CPU time significantly but generally resulted in slightly better predictions.
- The most challenging test was -P3-. Although RELAP5/Mod 3.2 calculated start-up of the two operational PCCs sufficiently, it under-predicted the final pressure of the system significantly (68 kPa for RELAP5 basic and 40 kPa for RELAP5-simple).
- Using the reduced nodalisation did not result in significant savings of computer time probably because maximum courant limit occurred in the unchanged parts of the system e.g. in the high steam velocity main steam lines or in the PCC tubes.
- There is no indication for a significant influence of the two different nodalisations on the mass error. It is in the order of 200 to 900 kg and generally a little bit smaller for calculations with simplified nodalisation.

REFERENCE

- [1] Carlson, K.E., et. al. "RELAP5/Mod 3 Code Manual NUREG/CR-4321 (1990)
- [2] Faluomi, V., Aksan, S.N. "RELAP5/Mod3.2 Model of PANDA Facility General Description and Steady State Qualification"; PSI internal report ALPHA-801-0 (TM-42-98-01)
- [3] Huggenberger, M. "TEPSS Project. Panda P-Series Specification"; PSI internal report ALPHA-703-0 (TM-42-97-05)
- [4] Huggenberger, M. et al. "TEPSS Project. Integral System test P2 Test Report"; PSI internal report ALPHA-816-0 (TM-42-98-16)
- [5] Luebbesmeyer, D.; "TEPSS Project. RELAP5/Mod 3.2 Post- Test Calculation of TEPSS Experiment -P2-"; PSI internal report ALPHA-824-0 (TM-42-98-25)
- [6] Huggenberger, M. et al. "TEPSS Project. Integral System test P3 Test Report"; PSI internal report ALPHA-819-0 (TM-42-98-19)
- [7] Huggenberger, M. et al. "TEPSS Project. Integral System test P5 Test Report"; PSI internal report ALPHA-823-0 (TM-42-98-24)
- [8] Luebbesmeyer, D. "TEPSS Project. RELAP5/Mod 3.2 Post- Test Calculation of TEPSS Experiment -P5-"; PSI internal report ALPHA-825-0 (TM-42-98-26)
- [9] Huggenberger, M. et al. "TEPSS Project. Integral System test P7 Test Report"; PSI internal report ALPHA-816-0 (TM-42-98-16)
- [10] Luebbesmeyer, D. "TEPSS Project. RELAP5/Mod 3.2 Post- Test Calculation of TEPSS Experiment -P7-"; PSI internal report ALPHA-826-0 (TM-42-98-27)

RELEVANT RESULTS OF PRE- AND POST-TEST ANALYSIS OF P3 AND P6 PANDA EXPERIMENTS



XA0055026

L. BATET, F. REVENTÓS
Department of Physics and Nuclear Engineering,
Polytechnical University of Catalonia,
Barcelona, Spain

Abstract

Polytechnical University of Catalonia (UPC) cooperates with different European research Centres and Universities in the framework of the TEPSS (Technology Enhancement of Passive Safety Systems) project, in the analytical support of PANDA tests. Analytical support of the tests consists of both pre and post-test calculations. The former to predict the expected behaviour for a defined scenario and the latter to confirm or discuss the recorded data and validate the models used for this purpose. Among all PANDA tests, it is UPC's responsibility to provide support of P3 and P6 experiments. Pre and post-test calculations have been performed with RELAP5/Mod3.2 using a base input-deck originally prepared by ECN, with minor changes performed in order to better predict the final configuration of the facility. This paper deals with the relevant results of the provided analytical support of tests P3 and P6. Due to the fact of having responsibility on two different tests, a comprehensive effort has been made in order to check the consistency of modelling recommendations. A short chapter is devoted to this purpose. Final discussion is focused on the capabilities of models and codes in order to correctly predict the behaviour of the plant. The advantages and disadvantages of using a one-dimensional view of an integral facility are presented along with different sensitivities related to the most significant phenomena. Finally, conclusions and open items are presented with the aim of summarizing results and identifying areas which need further work.

1. INTRODUCTION

1.1. Background and objectives

Polytechnical University of Catalonia (UPC) cooperates with different European research Centres and Universities in the framework of the "Technology Enhancement of Passive Safety Systems" project (TEPSS) [1], in the analytical support of PANDA tests.

PANDA facility is located in the "Paul Scherrer Institut" (PSI) and represents, in its TEPSS configuration, a simplified boiling reactor plant. It includes the reactor itself, the containment (drywell -DW- and wetwell -WW-) and the main safety features like the isolation condenser (IC), the passive containment cooling system (PCCS) and the gravity driven cooling system (GDCS).

The objective of PANDA tests [2] is to provide actual information (references [3-4]) in order to clarify the integral behaviour of the equivalent plant under accidental conditions in main steam line break (MSLB) scenarios and to collect data to validate or qualify the related codes and models.

Analytical support of the tests consists of both pre and post-test calculations. The former to predict the expected behaviour for a defined scenario and the latter to confirm or discuss the recorded data and validate the models used for this purpose.

Among all PANDA tests, it is UPC's responsibility to provide support of P3 and P6 experiments. The objective of P3 is to prove the PCCS capacity to start up under challenging conditions, with the containment and the condensers filled with noncondensable gas. The objective of P6 is to study the system interaction when the IC operates in parallel with the PCCS. It is also investigated the effect of a leakage between drywell and wetwell.

Pre and post-test calculations have been performed with RELAP5/Mod3.2 using a base input deck originally prepared by the Netherlands Energy Research Foundation ECN, with minor changes performed in order to better predict the final configuration of the facility.

Pre-test analysis were performed in 1997 with successful results as well as useful comments on test specifications. The experiments took place at the beginning of 1998 and experimental data were distributed to the analyst teams. Post-test calculations have been recently concluded and results and conclusions are presented here.

This paper deals with the relevant results of the provided analytical support of tests P3 and P6. Due to the fact of having responsibility on two different tests, a comprehensive effort has been made in order to check the consistency of modelling recommendations. A short chapter is devoted to this purpose.

Final discussion is focused on the capabilities of models and codes in order to correctly predict the behaviour of the plant. The advantages and disadvantages of using a one-dimensional view of an integral facility are presented along with different sensitivities related to the most significant phenomena.

Finally, conclusions and open items are presented with the aim of summarizing results and identifying areas which need further work.

1.2. Initial model

Initial nodalization, prepared by ECN, is a full RELAP5/Mod3.2 model that includes all the components of the facility [5]. A nodalization diagram is shown in Figure 1.

Modifications performed in the input deck are discussed in each specific chapter.

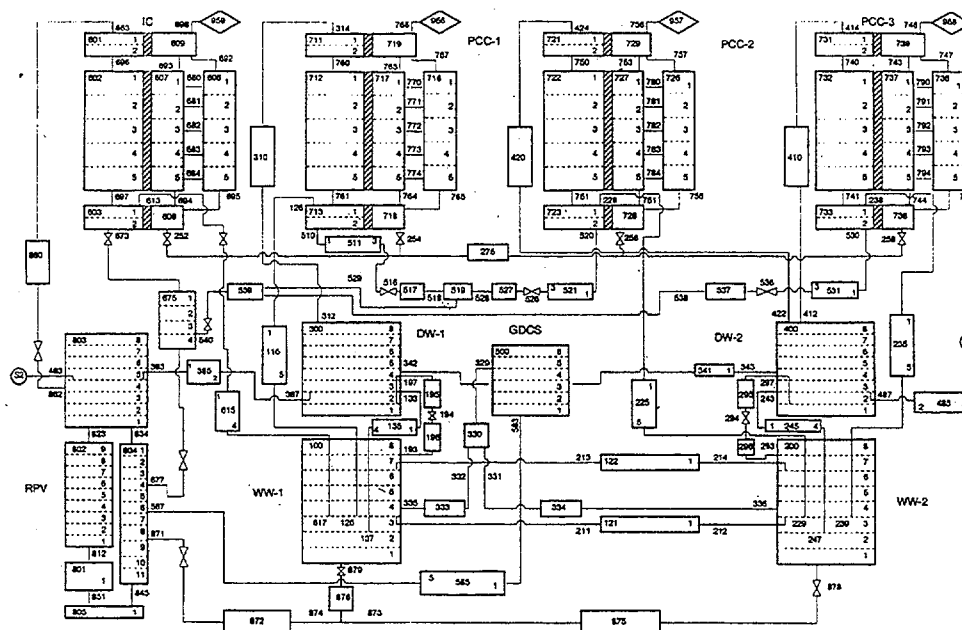


FIG. 1. Nodalization of ECN RELAP5/Mod3.2 model for PANDA facility [5].

2. ANALYTICAL SUPPORT OF TEST P3

2.1. Aims and test description

The aim of test P3 is to investigate the PCCS start up capability under challenging conditions. The drywell and the PCCS are initially filled with air. Only the two PCC units connected to DW2 are available and all the steam flow through the break is directed to DW2 [2].

After the break starts, there is a DW pressure increase that forces the air located in the DW to circulate to the WW through PCC vents. So, WW pressure increases too. During the first stage of the transient, sufficient amount of air is supposed to be in the DW to prevent the effective start up of the PCC system.

Once PCCS starts, condensation takes place inside the tubes, pressures stop increasing and the whole system reaches a quasi-steady situation.

2.2. Pre-test background

Pre-test calculation of P3 experiment [5-6] has been useful for general understanding of the expected behaviour of the plant. In order to improve the calculation speed all the components that did not take part in the test were removed.

The remaining components of the model were tested and the predicted behaviour of the plant was reasonably correct.

2.3. P3 post-test analysis

Taking advantage of pre-test background, and according to test initial specifications [2], some other components not taking part in the test were suppressed from the model and some minor changes were introduced.

After analyzing some sensitivities (see Section 2.4.) new important modifications were performed in the base deck:

- (a) the Main Vent lines, originally connected to the top of node 2 in the WW, have been redirected to the bottom of node 3,
- (b) WW water connecting volume, originally connected only to the top of node 3 in the WW, have been complemented with connexions to the bottom of node 4.

Figure 2 shows the pressure evolution in the containment. During the first stage of the simulation the calculated pressures increase at a greater rate than experimental ones. This is probably due to the fact that, in the calculation, a quite strong stratification of air-vapor mixture in DW2 is predicted (see Figure 3).

In the long term, although heater power is greater than total heat extraction, system pressures remain always below measured values. This seems to be related to the calculated stratification of water temperatures in the suppression pool (Fig. 4).

Both anomalous stratifications have to do with the fact of using a one dimensional model.

Two other discrepancies, related to code limitations, have been identified:

- (a) Gas temperatures predicted in PCCS tubes remain constant along them instead of decreasing to about pool temperatures (Fig. 5).

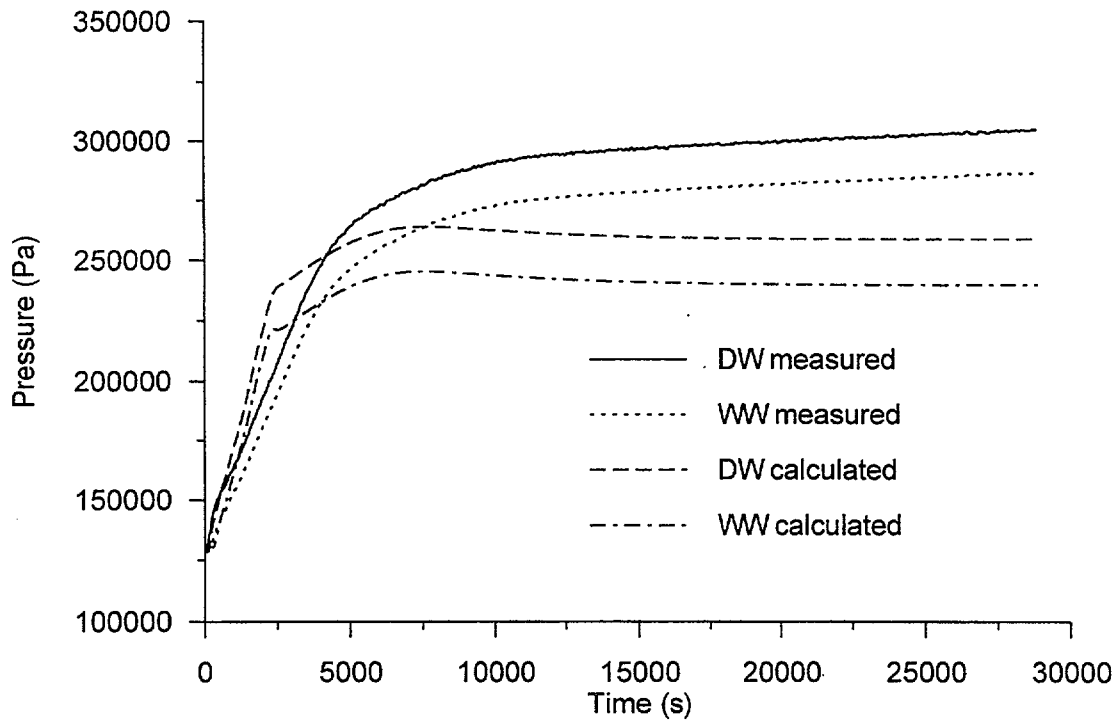


FIG. 2. P3 post-test calculation. Pressure evolution in the containment.

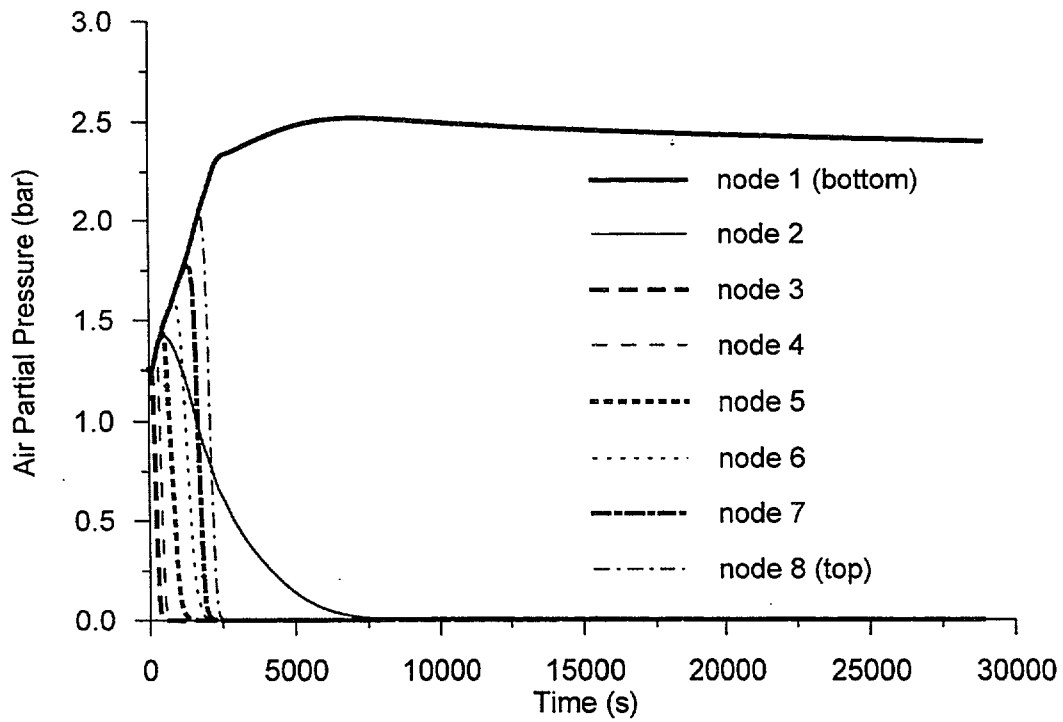


FIG. 3. P3 post-test calculation. Calculated air partial pressure evolution in DW2.

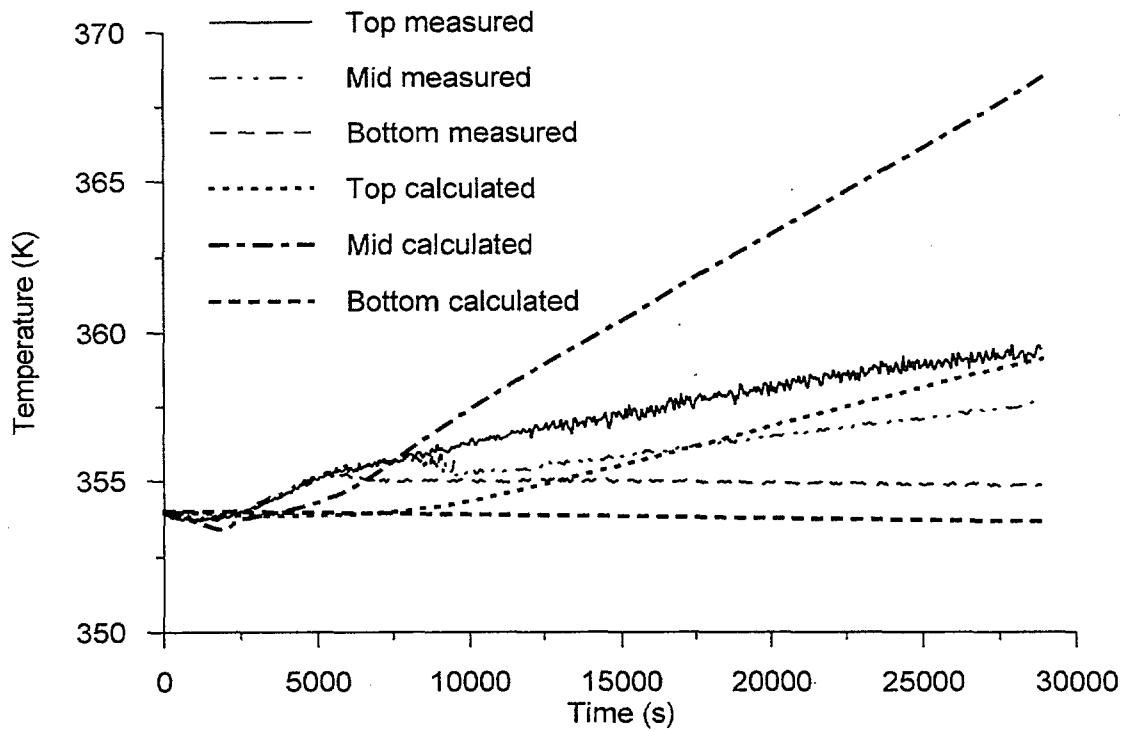


FIG. 4. P3 post-test calculation. Liquid temperature evolution in WW2.

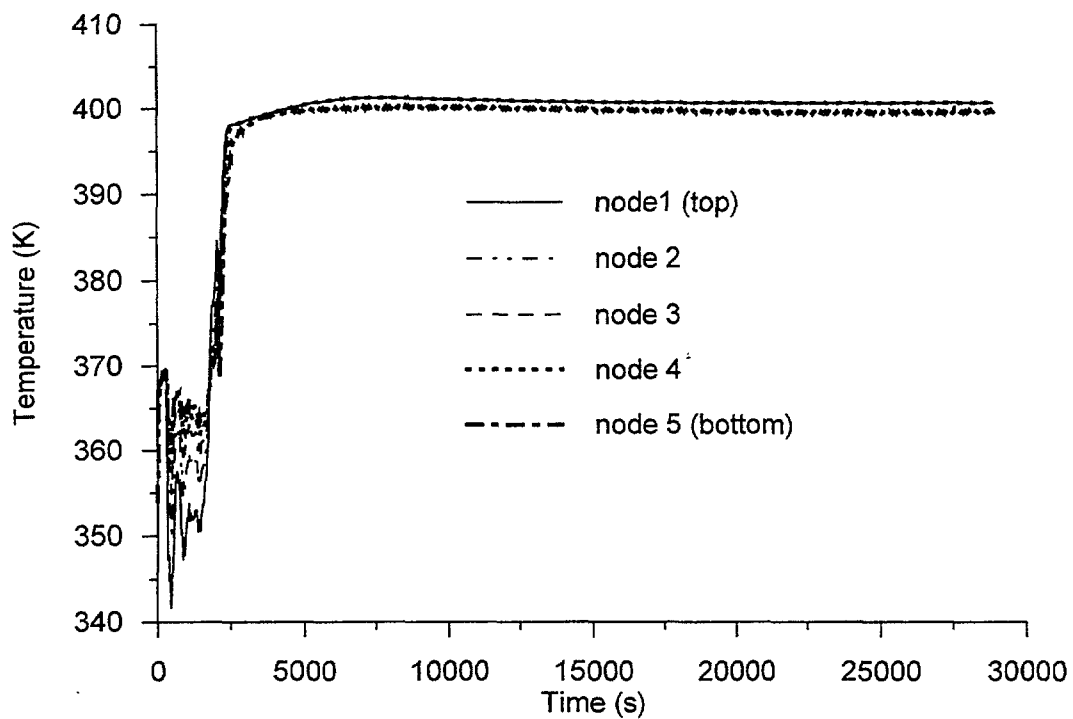


FIG. 5. P3 post-test calculation. Calculated gas temperature distribution in PCC2 tubes.

- (b) Temperatures in WW gas space reach unphysical values (about 20 K greater than saturation temperature at total pressure), as can be seen in Figure 6.

Despite of the anomalous predictions, the integral behaviour of the experimental facility is well simulated.

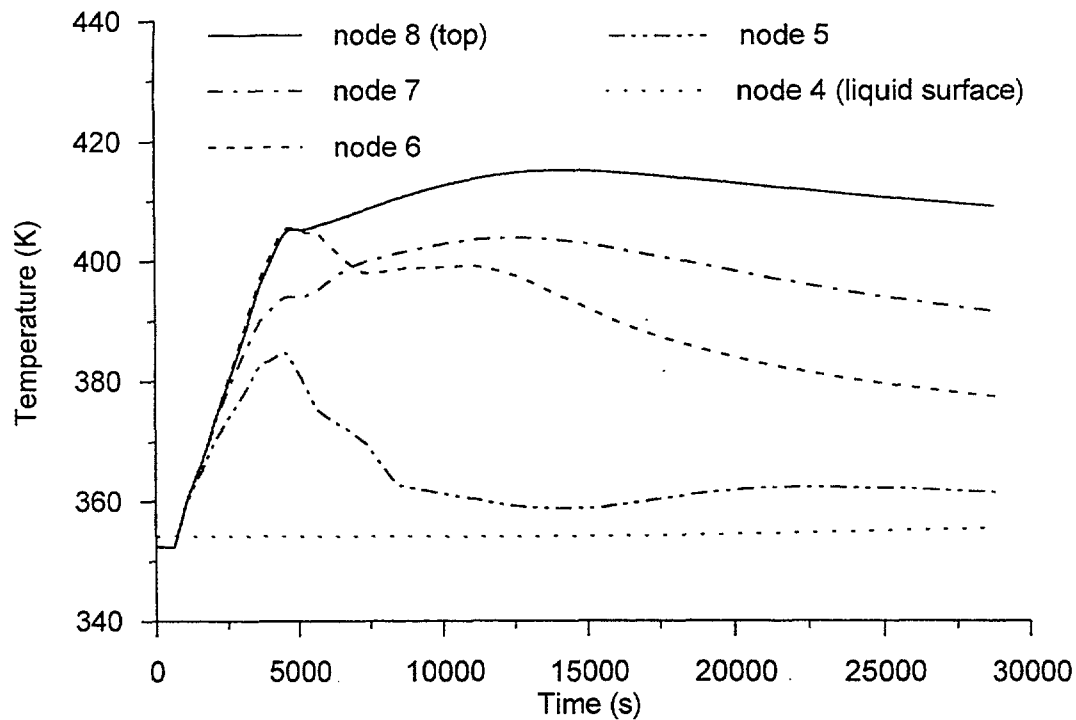


FIG. 6. P3 post-test calculation. Calculated gas temperature distribution in WW1.

2.4. Sensitivity studies related to P3 test

The following sensitivity studies have been performed:

- redirection of Main Vents connexions to WW (see above)
- redirection of PCC vent line connexions to WW (the lines, originally connected to the top of node 3 in the WW, were redirected to the bottom of node 4)
- improvement of connexions of WW water connecting volume (see above)
- changes in time step
- changes in initial temperatures of pools and RPV
- redirection of break flows (MSLs, originally connected to the bottom of node 3 in the DW, were redirected to the top of node 2).

Although it does not eliminate the temperature stratification, redirecting the Main Vents improves the temperature distribution in the suppression pool. For this reason this change has been maintained in the input deck.

The same is not true for the PCC vent lines. Redirecting the WW connexions leads to worst overall predictions.

In the original deck, WW water connecting volume was connected only to the top of node 3 in the WW. Because of it, air vented through the Main Vents was accumulated in that volume, causing a sharp increase of WW level by removing the liquid on it. This effect can be seen in Figure 7.

Test P3 calculation results have shown to be quite sensitive to the time step used. For this test is not recommended to use a time step greater than 0.025 s.

System behaviour has shown to be little sensitive to changes of few degree in initial liquid temperatures of PCCS pools and pressure vessel.

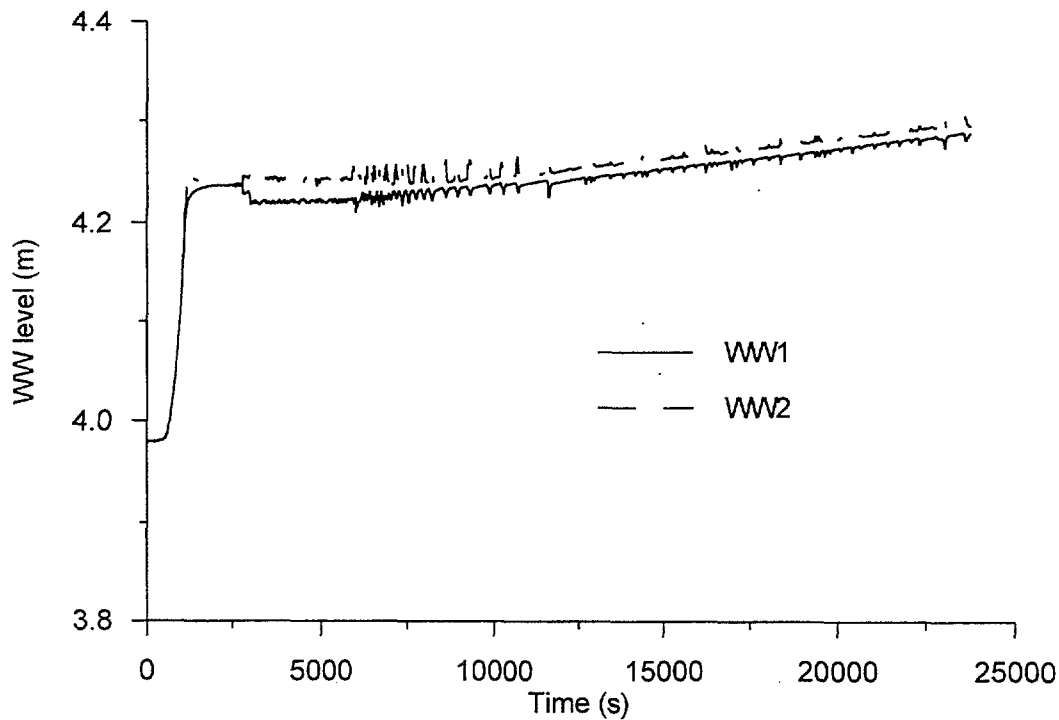


FIG. 7. P3 post-test calculation. Calculated WW levels using the original nodalization.

Redirecting the MSL connexions improve purging of air from DW to WW, leading to greater calculated system pressures in this test. This change has not been adopted in the input deck because its effects on test P6 need further investigation.

3. ANALYTICAL SUPPORT OF TEST P6

3.1. Aims and test description

The objective of this test is to investigate the interaction between the PCC system and the IC and to show the effect of this interaction on the containment and the reactor system performance. The specific objective of the second part of this test is to study the effect of a drywell-to-wetwell bypass leakage on containment performance [2].

Test P6 simulates a MSLB with flow directed to both drywell vessels. Simulation begins one hour after of the postulated break, at the end of GDCS injection phase, when boiling in reactor pressure vessel (RPV) resumes. Four hours after the beginning of the test a leakage path through Vacuum Breaker is assumed. Three hours later the IC is set off.

3.2. Pre-test background

Among the different lessons learned in the pre-test calculations (see references [5] and [7]), the strong relationship between the results and the initial conditions seems to be the most important. The sensitivity analysis performed showed quite different behaviours when starting with slightly different initial conditions. Further discussion on this point will be presented in Section 3.4.

Another finding of the pre-test analysis is the importance of the size of the leakage in the second part of the transient. Greater sizes produce quite greater increases in the calculated pressures.

3.3. P6 post-test analysis

Deck changes performed in P3 calculations have been kept in P6 post-test for consistency reasons. Other minor changes have been done, the most significant of them are:

- (a) IC lines and pool have been renodalized to fit them to the actual elevations
- (b) A new nodalization has been used for PCCS pools following the recommendations of other TEPSS partners [8].

Figure 8 shows the main pressures in the whole transient. Two different phases can be observed in this results.

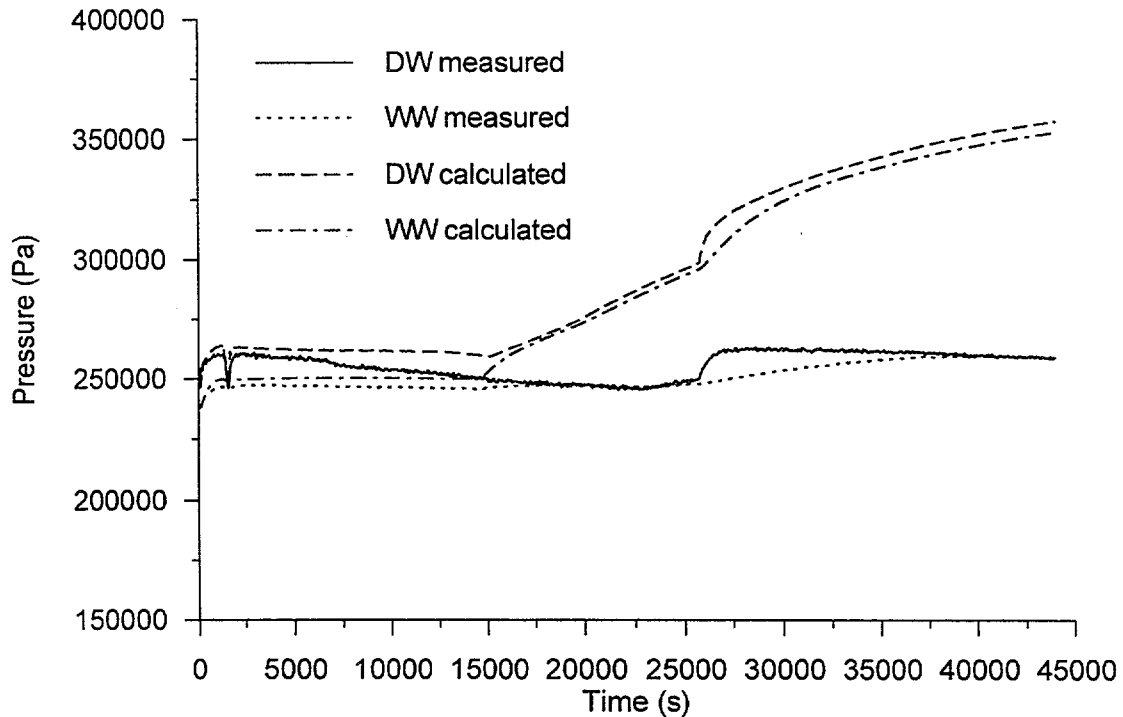


FIG. 8. P6 post-test calculation. Pressure evolution in the containment.

During the first phase, before the leakage, the calculated parameters are in close agreement with the experimental data (see also mass flow results in Figures 9 and 10). After the leakage, calculated pressures increase unexpectedly, even with the IC operating, and predicted global parameters do not match to experimental ones.

The results of different sensitivity studies presented in the next section will be helpful to establish the reasons of these discrepancies.

3.4. Sensitivity studies related to P6 test

The following sensitivity studies have been performed in order to clarify the origin of the discrepancies stated above:

- (a) initial amount of air in the DW
- (b) initial amount of air in the IC
- (c) DW nodalization
- (d) heat losses in the DW to WW leakage line
- (e) heat transfer options in condensers

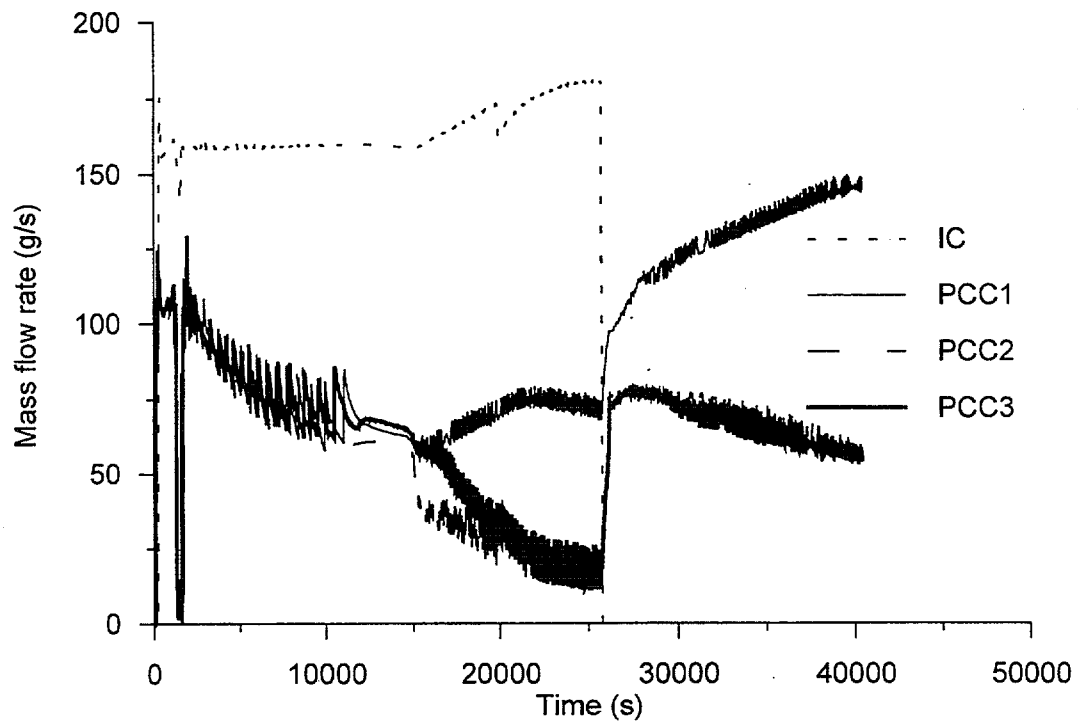


FIG. 9. P6 post-test calculation. Calculated steam supply mass flow to the condensers.

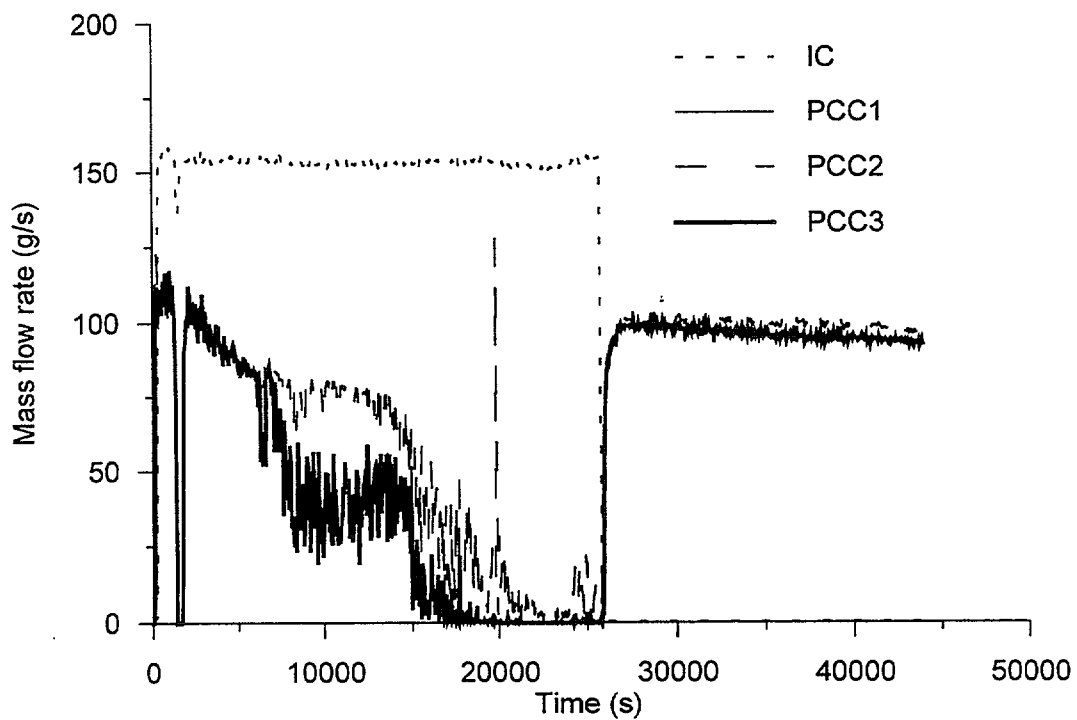


FIG. 10. Test P6 measured steam supply mass flow to the condensers [4].

A greater amount of air in the DW produces greater calculated pressures due to the following facts: more air is purged to WW and air presence in PCC tubes increases reducing its performance.

A greater initial mass of air in the IC causes a decrease in the corresponding mass flow and a reduction in heat extraction. If IC mass flow decreases steam flow through the MSLs increase. Then, steam flow through the PCCs is greater, enhancing their performance. So, the calculated global effect becomes less sensitive to initial amount of noncondensables in IC than expected.

The discrepancies after the leakage starts are related to a deficient heat extraction in PCCs due to air accumulation. A renodalization of DW bottom and MSL connexions to DW has been tested to improve air purging to WW and reduce the amount of noncondensable gas finally trapped in the PCC tubes. The effect of the new nodalization is positive during the first phase but not in the second phase of the transient (see Figure 11).

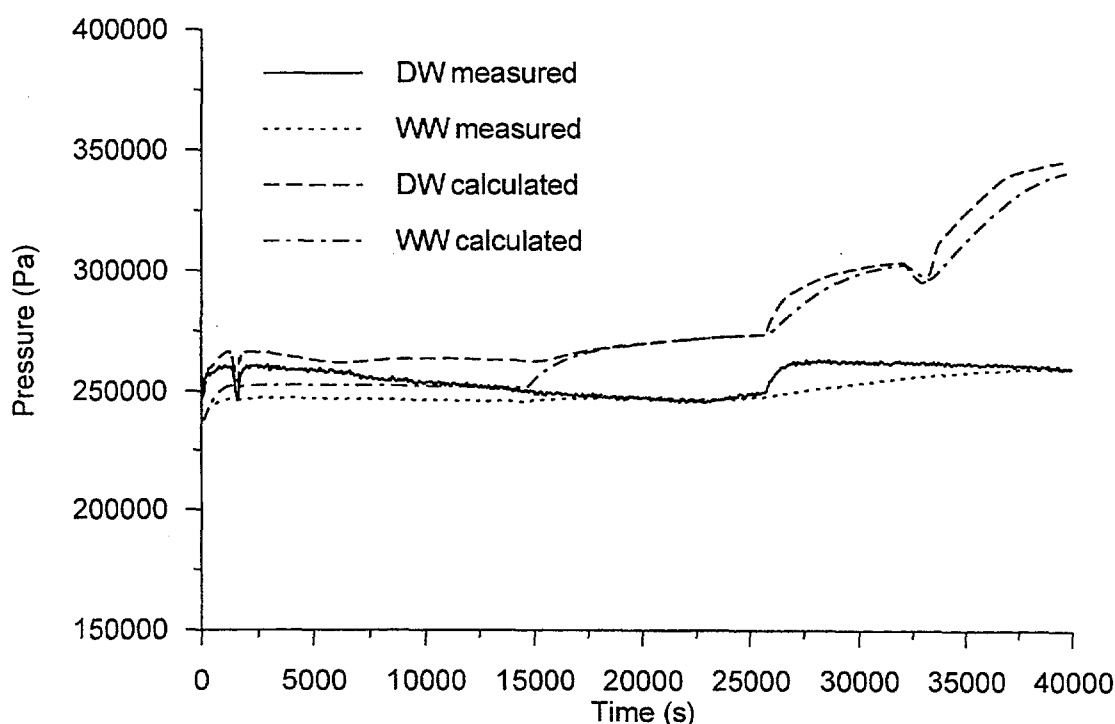


FIG. 11. P6 post-test calculation. Pressure evolution in the containment using a renodalized drywell and MSLs connexion.

Heat losses in the DW to WW leakage line have been introduced for two main reasons. The first of them is the anomalous WW pressure increase observed in the calculations when the leakage starts, and the second one is the fact the line itself is quite long. Although a certain improvement has been reached, the discrepancy is still not corrected.

The new heat transfer options of RELAP5/Mod3.2 have been tested in order to use more detail in the heat structures related with the condensers. No significant improvement has been reached.

4. COMPREHENSIVE CONSIDERATIONS

Although both analysis (P3 and P6) have been performed with the same deck and the same basic changes, the results of different sensitivities show that further considerations are needed.

The anomalous temperature increase detected in P3 calculations does not appear in P6 case and it is difficult to identify the reason of it.

PCC system behaviour is better predicted when it works by itself with no interaction with IC (see, for instance, references [8] and [9]).

Initial amount of air, that seems to be a significant parameter in P6 analysis becomes not so important in P3 results. More accurate actual values of partial pressures could be helpful in order to reduce the uncertainty on these results.

Redirecting MSLs connexion to DW has a significant effect in test P3 and not in other tests (see reference [10]). This is due to the important amount of air in this experiment.

All these comprehensive considerations have to be taken into account to establish the conclusions of this work or to suggest what it is needed to improve the simulation capabilities.

5. CONCLUSIONS.

Some advantages and disadvantages in using RELAP5/Mod3.2 models have been identified in this work.

As a general conclusion, both the code and the model are suitable for two main purposes in the framework of experiments like P3 and P6:

- (a) to investigate the general behaviour of the facility
- (b) to establish the significance of definite parameters like: amount of air, initial conditions, heat losses...

The fact of using a one-dimensional solution of general thermal-hydraulic equations appears normally as a limitation: natural circulation situations that have a strong probability to occur in containments and pools cannot be simulated with this tool. The same comment can be applied to other 3D effects like air purging. Anomalous stratifications or strange local temperature excursions are the results of this fact.

On the other hand, nevertheless, as most of the incorrect predictions are related to local phenomena, the code and the model are quite suitable to simulate the general interaction of all components of the facility.

The results of RELAP5/Mod3.2 and the model that has been used, are good enough in a long term basis and from the overall point of view.

The tool works better when it is used to simulate a complete purge of air (like in test P3, where Main Vents help to clear the DW) than when it is used to investigate the effect of dealing with an air-steam mixture with a small amount of air (like in test P6, where a considerable amount of air is trapped in the bottom of DW vessels and in Main Vent lines).

From future work point of view, although it is understood that improvements in the field of heat transfer with noncondensables will be welcome, it could be interesting to study the impact of using a 3D or a pseudo-3D (1D with interconnected channels) model in order to improve the predicted transport of noncondensables.

REFERENCES

- [1] STOOP, P.M., et al., "TEPSS-Technology Enhancement of Passive Safety Systems", 5th International Conference on Nuclear Engineering (Proc. ICONE5, Nice, 1997), ECN, 1996.

- [2] HUGGENBERGER, M., "TEPSS-Project: PANDA P-Series Test Specification", ALPHA-703-B, TM-42-97-05, PSI, September 1997.
- [3] HUGGENBERGER, M. et al., "TEPSS Project: Integral System Test P3 Test Report", ALPHA-819, PSI, 1998.
- [4] HUGGENBERGER, M. et al., "TEPSS Project: Integral System Test P6 Test Report", ALPHA-827, PSI, 1998.
- [5] HART, J., "TEPSS Project Yearly Progress Report 1997", FI4I-CT95-0008, ECN, 1998.
- [6] BATET, L., GAGO, J.L., REVENTÓS, F., "P3 Pre-Test Calculation Report", UPC, 1998.
- [7] BATET, L., GAGO, J.L., REVENTÓS, F., "P6 Pre-Test Calculation Report", UPC, 1998.
- [8] HART, J., "RELAP5/MOD3.2 Post-Test Analysis of PANDA P1/8 Tests", ECN, 1998.
- [9] HART, J., "TEPSS Project Technical Progress Report January 1 - June 30, 1998", FI4I-CT95-0008, ECN, 1998.
- [10] LÜBBESMEYER, D., "Post-test analysis for TEPSS test P2 (RELAP5/Mod3.2-Analysis)", PSI, 1998.

QUALIFICATION OF ANALYTICAL METHODS AND CODES

(Session 5)

Chairman

F. D'Auria
Italy

**NEXT PAGE(S)
left BLANK**



RELAP5 ANALYSIS OF PACTEL INJECTION TESTS

G.R. KIMBER, J.N. LILLINGTON
AEA Technology plc,
Winfrith Technology Centre,
Dorchester, Dorset, United Kingdom

Abstract

A characteristic feature of advanced reactor designs is their reliance on passive safety systems. It is important to assess both the operation of such systems and the ability of systems codes, such as RELAP5, to model them. In Finland VTT Energy, together with Lappeenranta University of Technology, is using the PACTEL facility for the investigation of passive core cooling systems. In particular, a core make-up tank (CMT) has been installed in the rig to operate in a similar manner to those in many Advanced PWR designs. Three small break tests, GDE-24, GDE-34 and GDE-43 in the PACTEL facility were chosen for modelling with RELAP5. The objective of GDE-24 was to investigate CMT behaviour and in particular the effects of condensation in the CMT. The second test, GDE-34, was similar except that it had a smaller CMT and at the start of the test the water in the CMT and connecting pipework was at an elevated temperature. Test GDE-43 focused on conditions when the driving force for flow through the passive system injection system (PSIS) slowly disappears. Analysis of all tests reported here was carried out with RELAP5/MOD 3.2.1.2.

The paper summarises the conclusions of all the tests. A critical part of the study revolved around modelling of the CMT. A model was developed to allow its detailed behaviour to be investigated more easily. This enabled recommendations for improving the condensation modelling in RELAP5 to be made. Apart from the wall condensation modelling issue, the implication of the work is that RELAP5/MOD 3.2.1.2 (a comparatively recent version of the code) is broadly adequate for these applications.

1. INTRODUCTION

The main objectives of the work presented in this paper are:

- To identify new phenomena associated with the performance of passive safety injection systems;
- To determine how well the RELAP5 code can simulate the behaviour of such systems.

Several series of tests have been performed in the PACTEL facility [1] sited at the University of Lappeenranta in Finland. The work is carried out as part of the European Commission 4th Framework Programme project "Assessment of Passive Safety Injection Systems of Advanced Light Water Reactors" (F I4I-CT95-0004). The work involves four partners: VTT, the project co-ordinator, AEA Technology, University of Lappeenranta and the University of Pisa. This paper is specifically concerned with the AEA Technology contribution to the project, the validation of the RELAPS code. The authors acknowledge the support of the UK Department of Trade and Industry and the EC in this project.

2. PACTEL FACILITY

The PACTEL Facility is a 1:305 volumetrically scaled full height model of a 6 loop VVER. It has 3 equal sized loops, each representing two of the reactor loops. Each loop has an active pump and steam generator. The core and downcomer are modelled as separate pipes.

The core is electrically heated with 144 fuel rod simulators in a triangular grid. The axial power profile is simulated. The steam generators have horizontal tubes with a single bend. The primary volume is accurately scaled, but the need to represent the plant elevations correctly means that the secondary side is larger than its true scaled size. A diagrammatic sketch of the facility with the CMT is shown in Figure 1.

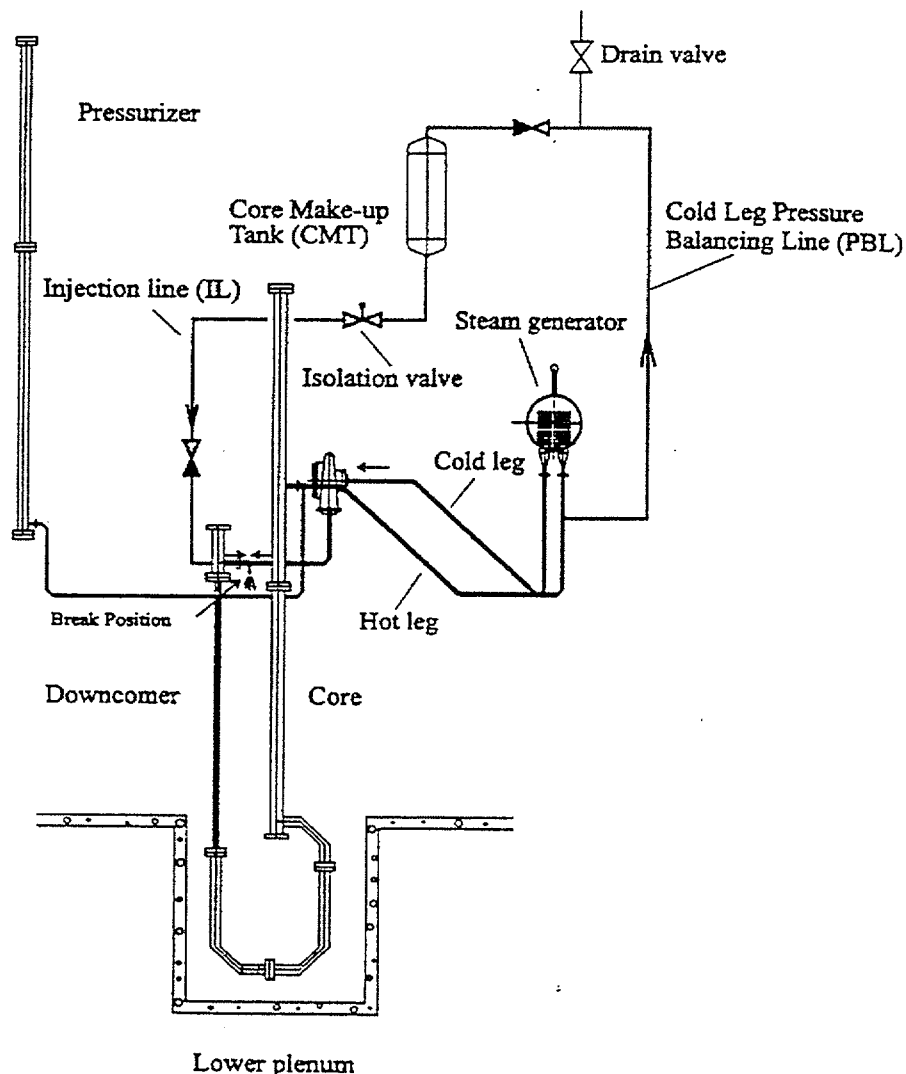


FIG. 1. PSIS Configuration (Third series).

3. PACTEL EXIPERIMENTS

3.1. Brief description of test programme and procedures

Within the project, three series of Small Break Loss-of-Coolant Accident (SBLOCA) tests were performed. Each series was designed to investigate the performance of the Passive Safety Injection Systems (PSIS) for different rig geometry or test conditions. The first series focused on the effect of break size, the second on the break location and the third on the Core Make-up Tank (CMT) elevation. Experimental parameters were varied to cover the range of conditions expected to exist in a plant and to provide relevant data for the important code models. Full details of the experiments are given in a number of internal references within the EC Project. References [2-5] include summary information together with the RELAP5 code comparisons.

In each experiment the primary and secondary system parameters were established to achieve the desired initial conditions. At the start of the test, there was no flow through the PSIS. It proved necessary, however, to preheat the PBL to ensure that the injection flow commenced when the Injection Line (EL) valve was opened. The valve opening was triggered by the fall in pressuriser level after the break was opened.

3.2. Description of key features and phenomena

Each experiment can be separated into three phases:

Recirculation - once the IL isolation valve is open, buoyancy driven single phase water circulates through the PSIS. The driving head is the density difference between the hot water in the PBL and the cold water in the IL and CMT.

Oscillation - two phase flow in the PBL resulting in an increased driving head and flow compared with the recirculation phase.

Injection - steam flows into CMT resulting in increased driving head. The magnitude of this may be adversely affected by steam condensation. Investigation of this feature is a key issue of the experiments and the analysis presented in this paper.

4. RELAP5 MODELLING

4.1. Physical models

The RELAP5 code has been developed over many years as a best estimate system thermal hydraulics code for PWR accident conditions. The mass, momentum and energy equations are solved for the steam and water phases. The model allows for thermal-disequilibrium between the phases and also for heat transfer between the fluid phases and heat structures. Current generation PWRs utilise powered ECCS for SBLOCA and hence the code models have been exercised and validated under flow conditions rather different from those encountered in these applications.

In general the key phenomena modelled by the code, including the wall, fluid heat transfer and shear require empirical correlations. These are flow regime and, therefore, applications dependent. It is not possible in this paper to provide detail on all the RELAP5 models and attention is concentrated on a few phenomena which are of importance in these tests.

A key consideration in the RELAP5 modelling concerns the behaviour of the CMT. The phenomena of interest and which it is crucial to model correctly include thermal stratification, condensation and the liquid and wall heat transfer. The performance of the code models are considered in more detail in the analysis results from the individual tests.

4.2. Numerical representation

The original deck for the analysis was supplied by VTT and was intended to be compatible with RELAP5 MOD 3.2. AEA Technology undertook a thorough review of the deck, making modifications to the pressuriser model and adding a model for the CMT and associated pipework.

A critical factor in this work was the nodalisation chosen to ensure appropriate representation of the physics and numerical stability for the solution scheme. More details are given in [3-5]. The basic nodalisation is shown in Figure 2. The same version of the code, RELAP5 MOD 3.2.1.2 was used for all the tests. The analyses are presented for three experiments GDE-24, GDE-34 and GDE-43.

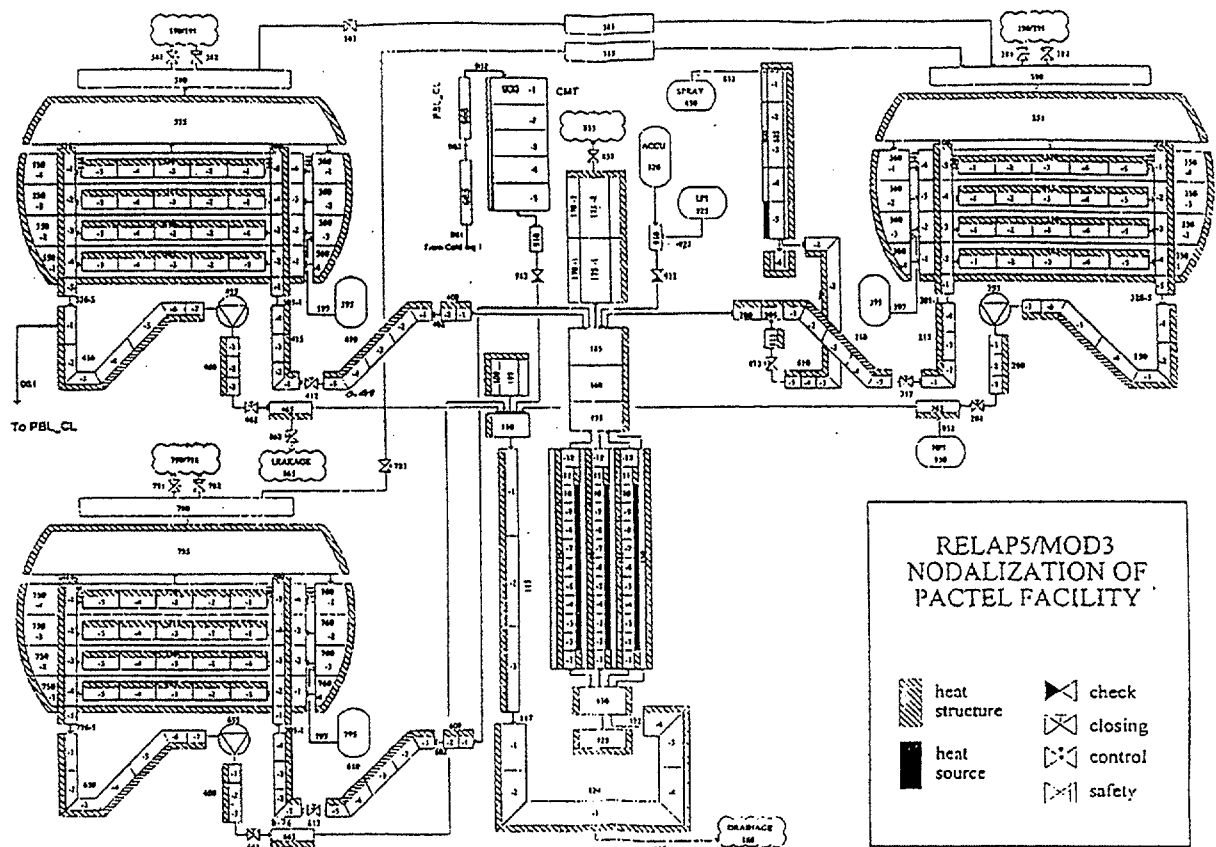


FIG. 2. RELAP5 Nodalisation of the PACTEL Facility.

5. CODE COMPARISONS WITH THE GDE-24 ~EXIPERIMENT

The GDE-24 experiment included a 3.5 mm cold leg break. The main objective was to investigate CMT behaviour and in particular the effects of thermal stratification and condensation in the CMT.

Results from calculations representing the full transient are shown in this paper, Figure 3. In the reference calculation there was a significant fall of pressure which occurred as the core make-up tank started to empty. In a second sensitivity calculation the rate of condensation in the core make-up tank was artificially reduced and it was found that the results followed the experimental data almost precisely. This highlighted some inadequacy in the wall condensation modelling in the RELAP5 code.

A study of how the code calculated the heat transfer coefficients revealed a deficiency in the model, the principal feature being that the thickness of the condensation film on the wall is not modelled realistically.

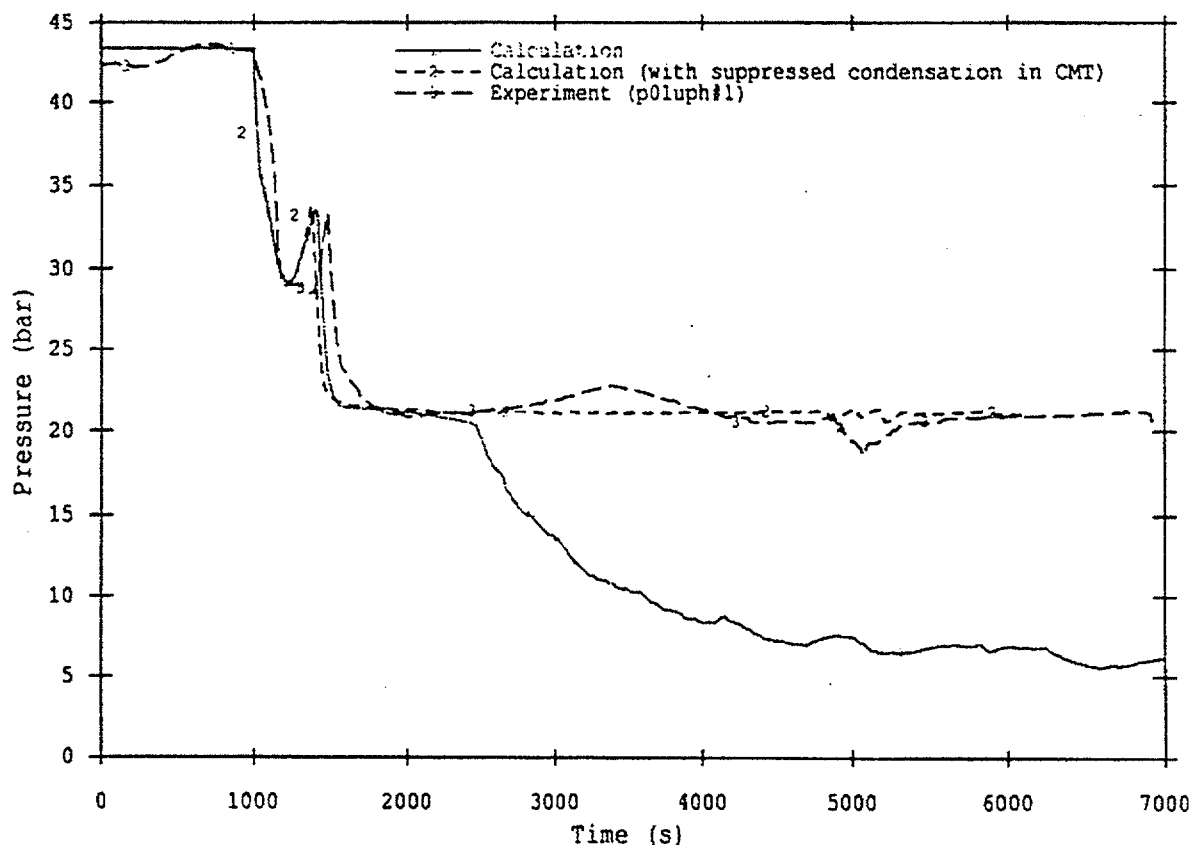


FIG. 3. Pressuriser Pressure.

Stand-alone modelling of the CMT was then carried out which indicated:

- that replacing the mesh in the CMT wall, over a practical range of sizes, produced little benefit. The implication is that it may be difficult to get the resolution necessary using a system code like RELAP5;
- flow oscillations could be reduced by refining the volumetric (vertical) mesh, but it was not possible to eliminate them altogether. Again this is a limitation of the approach inherent in system codes;
- the results were not sensitive to the nodding refinement in the PBL. This is comforting because of the practical limitations of running a complete rig model with fine nodding in the PBL.

The implication of the GDE-24 analysis was that, apart from the wall condensation modelling issue, the modelling in RELAP5 was broadly adequate for this experiment.

6. CODE COMPARISONS WITH THE GDE-34 EXPERIMENT

The second test analysed, GDE-34, was similar to GDE-24 but with a smaller CMT. It was initially full of hot water. The GDE-34 test represented the conditions that would prevail if a check valve in the pressure balance line had been leaking. The objective was to investigate the PSIS performance when the driving force for starting the recirculation was small.

Two calculations are again presented each representing the full transient. In the reference calculation there was a significant disturbance to the emptying of the core make-up tank due to condensation being calculated. In a second sensitivity calculation the rate of condensation in the core make-up tank was again artificially reduced (as in the previous study) and it was found that the results gave an improved agreement with the experiment.

Stand-alone modelling of the CMT indicated support for the conclusions drawn from the GDE-24 analysis performed previously.

- an alternative approach to the calculation of the wall heat transfer for condensation was tried making use of an input table in the input deck relating the heat transfer coefficient to the wall temperature. The heat transfer coefficients in the table were calculated from the average value obtained from the Nusselt theory [6]. Despite being only an approximate model, this showed, Figure 4, improved steadiness in the injection flow and could provide a possible resolution to the condensation problem if implemented in the code;
- a more detailed study of the conditions around the time of emptying of a cell revealed that the code was calculating the vapour to become superheated. This is not physically realistic and is the result of a code error in a condensation routine. A corrected version has been supplied by the code developer.

The implication remained that, apart from the wall condensation modelling issue, the modelling in RELAPS was broadly adequate for this experiment as well.

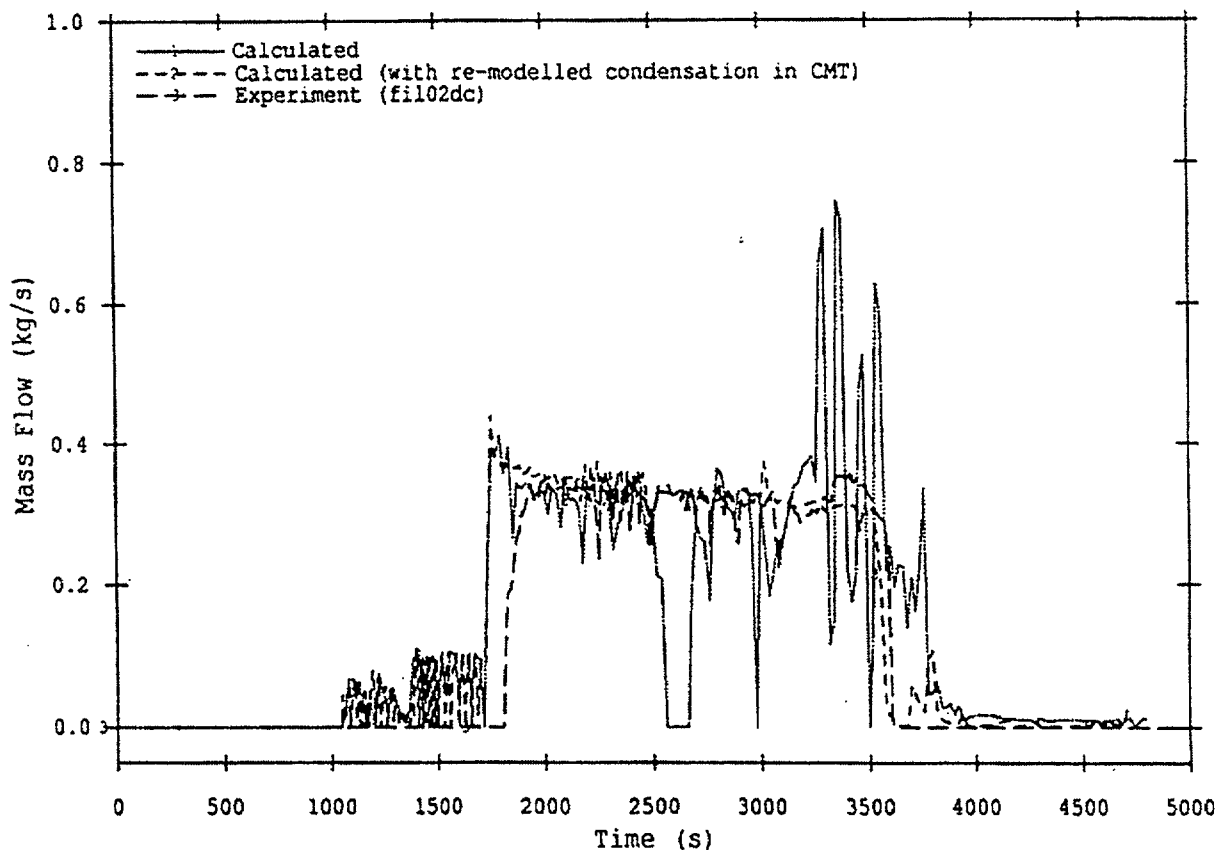


FIG. 4: CMT Injection Line Flows.

7. CODE COMPARISONS WITH THE GDE-43 EXIPEMMMENTS

The test conditions for this experiment were a very small break (0.13 %), the PSIS geometry was as for GDE-34. The steam generator tubes were kept covered. The objective of this test was to focus on a long natural re-circulation phase when the driving force for the flow slowly disappears.

As previously, a reference calculation and a number of sensitivity calculations were carried out.

These included a number of single parameter changes. Calculations investigating the effects of the thermal stratification model in the CMT, the number of nodes in pressuriser, the pressuriser heaters modelled individually, and with adjustment of the heat losses from pressuriser.

The conclusions from the analysis of this experiment were:

- RELAPS/MOD3.2.1.2 predicted the CMT flow behaviour with good accuracy.
- the injection flow rate was well predicted using the results of pressure loss tests in the CMT lines. A period when the recirculation ceased was also predicted, but only, within the timescale of the calculation, when the thermal stratification model was employed in the CMT and associated pipework, see Figure 5;

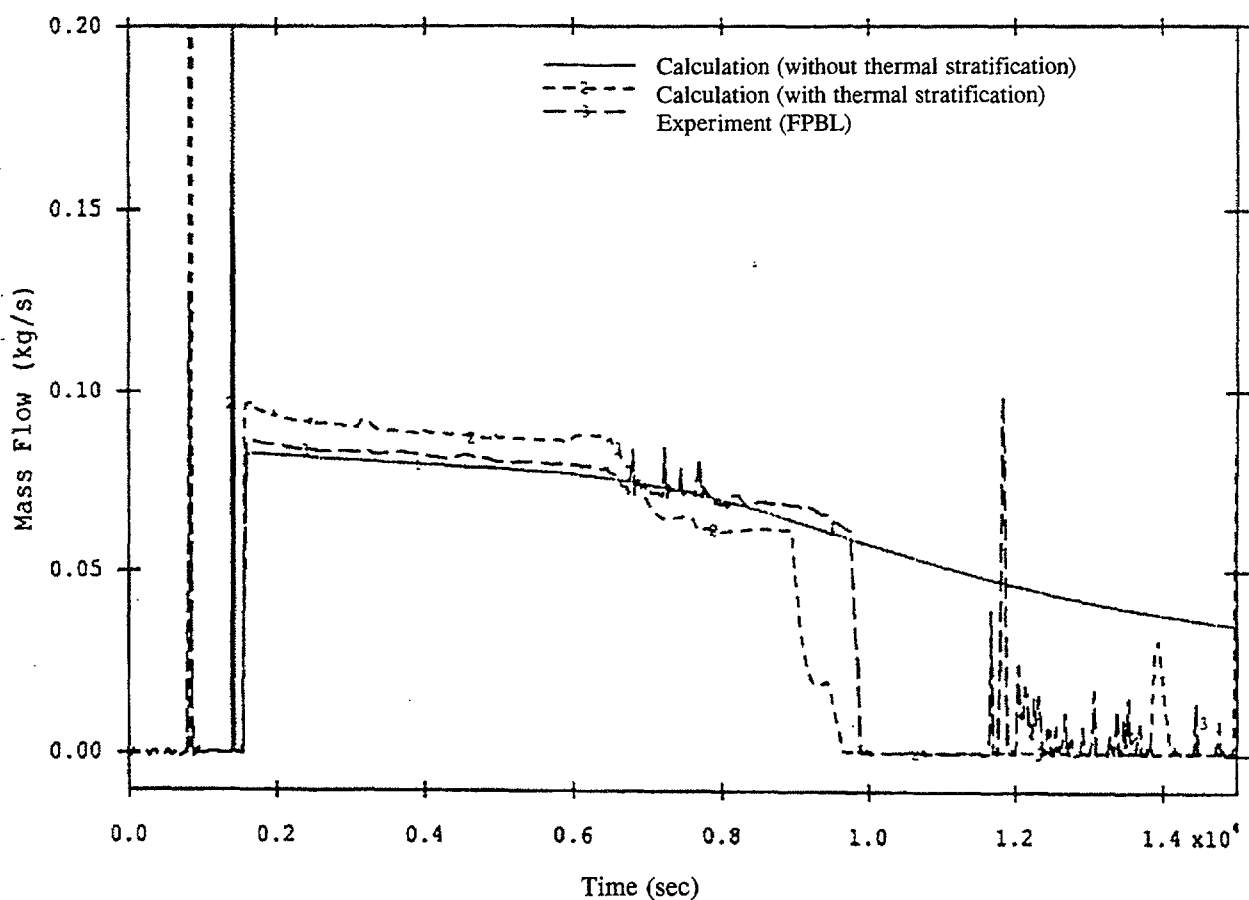


FIG. 5. CMT Pressure Balance Line Flow.

- the overall course if the transient was followed by the calculation. The behaviour of the pressuriser was particularly sensitive to the imposed heat losses;
- the CMT flow and its cessation were observed to be insensitive to the wide variations which occurred in different calculations.

8. CONCLUSIONS

The code was successful in calculating all three tests chosen for analysis. No code failures were encountered. All mass errors were small.

From the analysis of tests GDE-24 and GDE-34 it is clear that the modelling of wall condensation in the RELAPS code requires improvement for this application

The principal deficiency was shown to lie in the unrealistic modelling of the thickness of the condensate film on the wall.

Some benefits could be obtained from reducing mesh sizes but, within practical limitations, it was not possible to achieve a complete resolution this way.

An alternative model, not included in the code but applied as a revised boundary condition, successfully demonstrated a possible approach to overcoming the problem for this specific application.

A further observation of this work was some unphysical superheating of vapour in a cell just becoming empty. Modified coding to resolve this problem was received from the USNRC code development contractors.

The analysis of test GDE-43 successfully reproduced the following CMT parameters:

- (a) the single phase recirculation flow rate,
- (b) the cessation of this flow when the circuit was full of hot water during the recirculation phase of the experiment.

The agreement of these features with the experiment was good provided the thermal stratification model was invoked in the code.

All overall course of the transient was generally well reproduced but a particular sensitivity to heat losses in the pressuriser was observed.

Overall it is concluded that, subject to the particular issue of the condensation modelling noted above, the RELAP5 code is broadly suitable for the analysis of Passive Injection Systems of the type investigated here.

REFERENCES

- [1] TUUNANEN, J.; MUNTHER, R.; VIHAVAINEN, J.; "PACTEL Experiments for Investigation of Passive Safety Injection Systems for Advanced Light Water Reactors"; The 4th International Conference on Nuclear Engineering (ICONE-4). New Orleans, USA, March 10- 14, 1996.
- [2] KIMBER, G.R.; "PACTEL Passive Safety Injection System Test Analysis"; GNSR(DTI) P(96)265, March 1996.
- [3] KIMBER, G.R.; "Further Analysis of PACTEL Test GDE-24 with RELAP5/MOD3.2.1.2"; AEA Technology Report, January 1997.
- [4] KIMBER, G.R.; "Further Analysis of PACTEL Test GDE-34 with RELAP5/MOD3.2.1.2"; AEA Technology Report AEAT-2692, January 1997.
- [5] KIMBER, G.R.; "Further Analysis of PACTEL Test GDE-43 with RELAP5/MOD3.2.1.2"; AEA Technology Report, January 1997
- [6] ROGERS, G.F.C.; MAYHEW, Y.R.; "Engineering Thermodynamics, Work, and Heat Transfer"; Longmans Scientific and Technical Publications 4th Edition 1992.

NEXT PAGE(S)
left BLANK

A. BERGERON, D. CARUGE, E. ROYER
Commissariat à l'énergie atomique,
DRN/DMT/SERMA/LETR,
CE-Saclay, Gif-Sur-Yvette, France



XA0055028

Abstract

This paper presents the FLICA-IV three dimensional two-phase flow code devoted to steady state and transient thermal-hydraulic analysis of nuclear reactor cores. The first part deals with the main features of the code. Then the flow modeling is exposed. Follows a discussion relative to the closure models selection procedure. The advantages of the advanced numerical method based on an extension of Roe's approximate Riemann solver initially developed for Euler equations with ideal gases are shown. An overview of the program validation set-up for PWR core design is given. Finally some actual 3D applications to PWR and BWR flow rate oscillations are presented.

1. INTRODUCTION

This paper is devoted to the presentation of the FLICA-IV three dimensional thermal-hydraulic code dedicated to two-phase calculations required for the design and the safety analysis of nuclear reactor cores.

FLICA-IV has been developed to cover up some major deficiencies of the previous generation of thermal-hydraulic nuclear core codes based on subchannels analysis assumptions [1]. In those codes, any lateral flow is directed by the rod-to-rod gap through which it flows and loses it sense of direction far away from the gap region. This assumption leads to simplifications in the transverse momentum balance so situations in which axial flows are not preponderant over transverse flows cannot be well represented. Such examples of situations are reverse flow and recirculating loop occurring under natural circulation or downstream of an axial flow blockage. Moreover, FLICA-IV integrates new efficient numerical methods which leads to a good spatial and temporal accuracy of the solution and allows computation of reverse flow.

The code has been designed to suit to various reactors such as PWR, BWR, VVER, RBMK, and experimental reactors. Moreover the meshing capabilities of the code allow computations in the upper and lower plenum of the cores.

FLICA-IV is integrated to the Reactor Physics Analysis computer code system (SAPHYR). The code is now coupled via the ISAS software with CRONOS2, a neutronic diffusion code and with the CATHARE code(system transient analysis) to perform a best estimate analysis of 3D reactivity accidents [2].

The thermal-hydraulic model and the closure relationships are first presented. Then the validation program set up for PWR calculations is presented. The last part deals with some code advanced applications and capabilities for PWR and BWR reactors.

2. THERMAL-HYDRAULIC MODEL

2.1. The constitutive equations

FLICA-IV is a four equation code. The equations are space-time-averaged phase of the fundamental fluid dynamic equations over control volume. These are mixture mass balance, phasic mass balance, mixture momentum balance and mixture energy balance. A Drift-flux model is used to take into account the slip between the vapor and the liquid phase. The fluid is compressible and the two-phases are assumed to be at the same pressure. One of the phases is assumed to be saturated. The phasic mass balance aims to calculate thermal disequilibrium and subcooled boiling flows. The equations are written in a conservative form below :

$$\begin{aligned}
 \frac{\partial}{\partial t} \sum_k \alpha_k \rho_k + \nabla \sum_k (\alpha_k \rho_k \mathbf{u}_k) &= 0 \\
 \frac{\partial}{\partial t} \alpha_k \rho_k + \nabla (\alpha_k \rho_k \mathbf{u}_k + \alpha_k \mathbf{M}_k) &= \Gamma_{k'k} + \Gamma_{wk} \\
 \frac{\partial}{\partial t} \sum_k \alpha_k \rho_k \mathbf{u}_k + \nabla \sum_k (\alpha_k \rho_k \mathbf{u}_k \otimes \mathbf{u}_k + \alpha_k \Pi_k) &= \sum_k \alpha_k \rho_k \mathbf{g} - \tau \\
 \frac{\partial}{\partial t} \sum_k \alpha_k \rho_k E_k + \nabla \sum_k (\alpha_k \rho_k \mathbf{u}_k H_k + \alpha_k \mathbf{Q}_k) &= \sum_k \alpha_k \rho_k \mathbf{g} \mathbf{u}_k + q
 \end{aligned} \tag{1}$$

In above equations, the subscript k refers to the vapor phase (k=v) or the liquid phase (k=l). the nomenclature is given as follows : α is the void fraction ($\alpha_l + \alpha_v = 1$), ρ_k is the phasic density, \mathbf{u}_k is the phasic velocity, E_k is the phasic energy and H_k is the phasic enthalpy. \mathbf{M}_k is a phase mass diffusion term due to two-phase flow turbulence, Π_k contains the viscous stress tensor and turbulence effects modeling. \mathbf{Q}_k contains fluid heat conduction and energy turbulence diffusion terms. The $\Gamma_{k'k}$ term represents the interphase mass exchange and the Γ_{wk} term represents the vapor production at the heating surfaces. τ is the wall drag force, q is the volumic power density and \mathbf{g} is the gravity. Moreover in this drift flux model, the relative velocity between liquid and vapor phases ($\mathbf{u}_r = \mathbf{u}_v - \mathbf{u}_l$) is taken into account by a kinetic constitutive equation. The system of equations is completed by the closure models and the boundary conditions.

FLICA-IV may also compute the temperature field in nuclear fuel (rods and flat plates) for transient and steady state analysis. An additional equation relative to solute transport is also available in FLICA-IV to simulate for example boron transport in PWR cores during transient accidents.

2.2. Closure models

The closure models are relative to fluid data tables, axial and transverse frictional pressure losses, singular pressure losses (for example due to spacer and mixing grids), heat exchange between fluid and rods, subcooled boiling, turbulent mixing and slip ratio.

The singular pressure losses are treated using the following 3D tensor:

$$\begin{aligned}
 \tau_{\text{sing}} &= -\frac{1}{2} |\mathbf{U}| \bar{\Lambda} \begin{pmatrix} \rho \cdot \mathbf{u} \\ \rho \cdot \mathbf{v} \\ \rho \cdot \mathbf{w} \end{pmatrix} \text{ with } \bar{\Lambda} = \begin{pmatrix} k_z & k_{xz} & k_{yz} \\ -k_{xz} & k_x & -k_{xy} \\ -k_{yz} & k_{xy} & k_y \end{pmatrix} \text{ and } \rho = \alpha_l \cdot \rho_l + \alpha_v \cdot \rho_v \\
 u &= \frac{\alpha_l \cdot \rho_l \cdot u_l + \alpha_v \cdot \rho_v \cdot u_v}{\rho} \quad v = \frac{\alpha_l \cdot \rho_l \cdot v_l + \alpha_v \cdot \rho_v \cdot v_v}{\rho} \quad w = \frac{\alpha_l \cdot \rho_l \cdot w_l + \alpha_v \cdot \rho_v \cdot w_v}{\rho} \\
 |\mathbf{U}| &= \sqrt{u^2 + v^2 + w^2} \quad u, v, w \text{ refer respectively to the } z, x, y \text{ axes.}
 \end{aligned}$$

The diagonal coefficients represents the axial and the two radial pressure loss coefficients. The others are rotary coefficients which transfer momentum from one direction to an other one. They may be used for mixing vanes modeling.

The turbulent viscosity involved in the phasic mass balance, the energy balance and the momentum balance may either be computed as function of the local Reynolds number for the three directions or be transported by a turbulent viscosity equation derived from the k-ε model. This last code capacity is still under development.

The FLICA-IIIM models were first implemented in the code. FLICA-IIIM is a previous version of FLICA based on subchannel analysis and validated for PWR safety analysis [3]. This original set of models is currently being extended to take into account increasing accurate models and to adapt FLICA-IV to a wide range of nuclear cores.

2.3. Boundary conditions

The boundary conditions are relative to inlet repartition of mass velocities and temperatures, outlet repartition of pressures and heat flux distributions. Inlet transverse mass velocities are also available.

2.4. Numerical procedure

The numerical method is based on a finite volume discretization. The system of the 6 conservative variables $U = \left(\sum_k \alpha_k \rho_k, \alpha_v \rho_v, \rho \cdot u, \rho \cdot v, \rho \cdot w, \sum_k \alpha_k \rho_k E_k \right)$ are assumed to be constant over each control volume.

The system (1) is rewritten as below:

$$\frac{\partial U}{\partial t} + \nabla \cdot (F(U) + G(U, \nabla U)) = S(U)$$

where $S(U)$ is the source term, $F(U)$ is the inviscid flux vector and $G(U, \nabla U)$ is the viscous flux that is also dependant on ∇U . The following integral formulation is used for any volume Ω_i contained in the computation domain Ω .

$$\frac{\partial}{\partial t} \int_{\Omega_i} U d\Omega + \oint_{\partial\Omega_i} (F + G) \cdot n d\Gamma = \int_{\Omega_i} S(U) d\Omega$$

As the conservative variables are assumed to be constant over the volume, the resulting discretization leads to the following system of balance equations:

$$U_i' - U_i'^{-1} + \Delta t \sum_j (\Phi_i(U_i', U_j') + \Phi_v(U_i', U_j')) = S(U_i')$$

The numbers i and j are relative to adjacent hydraulic coupled volumes, $\Phi_i(U_i', U_j')$ and $\Phi_v(U_i', U_j')$ are respectively the inviscid and viscous contributions to the flux on the cell Ω_i in direction of the neighbor cell Ω_j .

The numerical fluxes at cell interfaces are calculated using an approximate Riemann solver. The method used is an extension of Roe's original scheme for Euler equations with ideal gases [4] to two-phase flow [5].

The method is fully implicit. The steady state is reached by a relaxed pseudo transient calculation, keeping constant the boundary conditions. More details concerning the numerical method may be found in reference [6].

The advantages of such a scheme consist in non-staggered grid and low numerical viscosity. The Figure 1 is relative to the comparison of FLICA-IV method against classical staggered grids and donor cell methods for the two-phase flow blow down problem proposed by Ransom and Hicks [7]. The calculations were made for a pipe 3m long, discretized with 50 cells and initially pressurized to 0.3 MPa. Boundary conditions were zero velocity at the closed end and constant ambient pressure at the open end. The Figure 1 shows the pressure versus time at the closed end of the pipe. It is clear that Riemann solver approach is superior.

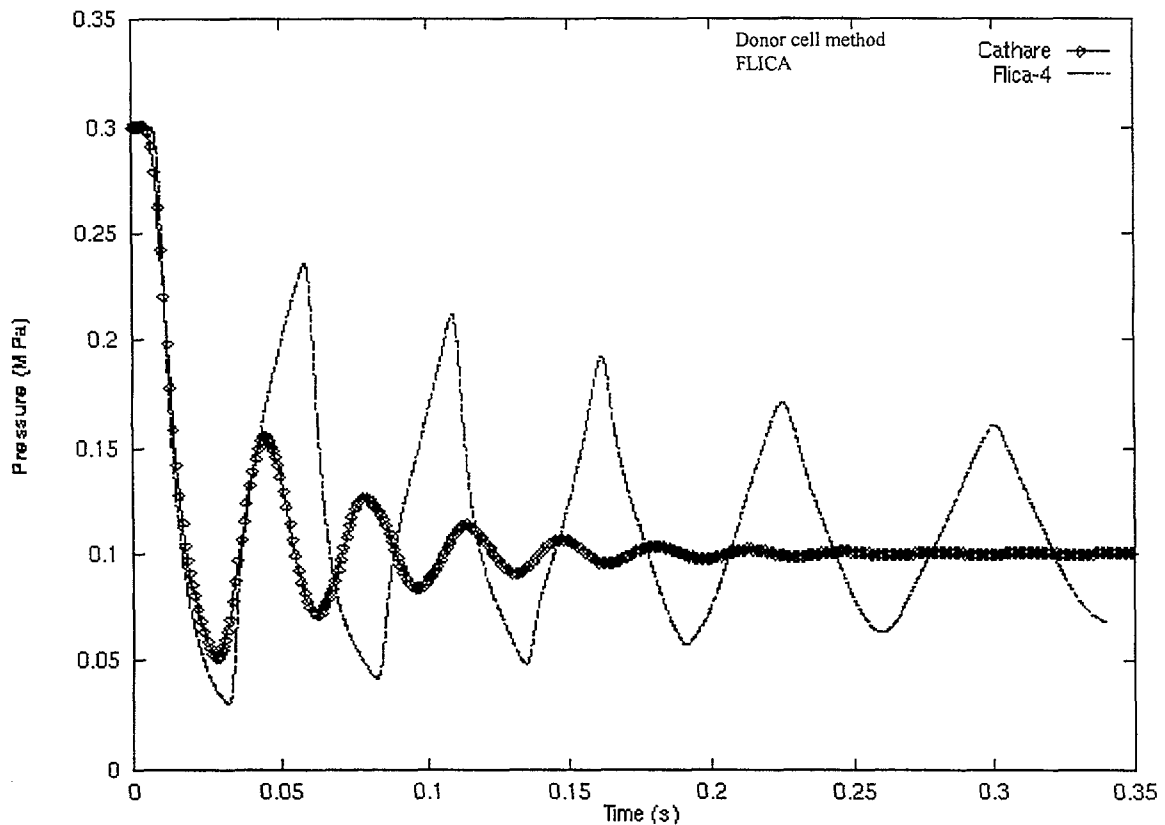


FIG. 1. Pressure at the closed end of the pipe.

2.5. Spatial description capabilities

The computation domain is divided into charged or free fluid volumes according to the core direction. An axial mesh is defined along the main direction and the radial description remains the same from the inlet to the core outlet. At the time being, the radial mesh must be conform.

The code allows different levels of refinement as shown on Figure 2.

At the time, as the radial mesh has to be conform, several computations increasing at each step the refinement level are successively performed for hot channel critical heat flux studies.

3. VALIDATION PROGRAM

3.1. Objectives

The code validation is needed to ensure that the thermal-hydraulic model and the closure models simulate well the experimentally observed trends.

The validation program, only relative to PWR reactors, deals with the improvement of closure models and with the experimental program set-up for performing the comparisons between calculations and experimental data.

3.2. Improving the closure models

For each model, systematic bibliographic studies have to be conducted. However the model found in the literature are most often 1D model and not always well adapted to thermal-hydraulic core computation. For example the transverse friction factor models in rod bundles usually do not take into account the coupled effects of axial and transverse flow.

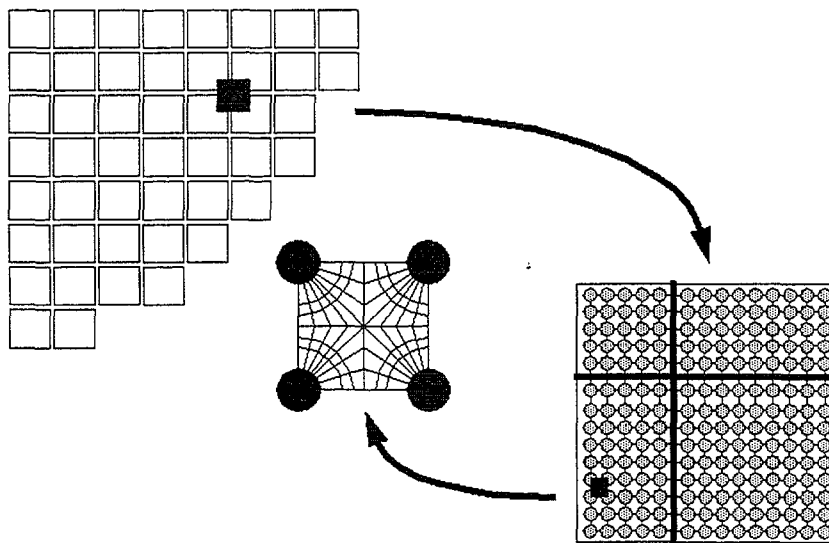


FIG. 2. Refinement level.

So when it is possible, the bibliographic studies should be completed either by analytical experiments or by simulations of analytical experiments by fine hydraulic computation in order to construct models available for FLICA-IV coarse meshing from the detail knowledge of the flow field between the rods within a wide range of thermal-hydraulic conditions.

The well developed fine hydraulic codes may be used to construct coarse models for the single phase axial and transverse pressure drop coefficients, the mixing vanes model (rotary coefficients) and the single phase flow turbulent mixing.

For two-phase flow, at the moment only bibliographic studies and specific experiments are foreseen.

3.3. Experimental program

3.3.1. Objectives

The objectives of the experimental program is to demonstrate that FLICA-IV suits well to calculate the fluid flow and the energy distribution in rod bundles for a wide type of thermal-hydraulical and geometric conditions.

For each experiment, the validation consists of optimizing the accordance between computed and experimental values following the procedure described below:

1. For each calculation, the spatial convergence is checked out by progressively decreasing axial and radial mesh sizes.
2. When spatial convergence is reached, studies involving for each closure laws several models is undertaken. Moreover some studies relative to the geometric description may also be performed. (For example to close or not the transverse surfaces at the grid levels)

These two steps are important to verify that the thermal-hydraulic model is able to compute accurately the experiment and for the positive cases allow the determination of the best accuracy FLICA-IV may reach. The cases in which great differences between computed data and experimental data are still observed, whatever the model used, are useful to determine FLICA-IV limitations.

However, it may occur that the refinement of the spatial description needed to ensure convergence leads to a prohibitive number of mesh for industrial applications. So it is the goal of the validation program to determine from sensitivities studies the sizes of axial and radial mesh needed to calculate the solution for a given accuracy.

3.3.2. Experimental facilities

FLICA-IV is a two-phase flow code which is mainly used to determine the flow redistribution in rod bundle induced by the differential pressure loss coefficients of the channels. The differences are both due to single phase and two-phase flow effects. Before introducing two-phase flow effects, it is important to verify that the redistribution computed for single phase flow without heat agrees with experiments. So, the experimental program has been divided into single phase flow and two-phase flow validation.

3.3.2.1. Single phase flow validation

The validation aims to assess the axial and transverse friction factor models, the singular pressure drop model, turbulent mixing between channels and to fit the right rotary coefficients.

The CEA's facilities AGATE(CE-Grenoble) and HERMES (CE-Cadarache) simulating full-scale vertical rod bundles(square lattice) are employed. The velocities are accurately measured between the rods by laser velocimetry techniques. Average area integration processes are applied to the measured velocities to compute the average axial and transverse velocities in channels and at the gaps between the channels, for direct comparisons with FLICA-IV results.

The AGATE mock-up is 1.5 meter high and simulates a 5X5 rod bundle. The experiments realized are relative to staggered spacer grids, axial flow blockage, transverse velocities induced by spacer grids and by grids supplied with mixing vanes.

The HERMES mock-up integrates two-full scale assemblies. Here, the experiments are relative to staggered spacer grids, hydraulic compatibility of assemblies supplied with different inlet nozzles, flow redistribution at the entrance of assemblies for non uniform inlet mass velocity.

3.3.2.2. Two-phase flow validation

For the moment, only two types of experiments are foreseen for the two-phase flow validation. The first one aims to measure the mass velocities and the enthalpies at the outlet of each channels of a 5X5 rod bundle by isokinetic sampling [8] for a wide range of thermal-hydraulical conditions and different types of grids. The facility may be used to assess the two-phase flow models relative to two-phase pressure drop, slip ratio and turbulent mixing. It is also a good tool to test the mixing vanes modeling for two-phase flow configurations.

The second type of experiment deals with subcooled boiling in a 3X3 rod bundle. Fast photographic techniques allow the visualization of the bubbles departure at the rod surfaces in order to validate subcooled boiling models.

3.3.3. First results

The experimental program has just begun, but some results are already available. Comparisons between computed and experimental values for staggered grids experiments in AGATE lead to very good agreements [9]. These experiments aim to simulate the mixed core configurations in which assemblies supplied with three supplementary mixing grids and assemblies without added grids are positioned side by side.

As shown on Figure 3, the axial velocities are carried out at 33 locations in all the inner subchannels. The transverse velocities are carried out at 3 locations for each gap between two rods.

The axial and radial map of the mock-up are represented respectively on Figure 4 and on Figure 5. The distance between the two spacer grids is 28 cm.

The different radial mesh sizes employed are given on Figure 5. Comparisons between computed and experimental values are performed for the transverses velocities at the gap pointed out on Figure 5. It can be seen on Figure 6 the very good agreement between the two plots.

The occurrence of reverse flow just downstream of an axial flow blockage in the AGATE facility has also be successfully simulated [9]. A small plate is inserted between four rods at 1 m from the rod bundle entrance. The computation is performed for radial mesh

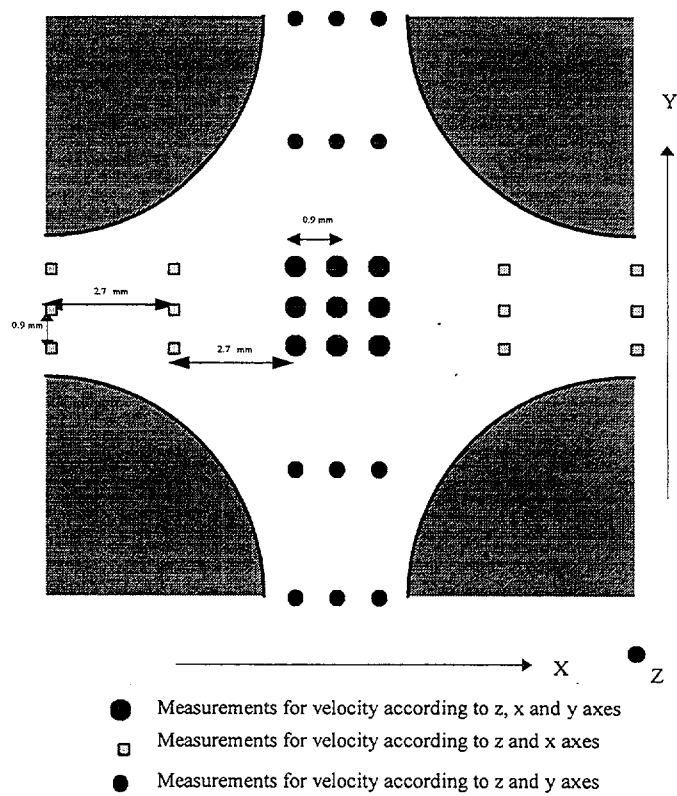


FIG. 3. Locations of velocities measurements.

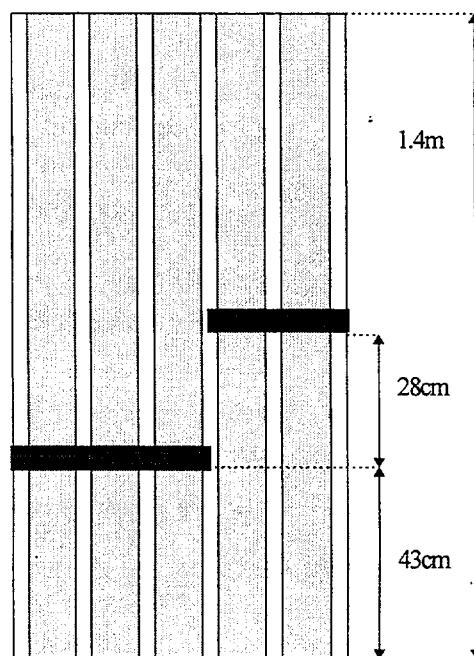
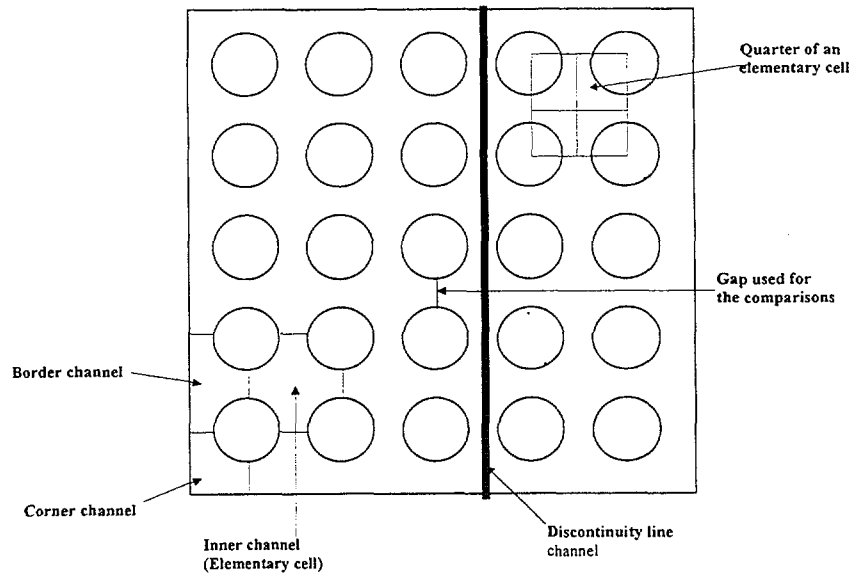


FIG. 4. Axial map of the mock-up.



N4

FIG. 5. Radial map of the mock-up

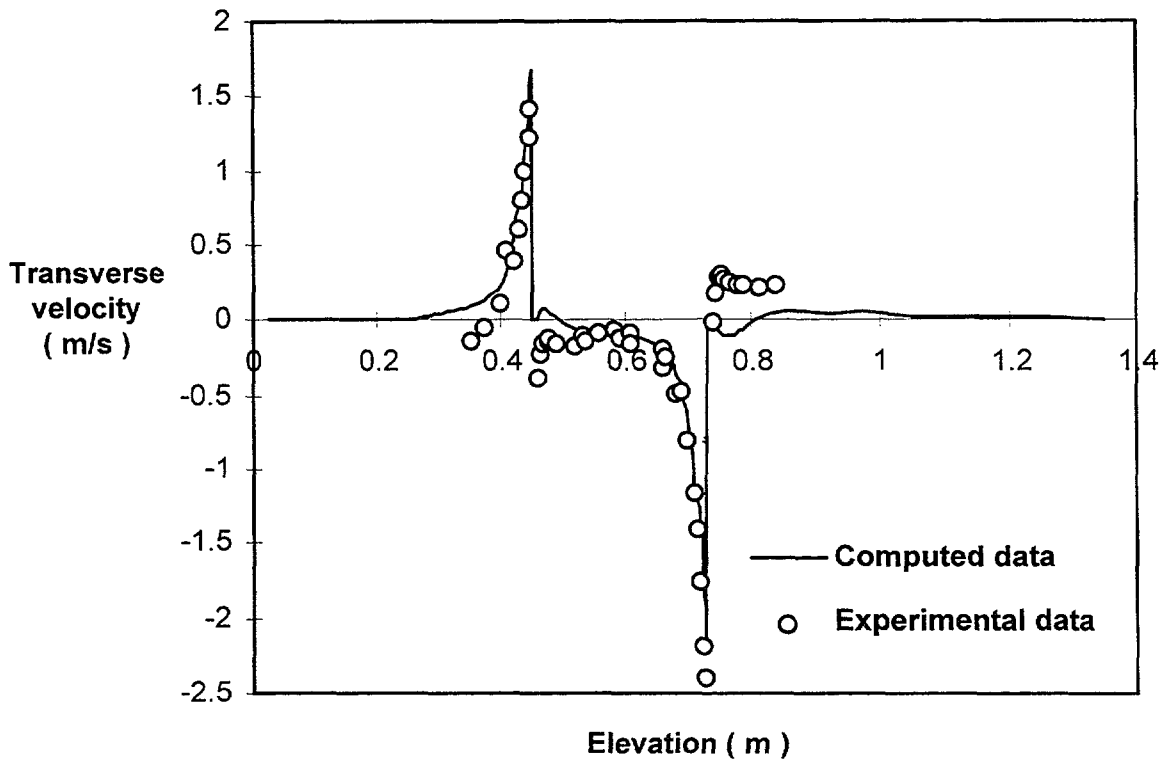


FIG. 6. Comparison between computed and experimental transverse velocities.

representing either an elementary cell (hydraulic space between four rods) or a quarter of an elementary cell (Figure 5). Turbulent mixing is not considered in the calculation. The Figure 7 shows the comparison on axial velocity between experiments and computed values for the two mesh. It turns out that the finest mesh is better without any models fitting, even if the predicted reverse flow is much larger than the experimental one. As the turbulent mixing

between the channels is not taken into account, the calculation length for the fluid to come back to its upstream value is too large.

4. APPLICATIONS TO NUCLEAR CORES

4.1. Overview of applications

The coupling between the FLICA-IV and CRONOS-2 codes has been successfully applied to Russian RBMK calculations, BWR flow rate oscillations and to the European Pressurized Reactor(EPR) [6]. Furthermore, applications to the future CEA's experimental reactor RJH in Cadarache is being processed. For PWR and Russian VVER design, a lot of comparisons with the FLICA-IIIM code have been realized to ensure that the two codes still agrees on classical PWR safety analysis. A challenging computation relative to a low flow Steam Line Break Accident in a French

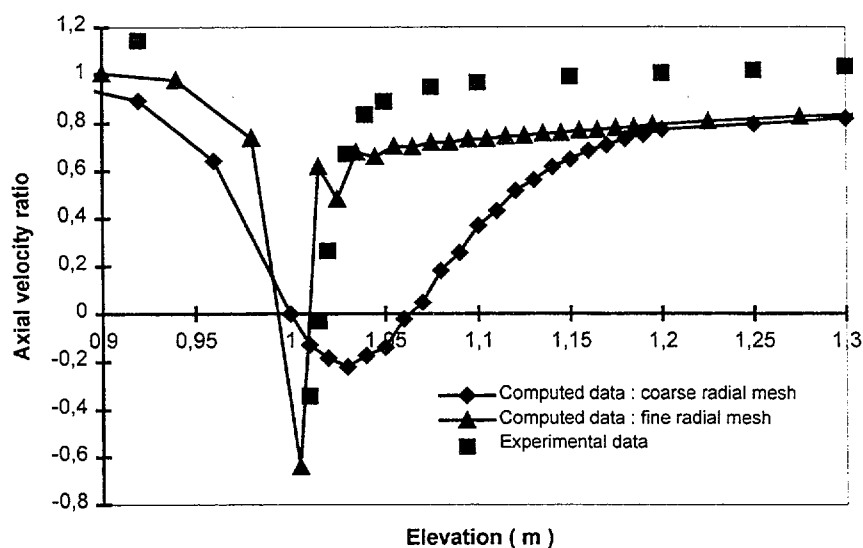


FIG. 7. Comparison between computed and experimental data for axial flow blockage.

reactor has been successfully performed [6]. Computation results concerning this accident are discussed in the next chapter. Chapter 4.3 deals with the first BWR flow rate oscillations calculated with FLICA-IV.

4.2. N4 Reactor Low Flow Steam Line Break Accident

An uncontrolled steam release in a secondary loop leads to core pressure and inlet core temperature drop in the corresponding primary loop. Because of the arrival of cold water, an heterogeneous distribution of power appears in the core which was initially in hot zero power state. In order to penalize the accident, a rod cluster assembly is supposed to remain fully withdrawn in the affected loop region. Furthermore, the primary pumps have been accidentally stopped. The core calculation is performed for an inlet flow rate which is only 3.4 % of nominal conditions.

As it is shown on Figure 8, natural circulation is preponderant and a recirculating flow loop appears in the core. The axial increase of hot assembly flow rate avoids CHF occurrence.

However most of the FLICA-IIIIM closure models employed for the computation are not available within the range of thermal-hydraulic conditions involved.

So the actual 3D capacity of the FLICA-IV numerical methods have been assessed but some more models adapted to low flow conditions have to be implemented in the code. Further, the computed natural circulation phenomena in rod bundles must be validated either on experimental simulations or by direct comparisons with validated hydraulic codes.

4.3. BWR calculations

The FLICA-IV code well suits to Boiling Water Reactor calculations, either by itself for thermal-hydraulics only, or used in conjunction with the CRONOS-2 code [10] for thermal-hydraulics and neutronics coupled applications.

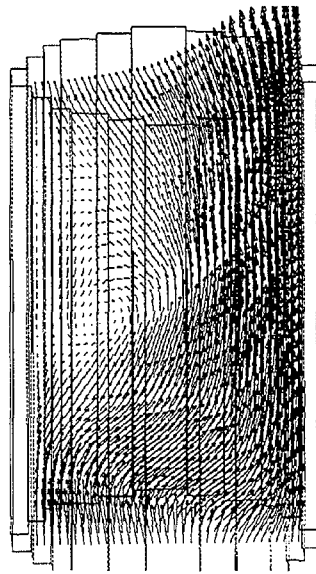


FIG. 8. Velocity field (xOz front cut).

4.3.1. Coupling to neutronics

The coupling between the FLICA-IV and CRONOS-2 codes is fully operable, thanks to the ISAS coupling software [11]. Standard coupling procedures are available for modeling the FLICA-IV thermal-hydraulics feedback on the CRONOS-2 nuclear power. The fuel temperature are computed by FLICA-IV, using its thermal module for solids.

ISAS

ISAS is a software designed to code management and data exchange between codes. It is based upon the PVM protocol, and provides a command language for an easy use. Each coupled code is considered as a slave process, receiving requests (or commands) from the ISAS supervisor, and exchanging data with it (input or output).

Such an external coupling method enables to run each code individually, as if it was run in stand alone, and to distribute the computing power on several machines (usually one per code).

CRONOS-2

CRONOS-2 is a 3D neutronics code developed by CEA/SERMA, and devoted to diffusion, transport, and kinetics. It provides two main numerical methods: the finite difference and the finite elements. CRONOS-2 is a modular code, including a simplified thermal-hydraulics module.

4.3.2. Instability occurrence

Instability occurrence related to thermal-hydraulics and neutronics coupling was studied with the FLICA-IV and CRONOS-2 codes [12]. Theoretical models show there are unstable operating conditions for BWR, due to the coupling between thermal-hydraulics and power (neutronics) [13]. For instance, a reactivity insertion can result in mass flow rate and power oscillations, instead of reaching another stable operating point. The instability threshold strongly depends on the physical models used for thermal-hydraulics, since neutronics is affected by void fraction and fuel temperature. Hence, such an accurate tool as FLICA-IV is of great interest for BWR calculations.

The first type of instability occurrence computed with the coupled FLICA-IV and CRONOS-2 codes is relative to reactivity insertion in a core. FLICA-IV uses a 1D model for the core and the CRONOS-2 point neutronics module is employed. The relative power oscillations obtained are shown on Figure 9.

In a second time, benchmark calculations [14] were performed to assess the FLICA-IV capacity to model 3D flow instabilities. The Figures 10 and 11 show the relative power evolution in center and border core assemblies. The oscillation phase computed depends on the channel position. This phenomena is particular to large cores with various channel types.

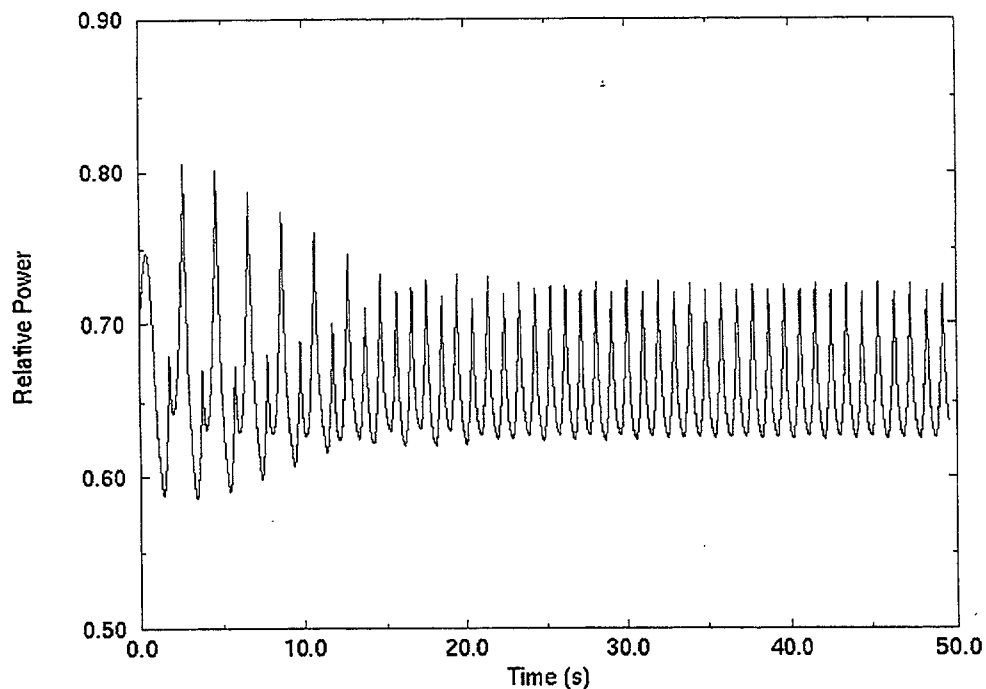


FIG. 9. Power evolution (FLICA-IV coupled with point neutronics module).

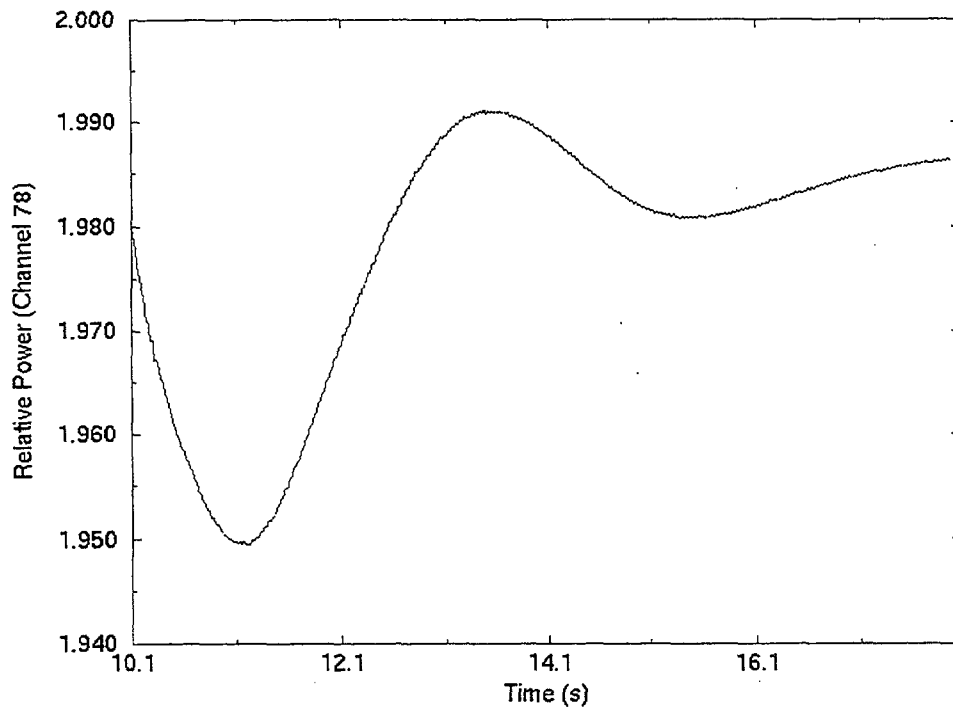


FIG. 10. Power evolution for center core assembly.

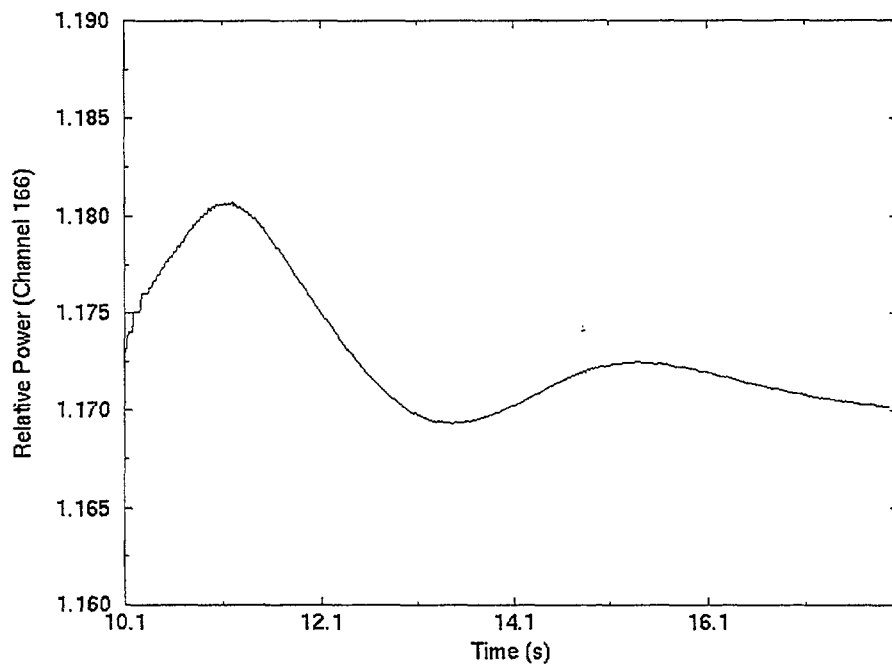


FIG. 11. Power evolution for border core assembly.

4.3.3. Validation effort

Particular care is necessary to validate BWR calculations, since the vapor phase is no more of minor issue like in PWRs. The net vapor generation point for instance largely affects the instability threshold. The drift flux model should also be well validated, since it conditions the void fraction, and then the power distribution.

5. CONCLUSIONS

FLICA-IV is a powerful tool for actual 3D thermal-hydraulic nuclear core computation. The validation program aims to use the most recent measurement techniques and fine hydraulic codes performances to increase the accuracy of industrial applications. The code has proved its capacity for advanced core analysis such as low flow Steam Line Break Accident in PWR and flow rate oscillations in BWR.

ACKNOWLEDGEMENT

The authors are grateful to CEA/SETEX/LTDF in GRENOBLE for permission to publish the experimental data included in this paper.

REFERENCES

- [1] TODREAS, N.E., N.E, KAZIMI, M.S., "Nuclear System II : Elements of Thermal Hydraulic design", HEMISPHERE, New York (1990).
- [2] ROYER, E., TOUMI, I., "CATHARE-CRONOS-FLICA coupling with ISAS : a powerful tool for nuclear studies" , ICONE-6, San Diégo, 10-15 May (1998).
- [3] RAYMOND, P., SPINDLER, B., LENAIN, R., "Pressurized Water Reactor Thermal-Hydraulic Core Analysis with the FLICA Computer Code", Nuclear Engineering and Design, 124, 299, (1990).
- [4] ROE, P.L., "Approximate Riemann Solvers Parameter Vectors and Difference Scheme", Journal of Computational Physics, 43, 357-372 (1981).
- [5] TOUMI, I., "A Weak Formulation of Roe's Approximate Riemann Solver", Journal of Computational Physics, 102, 360-373 (1992).
- [6] TOUMI, I., GALLO, D., ROYER, E., "Advanced Numerical Methods For Three Dimensional Two-Phase Flow Calculations In PWR", NURETH-8, Kyoto, Japan, Sept 30-Oct 4 (1997).
- [7] RANSOM, V.H., HICK, D.L., "Hyperbolic Two-Pressure Models for Two-Phase Flow", Journal of Computational Physics, 53, 14 (1984).
- [8] GARNIER, J., "Isokinetic Sampling of boiling R12 in a Rod Bundle : Methodology and First Results", ISSCA-4, Tokyo, September 25-26 (1997).
- [9] BERGERON, A., TOUMI, I., "Assessment of the FLICA-IV Code on Rod Bundle Experiments", ICONE-6, San Diégo 10-15 May (1998).
- [10] LAUTARD, J.J., LOUBIERE, S., FEDON-MAGNAUD, C., "CRONOS a modular computational system for neutronic core calculations", Specialist Meeting on Advanced Calculations Methods for Power Reactors, Cadarache (France), (1990).
- [11] TOUMI, I., and al., "Specifications of the general software architecture for code integration in ISAS", Euratom Fusion Technology, ITER Task S81TT-01/1, (1995) (also CEA internal report CEA/DMT/95-273).
- [12] CHAABOUNI, K., "Etude des instabilités liées au couplage neutronique thermohydraulique dans les REB", PhD thesis, (1998).
- [13] MARCH-LEUBA, J., CACUCI, D.G., PEREZ, R.B., "Nonlinear dynamics and stability of boiling water reactors - part 2 - quantitative analysis", Nuclear Science and Engineering, vol. 93, (1986).
- [14] FINNEMANN, H., GALATI, A., "NEACRP 3D LWR core transient benchmark - Final specifications", (1992).

PRIMARY COOLANT CIRCUIT COASTDOWN AND THERMOSYPHON MODE UNDER FAILURE OF FORCED CIRCULATION IN INDIAN PHWR

P. PRAMOD, A. DUBEY, H.P. RAMMOHAN, S.S. BAJAJ
Reactor Safety Analysis Group,
Nuclear Power Corporation,
Mumbai, India



XA0055029

Abstract

In Pressurised Heavy Water Reactor, in the absence of forced circulation in the Primary Cooling Circuit, the decay heat is removed by thermosyphoning. Accuracy in the prediction of thermosyphoning flow depends on the pressure drop model at low flow conditions. Behaviour of the plant under such condition is analysed using a transient analysis computer code "ATMIKA.T". Here, the analysis predicts thermosyphoning behaviour and compares with the plant transient data. Effect of different pressure drop models on the core flow is also studied.

1. INTRODUCTION

In concept, the Indian Pressurised Heavy Water Reactor (PHWR) is a pressure tube type reactor using heavy water moderator, heavy water coolant and natural uranium dioxide fuel. The reactor shown in the cut away view in Figure 1 consists primarily of calandria, horizontal cylindrical vessel. It is penetrated by a large number of zircaloy pressure tube (306 for 220 MWe reactor) arranged in square lattice. These pressure tubes also referred to as coolant channels contain the fuel and hot high pressure heavy water coolant. Each pressure tube is isolated from cold heavy water moderator present in calandria by concentric zircaloy calandria tube.

The Primary Heat Transport (PHT) System circulates high pressure coolant through the fuel channels to remove the heat generated in fuel. Major components of this System are the reactor fuel channels, feeders, two reactor inlet headers, two reactor outlet headers, four pumps and interconnecting pipes and valves. The headers, steam generators and pumps are located above the reactor and are arranged in two symmetrical banks at either end of reactor.

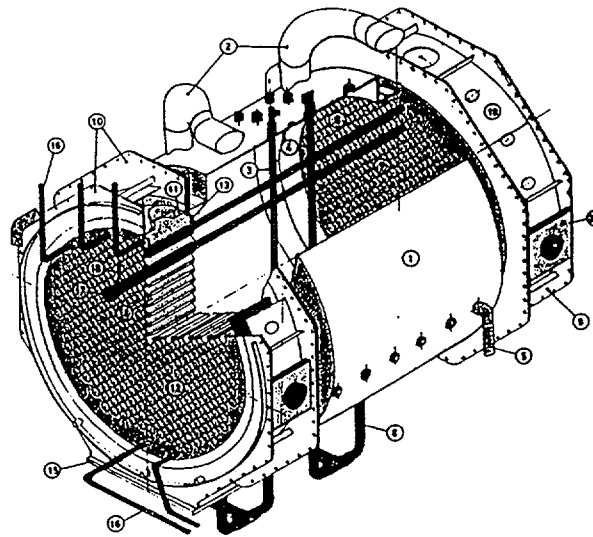
The headers are connected to fuel channels through individual pipes. The coolant flow in neighbouring fuel channel is in opposite directions. This arrangement results in a characteristic figure of 8 circuit layouts where coolant in each circuit makes two passes through the core as shown in Figure 2.

The coolant circulation is maintained during the reactor operation by four PHT Pumps. PHT pumps are provided with the flywheel so that initial heat generation is removed by primary coolant circuit coastdown and subsequent decay heat is removed by thermosyphoning whenever pumps trip. The reactor pressure is maintained by feed and bleed system.

2. PLANT TRANSIENT

To study the coastdown and thermosyphoning effect during a typical plant transient, Class IV power supply failure encountered at Kakrapar Atomic Power Station is selected. In this transient, the PHT Pumps (PCPs) which are on Class IV power supply, trip. This is followed by reactor trip and turbine also trips following reactor trip.

The Primary pressurising pumps which are powered by Class-III electric supplies comes on auto after 40 sec. The auxiliary feed water pump is also on Class III power supply. Initially,



- | | |
|-------------------------------------|------------------------------|
| 1. CALANDRIA SHELL | 11. MAIN SHELL ASSY. |
| 2. OVER PRESSURE RELIEF DEVICE | 12. TUBE SHEET F/M SIDE |
| 3. MECHANICAL SHUT OFF ROD | 13. TUBE SHEET CAL. SIDE |
| 4. LIQUID SHUT OFF SYSTEM | 14. LATTICE TUBE |
| 5. MODERATOR INLET | 15. END SHIELD SUPPORT PLATE |
| 6. MODERATOR OUTLET | 16. END SHIELD COOLANT PIPES |
| 7. CALANDRIA TUBE* | 17. END FITTING ASSY.* |
| 8. COOLANT TUBE* | 18. FEEDER PIPES* |
| 9. END SHIELD | 19. OUTER SHELL |
| 10. C.S. OCTAGONAL STRUCTURED ASSY. | 20. SUPPORT LUG |
- * ONLY ONE TYPICAL ASSY. SHOWN FOR CLARITY

FIG. 1. Cut-away view of reactor (Integral assay of Calandria and end shields).

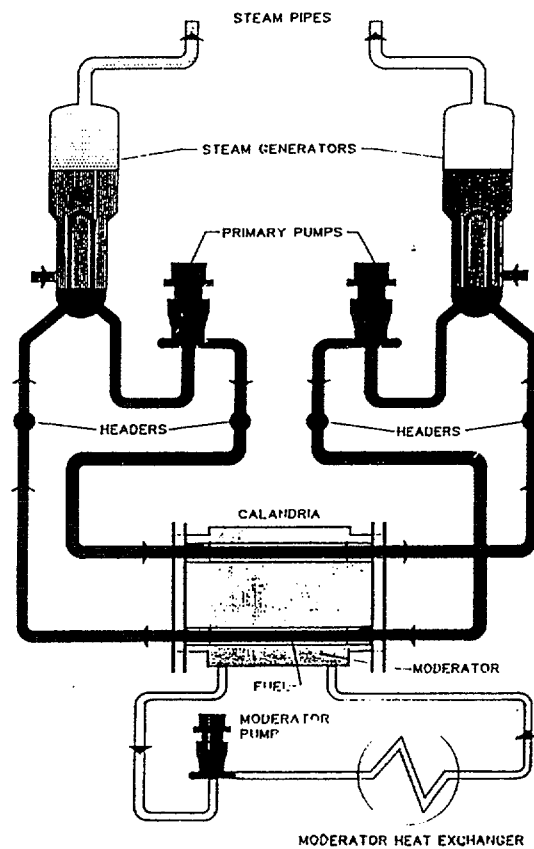


FIG. 2. PHWR simplified flow diagram.

coastdown of the main circulating pumps of PHT System (which are provided with flywheels) provides the flow and subsequently, thermosyphoning predominates.

3. ANALYTICAL TOOL

The above scenario of Class IV power supply failure is analysed with a transient code "ATMIKA.T". ATMIKA.T [1] is a general purpose thermal-hydraulics, neutronic computer code used for simulation of transients in PHWRs. Thermalhydraulic part of the code is based on Unequal Velocity Equal Temperature (UVET) model. The code uses 3 conservation equations alongwith Drift Flux Correlation. Neutro kinetic calculation is done using point kinetic model. The code has all the control system models. Important controls simulated are Boiler Pressure Control, Turbine Speed Control, Steam Generator Control, Boiler Level Control, Reactivity Control and PHT Pressure Control. Both primary heat transport system and secondary loop including turbine are simulated in the code.

4. ANALYSIS

Nodalization diagram used in simulation of above transient is shown in Figure 3. As pressure drop model plays a predominant role in thermosyphoning, the analysis is carried out

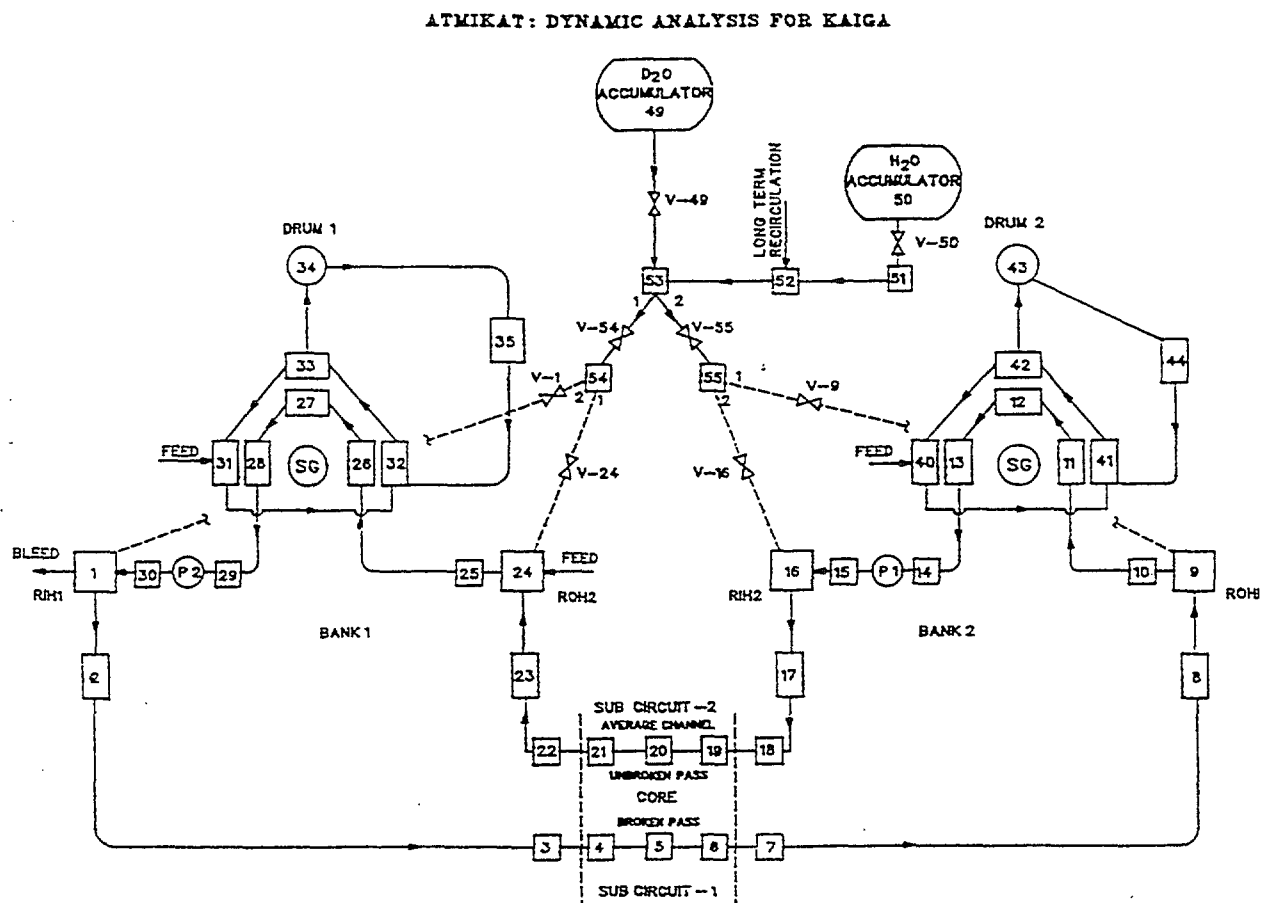


FIG. 3a. Nodalization scheme (PHT & ECC).

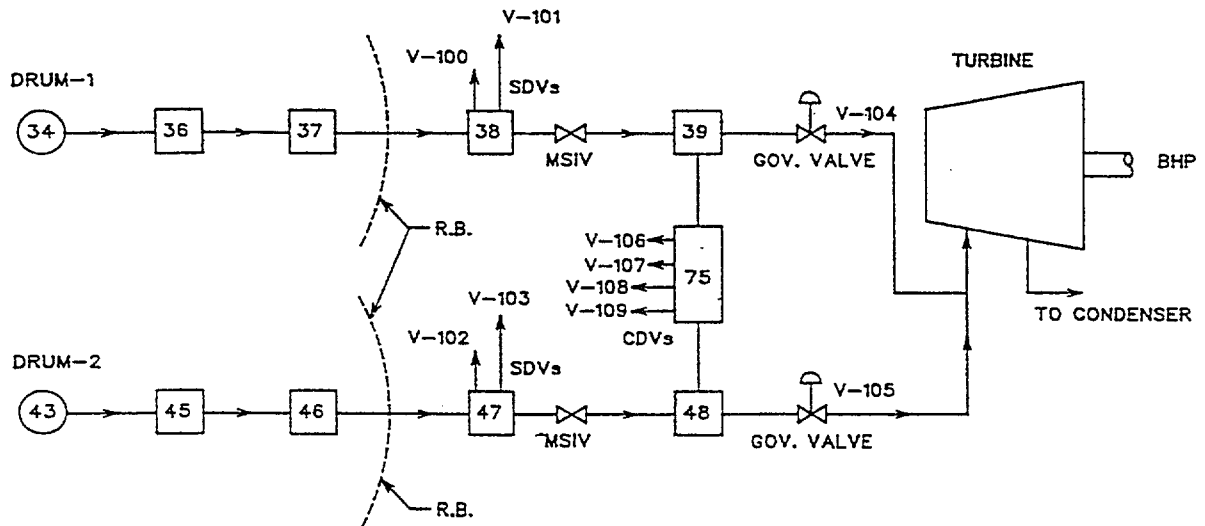


FIG. 3b. Nodalization scheme (SG drum to turbine).

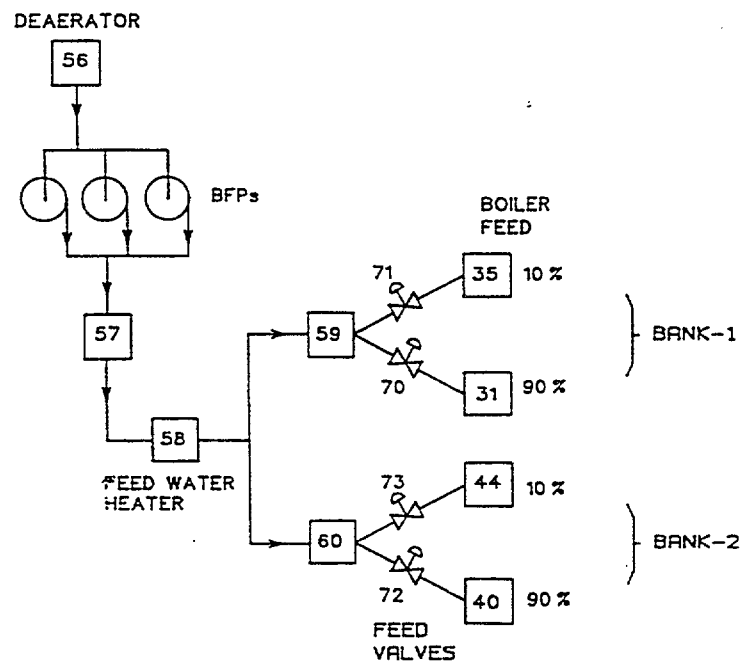


FIG. 3c. Nodalization scheme (deaerator to SG).

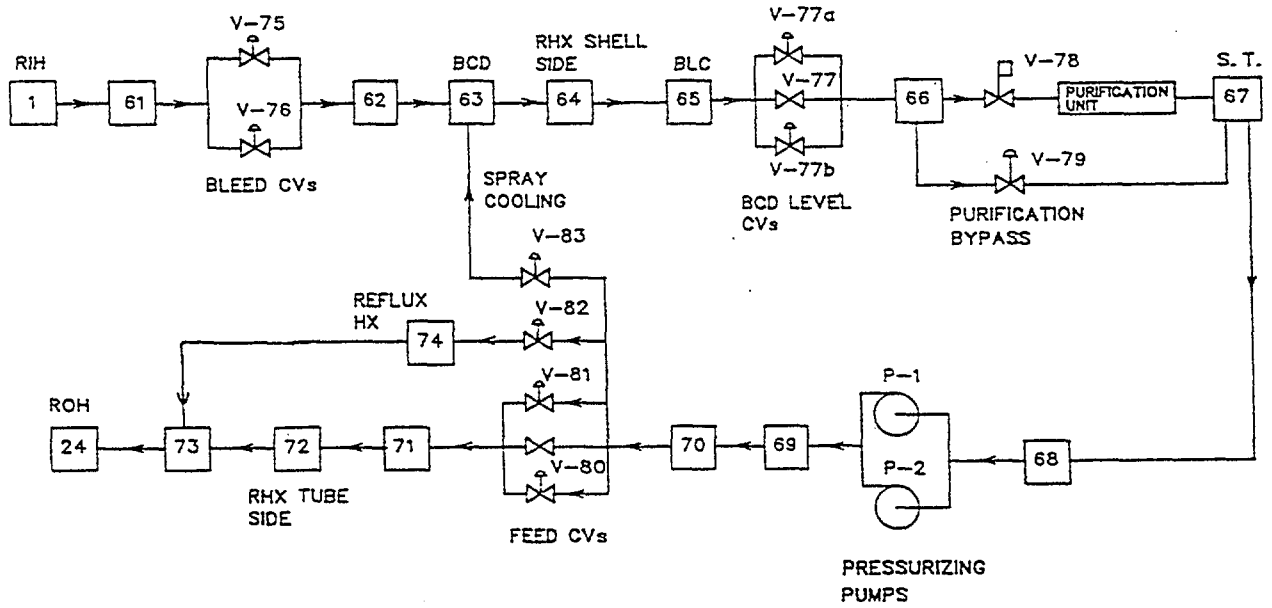


FIG. 3d. Nodalization scheme (Feed and bleed).

using various friction coefficient models. The models chosen are those which are applicable over a wide range of flow especially in a low flow regime. Following frictional coefficient models are selected for study.

CASE - I [2]

$$F = \left[\left(\frac{8}{\text{Re}} \right)^{12} + \frac{1}{(A+B)^{\frac{3}{2}}} \right]^{1/12}$$

$$A = \left\{ 2,457 \cdot \ln \left[\frac{1}{\left(\frac{7}{\text{Re}} \right)^{0.9} + 0.27 \left(\frac{\varepsilon}{D} \right)} \right] \right\}^{16}$$

and

$$B = \left(\frac{37530}{\text{Re}} \right)^{16}$$

Valid over complete range of Re.

CASE - II [3]

$$\frac{1}{\sqrt{f}} + 0.86 \cdot \ln(\text{Re} \sqrt{f}) - 0.8$$

$$f = \frac{64}{Re} \quad \text{for} \quad Re < 2000$$

$$f = 0.00056 + 0.5 \cdot Re^{-0.32} \quad \text{for} \quad 3000 < Re < 3 \times 10^6$$

Linear Interpolation for $2000 < Re < 3000$

where,

f = friction factor

Re = Reynold number

Both primary and secondary loops are modelled. The core of 306 channels is divided into two core passes of 153 channels each. The two pumps and steam generators in each bank are clubbed into thermal hydraulically equivalent ones. Feed and Bleed System is also modelled to simulate the PHT pressure control.

5. RESULTS

Following failure of Class IV power supply, Primary Circulating Pumps (PCPs) trip and reactor will trip (on signal of no PCP operating). Turbine trips following reactor trip after 500 msec, resulting in rise in boiler pressure. Sudden decrease in coolant flow and rise in boiler pressure causes PHT pressure to shoot up. Opening of Atmospheric Discharge Valves in response to boiler pressure controller (BPC) signal causes sudden dip in boiler pressure; hence, PHT pressure fails quickly. As the reactor power is reducing, the pressure fails further. As per BPC Scheme, with decrease in Boiler ΔT , the boiler pressure starts increasing, causing the PHT mean temperature to increase. Alongwith this pressurizing pump coming on Class-III electrical supply after 40 sec., the PHT pressure recovers and stabilizes.

Following turbine trip, boiler pressure rises immediately and dips quickly as ASDVs are opened (on BPC signal). As Boiler ΔT starts decreasing, the boiler pressure increases. At around 90 sec., due to reactor trip and PCP trip, enough heat is not available; hence, the boiler pressure starts failing.

As the rate of decrease in core flow due to coastdown is less than that of power, the boiler ΔT starts decreasing. As coastdown effect becomes less significant, at around 110 sec, the boiler ΔT starts increasing till thermosyphoning establishes itself. After that, boiler ΔT varies depending on reactor power and the S.G. temperature, i.e. boiler pressure.

The best way of assessing the thermosyphoning would be by comparing the core flow. As coreflow data from the plant is not available, header pressure and boiler ΔT are compared in Figures 4a, 4b and 5. Status of sink is depicted as boiler pressure in Figure 6. The slight variation with regard to Boiler ΔT and Boiler Pressure is due to minor difference in the characteristic of Auxiliary Feed Pump assumed in the analysis and that of plant. Otherwise, the predicted and actual data match fairly well. Thus, the transient analysed can predict thermosyphoning phenomenon close to reality. To see the effect of various frictional models, the core flow of various cases is shown in Figure 7. Case 3 seems to predict the lowest flow, thus, higher friction drop.

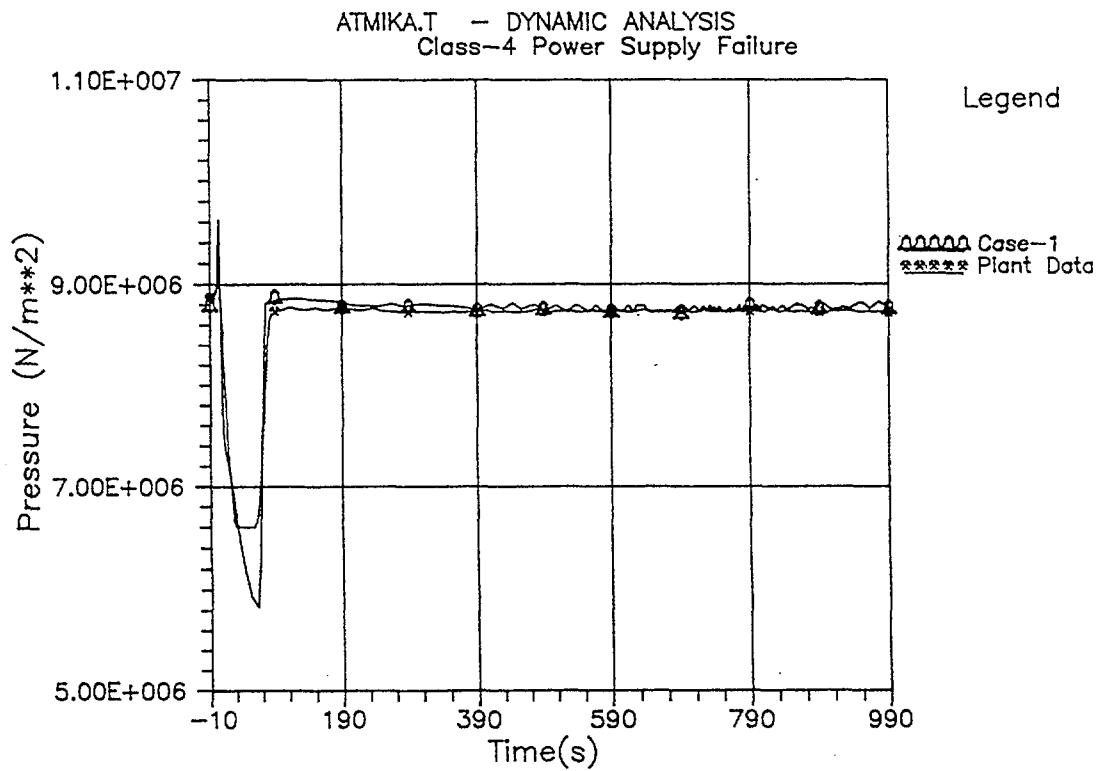


FIG. 4a. ROH pressure variation.

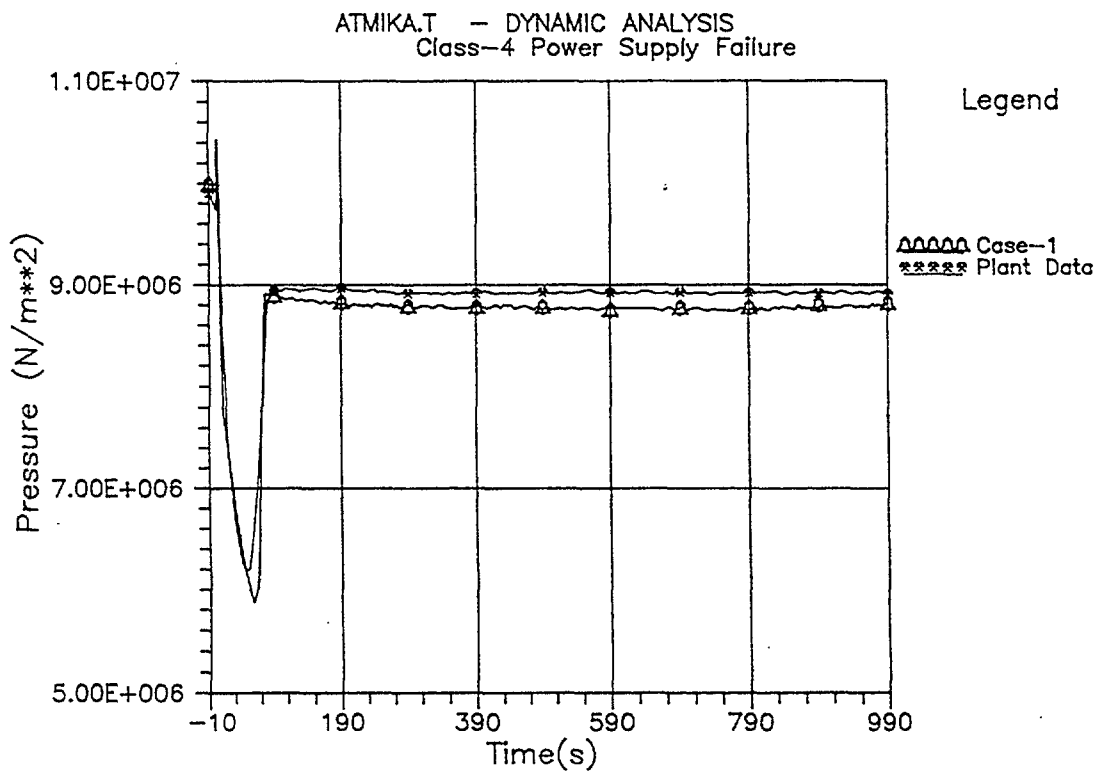


FIG. 4b. RIH pressure variation.

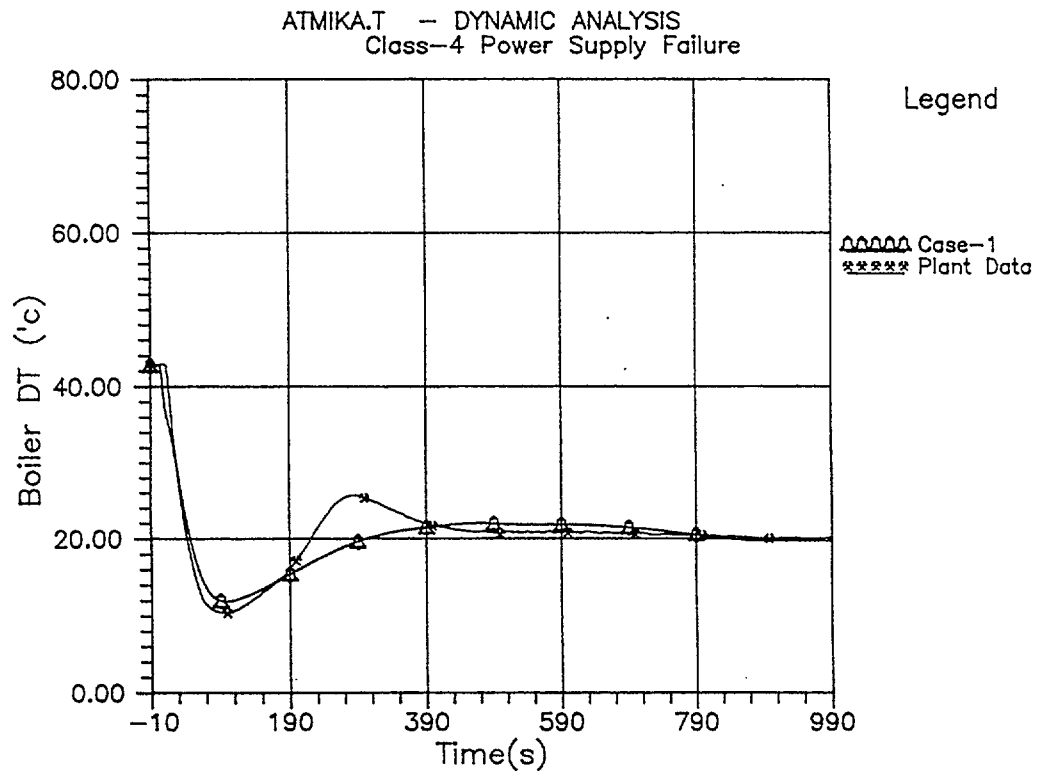


FIG. 5. Temperature difference across boiler.

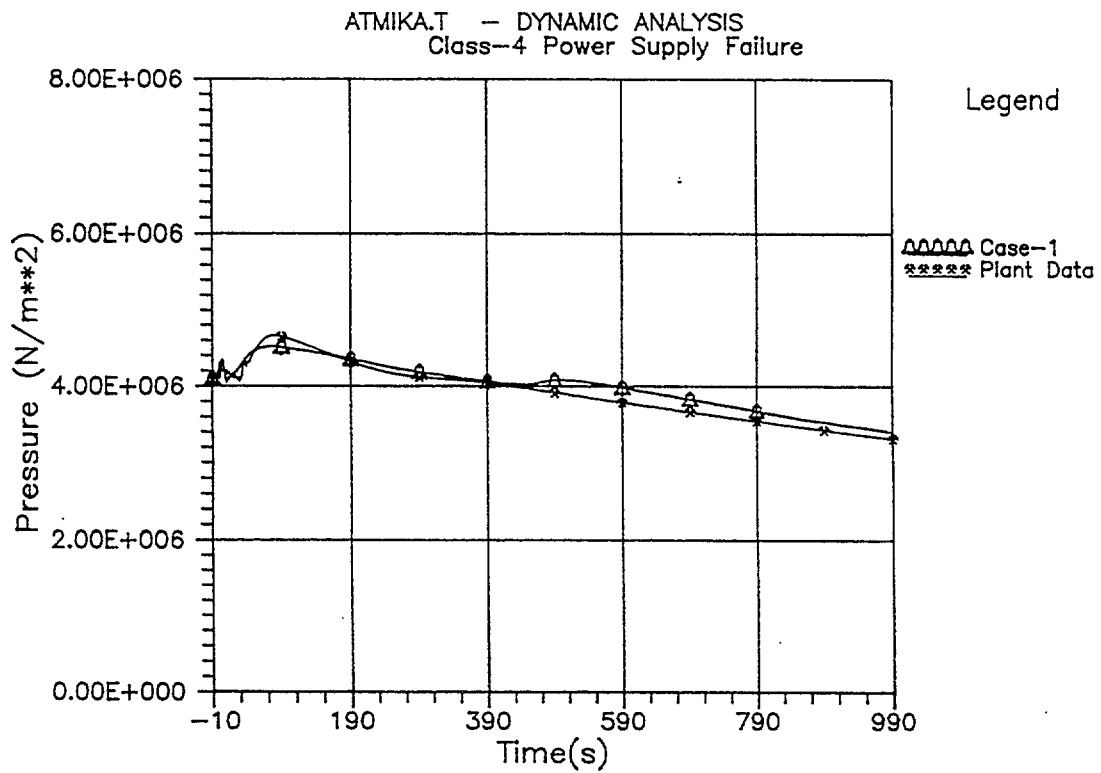


FIG. 6. Boiler pressure variation.

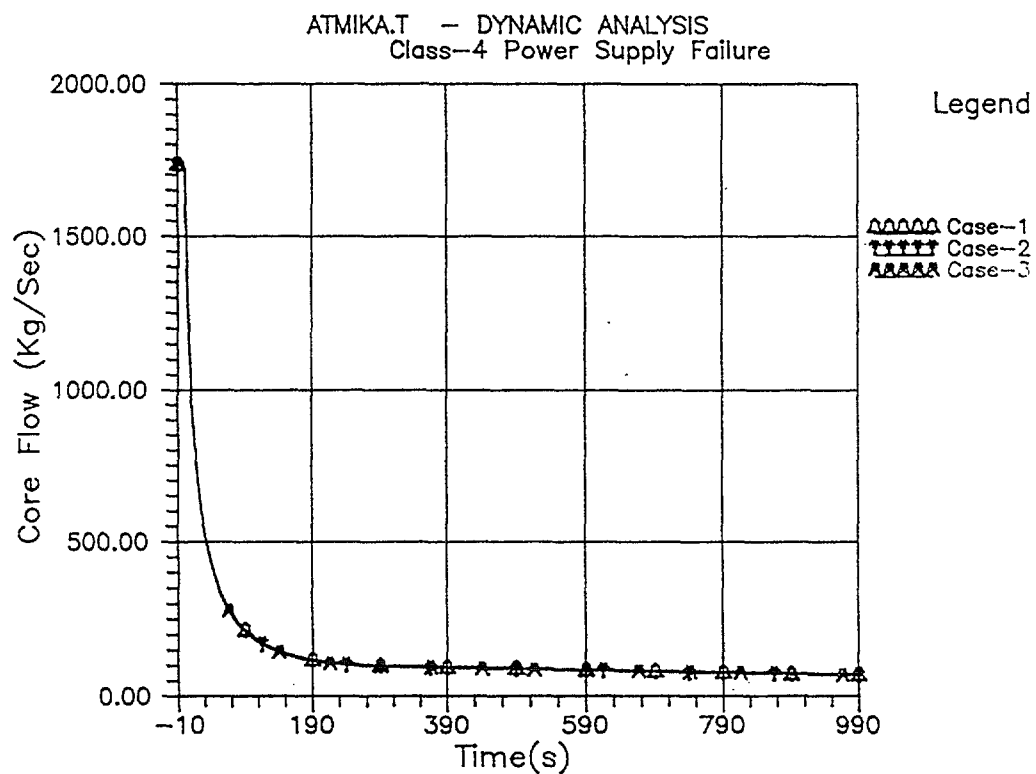


FIG. 7a. Core flow variation.

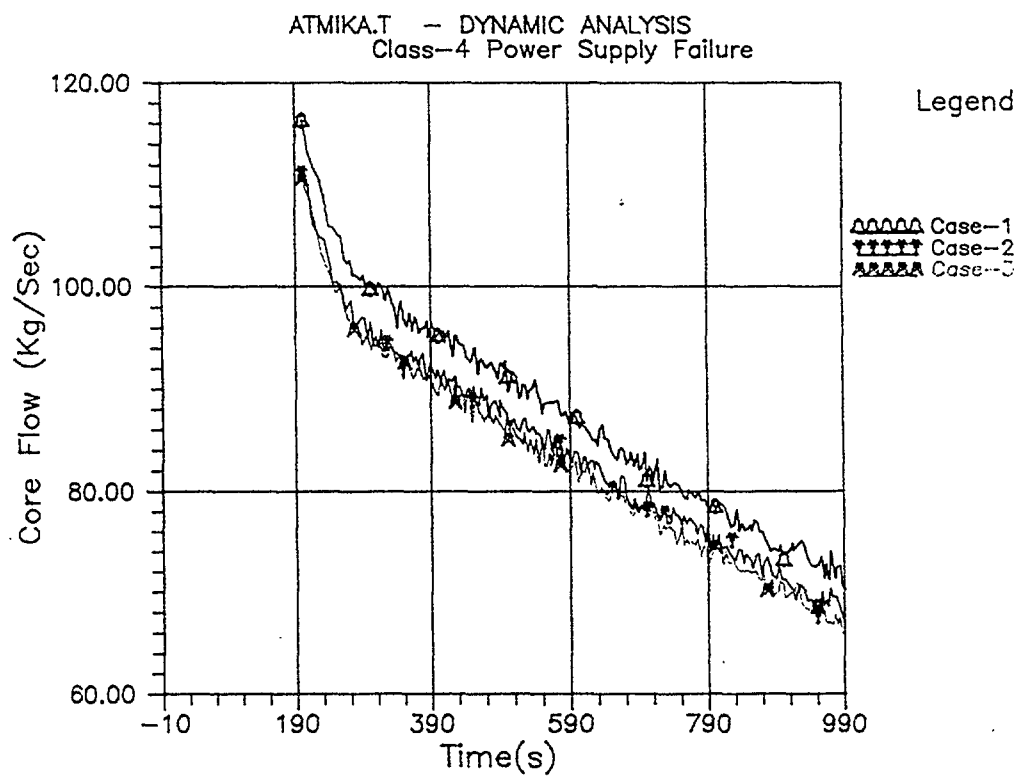


FIG. 7b. Core flow variation.

REFERENCES

- [1] RAMMOHAN, H.P.; BAJAJ, S.S.; 1996; "ATMIKA, a system thermal hydraulic computer code - model description", Nuclear Power Corporation, Mumbai, India.
- [2] CHURCHILL, S.W.; 1977; "Friction equation spans all fluid flow regimes", Chemical Engineering, Vol. 84(24) PP91-92.
- [3] NIKURADSE, J.; 1932, Mill. Forsch Geb. Ing.-Wesen 356, 1.
- [4] DREW, T.B.; KOO, E.C. and MCADAMS, W.H.; 1932; Trans AlchE -1932, 28, 56.



TRAC ANALYSES AND GIRAFFE TESTS FOR PCCS PERFORMANCE PREDICTION

K. KATAOKA, K. ARAI, S. YOKOBORI

Nuclear Engineering Laboratory,
Toshiba Corporation,
Yokohama, Japan

Abstract

The passive containment cooling system (PCCS) would remove decay heat by steam condensation without any electric power supply or operator's action if an accident should occur in nuclear reactors. There is, however, concern that non-condensable gas might influence the PCCS performance in the event of an accident. This paper summarizes Toshiba's activities respecting PCCS development, in particular those activities relating to TRAC qualification for PCCS performance prediction and the GIRAFFE tests. TRAC is a best estimate thermal hydraulic analysis code. GIRAFFE is a full-height test facility simulating the SBWR containment with the PCCS, at Toshiba's Ukishima site.

1. INTRODUCTION

1.1. Programme overview

The passive containment cooling system (PCCS) would remove decay heat by steam condensation without any electric power supply or operator's action if an accident should occur in nuclear reactors. This passive feature would enhance the reliability and simplicity of the safety systems since malfunction of active devices would be avoided as well as any operator's mistakes. The PCCS is being adopted for the advanced water-cooled reactors.

There is, however, concern that non-condensable gas might influence the PCCS performance in the event of an accident. The containment vessel of a BWR is filled with nitrogen, which is non-condensable; other non-condensable gases such as hydrogen might be released due to metal-water reaction under the conditions created by an accident. Non-condensable gases degrade steam condensation in the PCCS HX (heat exchanger).

This paper summarizes Toshiba's activities respecting PCCS development, in particular those activities relating to TRAC qualification for PCCS performance prediction and the GIRAFFE tests. TRAC is a best estimate thermal hydraulic analysis code. GIRAFFE is a full-height test facility simulating the SBWR containment with the PCCS, at Toshiba's Ukishima site [1].

Table I shows a timetable of Toshiba's PCCS development programme [2]. We have conducted the PCCS development since 1989 and focused on the thermal-hydraulics. Construction of the GIRAFFE test facility began in 1989. Various tests have been carried out at the GIRAFFE and many important data have been obtained and utilized for analytical code development.

An essential phenomenon governing the PCCS heat removal performance is steam condensation in the presence of non-condensable gas. First, a series of separate effect tests has been carried out to investigate the non-condensable gas effects and to develop a degradation model of steam condensation [2] [3].

Then small system-integral tests were conducted. The PCCS gas vent function and geometric effects of the PCCS-HX have been measured. Using these test results, the analytical models for the non-condensable gas effects have been validated.

TABLE I. PCCS DEVELOPMENT PROGRAMME

Programme	Item	89	90	91	92	93	94	95	96	97	98
GIRAFFE construction	Construction, upgrade	■	■	■	■						
Separate effect test	Nitrogen		■								
	Helium						■				
Small system test	Steam condensation		■	■							
	Gas venting, tubes etc.		■	■						■	■
Large system test	LOCA simulation		■		■	■	■	■			
	System optimization					■	■	■			
Analysis	Degradation model	■	■				■	■			
	Model validation		■	■	■	■	■	■		■	■
	GIRAFFE simulation		■	■	■	■	■	■		■	■
	TRAC qualification			■	■	■	■	■	■	■	■
	Adv. BWR simulation		■	■	■	■	■	■	■	■	■

Next, a series of system integral tests as well as analyses have been carried out to simulate thermal hydraulic behavior in the containment vessel with the PCCS following a loss-of-coolant-accident (LOCA) [2][4][5]. For the qualification of the analytical code, the analytical results have been compared with the test results.

Hydrogen effects on steam condensation and the PCCS performance have been investigated experimentally [6] and analytically. Hydrogen could be released into the containment vessel under the conditions created by a severe accident. We have used helium in the tests instead of hydrogen for reasons of safety.

1.2. PCCS configuration

The PCCS was originally designed for SBWR. The SBWR passive safety system consists of depressurization valves (DPVs), the gravity driven cooling system (GDSCS), the equalizing line (EQL) and the PCCS as shown in Fig. 1. The GDSCS injects water into the reactor pressure vessel (RPV) by gravity following a LOCA. The DPVs promote GDSCS injection by depressurizing the RPV. Long-term core coverage is achieved by the EQL, which allows suppression-pool water to flow into the RPV.

The PCCS consists of a steam supply-line, a vertical shell-and-tube-type heat exchanger in a large water pool (PCCS pool), a condensate drain-line and a non-condensable gas vent-line. Following a LOCA, high-pressure steam comes from the RPV to the drywell and raises pressure in the drywell. The resultant pressure difference between the drywell and the suppression-chamber (SC) drives mixture of steam and non-condensable gas in the drywell into the PCCS-HX through the steam supply-line.

Steam condenses in the PCCS-HX and the condensate drains into the GDSCS pool through the condensate-line by gravity. Non-condensable gas absorbed in the PCCS-HX is vented to the SC through the PCCS vent-line. The PCCS pool is located outside the drywell and serves as a heat sink for decay heat. The SBWR PCCS pool accommodates a sufficient amount of water to remove decay heat for three days following a LOCA.

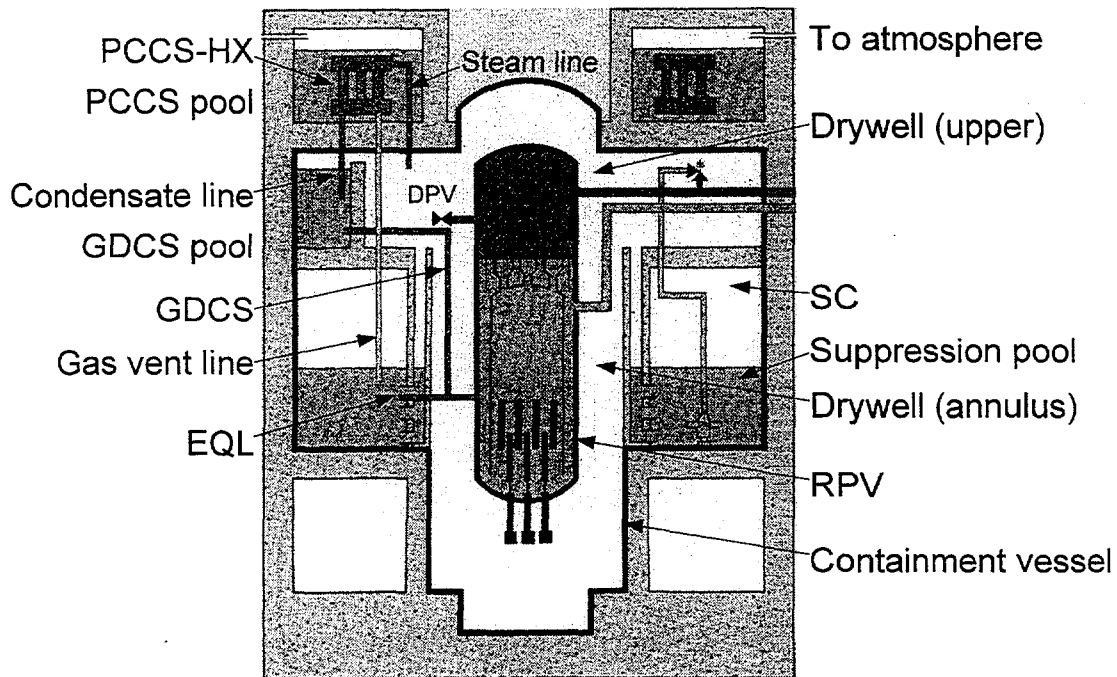


FIG. 1. Schematic diagram of SBWR safety systems [1].

1.3. GIRAFFE test facility

GIRAFFE (Gravity-driven integral full-height test facility for passive heat removal) is a full height integral system test facility located at Toshiba's Ukishima site. GIRAFFE primarily consists of five separate vessels, which are modeled on the PCCS pool, the RPV, the SC, the drywell and the GDCS pool designed for the SBWR. A photograph of GIRAFFE and its schematic diagram are shown in FIG. 2.

Since thermal hydraulic behavior is driven by gravity for long-term transients after a LOCA, GIRAFFE has 1:1 height scale to the SBWR design; the total height is 30 m. The volumetric scale is 1:400 to the SBWR design.

The PCCS-HX consists of a steam box, heat transfer tubes and a water box as shown in Fig. 2. The GIRAFFE PCCS-HX has three vertical heat-transfer tubes whose inner diameter is 0.046 m and the length is 1.8 m. The elevation of the HX tubes and the clearance between adjacent tubes are identical to those for SBWR.

In the PCCS pool, a chimney separates the boiling region along the HX tubes from the subcooled water region. The pool water circulates along the chimney and boils off to the atmosphere when the PCCS functions.

The RPV contains electric heater-rods simulating the SBWR core. The electric power is controlled to generate decay heat following a LOCA. Thermal insulators are wrapped around all the vessels to lower heat loss from them. The remaining heat loss is compensated by increasing the electric power in the RPV.

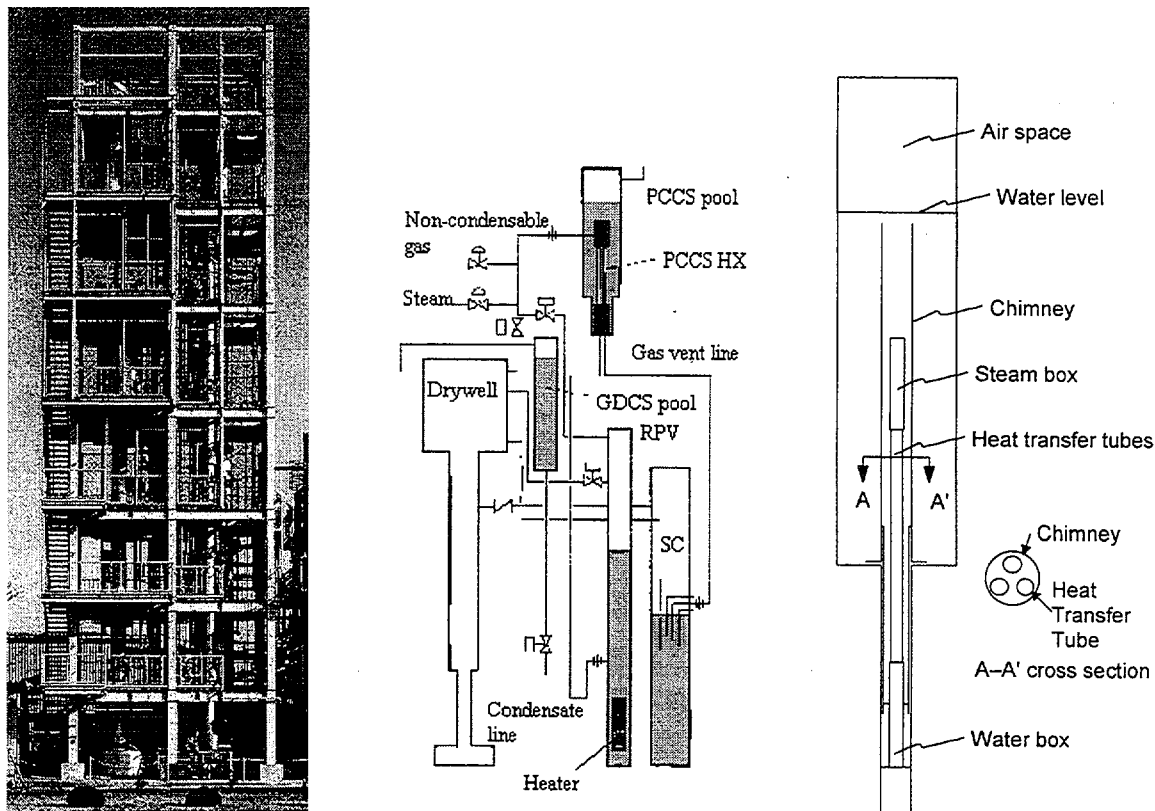


FIG. 2. GIRAFFE, the schematic diagram and the PCCS HX configuration [1][2].

2. SEPARATE EFFECT TESTS AND MODEL DEVELOPMENTS

2.1. Degradation by nitrogen

2.1.1. GIRAFFE data development

Degradation in steam condensation inside the PCCS-HX due to nitrogen was investigated under the forced convective flow condition as the first step of the development programme. These test conditions were chosen based on the analyses for thermal hydraulic behavior in the SBWR containment vessel under the long-term post-LOCA conditions (Table II).

First, condensation rates in the HX tube were measured for different flow-rates of pure steam. Then nitrogen was supplied into the steam flow and steam condensation rates were measured for different nitrogen partial pressures. The results are shown in Fig. 3 as degradation coefficients against nitrogen partial-pressure-fractions. The degradation coefficient (DC) is defined as follows. $DC = h_{cond}/h_{ps}$, where h_{cond} is condensation heat-transfer-coefficient in the presence of nitrogen and h_{ps} is pure-steam condensation heat-transfer-coefficient. This relationship between DC and nitrogen partial-pressure-fraction was named "GIRAFFE data" and incorporated in TRAC.

TABLE II. TEST CONDITIONS FOR THE HEAT REMOVAL DEGRADATION BY NITROGEN [3]

Condition	Unit	Value
Total pressure	MPa	0.2 - 0.4
Nitrogen partial-pressure-fraction (P_N / P_{total})	-	0 - 0.10
Steam flow-rate	kg/s	0.02 - 0.04

In 1960's, Sparrow gave two sets of degradation curves in steam condensation for stagnant flow condition and convective flow condition on a horizontal plate at 0.1 MPa with wall subcooling 11 K [7]. The GIRAFFE test conditions are close to Sparrow's convective flow condition. The GIRAFFE DCs are slightly higher than Sparrow's DCs for convective flow condition.

2.1.2. GIRAFFE data validation

A series of small integral tests were carried out to validate the GIRAFFE data. The test loop consists of a pure-steam supply-line, a nitrogen supply-line, a PCCS-HX submerged in the PCCS-pool, the vent-line to the SC, and the condensate-line to the RPV in the GIRAFFE (Fig. 2). The system pressure was controlled at 0.3 MPa.

First, overall pure-steam condensation rates were measured and compared with the analytical results with three steam condensation models: Nusselt's model, Uehara's correlation model, and Vierow's model [8][9]. Nusselt's model is applied for pure-steam condensation in the TRAC analyses. The other models were developed empirically to supplement Nusselt's model, which tends to underestimate steam condensation. Fig. 4 shows the comparison between the experimental data and the analytical results obtained with those models.

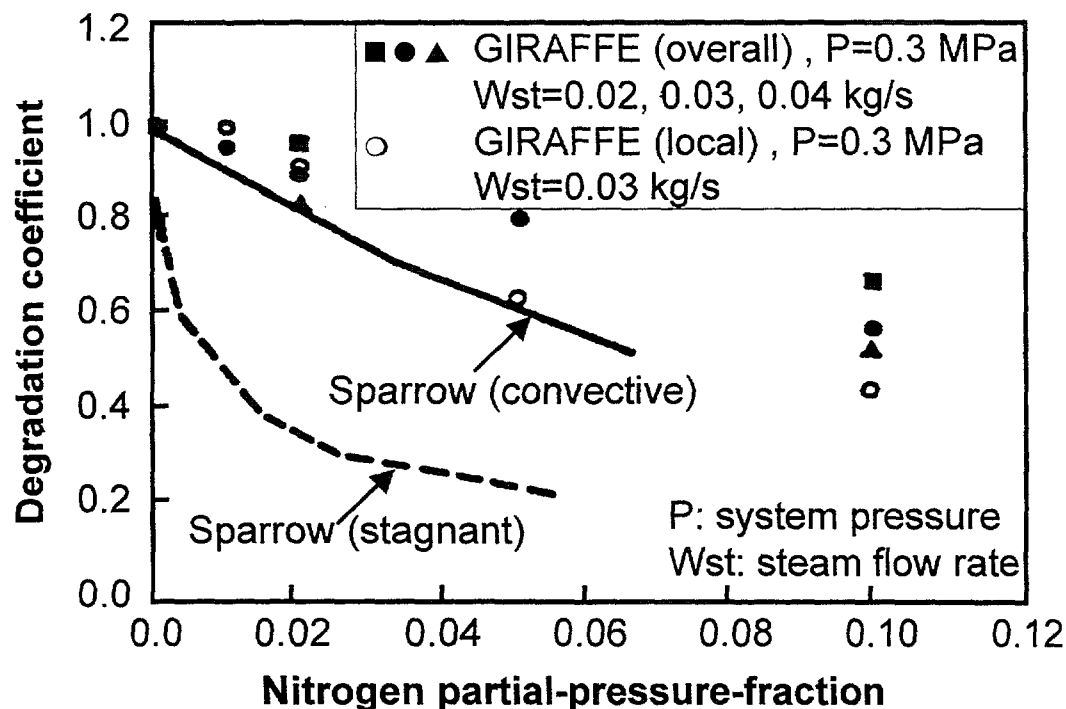


FIG. 3. Steam condensation degradation by nitrogen [3].

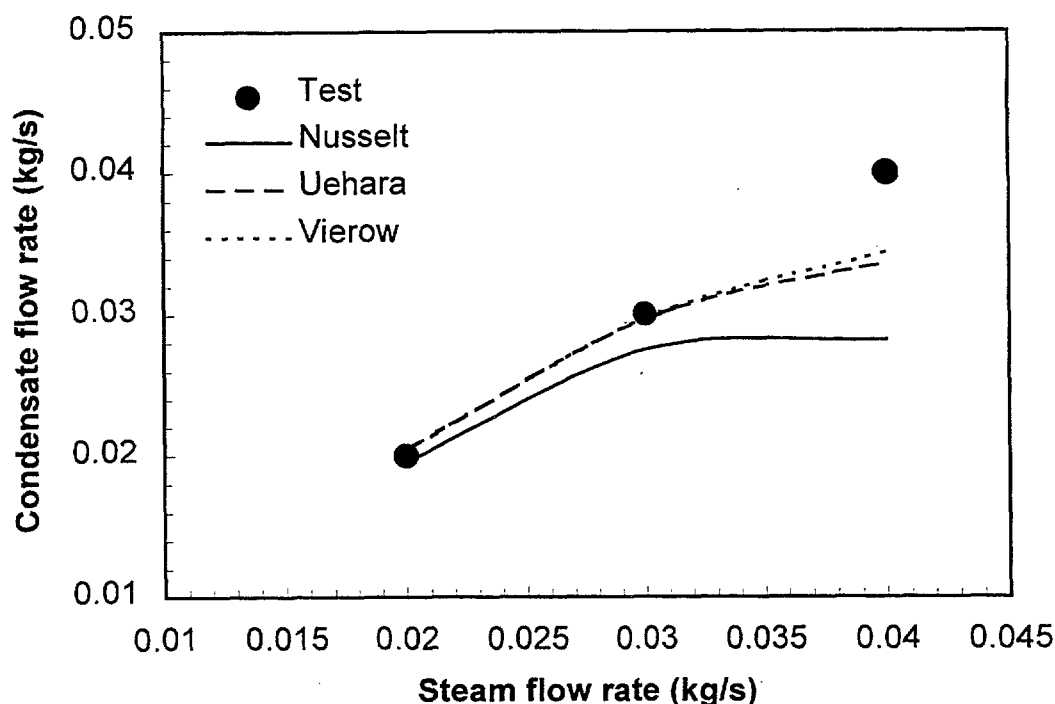


FIG. 4. Validation of the pure-steam condensation models.

The analytical results obtained with Uehara's model and Vierow's model are closer to the experimental results than those obtained with Nusselt's model. Uehara's model gives steam condensation rates and a trend against steam flow-rate similar to those given by Vierow's model. However, they still underestimate pure-steam condensation rate for relatively high steam flow-rate.

Next, overall steam-condensation-rates were measured in the presence of nitrogen with the steam flow-rate of 0.03 kg/s. To clarify the nitrogen effects on steam condensation, condensation ratio was defined as the ratio of steam condensation rate in the presence of nitrogen to pure steam condensation rate. Fig. 5 shows the comparison between the experimental and the analytical results.

The analytical results obtained with the GIRAFFE data and Vierow's model show a good agreement with the experimental results respecting condensation ratios versus nitrogen partial-pressure-fractions. The differences between the analytical results and the experimental results were below 15%. Nusselt's model underestimates the condensation ratios.

It is concluded that the GIRAFFE data would successfully estimate degradation of steam condensation in the presence of nitrogen since the design margin is about 15% for the containment. For pure-steam condensation, Uehara's correlation is recommended but it still gives conservative steam-condensation-rates for high steam flow-rates.

2.2. Degradation by hydrogen

The PCCS is expected to function in the event of a severe accident to maintain the containment integrity. Hydrogen might be released by metal-water reaction and influence the PCCS performance under the conditions created by a severe accident.

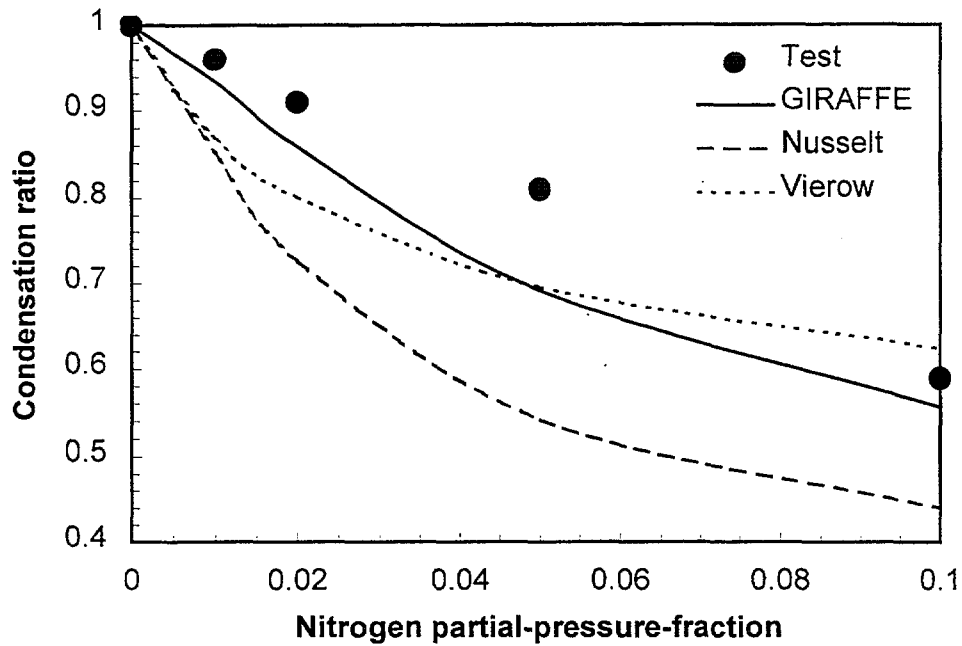


FIG. 5. Validation of degradation model for steam condensation in the presence of nitrogen.

Thermal properties of hydrogen are different from those of nitrogen (Table III). Because hydrogen is lighter than nitrogen and steam, it is liable to remain in the upper part of the containment vessel, where the PCCS-HX is accommodated. On the other hand, the thermal conductivity and the thermal diffusivity of hydrogen are higher than those of nitrogen. These characteristics make hydrogen more favorable than nitrogen respecting steam condensation.

To determine the hydrogen effects on steam condensation in the PCCS HX, separate effect tests have been conducted using helium for reasons of safety. The thermal properties of helium are close to those of hydrogen as shown in Table III. The system pressure was set to 0.3 MPa and the steam flow rate was controlled at 0.03 kg/s in the tests. These test conditions were chosen based on severe accident analyses and the earlier LOCA studies.

TABLE III. THERMAL PROPERTIES OF NON-CONDENSABLE GASES

Property	Unit	Nitrogen	Hydrogen	Helium
Density	kg/m ³	1.14	0.08	0.16
Thermal conductivity	mW/(m·K)	26	181	153
Thermal diffusivity	mm ² /s	22	155	181

Degradation coefficients (DCs), which are defined in the Section 2.1.1, for different helium partial-pressure-fractions were measured and they are plotted in Fig. 6. The trend of the helium DCs is similar to that of the nitrogen DCs in relation to non-condensable gas partial-pressure-fractions. The helium DCs are higher than those of nitrogen in relation to relatively higher partial-pressure-fractions.

This study shows that the GIRAFFE data with small modification would be applied to the PCCS performance prediction under the conditions created by a severe accident. It is noted, however, that the helium DCs in relation to non-condensable gas mass-fractions are lower than the nitrogen DCs. This is because helium molecular weight is one seventh of that of nitrogen.

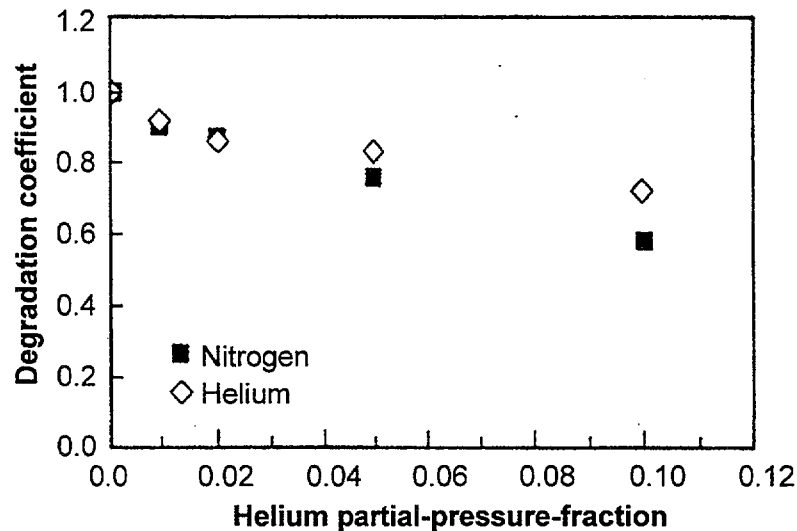


FIG. 6. Steam condensation degradation by helium [6].

3. SYSTEM INTEGRAL TESTS AND TRAC ANALYSES

3.1. PCCS performance in the presence of nitrogen

3.1.1. Experimental study

System integral tests have been carried out to investigate the PCCS performance under three LOCA conditions: main-steam-line break (MSLB) condition, GDCLB condition and the RPV bottom-drain-line break (DLB) condition. The MSLB represents a steam-phase large pipe-break located at the upper elevation of the drywell. The GDCLB represents a liquid-phase medium sized pipe-break in the drywell. The DLB represents a liquid-phase small pipe-break. The location and the size of pipe-break and the phase of the fluid influence nitrogen behavior in the containment following a LOCA.

The initial test conditions are summarized in Table IV. Those conditions simulate SBWR's conditions at one hour after a corresponding LOCA occurs. The conditions were chosen based on TRAC analyses for the corresponding LOCAs. The initial nitrogen partial-pressure-fraction in the drywell differs for each pipe-break location. The test results are described in the next section and compared with the analytical results.

3.1.2. Analytical study (TRAC qualification)

3.1.2.1. TRAC model

TRAC is a best-estimate computer code for BWR thermal hydraulic transient analysis. It employs a three-dimensional two-fluid non-homogeneous and non-equilibrium thermal hydraulic model of two-phase flow, supplemented by a non-condensable gas model. Non-

TABLE IV. INITIAL TEST-CONDITIONS FOR MSLB, GDCSLB AND DLB TESTS [4]

Condition	Unit	MSLB	GDCSLB	DLB
Drywell total pressure	MPa	0.19	0.19	0.20
Drywell nitrogen partial-pressure-fraction		0.28	0.21	0.09
Drywell temperature	K	381	383	389
Drywell collapsed water level	m	0	0.24	0.32
SC total pressure	MPa	0.17	0.19	0.20
SC nitrogen partial-pressure-fraction		0.94	0.95	0.96
SC temperature	K	326	325	324
RPV pressure	MPa	0.19	0.19	0.20
GDCS pool water level	m	2.8	1.0	2.2
PCCS pool temperature	K	373	373	373

condensable gas is assumed to be in thermal equilibrium with steam existing with the non-condensable gas and to move with the same velocity as the steam.

The GIRAFFE data for non-condensable gas effects as well as Uehara's model for pure steam condensation have been incorporated in TRAC to accurately evaluate the PCCS performance in the presence of non-condensable gas for convective steam flow. For stagnant steam flow, a conventional steam condensation model is applied in the presence of non-condensable gas. The conventional model consists of two parts: Nusselt film condensation model for pure-steam condensation and Sparrow's stagnant model for degradation of steam condensation in the presence of non-condensable gas.

3.1.2.2. TRAC nodalization

To analytically simulate the system integral tests, the GIRAFFE components were modeled by TRAC components. The RPV, SC, drywell GDCS pool and PCCS pool are simulated by independent cell/cells in a three-dimensional TRAC component (VESSEL) having three radial rings, one azimuthal sector and 12 axial levels. Connection lines between the major GIRAFFE components are built by one-dimensional TRAC components such as PIPE, VLVE and TEE. The boundary conditions are given by mass flow rate or pressure. The TRAC nodalization for the GIRAFFE tests is shown in Fig. 7.

The PCCS-HX tubes consist of a PIPE component with some modification, in which the total inner and outer heat-transfer area, and the thickness of the tubes are accurately set to simulate the PCCS-HX tube geometry. The PCCS pool is modeled to have flow paths so that natural circulation of water can occur around the PCCS-HX.

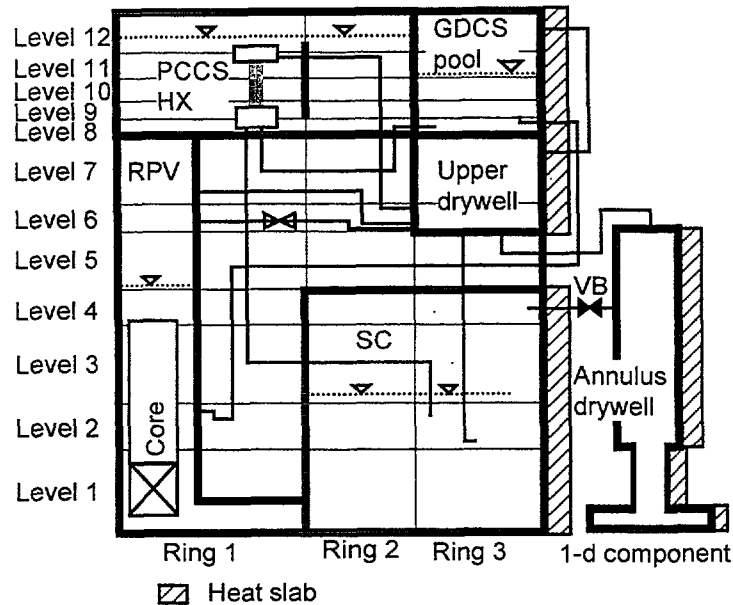


FIG. 7. TRAC nodalization for the GIRAFFE integral tests [5].

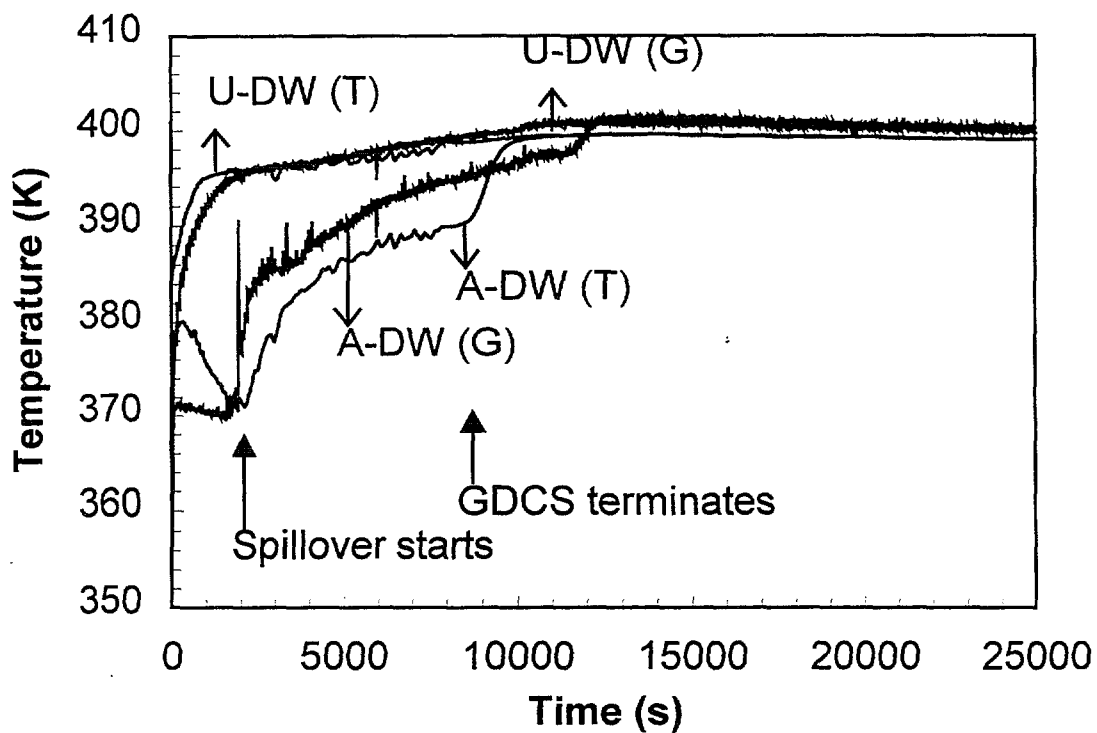
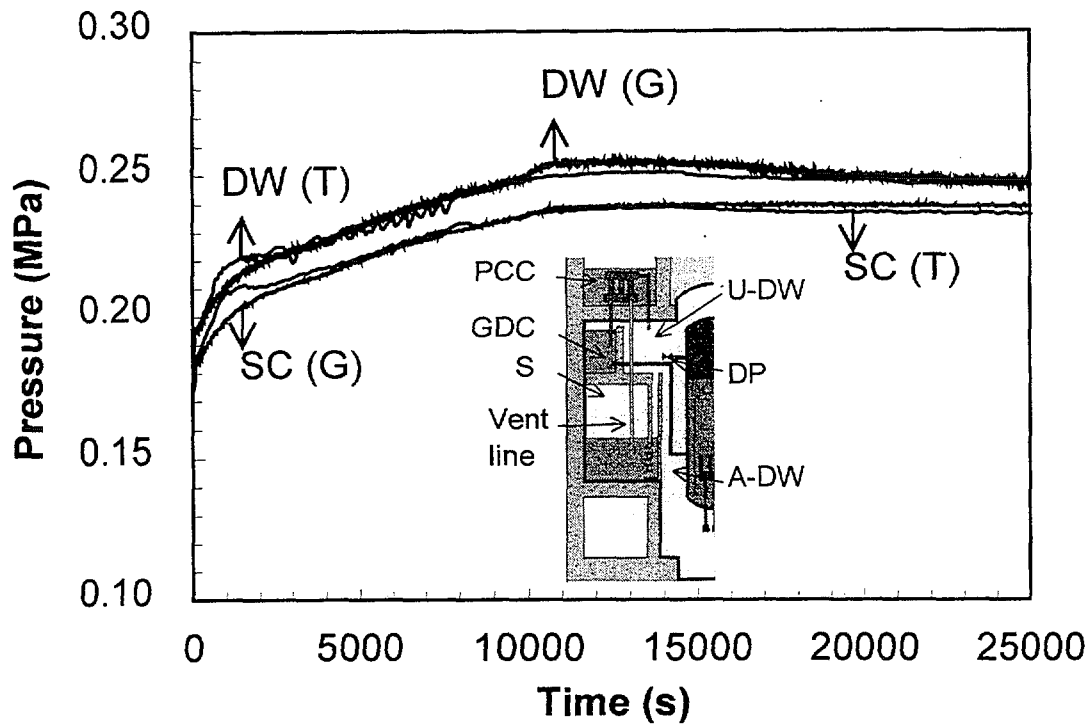
Heat loss from the GIRAFFE components to the ambient is taken into account by giving heat transfer coefficients to the outside wall of the TRAC components. The heat transfer coefficients have been determined based on the GIRAFFE heat-loss data.

3.1.2.3. Test and analytical result

The main function of the PCCS is to keep the containment pressure below the design pressure (0.48 MPa for the SBWR containment) following a LOCA. The PCCS performance is influenced by non-condensable gas behavior. To evaluate the PCCS performance and the non-condensable gas behavior, comparisons between the GIRAFFE test results and the TRAC analyses were made, focusing the containment pressure responses and the containment temperature responses. The lower the containment temperature is, the richer non-condensable gas is in the containment.

The TRAC analysis shows a good agreement with the GIRAFFE test result for the containment pressure and temperature responses following an MSLB as shown in FIG. 8. After the MSLB blowdown phase, steam generated by decay heat in the RPV flows out to the drywell. The PCCS-HX begins to absorb steam in the drywell without any active devices or operator's action. Since the decay heat rate is larger than the PCCS heat removal rate before 13,000 sec, the drywell pressure is gradually increased as well as the SC pressure and reaches a maximum pressure of 0.26 MPa at 13,000 sec.

Due to the GDCS injection, the RPV water level increases and reaches the DPVs elevation at 2,000 sec. The continuous GDCS injection has forces the coolant spillover from the RPV to the drywell through the DPVs. The water spilt at the bottom of the drywell evaporates and makes upward flow of steam accompanying non-condensable gas accumulated in the bottom of the drywell. According to this non-condensable gas behavior, temperature in the annulus drywell suddenly rises at 2,000 sec and increases until the GDCS termination at 13,000 sec as shown in Fig. 8.



DW: drywell, U-: upper, G: GIRAFFE,
 SC: suppression chamber, A-: annulus, T: TRAC

FIG. 8. Containment pressure (left) and temperature (right) response following an MSLB [4] [5].

The pressure difference between the drywell and the SC is so large before 13,000 sec that the PCCS vent line is cleared. Through the vent line, most non-condensable gas is transferred from the drywell to the SC. Consequently, the SC pressure increases as shown in Fig. 8; the annulus-drywell temperature rises to the steam saturation temperature.

Then the drywell pressure decreases gradually and flattens out as shown in Fig. 8 because the PCCS heat removal rate gradually catches up and eventually exceeds the decay heat rate. Most non-condensable gas is already transferred to the SC and the remaining gas starts to fall to the bottom of the drywell since the steam upward flow begins to weaken and nitrogen is heavier than steam. Although the PCCS vent line is no longer cleared and a little nitrogen accumulates in the PCCS-HX, the heat transfer rate of the PCCS is sufficient to remove decay heat.

For the GDCSLB case, the TRAC analysis also shows a good agreement with the test result (Fig. 9). The containment pressure responses are similar to those for the MSLB case but milder. The peak pressure in the drywell is 0.24 MPa in the test.

Because a GDCS line breaks, the RPV coolant-make-up is smaller than that for the MSLB case and coolant does not spill over from the RPV through the DPVs. Little upward flow occurs at the bottom of the drywell so that non-condensable gas accumulates there as shown in Fig. 9.

Consequently, the PCCS absorbs a small amount of non-condensable gas and the heat removal rate exceeds the decay heat rate after 10,000 sec. The drywell pressure gradually decreases and remains far below the design pressure.

For the DLB case, the TRAC analysis shows milder pressure response than the test result but the differences between them are small. The drywell pressure rises slowly and reaches 0.24 MPa then decreases. These responses are slow because the PCCS heat removal performance is better than those in other cases. The initial non-condensable gas inventory in the drywell is smaller than those in other cases; the coolant evaporation is larger due to a bottom line break.

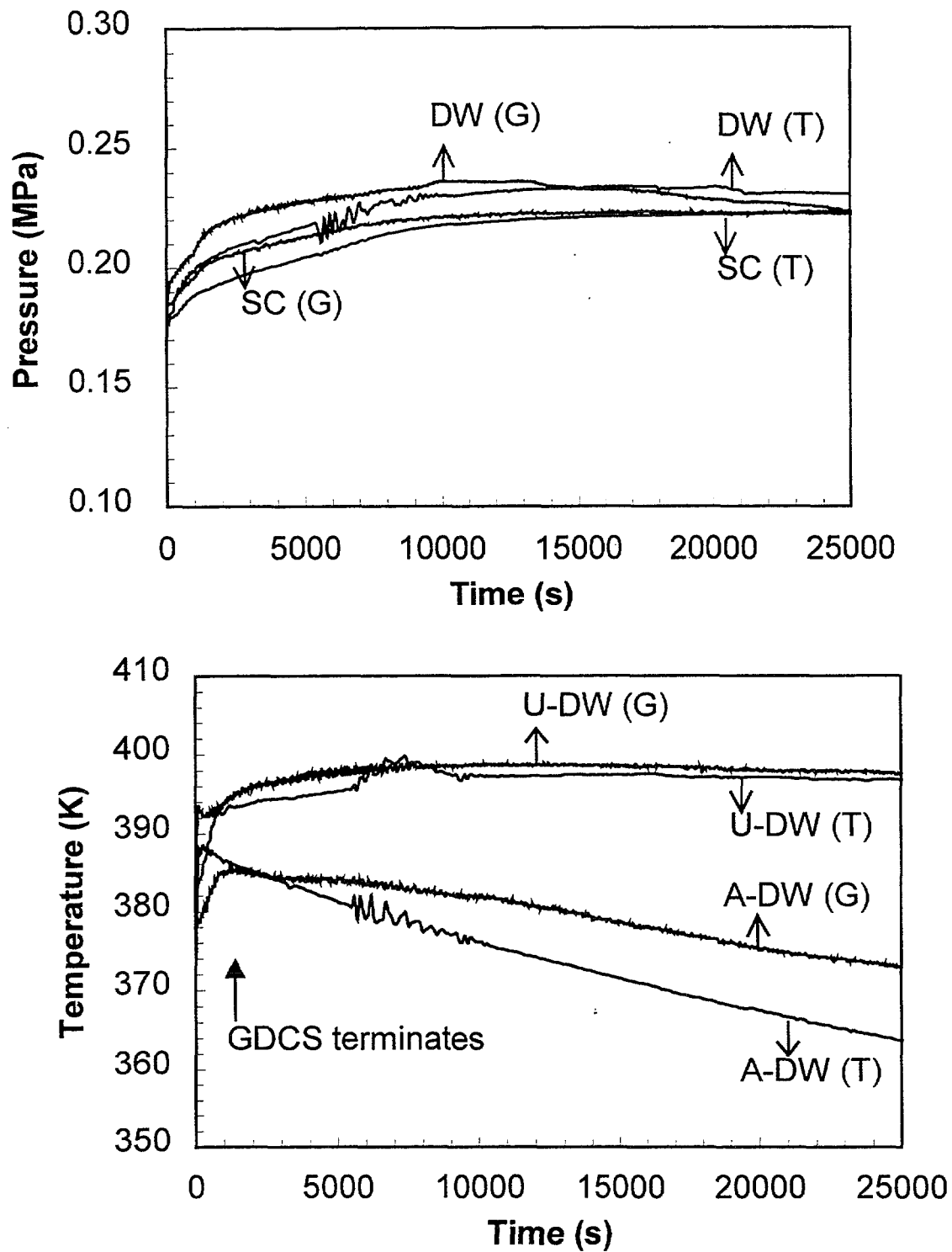
From these comparisons between the TRAC analyses and the GIRAFFE tests for the MSLB, GDCSLB and DLB cases, it is concluded that the PCCS would remove decay heat following a LOCA. Most non-condensable gas would be transferred to the SC, and therefore the PCCS performance would not be deteriorated by non-condensable gas.

TRAC reproduces the non-condensable behaviors and pressure responses in the GIRAFFE containment following a LOCA. TRAC incorporating the GIRAFFE data is qualified to predict the PCCS performance following a LOCA in the presence of nitrogen.

3.2. PCCS performance in the presence of hydrogen

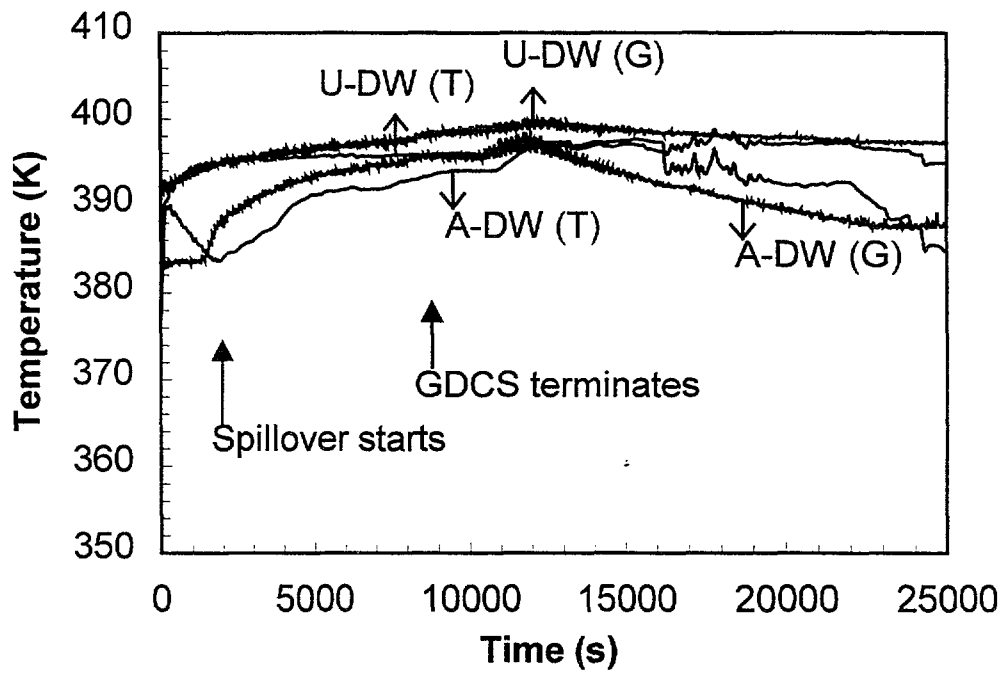
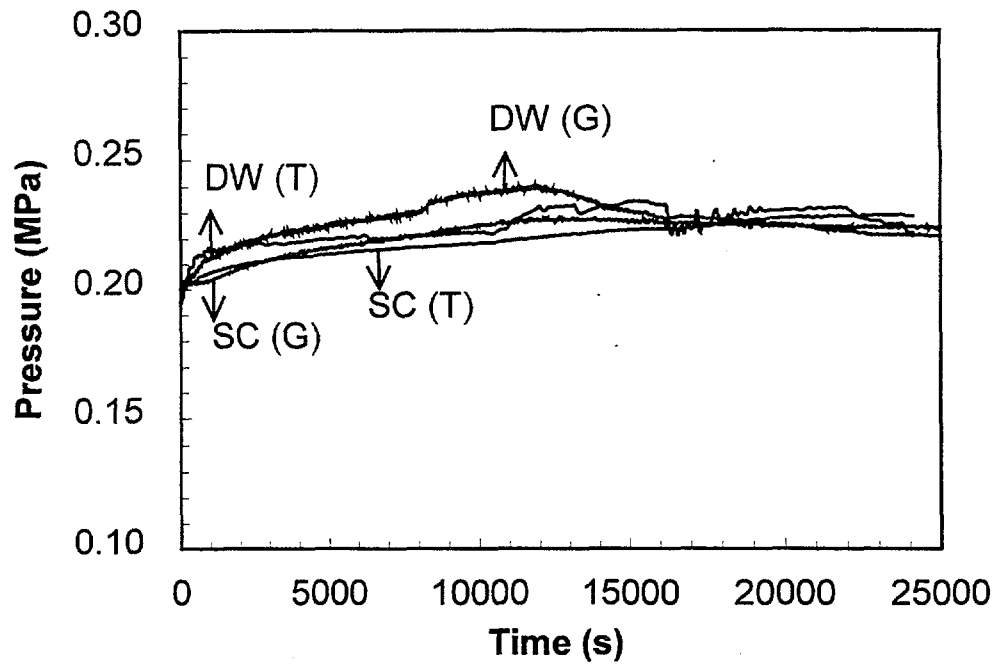
Hydrogen might be released during a severe accident and its behavior might differ from that of nitrogen in the containment. Consequently, the PCCS performance might be different in the presence of hydrogen.

To determine the hydrogen effects on the PCCS performance, another series of system integral tests was conducted using helium instead of hydrogen for the reasons of safety. The test simulated thermal hydraulic behavior in the SBWR containment following an MSLB. The test conditions were identical to those of the MSLB test in the presence of nitrogen (Table IV).



DW: drywell, U-: upper, G: GIRAFFE,
 SC: suppression chamber, A-: annulus, T: TRAC

FIG. 9. Containment pressure (left) and temperature (right) response following a GDCSLB [4] [5].



DW: drywell, U-: upper, G: GIRAFFE,
 SC: suppression chamber, A-: annulus, T: TRA

FIG. 10. Containment pressure (left) and temperature (right) response following a DLB [4][5].

TRAC analyses were also carried out with the modified GIRAFFE data obtained from the GIRAFFE separate effect test of helium (Section 2.2). The analytical results show a good agreement respecting the containment pressure responses with the test results as shown in Fig. 11.

The drywell pressure increases following an MSLB and reaches a maximum pressure of 0.25 MPa at 10,000 sec. During this period, most helium in the drywell is transferred to the SC and the SC pressure increases (Fig. 11). These pressure responses are similar to those in the nitrogen case.

After the drywell pressure reaches the maximum pressure, however, the pressure responses are slightly different from those in the nitrogen case. Since helium is lighter than steam, the remaining helium in the drywell continues to rise after the GDCS termination. Helium begins to accumulate in the upper part of the PCCS-HX and to deteriorate steam condensation. However, some steam condenses in the PCCS vent line and at the PCCS pool surface since helium does not accumulate there. Consequently, the PCCS heat removal rate does not fall below the decay heat rate and the drywell pressure flattens out.

TRAC underestimates temperatures in the containment. This implies that the more helium remains in the drywell than during the test. A more accurate helium diffusion model might be needed for TRAC to analyze helium behavior in the containment.

From these results, it is concluded that the PCCS would remove decay heat following an MSLB in the presence of hydrogen. Although a little hydrogen would be accumulated in the PCCS-HX, the PCCS performance would be sufficient to remove decay heat.

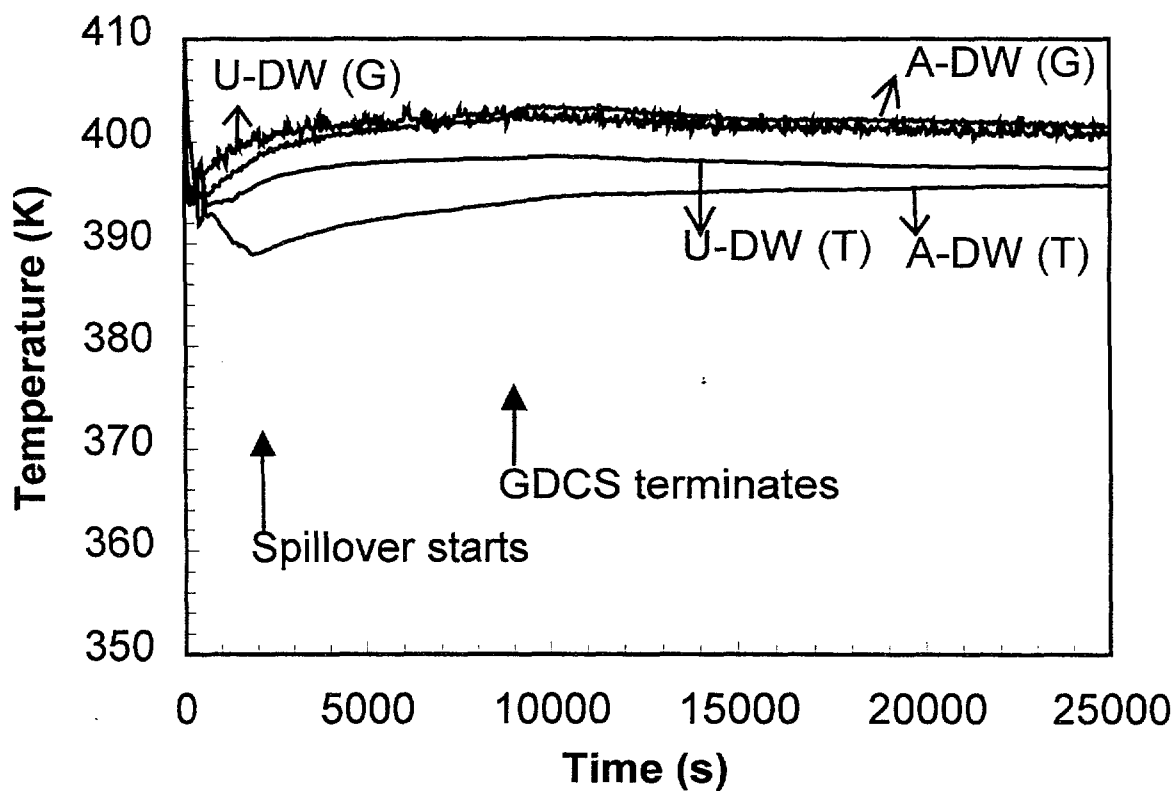
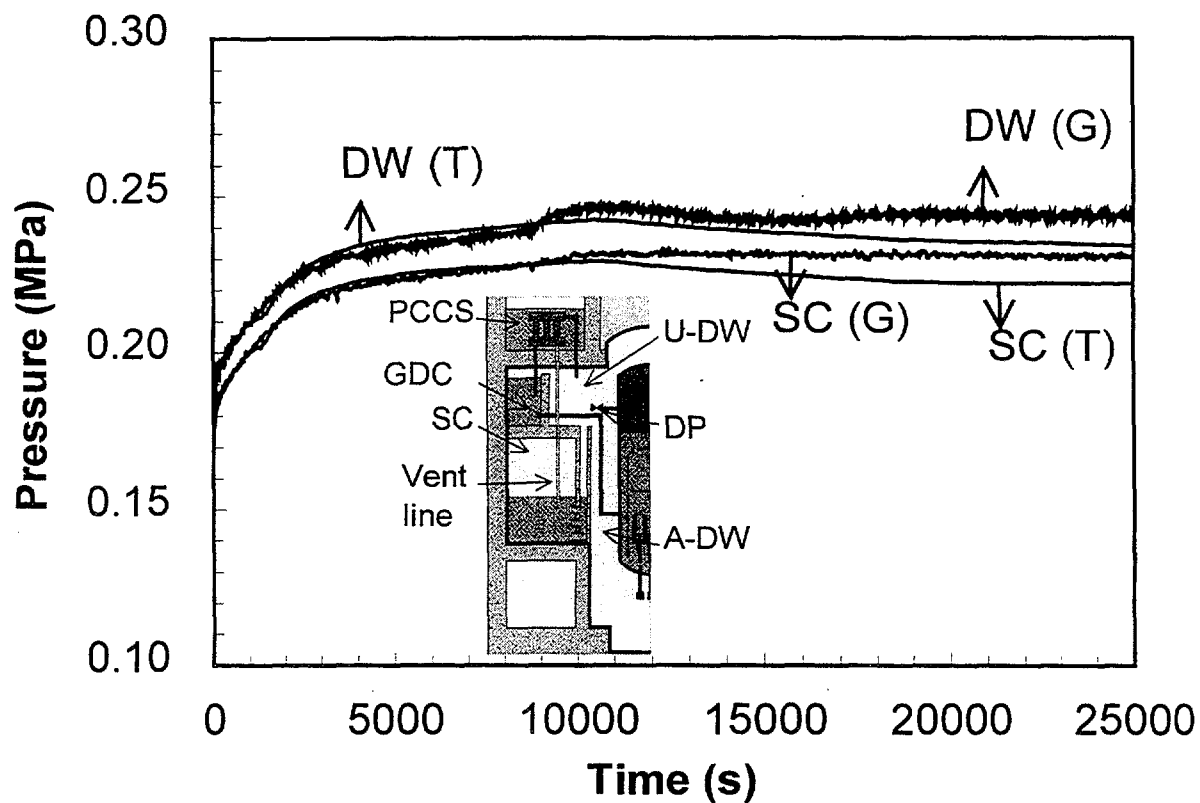
TRAC with the GIRAFFE data reproduced the GIRAFFE test in the presence of helium following an MSLB LOCA. Therefore, TRAC with the GIRAFFE data has the potential to predict PCCS performance in the event of a severe accident.

4. CONCLUSION

Toshiba has been carrying out a PCCS development that combines experimental and analytical approaches. First, the nitrogen effects on steam condensation were identified from the GIRAFFE separate effect tests; a degradation model of steam condensation was developed, namely, the GIRAFFE data. Then small system-integral tests have been conducted to validate the degradation model. The GIRAFFE data are also applicable to the prediction of light non-condensable gas effects with small modification.

Next, a series of GIRAFFE system integral tests has been carried out to simulate thermal hydraulic behavior in the containment with the PCCS following a LOCA. The test results showed that the PCCS could successfully absorb and condense steam generated by decay heat and keep the containment pressure far below the design pressure in the presence of non-condensable gas.

TRAC could reproduce non-condensable behaviors and pressure responses observed in the GIRAFFE system integral tests. TRAC incorporating the GIRAFFE data was qualified to predict the PCCS performance following a LOCA in the presence of nitrogen. It also has the potential to predict PCCS performance under the conditions created by a severe accident.



DW: drywell,

U-: upper,

G: GIRAFFE,

SC: suppression chamber,

A-: annulus,

T: TRAC

FIG. 11. Containment pressure (left) and temperature (right) responses following an MSLB in the presence of helium [6].

REFERENCES

- [1] TOSHIBA, SBWR pamphlet, (1993)
- [2] TSUNOYAMA, S., YOKOBORI, S., ARAI, K., Development of passive containment cooling system, ARS'94 (1994) 240-248
- [3] NAGASAKA, N., YAMADA, K., KATOH, M., YOKOBORI, S., Heat removal tests of isolation condenser applied as a passive containment cooling system, ICON-1, Vol. 1 (1991) 257-263
- [4] YOKOBORI, S., TOBIMATSU, T., KURITA, T., OIKAWA, H., System response tests of passive containment cooling system (PCCS) heat removal performance against major three break scenarios, ICON-3, Vol.2 (1995) 1041-1046
- [5] ARAI, K., TRAC qualification for passive containment cooling system performance prediction against the GIRAFFE tests, ICON-3, Vol.2 (1995) 1035-1040
- [6] YOKOBORI, S., TOBIMATSU, T., KURITA, T., OIKAWA, H., System response tests of PCCS performance with light noncondensable gas considering severe accident conditions, ICON-3, Vol.2 (1995) 1047-1052
- [7] SPARROW, E. M., MINKOWYCZ, W. J., SADDY, M., Forced convection condensation in the presence of non-condensables and interfacial resistance, Int. J. Heat Mass Transfer, 10 (1967) 1829-1850
- [8] VIEROW, K. M., SCHROCK, V. E., Condensation in a natural circulation loop with noncondensable gases. Part I - Heat transfer, ICMF'91, Vol. 1 (1991) 183-186
- [9] UEHARA, H., MIYAYOSHI, A., NAKAGAWA, S., Gravity controlled film condensation on a vertical plate (Empirical equations for harmonic wavy and turbulent flow, Proc. 28th National Heat Transfer Symposium of Japan, Vol. III (1991) 883-891

APPLICATION OF METHODS IN DESIGN AND SAFETY ANALYSES

(Session 6)

Chairman

Y. Hassan
United States of America

NEXT PAGE(S)
left BLANK



UNCERTAINTY METHODOLOGY APPLIED TO LARGE BREAK LOCA ANALYSIS

C.F. FREIRE, E. KURAMOTO
Eletronuclear S.A.,
Rio de Janeiro, Brazil

G. SEEBERGER, S. BLANK
Siemens/KWU,
Erlangen, Germany

Abstract

The USNRC developed the Code Scaling, Applicability, and Uncertainty (CSAU) Methodology, which provides a formal structure for selecting a computer code to evaluate an event, establishing the adequacy of the performance of these uncertainties in the calculated results. Siemens/KWU and Eletronuclear had developed a methodology and adapted to Angra2 four loops PWR based on CSAU approach with some differences in the application of some steps. The uncertainties are grouped into three basic categories: code uncertainties, fuel uncertainties and plant uncertainties.

Code uncertainties are related to the capabilities to predicted basic key PWR Large Break Loss of Coolant Accident (LOCA) phenomenology. These uncertainties are included in the determination of uncertainties from assessment calculations against LBLOCA experiments and apply for PWR which are predicted to exhibit this basic LBLOCA phenomenology.

Fuel related uncertainties take in account core power, total power peaking factor, stored energy in fuel and decay heat.

Plant uncertainties relate to uncertainties in predicting the Peak Cladding Temperature (PCT) due to the design and operational characteristics of a specific PWR.

1. INTRODUCTION

This methodology is applied to 4-loop Angra2 PWR to demonstrate the realistic existing margin to the fuel cladding temperature limits and other licensing criteria in case of a LBLOCA and to remove unnecessary conservatism from the initial and boundary conditions of the analysis and hence of the analytical results [1]. The realistic LBLOCA methodology consists of the LOCA codes to be applied, the assessments which support the methodology, and quantification of the uncertainties. The result provides a range and distribution of blowdown and reflood peak cladding temperatures and provides a high probability that the 95/95% upper band (PCT) will not be exceeded in case of a LBLOCA and thus remains below 1200°C.

2. DESCRIPTION OF THE UNCERTAINTIES METHODOLOGY

The uncertainties methodology follows essentially the structured CSAU [2] approach, but differs from CSAU in the application of some of the steps. The uncertainties are grouped into three basic categories: code uncertainties, fuel uncertainties and plant uncertainties.

Code uncertainties relate to the capabilities to predict basic key PWR LBLOCA phenomenology. The uncertainties in fuel relate to the initial stored energy, however much of this uncertainty is due to the prediction of power during irradiation histories for the rods from which the data are derived. Thus, separation of fuel related uncertainties from the power uncertainties is not possible. Plant uncertainties relate to uncertainties in predicting PCT due to the design and operational characteristics of a specific PWR.

Some additional parameters related to uncertainties exist, which typically have been required by regulation to be run at combined worst case conditions. These are:

- Break size, break location
- Axial core power distribution
- Worst single failure and repair assumption
- Loss of offsite power
- Reactor Kinetics

Applying these boundary conditions and realistic ones for all other input parameters, results in the LBLOCA base case for which the sensitivity studies and the uncertainties analyses are performed.

The three elements of CSAU structure:

- Requirements and Code Capabilities,
- Assessment and Ranging Parameters, and
- Sensitivity and Uncertainty Analysis,

were evaluated to identify where these steps are addressed in the realistic LBLOCA methodology.

3. APPLICABILITY EVALUATION

The applicability of the Uncertainty methodology to the LBLOCA analysis for the Angra2 NPP strongly depends on the plant modeling, which has also to be consistent with those used for the validation calculations and the capability of the used code to represent the anticipated phenomena. The requirement of consistent nodalizations is based on the fact that the code uncertainties are determined from validation calculations and influences from different nodding methods must be excluded to the extent possible. The plant analysis must show all important phenomena expected during a LBLOCA.

To perform the LBLOCA analysis the codes S-RELAP5 [3], RODEX3 [4] and COCO [5] were used. The S-RELAP5 code, developed by Siemens, incorporates features of RELAP5/MOD2 and RELAP5/MOD3, and specific improvements. The RODEX3 calculates the initial fuel state at power and the transient fuel behavior. The cold initial fuel conditions at the burnup of interest for input to S-RELAP5 are computed using the realistic fuel performance from RODEX. Containment pressure boundary conditions during LBLOCA transient are provided by COCO, which is run concurrently with S-RELAP5 using realistic values for parameter input.

4. SELECTION AND QUANTIFICATION OF UNCERTAINTY PARAMETERS

The capability of the base RELAP5/MOD2 code to realistically calculate LOCA phenomena has been assessed by various organizations which have performed numerous analyses of many LOCA experiments and compared calculated results against experiments data. The RELAP5/MOD2 capabilities are inherent in S-RELAP5, and the generic

assessments of these features apply for S-RELAP5. The experiment data sets are used to support the PWR plant model nodalization scheme, to investigate the scale uncertainty, and to evaluate the code accuracy.

5. SENSITIVITY STUDIES

Based on the CSAU procedure the important phenomena are established from the Phenomena Identification and Ranking Table (PIRT). Parameters in the analyses codes and input used to compute these important phenomena are identified. Uncertainties in those identified parameters which significantly affect PCT's must be addressed in determining the overall model uncertainty. Sensitivity studies are used to determine which parameters are significant and must be addressed regard to uncertainties. The analyses performed for Angra2 NPP have shown that PCT is the most limiting of the licensing criteria, and therefore cladding temperature is the criterion used to determine significance of a parameter variation from the sensitivity studies.

5. ANALYSIS OF UNCERTAINTIES

The 95% probability upper bound PCT's were generated by using Monte Carlo calculations to convolve uncertainties from three sources. The three sources of uncertainties which were convolved in the Monte Carlo calculations are: (1) The integral uncertainty parameter generated by comparison of S-RELAP5 to LOFT and CCTF experimental data, (2) Parameter which are important to PCT, but are not included in the integral uncertainty parameter, and (3) Additional uncertainties which are of lesser importance to PCT, and are not included in the integral uncertainty parameter. Parameters which are important to PCT but not included in the integral uncertainty parameter were treated by generating blowdown and reflood PCT response surfaces. The integral uncertainty factor and the additional uncertainty parameters were used which the response surfaces in the Monte Carlo calculations to generate upper 95% probability blowdown and reflood PCT's.

Monte Carlo calculations were performed for both blowdown and reflood using 50000 trials for each of the calculations. In each trial, each of the parameters used in the response surface, including the term which accounts for the fit, the integral uncertainty factor, and the additional uncertainties factor parameters were sampled from their respective distributions, and the resultant PCT was tabulated. The blowdown calculation Monte Carlo frequency distribution for total PCT uncertainty is shown in Fig. (1), and the cumulative distribution is shown in Fig. (2). The reflood calculation Monte Carlo frequency distribution for total PCT uncertainty is shown in Fig. (3), and the cumulative distribution is shown in Fig. (4).

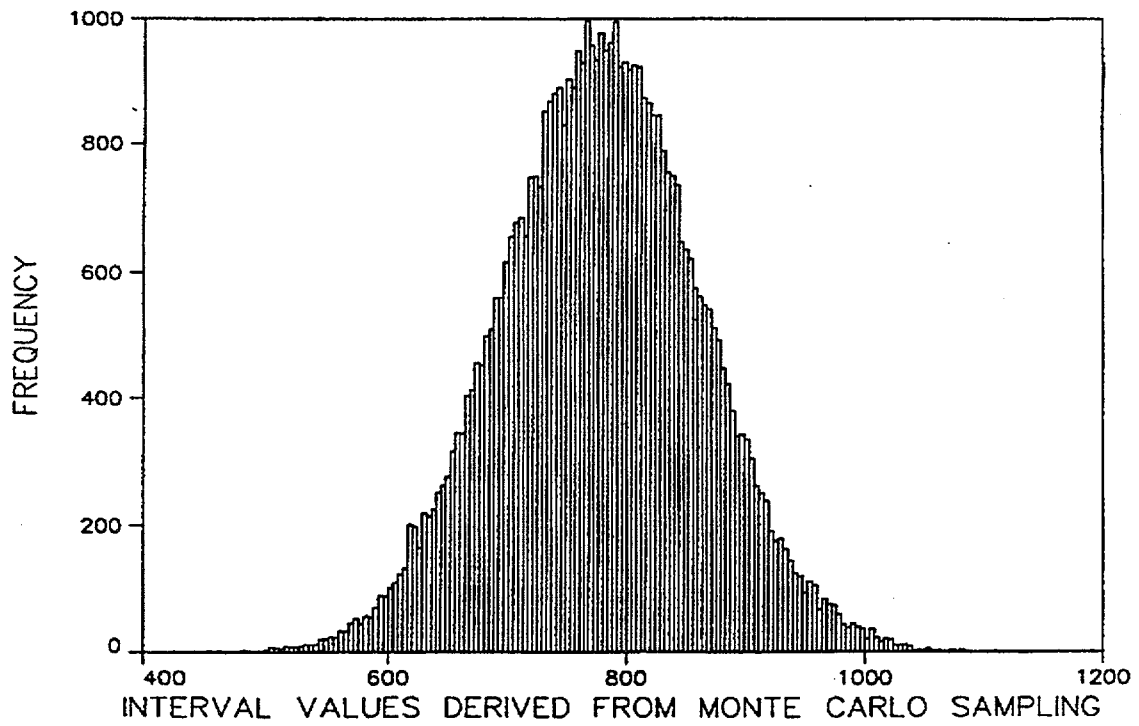


Fig. 1: Blowdown total PCT (°C) uncertainty frequency distribution.

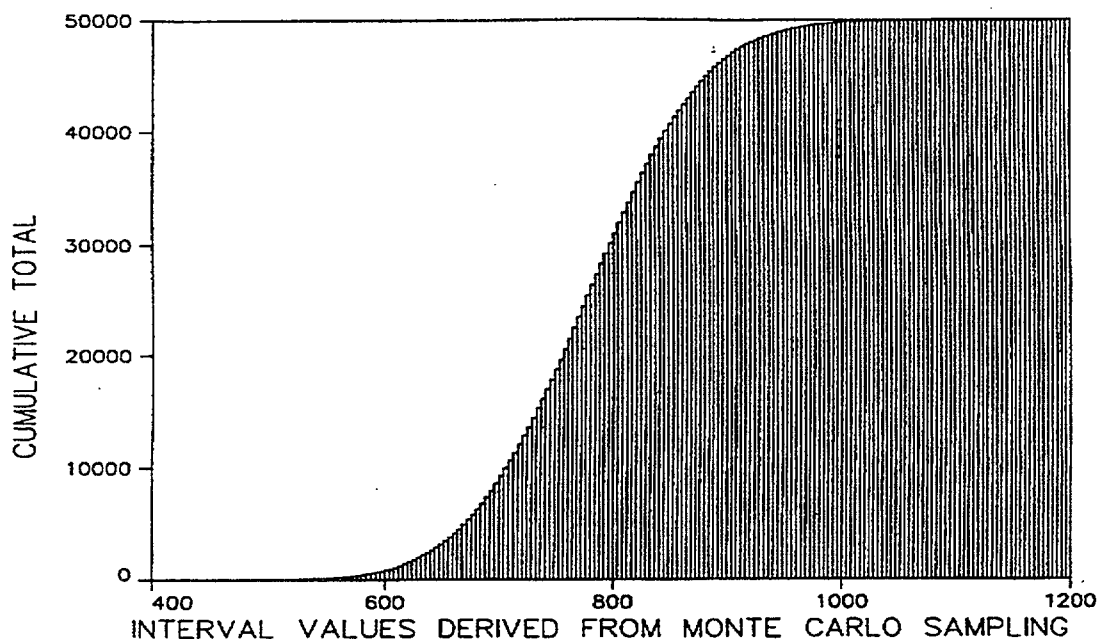


Fig.2: Blowdown total PCT (°C) uncertainty cumulative distribution.

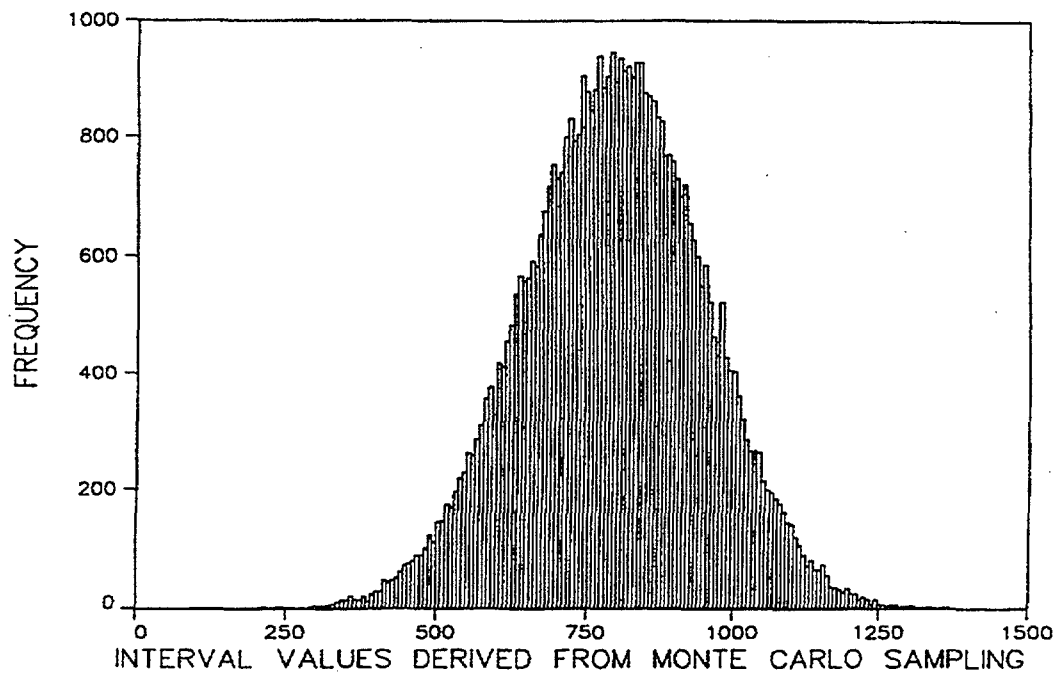


Fig. 3: Reflood total PCT ($^{\circ}\text{C}$) uncertainty frequency distribution.

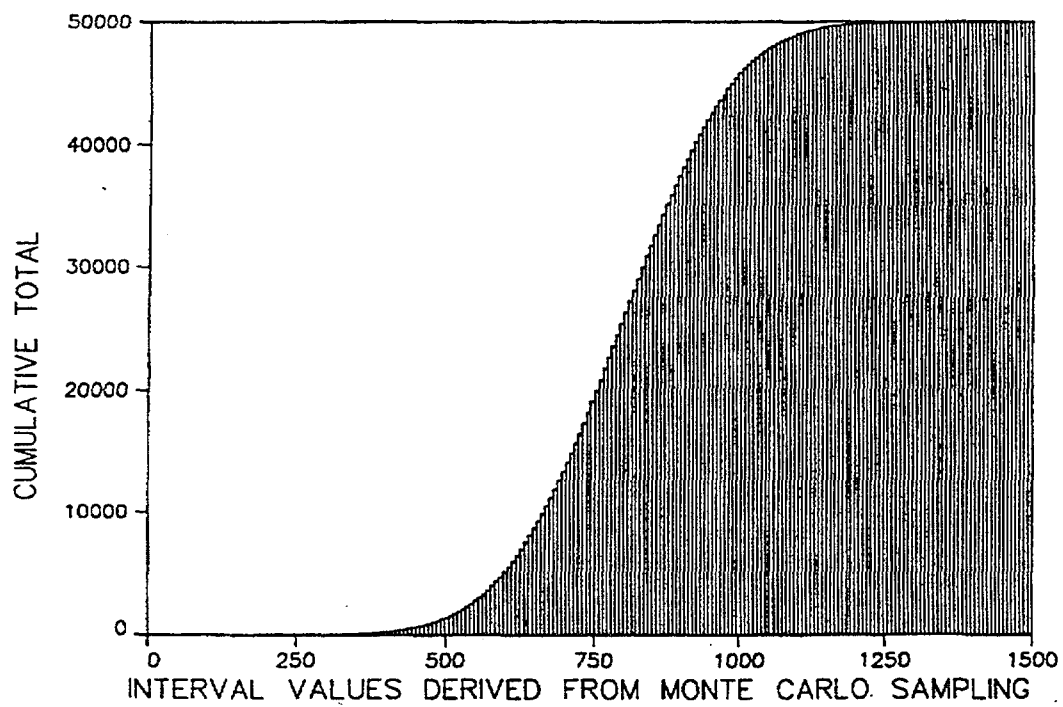


Fig. 4: Reflood total PCT ($^{\circ}\text{C}$) uncertainty cumulative distribution.

6. CONCLUSIONS

The analyses result in a PCT of 915 °C for the blowdown and 1046 °C for the reflood phase, which considers the 95% confidence bounds on the 95% probability point. For the determination of the cladding oxidation a deterministic approach was used. For the combination of maximum reactor power, maximum initial stored energy, maximum linear heat generation rate and decay heat according to DIN 25463+2 σ the maximum local oxidation depth is 9.34 μ (1.3%). The total cladding material oxidation for this rod is 0.53%, the total oxidation for an average rod is only 0.15%. Hence, is proved that the entire cladding material oxidation is less than 1%.

From this it can be concluded that the Angra2 NPP emergency core cooling system is designed sufficiently to keep the peak cladding temperature and the local and total oxidation rate in case of a LBLOCA clearly bellow the required licensing limits.

REFERENCES

- [1]SEEBERGER, et al, "Efficiency of the emergency core cooling system in case of large break LOCA for NPP Angra2 considering the analysis uncertainty", Siemens WR NDS1/97/E2125a, 04/09/97
- [2]USNRC, NUREG/CR 5249 EGG-2552, "Quantifying reactor safety margins, application of code scaling, applicability, and uncertainty evaluation methodology to large break LOCA", December 1989.
- [3]DEPISCH, S.; "RELAP5 Manual: code description system models and solution methods", Siemens TR NDS1/95/E2125, 13/12/95.
- [4]MERCKX, et al, "RODEX3 fuel rod thermal-mechanical response evaluation model", Advanced Nuclear Fuels Company, March 1991.
- [5]MASSIG, "COCO – A computer program for analyzing changes in pressure, temperature, and humidity in a containment building and for designing the containment building for loss of coolant accidents", Siemens/KWU R61,62/83/E007.

APPLICATION OF DATA ANALYSIS TECHNIQUES TO NUCLEAR REACTOR SYSTEMS CODE TO ACCURACY ASSESSMENT

R.F. KUNZ, G.F. KASMALA, C.J. MURRAY, J.H. MAHAFFY
Applied Research Laboratory,
Pennsylvania State University,
University Park, Pennsylvania,
United States of America



XA0055032

Abstract

An automated code assessment program (ACAP) has been developed by the authors to provide quantitative comparisons between nuclear reactor systems (NRS) code results and experimental measurements. This software was developed under subcontract to the United States Nuclear Regulatory Commission for use in its NRS code consolidation efforts. In this paper, background on the topic of NRS accuracy and uncertainty assessment is provided which motivates the development of and defines basic software requirements for ACAP. A survey of data analysis techniques was performed, focusing on the applicability of methods in the construction of NRS code-data comparison measures. The results of this review process, which further defined the scope, user interface and process for using ACAP are also summarized. A description of the software package and several sample applications to NRS data sets are provided. Its functionality and ability to provide objective accuracy assessment figures are demonstrated.

1. INTRODUCTION

In recent years, the commercial nuclear reactor industry has focused significant attention on NRS code accuracy and uncertainty issues. There are several reasons for this including the inherent safety (and concomitant code reliability and licensing) concerns associated with nuclear reactors. Over a decade ago, the United States Nuclear Regulatory Commission (hereafter NRC) initiated an international effort to improve and standardize the assessment of thermal hydraulic (TH) systems codes ([1, 2], for example). Prior to that, processes for assessing the performance of TH codes were largely qualitative and subjective, and thereby difficult to use in plant safety certification. In 1984, the NRC organized the International Thermal Hydraulic Code Assessment and Applications Program (ICAP), a major goal of which was the assessment of TH codes using relevant data from a wide range of international experimental facilities. Since that time, a large amount of work has been carried out domestically and internationally in this area (see [3-9], for examples).

In 1997, the NRC contracted with the present authors to:

- 1) Survey available data conditioning and analysis techniques, focusing on their appropriateness in NRS code accuracy and uncertainty assessment
- 2) Develop software to deploy recommended techniques

This software was to be used for validation in NRC code consolidation efforts and have the potential to be expanded to play a role in determining code adequacy. The ACAP software described herein represents the outcome of this code development effort.

2. NRS CODE ACCURACY ASSESSMENT

2.1. Issues and needs

The issues associated with nuclear reactor systems (NRS) code accuracy and uncertainty assessment are numerous and complex. They include:

- 1) Scaling of test data.
- 2) Discretization, model setup and other "user issues".

- 3) Software reliability.
- 4) The move towards best estimate vs. conservative acceptability criterion in licensing decisions.
- 5) Key parameter selection.
- 6) The wide variety and complex features of the modeled transient physics and experimental data.
- 7) The inconsistency of measured and computed comparison quantities.
- 8) The inherent subjectivity of code – experimental comparisons.
- 9) Uncertainty in experimental measurements.
- 10) The large and growing available test matrix data base.
- 11) The lack of a generally applicable suite of code-data assessment tools.

These issues collectively motivate the need for automated code assessment in code consolidation and future development efforts. Ideally, in the future, when assessing a systems code, a single post-processor would be deployed. Based on *all* uncertainties involved, this post-processor would return, at a given confidence level, the maximum expected deviation between code results and reactor for several key parameters [3]. The methodologies embodied in this “ideal” post-processor must address each of the uncertainty components summarized above. The need for such a capability, has motivated a vast amount of research in the past decade (see [4] for a review of much of this work).

Though significant progress has been made in addressing most assessment issues, reliable and general tools to quantify NRS code accuracy are not available today. An important contribution to meeting this ideal would be a universally available assessment tool for the users of NRS codes to post-process results in a way that would return quantitative accuracy measures of code-data comparisons. Such a tool would only address some of the uncertainties in real plant analysis. However, it would be part of a process which validates a code with scaled facility data, contributing an important component to total uncertainty in full scale plant simulations.

Consistent with this view, the goal of the present work has been to initiate a software framework to automatically assess several of the NRS code uncertainty issues summarized above. In particular, the ACAP software package has been developed to objectively and quantitatively compare NRS simulations with data. This package was designed to:

- Draw upon a mathematical toolkit to compare experimental data and NRS code simulations.
- Return quantitative figures of merit associated with individual and suite comparisons.
- Accommodate the multiple data types encountered in NRS environments.
- Incorporate experimental uncertainty in the assessment.
- Reduce subjectivity of comparisons arising from the “event windowing” process.
- Accommodate inconsistencies between measured and computed independent variables (i.e. different time steps).
- Tie into data bases of NRC test data and code results.
- Provide a framework for automated, tunable weighting of component measures in the construction of overall accuracy figures of merit for a given comparison.

So the ACAP tool has been developed to address issues 6-11 summarized above. The scope of this project did *not* include the quantification of the uncertainties introduced by user training issues, discretization issues or code operational issues. Nor has the present work addressed quantification of uncertainty associated with physical models being used on a best estimate basis, nor on scaling uncertainties. However, the present investigators feel that with modest modifications the package could be applied parametrically to complement uncertainty assessment in each of these other areas.

In summary, our fundamental goal has been to develop a numerical toolkit to analyze discrete computational and experimental NR systems data, and, in particular, to use these data analysis procedures to develop code-data and code-code comparison measures. The remainder of this paper summarizes this development effort.

2.2. Categorization of NRS data

NRS data types are classified here into five categories, in order to provide a basis for assessing individual comparison methods. Specifically, scaled NR facilities are instrumented to provide a fairly wide array of key parameter and other data. These include:

- I. Key parameters tables.
- II. Timing of events tables.
- III. Scatter plots of nominally 0-D data (e.g., see Figure 4)¹.
- IV. 1-D (in space) steady state data.
- V. Time record data (e.g., see Figure 5).

Each of these data types is potentially important in any particular NRS code analysis. The emphasis of the ACAP project is on the latter three. In particular, data conditioning and analysis techniques were assessed and deployed within ACAP for code-data comparisons of data Types III, IV and V. Type V data in particular provides a significant challenge for several reasons:

- 1) The ubiquitous appearance and relevance of these transient data in NR systems.
- 2) The typically long record (often $O(10^5)$ time steps) nature of these data, complicated significantly by their *non-stationarity* and *diversity in characteristic features* (long time scale damping, local quasi-periodicity, sudden changes due to active or passive phenomena, chatter (often of high amplitude), dependent variable limits (for volume fraction) between 0 and 1).
- 3) The fairly significant differences that often appear between computed and measured time trace data (e.g., see Figure 5).

2.3. Data analysis methods

Discrete data analysis is an important element in a wide array of technical disciplines. Techniques to analyze data samples or records lie within the scope of the three overlapping fields: probability and statistics, approximation theory, and time-series analysis. Also, the needs of several engineering and scientific communities have motivated the development of data analysis techniques, which although falling within the three general categories mentioned, are characterized by unique or extended features of relevance to the present research. In particular, methods developed in atmospheric/geologic sciences, economic forecasting, aerodynamic stability, demographics, digital signal processing, pattern (i.e., speech/optical/character) recognition and other fields have relevance to the analysis of NRS data, and could be plausibly adapted to construct systems code-data or code-code comparison measures.

A number of mathematical data analysis methods from these various fields were reviewed for their applicability in the construction of NRS code-data and code-code comparison measures. The goal of the review was to identify issues and techniques to be considered in the development of an automated simulation rating procedure. Details of that review are the subject of a forthcoming publication. These findings defined the scope, user interface and a recommended process for using ACAP. A summary of these issues and findings is provided here:

- 1) Most of the methods considered can be applied to provide useful quantitative measures of accuracy for at least a subset of NRS data Types III, IV and V.
- 2) Inappropriate use of some methods can yield incorrect results, that is, return figures of merit that are worse for more accurate simulations. This motivates:
 - Definition of a *robust* comparison measure or suite of measures as one that reliably return bet-

¹ Often these data are rendered “0-D” by collapsing data obtained at multiple space-time coordinates to a single scatter plot.

ter figures-of-merit for superior comparisons and worse figures-of-merit for inferior comparisons.

- That great care be taken in the selection of the suite of analysis tools chosen *for each particular comparison*.
- 3) The inherent limitations to stationary data of most available methods render straightforward application to NRS Type V data less than rigorous. Trend removal techniques can be brought to bear to preprocess the data, thereby yielding more robust comparison measures, especially when deployed in concert with time-windowing.
- 4) Experimental uncertainty can be effectively incorporated in code-data accuracy assessment within the framework of the “toolkit” of analysis procedures considered. Experimental uncertainty should be included with the “raw” experimental data in the code reassessment test matrix.
- 5) Inconsistency between the computed and measured independent variable range and basis (i.e. different time steps) motivates the incorporation of resampling and range trimming conditioners within ACAP. Such “synchronization” is required for most comparisons.
- 6) For Type V data, techniques that are intrinsically appropriate for *non-stationary* data analysis can be utilized in the construction of comparison measures. These include best approximation fits and, most promising in the view of the present investigators, time-frequency techniques.
- 7) There is a fundamental lack of rigor in applying basic statistical analysis procedures to most NR systems data. This arises due to non-stationarity of the data and the unavailability of a known distribution of error about its mean. This renders the construction of statistical *inference* measures suspect at best. Basic statistical difference and correlation measures can be deployed to construct *useful* figures of merit, but uncertainty bounds should not be inappropriately constructed.
- 8) The methods vary widely in range/dimensionality of their returned metrics. This complicates the definition of an overall figure-of-merit, and thereby motivated normalization and range limit scaling in constructing component figures of merit. Specifically, each individual comparison measure is redefined to range from 0 to 1.
- 9) As indicated in conclusion 2 above, great care must be taken in deploying comparison measures. In particular, for each experimental data set, a demonstrably robust assessment strategy must be developed. The present investigators feel that this requirement defines a *process* whereby expert assessors “calibrate” and document a suite of robust data analyses for each experimental data set in the code reassessment matrix. This assessment *configuration* will in general include preconditioning strategies, data comparison measures, figure-of-merit weighting assembly factors, and should be included with the “raw” experimental data in the reassessment matrix. Such configured assessments will then be used to define ACAP sessions in future code *re-assessments*.

In concert with the above design criteria and method assessment findings, a set of baseline techniques for code-data (or code-code) comparisons, data preconditioning, figure-of-merit-assembly and incorporation of experimental uncertainty were selected and implemented in ACAP. These are listed below. For brevity, the details of the mathematics associated with these methods are not provided in this paper - the reader is referred to forthcoming references including the formal documentation of ACAP.

3. OVERVIEW OF ACAP

3.1. Program description and mechanics

ACAP is a PC and UNIX station based application which can be run interactively on PCs running WINDOWS 95/98/NT or in batch mode on PCs as a WINDOWS console application or in batch mode on UNIX stations as a command line executable. The code will be delivered to NRC with full source code. The interactive and batch PC versions can be modified and recompiled from a WINDOWS “folder” under the Microsoft Visual C++ environment. The batch UNIX version can be modified and recompiled using any C++ compiler which conforms to the C++ draft standard (including the freely available g++/gcc compilers).

A brief summary of the operation of the ACAP is provided here. Figure 1 shows a schematic overview of the structure of the code. Experimental and computational NRS data are input through ACAP data files, which, in their simplest form, contain a table of x-y data and a few data descriptor keywords. The user specifies, either interactively or through front end script files, a suite of data conditioning and data analysis methods to be deployed in quantifying the correspondence between the measurements and the (one-or-more) simulation data sets. This suite of methods is termed the ACAP *configuration*, which can be saved in a file for later use on the current or other data sets. In interactive mode, ACAP displays the data sets and provides standard windows environment interfaces to select and adapt the mathematical methods to be deployed. The code then executes specified data conditioning processes and data comparison measures. Lastly, with user selected weighting, an overall figure-of-merit is constructed quantifying the accuracy of the individual code runs. The results of the ACAP session, including a summary of all selections made, and the component and overall figures-of-merit are output to screen and file.

ACAP is also currently being incorporated within a global auto-validation tool, being developed by Scientech Inc., under separate contract to NRC. That tool automatically runs systems code simulations for a (growing) palette of test cases and generates a prespecified series of plots which include experimental measurements and the results of the multiple simulation runs. ACAP will be invoked in batch mode from this auto-revalidation tool to provide concomitant quantification of the correspondence between each simulation run and, where available, experimental measurements.

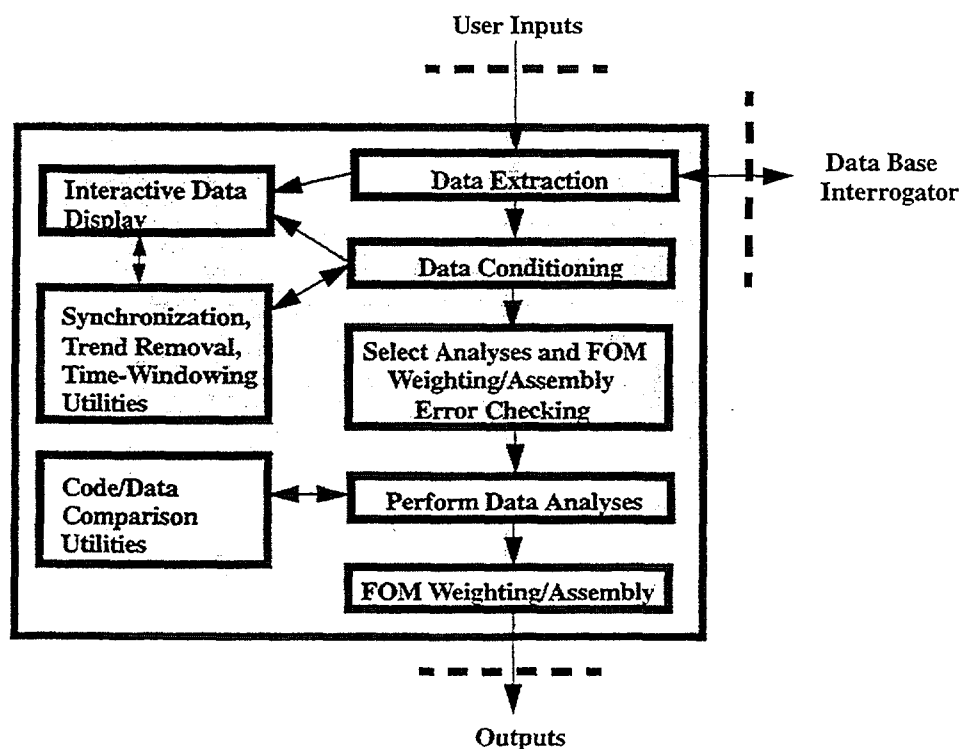


Figure 1. Schematic overview of the structure of ACAP.

3.2. ACAP Methods

Table I summarizes the methods currently installed in ACAP. There are three data conditioning utilities and sixteen data comparison utilities.

Table I. ACAP Methods

	Method	Utility Class
1	D'Auria FFT (DFFT)	Data Comparison Utility
2	Mean Error (ME)	Data Comparison Utility
3	Variance of Error (VE)	Data Comparison Utility
4	Mean Square Error (MSE)	Data Comparison Utility
5	Mean Error Magnitude (MEM)	Data Comparison Utility
6	Mean Relative Error (MRE)	Data Comparison Utility
7	Index of Agreement (IA)	Data Comparison Utility
8	Systematic Mean Square Error (SMSE)	Data Comparison Utility
9	Unsystematic Mean Square Error (UMSE)	Data Comparison Utility
10	Mean Fractional Error (MFE)	Data Comparison Utility
11	Cross-Correlation Coefficient (ρ_{xy})	Data Comparison Utility
12	Standard Linear Regression (L_2 -standard)	Data Comparison Utility
13	Origin Constrained Linear Regression (L_2 -constrained)	Data Comparison Utility
14	Perfect Agreement Norm (L_2 -perfect agreement)	Data Comparison Utility
15	Continuous Wavelet Transform (CWT)	Data Comparison Utility
16	Percent Validated (PV)	Data Comparison Utility
A	Resampling	Data Conditioning Utility
B	Trend Removal	Data Conditioning Utility
C	Time-Windowing	Data Conditioning Utility

Among the data *comparison* utilities, the reader will likely recognize the FFT method of D'Auria [5]. Also available are a number of baseline statistical techniques (methods 2-5, 11-14), Willmott's Index of Agreement (method 7, [10]) and several adapted statistical methods utilized by the atmospheric sciences community (methods 6, 8-10, see [11] for example). Experimental uncertainty is incorporated in a fashion consistent with recent computational fluid dynamic (CFD) code validation work undertaken by Coleman and Stern [12], where a "Percent Validated" metric (method 16) is defined from the fraction of simulation data in a trace which falls within the uncertainty bands of the measurements.

In the authors' view, a particularly attractive comparison tool for NRS code accuracy assessment is the continuous wavelet transform (CWT) measure installed in ACAP (method 15), and some further discussion of this method is provided here. Wavelet transforms are time-frequency techniques which are directly applicable to non-stationary data. As such, if applied consistently, they can provide more accurate representation of local features in a time trace than global transforms (such as the FFT), especially when important features appear at widely varying time scales (as is characteristic of NRS data traces, e.g., see Figure 5). Also, a variety of CWTs are available, each targeting particular features in a signal (the *Morlet* wavelet is implemented in the first ACAP release.)

The available data *conditioning* utilities include particular choices of resampling, trend removal and time windowing methods. A number of authors have observed the usefulness of time-windowing of transient NRS data in order to isolate distinct physical processes, and thereby provide a more focused assessment of simulation strengths and weaknesses. In ACAP, the user may specify up to six time windows. For each window, a fully configured ACAP session is specified. Individual figures-of-merit are computed for each window and a global figure-of-merit is constructed based on a weighted sum of these contributions.

As mentioned above, resampling of the computed data traces is usually appropriate in order that the experiment and simulation have a consistent independent variable basis (i.e. time steps). This issue is relevant only to Types IV and V data where discretization choices and/or numerical stability issues will generally give rise to NRS predictions of dependent variables at different locations in space-time than where the data was taken. Basis consistency is required for all data comparison utilities except methods 1, 8, 15 and 16, though the DFFT and CWT methods can be more accurately deployed if samples are taken at the same time steps. Also, valid application of some trend removal processes, including running averages, require independent variable consistency. As illustrated below, ACAP provides a palette of resampling options to perform this task.

As also mentioned previously, trend removal techniques can be useful in analyzing non-stationary NRS data. For example, a computed time trace may be characterized by a relatively constant underprediction of, say, pressure and also exhibit higher frequency oscillatory differences from measurements. The authors have found that deploying a trend removal step allows these separate effects to be analyzed individually resulting in a more robust code-data comparison configuration. A running-average smoother is installed in ACAP for trend definition and the mechanics are available to separately analyze both differences in the trend itself and in the more nearly stationary “low-pass-filtered” traces. Generally, different data comparison utilities are deployed for the trend and filtered traces, consistent with their differing features and stationarity.

Another issue related to the baseline ACAP methods, mentioned above, is the widely varying range and dimensionality of the various data comparison measures. This complicates the definition of an overall figure-of-merit, and thereby motivated normalization and range limit scaling in constructing component figures of merit. Specifically, each individual comparison measure was redefined to range from 0 to 1, corresponding to worst possible and best possible agreement between a given computed trace and experiment. The process implemented to do so comprised two steps. First, all dimensional figures-of-merit are non-dimensionalized with respect to the experimental dependent variable range $|O_{\max} - O_{\min}|$. This “sizes” the different metrics such that $O(10^0)$ errors (i.e. order of 100 % errors) between traces will give rise to $O(10^0)$ metric values. The second step is to, where necessary, modify these “sized” metric definitions so that they independently return figures of merit between 0 and 1. Several of the comparison metrics have ranges between 0 and ∞ or $-\infty$ and ∞ . For all of these except the DFFT and CWT measures, a method for achieving the desired range of [0,1] is implemented, somewhat arbitrarily, as $FOM = 1/(|\eta|+1)$, where η is the non-dimensionalized metric. The DFFT, CWT, MRE and ρ_{xy} metrics require somewhat different treatment, the form of which will be available in forthcoming references including the formal documentation of ACAP. Since chosen normalization and range limit scaling of the data comparison utilities in ACAP are somewhat arbitrary, ACAP users may wish to invoke alternate definitions or simply consider the “raw” metrics returned by the baseline methods. This latter option is available in the code, the former would require some modest C++ code modifications.

4. SAMPLE ACAP SESSIONS AND RESULTS

To date, ACAP has been deployed on a large number of test cases, as we evolve the capabilities of, and our own experience with, the tool. Several example applications are presented in this section. The purpose of these demonstration cases is to illustrate the functionality of the code and its ability to provide objective accuracy measures.

4.1. D’Auria sample experimental and calculated time traces

The functionality of ACAP is demonstrated using the D’Auria “sample” data used by the University of Pisa group in numerous recent publications ([5], for example). This data (which was digitized here from the cited reference) provides one experimental and six representative “systems code” data traces. This artificial data was originally constructed to capture several features of typical NRS transients, as well as the widely varying differences between simulation and experiment that can occur.

The data was input to ACAP and displayed graphically as reproduced in Figure 2. Four component figures-of-merit were chosen: DFFT, MSE, ρ_{xy} and CWT. These were selected and each given a

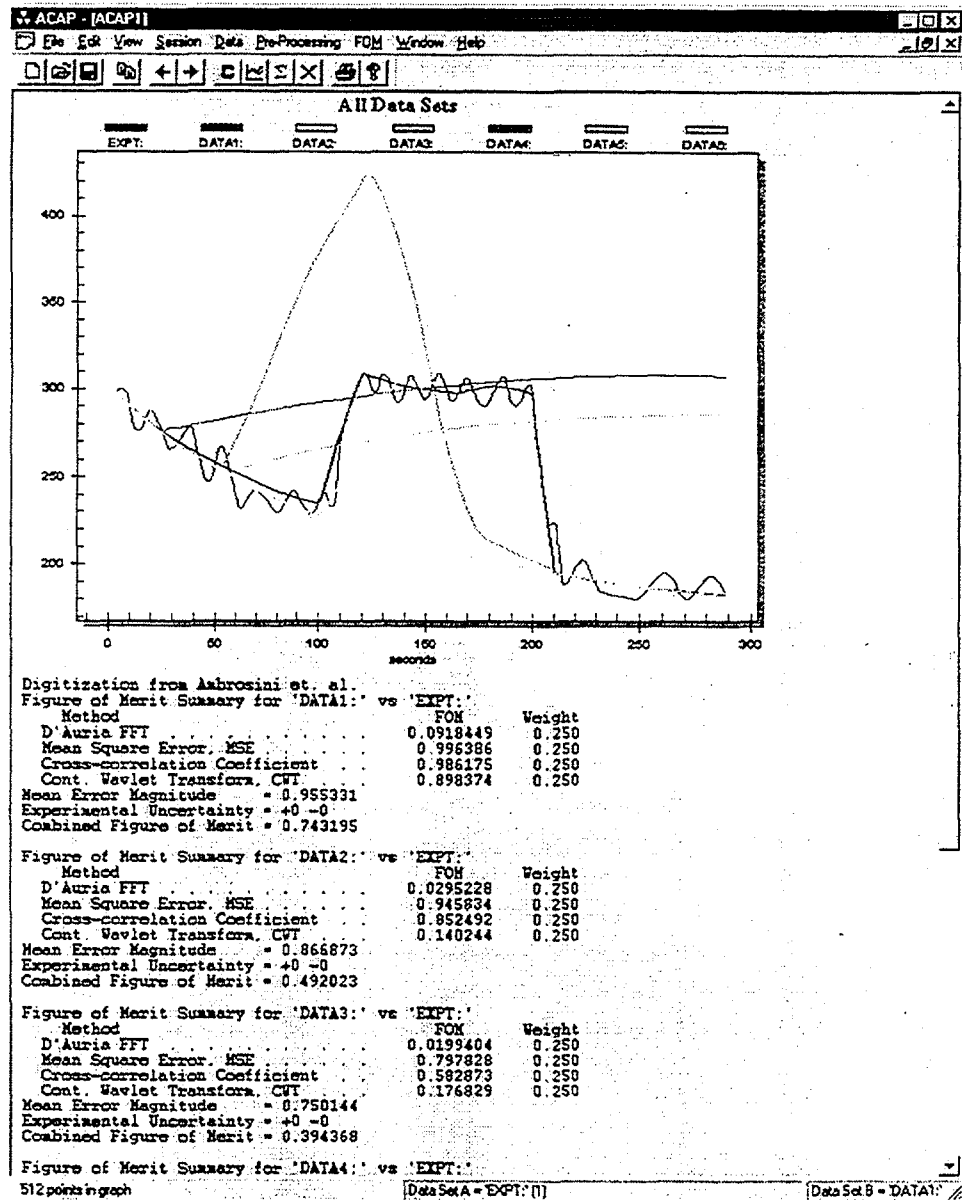


Figure of Merit Configuration

Methods

Measure	Weight	Measure	Weight
<input checked="" type="checkbox"/> D'Auria FFT	[0.25]	<input type="checkbox"/> Constrained Linear Reg. (L2)	
<input type="checkbox"/> Mean Error, ME		<input type="checkbox"/> (Predicted - Perfect) Norm (L2)	
<input type="checkbox"/> Variance of Error, VE		<input type="checkbox"/> Percent Validated, PV	
<input checked="" type="checkbox"/> Mean Square Error, MSE	[0.25]	<input checked="" type="checkbox"/> Cont. Wavelet Transform, CWT	[0.25]
<input type="checkbox"/> Mean Error Magnitude, MEM			
<input type="checkbox"/> Mean Relative Error, MRE			
<input type="checkbox"/> Index of Agreement, IA			
<input type="checkbox"/> Systematic MSE, MSEs			
<input type="checkbox"/> Unsystematic MSE, MSEu			
<input type="checkbox"/> Mean Fractional Error			
<input checked="" type="checkbox"/> Cross-correlation Coefficient	[0.25]		
<input type="checkbox"/> Standard Linear Regression (L2)			

Experimental Uncertainty: + [0] - [0]

Reference Offset: [0]

Select All Reset Weights Normalize

OK Cancel Help

Resampling parameters

Interpolation Method

☒ Linear

☐ Cubic spline

Independent Variable

☒ Unrestricted

☐ Overlapping range of all sets

☐ Full extent of all sets

☐ Set A range (uniform sampling)

☐ Set A sample points

Independent Variable Min. [0]

Independent Variable [288.5]

Number of samples in new sets [512]

☐ Round up to power of 2

OK Cancel Help

Figure 2. Elements of ACAP Interface. a) D'Auria data displayed in ACAP main window with results of comparison assessment for sample "code" results. b) Figure-of-merit configuration dialog. c) Resampling dialog.

weight of 0.25 in the *Figure of Merit Configuration* dialog box, as also shown in the figure. The assessment analysis was then run and the results displayed below the data plot. For the rather arbitrary selections made here, ACAP returns consistently superior component and overall figures-of-merit for sample trace 1. The CWT measure is illustrated in Figure 3, where the locus of points generated by the CWT for each time trace is plotted in the AA (average amplitude), 1/WF (inverse frequency) plane. The percentage of points within the illustrated acceptance boundary defines the figure-of-merit.

4.2. Type III data assessment

In order to illustrate the use of ACAP for producing figures-of-merit for Type III data, use is made of an, as yet, unpublished two-phase pressure drop analysis performed at Penn State. Several different popular empirical correlations were used to predict the two-phase pressure drop for water flowing upwards through a heated tube at 1000 psia. Comparisons were made against experimental data from [13]. Figure 4a shows a predicted vs. measured scatter plot comparison of the experimental data against Martinelli-Nelson correlation predictions. Figure 4b shows a similar comparison using results from the Freidel empirical correlation.

Visual inspection of the data illustrates that the Freidel model is clearly more accurate over the entire range of pressures analyzed. The issue here is whether this behavior can be captured quantitatively through some figure-of-merit strategy using ACAP. After importing the relevant data into the code, the ACAP session was configured to make use of the metrics that may reasonably be applied to Type III data. No data preconditioning was necessary because the data were already synchronized before being imported into the code. Table II provides a summary of the individual figures-of-merit returned by ACAP for each metric, the weighting factors used, and an overall assessment value, for each pressure drop correlation.

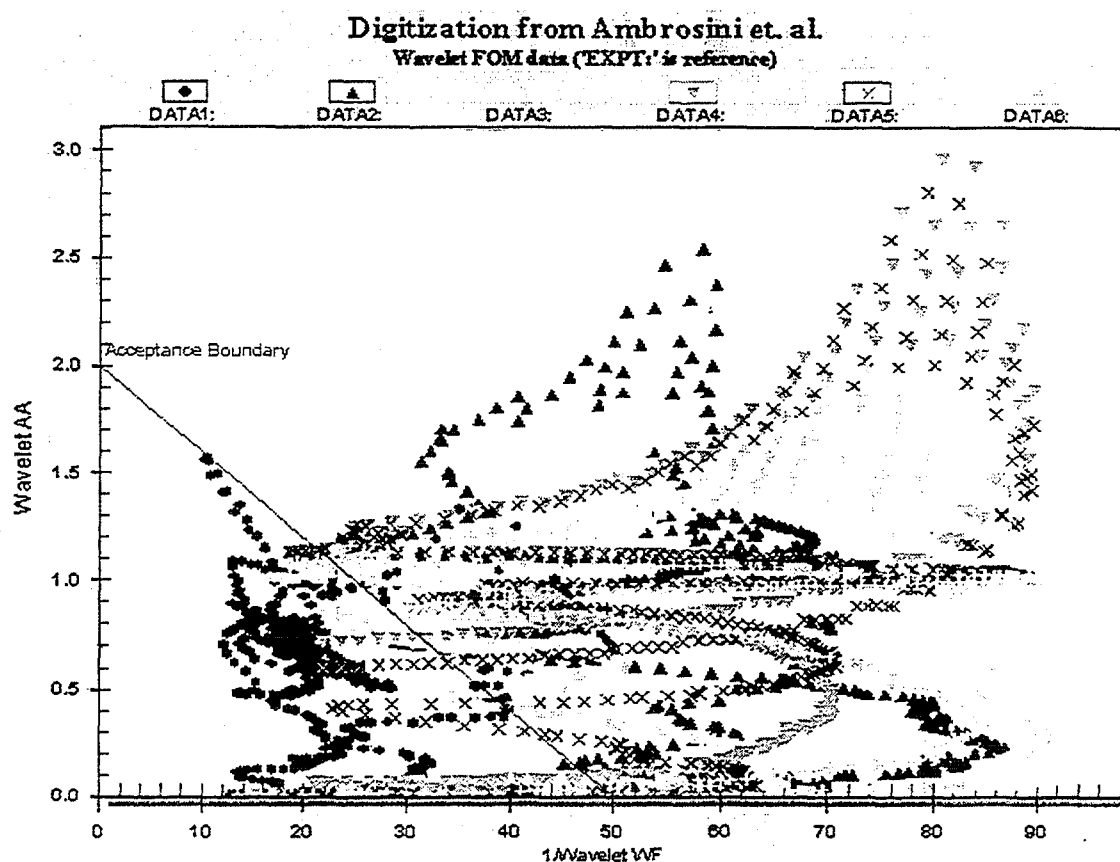


Figure 3. Display of continuous wavelet transform applied to D'Auria data, illustrating locus of points in AA-1/WF plane and acceptance boundary.

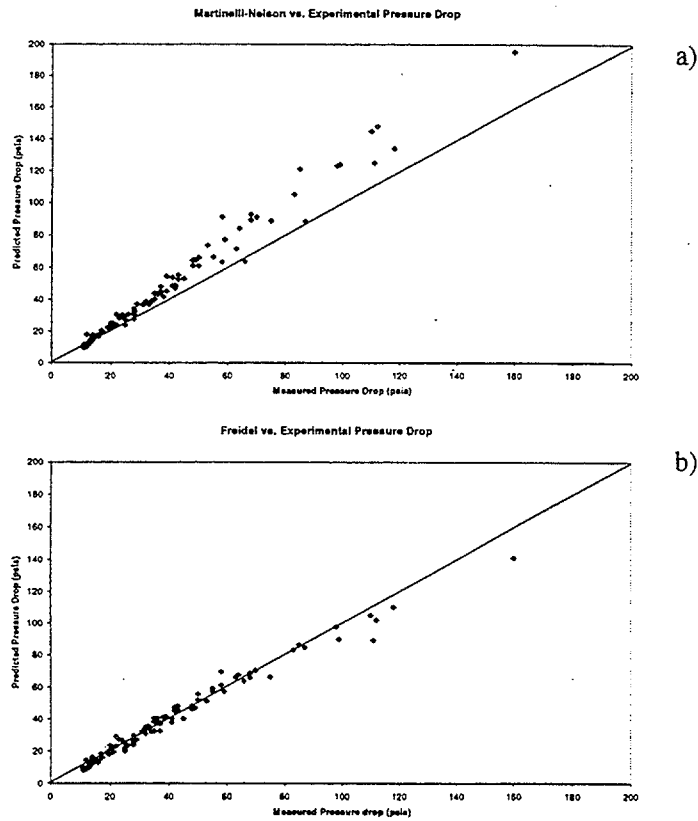


Figure 4. Sample Type III data comparisons. Predicted vs. measured scatter plot comparison of pressure drop experimental data [13] against a) Martinelli-Nelson correlation predictions and b) Freidel empirical correlation.

Table II. Comparison of ACAP Results for Presented Type III Data

Method	M-N Model	Freidel Model	Weight
Mean Error	0.948	0.995	0.077
Variance of Error	0.996	0.999	0.077
Mean Square Error	0.994	0.999	0.077
Mean Error Magnitude	0.947	0.980	0.077
Mean Relative Error	0.923	0.984	0.077
Index of Agreement	0.965	0.993	0.077
Systematic Mean Square Error	0.956	0.999	0.077
Unsystematic Mean Square Error	0.974	0.999	0.077
Mean Fractional Error	0.484	0.882	0.077
Cross-Correlation Coefficient	0.990	0.989	0.077
Standard Linear Regression	0.984	0.997	0.077
Origin Constrained Linear Regression	0.996	0.997	0.077
Perfect Agreement Norm	0.992	0.997	0.077
Combined Figure-of-Merit	0.935	0.986	

For each method, except one, the figures-of-merit are seen to be closer to unity for the Freidel case, indicating better agreement to the experimental data. The exact sensitivity of a particular metric to changes in the pressure drop correlation is seen to vary significantly. In some cases, the figures-of-merit only differ in the third decimal place while for others, the differences occur in the first or second decimal place. While it is not the purpose of this paper to present a detailed discussion of this behavior, these differences in sensitivity derive, in part, from the ability, or lack thereof, of a particular metric to capture a particular trait of the data set. For example, the closely corresponding values of the ρ_{xy} and L_2 -constrained metrics suggest that both models *correlate* quite well with data. Taken with the significant differences in MFE, which is a good measure of *bias* in the predictions, one can conclude that the shortcomings of the Martinelli-Nelson model are principally due to a consistent over-prediction of the pressure drop. These observations, and other which can be drawn from the results in Table II, illustrate the utility of selecting multiple figures-of-merit to capture different features in NRS code comparisons. Here, equal weighting was arbitrarily given to each method in constructing the overall merit value. In general, when constructing figure-of-merit configurations, the user would need to analyze the data, identify the traits which need to be captured, and make appropriate decisions as to which metrics ought to be used and how they should be weighted.

4.3. Type V data assessment

This next example illustrates the use of ACAP with Type V data. Figure 5 shows a comparison between the predicted and measured rod surface temperature at a particular axial level during the core heatup and reflood stages of a FLECHT SEASET vs. TRAC-B simulation [14]. Two different reflood heat transfer models within TRAC-B were deployed - the original and a newer model.

Again, after importing the relevant data into the code, methods were selected to construct a figure-of-merit. In particular, most of the metrics used in the previous example were retained and the DFFT and CWT methods were also implemented. Because the data were not synchronized before being imported, ACAP's resampling feature was used to linearly interpolate between each respective model's data points, and subsequently generate new "predicted" data points which correspond in time to those in the experimental data set. Furthermore, because the original reflood model results only ran out to about 330 seconds, the data used to construct the figures-of-merit was limited to $t < 330$ using ACAP's time-windowing feature. After these configuration steps were performed, ACAP generated the figures-of-merit for each simulation and these are summarized in Table III.

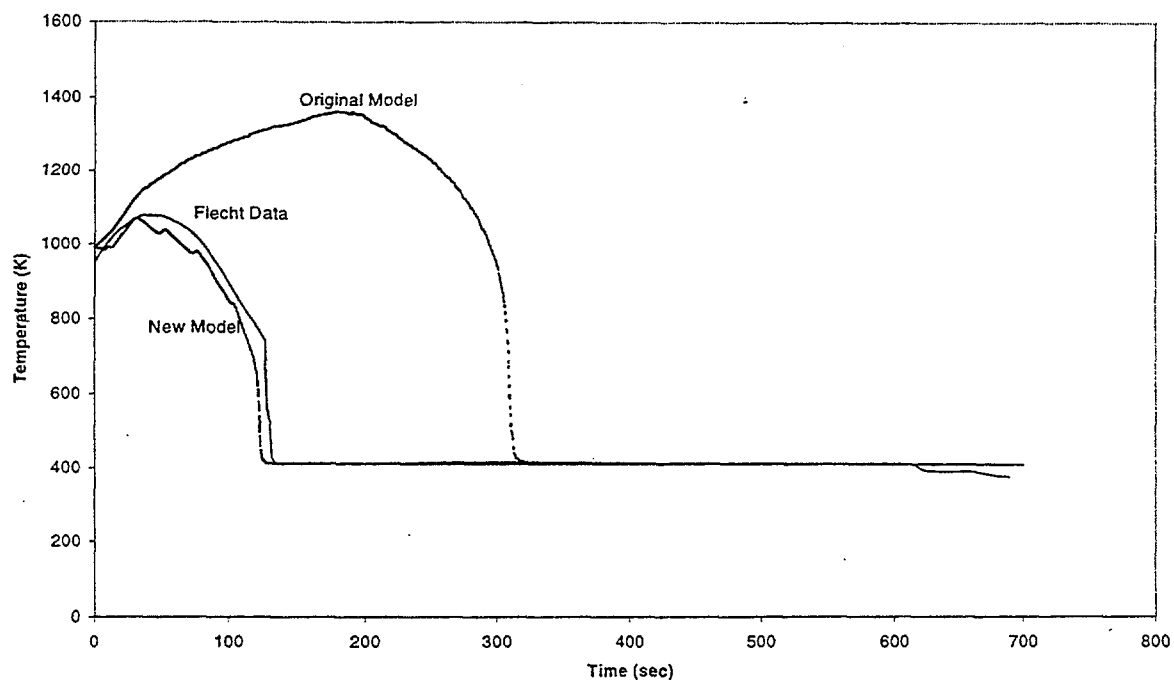


Figure 5. Sample Type V data comparisons. Predicted vs. measured rod surface temperatures during heatup and reflood of a FLECHT SEASET transient.

Table III. Comparison of ACAP Results for Presented Type V Data

Method	Original Model	New Model	Weight
D'Auria FFT	0.035	0.141	0.077
Mean Error	0.555	0.969	0.077
Variance of Error	0.779	0.996	0.077
Mean Square Error	0.519	0.995	0.077
Mean Error Magnitude	0.555	0.967	0.077
Mean Relative Error	0.689	0.985	0.077
Index of Agreement	0.421	0.992	0.077
Mean Fractional Error	0.052	0.556	0.077
Cross-Correlation Coefficient	0.037	0.988	0.077
Standard Linear Regression (L_2 Norm)	0.926	0.998	0.077
Origin Constrained Linear Regression (L_2 Norm)	0.981	0.999	0.077
Perfect Agreement Norm (L_2 Norm)	0.979	0.998	0.077
Continuous Wavelet Transform	0.665	0.864	0.077
Combined Figure-of-Merit	0.553	0.880	

For each case, the merit values do generally get better for the modified reflood model simulation, as expected. The overall figure of merit for the new reflood model is 0.880 while for the original code case, it is only 0.553.

4.4. Type V data assessment including experimental uncertainty

As a final demonstration example, a Type V data assessment is performed for a case which has an experimental uncertainty available. Integrated mass flow through an automatic depressurization system for an OSU SBLOCA case is considered (NRC12). An experimental uncertainty is known for this quantity. Figure 6a shows the ACAP interface display of the experimental data with a RELAP5 solution and an artificial systems code solution (here simply a straight line). The percent validated metric, defined above (section 3.2), is utilized to assess the relative accuracy of the two simulations. Though the artificial code solution exhibits significant differences from both RELAP5 and measured values, the RELAP5 and artificial simulations return PV values of 0.42 and 0.40 respectively. Therefore the artificial data cannot be deemed much less accurate than the RELAP5 simulation if taken in light of the experimental uncertainty. This is further illustrated in Figure 6b where the absolute error of the two simulations is plotted with the experimental uncertainty bands.

5. CONCLUSIONS

An automated code assessment program (ACAP) developed under subcontract to the United States Nuclear Regulatory Commission for use in its NRS code consolidation efforts was presented in this paper. Some background on the topic of NRS accuracy and uncertainty assessment was provided which motivated the development of and defined basic software requirements for ACAP. A description of the software package and several sample applications to NRS data sets were provided. Its functionality and ability to provide objective accuracy assessment figures were demonstrated.

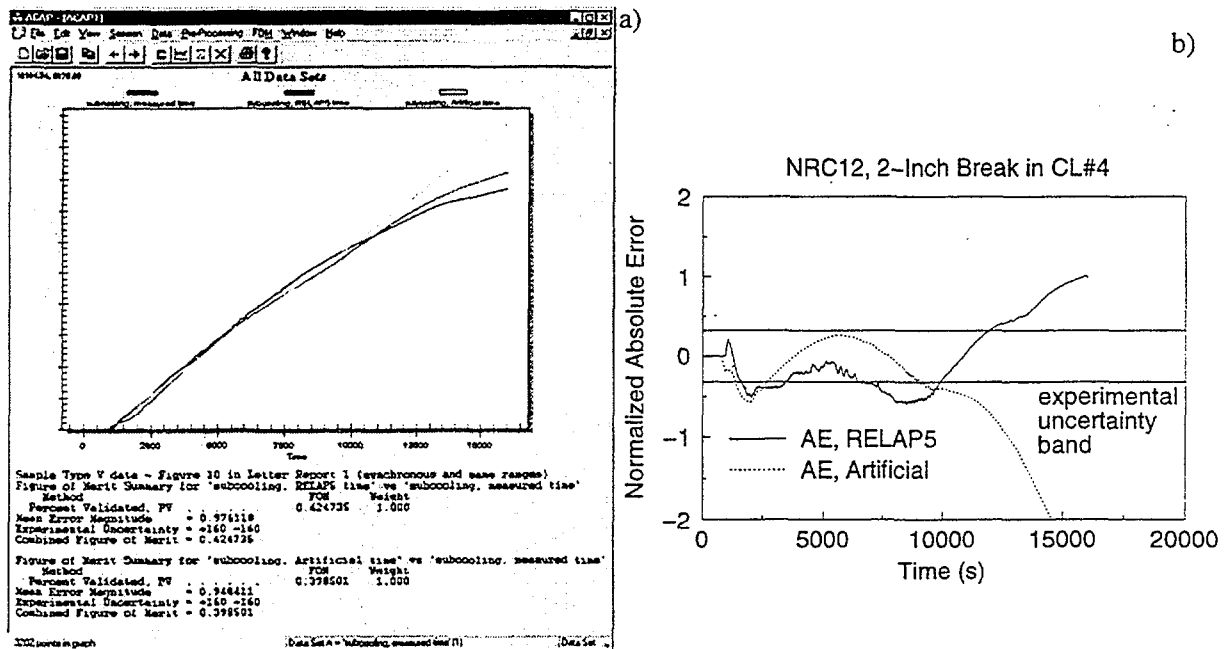


Figure 6. Sample Type V data comparisons. Predicted vs. measured integrated mass flow through an ADS vs. time for NRC12 case. a) ACAP display of data and assessment output. b) Plot of absolute error for two simulations with experimental uncertainty.

ACKNOWLEDGEMENTS

This work was performed under United States Nuclear Regulatory Commission Contract NRC-04-97-046, Task Order #3, with contract monitor Dr. Jennifer Uhle.

REFERENCES

- [1] BESSETTE, D.E., ODAR, F., "The U.S. Nuclear Regulatory Commission (NRC) Program on the Development and Assessment of Thermal Hydraulic Systems Codes," NUREG/CP-0080, Vol. 1 (1986).
- [2] KMETYK, L.N., BYERS, R.K., ELRICK, M.G., BUXTON, L.D., "Methodology for Code Accuracy Quantification," NUREG/CP-0072, Vol. 5 (1985).
- [3] WILSON, G.E., CASE, G.S., BURTT, J.D., EINERSON, J.J., HANSON, R.G., "Development and Application of Methods to Characterize Code Uncertainty," NUREG/CP-0072, Vol. 5 (1985).
- [4] D'AURIA, F., LEONARDI, M., GLAESER, H., POCHARD, R., "Current Status of Methodologies Evaluating the Uncertainty in the Prediction of Thermal-Hydraulic Phenomena in Nuclear Reactors," from Two-Phase Flow Modeling and Experimentation, 1995, ed: Celata, Shah, pp. 501-509 (1995).
- [5] AMBROSINI, W., BOVALINI, R., D'AURIA, F., "Evaluation of Accuracy of Thermal-Hydraulics Code Calculation," *Energianucleare*, Vol. 7, No. 2, pp. 5-16 (1990).
- [6] D'AURIA, F., GALASSI, G.M., "Code Assessment Methodology and Results," IAEA Technical Committee/Workshop on Computer Aided Analysis, Moscow (1990).
- [7] D'AURIA, F., DEBRECIN, N., GALASSI, G.M., "Outline of the Uncertainty Methodology Based on Accuracy Extrapolation," *Nuclear Technology*, Vol. 109, January, pp. 21-38 (1995).
- [8] D'AURIA, F., GALASSI, G.M., "Code Validation and Uncertainties in System Thermalhydraulics," submitted *Journal of Progress in Nuclear Energy* (1997).
- [9] SCHULTZ, R.R., "International Code Assessment and Applications Program: Summary of Code Assessment Studies Concerning RELAP5/MOD2, RELAP5/MOD3, and TRAC-B," NUREG/IA-0128 (1993).
- [10] WILLMOTT, C.J., "Some Comments on the Evaluation of Model Performance," *Bulletin of the American Meteorological Society*, Vol. 63, No. 11, pp. 1309-1313 (1982).

- [11] KU, J.Y., RAO, S.T., RAO, K.S., "Numerical Simulation of Air Pollution in Urban Areas: Model Performance," *Atmospheric Environment*, Vol. 21, No. 1, pp. 213-232 (1987).
- [12] COLEMAN, H.W., STERN, F., "Uncertainties and CFD Code Validation," *Journal of Fluids Engineering*, Vol. 119, No. 4 (1997).
- [13] MATZNER, B., J. E. CASTERLINE, E. O. MOECK, AND G. A. WIKHAMMER, "Critical Heat Flux in Long Tubes at 1000 psi With and Without Swirl Promoters," Presented at the Winter Annual Meeting of the ASME, Chicago, Illinois, November 7-11 (1965).
- [14] PAIGE, D.R., "Assessment of Improved Reflood Model in TRAC-BF1/MOD1", MS Thesis in Nuclear Engineering, The Pennsylvania State University, (1998).

ANALYSIS OF EXCESSIVE INCREASE IN SECONDARY STEAM FLOW TRANSIENT IN CHASHMA NUCLEAR POWER PLANT



XA0055033

INTSAR-UL-HAQ
Institute for Nuclear Power,
Islamabad, Pakistan

ABSTRACT

Excessive increase in secondary steam flow transient is analyzed for 300 MWe Chashma Nuclear Power Plant, using RELAP5/MOD2 code. The DNB analysis is performed using, COBRA IV code. Four cases are analyzed to demonstrate the plant behavior following a 10% step load increase from the full load. The analysis shows that for a 10% step load increase, with minimum and maximum reactivity feed back, the DNBR remains above the limiting value, which is the design basis for DNBR. In all four cases the plant reaches a stabilized condition following the load increase.

INTRODUCTION

Chashma Nuclear Power Plant (CHASNUPP) is the first light water reactor in Pakistan. This is a 300 MWe nuclear reactor designed by China. The plant is under construction and expected to be critical in 1999. It consists of a reactor core and two closed reactor coolant loops connected in parallel to the reactor vessel, each loop contains a reactor coolant pump and a steam generator. An electrically heated pressurizer is connected to one of the two hot legs. The reactor coolant pumps are vertical, centrifugal, equipped with a non-reverse mechanism to prevent reverse rotation. The steam generators use vertical U-tubes made of inconel.

The reactor vessel encloses the reactor core. The core consists of 121 fuel assemblies, with each assembly having 204 fuel rods and 21 thimble tubes arranged in a 15x15 array. The fuel used in the core consists of slightly enriched uranium dioxide fuel pellets contained with a Zircaloy-4 cladding. The reactor power is controlled by the coordinated combination of chemical shim and mechanical control rods.

The final safety analysis report of Chashma Nuclear Power Plant has been submitted. It is required to verify the design calculations and the accidents analyzed. The RETRAN code has been used for most of the accident analysis in final safety analysis report, but now RELAP5/MOD2 code for accident analysis and COBRA IV for DNB analysis are being used. Excessive increase in secondary steam flow transient is analyzed.

PLANT NODALIZATION

Plant nodalization for RELAP5/MOD2 model is shown in fig. 1. The plant primary and secondary systems are split into volumes interconnected by junctions. The balance of plant components is represented by the dependent boundary conditions. The reactor core contains four fluid volumes and one bypass volume. The core heat structure having eight nodes, that uses point kinetics and ANS recommended decay heat as a power source, represents the fuel rods. The downcomer of the reactor vessel contains five fluid volumes. These five stacked nodes represent any temperature stratification that could not be predicted with a single node downcomer volume. The heat structures attached to appropriate volumes are incorporated in the problem. The lower

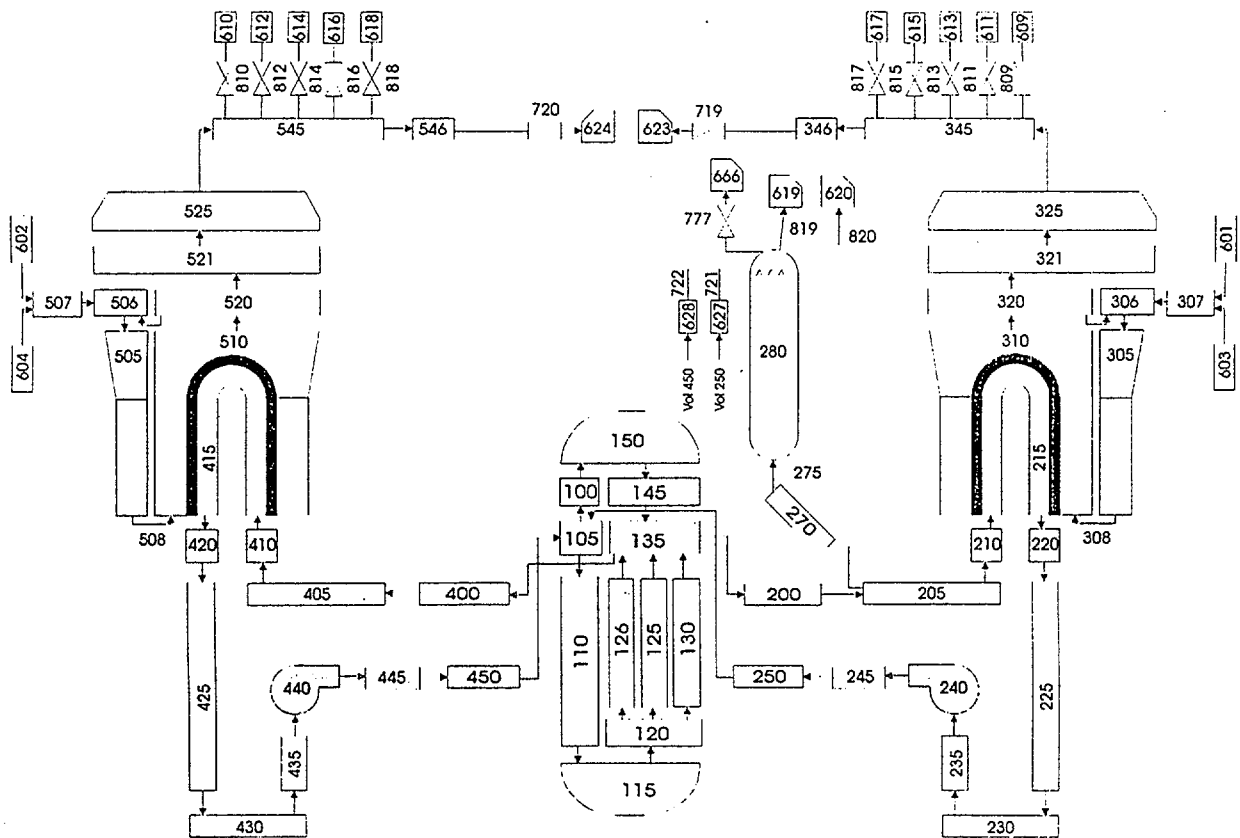


Fig. 1 CHASHMA NPP Nodalization for RELAP5Mod2

plenum, upper plenum and upper head are modeled with single fluid volume. The hot leg is represented by two hydrodynamic volumes, with one of the junctions being located at the point where the pressurizer surge line connects to the hot leg. Pressurizer connected to one of the two loops is modeled as a non-homogeneous control volume, divided into eight sub-volumes. The surge line, connecting the hot leg, is divided into two volumes. Primary safety and relief valves are also simulated.

The steam generator primary side contains fluid volumes for the inlet and outlet plenum. The tube region is divided into eight volumes, with four up and four down volumes. The boundaries between volumes on secondary side are at the same elevations as boundaries on primary side. Heat structures of tube walls are also modeled. The separator is a specialized hydrodynamic component having three junctions vapor outlet, liquid fallback and separator inlet. Two fluid volumes represent the steam line to turbine. Reactor coolant pump component is indicated by pump. A pump consists of one volume and two junctions, one attached to each end of the volume. The pump suction piping is modeled with three volumes, while the pump discharge piping is modeled with two hydrodynamic volumes. Feed water is supplied at a constant rate during normal operation.

ACCIDENT DESCRIPTION

An excessive increase in secondary system steam flow (excessive load increase incident) is defined as a rapid increase in steam flow that causes a power mismatch between the reactor core power and the steam generator load demand. The reactor control system is designed to accommodate a 10% step load increase and a 5% per minute ramp load increase in the range of 15% to 100% of full power. Any loading rate in excess of these values may cause a reactor trip actuated by the reactor protection system. This accident could result from either an administrative violation such as excessive loading by the operator or an equipment malfunction in the steam dump control or turbine speed control.

During the power operation, steam dump to condenser is controlled by reactor coolant condition signals, i.e. high reactor coolant temperature indicates a need for steam dump; an interlock is provided which blocks the opening of the valves unless a large turbine load decreases or turbine trip occurs. Protection against an excessive load increase accident is provided by the following reactor protection system signals:

- Overpower ΔT
- Overtemperature ΔT
- Power range high neutron flux

Four cases are analyzed to demonstrate the plant behavior following a 10% step load increase from rated load.

1. Reactor control in manual with minimum moderator reactivity feed back.
2. Reactor control in manual with maximum moderator reactivity feed back.
3. Reactor control in automatic with minimum moderator reactivity feed back.
4. Reactor control in automatic with maximum moderator reactivity feed back.

For the minimum moderator feedback cases, the core has the least negative moderator temperature coefficient of reactivity and therefore, the least inherent transient capability. For the maximum moderator feedback cases the moderator temperature coefficient of reactivity has its highest absolute value. This results in the largest amount of reactivity feedback due to changes in coolant temperature.

Normal reactor control systems and engineered safety systems are not required to function. The reactor protection system is assumed to be operable. However reactor trip is not encountered due to the error allowances assumed in the setpoints. No single active failure will prevent the reactor protection system from performing its intended function.

RESULTS

For the minimum moderator feedback manually control case, there is slight power increase, and the average core temperature shows a large decrease. This results in a DNBR, which increases above its initial value. For the maximum moderator feedback, manually controlled case there is much larger increase in reactor power due to the moderator feedback. For both of these cases, the minimum DNBR remains above the limit value. For these cases the plant reaches a stabilized condition at the higher power level.

Both the minimum and maximum moderator feedback cases with automatic power control, the core power increases thereby reducing the rate of decrease in coolant average temperature and pressurizer pressure. For both of these cases, the minimum DNBR remains above the limit value. The results of the case with maximum moderator feed back are shown in fig. 2 to 5.

The excessive load increase incident is an overpower transient for which the fuel temperature will rise. Reactor trip may not occur for the cases analyzed and the plant reaches a new equilibrium condition at the higher power level corresponding to the increase in steam flow. Since DNB does not occur at any time during the excessive load increase transients, the ability of the primary coolant to remove heat from the fuel rod is not reduced. Thus the fuel cladding temperature does not rise significantly above its initial value during the transient.

Excessive Increase In Steam Flow

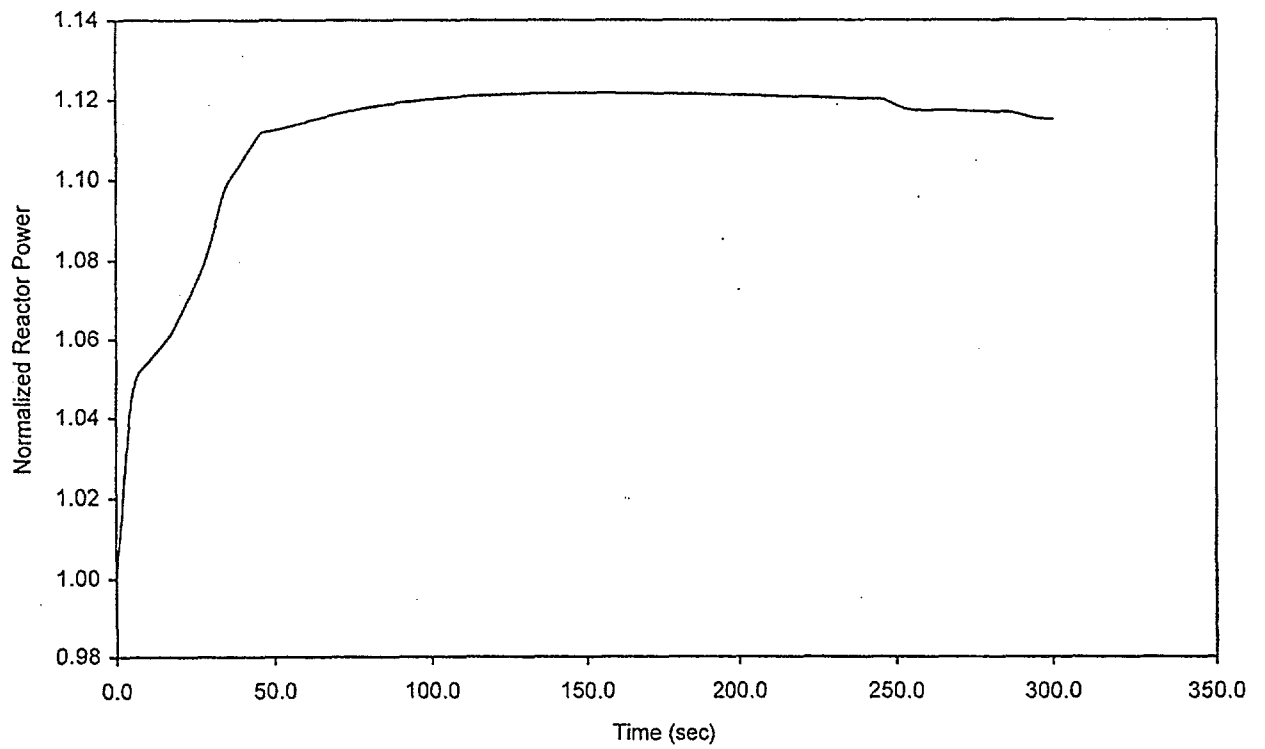


Fig. 2 Normalized Reactor Power

Excessive Increase In Steam Flow

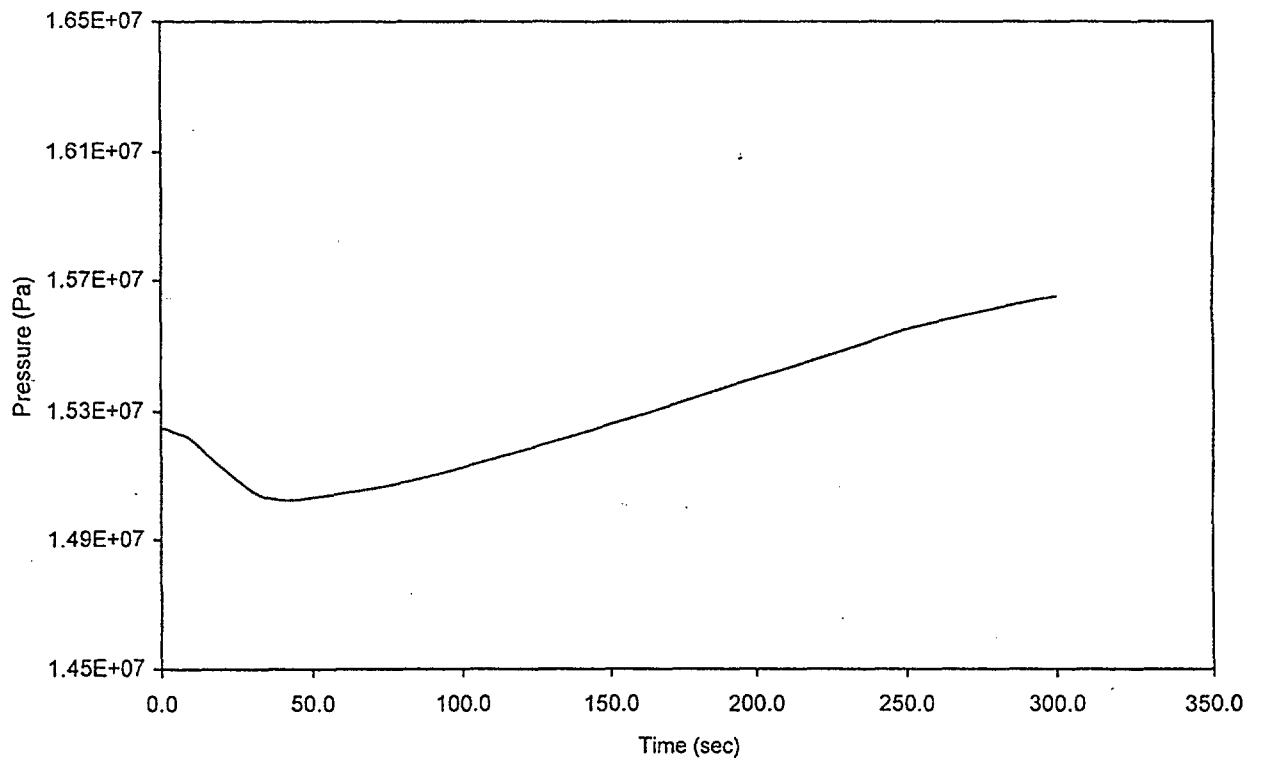


Fig. 3 Core Inlet Pressure

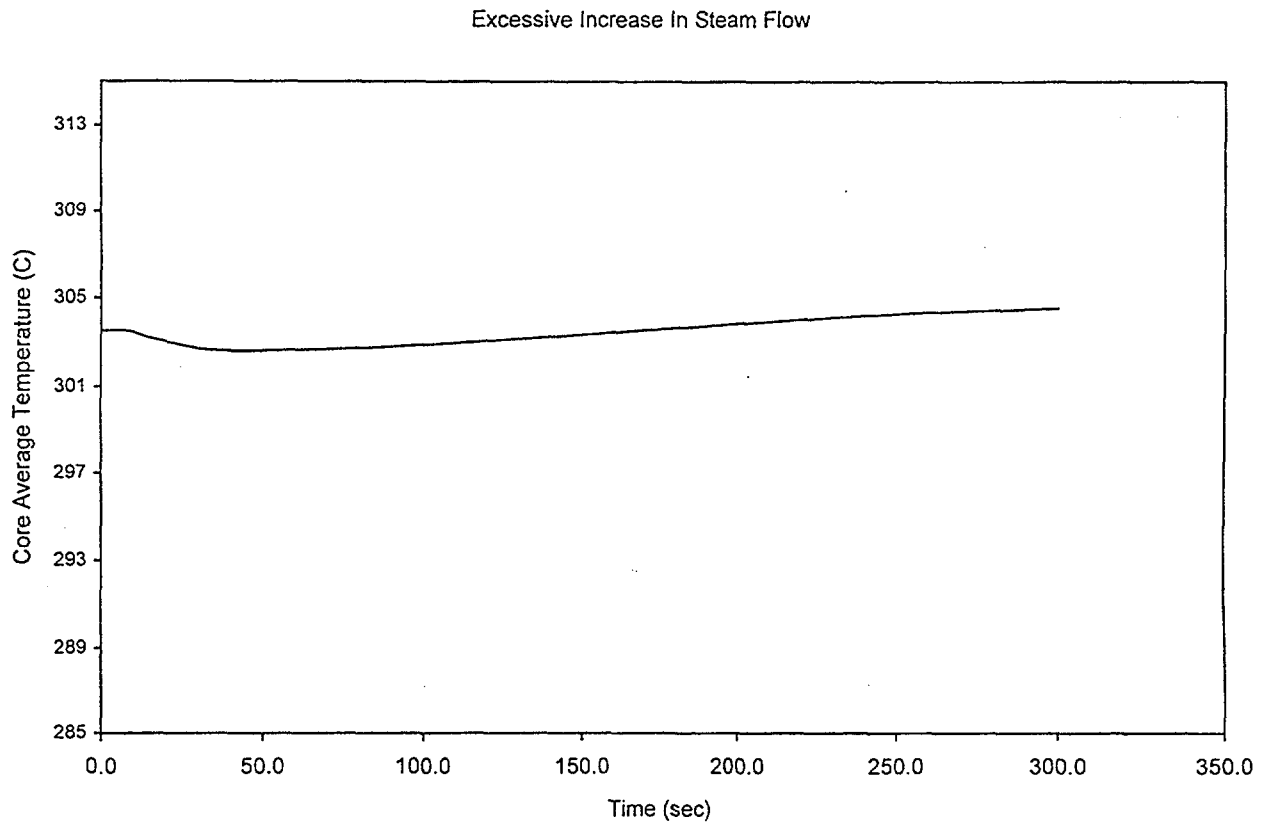


Fig. 4 Core Average Temperature

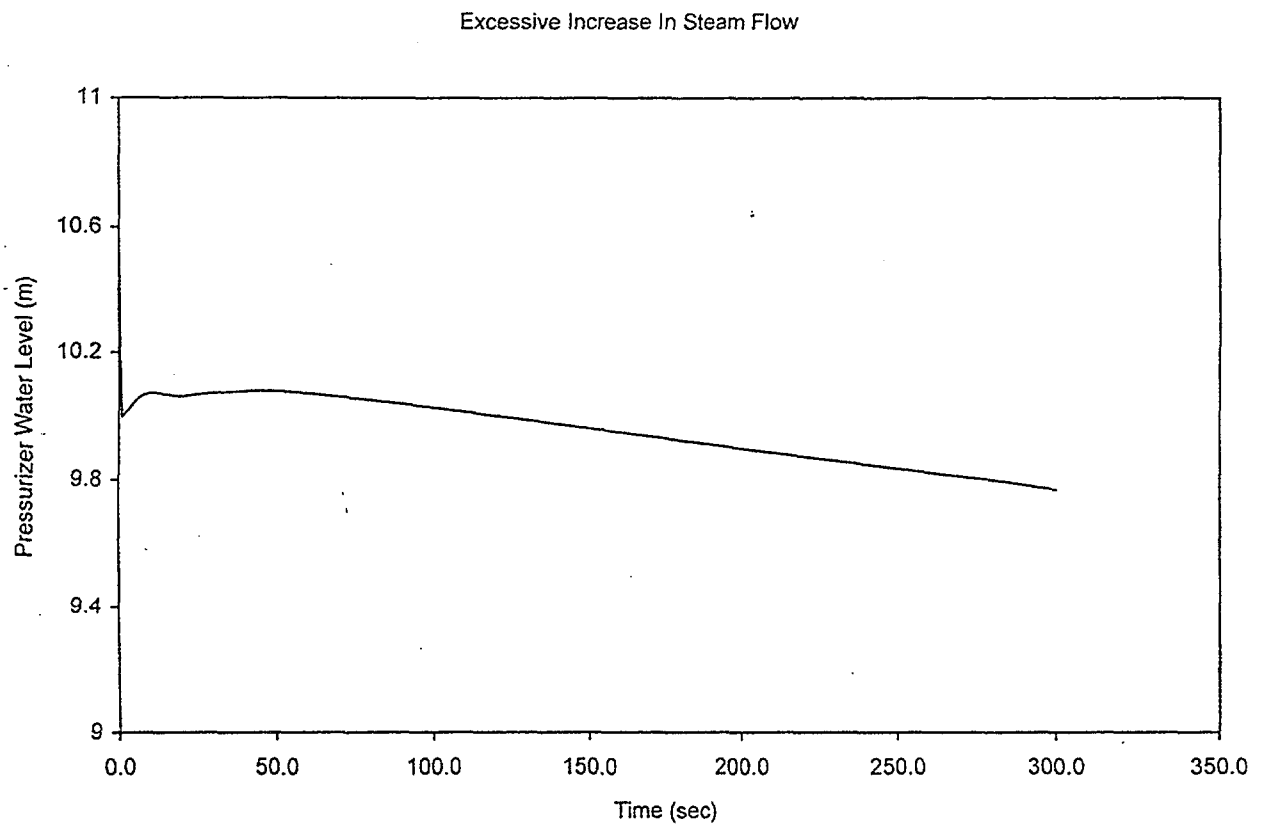


Fig. 5 Pressurizer Water Level

CONCLUSIONS

The analysis presented above shows that for a 10% step load increase, the DNBR remains above the limit value, thereby precluding fuel or clad damage. The plant reaches a stabilized condition rapidly following the load increase.

REFERENCES

- [1] Victor H. Ransom; RELAP5/MOD2 computer code manuals, 1985
- [2] Nuclear system flow diagrams of 300 MWe nuclear power plant, SNERDI, 1993
- [3] 300 MWe Chashma Nuclear Power Plant FSAR, 1998.
- [4] Full scope training simulator of Chashma Nuclear Power Plant, ICCC/SNERDI/8.4



ANALYSIS OF SGTR IN AP-600 BY RELAP5/MOD3.2 CODE

F. D'AURIA, G. FRUTTUOSO, G.M. GALASSI, F. ORIOLO

Dipartimento di Costruzioni Meccaniche e Nucleari,
Università di Pisa,
Pisa

I. BASSANELLI

Ente Nazionale Energia Elettrica (ENEL),
Rome

Italy

Abstract

Five SGTR (Steam Generator Tube Rupture) sequences assumed to occur in the AP-600 system have been analysed in the present framework. These came from PSA (Probabilistic Safety Assessment) studies performed at ENEL in Rome; however, the bounding properties or the realism of the sequences are not discussed hereafter. Rather, the attention is focused toward the thermohydraulic performance of the system.

In all the considered sequences, the break is a double ended at the top bend of a single U-tube: this is done to maximise the I131 release to the environment. The break model in the code input deck consists of two pipes having the cross section area equal to that of a single U-tube. These are connected to the primary side in the position of the steam generator plena and to the secondary side at the bottom of the riser zone separating the U-tubes bundle from the steam separator.

1. INTRODUCTION

The design and the safety characteristics of innovative reactors, essentially based upon passive emergency core cooling systems, have been studied at Dipartimento di Costruzioni Meccaniche e Nucleari of the University of Pisa (DCMN) since 1986, i.e. soon after the Chernobyl accident. Experimental activities, code assessment activities and development of phenomenological models have been conducted and are in progress. Most of the researches in the area, have been supported, supervised or stimulated by ENEL (Ente Nazionale Energia Elettrica).

The present activity deals with an application of system codes finalised at the demonstration of safety and at the same time to the optimisation of the emergency procedures for the AP-600 plant. The study needs the availability of qualified code, nodalisation, code-user and computer-compiler installation. Basically, before achieving results of potential interest to the technology, like those foreseeable from the present code application, the above conditions must be proven.

The code qualification (first condition) stems from the use of an internationally recognised code version, the Relap5/mod3.2, ref. [1]. The quality of the code derives from the demonstration of capabilities in predicting suitable sets of experimental data. This can be achieved by considering the results of different groups of qualified code users (see below). Published papers in international Journals or Conferences, as well as conclusions or discussions from working Seminars (e.g. CAMP meetings or Relap5 Seminars), support the conclusion that the first condition is met. The specific activities carried out at DCMN finalised either to the identification and characterisation of phenomena expected to be important for new generation reactors, [2], and to the assessment of the code capabilities against the same phenomena, [3], constitute an independent confirmation of the same finding. A proposal for a comprehensive code qualification procedure, i.e. to demonstrate in a traceable and reproducible way code limits and capabilities, has also been recently proposed by DCMN, ref. [4]; the considered 'quality' criteria have basically been met.

The availability of a qualified code does not imply quality of results unless a qualified nodalisation is available (second condition). Nodalisation qualification criteria have been proposed dealing with the development, the "steady-state" and the "on-transient" acceptability of a nodalisation, ref. [5]. Those criteria are considered for the development and the qualification of the AP-600 noding scheme.

The availability of qualified code and nodalisation does not imply quality of results unless the code user, or better the group of code users, is qualified (third condition). The user may "interpret" boundary and initial conditions as well as code options available from the code manual, supplying wrong or inadequate information in the input deck; user effects upon predicted results are extensively discussed in ref. [6]. The problem of user qualification is a critical one to be solved or even to be addressed, e.g. ref. [7].

The last condition to be met is concerned with the availability of a qualified computer/compiler installation (fourth condition). The code released by developers can be used in different computers. The results may be

largely affected by the computer/compiler, e.g. ref.. [8]. The solution to the problem is the execution of relevant 'benchmarks' showing that code developers results are "the same" as produced from the concerned installation.

A comprehensive description of conditions I to IV can be found in ref. [9]. All the conditions are supposed to have been met before starting the present investigation, e.g. refs. [2], [3] and [10] to [12]. This is focused toward the analysis of AP-600 performance during Steam Generator Tube Rupture (SGTR) transient; the results can be used to optimise Emergency Operating Procedures.

2. CODE AND INPUT DECK

The Relap5/mod3.2 is a well known code based upon 1-D thermalhydraulics and 0-D neutron kinetics equations. The adopted one is the latest version of a series of codes distributed since 1980. The code is widely used by several Organisations all over the world. Wide range assessment programs like CAMP (Code Assessment and Maintenance Programme) are in progress that may give an idea of the interest of the scientific community toward this code and, at the same time, of its capabilities.

Independent assessment activities have been carried out at DCMN as already mentioned (e.g. ref.. [9]); these also brought to the proposal for a methodology for the evaluation of the error made by a generic code calculation in predicting a transient scenario in a Nuclear Power Plant (NPP): uncertainty evaluation. With main reference to the area of advanced reactors, the code capabilities were characterised: basically, it was found that Relap5 performance is the same in case of applications to present generation and future generation NPP, provided the pressure is above 0.5 Mpa; however, areas for improvements connected with the simulation of components and systems introduced in advance reactors, have been identified, refs. [3] and [10]. Looking at the present application, it may be concluded that the adopted code is fully able to represent physical phenomena relevant in the case of SGTR scenarios here considered: the primary loop remains in nearly single phase condition at high pressure for the entire duration of the transients.

2.1 Nodalisation

A detailed nodalisation has been developed at DCMN for simulating the AP-600. This is described into detail in ref. [13]. It consists of more than 400 hydraulic nodes and 1200 meshes for conduction heat transfer. All the Engineered Safety Features of AP-600 design are part of the nodalisation including CMT (Core Make-up Tanks), PRHR (Pressurised Residual Heat Removal system), IRWST (In-Reactor Water Storage Tank), Accumulators, ADS 1 to 4 (Automatic Depressurisation System from 1 to 4), Pressuriser PORV (Pilot Operated Relief Valve), steam generator PORV and SRV (Steam Relief Valve) and SFW (Start-up Feedwater). In addition, systems for the nominal reactor operation like CVCS (Chemical and Volume Control System), MSIV (Main Steam Isolation Valves), turbine inlet and turbine bypass valves are included into the code model together with full control logic of operation of the various systems.

Special attention has been paid in modelling components like CMT and PRHR, specifically considering the experience gained in simulating the related phenomena measured in Spes-2 facility: CMT recirculation and draining phases controlled by thermal stratification of the fluid and pool side heat transfer in the case of PRHR, are examples of such phenomena.

The nodalisation underwent the qualification process at the steady state level as discussed in ref. [9]; the related results are given in ref. [13]; information suitable for the 'on-transient' qualification of the nodalisation can be derived from ref. [14]. The transformation from Relap5/mod2.5 to Relap5/mod3.2 was carried out utilising a standard procedure, basically considering the new capabilities of the Relap5/mod3.2 and the (slightly) different code input options. A new steady state was run; the related results demonstrated to be consistent with the requirements settled in ref. [9].

The nodalisation dimensions are given in Tab. 1; the related sketch and the utilised boundary and initial conditions can be seen in Fig. 1 and Tab. 2, respectively.

3. IMPOSED SEQUENCES OF EVENTS FOR SGTR

The imposed sequence of events for five SGTR sequences in the AP-600 can be deduced from Tab. 3, where the actuated systems are listed together with the relevant or adopted conditions for actuation. The sequences are identified with labels from SGT1 to SGT5.

Tab. 1 - AP-600 Nodalization dimensions

PARAMETER	VALUE
Number of volumes	416
Number of junctions	450
Number of heat structures	367
Number of mesh points	1214

Tab. 2 - Relevant boundary and initial conditions for the AP-600 SGTR calculations.

Quantity	Unit	Calculated value	Reference value
Reactor thermal power	Mw	1971.7	1971.7
PRZ pressure	MPa	15.51	15.51
Loop mass flowrate a	kg/s	4416.4	-
Loop mass flowrate b	kg/s	4450.1	-
Primary coolant mass	kg	150848	-
SGa exchanged power	Mw	985.83	985.85
SGb exchanged power	Mw	990.50	985.86
SG secondary side pressure	MPa	5.48	5.40
MFWa mass flowrate	kg/s	542	542
MFWb mass flowrate	kg/s	542	542
SGa secondary side coolant inventory	kg	52994.2	51397.8
SGb secondary side coolant inventory	kg	52909.6	51397.8
PRZ level	m	6.32	6.33
Core inlet mass flowrate	kg/s	8263.2	8549
Core bypass mass flowrate	kg/s	347.94	693
Core inlet fluid temperature	K	550.9	549
Core outlet fluid temperature	K	592.1	591
SGa DC level	m	13.46	13.46
SGb DC level	m	13.46	13.46
MFWa fluid temperature	K	499	499
MFWb fluid temperature	K	499	499

In all cases the break is a double ended at the top bend of a single U-tube. The break position has been chosen as the most critical one as far as iodine release is concerned. In the code input deck this is achieved by adding two pipes having the cross section of a single tube connected to the primary side in the position of the Steam Generator (SG) inlet and outlet plena and to secondary side at the bottom of the riser zone separating the U-tubes bundle from the steam separator.

Following the break occurrence in SGT1 at time $t=0$ s in the SG No. B (or b), pressure decrease in pressuriser is assumed to cause scram. Turbine isolation occurs followed by condenser bypass opening and main feedwater blockage. Primary pumps are also stopped and SFW comes into operation as scheduled. PRHR and CMT systems work as from the design. One CVCS pump is assumed to start following low level in pressuriser.

At $t=1800$ s (30'), after scram, a planned 55 K/hr equivalent depressurisation rate is assumed for both steam generators.

The affected steam generator is isolated (isolation of SFW) following high level in SG No. B; an operator action is assumed for the isolation of the MSIV. CVCS is isolated on the basis of the same signal controlling SFW.

The calculation ends at 10000 s.

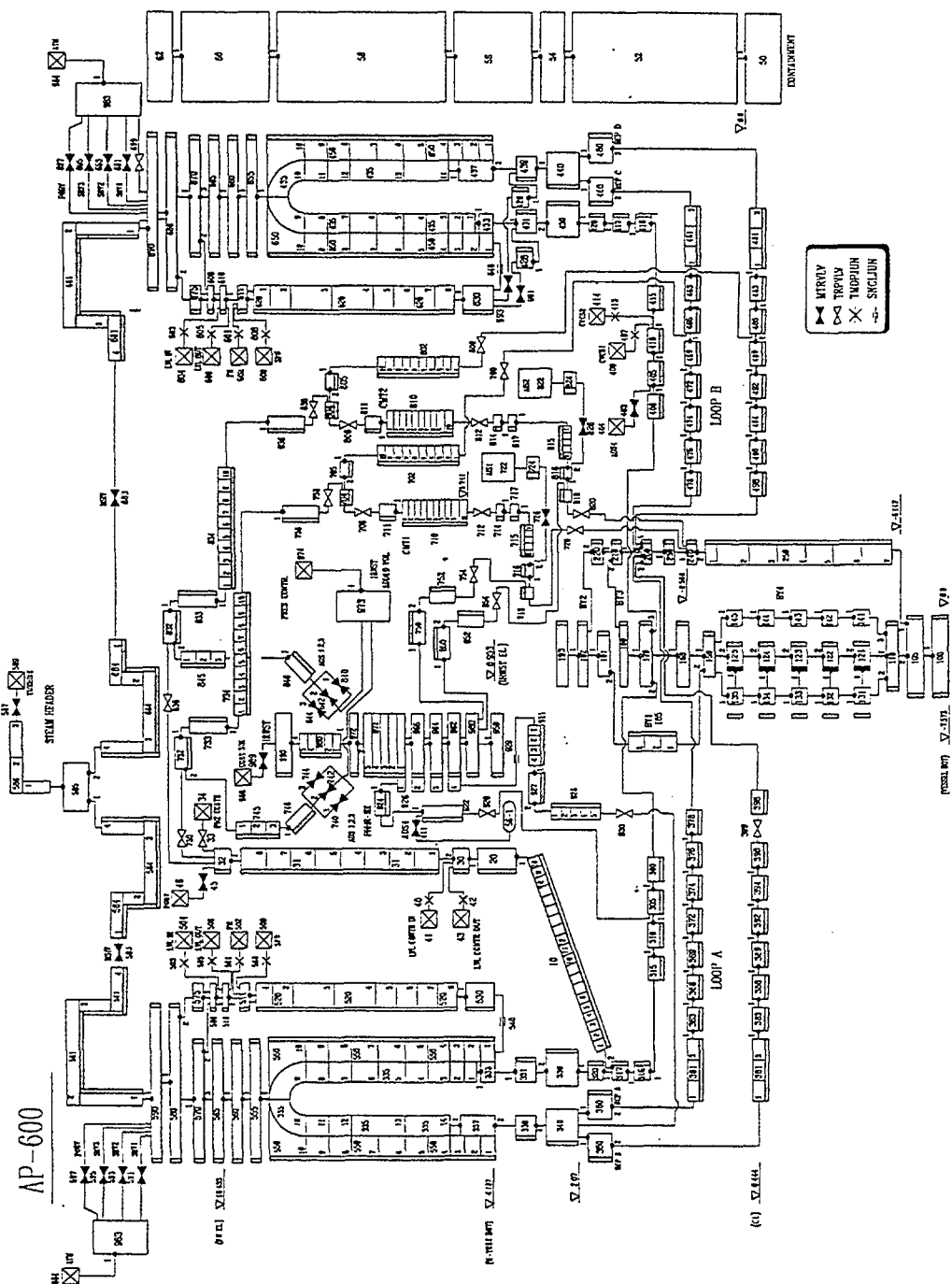


Fig. 1 - Nodalization for RELAP5/Mod2.5 code of the Westinghouse AP-600 plant

Tab. 3 - List of imposed events for AP-600 SGTR transients.

SYSTEM	TRIP	VALUE	DELAY	ACTION
RCP trip	scram time	-	17s	RCP coastdown-table
CMT injection	scram time	-	22s	valve opening
PRHR actuation	CMT opening	-	60s	valve opening
SI signal	Low PRZ pressure Low SG pressure Low CL temperature	<11.7MPa <3.7MPa <554 K		
ADS actuation	-	-	-	not foreseen
Reactor trip	Low PRZ pressure	<12.41MPa	3.5s	
MSL isolation (only SGb)	manual closure	30 min after scam signal	-	
CVCS flow isolation	High narrow level in SGb	>14.97m	10s	valve closure
CVCS flow actuation	Low PRZ level	<0.823m	2s	valve opening
SFW activation	Low level in SGa or SGb Low FW flow	<12.57m	2s	flowrate 12.5 kg/s
SFW isolation (SGb only)	High level SGb	>14.97m	-	valve closure
Turbine trip	Scram time	-	5s	valve closure
Feedwater isolation	Scram time	-		complete valve closure in 15s
Steam dump to condenser actuation	turbine isolation time not actuated in SGT3	-	-	depres. rate corresponding to 55 K/hr

AP600 Plant - SGTR Transient - SGT1 and SGT3 calculations : Trips List

SYSTEM	TRIP	VALUE	DELAY	ACTION
RCP trip	scram time	-	17s	RCP coastdown table
CMT injection	scram time	-	22s	valve opening
PRHR actuation	CMT opening	-	60s	valve opening
SI signal	Low PRZ pressure Low SG pressure Low CL temperature	<11.7MPa <3.7MPa <554 K		
ADS actuation	Low CMT level	<1.26m	120s	2 out of 4 stage four
Reactor trip	Low PRZ pressure	<12.41MPa	3.5s	
MSL isolation (only SGb)	manual closure	30 min after scam signal	-	NOT ACTUATED
CVCS flow isolation	High narrow level in Sgb Only for SGT2 case: after 6 hours from activation	>14.97m	10s	NOT ACTUATED (used for SGT2 case only)
CVCS flow actuation	Low PRZ level	<0.823m	2s	valve opening
SFW activation	Low level in SGa or SGb Low FW flow	<12.57m	2s	flowrate 12.5 kg/s
SFW isolation (SGb only)	High level SGb	>14.97m	-	NOT ACTUATED
Turbine trip	Scram time	-	5s	valve closure
Feedwater isolation	Scram time	-		complete valve closure in 15s
Steam dump to condenser actuation	turbine isolation time not actuated in SGT4	-	-	depres. rate corresponding to 55 K/hr
SRV stuck open	transient beginning	time = 0.0	-	actuated only in SGT5 case

AP600 Plant - SGTR Transient - SGT2, SGT4 and SGT5 calculations : Trips List

The SGT2 calculation proceeds in the same as SGT1. However, SFW and MSIV of the affected steam generator are not isolated. CVCS is isolated six hours following the scram.

The calculation ends at 30000 s (this is the only calculation allowed to reach 30000 s from the time of the break occurrence: this was done to evaluate the test scenario consequent to the failure of CVCS).

The SGT3 calculation is similar to the SGT1 with the only difference that the turbine bypass valves do not open. This is done to check the possibility that broken steam generator pressure reaches the SRV opening set point (this did not occur as the result of the calculation).

The SGT4 calculation is similar to the SGT2 with the only difference that the turbine bypass valves do not open. This is done, again, to check the possibility that broken steam generator pressure reaches the SRV opening set point (this did occur toward the end of the calculation).

The SGT5 calculation is similar to the SGT2 with the only difference that one SRV in the steam generator No. B remains stuck open starting from $t=0$ s. This is done to simulate a situation where the tube break is caused by the dynamic loads consequent the SRV opening. In such a situation, the lack of a qualified model for neutron kinetics, suggested to impose the scram at 200's into the transient (operator action).

In addition, in order to avoid back flow from the system controlling the steam generators pressure at 55 K/hr into the broken steam generator (in the present case, this attains a pressure much lower than in the case of SGT2), the MSIV of the broken steam generator has been assumed to close at $t=0$.

4. SUMMARY OF RESULTS

The resulting time sequences of events for steam generator tube rupture calculations in AP-600 identified as SGT1 to SGT5 are given in Tab. 3. Each transient scenario is documented and characterised by more than thirty time trends in ref. [16]. However, only four of these are shown hereafter per each calculation (Figs. 2 to 21). It can be premised that in all cases the CMT and the PRHR interventions were (as expected) successful: in other terms, the sum of the power exchanged through PRHR and used for CMT liquid heating up, was larger than core decay power. This basically prevented the possibility of steam generator SRV opening as mentioned before.

Needless to say, the core remained covered during the entire duration of the different transients; so, the only safety concern remained the iodine release outside the secondary loop, and eventually that transferred from the primary to the secondary loop.

The main observations from the performed analyses as reported below.

- Only in the SGT1 calculation reverse flow is calculated at the break at about 5000 s into the transient; in the case SGT2, the heat sink constituted by the 55 K/hr system prevents pressure reversal between primary and secondary systems; in cases SGT3 and SGT4, SFW is sufficient to keep secondary pressure below primary pressure (in the case SGT3, an anticipation of the isolation of SFW would have been caused pressure reversal); in the case SGT5, the same effect is due to the SRV stuck open (Figs. 3, 7, 11, 15, 20).
- In SGT1 and SGT2 the primary pressure achieves low value to cause accumulator actuation, before the end of the calculated transient. The 4.2 MPa value is reached at about 4100 and 22000 s into the transient, respectively (Figs. 2, 6, 10, 14 and 18, see also Tab. 4).
- In both SGT2 and SGT4 calculations, solid condition occurs in the affected (broken) steam generator. This event occurs at a pressure below the SRV set-point in the SG No. B in the case SGT2; however, in both cases primary pressure at the time of this event is above 10 MPa causing the potential for failure of other tubes and/or opening of the SRV: this could be damaged by the crossing of liquid. It must be emphasised that no signal was assumed for SRV opening based on high downcomer level in the steam generator, if the pressure remained below the set-point. The flowrate delivered by CVCS is at the origin of such scenario.
- In the case SGT3, the pressure equalisation between primary and secondary system occurs earlier than in the case SGT1: this is due to the operation of the condenser dump, not available in SGT3.
- In the case SGT4, steam passes from steam generator No. A to No. B: this limits the overpressurisation in the steam generator No. B caused by the overfilling condition discussed above.
- In all cases, with the exception of the SGT5, the level in the steam generator No. B overpasses the break elevation soon after the scram (see also Tab. 3) and remains above that position for the entire duration of the transient.
- Related to CMT, a recirculation period can be observed in all cases: the recirculation rate decreases during the transient; however, only in the case SGT2, draining of CMT starts at about 25000 s into the transient following isolation of the CVCS.
- The integrals of mass lost from the primary into the secondary loop and of mass exiting from the steam line of the broken steam generator, are given in Tab. 4. These can be assumed as representative of iodine diffusion from primary to secondary system and of iodine lost from secondary system, respectively, though only in case SGT4 an actual release is calculated.

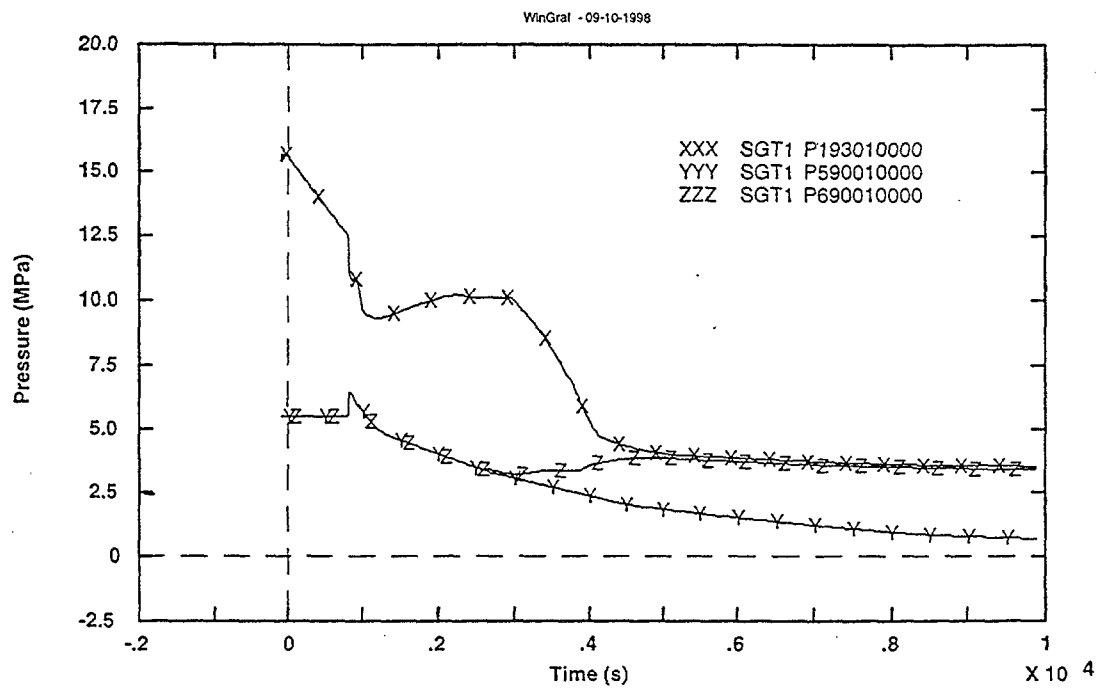


Fig. 2- Primary and secondary side pressures

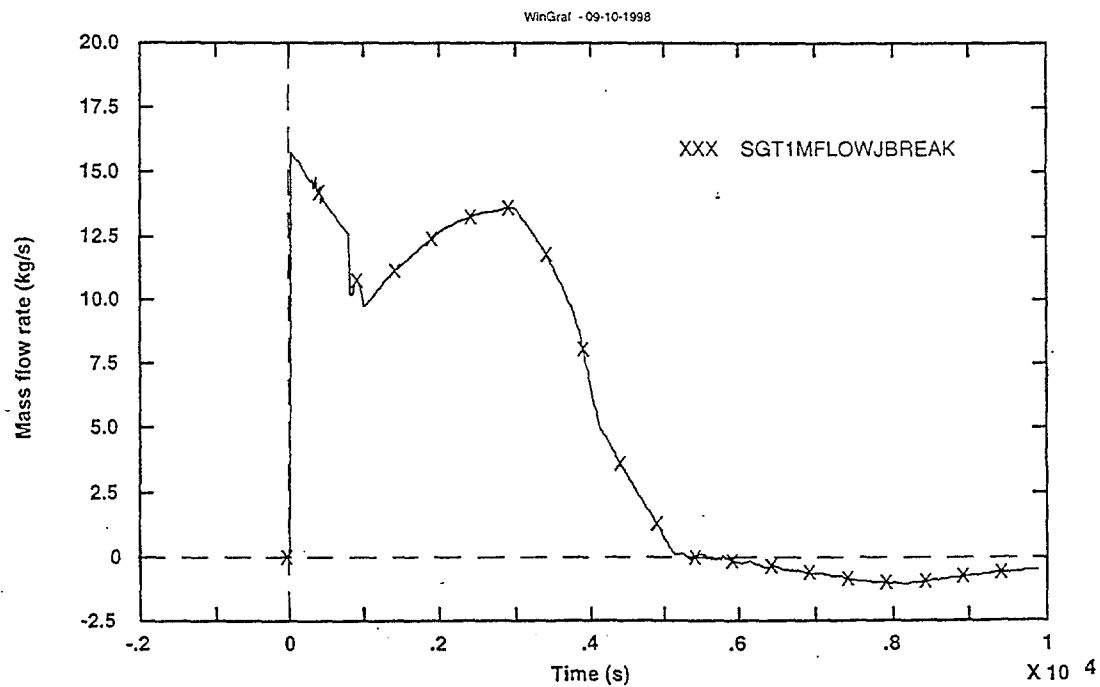


Fig. 3 - Break total mass flow rate

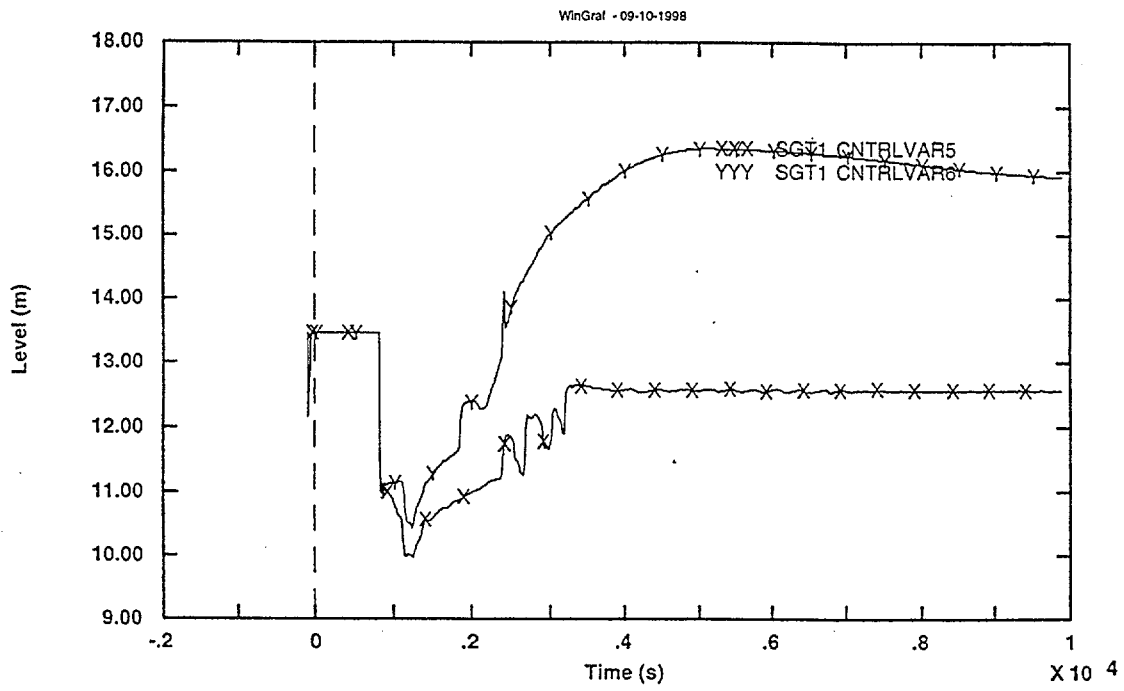


Fig. 4- Downcomer SGs collapsed level

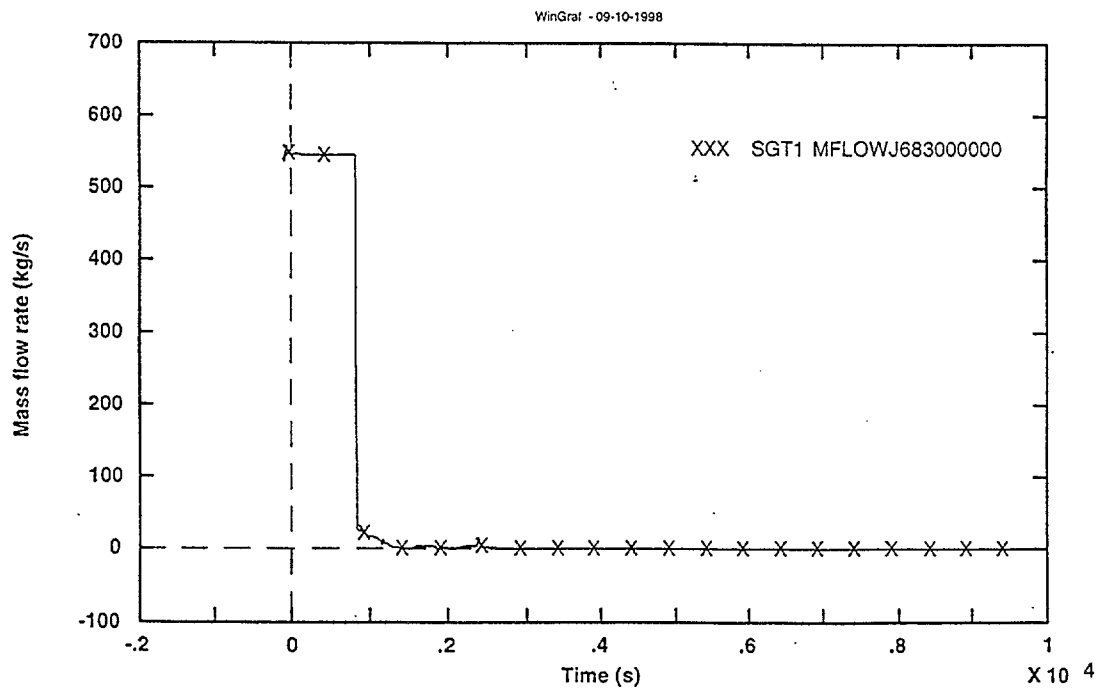


Fig. 5- Mass flow rate from SGB

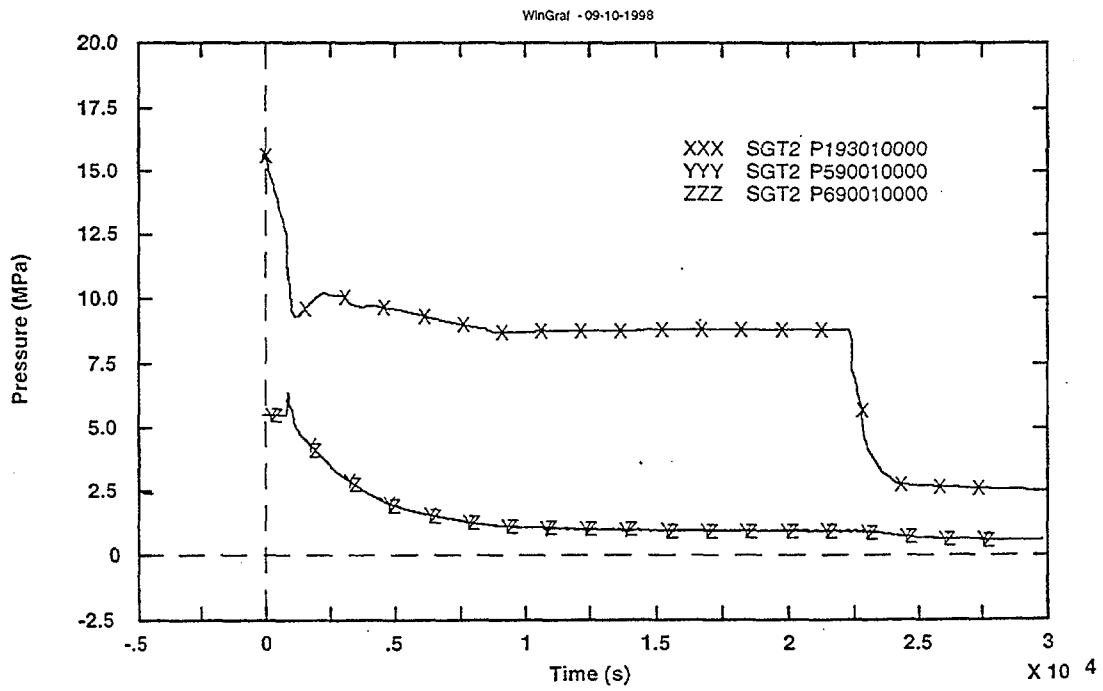


Fig. 6- Primary and secondary side pressure

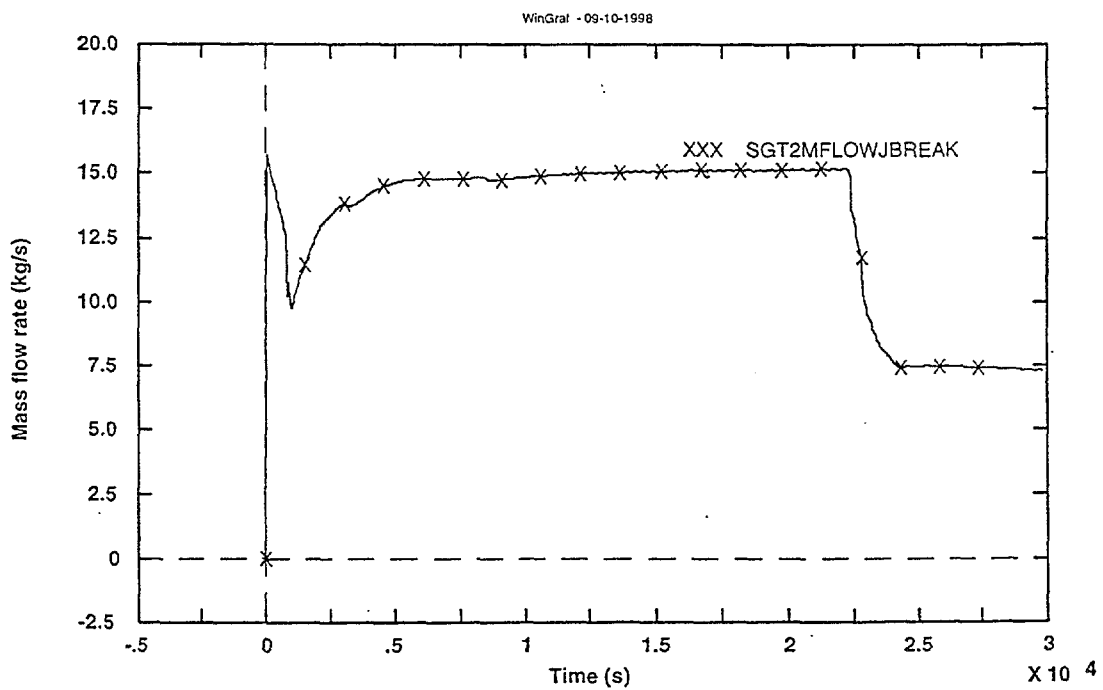


Fig. 7- Break total mass flow rate

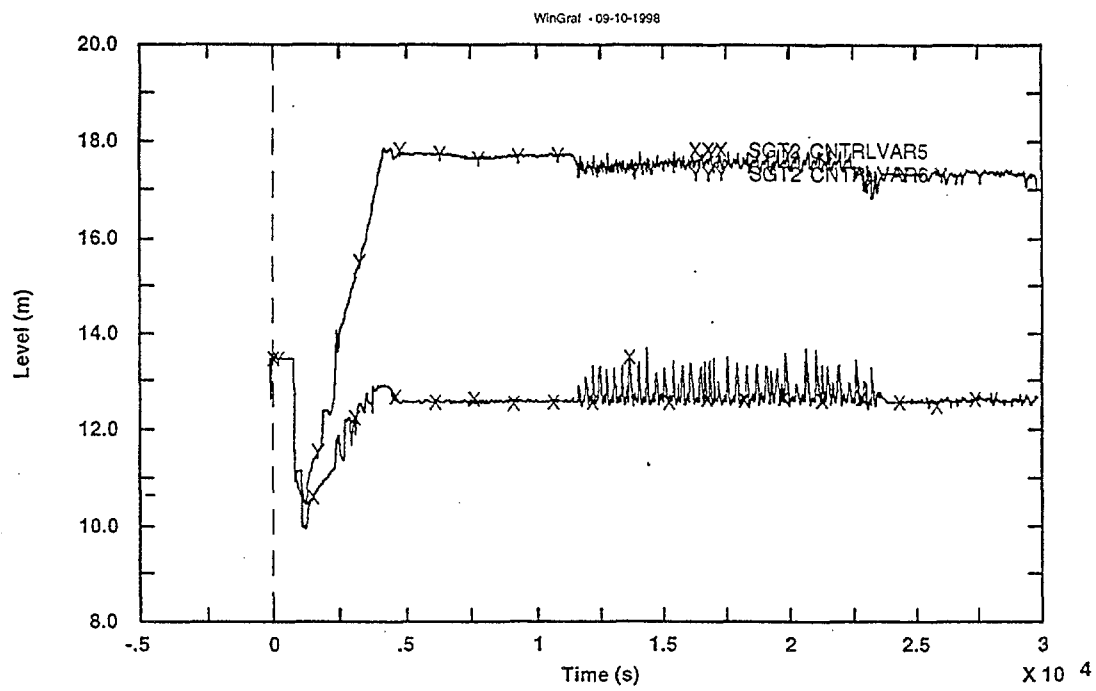


Fig. 8- Downcomer SGs collapsed level

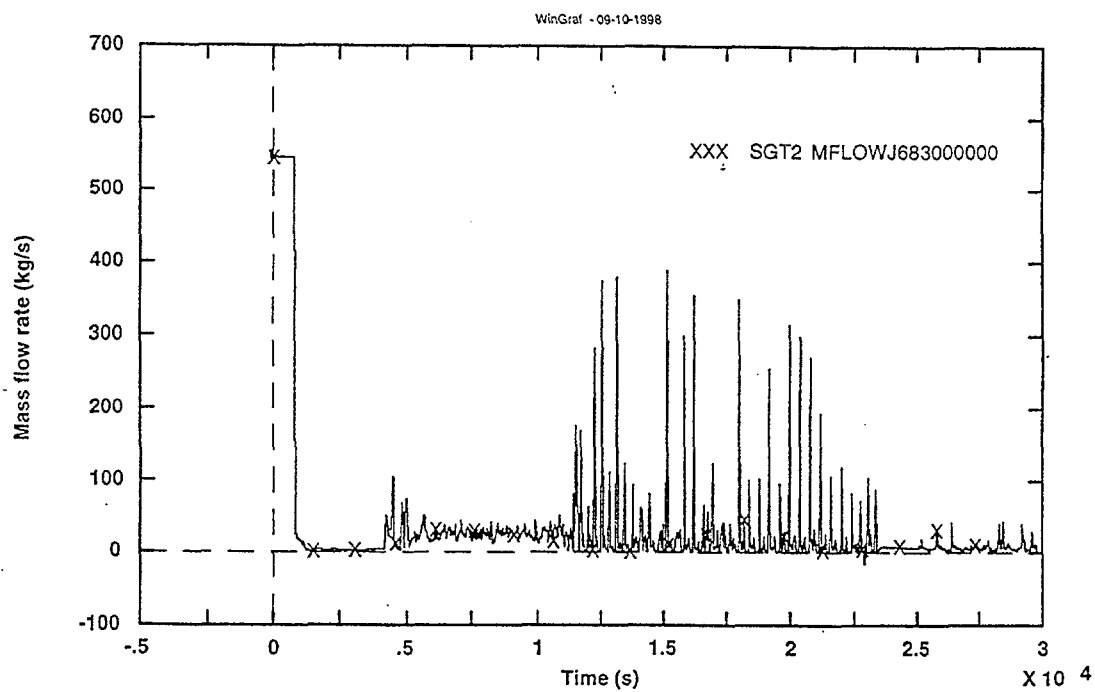


Fig. 9- Mass flow rate from SGB

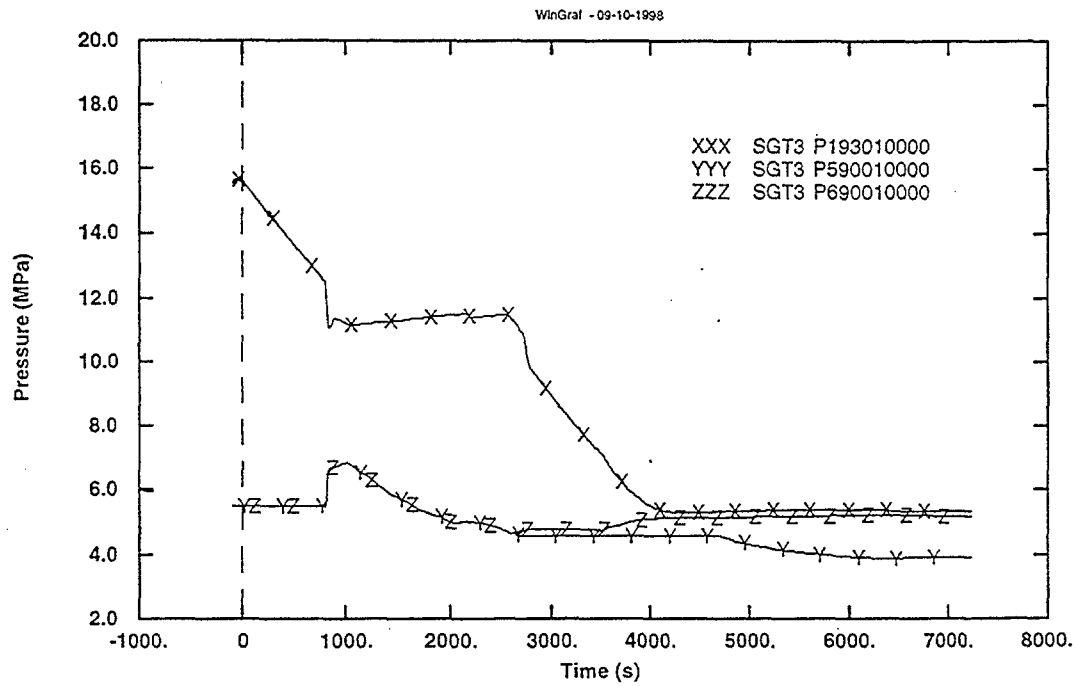


Fig. 10- Primary and secondary side pressure

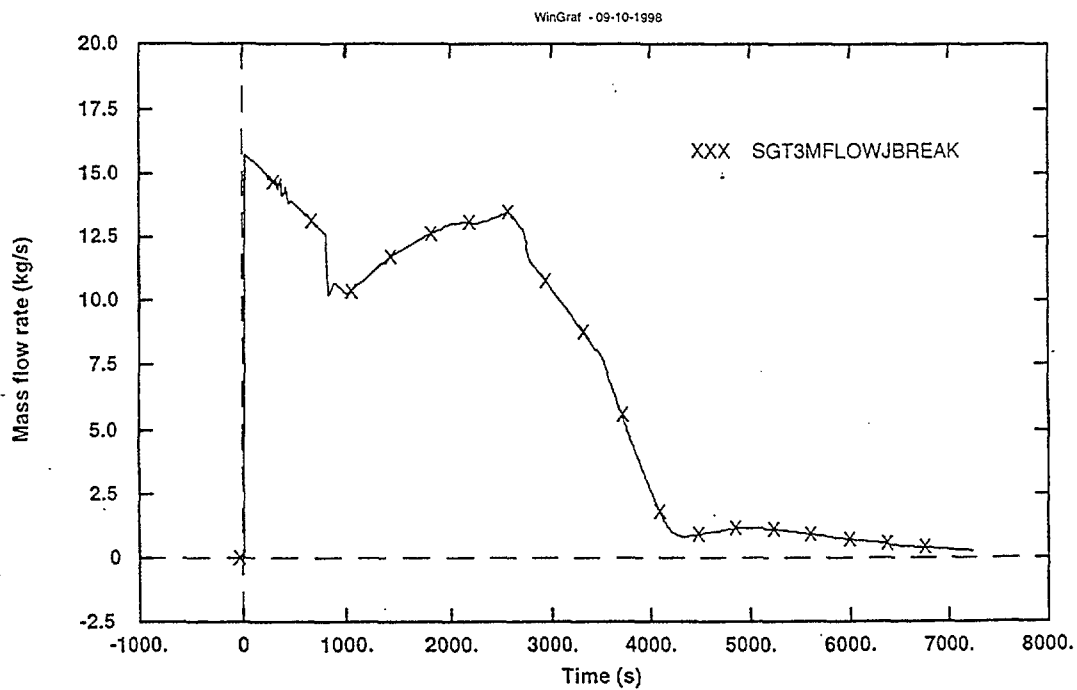


Fig. 11- Break total mass flow rate

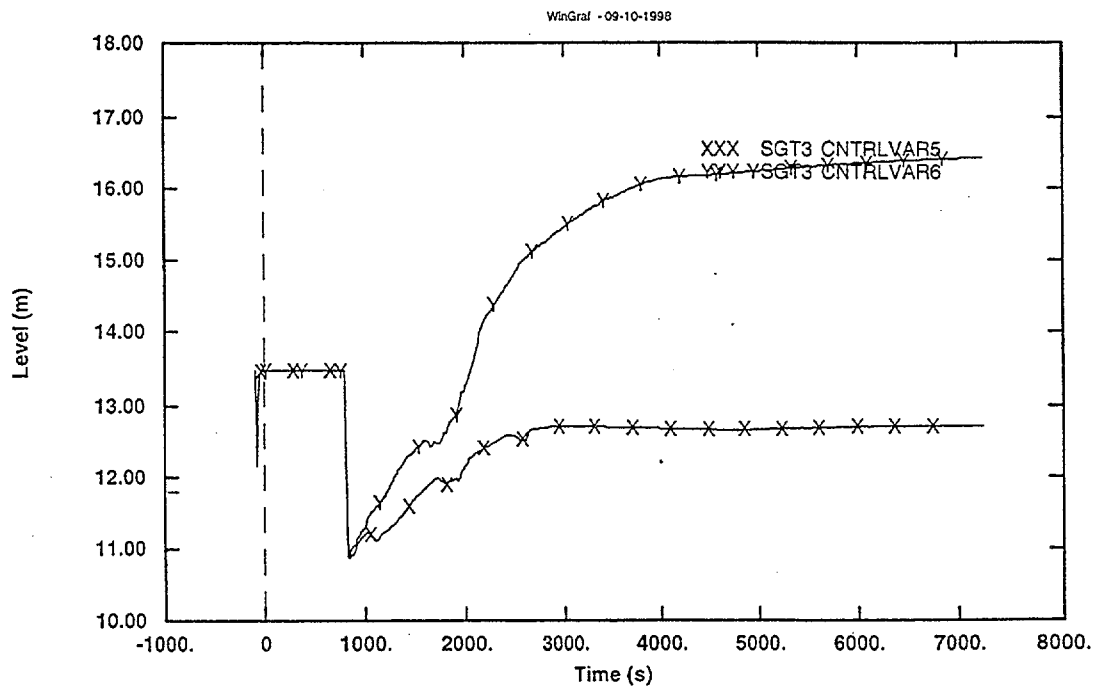


Fig. 12- Downcomer SGs collapsed level

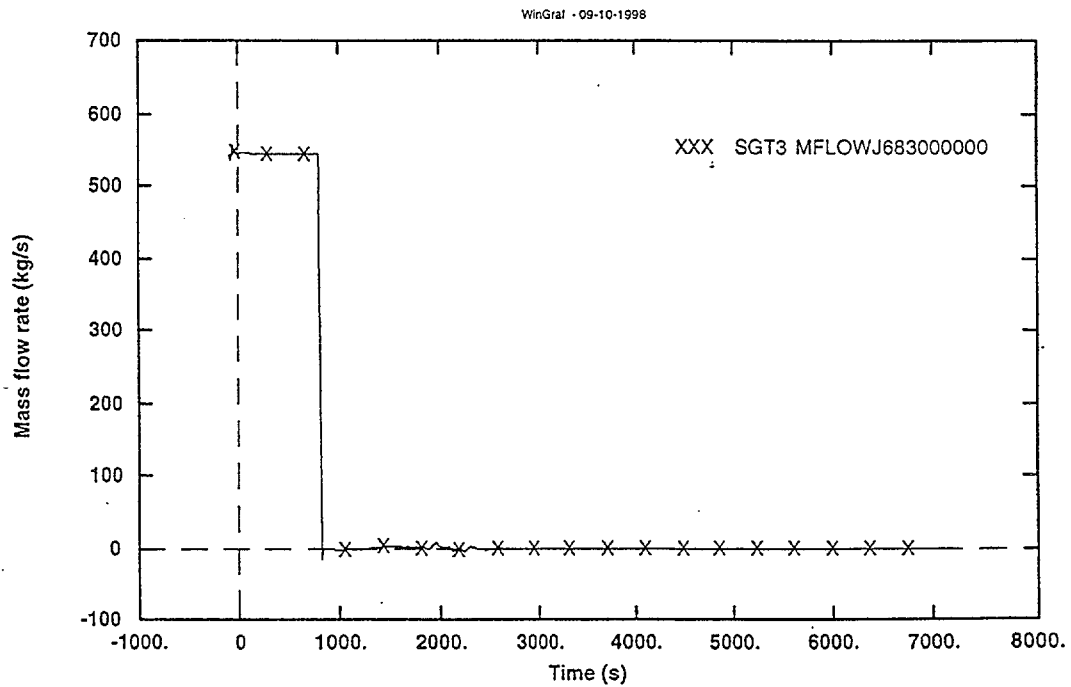


Fig. 13- Mass flow rate from SGB

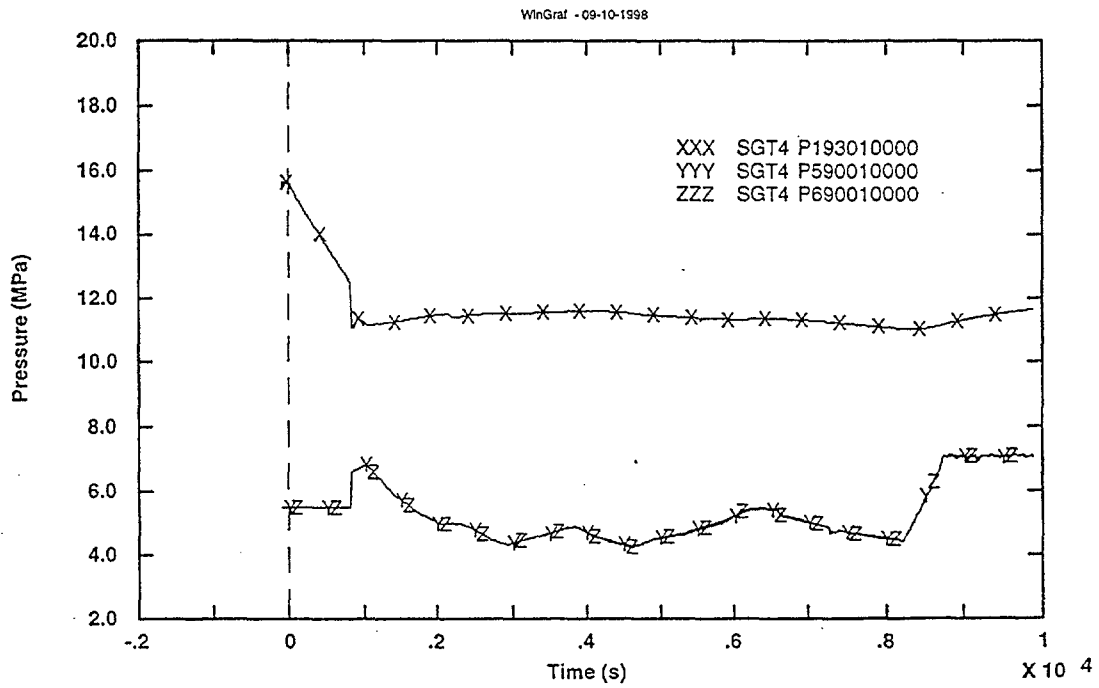


Fig. 14- Primary and secondary side pressure

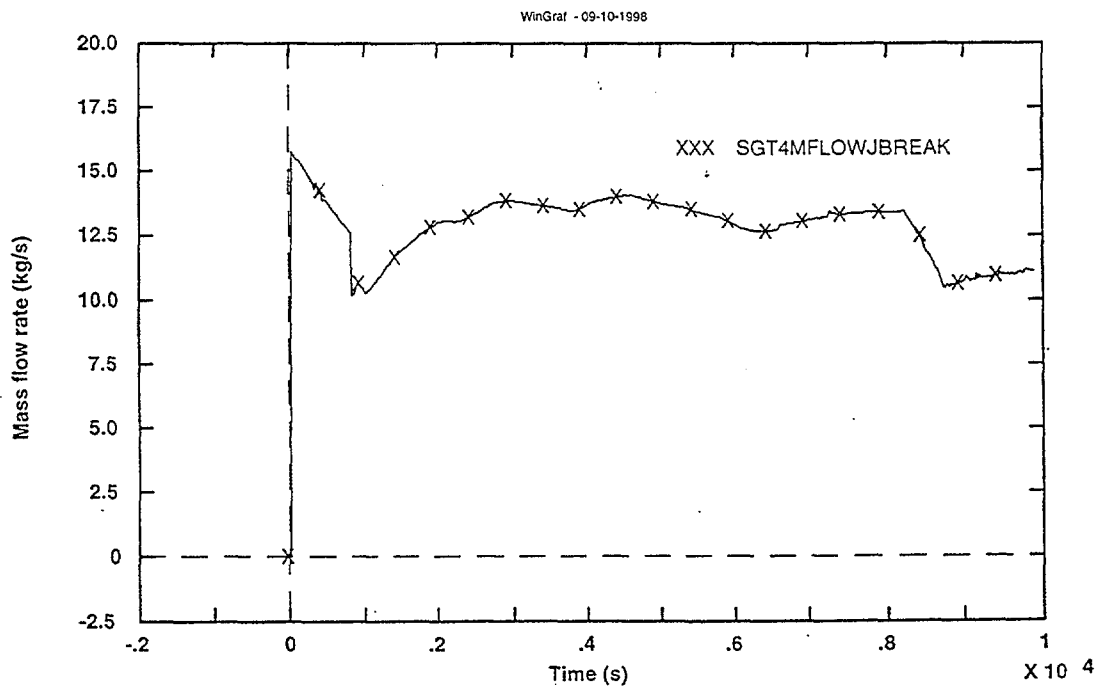


Fig. 15- Break total mass flow rate

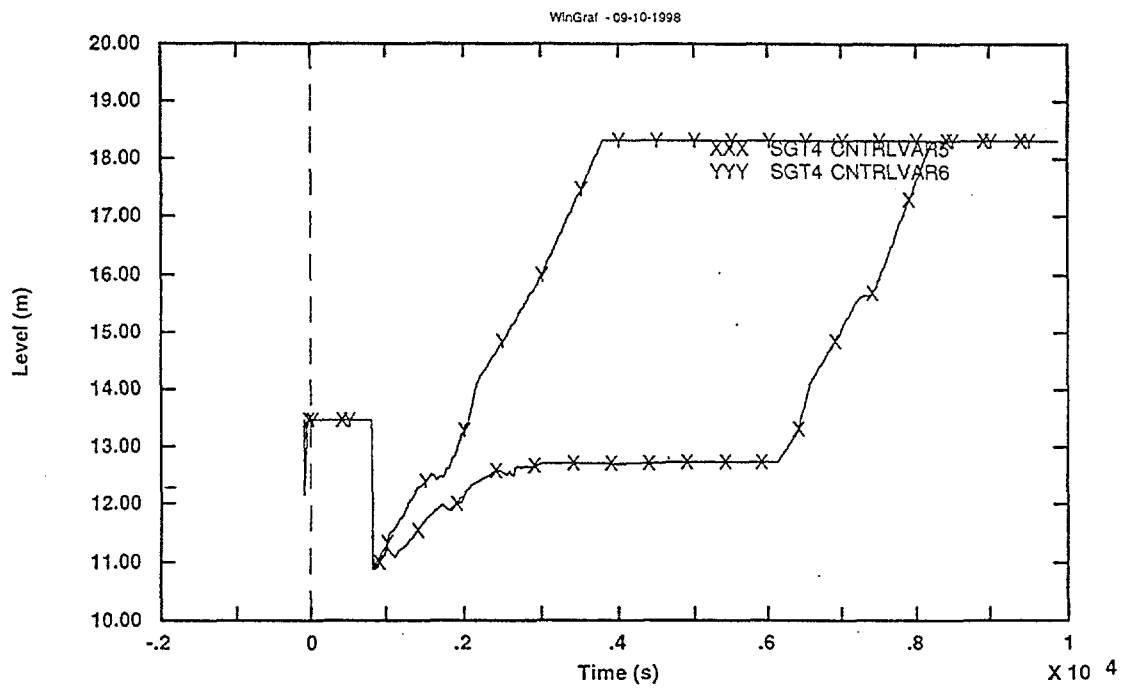


Fig. 16- Downcomer SGs collapsed level

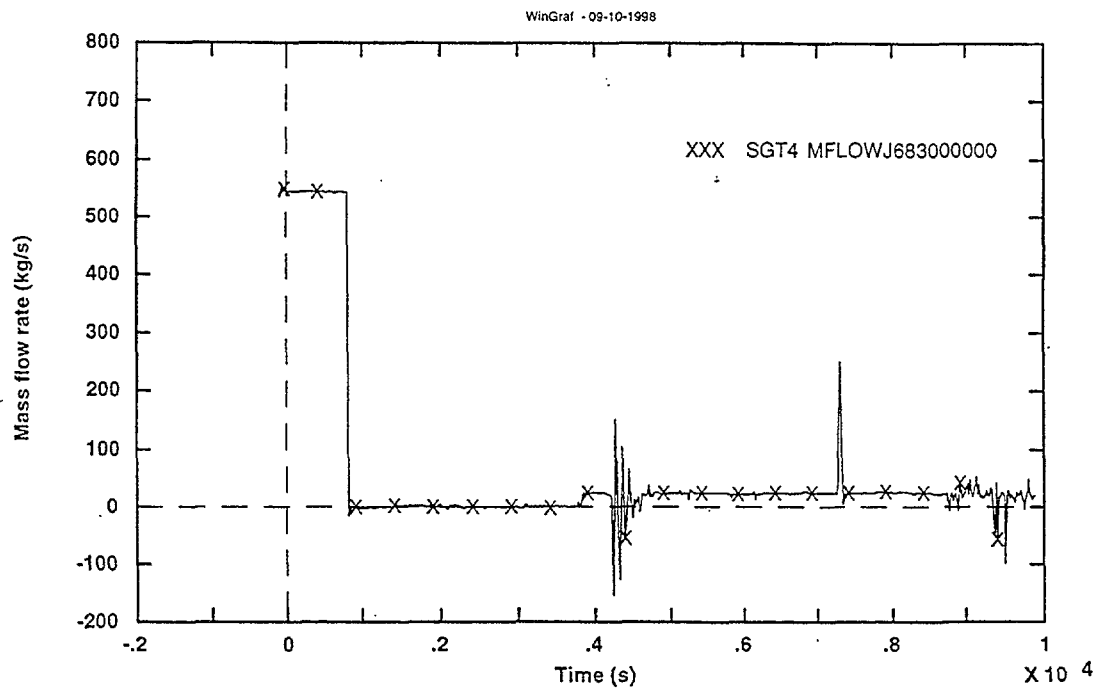


Fig. 17- Mass flow rate from SGB

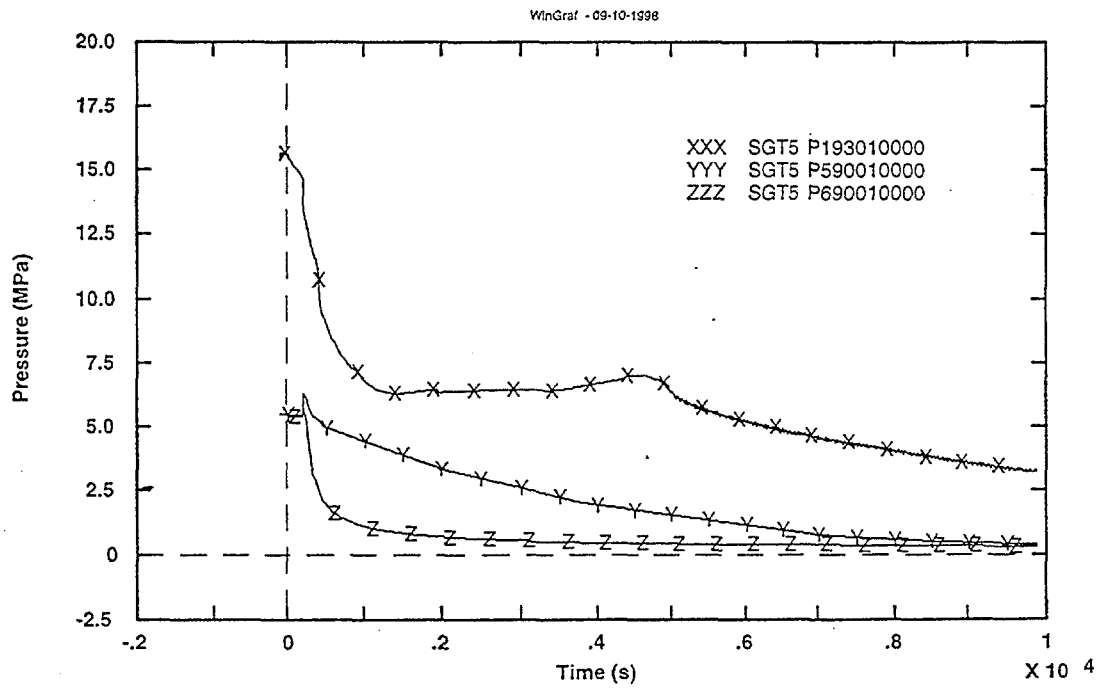


Fig. 18- Primary and secondary side pressure

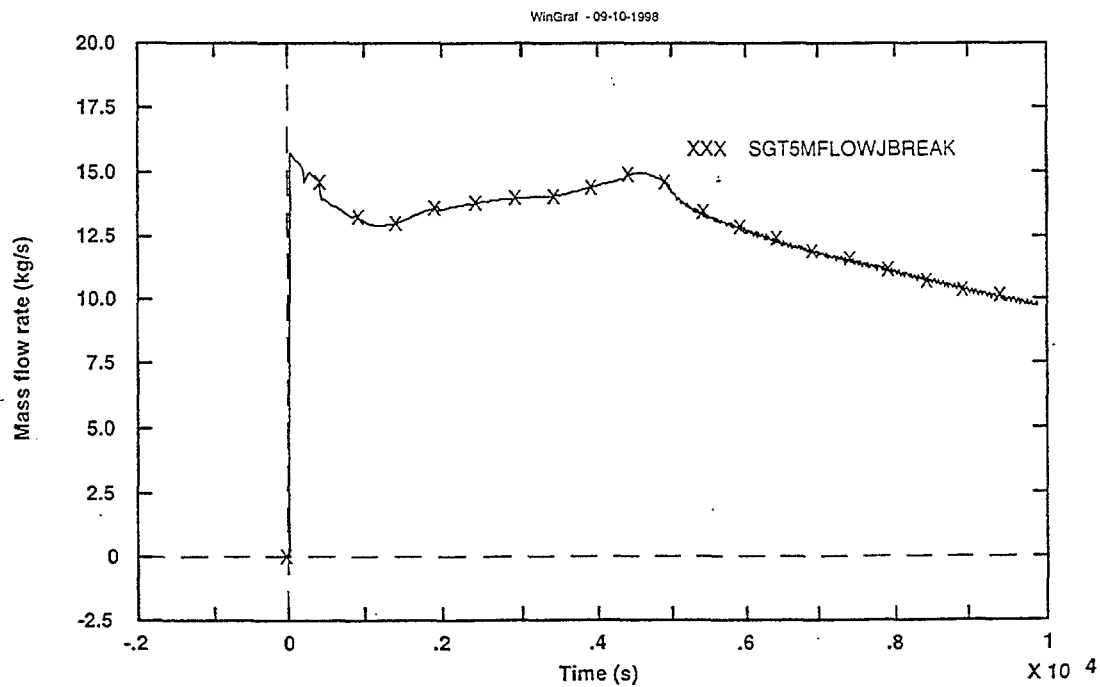


Fig. 19- Break total mass flow rate

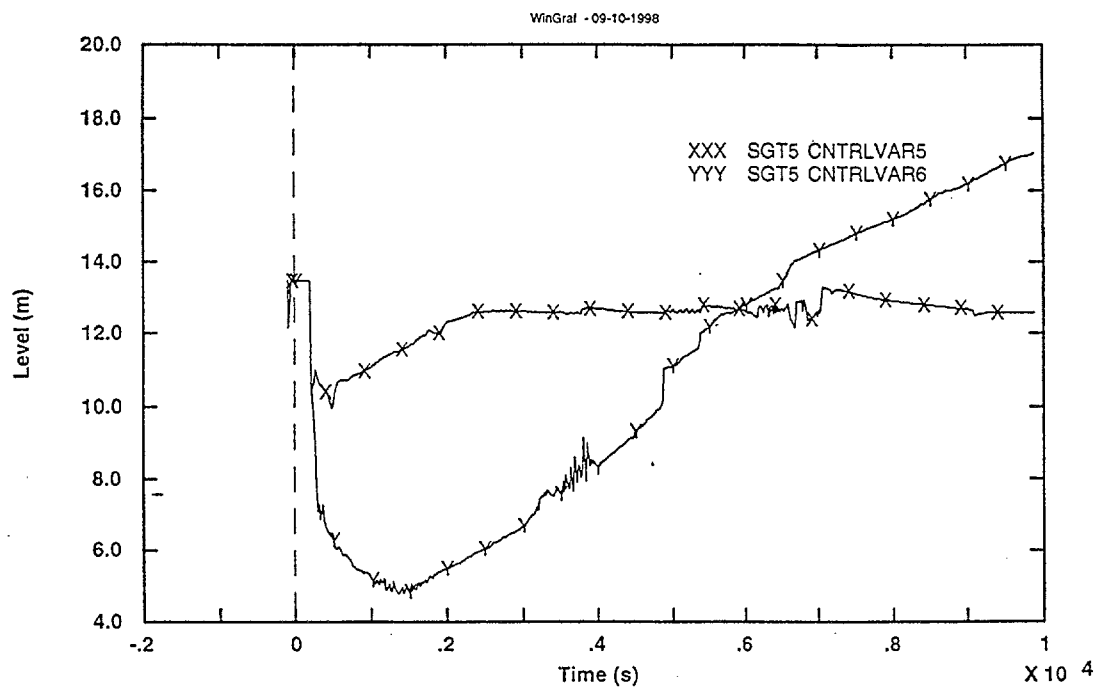


Fig. 20- Downcomer SGs collapsed level

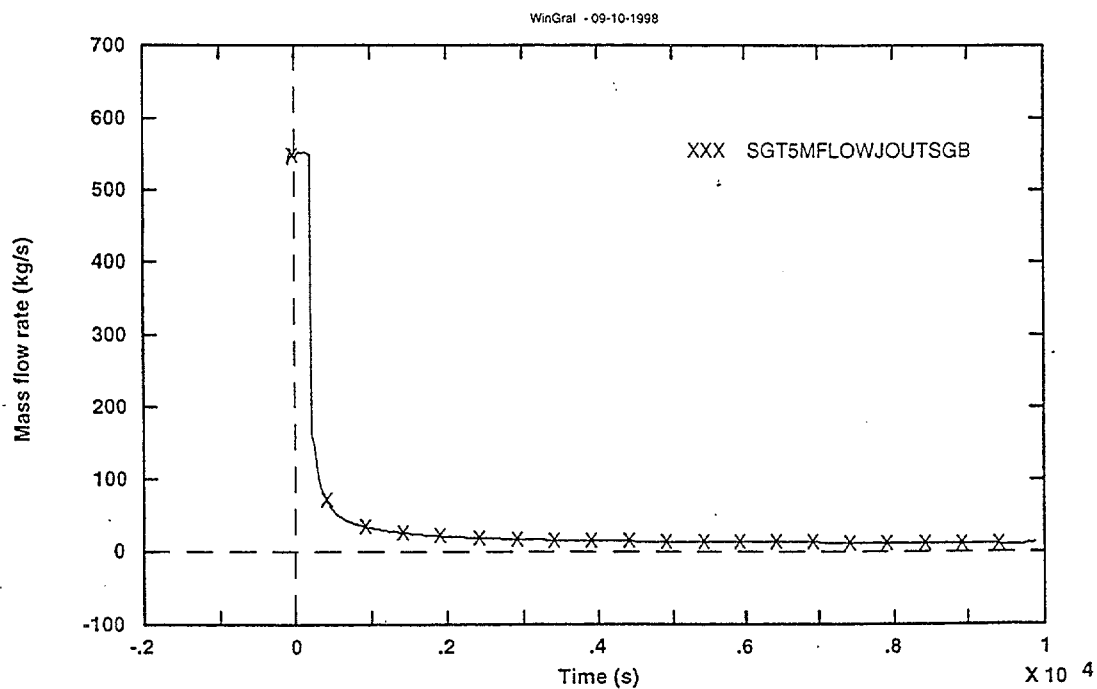


Fig. 21- Mass flow rate from SGB

Tab. 4 - Break and MSIV mass flow rate integrals

QUANTITY	SGT1	SGT2	SGT3	SGT4	SGT5
Break integral (Mg)	52.2	139.9/384.9*	47.4	127.1	126.4
MSIV integral from SG No. B (Kg)	443.5	593.6/1005.6*	435.2	572.5**	86.3/197.5***

* value at 30000 s into the transient

** some mass is lost from the SRV (cycling)

*** value from the SRV stuck open

5. CONCLUSIONS

A qualified AP-600 nodalisation has been adopted for performing scoping calculations concerned with steam generator tube rupture transient in AP-600. The analysis confirmed the quality of the AP-600 safeguards during this kind of transient: mainly CMT and PRHR system design parameters are concerned in this case. In particular, core level remains above the top of active fuel at each time during any of the calculated transient scenarios.

In relation to iodine release from primary to secondary side and across the MSIV of the broken steam generator, the following can be noted:

1. The closure of the MSIV of the affected steam generator is essential for limiting primary coolant mass leakage; clearly, this result must be evaluated considering the status of the primary and secondary loops at the end of the calculated transients.
2. The occurrence of 'solid condition' should be avoided with improved design of Emergency Operating Procedures;

Only in one calculation, i.e. SGT4, SRV cycling (i.e. direct release of iodine to the atmosphere) has been calculated toward the end of the transient.

REFERENCES

- [1] US NRC
"Relap5/mod3 Code Manual"
NUREG/CR-5535, 1995
- [2] D'Auria F., Galassi G.M.
"Experience gained in the application of Relap5 and Cathare codes to situations relevant to the new generation reactors"
Post-Smirt Seminar 14, Pisa (I) Aug. 25-27, 1997
- [3] D'Auria F., Modro M., Oriolo F., Tasaka K.
"Relevant thermalhydraulic aspects of new generation reactors"
J. Nuclear Engineering and Design, vol 145, Nrs 1&2, 1993
- [4] D'Auria F., Marsili P., Frogheri M., Giannotti W.
"Standardised procedure for thermalhydraulic system code assessment"
Spring 1998 CAMP meeting, Ankara (Tr), June 24-26 1998-09-09
- [5] Bonuccelli M., D'Auria F., Debrecin N., Galassi G.M.
"A methodology for the qualification of thermalhydraulic codes nodalisations"
NURETH-6 Conference, Grenoble (F), Oct. 5-8, 1993
- [6] Aksan S.N., D'Auria F., Staedtke H.
"User effect on the thermalhydraulic transient system codes calculations"
J. Nuclear Engineering and Design, vol 145, Nrs 1&2, 1993
- [7] D'Auria F.
"Proposal for training of thermalhydraulic system code users"
IAEA SM on User Qualification and User Effects on Accident Analysis for Nuclear Power Plants",
Vienna (A), Aug. 31-Sept. 4, 1998
- [8] Trambauer K.
"Computer and Compiler Effects on Code Results"
OCDE/CSNI Status Report NEA/CSNI R(96) 15, Paris (F), 1996

- [9] D'Auria F., Galassi G.M.
"Code Validation and Uncertainties in System Thermalhydraulics"
J. Progress in Nuclear Energy, Vol 33, No 1&2, 1998
- [10] Aksan S.N., D'Auria F.
"Status Report on Relevant Thermalhydraulic Aspects of advanced Reactor Design"
OECD/CSNI Report NEA/CSNI R(96)22, Paris (F), Nov. 1996
- [11] D'Auria F., Fruttuoso G., Oriolo F., Bella L., Cavicchia V., Fiorino E.
"Spes-2: AP-600 integral test facility results: confirmatory plant behaviour and Relap5/mod2.5 code assessment"
ICONE-3 Conf. – Kyoto (J), April 23-27, 1995
- [12] D'Auria F., Fruttuoso G., Galassi G.M., Oriolo F.
"AP-600 transient behaviour: evaluation of Spes-2 data and of code capabilities in reproducing relevant phenomena"
University of Pisa Report, DCMN NT 262(95), Pisa (I), July 1995
- [13] Bajs T., D'Auria F., Fruttuoso G., Galassi G.M., Oriolo F.
"Update of the Relap5 nodalization of the Westinghouse AP-600 plant"
University of Pisa Report, DCMN RL 644(94), Pisa (I), Aug. 1994
- [14] Bajs T., D'Auria F., Fruttuoso G., Galassi G.M., Oriolo F.
"Analysis by Relap5/mod2.5 code of a 1 tube SGTR in the Westinghouse AP-600 plant"
University of Pisa Report, DCMN RL 645(94), Pisa (I), Aug. 1994
- [15] Bajs T., D'Auria F., Fruttuoso G., Galassi G.M., Oriolo F.
"Analysis by Relap5/mod2.5 code of a 2" cold leg break in the Westinghouse AP-600 plant"
University of Pisa Report, DCMN RL 646(94), Pisa (I), Aug. 1994
- [16] Ambrosini W., D'Auria F., Fruttuoso G., Oriolo F.
"AP-600 overall analyses evaluation: ENEL activity Final Report" (in italian)
University of Pisa Report, DCMN RL 648(94), Pisa (I), Sept. 1994

LIST OF PARTICIPANTS

Aksan, N.	Paul Scherrer Institute, Department of Nuclear Energy/Safety, Thermal-Hydraulics Laboratory, CH-5232 Villigen, Switzerland
Analytis, G.Th.	Paul Scherrer Institute, Department of Nuclear Energy/Safety, Thermal-Hydraulics Laboratory, CH-5232 Villigen, Switzerland
Andreani, M.	Paul Scherrer Institute, Department of Nuclear Energy/Safety, Thermal-Hydraulics Laboratory, CH-5232 Villigen, Switzerland
Bandurski, T.	Paul Scherrer Institute, Department of Nuclear Energy/Safety, Thermal-Hydraulics Laboratory, CH-5232 Villigen, Switzerland
Barnea, J.	IAEC, P.O. Box 7061, Tel Aviv, Israel
Batet, L.	Universitat Politecnica de Catalunya, Seccio Enginyeria Nuclear, EDIFICI ETSEIB, Av Diagonal, 647, E-08028 Barcelona, Spain
Bergeron, A.	CEA/DRN/DMT/SERMA/LETR, Centre d'Etudes de Saclay, F-91191 Gif-sur-Yvette Cedex, France
Bermejo, J.M.	European Commission, DGXII/F/5, Eue de la Loi 200, B-1049 Brussels, Belgium
Chen, Y.	China Institute of Atomic Energy, P.O. Box 275(59), 102413 Beijing, China
Cleveland, J.	International Atomic Energy Agency, Wagramer Strasse 5, P.O. Box 100, A-1400 Vienna, Austria
Chung, M.K.	Korea Atomic Energy Research Institute, Yusung, P.O. Box 105, Taejon 305-600, Republic of Korea

- D'Auria, F. University of Pisa,
Dipartimento di Costruzioni Meccaniche E Nucleari,
Via Diotisalvi, 2, I-56126 Pisa, Italy
- Dreier, J. Paul Scherrer Institute,
Department of Nuclear Energy/Safety,
Thermal-Hydraulics Laboratory,
CH-5232 Villigen, Switzerland
- Dumaz, P. Commissariat à l'Energie Atomique,
CEA Cadarache DRN/DER/SIS,
F-13108 St. Paul-lez-Durance, France
- Faluomi, V. Energy and Environment Technology Center (TEA),
Consorzio Pisa Picerche, Piazza d'Ancona 1,
I-56126, Pisa, Italy
- Foskolos, K. Paul Scherrer Institute,
Deputy Head of Nuclear Energy
and Safety Department,
CH-5232 Villigen, Switzerland
- Freire, C.F. Electronuclear,
Rua da Candelária, 65/7º andar
20091-020, Rio de Janeiro - RJ, Brazil
- Gamble, R. GE Nuclear Energy,
175 Curtner Avenue, MC 365,
San Jose, California 95125,
United States of America
- van der Hagen, T. Delft University of Technology/IRI,
Mekelweg 15, NL-2629 JB Delft,
Netherlands
- ul-Haq, I. Institute for Nuclear Power,
P.O. Box 3140, Islamabad, Pakistan
- Hart, J. Netherlands Energy Research Foundation,
Westerduinweg 3, NL-1755 ZG Petten,
Netherlands
- Hassan, Y.A. Department of Nuclear Engineering,
Texas A&M University,
College Station, Texas 77843-3133,
United States of America
- Herranz, L.E. CIEMAT,
Department of Nuclear Fission (Ed.12),
Avda. Complutense 22,
E-28040 Madrid, Spain

Hicken, E.F.	Forschungszentrum Jülich GmbH, Institut für Sicherheitsforschung und Reaktortechnik, Jülich, Germany
Van Hove, W.A.M.	Tractebel N.V., Arianelaan 7, B-1200 Brussel, Belgium
Huggenberger, M.	Paul Scherrer Institute, Department of Nuclear Energy/Safety, Thermalhydraulics Laboratory, CH-5232 Villigen, Switzerland
Ingham, P.J.	Atomic Energy of Canada Ltd, Whiteshell Laboratories, Pinawa, Manitoba, ROE ILO, Canada
Jackson, J.D.	University of Manchester, School of Engineering, Oxford Road, Manchester M13 9PL, United Kingdom
Ji, F.	Senior Engineer, Nuclear Power Institute of China, P.O. Box 622-203, Chengdu, China
Kataoka, K.	Deputy Manager, Mechanical Engineering and Reactor System Group, Nuclear Engineering Laboratory, Toshiba Corporation, 8, Shinsugita-cho, Isogo-ku, Yokohama 235-8523, Japan
Ketelaar, K.	Netherlands Energy Research Foundation, Westerduinweg 3, NL-1755 ZG Petten, Netherlands
Khartabil, H.F.	Atomic Energy of Canada Ltd, Chalk River Laboratories, Chalk River, Ontario KOJ 1JO, Canada
Kirillov, P.	State Scientific Centre, Institute of Physics and Power Engineering, Bondarenko Sq. 1, 249020 Obninsk, Kaluga Region, Russian Federation
Knebel, J.U.	Forschungszentrum Karlsruhe GmbH, Technik und Umwelt, Institut für Angewandte Thermo- und Fluidodynamik, Postfach 3640, D-76021 Karlsruhe, Germany
Kunz, R.	Applied Research Laboratory, Garfield Thomas Water Tunnel, 3rd Floor, Pennsylvania State University, University Park, PA 16802, United States of America

Kuramoto, E.	Electronuclear, Rua da Candelária, 65 – Centro, 20091-020, Rio de Janeiro - RJ, Brazil
Lillington, J.	AEA Technology, 364/A32, Winfrith Technology Centre, Dorchester, Dorset DT2 80H, United Kingdom
Lübbesmeyer, D.	Paul Scherrer Institute, Department of Nuclear Energy/Safety, Thermalhydraulics Laboratory, CH-5232 Villigen, Switzerland
Maheshwari, N.K.	Bhabha Atomic Research Centre, Reactor Engineering Division, Hall No. 7, B.A.R.C., Mumbai - 400 085, India
Mazufri, C.M.	INVAP, F.P. Moreno 1089, 8400 S.C de Bariloche, Rio Negro, Argentina
Meseth, J	Siemens AG, KWU NAPS, P.O. Box 3220, D-91050 Erlangen, Germany
Nitheanandan, T.	Atomic Energy of Canada Ltd, Whiteshell Laboratories, Pinawa, Manitoba, ROE ILO, Canada
Nunez-Carrera, A.	National Commission of Nuclear Safety and Safeguards (CNSNS), Dr. Barragan No. 779, Col. Narvarte, C.P. 03020, Mexico, D.F.
Oriolo, F.	University of Pisa, Dipartimento di Costruzioni Meccaniche E Nucleari, Via Diotisalvi, 2, I-56126 Pisa, Italy
Rammohan, H.P.	Nuclear Power Corporation of India Ltd, Vikram Barabhai Bhavan, Anushaktinagar, Mumbai - 400 094, India
Rao, A.	GE Nuclear Energy, 175 Curtner Avenue, MC 365, San Jose, California 95125, United States of America
Reventos, F.	Universitat Politècnica de Catalunya, Secció Enginyeria Nuclear, EDIFICI ETSEIB, Av Diagonal, 647, E-08028 Barcelona, Spain

Song, C.H.	Korea Atomic Energy Research Institute, Yusung, P.O. Box 105, Taejon 305-600, Republic of Korea
Tanrikut, A.	Turkish Atomic Energy Authority, P.K. 249, Kavaklıdere, 06693 Ankara, Turkey
Tóth, I.	KFKI Atomic Energy Research Institute, H-1525 Budapest POB 49, Hungary
Yadigaroglu, G.	Paul Scherrer Institute, Department of Nuclear Energy/Safety, Thermalhydraulics Laboratory, CH-5232 Villigen, Switzerland
Yesin, A.O.	Turkish Atomic Energy Authority, Middle East Technical University, Mechanical Engineering Department, 06531 Ankara, Turkey
Yonamoto, T.	Senior Engineer, Thermohydraulic Safety Research Laboratory, Department of Nuclear Engineering, Tokai Research Establishment, Japan Atomic Energy Research Institute, 2-4 Shirakata-shirane, Tokai-mura, Naka-gun, Ibaraki-ken 319 1195, Japan

The IAEA does not normally maintain stocks of reports in this series. They are however collected by the International Nuclear Information System (INIS) as non-conventional literature. Should a document be out of print, a copy on microfiche or in electronic format can be purchased from the INIS Document Delivery Services:

INIS Clearinghouse
International Atomic Energy Agency
Wagramer Strasse 5
P.O. Box 100
A-1400 Vienna, Austria

Telephone: (43) 1 2600 22880 or 22866
Fax: (43) 1 2600 29882
E-mail: chouse@iaea.org

Orders should be accompanied by prepayment of 100 Austrian Schillings in the form of a cheque or credit card (VISA, Mastercard).

More information on the INIS Document Delivery Services and a list of national document delivery services where these reports can also be ordered can be found on the INIS Web site at http://www.iaea.org/inis/dd_srv.htm.